HIGH-RESOLUTION SPELEOTHEM-BASED PALAEOCLIMATE RECORDS FROM NEW ZEALAND REVEAL ROBUST TELECONNECTION TO NORTH ATLANTIC DURING MIS 1-4

A thesis
submitted as required for the degree
of

Doctor of Philosophy in Chemistry and Earth and Ocean Sciences

at

The University of Waikato

by

THOMAS EDWARD WHITTAKER

The University of Waikato
2008

Abstract

Growth rates, $\delta^{18}O$ and $\delta^{13}C$ of five stalagmites from the west coasts of North and South Islands, New Zealand, provide records of millennial-scale climate variability over the last ~75 kyr. Thirty-five uranium-series ages were used to provide the chronology. $\delta^{18}O$ of stalagmite calcite was influenced by changes in moisture source region, temperature and both $\delta^{18}O$ and $\delta^{13}C$ primarily display a negative relationship with rainfall. To assist interpretation of climatic signals $\delta^{18}O$ profiles were adjusted for the ice-volume effect. Changes in these proxies reflect changes in the strength of the circumpolar westerly circulation and the frequency of southwesterly flow across New Zealand.

MIS 4 was a period of wet and cool climate lasting from 67.7 to 61.3 kyr B.P., expressed in the stalagmites by an interval of strongly negative isotope ratios and increased growth rate. This contrasts with less negative $\delta^{18}O$ and $\delta^{13}C$, and slow growth, interpreted as dry and cold climate, during much of MIS 2. This difference between MIS 2 and MIS 4 provides an explanation for why glacial moraines in the Southern Alps of MIS 4 age lie beyond those deposited during the last glacial maximum (MIS 2).

Heinrich events, with the exception of H0 (the Younger Dryas), are interpreted from high-resolution South Island stalagmite HW05-3, from Hollywood Cave, West Coast, as times of wetter and cooler climate. Minima in $\delta^{18}O$ and $\delta^{13}C$ (wet periods) occurred at 67.7-61.0, 56-55, 50.5-47.5, 40-39, 30.5-29, 25.5-24.3 and 16.1-15. kyr B.P. matching Heinrich events H6-H1 (including H5a) respectively. This demonstrates a robust teleconnection between events in the North Atlantic and New Zealand climate. Minima in $\delta^{18}O$ also occurred at similar times in less well-dated North Island stalagmite RK05-3 from Ruakuri Cave, Waitomo. Speleothems from low-latitudes have revealed that Heinrich events forced southerly displacement of the Intertropical Convergence Zone. This caused steepening of the temperature gradient across mid-southern latitudes, increased westerly circulation and resulted in wet conditions on the west coast of both islands.

Immediately following H1 in the HW05-3 stable isotope profiles is another excursion to more negative isotopic values, suggesting wet and cold climate,

lasting from 14.6 to 13.0 kyr B.P. Such a climate on the West Coast at this time has been previously suggested from glacier advance (e.g. Waiho Loop moraine) and decreased abundance of tall trees on the landscape. This event occurred too early to be a response to H0, but is synchronous with a return to cool climate in Antarctica. Thus West Coast climate appears to have been sensitive to changes in Antarctica as well as the North Atlantic.

Isotopic minima (wet and cool climate) in South Island stalagmite GT05-5, which formed during the Holocene, first occurred 4.6 kyr B.P. This began a series of four oscillations in isotope ratios, the last terminating when the stalagmite was collected (2006). Onset of these oscillations is associated with initiation of ice advance in the Southern Alps, and beginning of the Neoglacial. The last oscillation displays enriched isotope ratios lasting from 1.2 to 0.8 kyr B.P. succeeded by depleted ratios lasting until 0.15 kyr B.P., mirroring the Medieval Climate Optimum and Little Ice Age, respectively, of European palaeoclimate records.

Acknowledgements

Completion of this thesis would not have been possible without the help and support of a great many people. First and foremost this project would not have existed but for the vision and financial support of Gary Comer. I hope that the work contained within this thesis is a rewarding result for his investment in abrupt climate change research through grants from the Gary Comer Educational Foundation. Second, I would like to thank my primary supervisor Chris Hendy for providing me with the opportunity to be involved in such an exciting project. Third, I doubt that the fieldwork for this project could ever have gone so well, so smoothly, or with so much fun without the inextinguishable enthusiasm of Russell Bromley.

Thank you also to Cam Nelson for providing invaluable advice when things didn't run so smoothly and for ensuring that the manuscript was suitable for submission; Deborah Carden (Buller-Kawatiri Office, Department of Conservation) for assistance in the permit application process; Jane Furkert and Dawn Mazzagetti for help in the field; Steve Cooke for teaching me more mass spectrometer operating idiosyncrasies than I ever thought possible; John Hellstrom for dedicating time to teach me the ins and outs of uranium-thorium dating; and to Marcus Vandergoes for many discussions on current thinking of New Zealand palaeoclimate research and for assisting in editing the manuscript.

I wish to acknowledge John Ash and Van Watson (tourism Holdings Limited) and Dave Smith (Department of Conservation for the generous access to stalagmites recovered during the redevelopment of Ruakuri Cave, Waitomo. I also acknowledge Timberlands West Coast (Greymouth office) for allowing access to the land surrounding Whiskey Cave and Mr and Mrs Hunter of Springs Junction for granting permission to cross their land in order access Guillotine Cave.

Lastly, I am especially grateful to my wife, Amber, for her unending support throughout this project. I only hope I can return in kind when she does her Ph.D.

Table of Contents

List of Figures

List of Tables

Glossary of Abbreviated Terms

ACR	Antarctic Cold Reversal
AIM	Antarctic Isotope Maximum
B.P.	Before Present (an attempt has been made to ensure that in all cases "present" is equivalent to 2000 A.D.)
D-O event	Dansgaard-Oeschger event. Equivalent to GIS
eLGM	Extended Last Glacial Maximum
GIS	Greenland Interstadial
H event	Heinrich event. Massive iceberg discharge into the North Atlantic (numbered sequentially from 0)
ICP-MS	Inductively Coupled Plasma Mass Spectrometer
ITCZ	Intertropical Convergence Zone
kyr	Thousand year(s)
LGM	Last Glacial Maximum as defined by EPILOG (Environmental processes of the ice age: land, oceans, glaciers; Mix *et al.*, 2001)
MIS	Marine Oxygen Isotope Stage [numbered sequentially from 1, after Emiliani (1955)]
STF	Subtropical Front
VPDB	Vienna Peedee Belemnite
VSMOW	Vienna Standard Mean Ocean Water
YD	Younger Dryas Chronozone

1 Background

1.1 Milankovitch Theory and Global Climate (A)Synchrony

A characteristic of many Quaternary climate records are the asymmetric, ~100 kyr and 40 kyr long glacial-interglacial cycles. These asymmetric records were first observed by Emiliani (1955) in oxygen isotope measurements undertaken on planktonic foraminifera from deep-sea sediment cores and later developed by Broecker and van Donk (1970), Shackleton and Opdyke (1973) and many others. Following the development of dating of marine cores with a combination of ^{14}C for the first 30 kyr, $^{230}Th/^{234}U$ of interglacial high sea levels in Barbados (Fairbanks and Matthews, 1978) and palaeomagnetic stratigraphy, the oxygen isotope records were correlated with variations in orbital forcing, so-called Milankovitch theory (Shackleton and Opdyke, 1973). From this stage it was widely accepted that changes in insolation were responsible for the timescale of these cycles. More recently a few long cores have been obtained through packages of marine sediments of unusually high sedimentation rate, which have provided high-resolution records. These and continuous, high-resolution records from other deposits, such as ice cores, show that at shorter timescales this simple relationship cannot explain many of the climate patterns observed in developed palaeoclimate records. A significant example is the onset of deglaciation following the last glacial period, an event which occurred synchronously at multiple locations in both Northern and Southern Hemispheres (Denton *et al*., 1999a; Schaefer *et al*., 2006; Easterbrook, 2007). Orbital theory adequately explains the termination of the last glacial maximum (LGM) in the Northern Hemisphere as the result of increasing insolation. However, the same reasoning cannot be applied globally as at the same time in the Southern Hemsiphere insolation began a decreasing trend (Berger and Loutre, 1991) so application of the same logic would have predicted cooling (accompanied by glacial expansion). A possible solution to this dilemma is that the Earth's own atmosphere-ocean system is capable of rapidly redistributing incoming solar energy to the extent that it becomes the main driver of short-term climatic variability. In order to understand better how this system operates today, and has in the past, it is necessary to obtain many geographically

disparate palaeoclimate records and to observe regional, hemispheric and global patterns of climate (a)synchrony.

In the palaeoclimate literature there is conflicting evidence regarding the relative (a)synchrony of past climatic events between Northern and Southern hemispheres. Particular focus has been applied to investigating the timing and structure of climate changes during the latter stages of the last glacial period and the transition into the present interglacial. Significantly, determination of the relative timings of hemispheric-scale climate events is required to allow better understanding of the cause(s) of abrupt climate change.

There is evidence to suggest that at least during the last deglaciation climate change in the Southern Hemisphere, across all latitudes, was synchronous with events in the Northern Hemisphere (Denton and Hendy, 1994; Steig *et al*., 1998; Moreno *et al*., 2001; Schaefer *et al*., 2006). However, other records, in particular those from the Antarctic interior, display climate events independent of those operating in the North Atlantic (Blunier *et al*., 1998; Singer *et al*., 1998; Bennett *et al*., 2000; Turney *et al*., 2003), or that suggest a lead-lag relationship, with events in the south preceding those in the north (Charles *et al*., 1996; Morgan *et al*., 2002).

During the last glacial period, particularly throughout marine isotope stage (MIS) 3, there is also evidence for global climate synchrony (Kanfoush *et al*., 2000). An ice core recently drilled from Antarctica's Atlantic sector revealed minor millennial-scale variability similar in timing and duration to the Dansgaard-Oeschger (D-O) events that mark the Greenland ice core records (EPICA Community members, 2006). However, the structure of the LGM and the timing of the initiation of deglacial warming are not common to both Antarctic and Greenland records. Furthermore there is uncertainty surrounding the timing of the LGM at lower latitudes (Mix *et al*., 2001; Newnham *et al*., 2007a).

Comparatively little is understood of the relative timing of abrupt climate changes that affected extra-polar locations prior to the LGM, particularly in the Southern Hemisphere (Voelker *et al*., 2002). There is thus a need for other long, continuous records of climate change from the Southern Hemisphere to investigate whether global climate synchrony existed throughout the past or if synchrony occurred between times of asynchrony during the last glacial period and deglaciation.

1.2 New Zealand Climate History

New Zealand (approximately 34-47°S) is one of few landmasses in the largely oceanic province that occupy the mid southern latitudes. As such it is a prime location from which to develop terrestrial-based palaeoclimate records that can be used to test climate (a)synchrony. Furthermore, such datasets are valuable for the reasons that (1) New Zealand is far removed from North Atlantic origins of thermohaline convection and the large ice sheets of the Northern Hemisphere and therefore arguably only going to be influenced by events there if they are global in extent, (2) it lies directly in the path of, and will therefore be sensitive to changes in, the circumpolar westerly circulation, and (3) the annual pattern of Southern Hemisphere insolation is out of phase with that of the Northern Hemisphere, a significant point to consider when attempting to determine the cause of synchronous climate change between the hemispheres.

A palaeoclimate framework for New Zealand, covering the most recent 30 kyr, has been published by Alloway *et al*. (2007). The work attempts to draw a consensus on the millennial-scale structure of events occurring during the LGM, deglaciation and the Holocene from the terrestrial and marine palaeoclimate records developed from the region. Comparisons are made to Greenland and Antarctic ice cores, although it is unclear to what extent the New Zealand climate is forced by events at either location. A prime example of this is the definition of a New Zealand Late Glacial Reversal for a cooling event ~14-10 kyr B.P. which matches neither the Antarctic Cold Reversal (ACR) nor the Younger Dryas chronozone (YD), yet straddles both (Alloway *et al*., 2007).

Prior to 30 kyr B.P. there is a distinct lack of continuous, precisely-dated palaeoclimate records that are resolvable at millennial-scale resolution or better. This is particularly true for the terrestrial realm, with perhaps the only exception being the Okarito pollen sequence (Vandergoes *et al*., 2005; Newnham *et al*., 2007b). Offshore, high resolution marine sediment proxy records have been recently developed from locations in the Pacific Ocean and the Tasman Sea (Pahnke *et al*., 2003; Pahnke and Zahn, 2005; Pahnke and Sachs, 2006; Barrows *et al*., 2007). However, none of the datasets present information from marine oxygen isotope stage (MIS) 3 (or earlier) that is based on an independent

chronology. The reliance on “tuning” the data to other palaeoclimate records limits their use in helping to interpret (a)synchrony of regional and global climate change.

The continuous record of early last glacial climate change at Okarito displays only small variations in relative pollen abundances suggesting either that this interval was marked by minor climate variability or that the available vegetational assemblages are insufficiently sensitive. However, glacial features on both sides of the Southern Alps indicate multiple advances and retreats of ice during this time, including the most extensive advance of the last glacial period (Suggate, 1990; Williams, 1996; Preusser *et al*., 2005; Denton *et al*., unpublished data). A record of more responsive proxies is required to relate the apparent climatic changes with observed glacial fluctuations.

The New Zealand moraine record has been extensively investigated and a robust chronology of events has been determined (Suggate, 1965; Gellatly *et al*., 1988; Suggate, 1990; Denton and Hendy, 1994; Denton *et al*., 1999a; Suggate and Almond, 2005, and references therein). Significantly many of these events are consistent with glacier mass balance fluctuations in other regions of the globe (Denton *et al*., 1999a; Schaefer *et al*., 2006; Easterbrook, 2007). An interesting feature of the New Zealand moraine record is the discovery that ice advances on both sides of the main divide during MIS 4 were of greater extent than at the last glacial maximum (Suggate, 1990; Putnam *et al*., 2007). This raises an important question. During the last glacial was the period of maximum cooling during MIS 4 or MIS 2? On the global scale MIS 2 has generally been recognized as the coolest interval of the last glacial period in association with greatest sea level lowering and the concurrent maximum in global ice volume. Although, as in New Zealand, Chilean MIS 4 glaciers also extended beyond their MIS 2 extremes (Denton *et al*., 1999b). Relatively small sized ice fields extending from high mountain chains and exposed to maritime climates, such as those in New Zealand and Chile, would have been much more sensitive and responded quicker to climate variability than the large Northern Hemisphere ice sheets. Anderson and Mackintosh (2006) found temperature to have been the dominant influence on the modern glacier mass balance on the Franz Josef Glacier, Westland, and suggest that this relationship should hold for the past. Coupled with the evidence from glacial geomorphology this may indicate that MIS 4 was colder than MIS 2.

However, glacier expansion is also driven by increased precipitation and greater expanse of ice at MIS 4 relative to MIS 2 could indicate decreased mean annual precipitation volumes during MIS 2 (Hooker and Fitzharris, 1999). In order to understand behaviour of glaciation in New Zealand the relative significnce of temperature changes versus precipitation needs to be determined.

1.3 Speleothems

Speleothems have the potential to yield long, continuous, high-resolution palaeoprecipitation/palaeotemperature datasets, from multiple proxies including stable isotopes of carbon and oxygen and trace elements (Fairchild *et al*., 2006). Furthermore, through the application of U-Th dating techniques these datasets may be supported by absolute and precise chronologies which extend far beyond the limit of radiocarbon dating, the mainstay of most New Zealand palaeoclimate records.

The value of such records to the understanding of New Zealand palaeoclimate has previously been demonstrated (Hendy and Wilson, 1968; Wilson *et al*., 1979; Hellstrom *et al*., 1998; Williams *et al*., 2004, 2005). However opportunities remain to investigate in finer scale the climate changes of the Holocene and deglaciation, and to extend the record beyond the last glacial maximum.

1.4 Research Objectives

In this research I present palaeoclimate data from the last glacial-interglacial cycle archived in stalagmites from North and South Islands of New Zealand. These records are used to investigate patterns of millennial-scale climate variability and abrupt climate changes that have influenced New Zealand in the past. Contemporaneous records from North and South Islands will be used to test regional climate synchrony and gauge the relative influences of polar and subtropical climate at these sites. Furthermore, the potential to determine the timing and causes (temperature and/or precipitation) of glacier advance and retreat in the Southern Alps during the last glacial period and the Holocene using speleothem proxy records will be investigated. Lastly, the timing and structure of abrupt climate events will be compared to similar events (e.g. Heinrich events, D-

O events and Antarctic Interstadials) in records from the North Atlantic and Antarctica. This will allow an assessment of the relative influence on the past climate of New Zealand of Northern and Southern Hemisphere climate dynamics and therefore allow a greater understanding of global climate (a)synchrony during the last glacial-interglacial cycle.

2 Literature Review

2.1 Climate Events of the Last Glacial-Interglacial Cycle

2.1.1 Background

The theory of the ice ages was introduced to the scientific community by Louis Agassiz in 1837. In his presentation he proposed that continent-sized ice sheets were responsible for the deposits widely thought to have been laid down during the biblical flood. Despite early opposition, it wasn't long before most researchers recognized that it could explain many more of their findings than could a flood.

Subsequently, it was determined that in at least Europe and North America four separate drift sheets could be identified. In some instances these deposits were separated by peat, an indication that warm climate intervened between ice ages. From this was born the idea that ice volumes had waxed and waned multiple times during recent Earth history and that the Earth had not experienced one ice age, but many.

James Croll (1864; cited in Imbrie and Imbrie, 1979) and, later, Milutin Milankovitch (Köppen and Wegener, 1924) suggested that temporal cyclicity in the variation of the Earth's orbit around the sun, its angle of tilt and the precession of the equinoxes were capable of driving climate changes on Earth. Milankovitch's calculations were the first to show that the magnitude of change in incoming solar radiation was sufficient to drive the ice ages. Furthermore he demonstrated that obliquity (tilt), the ~41 kyr cycle, was the dominant cycle at high latitudes, while precession, the ~21 kyr cycle, was dominant at low latitudes.

In the 1970s the CLIMAP initiative was undertaken (Hays *et al*., 1976). This multi-institutional effort aimed to determine the pacemaker of the ice ages from marine sediment cores. It soon became clear that for at least the last 500,000 years Earth had gone into and come out of ice ages on a ~100,000 year timescale, following the eccentricity frequency calculated by Milankovitch. Furthermore the detail of the isotopic variability described not only a 100 kyr periodicity, but also 43, 24 and 19 kyr cycles as being important. This was clear evidence that changes

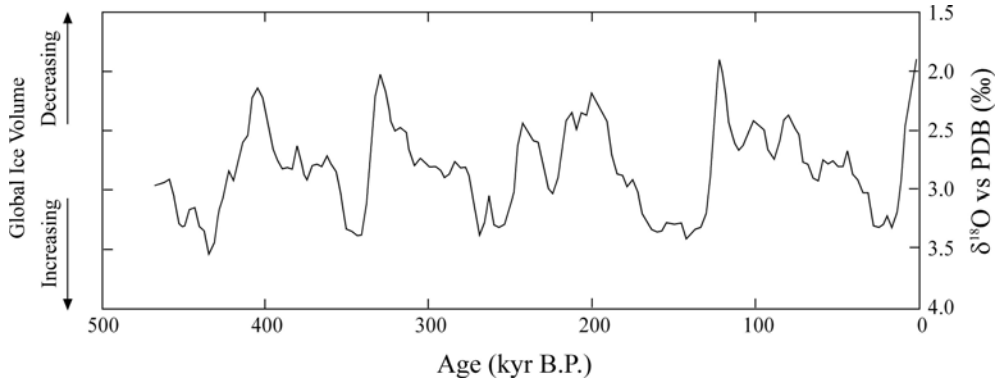

Figure 2.1: The characteristic "sawtooth" pattern of Quaternary glacial-interglacial cycles. Figure modified from Imbrie and Imbrie (1979); data from Hays *et al*. (1976).

---

in eccentricity, obliquity and precession were largely responsible for the timing of ice ages.

Each ~100 kyr glacial-interglacial cycle can be recognized from the "sawtooth" pattern in the oxygen isotope record of oceanic calcareous sediment (Figure 2.1). The pattern derives from the slow build up and subsequent rapid melting of large continental ice sheets (Broecker and Van Donk, 1970), although much of the pattern described by Broecker and van Donk can be attributed to their use of "Terminations" as tie points in tuning their records. The most recent of these periods of ice accumulation began 115-120 kyr B.P. at the end of the last interglacial (MIS 5e). Ice build up reached a maximum approximately 21 ± 3 kyr B.P. (Mix *et al*., 2001), although there may have been regional differences in the exact timing of glacier maxima. Rapid deglaciation followed the LGM, and the present interglacial (the Holocene) began ~10,000 years ago.

Another significant finding to emerge was the discovery that oxygen isotope ratios of fossilized marine plankton and benthos (specifically foraminifera) could be used to chart global ice volume through time (Shackleton, 1967). The CLIMAP project exploited this, demonstrating that at the time of the most recent radiation minimum in the Northern Hemisphere (~20 kyr B.P.) global ice volume, or at least its impact on oceanic oxygen isotopes, had reached a maximum for the last glacial phase (MIS 2-4).

Both Milankovitch and Croll recognized that the changes in incoming radiation in each hemisphere were opposite. Logically this would suggest that

while one hemisphere was in the grip of a glacial period the other should be experiencing an interglacial. However, following the advent of radiocarbon dating in the 1950s and the analysis of a significant number of marine sediment cores from around the world it became clear that the major glacial and interglacial climates occurred more or less synchronously in both hemispheres, and that both hemispheres were following the Northern Hemisphere radiation pattern.

At the same time that the CLIMAP hypothesis suggested that ice ages of the Quaternary were driven by variability in the Earth's position relative to the Sun, it was also becoming clear that past climate changes had occurred at timescales far shorter than that associated with orbital parameters.

In 1954, Iversen identified distinct pollen zones in Danish peat that were dominated by *Dryas octopetala*, an arctic-alpine flowering plant. Following the application of radiocarbon chronology to similar peat sequences in other parts of Scandinavia, Mangerud *et al*. (1974) assigned ages to each of these zones and discovered that oscillations between full glacial and interglacial climates had occurred on millennial timescales. The names of these (chrono)zones are now familiar to palaeoclimate researchers as the Bölling-Alleröd, a double-peaked warm interval, and the Younger Dryas, a cool interval.

In 1965 H. H. Lamb had identified a cool climate interval that occurred between ~1450 and 1850 A.D., now commonly referred to as the Little Ice Age, which followed a warm period, "The Medieval Warm Period", which peaked ~0.8 kyr B.P. Subsequently, Denton and Karlén (1973) demonstrated that during the Little Ice Age, and on four other occasions during the last 11,000 ^{14}C years, glaciers around the world underwent periods of expansion and retreat. These changes could not be explained by Milankovitch radiation forcing alone and it was therefore necessary to reconsider the interactions and feedbacks between elements of the global cryosphere-hydrosphere-atmosphere system. The importance of this system had already been recognized from the global synchroneity of the ice ages, however it now appeared as if it could be responsible for generating climate changes without the aid of Milankovitch variability.

As advances have been made in the precision of dating of climate proxy records, evidence for rapid atmosphere-ocean reorganizations has been revealed. Such "abrupt" climate changes were first revealed in cores obtained from the Greenland ice sheet (Dansgaard *et al*., 1982, 1989, 1993; Johnsen *et al*., 1992;

Grootes *et al*., 1993; also reviewed in Johnsen *et al*., 2001) and have since been duplicated in other high-resolution proxy records, including from speleothems (e.g. Wang *et al*., 2001). These abrupt events occur, and in some cases recur, at millennial and sub-millennial timescales. There is some debate in the scientific literature regarding whether these events are global, hemispheric or merely regional in extent. Furthermore there is even less understanding of the drivers of these events. It is for these reasons that new, continuous, long, high-resolution, absolute-dated records of past climate are sought and developed. Greater spatial and temporal coverage of palaeoclimate records will allow a better insight into the forcings and feedbacks that drive the Earth climate system.

The following sections will review in further detail the timing and finer-scale events of the last glacial-interglacial cycle as reported in the scientific literature. For ease of discussion this period is subdivided chronologically into the "Last Glacial Period" (~115-10 kyr B.P.), the LGM (30-18 kyr B.P.), "Deglaciation" (18-10 kyr B.P.) and "The Holocene" (10-0 kyr B.P.). In each case, particular effort will be made to focus on those events of specific importance to New Zealand.

2.1.2 Last Glacial Period (~115-10 kyr B.P.)

Following the work of Emiliani (1955), commonly recognized variability in planktonic foraminiferal $\delta^{18}O$ from marine sediments is used to subdivide the Quaternary into periods called marine oxygen isotope stages (abbreviated to MOIS or simply MIS in the literature). Under this nomenclature less positive $\delta^{18}O$ (warm periods) are assigned odd numbers and more positive $\delta^{18}O$ (cool intervals) even numbers. The Last Glacial Period, or Otiran in the New Zealand stratigraphy, covers marine oxygen isotope stages 2, 3, 4 and 5a-d. Within this, stages 2 and 4 represent the coldest climates and each is likely to have lasted for ~10,000 years.

Superimposed upon this broad framework of climate change are many smaller scale fluctuations. These are most easily recognized in high-resolution, continuous records from ice cores drilled in Antarctica and Greenland. It is widely accepted that the poles are acutely sensitive to climate change, therefore variability in the proxies obtained from these sites provides evidence for

hemispheric, if not global climate change. As such, polar ice cores are regularly used for inter-comparison with other proxy records from lower latitudes.

Ice cores retrieved from Greenland have revealed that climate during the Last Glacial Period was characterized by recurring, large, abrupt warming events lasting several hundred years or longer (Johnsen *et al*., 1992; Dansgaard *et al*., 1993; Mayewski *et al*., 1997; NGRIP Members, 2004). Twenty-five such oscillations, known as Dansgaard-Oeschger (D-O) events or Greenland interstadials (GIS), have been identified in Greenland ice over the period 115-14 kyr B.P. (Figure 2.2).

In addition to (and likely related to) D-O events, the North Atlantic experienced periodic large influxes of icebergs, known as Heinrich events (Heinrich 1988; McManus *et al*., 1994; Bond and Lotti, 1995; Rashid *et al*., 2003). Eight Heinrich events occurred during the Last Glacial Period (Figure 2.2). Each iceberg discharge followed a relatively long stadial and immediately preceded (or initiated) warming associated with the onset of a D-O event.

The long Antarctic ice core records [Byrd (Blunier *et al*., 1998; Blunier and Brook, 2001); Vostok (Petit *et al*., 1999); Taylor Dome (Steig *et al*., 1998; 2000); Dome Concordia (EPICA Community Members, 2004), Dronning Maud Land (EDML; EPICA Community Members, 2006), Dome Fuji (Watanabe *et al*., 2003)] display a more settled Last Glacial Period with variability of climate proxies being much less than that seen in Greenland. Blunier and Brook (2001) identified the seven largest positive excursions in $\delta^{18}O$ as Antarctic interstadials (A1-A7). These preceded by 1500 to 3000 years the longest of the D-O events in Greenland. More recently an ice core drilled in the Atlantic sector of the East Antarctic Ice Sheet has demonstrated that there were likely as many Antarctic interstadials (which they name Antarctic Isotope Maxima – AIMs) as there were D-O events (EPICA Community Members, 2006). Again, the onset of each Antarctic interstadial preceded its Greenland counterpart although there was particularly close correspondence between the timing of D-O and AIM events during MIS 3. A bipolar seesaw model of reduced North Atlantic circulation (meridional overturning circulation) and build-up of heat in the Southern Ocean has been invoked to explain the coupling of climate at both poles and also the phase relationship between AIMs and D-O events (Broecker, 1998; EPICA Community Members, 2006). It is hypothesized that the reduced magnitude of

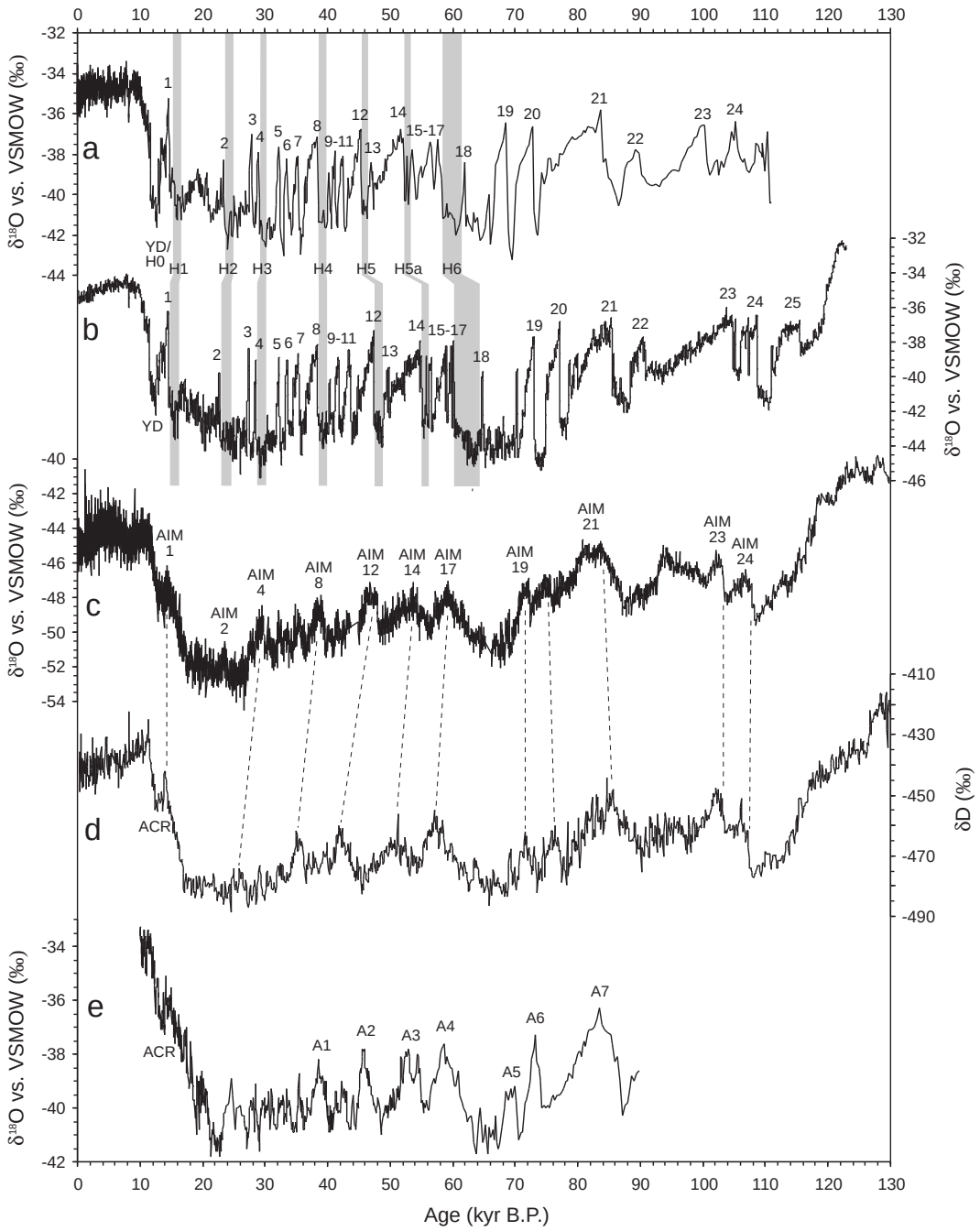

Figure 2.2: Comparison of ice core records from Greenland and Antarctica. Shown are (a) GISP2 (Grootes et al., 1993), (b) NGRIP (NGRIP Members, 2004), (c) EDML (EPICA Community Members, 2006), (d) Vostok (Petit et al., 1999), and (e) Byrd (Blunier and Brook, 2001). Greenland interstadials (D-O events) 1 to 25, the Younger Dryas chronozone (YD) and the relative timing of Heinrich events H1-H6 are indicated on the Greenland records. Antarctic interstadials A1-A7 and Antarctic Isotope Maxima (AIMs) defined in the Byrd and EDML records are shown, as well as the timing of the Antarctic Cold Reversal (ACR).

Antarctic events relative to their Greenland counterparts occurred as a result of amplification of the Antarctic signal or from overprinting of highly variable winter temperatures on annual temperature signals on the Greenland summit (Denton *et al*., 2005).

The large, abrupt climate changes that characterize the Greenland record for the Last Glacial Period are duplicated in records from across the Northern Hemisphere (Wang *et al*., 2001; Peterson *et al*., 2000; Hendy and Kennett, 2003; Shackleton *et al*., 2000; and others cited in Voelker, 2002), as well as at least one Southern Hemisphere location (Wang *et al*., 2006). The extent of Antarctic forcing is less well defined although Shackleton *et al*. (2000) identified evidence for it from varying extent of Antarctic Bottom Water in the North Atlantic.

Continuous series of high-resolution palaeoclimatic data covering the last glacial period are still rare in the Southern Hemisphere (Voelker, 2002) and clearly more are required before adequate testing of regional and global climate models can be accomplished.

Climate records from New Zealand (Figure 2.3) that cover some of the last glacial period are few, with many focusing on events that occurred during the late-glacial. Furthermore, the data available yields a relatively coarse resolution view of past climate. Only a handful of long (> 20 kyr) palaeoclimate records confidently resolve events at (sub) millennial scales (Nelson *et al*., 1993; Pahnke *et al*., 2003; Vandergoes *et al*., 2005; Carter *et al*., 2008). Despite this, a coherent picture of climate change throughout the last glacial period is emerging, particularly for South Island. Luminescence dates on glacial deposits in North Westland indicate that ice expansion in the Southern Alps began during MIS 5 (Preusser *et al*., 2005). This advance was accompanied by partial replacement of forest by shrubland further indicating weak cooling at this time (Newnham *et al*., 2007b).

Glaciers on both sides of the Southern Alps achieved their greatest extent of the entire last glacial period during MIS 4 (Suggate and Almond, 2005; Preusser *et al*., 2005; Schaefer *et al*., 2006). Further evidence for cooling at this time comes from glacially derived sediment deposits in Aurora Cave, Fiordland, sub-fossil coleoptera (beetles) assemblages at a site near Westport, increased accumulation of aeolian quartz in Taranaki soils, and pollen assemblages at Lake Tangonge in Northland (Figure 2.3; Alloway *et al*., 1992; Williams, 1996; Elliot *et al*., 2005;

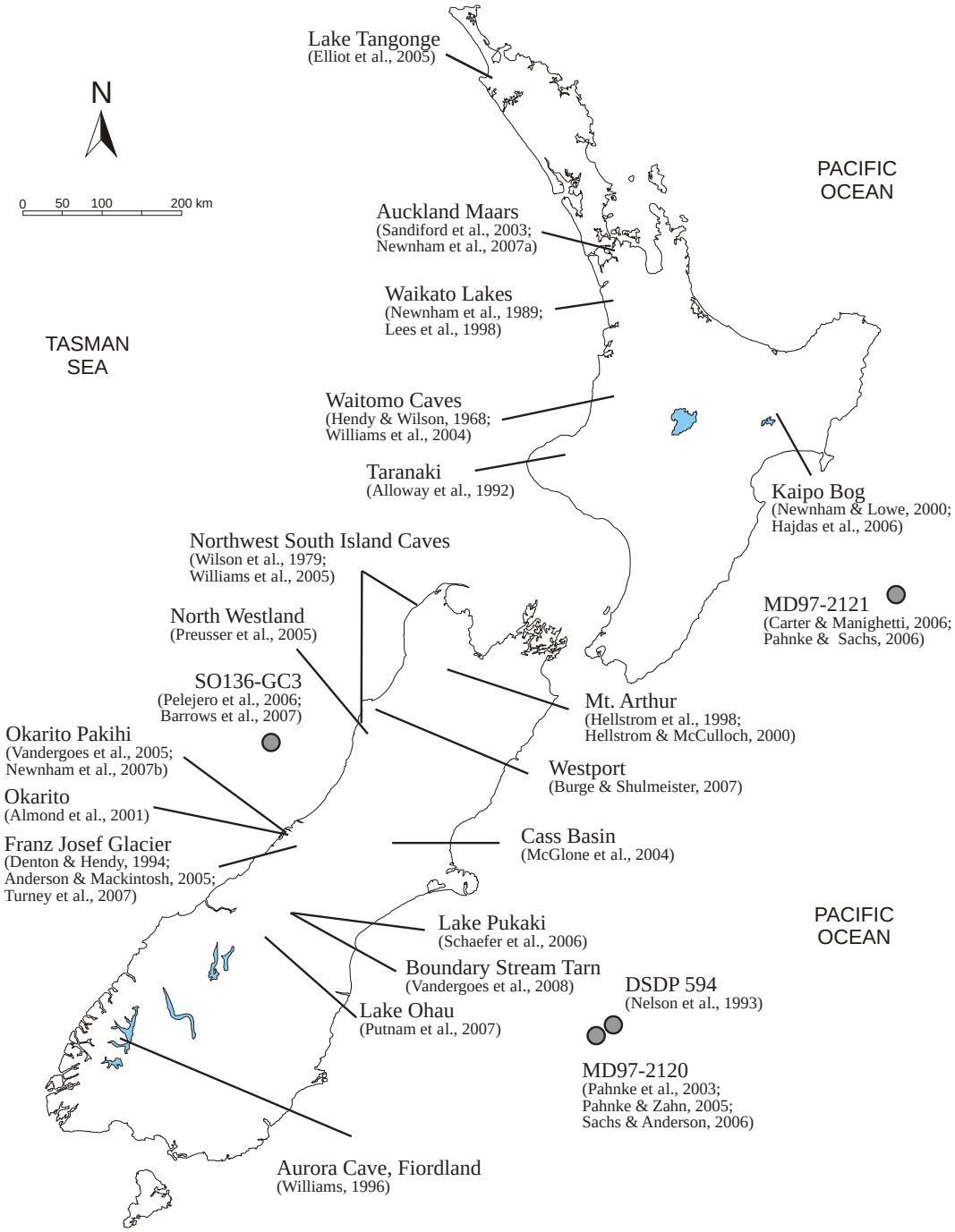

Figure 2.3: Locations of New Zealand palaeoclimate records mentioned in the text. Marine sediment cores are identified by filled circles.

Burge and Shulmeister, 2007). Despite the large extent of glaciers during MIS 4, mean annual temperatures were not as cool as they were in MIS 2 (Pahnke *et al*., 2003; Pelejero *et al*., 2006), although it was cold enough to almost entirely remove forest from parts of Westland (Vandergoes *et al*., 2005).

Unfortunately a lack of independent dates and/or poor dating precision affects all the records from New Zealand that cover MIS 4. This prevents the determination of the onset, character and termination of this event, important information needed for a greater understanding of the drivers affecting regional and global climate.

In the interval between the termination of MIS 4 glaciation and the significant re-advance of glaciers at ~34 kyr B.P., marking the onset of the LGM (Suggate and Almond, 2005), there is little preserved evidence for climate change. Williams (1996) and Vandergoes *et al*. (2005) each independently identify two periods of cool climate during MIS 3, with associated glacier advance and expansion of grassland occurring at 46-48 and ~ 40 kyr B.P. Further support for the earlier event is provided by increased loess accumulation in Westland between 45 and 50 kyr B.P. (Almond *et al*., 2001).

2.1.3 The Last Glacial Maximum (LGM)

The LGM is defined as the period of maximum sea level lowering during the last glacial period, which according to Mix *et al*. (2001) occurred 24-18 kyr B.P. While this provides an assessment of the timing of maximum global ice volume it would appear to not fully coincide with the timing of maximum cooling as recorded by the polar ice cores. Minimum isotopic values of ice at Greenland sites occurred ~30 kyr B.P. (Figure 2.2a,b; NGRIP Members, 2004). In Antarctica several ice core records display periods of maximum cooling beginning ~28 kyr B.P. (Figure 2.2c,d; Petit *et al*., 1999; Watanabe *et al*., 2003; EPICA Community Members, 2006).

Although there may be some debate surrounding the onset of LGM conditions on the global scale, the timing of its termination is well known. Warming, associated with deglaciation, was underway in Antarctica ~18 kyr B.P. (Petit *et al*., 1999; Morgan *et al*., 2002; EPICA Community Members, 2006); in the mid-

latitudes of both hemispheres retreat of glaciers from their LGM positions took place 18-17 kyr B.P. (Schaefer *et al*., 2006; Easterbrook, 2007); and sea level rise from the LGM lowstand began also ~18 kyr B.P. (Mix *et al*., 2001). However, significant warming is not observed at Greenland sites until the onset of the Bølling (D-O 1) at 14.7 kyr B.P. (Figure 2.2). Schaefer *et al*. (2006) suggest that unusually extensive sea ice in the North Atlantic during the period 18-14.7 ka may have isolated Greenland climate creating the apparent delayed response to global warming.

In New Zealand, evidence from South Island (east and west of the main divide) and North Island points to the onset of significant regional cooling between 34 and 28 kyr B.P., in line with polar ice core records but earlier than the defined LGM (Alloway *et al*., 1992; Suggate and Almond, 2005; Vandergoes *et al*., 2005; Newnham *et al*., 2007a; Putnam *et al*., 2007). Drost *et al*. (2007) modelled New Zealand's LGM climate and determined that temperatures were cooler than present in all areas with some regions colder (ΔT -4°C) than others (ΔT -2.5°C). Termination of the LGM at ~18 kyr B.P. is well supported through a range of proxies at sites across New Zealand and thus agrees with the global model.

Two recent studies have suggested that the LGM, as defined by Mix *et al*. (2001), is not directly applicable to the New Zealand palaeoclimatic record (Alloway *et al*., 2007; Newnham *et al*., 2007a). Therefore phrases such as Last Glacial Coldest Period (LGCP; Alloway *et al*., 2007) and extended LGM (eLGM; Newnham *et al*., 2007a) have been created. In this manuscript the term LGCP will be adopted when referring to the period of maximum cooling at the end of the last glacial period.

Polar ice core records demonstrate that the LGCP was not uniformly cold. Greenland climate experienced three millennial-scale warmings (D-O events 2-4) which occurred close to 23, 27 and 28 kyr B.P. (Figure 2.2). In contrast there is evidence from Antarctica for only a single, minor, warming event (AIM2 – 23-25 kyr B.P.). These records highlight a de-coupling of polar climate during the LGCP following the relative synchrony apparent during MIS 3.

A complex of warmer and cooler intervals comprises the LGCP in New Zealand. There is strong evidence from pollen records, glacial deposits and chironomid assemblages for a mild interval (possibly an interstadial) between 24

and 26 kyr B.P. (Suggate and Almond, 2005; Vandergoes *et al*., 2005; Woodward and Shulmeister, 2007; Newnham *et al*., 2007a). Perhaps significantly the timing of this event does not appear to coincide with documented millennial-scale warmings elsewhere around the globe, which may support this event being only regional in extent.

At Okarito, Westland, South Island, a decrease in herb pollen abundance between 23 and 21.5 kyr B.P. might indicate a second warm period during the LGCP (Vandergoes *et al*., 2005). Support for this is found in a speleothem record from Mt Arthur which displays a negative oxygen isotope anomaly from 23-21 kyr B.P. (Hellstrom *et al*., 1998). However, on the global scale, the period 23-21 kyr B.P. is commonly recognized as one of cool climate associated with maximum glacier extent (Blunier and Brook, 2001; Easterbrook, 2007), a view supported by several New Zealand studies (Suggate and Almond, 2005; Newnham *et al*., 2007a).

2.1.4 Deglaciation

The timing and character of deglaciation following the LGCP (also known as Termination I) was not synchronous across the globe. Palaeoclimate records that cover this period appear to follow one of two patterns, the differences between which are most clearly highlighted in the ice core records from Greenland and Antarctica.

The first significant discrepancy between the deglacial sequences is in the rate of warming. In Antarctica the warming that follows the termination of the LGCP at ~18 kyr B.P. is gradual and relatively constant. In Greenland significant warming did not take place until ~14.7 kyr B.P. and when it did it was abrupt (Figure 2.2).

A second difference in the style of deglaciation between Antarctic and Greenland is the timing and magnitude of a brief return to cooler conditions during the later stages of the warming. Immediately after the onset of the Bølling warming (D-O 1) in Greenland much of Antarctica experienced a small temperature decline that lasted for approximately 1500 years, known as the Antarctic Cold Reversal (ACR). Just prior to the resumption of warming at the

end of the ACR, Greenland experienced a dramatic cooling. This event lasted for 1300 years and is referred to as the Younger Dryas (YD) or, more correctly, the Younger Dryas chronozone (12.8-11.5 kyr B.P.).

One of the major objectives of palaeoclimate research has been to determine the regional extent to which Antarctic and Greenland late-glacial climate cooling has been experienced. The YD is widely recognized in climate archives from across the Northern Hemisphere and, more significantly for this study, at some Southern Hemisphere locations (Lowell *et al*., 1995; Goede *et al*., 1996; Ariztegui *et al*., 1997; Abell and Plug, 2000; Moreno and Leon, 2003). However, Bennett *et al*. (2000) find no evidence for YD cooling in southern Chile (44-47°S), perhaps placing a southern limit on its influence of climate. Interestingly though, Bennett *et al*. (2000) do not observe an ACR signal in its stead.

Good evidence for a late-glacial reversal exists in New Zealand. In a recent review Alloway *et al*. (2007) assimilated the available data and suggested that shortly after the onset of the ACR in Antarctica, New Zealand climate experienced minor cooling which continued to the end of the YD. The individual records which went into this determination are presented briefly here. Westland and Nelson speleothem records show temporary climate cooling from 13.8-11.7 (Hellstrom *et al*., 1998) and 13.5-11.1 kyr B.P. (Williams *et al*., 2005), while at Kaipo Bog on North Island minor late glacial cooling from 13.8-12.4 kyr B.P. is interpreted from an increase in abundance of grass pollen (Hajdas *et al*., 2006).

It was initially thought that the Waiho Loop moraine in South Westland was deposited in response to Younger Dryas cooling (Denton and Hendy, 1994; Turney *et al*., 2006), although its calendar age of ~13 kyr B.P. could also place it at the end of the ACR (Turney *et al*., 2007). Other glacial deposits from the West Coast, Fiordland and Arthur's Pass indicate minor advances or stillstands during retreat occurred within the interval 14-11 kyr B.P (Williams 1996; Denton *et al*., 1999; Ivy-Ochs *et al*., 1999). In each of these studies the magnitude of late-glacial cooling is relatively minor in comparison to LGCP conditions.

Not considered in the review was the high-resolution planktonic foraminiferal $\delta^{18}O$ data from marine sediment core MD97-2120 recovered off the east coast of South Island (Pahnke *et al*., 2003). The record displays a brief reversal during Termination I that is similar in timing and structure to the ACR. An ACR signal also appears in the benthic foraminiferal $\delta^{18}O$ of core MD97-2121, east of North

Island (Carter *et al*., 2008). However, $\delta^{18}O$ of planktonic foraminifera at this site indicate surface water cooling was delayed until 13.5 kyr B.P. Carter *et al*. (2008) suggest that cool air temperatures associated with the ACR were initially offset by strengthened inflow of subtropical water generated by increased wind strength in the region.

2.1.5 The Holocene

Holocene climate, although relatively stable in comparison to both glacial and previous interglacial climates, is nevertheless also affected by climate fluctuations. The most significant of these, in terms of their magnitude, large spatial nature and/or specific relevance to New Zealand, are discussed below in order of occurrence in the palaeoclimate record.

Bond Cycles (Bond *et al*., 1997, 2001) are a potential continuation into the Holocene of D-O events. Each cycle lasts ~1500 yr, with the most recent anomaly coinciding with the Little Ice Age (LIA; discussed below). Evidence for these events come primarily from layers of ice rafted detritus in North Atlantic deep-sea sediments, but are also represented in sea surface temperature (SST) changes off the west coast of Africa (deMenocal *et al*., 2000). However, Bond Cycles are absent from records of North Atlantic planktonic foraminiferal $\delta^{18}O$, and the isotopic composition of Greenland ice (Bond *et al*., 1997), and have not previously been recognized in New Zealand palaeoclimate studies.

An early Holocene climate optimum is widely observed in New Zealand palaeoclimate records between 11 and 10 kyr B.P. (Sandiford *et al*., 2003; Pahnke *et al*., 2003; McGlone *et al*., 2004; Williams *et al*., 2004). This is likely a global signature with similar events apparent in Greenland (GISP2) and Antarctic (EPICA Dome C) ice cores between 11 and 9.5 kyr B.P.

The moderate cooling that succeeded the early Holocene warmth and lasted until 7.5 kyr B.P. is most clearly demonstrated in New Zealand in speleothem isotope records from northwest Nelson (Hellstrom *et al*., 1998). There is also limited evidence for glacier advance in the Southern Alps at this time [summarized by Gellatly *et al*. (1988)]. Within this cool interval is the 8.2 ka event (Alley *et al*., 1997) which represents an abrupt 200 year long cooling in the Greenland ice cores. Further evidence for this event is compiled and reviewed by

Rohling and Pälike (2005), and includes sites as distant as Cariaco Basin (Hughen *et al*., 1996) and Dongge Cave (China; Dykoski *et al*., 2005). No firm evidence for it has yet been found in New Zealand.

Mid-Holocene warming is observed at two sites in New Zealand with peak conditions occurring 6.8-6.2 kyr B.P. (Sandiford *et al*., 2003; Williams *et al*., 2005). However, this event is missing from many other New Zealand palaeoclimate records and further research is required to determine whether it is of local or regional significance.

Eleven periods of glacier advance in the Southern Alps from 5.0-0.1 kyr B.P. demonstrate that cool climate characterised much of the latter stages of the Holocene (Gellatly *et al*., 1988). Cold temperatures were not uniform throughout this interval and the most extensive periods of glacier advance occurred between 4.5 and 2.2 kyr B.P. This is supported by speleothem records from both South Island and North Island which display a cool interval from 4.5-3 kyr B.P. (Hellstrom *et al*., 1998) and minimum Holocene temperatures ~3 kyr B.P. (Williams *et al*., 2004), respectively.

Among the fluctuations toward warmer climate that intersperse the broad mid-to-late Holocene cooling is the Medieval Climate Optimum (MCO), defined as the interval 1.1-0.8 kyr B.P. (or 900-1200 AD) and recognized primarily at locations in the North Atlantic (Osborn and Briffa, 2006). Wilson *et al*. (1979) and Williams *et al*. (2004) observe it ~0.75 kyr B.P. on North Island, but Williams *et al*. (2005) suggest its influence on South Island climate was delayed until the period 0.7-0.57 kyr B.P. Few other records are resolved at sufficient resolution to determine the true extent of this climate anomaly in New Zealand.

The Little Ice Age (LIA) is roughly the period 1200-1850 AD and represents a period of cooler-than-present temperatures (Lockwood, 2001). As for the MCO, it is most often recognized in palaeoclimate records from Europe and the North Atlantic but may potentially be of global extent (Broecker, 2000). There is evidence for LIA cooling in New Zealand from the South Island moraine record (Gellatly *et al*., 1988) and also from Waitomo speleothems (Williams *et al*., 2004).

2.1.6 Summary

The broad scale climate changes of the last glacial period indicate intensely cold periods during MISs 2 (LGCP; 30-18 kyr B.P.) and 4 (~72-60 kyr B.P.), separated by the slightly milder MIS 3. Superimposed on this pattern are a significant number of abrupt, short-duration climate events. There is evidence to suggest that these events are global in extent although the magnitude of the climate response is greatest in the North Atlantic/Greenland and least in Antarctica. Currently there are insufficient high-resolution palaeoclimate records to determine how these events affected New Zealand climate during the last glacial period. Therefore questions remain as to whether or not abrupt climate changes affected New Zealand, and if so when and how frequently?

While there may be some argument for an in-phase relationship between similar climate events in Antarctica and Greenland during the last glacial period, this does not appear to be the case for the LGCP. The onset of this event is not synchronous at both locations, and neither is its termination. Furthermore, there are discrepancies on millennial-scales of abrupt warmings and coolings experienced at the poles. This millennial-scale asynchrony of polar climates during the LGCP is significant for New Zealand palaeoclimate studies as mid and low latitude records covering this period must be sought to determine the extent of influence of each climate pattern. Existing high-resolution records do identify millennial-scale climate change during the LGCP in New Zealand. However, the timing of these events does not appear to closely match those evident in Antarctic or Greenland records.

The palaeoclimate record for New Zealand during Termination I displays two features that appear to link it more closely to Antarctic climate than to Greenland. First, the onset of deglaciation occurs close to 18 kyr B.P. Second, the magnitude of the late-glacial cooling is relatively minor. However, the timing of this reversal straddles both ACR and YD perhaps indicating a weak connection to Greenland or that the mechanism of the climatic connection is more complex involving a component with significant thermal inertia.

The Holocene, both in New Zealand and global palaeoclimate records, is marked by a number of significant climatic events. There is strong evidence for an early Holocene optimum ~11-10 kyr B.P. and some support for a second warm

interval 6.5 ± 0.3 kyr B.P. The latter half of the Holocene is characterized by cool climate conditions although it is occasionally interrupted by warm periods such as the Medieval Warm Period.

While a number of climate events are recognized from New Zealand palaeoclimate records covering the Holocene and last glacial period, there remain uncertainties in the spatial extent, significance (in the global setting) and, perhaps most importantly, timing of these events. Furthermore, there is a dearth of information on pre-LGCP (prior to 30 kyr B.P.) climate, little of which is based on continuous data plotted against an independent and absolutely-dated chronology. This has led to a lack of knowledge of events, particularly those operating at the millennial-scale, which affected New Zealand during this time.

2.2 Speleothems

2.2.1 Introduction

Caves are known on every continent on Earth, including Antarctica (Middleton & Waltham, 1992), and come in a variety of types (Figure 2.4). Solution caves found in carbonate rocks (e.g. limestone, dolomite and marble) are the most abundant cave type, primarily because they account for 10-15% of all sedimentary rocks at the Earth's surface (Gillieson, 1996; Christie, 2001). However, many significant subterranean cavities, including some of the world's longest solution caves, are found in gypsum deposits (Klimchouk, 2005).

The typical requirements for cave development are a pure, hard calcium carbonate bedrock with well developed secondary porosity, that is located in an area of hilly or mountainous local relief that also receives at least periodic heavy rainfall (Ford and Williams, 1989). The formation is then driven by solution of the rock by an acid. Typically this role is fulfilled by carbonic acid (H_2CO_3) which is readily formed in soils following the dissolution of respired CO_2 in water.

As well as having the ability to dissolve carbonate, groundwater entering a cave may also form new calcium carbonate, infilling the void. These precipitates are known as speleothems. The term speleothem derives from the Greek "speleux" meaning cave and "them" meaning deposit. Most commonly, speleothems formed in carbonate rocks are composed of calcite ($CaCO_3$) although in many caves in arid regions aragonite (another polymorph of calcium carbonate) may be preferentially precipitated. In addition where there are sulphide-rich bedrock layers within the path of seepage waters, gypsum ($CaSO_4.2H_2O$) may be precipitated. Many speleothems accumulate layer upon layer to create formations such as stalagmites, stalactites and flowstones. The composition, thickness and structure of each of the layers that compose a speleothem is usually in some way influenced, to a greater or lesser extent, by climate at the surface. It is because of this, and our ability to date them, that speleothems are considered such valuable archives of past climate.

In the following sections I will describe further the process of speleothem formation and explore the various proxies contained within them from which climate information can be extracted.

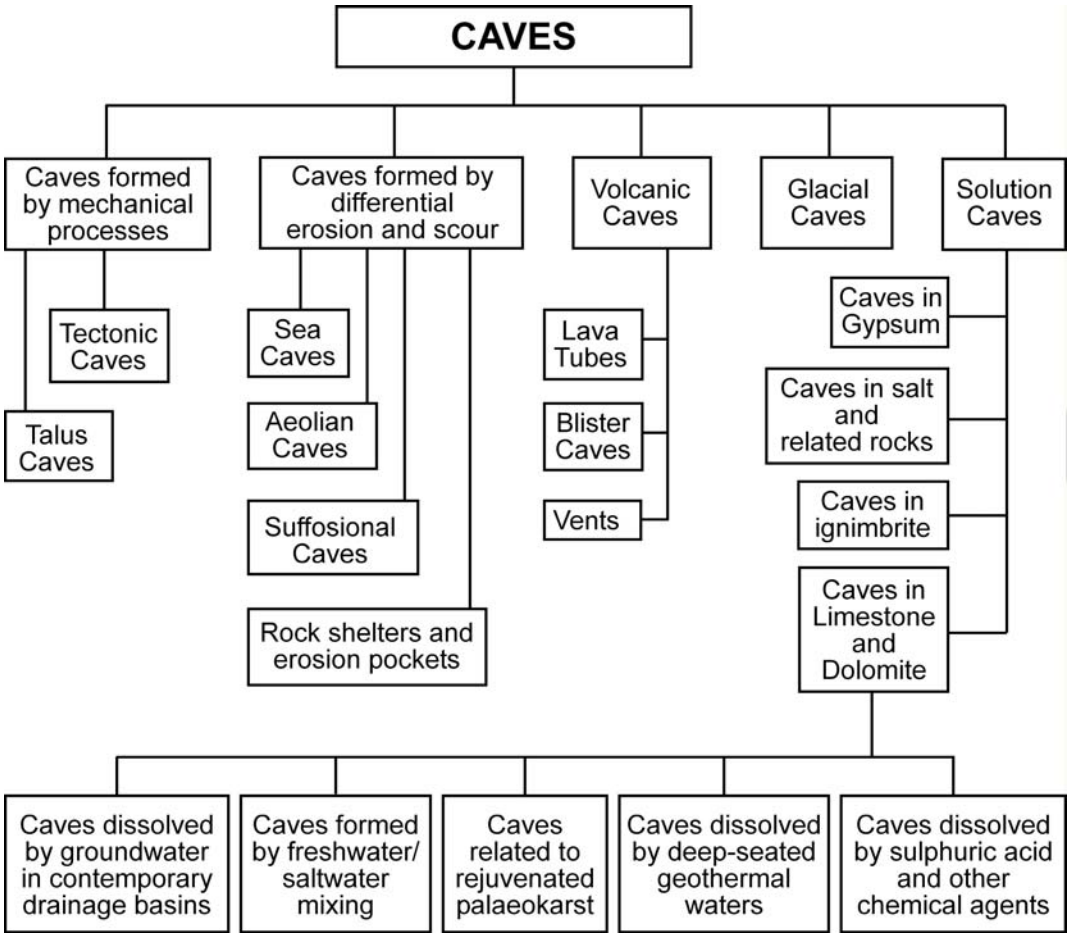

Figure 2.4: Types of caves [modified from White and Culver (2005)].

2.2.2 Speleothem Formation

Caves and speleothems develop because calcareous rocks are soluble in natural waters. Carbon dioxide when dissolved in water produces a weak acid called carbonic acid (H_2CO_3). Modern atmospheric carbon dioxide concentrations are currently ~380 ppm (IPCC, 2007), although concentrations more appropriate for this study are typical interglacial values of ~280 ppm, and typical glacial values of ~180 ppm (Petit *et al.*, 1999; EPICA community members, 2004). Therefore rainfall is capable of dissolving small amounts of carbonate bedrock. However, atmospheric pCO_2 cannot easily drive speleothem formation as cave carbon dioxide concentrations are typically 2 to 20 times greater than in the open

atmosphere and carbon dioxide has to be lost to the cave atmosphere from the seepage water to precipitate calcium carbonate (Ek and Gewelt, 1985; Baldini *et al*., 2006).

If rainfall washes through soil before reaching bedrock more carbon dioxide can be dissolved and the potential for bedrock dissolution increases. High pCO_2 in soil atmospheres is the result of bacterial respiration of organic material and direct respiration from plant roots. In fertile soils with high carbon content or vigorous plant growth, carbon dioxide concentrations can be in excess of 50,000 ppm (Ek and Gewelt, 1985; C. Hendy, pers. comm.).

Carbonic acid percolating through carbonate rock dissolves the bedrock as it moves until the acid is neutralized. The formation of speleothems occurs when this carbonate saturated seepage water enters a subterranean cavity which has a pCO_2 lower than its own. In an attempt to achieve equilibrium with the cave atmosphere the excess CO_2 diffuses out of the seepage water. This process raises the pH of the seepage water, forcing the precipitation of calcium carbonate. For every mole of CO_2 that is degassed one mole of $CaCO_3$ is precipitated.

If the seepage water is not saturated, or pCO_2 is lower than the cave atmosphere speleothem, deposition may not occur or there may be corrosion of speleothems. No seepage water will also result in no deposition. This has important implications for palaeoclimate studies using cave deposits as not only is it important to be able to identify hiatuses within a record, the hiatus itself has likely occurred in response to climate change. One must then consider factors that may cause there to be no dripwater, low seepage water pCO_2 or undersaturation of seepage water with respect to calcium carbonate.

Over time the source of water for drips in caves may change and in some instances this may lead to a cessation of dripwater at given locations. The simplest mechanism that will lead to no dripwater entering the case is removing the water supply to the surface. In an environmental sense, this may occur if the region surrounding the cave becomes arid (i.e. evaporation greatly exceeds precipitation), or if water can no longer penetrate into the ground (e.g. as a result of permafrost, or being overridden by a glacier). Alternative mechanisms surround the diversion of seepage water. For example, the paths by which surface precipitation makes its way to the drip site may become blocked by calcite deposition, or new paths created by more recent dissolution may divert water away from the seepage site.

Seepage waters with low pCO_2, relative to the cave atmosphere, that may result in no deposition or corrosion of speleothem carbonate can result from several factors. These include:

1) There being only a thin layer, or complete lack, of soil at the surface
2) Fast throughput of rainfall through the soil column (which may occur in areas that receive high annual rainfall, brief periods of intense rainfall or have soils with poor moisture retention).
3) Dripwater passing through other cave galleries and precipitating calcite prior to reaching the one in which the drip is being measured.

Undersaturation of seepage waters with respect to calcium carbonate can occur when the residence time of the water within the bedrock is short. This can be caused if the water travels along flowpaths that are short and/or large and unconfining.

Considering only the cases where seepage waters entering a cavity are saturated or super-saturated with respect to calcium carbonate, a variety of deposits may be formed. Dreybrodt (1999) describes the diversity of speleothem shapes as overwhelming. Some of the often seen (and therefore named) formations include stalagmites, stalactites, flowstones, soda straws, helictites, shields, columns, shawls, anthodites, cave pearls and moonmilk. However, of these, only the first three are of significant interest to palaeoclimate research.

The shapes of stalagmites and stalactites depend on the amount of water supplied to them (Franke, 1965). Dreybrodt (1999) investigated the effects of varying drip rates on stalagmite morphology and growth rate. Stalagmite layers form as dripwater falls onto a point and spreads out as a thin film across the surface. With increasing distance from the point of impact the thickness of deposited calcite decreases. With increasing drip rate the lateral extent of the deposited layer increases and, to a much lesser extent, so does the layer thickness. Growth rates of stalagmites are typically in the range 0.01-1.0 mm/year (McDermott, 2004). In addition to the drip rate, temperature and the amount of carbon dioxide available in the soil strongly influence growth rate (Kaufmann and Dreybrodt, 2004).

2.2.3 Speleothems as Archives of Past Climate

In the late 1960s the potential for using speleothems to develop records of past climate was realized (Galimov and Grinenko, 1965; Hendy and Wilson, 1968; Duplessy *et al*., 1970). In the roughly forty years since then a wide range of techniques have been applied to understand more about the records they contain. A variety of speleothem properties are proxies for mean annual temperature, rainfall and surface vegetation (McDermott, 2004) and this information is recorded in successive growth layers, often with annual and even sub-annual resolution (Baker *et al*., 1998; Frappier *et al*., 2007). Speleothems can respond rapidly to changing climatic conditions and may remain very well preserved for many millions of years (Woodhead *et al*., 2006), making them ideal for palaeoclimate research.

Of the three main speleothem types useful for palaeoclimate research (stalagmites, stalactites and flowstones), stalagmites are the simplest to work with. Primarily this is because each new layer is deposited on top of the previous deposit allowing a simple interpretation of the stratigraphy. Stalactites on the other hand may drip through the centre or along the outside which results in a discontinuous stratigraphy. Furthermore, the area over which deposition of new layers may occur is typically less for stalagmites than for stalactites of the same size. This occurs because the dripwater is focused to a point on the stalagmite whereas it is spread around the outside of a stalactite. Often this provides the researcher a greater amount of material to work with for each layer if stalagmites are chosen.

In situ flowstone must be cored for a paleoclimate record to be obtained. While this has the distinct advantage of being less destructive than the removal of entire stalagmites or stalactites for analysis, the researcher is left with far less material to work with. In addition the speleothem is often fractured and broken as a result of the coring action, and therefore there exists the potential for some of the record to be lost.

Once a speleothem sample has been obtained and brought back to the laboratory there are a wide variety of analytical techniques that can be applied to extract climate information. Typically, records of stable carbon and oxygen isotope and trace element variability are developed, although speleothems contain

a much wider range of proxies than just these three. The following sections contain a description of the physical, chemical and biological processes that drive temporal variability in these proxies and how they influence the interpretation of speleothem-based palaeoclimate records.

2.2.3.1 Factors Influencing Speleothem $\delta^{18}O$

For a robust climate signal to be extracted from a speleothem oxygen isotope record, deposition of the calcium carbonate must have occurred under conditions of isotopic equilibrium with the dripwater, and there was no subsequent alteration of the deposit. In a poorly ventilated cave where air temperature is constant, relative humidity is approximately 100% and there is little or no air movement, the diffusion of carbon dioxide from dripwater will be sufficiently slow to ensure that equilibrium conditions are maintained.

Non-equilibrium or 'kinetic' fractionation refers to situations where the rate of loss of carbon dioxide exceeds the capacity of the solution to maintain isotopic equilibrium between aqueous carbon dioxide and bicarbonate ions (Hendy, 1971). This may occur if there is a significantly large contrast between seepage water pCO_2 and that of the cave atmosphere, which itself may be the result of regular flushing of cave CO_2 by air movements. Alternatively, the precipitation of calcium carbonate from a dripwater solution could occur as a result of evaporative water loss. It is therefore advisable that only those speleothems in chambers where the relative humidity is close to 100% are selected for sampling, to eliminate the possibility of this effect overprinting the preserved paleoclimate signal. Fortunately speleothems formed through evaporative water loss develop distinctive morphologies as water moving through capillary action results in calcite growing to form a rough surface (Hendy, 1969). This contrasts with calcite formed from water flowing under gravity which produces smooth surfaces.

Under disequilibrium conditions precipitated calcium carbonate will become increasingly enriched in the heavier isotopes (^{13}C and ^{18}O) with increasing distance from the point at which the drip was incident. This is significant for helping to determine whether equilibrium conditions existed in the past. A simple test, often referred to as the "Hendy Test", involving stable isotope analysis of small samples collected along a single growth layer, allows the researcher to get

an indication of whether or not the isotopic signature of the speleothem is affected by kinetic fractionation effects. However, it is often the case that individual growth layers are thinner (particularly at increasing distances from the growth axis) than the tool being employed to extract the calcite for analysis, making accurate sampling somewhat challenging. It should be noted that failure to 'pass' the Hendy Test does not invalidate a paleoclimate record, but merely reduces the degree of confidence one can place in any climate interpretations made from it.

Isotopic disequilibrium is further indicated by strong correlation between paired $\delta^{13}C$ and $\delta^{18}O$ analyses (of samples collected along the growth axis) where the slope of the regression is close to three (Hendy, 1971; Treble *et al*., 2005). However, the closer each collected sample was to the growth axis the smaller the impact of disequilibrium fractionation on the isotopic composition of the calcite. Furthermore, climatic factors conceivably can simultaneously affect axial profiles of both $\delta^{13}C$ and $\delta^{18}O$ (Treble *et al*., 2005).

Returning to the situation where isotopic equilibrium is maintained between seepage water and calcium carbonate, two climatically-dependent variables determine the oxygen isotopic composition of speleothem calcite: cave temperature and rainfall (Lauritzen and Lundberg, 1999; Williams *et al*., 2005).

Urey (1947) first theorized that the temperature-dependent fractionation of oxygen isotopes could be useful as an indicator of past temperatures. This finding opened the door to the development of records of past climate from terrestrial deposits such as speleothems. This concept was the basis for a Ph.D. undertaken by Hendy (1969) which sought to develop palaeotemperature records from New Zealand speleothems.

The *cave temperature effect* is the name given to the temperature dependent fractionation of oxygen isotopes between aqueous bicarbonate and calcite. Under typical cave conditions the fractionation of oxygen isotopes is -0.24 ‰/°C (O'Neil *et al*., 1969). Simplified, this means that for every increase in cave temperature of 1°C there is a decrease in the oxygen isotopic value of the precipitated calcium carbonate of 0.24 ‰ (assuming all other variables are held constant).

In the deep, poorly ventilated interior of most caves the air temperature is reasonably constant and closely approximates mean annual temperature at the surface. If this temperature is known and the $\delta^{18}O$ of currently precipitating calcite measured then a simple relationship can be determined for past isotopic values.

Lighter than modern values should indicate warmer temperatures while heavier values are the result of cooler climate.

Unfortunately, precipitation has an opposing and greater influence on speleothem $\delta^{18}O$. Despite the early promise it is now recognised that palaeotemperatures cannot be directly determined from the isotopic ratio of speleothem calcite alone. However, stable isotope analysis of fluid inclusions within the speleothem may resolve this problem (McDermott (2004) and references therein).

The oxygen in speleothem carbonate has three sources: water (precipitation), carbon dioxide (soil respiration) and carbonate (dissolved from the calcareous bedrock). However, the amount of oxygen contributed by the water far exceeds that added by soil CO_2 and bedrock such that water entering the cave will have the same isotopic signature of the precipitation from which it originated (Hendy, 1969), unless the water was subject to significant evaporation at the surface. Cave dripwaters represent an integration of rainfall over time. If drip rates are slow and/or the seepage water takes a long route to the drip site the isotopic composition of the dripwater will more closely reflect the mean annual or seasonal $\delta^{18}O$ of precipitation (Yonge *et al*., 1985). Usually drips from fast throughflow show greater variability and are more sensitive to short-term climatic changes (Lauritzen and Lundberg 1999). In such cases where the speleothem captures this high-frequency variability it is possible to identify individual rainfall events (Frappier *et al*., 2007).

Not only is it important to consider the temporal variability of $\delta^{18}O$ of precipitation when interpreting speleothem stable isotope records, but it is also necessary to be aware of the factors that cause the changes. The isotopic composition of rainfall above a cave is the summation of 5 separate factors (the *precipitation effect*), three of which relate to the water source at the time of evaporation, and two relating to atmospheric conditions at the time of precipitation.

The oceans are the source of almost all atmospheric moisture. As such they represent the first cause for diversity in $\delta^{18}O$ of precipitation. First, there is minor spatial variability in the oxygen isotopic composition of ocean surface waters. Second, sea surface temperatures (SSTs) can also influence the $\delta^{18}O$ of evaporated water vapour. Warmer SSTs lead to heavier isotopic ratios than cooler SSTs. It is

therefore important to consider the possible oceanic sources of atmospheric moisture above the cave.

Third, when considering speleothem records that cover periods of significant global sea level change one must also consider the *ice-volume effect*. During glacial periods large volumes of ice built up at high latitudes in both hemispheres. The water evaporated from the oceans and incorporated into these ice masses had the effect of lowering sea level ~140 m at times of peak ice volume (Lambeck and Chappell, 2001). As a result of Rayleigh distillation the evaporated ocean water became isotopically lighter (^{16}O enriched) before being precipitated as snow on the building ice caps. As a result, much ocean ^{16}O was sequestered in the ice and the oceans became isotopically heavy (^{18}O enriched). Schrag *et al*. (2002) estimated the global average of this effect (the change in seawater $\delta^{18}O$) during glacial-interglacial cycles to be 1.0 ± 0.1 ‰.

Once evaporated, the water is then transported through the atmosphere and is deposited above the cave. At the point at which atmospheric water vapour condenses to form precipitation the fractionation of oxygen isotopes is again controlled by temperature. This may be referred to as the *precipitation temperature effect*. Dansgaard (1964) demonstrated empirically that for every 1°C decrease in mean annual air temperature the average $\delta^{18}O$ of precipitation decreases by 0.69 ‰. Therefore it acts in the opposite direction to the cave temperature effect and in most cases will be the dominant influence on speleothem $\delta^{18}O$ (Lauritzen and Lundberg, 1999).

It is also necessary to consider the *amount effect*. This is the process by which the isotopic composition of precipitation is controlled by the altitude at which it formed, as opposed to the mean annual temperature of the latitude where it falls. The amount effect therefore tends to have increased influence on mean $\delta^{18}O$ of precipitation in tropical regions that experience monsoons or frequent thunderstorms. Williams and Fowler (2002) suggest that the amount effect could have a weak influence on $\delta^{18}O$ of precipitation at northern New Zealand locations, but is statistically insignificant at South Island sites.

As a point of further interest, although speleothems are typically composed of calcite, aragonite forms occur occasionally, particularly in association with a high-Mg bedrock and dry/arid climate (Holmgren *et al*., 1995, 2003). It is important to determine whether speleothem layers are composed of aragonite or calcite as

oxygen isotopes are fractionated differently from dripwater into the two minerals. To be able to compare aragonite and calcite $\delta^{18}O$, aragonite values are adjusted by -0.6 ‰ (Tarutani *et al*., 1969; Grossman and Ku, 1986). However, from the literature it appears that aragonite speleothems are rare, if present at all, in New Zealand caves.

2.2.3.2 Factors Influencing Speleothem $\delta^{13}C$

The carbon isotopic signal of dissolved inorganic carbon in cave seepage waters is the result of processes occurring within the epikarst between biogenic and atmospheric carbon dioxide, water and carbonate bedrock (Hendy, 1971; Harmon *et al*., 2004). The carbon isotopic composition of the bedrock can be held constant, therefore variability in seepage water $\delta^{13}C$ is a function of the relative contributions of atmospheric and soil-bacteria respired carbon dioxide.

The $\delta^{13}C$ of atmospheric CO_2 is -7 ‰ (Deines *et al*., 1974; Faure, 1986) although there is some suggestion that this value varied by as much as 0.7 ‰ across glacial-interglacial transitions (Marino *et al*., 1992).

The $\delta^{13}C$ of biogenic soil CO_2 can vary significantly as a result of the types of vegetation present at a given site. Almost all terrestrial plants can be divided into two groups based on their method of carbon fixation during photosynthesis: Calvin Cycle (C3) and Hatch-Slack (C4). Those plants that use the C3 photosynthetic pathway have $\delta^{13}C$ values ranging from -34 to -24 ‰ (Faure, 1986), while those plants that use the C4 pathway typically have $\delta^{13}C$ values of -14 to -10 ‰ (Harmon *et al*., 2004). Respiration of these plants following their incorporation into the soil organic matter has a strong influence on the $\delta^{13}C$ of soil CO_2. Hendy (1971) calculated the likely $\delta^{13}C$ of speleothem calcite under soils supporting only C3-type vegetation at Waitomo, New Zealand, to be between -13 and -11 ‰. In caves beneath soils where plants utilising the C4 pathway are abundant, the $\delta^{13}C$ of speleothem calcite will theoretically fall in the range -7 to -5 ‰ (Talma *et al*., 1974).

A number of studies have interpreted speleothem $\delta^{13}C$ records in terms of switches between C3 and C4 dominated vegetation, with some success (Dorale *et al*., 1992, 1998; Holmgren *et al*., 1999). However, New Zealand vegetation is almost entirely composed of those plants which utilize the C3 photosynthetic

pathway. Only two species are known to use the C4 pathway and these plants are coastal dune dwelling (Wardle, 1991). Therefore it is extremely unlikely that they will influence speleothem $\delta^{13}C$ and thus the impact of C4 vegetation on $\delta^{13}C$ will not be considered further in this study.

The $\delta^{13}C$ of soil CO_2 is also determined by the relative contribution of biogenic CO_2 to total CO_2 in the soil atmosphere. Over long timescales (e.g. > 100 years) this is typically a function of climate although other methods of land disturbance (e.g. volcanic eruptions, fires, and land clearance for farming) should also be considered. In arid and/or cold regions soils typically are poorly developed, have little organic activity and sparse vegetation cover. As a result the majority of soil CO_2 is atmospheric in origin and the $\delta^{13}C$ of soil CO_2 reflects this. With increasing mean annual temperature and precipitation, soil productivity increases and bacterially-respired CO_2 makes a greater contribution to the soil atmosphere, simultaneously adjusting the $\delta^{13}C$ of the soil towards that of the dominant vegetation types.

Following movement of dissolved soil CO_2 into the epikarst, dissolution of the bedrock occurs. This process can take place in an environment containing excess CO_2 gas (open system), an environment isolated from the gas phase (closed system), or some intermediate scenario (Hendy, 1971). These alternative processes affect the $\delta^{13}C$ of bicarbonate in solution, such that solutions that experienced closed system conditions will have a heavier isotopic signature than those that formed in an open system. Harmon *et al*. (2004) suggest that open system conditions would be realised during times of high precipitation, and closed system conditions would likely occur with diminished or highly seasonal precipitation. Implicit in these statements is that the commonly experienced environment is that of an intermediate state between open and closed systems.

At the point of calcium carbonate deposition, rapid CO_2 loss, as a result of evaporation or high drip rate, can modify the $\delta^{13}C$ of precipitated speleothem calcite (Hendy, 1971). Furthermore, if prior calcium carbonate precipitation took place in another cavity before the seepage water emerged into one where the $\delta^{13}C$ of bicarbonate is being measured the isotopic composition may have changed considerably from that of the original solution.

As discussed above, and similar to speleothem $\delta^{18}O$, $\delta^{13}C$ in speleothem calcite is a composite signal. However, the many factors that influence this value

appear more apt to be highly variable and are difficult to measure (Harmon *et al*., 2004). As a result, few interpretations of $\delta^{13}C$ data are made in the literature. Despite this two general trends have been identified. First, heavier $\delta^{13}C$ values in speleothems forming beneath sites where soil biogenic activity is high generally indicates past cool and/or dry climate intervals. This occurs for three compounding reasons: (a) cold and dry conditions reduce the ability of soil bacteria and plant roots to respire reducing the contribution plant-derived CO_2 to the soil atmosphere, (b) these conditions are not favourable to plant growth limiting the input of organic material to the soil, thus further reducing the potential for bacterial respiration, and (c) as the soil degrades following lack of input of organic material, the residence time of water percolating through the soil is reduced preventing complete isotopic equilibration between soil CO_2 and dissolved atmospheric CO_2 in the soil water. Second, at sites where transitions between C3 and C4 dominated vegetation can occur, heavier $\delta^{13}C$ values indicate the presence of C4 plants and a warm and dry climate.

Not considered above is the case of aragonitic speleothems. To be able to compare $\delta^{13}C$ of aragonite and calcite, the aragonite values must be adjusted by -1.8 ‰ (Tarutani *et al*., 1969; Grossman and Ku, 1986). However, as stated in the previous section (on $\delta^{18}O$), no aragonite speleothems have been reported from New Zealand.

2.2.3.3 Chronology

The current strong interest in speleothem palaeoclimate records has stemmed from the development in the 1980s of thermal ionization mass spectrometry (TIMS) and its ability to routinely deliver high-precision, absolute ages from relatively small samples that are as much as 500,000 years old (Edwards *et al*., 1987; Li *et al*., 1989). Chronological control can be better than ± 0.5 % in 'clean' samples (Lauritzen and Lundberg, 1999) which allows speleothems to compete favourably with other high-resolution climate proxies such as ice and marine-sediment cores.

Previously speleothem chronologies had relied on radiocarbon and uranium-series alpha-spectrometry (decay counting) dating techniques (Hendy and Wilson,

1968; Gascoyne, 1992). Both methods have significant drawbacks for those wishing to develop precise chronologies covering the mid-to-late Quaternary.

Radiocarbon dating of speleothems has two limitations. The most significant is the unknown quantity of carbon in speleothem calcite derived from the ^{14}C-free carbonate bedrock. Incorporation of "dead" carbon into speleothem calcite results in age determinations that are too old. The second problem is that the range of samples that can be accurately and precisely dated by this technique is limited to those that formed within the last *ca*. 45 kyr (~8 half-lives).

Measurement of uranium and thorium concentrations by alpha spectrometry is a reliable, if not overly precise, method for dating speleothem material. Speleothems readily incorporate uranium (as UO_2^{2+} ions) and only negligible amounts of thorium which acts conservatively in solution. Therefore all thorium within the calcite ought to be produced through alpha decay of the uranium. Furthermore, speleothem calcite is typically contaminant-poor and contains sufficient uranium (> 1 ng/g) to allow measurement. However, measurement of uranium and thorium concentrations by alpha spectrometry requires counting of alpha emissions from relatively large samples over long periods (1 to 28 days; Gascoyne, 1992; Goldstein and Stirling, 2003). Because of the relatively long half lives of ^{234}U (~245 kyr) and ^{230}Th (~75 kyr), decay counting is on the order of 10^4 times less efficient than mass spectrometry at measuring the abundance of these isotopes (Chen *et al*., 1992; Dorale *et al*., 2004). Hence prior to the advent of thermal ionization mass spectrometry (TIMS), precise ages on speleothem calcite were difficult to achieve, particularly on older (> 200 kyr) samples.

There have been further developments in dating of speleothems since the advent of TIMS in the mid-1980s that mean the modern researcher has several options for obtaining a uranium-series age estimate from a carbonate sample. Each comes with relative advantages and disadvantages relating to sample size requirement, analytical precision and duration of sample preparation and measurement. Of these alternative techniques, perhaps the most widely applied is the use of multi-collector inductively coupled plasma mass spectrometers (MC-ICP-MS) to measure uranium-series isotopes. Its advantages over TIMS are (1) higher total system efficiency, (2) smaller sample size requirement, (3) less sample wastage, (4) higher sample throughput, and (5) comparable or better precision (Hellstrom, 2003; Goldstein and Stirling, 2003). The most significant

weakness of MC-ICP-MS is the inefficiency of the transfer of ions from the plasma source to the mass spectrometer.

In a recent development, MC-ICP-MS has also facilitated the development of U-Pb dating of speleothems (Woodhead *et al*., 2006). The U-Pb decay scheme offers the possibility to extend the use of speleothems in palaeoclimate and other studies back many millions of years.

2.2.3.4 Trace Elements

Minor and trace elements may be incorporated into speleothems in several ways: (1) by direct substitution for Ca^{2+} ions, (2) by dry deposition of fine particulates (clays) onto the speleothem surface between periods of calcite precipitation, and (3) by adsorption onto the speleothem surface from dripwater solution (Gascoyne, 1983).

The concentration of these elements in speleothems is controlled by a number of factors. Primary amongst these are the element concentrations in dripwaters. These are variable over time in response to changes in (1) the residence time of the seepage water in the epikarst, (2) prior calcite precipitation along the flowpath and (3) selective leaching of some ions with respect to Ca (Fairchild *et al*., 2000). Second, physical conditions at the time of crystallization, notably temperature and growth rate, are known to affect partition coefficients (between solution and precipitate) of some elements. For example, the concentration of Mg in calcite precipitated from solution is temperature dependent and it has been demonstrated experimentally that Sr concentrations in speleothems increase with higher growth rate (Huang and Fairchild, 2001). However, for both Mg and Sr in speleothem calcite most of the observed variation in concentration is likely the result of changes in seepage water Mg/Ca and Sr/Ca (Fairchild *et al*., 2000). Third, the nature of crystallographic sites that can accommodate trace elements also influences the concentration of elements in speleothem calcite. Defects in the crystal lattice promote the adsorption of phosphorus (as phosphate) and other elements that may act conservatively (e.g. thorium).

Therefore, as natural components of speleothem calcite present in varying concentrations, trace elements have the potential to record long-term, high-

resolution climatic data. This provides the researcher with an additional or alternative tool to stable isotope measurement.

Recent studies have focused on developing sub-annually resolved climate records from micro-sampling of speleothem calcite. This has been achieved following the application of (excimer) laser ablation technology coupled to either multi- or single collector ICP-MS (Treble *et al*., 2003; Desmarchelier *et al*., 2006). The ability of ICP-MSs to measure the abundance of a wide variety of elements in a given sample in a short period of time (seconds) has allowed researchers to investigate the variability of just about every element over time in speleothems (Hellstrom, pers. comm.). Most of these are not thought to be influenced by climate either directly or indirectly and hence only a handful of elements (Mg, Sr, Ba, U and P) are routinely analysed for.

Early studies investigated the possibility of using Mg as a palaeothermometer in light of the temperature dependence of its partition coefficient (Gascoyne, 1983; Goede, 1994). However, these found that natural variations in the dripwater masked any temperature signal. More recently, Treble *et al*. (2003) suggested that Mg concentration responds positively to increased groundwater residence times, which in turn is a function of decreased precipitation volumes at the surface. This interpretation is supported by data in Hellstrom and McCulloch (2000) who further demonstrated that enrichment of Mg relative to Sr occurs at the same time. This happens because the dissolution of dolomite (approximately $MgCa(CO_3)_2$) phases can take place when seepage water is already saturated with respect to calcite, thus leading to an enrichment in Mg relative to Sr (Verheyden, 2004). If recharge is greater, and therefore groundwater residence times are decreased, Sr may become enriched relative to Mg in solution as dissolution of dolomite takes longer than the dissolution of calcite (Roberts *et al*., 1998; Fairchild *et al*., 2006).

Prior precipitation of low-Mg calcite along the flowpath complicates this simple relationship. The process is recognized as a mechanism for generating enriched and covarying Mg/Ca and Sr/Ca ratios in speleothem calcite (Bar-Matthews *et al*., 1991; Fairchild *et al*., 2000; Verheyden, 2004).

Galy *et al*. (2002) provide some preliminary investigation into the potential use of Mg isotopes to determine past environmental changes from speleothems. They identify considerable variation (relative to measurement uncertainty) in Mg isotopes in four speleothems, a weak influence of temperature on Mg isotope

fractionation and a strong fractionation during carbonate precipitation. Further research is needed to determine whether there is further potential with this proxy.

As with Mg, Sr is also easily incorporated into the calcite lattice, typically in minor amounts (ppm to ‰), and has measurable isotopes (^{86}Sr and ^{87}Sr). An inverse relationship between Sr/Ca and Mg/Ca has been observed in several studies, which publish data at sub-annual to millennial scales, and this has been explained in terms of groundwater residence times (Roberts *et al*., 1998; Hellstrom and McCulloch, 2000; Treble *et al*., 2003). No further interpretations of Sr data are made in the literature although it is worth noting that Ba often displays a strong covariance with Sr (Hellstrom and McCulloch 2000, Treble *et al*., 2003).

It has been suggested that speleothem strontium isotope ratios may be used as indicators of past soil moisture conditions (Banner *et al*., 1996; Ayalon *et al*., 1999). However, Goede *et al*. (1998) used Sr and Sr isotope variations to infer changes in paleowind direction. It should be noted that these two interpretations of strontium isotope variability are not mutually exclusive and could in fact act in synchrony (Frumkin and Stein, 2004).

Uranium in speleothems has also been measured and has been shown to correlate with strontium and barium (Ayalon *et al*., 1999; Hellstrom and McCulloch, 2000). It is thought that the abundance of uranium is a measure of soil redox conditions, which in turn are driven by soil productivity. Uranium isotopes have been used as an indicator of local hydrological conditions. Both Frumkin and Stein (2004) and Hellstrom and McCulloch (2000) suggest elevated ratios occur following increased recharge and short groundwater residence times in association with past pluvial intervals.

Measurement of phosphorus has been undertaken in high-resolution studies attempting to identify seasonal climate changes. Due to its role as a nutrient, groundwater phosphorus concentrations are believed to be lowest during summer and greatest in the autumn (Huang *et al*., 2001; Treble *et al*., 2003). Further research is required to confirm this.

There is much potential for trace element analyses to complement stable isotope measurements of speleothem calcite. This can be achieved simply in a couple of ways. First, an important finding is that the processes that lead to kinetic (non-equilibrium) isotope fractionation (i.e. rapid degassing of CO_2 and evaporation) have little or no effect on trace element concentrations. Therefore

speleothem samples previously demonstrated to have failed the Hendy Test may still yield palaeoclimate information (Goede and Vogel, 1991).

Second, multiple proxy records from a single speleothem will allow for the investigation of relationships between stable isotope and trace element variability. As discussed above, and as is the case for stable isotope ratios in speleothems, the relationship between trace element concentrations of speleothem calcite and climate is not straightforward. It is likely that combined records will be able to separate the influence of climatic change from unrelated physical and chemical processes affecting seepage water in the soil and epikarst.

Third, an advantage to conducting trace element work in association with stable isotope measurements is that growth hiatuses are typically highlighted by greater abundance of trace elements that do not typically associate with carbonate (e.g. Si or Al), or that are conservative in solution (e.g. Th) (Ayalon *et al*., 1999).

Two drawbacks relating to trace elements as climate proxies have been identified in the literature. Both relate to reproducibility, although at different scales. Roberts *et al*. (1999) measured trace element compositions of three coeval stalagmites from a British cave by laser ablation ICP-MS and found no coherence between records. This brings into question whether trace element variability in speleothem calcite does in fact reflect changes in the palaeoenvironment. The authors argue that it is possible that the flow paths leading to the drip sites above each stalagmite might have intersected geochemically distinct source rocks, the dissolution of which have overwritten any potential climate signal.

At least two authors have also demonstrated that reproducibility is challenging on the micro scale. Finch *et al*. (2003) highlight the complex compositional heterogeneity of aragonitic speleothems involving both climate-derived and disequilibrium growth zoning. They suggest that a single line of analyses performed parallel to the growth axis is unlikely to provide reliable climatic proxy data, since even the most carefully positioned analysis track will move across laterally zoned crystallites. Reproducible trace element sections can therefore only be achieved by the averaging of several parallel analytical stepscans. This same drawback was encountered by Treble *et al*. (2003) who determined the mean of 11 parallel analyses before discussing the observed trends with confidence.

2.2.3.5 Other Proxies

Speleothems archive palaeoenvironmental changes in many other ways than just through their geochemistry. In the following paragraphs I will briefly outline a number of studies which have exploited these alternative proxies.

Dreybrodt (1999) summarises many studies that have used a combination of mathematics and modeling to determine factors influencing stalagmite morphology. Drip rates, and hence growth rates, were determined to be significant. Kaufmann and Dreybrodt (2004) took this a step further and assumed that drip rates were a direct function of climate. By doing this, stalagmite stratigraphy (layer thickness/growth rate) can be used to infer climate change.

With further developments in technology it may be possible in the future to determine layer thickness and growth rates without cutting the speleothem. Mickler *er al*. (2004) were able to 'view' the internal structure of a stalagmite using X-ray tomography. This technique has further applications in helping to determine the best angles to cut a speleothem such that samples for stable isotope and trace element analyses may always be taken from the growth axis.

Frequency histograms of speleothem ages have been used extensively to determine periods when speleothems did or did not form as a result of changing climatic conditions (Atkinson *et al*. 1978; Hennig *et al*. 1983; Goede *et al*., 1990a; Baker *et al*., 1995; Williams, 1996; Lauriol *et al*., 1997; Ayliffe *et al*., 1998; Spötl *et al*., 2002; Polyak *et al*., 2004; Wang *et al*., 2004). Such climate changes may be a switch to more moist conditions (e.g. from migration of the inter-tropical convergence zone across monsoon regions) or more indirectly through the thawing of permafrost or ice overlying a cave. Alternatively, too much water, specifically submergence of the speleothem, will lead to cessation of growth. Several researchers have visited submarine caves and dated speleothems in them that formed during glacial periods when sea level was lower than at present (Gascoyne *et al*., 1979; Richards *et al*., 1994). In doing so, understanding of the timing of past sea level changes can be improved.

Growth rates of speleothems also reveal palaeoclimate changes. Rates vary as a function of the degree of supersaturaion of carbonate (measured as pCO_2) and the drip rate (itself a function of rainfall amount) (Baker *et al*., 1993). Zhao *et al*. (2001) were able to determine the onset and duration of the previous interglacial (MIS 5e) from growth rates in a Tasmanian speleothem.

In speleothems where annual layering can be determined, growth rates can be more accurately measured through layer thickness. This method has been used to investigate the strength and frequency of El Niño at several locations in tropical latitudes (Brook *et al*., 1999; Rasbury and Aharon, 2006).

Williams (1982) used speleothem ages to determine the time at which cave passages had been abandoned by active streams in caves on the west coast of South Island, New Zealand. Abandonment occurred in conjunction with regional uplift and the development of new passages at lower elevations. By accumulating ages from passages at different elevations, uplift rates were determined for the region for the mid-late Quaternary. Similarly, valley incision which exposes limestone outcrops at lower elevations can lead to cave passage abandonment (Atkinson *et al*., 1978; Haeuselmann *et al*., 2007).

Variability in speleothem layers (stratigraphy) can be manifest as changes in mineralogy, crystal structure, colour or detrital content. The different layers may be visible in natural light or only under UV light (Shopov *et al*., 1994). Ultra-violet light causes fluorescence of organic material in the calcite such that different concentrations of these compounds lead to greater or lesser degrees of fluorescence (Shopov *et al*., 1994). The brightness, recurrence interval and thickness of bands can be measured and developed into a record of past climate, sometimes revealing annual resolution (Baker *et al*., 1993; Shopov *et al*., 1994).

Lee-Thorp *et al*. (2001) photomicrographed a speleothem and measured the grey level of the visible layers, a proxy for organic content. Darker layers were taken to indicate higher productivity at the surface in response to wetter climate.

Carbonate speleothems are composed of either calcite or aragonite. Crystals of both of these minerals can occur in a variety of fabrics. Calcite formed under evaporative conditions is often microcrystalline and soft. In contrast, calcite formed by slow degassing of CO_2 is usually hard and massively crystalline (Gillieson, 1996). Aragonite precipitation is driven by either, or a combination, of the following: (1) low relative humidity of the cave atmosphere, (2) rapid CO_2 loss from the seepage water, and (3) high Mg content of seepage water (Gonzalez and Lohmann, 1988; Gillieson, 1996). In some cases both aragonite and calcite may be present in the same speleothem which thus provides extra climate information (Holmgren *et al*., 1995).

Pollen grains may be transported into caves and deposited onto speleothems by seepage waters. A couple of studies have attempted to infer past climate changes from pollen preserved in speleothems (Brook *et al*., 1990; Lauriol *et al*., 1997).

2.2.4 Speleothem Collection

A factor in the success of extracting long-term palaeoenvironmental records from cave speleothems lies, quite simply, in choosing the right samples to start with (Holmgren and Shaw, 1999). The choice of speleothem and the method by which the sample is extracted are typically determined by factors such as cave access, conservation policy and experience of the sampler. For palaeoclimate studies, often the age and internal structure of speleothems are significant in the ability to develop a record that meets the research objectives. Neither of these can be determined in the field and therefore the potential and problems of the sample are frequently not recognized until it has been removed from the cave and undergoing analysis. Inevitably this leads to some samples being collected and never used (Frappier, in press).

From a logistical as well as a conservation point of view, cores taken from speleothems may serve as an alternative to the removal of whole specimens, particularly where those speleothems are large. Coring of speleothems has been conducted in several previous studies (Brook *et al*., 1990; Hellstrom *et al*., 1998; Holmgren and Shaw, 1999; Oster *et al*., 2006). In each of these studies palaeoclimate records were derived from material in the collected cores. However, a number of problems may be encountered by such methods. Asymmetric growth of stalagmites is common. In such cases it is not possible to capture the growth axis for the full length of the core when drilling vertically. Neither is it possible to conduct Hendy Tests as there is little lateral extension of layers in captured vertical cores.

2.2.5 Summary

Through their formation, many speleothems are inherently archives of past climate. This information is recorded in a variety of different proxies incorporated into the crystal structure, or manifest as the shape or growth rate of the speleothem. However, direct climate interpretations of many (if not all) speleothem records are not possible. This is particularly true where only subtle shifts over short time periods are recognized in the record (Fairchild *et al*., 2006). The use of multiple proxies, most notably combinations involving trace element records, offers the possibility of achieving greater understanding of formation mechanisms and untangling the various influences on individual proxies (e.g. $\delta^{13}C$).

Significantly, the global distribution of caves yields the potential to acquire multi-proxy speleothem records from almost every continent. This coupled with the ability to apply absolute and precise chronologies to these datasets, that may extend into the millions of years, makes them comparable to, if not better than, other proxy climate records from the terrestrial and marine realms.

However, the removal of speleothems for palaeoclimate research and its conflict with conservation ethics is becoming increasingly important. It is rapidly being recognized that methods for obtaining speleothems need to be improved, primarily in terms of minimizing impacts to the cave environment. Analysis of material cored from whole speleothems is potentially one way to achieve this goal.

2.3 Review of Southern Hemisphere Speleothem Records

2.3.1 Introduction

It is important to be able to place any new work on speleothems in relation to the existing published literature. In addition a good knowledge of the literature is required to prevent duplicating existing studies and to discover gaps in understanding that need to be filled in. Although pioneering work on palaeoclimates from speleothems was conducted in New Zealand, Southern Hemisphere speleothem research has lagged behind that of the Northern Hemisphere. In the following sections a review of all Southern Hemisphere speleothem-based palaeoclimate records is attempted.

2.3.2 New Zealand

2.3.2.1 Introduction

New Zealand, which extends from about 34°30′ to 47°30′ south latitude, has abundant carbonate rocks which crop out widely throughout the country (Figures 2.5a and 2.5b). These are predominantly Oligocene to earliest Miocene age limestones, but mixed with a scattering of Devonian marbles (Nelson region) to relatively unconsolidated Plio-Pleistocene deposits (Hawke's Bay) (Nelson, 1978). There are several major karst regions and caves are known from Waiomio Valley in the north to Clifden in the south (Crossley, 1988; Smith, 2004).

The use of speleothems for the purpose of determining past climates was pioneered in New Zealand, and the Southern Hemisphere, by Hendy and Wilson (1968). Although only a preliminary report, it suggested that at least in terms of sample resolution speleothem records held a significant advantage over marine sediment cores, the primary means of creating long palaeoclimate records at the time. The early promise was not realized, primarily due to a lack of confidence in radiocarbon-based chronologies, and speleothem-based palaeoclimate records from New Zealand were relatively rare in the literature in subsequent decades. However, with the introduction of TIMS uranium-thorium dating techniques to speleothems in the 1980s (Edwards *et al*., 1987), it became possible for high-

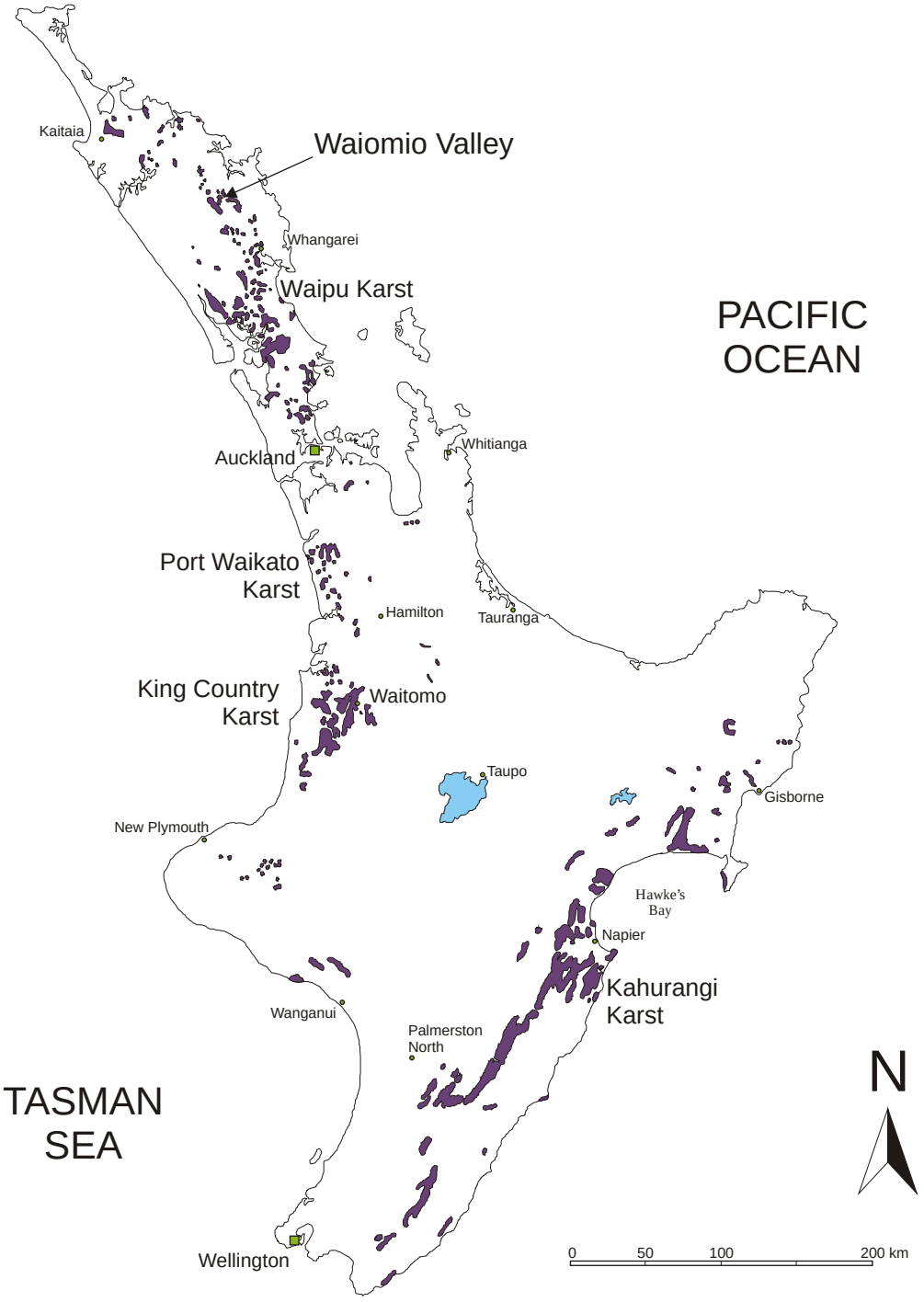

Figure 2.5a: Distribution of carbonate rocks in North Island, New Zealand. Modified from Williams (1992). Most North Island speleothem records are developed from deposits in caves near Waitomo in the King Country Karst.

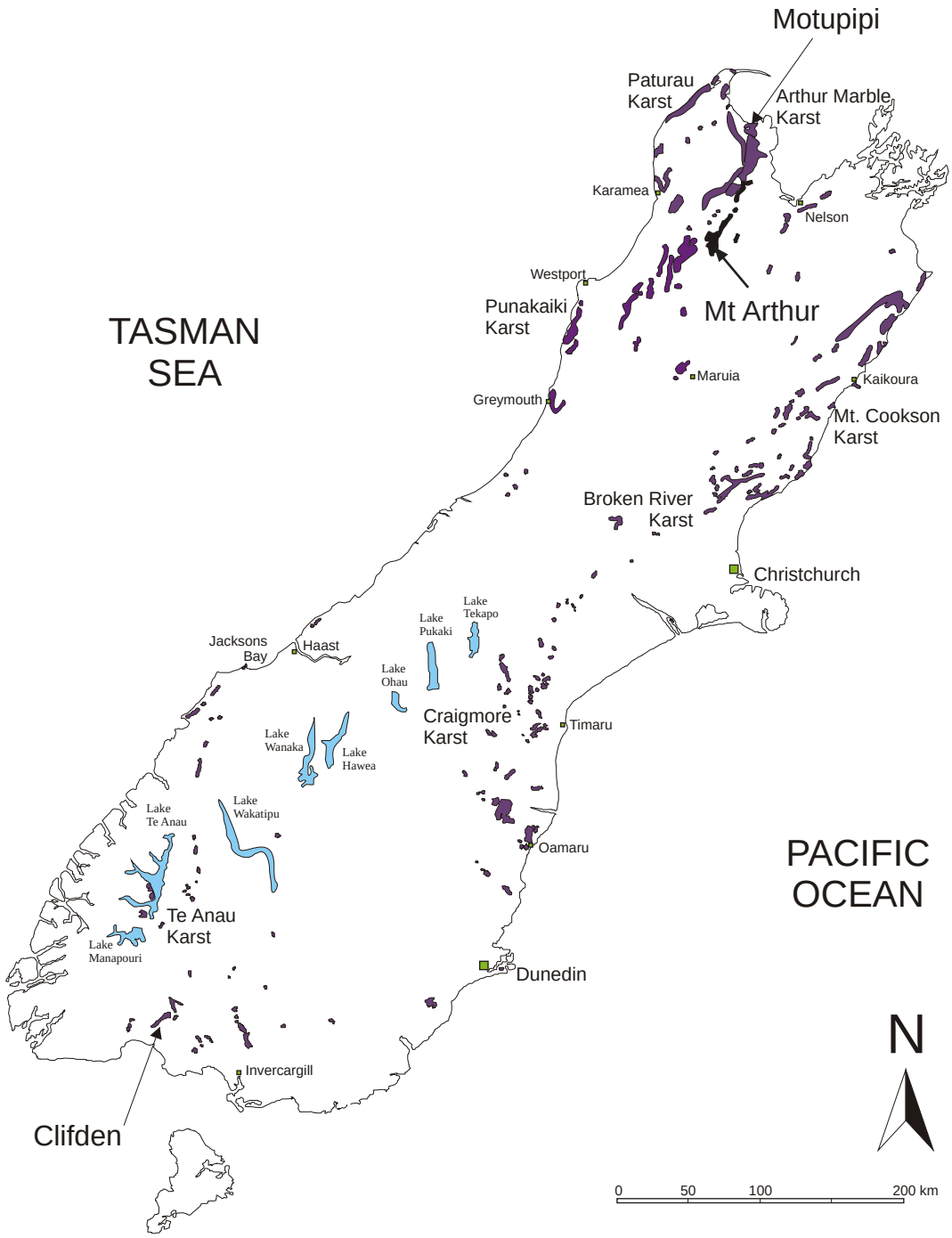

Figure 2.5b: Distribution of carbonate rocks in South Island, New Zealand. Modified from Williams (1992). Outcrops of Arthur Marble are highlighted by the vertical stripe pattern. Karsts in north-west South Island, and the Te Anau Karst in the south-west, have yielded palaeoclimate records.

resolution stable isotope records to be supported by precise, absolute chronologies. Since then there has been a resurgence in speleothem studies from New Zealand which, along with the early material, is reviewed in the following pages.

2.3.2.2 Late Pleistocene Records

Williams (1996) U-Th dated speleothems interbedded with glaciofluvial deposits in Aurora Cave, Te Anau Karst, in southern South Island (Figures 2.3, 2.5b). During periods of local glacier advance, ice-damming of cave resurgences occurred resulting in the accumulation of sediments within the cave. Glacier down-wasting during warm and/or dry phases to elevations below the level of cave resurgences allowed the cave to drain and speleothems formed on the deposited glacial sediments. Twenty-six alpha-spectrometry U-Th dates on buried flowstones and stalagmite tips allowed a 230 kyr glacial history of the Te Anau region to be determined. Seven glacier advances were reported, six of which took place during the last glacial period. The earliest of those six advances, Aurora 6, occurred between 91 and 67 kyr B.P. and appears to have been the largest event of the last glacial period. Subsequent glacier advances occurred from 48-46, 41-40, 20-18, 17-15 and 14-11 kyr B.P. (Williams, 1996).

Hendy and Wilson (1968) analysed two stalactites from Waipuna and Gardners Gut caves in the Waitomo region, North Island (Figure 2.5b) for $\delta^{18}O$ along the growth axis and dated them by means of the radiocarbon (^{14}C) technique. Where the two records overlapped (~35-10 ka) they were in good agreement. Much of the Waipuna Cave stalactite record was beyond the limit of radiocarbon dating and, through comparison with other long climate records, was shown to potentially represent the entire last glacial period. If so, it appeared as though there was little other than sea-level change driving variability in $\delta^{18}O$ at Waitomo.

As part of the same research project Hendy (1969) presented a further two speleothem $\delta^{18}O$ records from caves in northwest Nelson. A stalagmite from Council Cave, Motupipi (Figure 2.5b), formed over the period 30-0 kyr B.P. (as determined from radiocarbon dates). Isotopic minima at 20-17 and 30-25 kyr B.P. would appear to closely match the timing of temperature minima of the LGCP.

The second stalagmite record (Twin Forks Cave, Paturau) covered the late Holocene and is discussed in the next section (2.3.2.3).

At Mt Arthur, in northern South Island (Figure 2.5b), Hellstrom *et al*. (1998) sampled active flowstones ~200 m below the ground surface in two high-elevation caves, Exhaleair and Nettlebed. The Nettlebed flowstone (MD3) formed continuously from 31 kyr B.P. to the present, whereas ED1 (Exhaleair flowstone) ceased growth from 73-16 kyr B.P. and then grew continuously to the time of collection. The hiatus in ED1 represents the last glacial period. A likely scenario for non-deposition at this site is that regional climate cooling led to retreat of the treeline such that vegetation and soils did not persist above the cave causing a change to weakly acidic seepage waters. MD3 formed at a lower elevation and was not affected by this process, constraining the treeline lowering to no more than 600 m. Assuming an adiabatic lapse rate of 6°C/km this represents a maximum cooling of ~3.5°C for the period 73-16 kyr B.P.

Where the MD3 and ED1 isotope records overlap they showed good agreement. Data resolution in the MD3 record during the LGCP is ~60-500 yr/sample which provides definition of several prominent millennial-scale climate fluctuations, including some evidence for a late glacial reversal (Figure 2.6).

Hellstrom and McCulloch (2000) analysed, using ICP-MS, 117 consecutive homogenized 5 mm increments of the MD3 flowstone core for magnesium (Mg), strontium (Sr), barium (Ba), and uranium (U). To date, these remain the only published trace element data from New Zealand speleothems. The concentrations of Ba and Sr were strongly correlated ($r = 0.90$), indicating a common forcing factor. The fluctuations in concentrations of these elements also showed good agreement with the variability displayed in the MD3 $\delta^{13}C$ record (Hellstrom *et al*., 1998). These results are consistent with reduced temperature, precipitation, vegetation cover, and soil organic content during the LGCP relative to the Holocene.

Williams *et al*. (2005) measured stable isotope ratios in eight stalagmites from six caves in the Paturau (Creighton's Cave, Wet Neck Cave and Twin Forks Cave) and Punakaiki (Babylon Cave, Wazapretti Cave and Hollywood Cave) karsts, all at low elevation sites, along the northern west coast of South Island (Figure 2.5b). The results were compiled as a composite record that covers the last 23.4 kyr, although no single record covers the entire period. The master $\delta^{13}C$ and

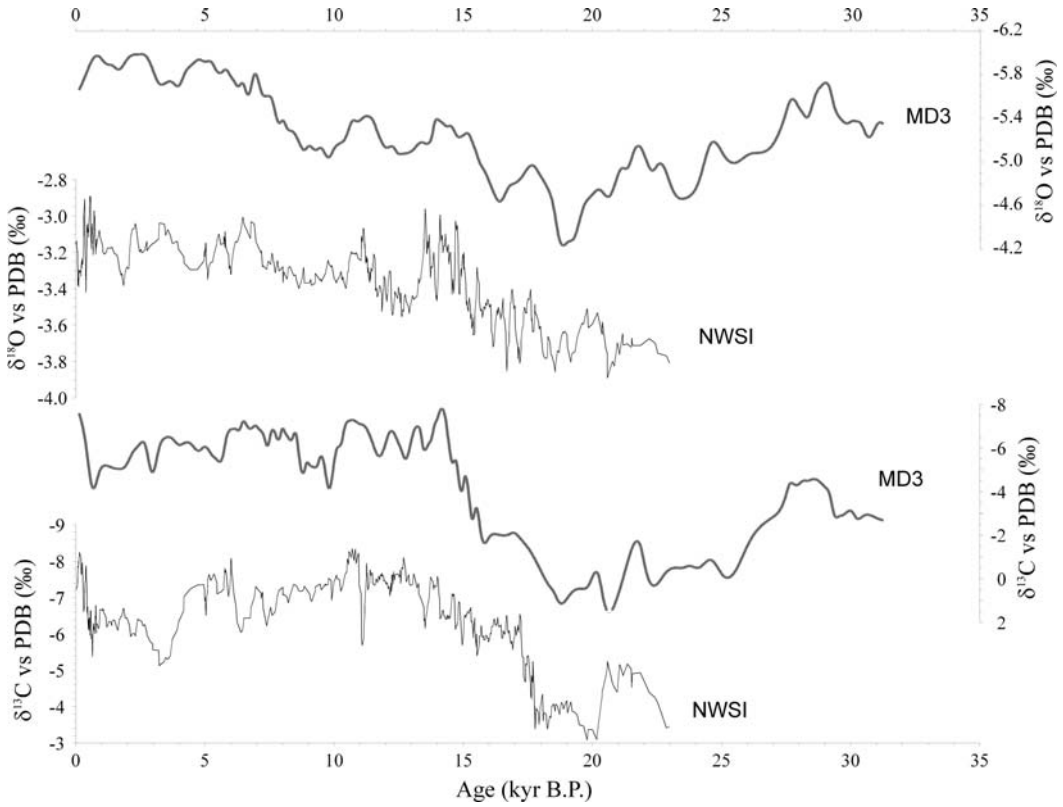

Figure 2.6: Comparison of $\delta^{18}O$ and $\delta^{13}C$ profiles from northwest South Island speleothems (MD3 from Hellstrom *et al*., 1998; NWSI from Williams *et al*., 2005).

$\delta^{18}O$ curves are composed of 573 paired stable isotope measurements tied to a chronology based on 43 TIMS dates (Figure 2.6). This yielded an average data resolution of 41 yr/sample, although the authors cautioned against too fine an interpretation of the record due to the possible errors associated with the linear interpolation of ages between TIMS dates. The $\delta^{18}O$ record was then corrected for the ice volume effect and yielded what appears to be a precipitation-driven signal. From the stable isotope data the LGCP was interpreted as cold and relatively dry, but with an interstadial event between about 20.4 and 19.7 kyr B.P. Deglaciation commenced ~18.2 kyr B.P. with the most rapid warming occurring between 16.7 and 14.7 kyr B.P. Between 14.7 and 13.53 kyr B.P. there was a 'climatic optimum' during which time temperatures similar to those in the Holocene occurred. The timing coincided with the Bølling/Allerød warm event of Europe. The subsequent cooling was of further interest as it overlapped both the Antarctic

Cold Reversal (ACR) and the Younger Dryas (YD). However, it began almost 1 kyr after the onset of the ACR and ended 0.36 kyr after the termination of the YD. It did, however, closely match a cold event recognized in Kaipo Bog sediments (Newnham and Lowe, 2000) leading to the conclusion that New Zealand had a palaeoclimate history distinct from either pole at this time. Subsequently this speleothem record was adopted by NZ-INTIMATE members to provide the framework for a New Zealand 'event stratigraphy' for the last 30 kyr (Alloway *et al*., 2007).

2.3.2.3 The Holocene

Hendy (1969) presented oxygen isotope data from a stalagmite from Twin Forks Cave, northwest Nelson, shown to have grown over the last 4500 ^{14}C years. In combination with the Gardner's Gut stalactite from Waitomo (Hendy and Wilson, 1968) a palaeotemperature curve for the past 10 kyr was constructed. Of note is a negative δ^{18}O excursion, or warm period, ~1000 years ago that is roughly correlative to the Medieval Climate Optimum (MCO) recognized in the Northern Hemisphere (also referred to as the Medieval Warm Period). The apparent discovery of a global MCO signal, and the possible effect that this may have had on the peopling of New Zealand by Polynesian explorers (Wilson and Hendy, 1971) prompted Wilson *et al*. (1979) to develop the most recent ~1000 year period of the Twin Forks speleothem record. Although the variability in the oxygen isotopes is small (~0.4 ‰), and the chronology is based on radiocarbon dates, the authors suggested that both the MCO and Little Ice Age (LIA) were represented in the record.

Williams *et al*. (1999) reported δ^{18}O records from three stalagmites and a straw stalactite in the Waitomo region of North Island, that covered the Holocene. The chronology for each stalagmite was created using one basal alpha-counting U-Th date, and a suite of AMS ^{14}C dates. In Williams *et al*. (2004) the same three stalagmites were dated again, this time using the TIMS method. The resulting chronology did not match that of the original study. Only the TIMS dates were retained.

As well as the three stalagmites in Williams *et al*. (1999), Williams *et al*. (2004) added a fourth from Ruakuri Cave (also in the Waitomo region). Nineteen

U-Th dates are used to create the chronologies for the stalagmites. The four oxygen isotope records showed relatively consistent long-term variability, but considerable disparity in the finer detail. There was less coherence among the carbon isotope curves, although major trends were still discernable. The resulting Waitomo master chronology covered the period 0-11.7 kyr B.P. and displayed a total range in $\delta^{18}O$ of 1.13 ‰ (following adjustment of the early part of the record for the ice volume effect), and of 3.63 ‰ in $\delta^{13}C$. An early Holocene thermal maximum, ~10.8 kyr B.P. was observed in the Waitomo record. This agreed well with observations from Antarctic ice core records and New Zealand palynological evidence (Petit *et al*., 1999; Newnham and Lowe, 2000). There was also a broad Holocene temperature minimum from 6-2 kyr B.P. In the most recent part of the Waitomo $\delta^{18}O$ record a clear positive excursion between 0.9 and 0.6 kyr B.P. closely corresponded to the MCO, and a subsequent fall in $\delta^{18}O$ values to a low point ~325 yrs B.P. could suggest that New Zealand experienced the LIA.

Williams *et al*. (2004) suggested that the differences in fine scale of the four separate $\delta^{13}C$ curves from Waitomo, resulted from strong local forcings and therefore no solid conclusions regarding regional climate could be drawn from the composite data.

2.3.2.4 Discussion

Early palaeoclimate records from New Zealand speleothems suffered from the use of radiocarbon dates as the basis of their chronology. In addition, only $\delta^{18}O$ was reported. Not until Hellstrom *et al*. (1998) were $\delta^{13}C$ values published, and trace element data have only been reported for one stalagmite (Hellstrom and McCulloch, 2000).

The inaccuracies inherent in using radiocarbon dates, and also uranium-thorium dates calculated using the alpha-counting technique (New Zealand speleothems generally have rather low uranium content), are highlighted in the discrepancies between chronologies of three speleothem records reported first in Williams *et al*. (1999) and then amended using uranium-thorium TIMS dates in Williams *et al*. (2004).

Although the use of TIMS dates created a much more robust chronology than one based on radiocarbon dates, it was still limited by the low density of dates.

Changes in speleothem growth rate are assumed to be negligible when linearly interpolating between dates. Naturally the more dates used to create a chronology the smaller the error incurred by ignoring growth rate changes. For example, Williams *et al*. (2004, 2005) cautioned against fine-scale interpretation of their master chronologies due to having only ~5 dates per speleothem.

Not withstanding the uncertainties inherent in the chronologies of the speleothem records, many climate events are recognised as having affected New Zealand in the past. Several records show MCO and LIA-like anomalies in the $\delta^{18}O$ record.

In New Zealand speleothem $\delta^{18}O$ records, LGCP values are typically offset from those of the Holocene by 0.5-1.0 ‰, in either the positive (Hellstrom *et al*., 1998) or negative (Williams *et al*., 2004, 2005) sense. Compared to speleothem records from around the world, particularly those from monsoon-affected sites, an LGCP shift of this magnitude is relatively small (Wang *et al*., 2001; Frumkin and Stein, 2004; Dykoski *et al*., 2005). This requires that interpretation of minor oscillations be made with care so as to not be confused with noise.

Hellstrom *et al*. (1998) indicated from oxygen isotope results that the most extreme glacial conditions were reached ~19 kyr B.P. (Figure 2.6), although this was a short-lived event. The ^{13}C data showed a much more familiar LGCP trend. Termination I began at ~15 kyr B. P. (Hellstrom and McCulloch, 2000). Evidence from the west coast of the South Island suggested that the duration of the LGCP was much greater than that indicated by the Mt. Arthur speleothems, and persisted until 18.2 kyr B.P.

The Younger Dryas is traditionally thought to have persisted from ~12.7 to 11.6 kyr B.P. (Johnsen *et al*., 1992; Wurth *et al*., 2004). Its imprint on palaeoclimate records was most noticeable in Europe, but has been recognised across the Northern Hemisphere (Hughen *et al*., 1996; Wang *et al*., 2001; Dykoski *et al*., 2005) and parts of the Southern Hemisphere (Lowell *et al*., 1995; Ariztegui *et al*., 1997; Moreno and León, 2003). There is considerable debate as to whether or not it was global in effect, particularly in New Zealand (McGlone, 1995; Turney *et al*., 2003). Hellstrom *et al*. (1998) found an oxygen isotope excursion towards colder climate at 13.8 to 11.7 kyr B.P. The onset of this event prior to the Younger Dryas would suggest that the two events may not be related. A similar conclusion was reached by Williams *et al*. (2005) who dubbed a major reversal in

$\delta^{18}O$ between 13.5 and 11.1 kyr B.P. the New Zealand Late Glacial Reversal (NZLGR). Despite not having a clear-cut YD signal, the correlation of the West Coast and Mt. Arthur speleothem records supports the notion that New Zealand was affected by its own cool climate anomaly at this time. This is further supported by glacial evidence on South Island, including the Aurora 1 glacial advance in Fiordland (Williams, 1996) which occurred after 13.8 kyr B.P., and the Waiho Loop advance at 11,050 ± 14 ^{14}C yr B.P. (Denton and Hendy, 1994). Furthermore, at Kaipo Bog on North Island the ratio of lowland podocarp to grass pollens was relatively low between 13.9 and 11.6 kyr B.P., indicating cooler climate at this time (Newnham and Lowe, 2000).

Wilson *et al*. (1979) suggested that the MCO and LIA could have been global in extent based on a $\delta^{18}O$ record from northwest South Island. Peak MCO conditions occurred around 1400 A.D., and maximum cooling associated with the LIA happened ~1650 A.D. The chronology of this record was based on radiocarbon dates and therefore some caution should be used when closely interpreting the record. However, Williams *et al*. (2004, 2005) found further, albeit weak, evidence of both the MCO and LIA in New Zealand.

Despite the close agreement among NZ $\delta^{18}O$ records around the time of the YD, MCO and LIA, there are no close correlations during the remainder of the Holocene in either $\delta^{18}O$ or $\delta^{13}C$.

2.3.2.5 Further Research Opportunities

The limited number of records, the brief period of time covered by each, and the inability to find correlative records opens up possibilities for further speleothem studies based in New Zealand. On North Island all existing records are from Waitomo, which yields poor geographic coverage. In addition, only four records have absolute chronologies and none extend beyond ~12 kyr B.P. Therefore there is opportunity to investigate the effect of glacial conditions on North Island climate. This can be compared to existing proxy records from North and South Islands and tested against global models of climate change.

On South Island there appears to be much potential given that there are no isotopic records that cover the period prior to 31 kyr B.P., and furthermore that

results in the current literature do not agree at the millennial-scale where they overlap.

2.3.3 Australia

2.3.3.1 Introduction

Australian caves have yielded speleothem records of past climate that cover much of the last 500 kyr. Furthermore, recent work has shown that many speleothems from caves in the Nullarbor are millions of years old which offer the possibility of extending records of Australian climate change back to the Pliocene (Woodhead *et al*., 2006). At the opposite end of the timescale are several studies which have sought to match speleothem records to meteorological observations of the last century (Treble *et al*., 2003; 2005; Desmarchelier *et al*., 2006).

It is important to look at Australian and in particular Tasmanian speleothem palaeoclimate records for two reasons. First, it is the nearest land mass to New Zealand. Second, the westerly circulation that affects at least the southernmost parts of Australia also influences New Zealand's climate. Therefore it is likely that at least major climate shifts observed in Australian records may also be present in records from New Zealand. Furthermore, it has been demonstrated that Tasmanian speleothem $\delta^{18}O$ values show a positive relationship to temperature (Goede *et al*., 1998), as do a number of South Island, New Zealand, samples (Williams *et al*., 2005). This might further indicate a common precipitation-driven climate forcing.

A summary of the locations of Australian and New Zealand speleothem studies is presented in Figure 2.7. The studies present inferences of past climate based on speleothem growth periods, stable isotopes of oxygen and carbon, and trace element concentrations in the speleothem calcite. The publications are reviewed here in order of age of the speleothems studied from the oldest to the youngest. Table 2.1 provides further information on each of the studies.

2.3.3.2 Pre- and Early Pleistocene

In the Nullarbor region of Australia there is a ~200,000 km^2 area of relict karst. Goede *et al*. (1990a) attempted to determine the ages of speleothems within

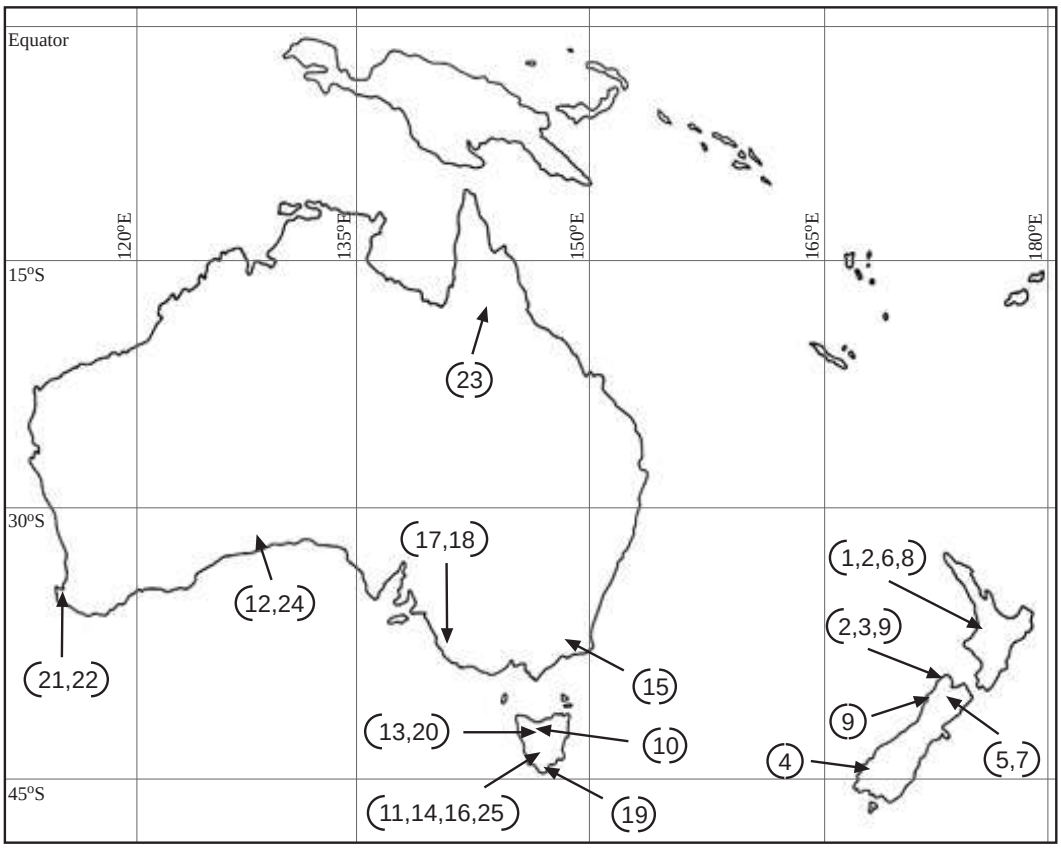

Figure 2.7: Locations of caves in Australia and New Zealand for which records of past climate change have been developed. Numbers are linked to references compiled in Table 2.1.

Table 2.1: A compilation of Southern Hemisphere speleothem research locations. The # value corresponds to locations on maps of Australia and New Zealand (Figure 2.7), Africa (Figure 2.9) and South America (Figure 2.11), with the exception of #47 which is not shown.

#	Author(s)	Publ. Year	Cave	Country	Latitude	Longitude	Elevation (masl)	Cave Temp. (°C)	Age of Deposits (kyr)	Comments
1	Hendy & Wilson	1968	Gardners Gut	New Zealand	38°16'S	175°01'E	60-100		0-40	^{14}C dates, stalactite
			Waipuna	New Zealand	38°18'S	175°01'E	240-270		0-100	^{14}C dates, stalactite
2	Hendy	1969	Gardners Gut	New Zealand	38°16'S	175°01'E	60-100		0-42	^{14}C dates, stalactite
			Waipuna	New Zealand	38°18'S	175°01'E	240-270		11-100	^{14}C dates, stalactite
			Twin Forks	New Zealand	40°40'S	172°26'E	30-60		0-4.5	^{14}C dates
			Council	New Zealand	40°53'S	172°51'E	15		0-32	^{14}C dates
3	Wilson *et al*.	1979	Twin Forks	New Zealand	40°40'S	172°26'E	30-60		0-1	^{14}C dates
4	Williams	1996	Aurora	New Zealand	45°17'S	167°42'E	200-400		11-230	Record of glacier activity
5	Hellstrom *et al*.	1998	Nettlebed	New Zealand	41°13'S	172°43'E	390	~8.3	0-31	Flowstone
			Exhaleair	New Zealand	41°15'S	172°41'E	685		0-16	Flowstone
6	Williams *et al*.	1999	Gardners gut	New Zealand	39°15'S	175°01'E	120	13.3		^{14}C dates
			Max's	New Zealand	38°16'S	175°01'E	340	11.5		^{14}C dates
			Waipuna	New Zealand	38°19'S	175°01'E	380	11.5	0	Straw tip
			Aurora	New Zealand	45°20'S	167°42'E	320	8.5	0	Straw tip
			Luxmore	New Zealand	45°22'S		1060	4.5	0	Straw tip
			Luxless	New Zealand	45°22'S		1060	4.5	0	Straw tip
			Waiau	New Zealand	46°S		100	9.3	0	Straw tip
7	Hellstrom & McCulloch	2000	Nettlebed	New Zealand	41°13'S	172°43'E	390		0-31	
8	Williams *et al*.	2004	Gardners Gut	New Zealand	39°15'S	175°01'E	60-100		0-9.7 & 0-11.8	Stacked record
			Max's	New Zealand	38°16'S	175°01'E	325		2.6-6.2	
			Ruakuri	New Zealand	38°16'S	175°04'E	60-100		6.1-11.1	
9	Williams *et al*.	2005	Wet Neck	New Zealand	~40°40'S	~172°25'E	60		13.8-17.1 & 15.5-21.2	Stacked record
			Creighton's	New Zealand	~40°40'S	~172°25'E	<170		6.9-16.1	
			Twin Forks	New Zealand	40°40'S	172°26'E	30-60		17.7-23.2	
			Babylon	New Zealand	42°02'S	171°25'E	~150		0.1-10 & 11.1-23.4	
			Wazapretti	New Zealand	42°06'S	171°24'E	~100		5.0-13.9	
			Hollywood	New Zealand	41°58'S	171°28'E	~100		0-4.2	

Continued on next page

Table 2.1 (continued)

#	Author(s)	Publ. Year	Cave	Country	Latitude	Longitude	Elevation (masl)	Cave Temp. (°C)	Age of Deposits (kyr)	Comments
10	Goede *et al.*	1986	Little Trimmer	Australia (Tas)	41°34'S	146°15'E	460	9.5 ± 0.5	76-109	
11	Goede *et al.*	1990a	Frankcombe	Australia (Tas)	42°32'S	146°27'E	360	8.3 ± 0.2	2.9-4.3 & 55-98	Re-dated: # 16
12	Goede *et al.*	1990b	(Nullarbor)	Australia (WA)			90-240	16-18	> 400	
13	Goede & Vogel	1991	Lynds	Australia (Tas)	41°35'S	146°15'E	300	9.5 ± 1	11.7-15.0	
14	Goede	1994	Frankcombe	Australia (Tas)	42°32'S	146°27'E	360	8.3 ± 0.2	55-98	High-res ^{18}O,^{13}C; Mg, Sr data
15	Goede *et al.*	1996	Royal Cave	Australia (Vic)	37°30'S	148°10'E	80	~15	2.1-3.2, 10.6-13.4	
16	Goede *et al.*	1998	Frankcombe	Australia (Tas)	42°32'S	146°27'E	360	8.3 ± 0.2	76.2-84	Sr, Sr isotope data
17	Ayliffe *et al.*	1998	Victoria Fossil	Australia (SA)	36°58'S	140°45'E	75	16.8	0-500	Growth frequency study
18	Desmarchelier *et al.*	2000	Victoria Fossil	Australia (SA)	36°58'S	140°45'E	75	16.8	157-185	
19	Zhao *et al.*	2001	Newdegate	Australia (Tas)	43°23'S	146°56'E			100-155	Growth rate study
20	Xia *et al.*	2001	Lynds	Australia (Tas)	41°35'S	146°15'E	300	9.5	5.1-9.2	
21	Treble *et al.*	2003	Moondyne	Australia (WA)	34°16'S	115°05'E		15.9-16.5	0-0.1	Trace elements, 1911-1992
22	Treble *et al.*	2005	Moondyne	Australia (WA)	34°16'S	115°05'E		15.9-16.5	0-0.1	Stable isotopes, 1911-1992
23	Turney *et al.*	2006	Chillagoe	Australia (Qld)	17°09'S	144°31'E			8-16	Within paleoclimate review
24	Woodhead *et al.*	2006	Leana's Breath	Australia (WA)	~31°S	~128°E			~4000	U-Pb dated
25	Desmarchelier *et al.*	2006	Frankcombe	Australia (Tas)	42°32'S	146°27'E	360	8.3 ± 0.2	0-0.23	Straw; trace elements
26	Talma *et al.*	1974	Wolkberg	South Africa	24°06'S	29°53'E	1486	20-22	1.5 - >45	^{14}C dates; growth freq. study
27	Brook	1982	Echo	South Africa	24°31'S	30°56'E	~1000		0-35	^{14}C dates; growth freq. study
28	Vogel	1983	Cango II	South Africa	33°23'S	22°13'E		17.5	0-40	^{14}C calibration for speleothem
29	Heine & Geyh	1984	Rössing	Namibia	22°32'S	14°48'E	338		0-40	^{14}C dates; growth freq. study
30	Brook *et al.*	1990	Drotsky's	Botswana	21°27'S	21°40'E			2-15 & 197	Flowstone
			Lobatse II	Botswana	~25°S	~26°E			0-45, 197	Growth frequency study
			Matupi	Zaire	1°30'N	36°E	1100		0-40	Pollen analysis
			Galweda	Somalia	~11°N	~48°E	20		4-116	Growth frequency study
			Hayla	Somalia	~11°N	~48°E	1800		4 - >250	Growth frequency study
31	Talma & Vogel	1992	Cango II	South Africa	33°23'S	22°13'E		17.5	0-5, 13.8-30	
32	Holmgren *et al.*	1994	Lobatse II	Botswana	~25°S	~26°E		20.6	21.6-50	Updated: # 33
33	Holmgren *et al.*	1995	Lobatse II	Botswana	~25°S	~26°E		20.6	21-27, 43-51	

Continued on next page

Table 2.1 (continued)

#	Author(s)	Publ. Year	Cave	Country	Latitude	Longitude	Elevation (masl)	Cave Temp. (°C)	Age of Deposits (kyr B.P.)	Comments
34	Holmgren & Shaw	1999	Lobatse II	Botswana	~25°S	~26°E		20.6	22-26, 40, 50	Stalagmite cores; some trace element data
35	Holmgren *et al*.	1999	Cold Air	South Africa	24°S	29°11'E	1420	~18	0-3	Updated: # 39
36	Repinski *et al*.	1999	Cold Air	South Africa	24°S	29°11'E	1420	~18	0-0.8, 4-4.4	
37	Brook *et al*.	1999	Anjohibe	Madagascar	15°33'S	46°53'E	~100		0-0.45	ENSO-controlled layer thickness’
38	Piketh *et al*.	1999	Cold Air	South Africa	24°S	29°11'E	1420	~18	0-1	Microprobed trace elements
39	Lee-Thorp *et al*.	2001	Cold Air	South Africa	24°S	29°11'E	1420	~18	0-6.5	
40	Finch *et al*.	2001	Cold Air	South Africa	24°S	29°11'E	1420	~18	6.2-6.4	Trace elements; aragonite
41	Finch *et al*.	2003	Cold Air	South Africa	24°S	29°11'E	1420	~18	0-0.05 & 0-0.05	Trace elements; aragonite
42	Holmgren *et al*.	2003	Cold Air	South Africa	24°S	29°11'E	1420	~18	0-10.2, 12.7-24.4	
43	Bertaux *et al*.	2002	João Arruda	Brazil	~21°S	~57°W	~300		0-3.8	Aragonite. Layer study
44	Wang *et al*.	2004	Toca da Boa Vista	Brazil	10°10'S	40°50'W	~500		10-210	Speleothems & travertine
			Lapa dos Brejões	Brazil	10°10'S	40°50'W	~500		10-210	Growth frequency study
			Toca da Barriguda	Brazil	10°10'S	40°50'W	~500		10-210	
45	Cruz *et al*.	2005	Botuverá	Brazil	27°13'S	49°09'W	230		0-116.2	Insolation influenced
46	Wang *et al*.	2006	Botuverá	Brazil	27°13'S	49°09'W	230		0-9.9 & 0-6.4, 8.1-10.9, 14-14.4, 17.4-36	North Atlantic influence?
47	Rasbury & Aharon	2006	Avaiki	Niue	19°00'S	169°55'W	2-4	~26	0-0.18, 0-0.26, 0-0.13, 0-0.12	ENSO-controlled layer thickness’

caves of the Nullarbor and found them to be beyond the range of U-Th dating by alpha spectrometric techniques. It has recently been shown that little if any speleothem development has occurred since ~500 kyr B.P., and that some stalagmites were forming ~4.0-3.7 million years ago (Woodhead *et al*., 2006).

2.3.3.3 Late Pleistocene

Two studies from caves in the vicinity of Naracoorte, South Australia (# 17 and 18 in Table 2.1), present palaeoclimate information for parts of the past ~500 kyr. Ayliffe *et al*. (1998) identified four main periods of speleothem development during this time (420-340 kyr B.P., 300-270 kyr B.P., 220-155 kyr B.P. and 115-20 kyr B.P.), each interpreted as cooler and wetter than today. Noticeably several glacial maxima are absent and they are inferred to have been arid, as it is unlikely that the area would have been affected by frozen ground/permafrost. Desmarchelier *et al*. (2000) presented $\delta^{13}C$ and $\delta^{18}O$ records for a speleothem that formed between 185 and 157 kyr B.P. Speleothem growth appears to have begun at the inception of MIS 6 and ceased shortly after the onset of full glacial conditions. There was significant correlation between $\delta^{13}C$ and $\delta^{18}O$ ($r^2 = 0.6$) which indicated that there was an increase in precipitation and vegetation density above the site during at least the period 178-162 kyr B.P. This supports the inferences of Ayliffe *et al*. (1998) that both interglacial and glacial climates in South Australia were arid while wetter climates, suited to speleothem development, were confined to the periods in between.

There is an abundance of speleothem-based palaeoclimate records from Tasmania (Figure 2.7). Zhao *et al*. (2001) presented a record of growth rate over time for a speleothem from Newdegate Cave (#19 in Table 2.1) that formed 155-100 kyr B.P. It began to grow at the onset of full glacial conditions in MIS6 and ceased during MIS 5, encompassing the previous interglacial and penultimate deglacial (Termination II). The period of most rapid growth was ~129-122 kyr B.P., coincident with peak interglacial conditions. Goede *et al*. (1986) provide stable isotope records for a stalagmite from Little Trimmer Cave in northern Tasmania (#10 in Table 2.1) which formed between 109 and 76 kyr B.P. The earliest 9 kyr were omitted from their discussion as that material was found to have formed out of isotopic equilibrium. The remainder of the record was

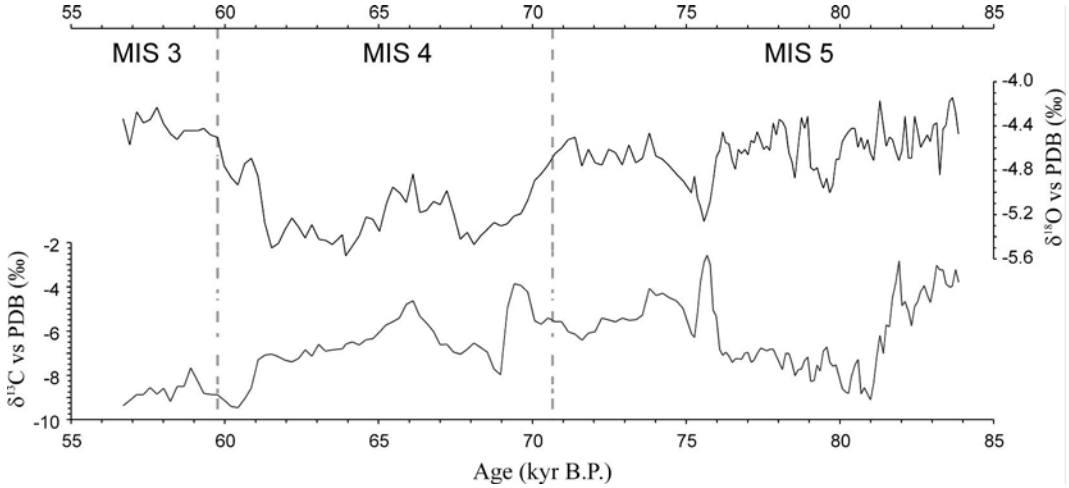

Figure 2.8: Stable isotope records from a speleothem from Frankcombe Cave, Tasmania (Goede *et al*., 1998). These data represent the longest continuous speleothem-based palaeoclimate record for the last glacial period from Australia. Note, that the $\delta^{18}O$ curve is not corrected for the ice volume effect.

---

interpreted as though more negative values were deposited at colder temperatures. Despite this, there was a general trend in $\delta^{18}O$ toward less negative values from 100 to 76 kyr B.P., which coincided approximately with the transition into the last glacial period.

A succession of papers have been published on a stalagmite from Frankcombe Cave in central Tasmania (#11, 14 and 16 in Table 2.1) which, it was eventually determined, formed between 84 and 56.5 kyr B.P. (Figure 2.8; Goede *et al*., 1990b, 1998; Goede, 1994). In addition to $\delta^{18}O$ and $\delta^{13}C$ variability, Mg, Sr (Goede, 1994) and strontium isotope ($^{87}Sr/^{86}Sr$; Goede *et al*., 1998) data are also presented. The oxygen isotope data appear to show a cooling into MIS 4, and eventual warming at the MIS 3/4 boundary, at which point growth ceased. There is little correlation with $\delta^{18}O$ of ice at Vostok suggesting a weak link to at least climate recorded at central Antarctic sites. A better match may be found in the isotopic records from Greenland ice cores although such a comparison was not attempted by the authors. Mg variations show a significant relationship to $\delta^{13}C$ ($r = 0.644$) and there is an almost equally strong correlation between Sr and $\delta^{18}O$ (Goede, 1994).

2.3.3.4 Termination I (Deglaciation)

Three partial records of Termination I from Australian have been published. They are from Lynds Cave, Tasmania (15.0-11.7 kyr B.P.; Goede and Vogel, 1991), Royal Cave, Victoria (13.4-10.6 kyr B.P.; Goede *et al*., 1996), and Chillagoe, Queensland (15.8–8 kyr B.P.; Turney *et al*., 2006) (Figure 2.7; #13, 15 and 23 respectively in Table 2.1). The Lynds Cave speleothem failed the Hendy Test and also had a highly significant positive correlation between $\delta^{18}O$ and $\delta^{13}C$. However trace element concentrations are not affected by isotope fractionation processes and as a result can still yield reliable palaeoclimate data. The authors conducted a coarse resolution analysis of the abundance of twelve elements. No attempt was made to interpret these results other than to comment that, in future, studies trace element compositions of speleothem calcite could be used to gain palaeoenvironmental information. Goede *et al*. (1996) presented evidence of Younger Dryas cooling in southeastern Australia from a speleothem that grew between 13.4 and 10.6 kyr B.P. A deviation towards less negative $\delta^{18}O$ values between 12.3 and 11.4 kyr B.P. was interpreted as evidence for a cool climate, and coincided with the Younger Dryas chronozone in North Atlantic palaeoclimate records.

Further to the north, bordering the tropics, are Chillagoe Caves (#23) from which a third speleothem record of Australian deglacial climate exists (Turney *et al*., 2006). Both $\delta^{13}C$ and $\delta^{18}O$ data were presented for the period ~15.8 – 8 kyr B.P. The data was interpreted as showing 'mild' climate between 15.4 and 14 kyr B.P. and a relatively dry phase from 14-10 kyr B.P. (interpreted from more enriched $\delta^{18}O$). There was no clear indication of either YD or ACR being the dominant influence on climate, but rather there being a broadscale climate event similar to that observed in several New Zealand records.

2.3.3.5 The Holocene

Within the current literature there are no Australian speleothem records that cover the entire Holocene. Furthermore, when all of the available data are combined, there were still gaps in the latter part of the Holocene. Xia *et al*. (2001) presented an early Holocene (9.2-5.1 kyr B.P.) record from Tasmania (#20 in Table 2.1) that showed much climate variability. Seven episodes were recognised

with greatest warmth interpreted as occurring between 8 and 7.4 kyr B.P. and highest precipitation between 7.4 and 7 kyr B.P.

Goede *et al*. (1990b) presented a radiocarbon-dated isotope record that covered approximately the mid- to late-Holocene. For almost the entire length of the record cooler than present climates were inferred. In addition there was a short (10 sample) speleothem isotope record from southeastern Victoria, Australia, covering the period 3.2 to 2.1 ka (Goede *et al*., 1996). The authors suggested that this period had been one in which climate was perhaps cooler than at present.

2.3.3.6 Contemporary

Two rapidly growing Australian speleothems have been used to look at contemporary climate variability at annual to sub-annual scales. The first is a 33 mm tall stalagmite that grew on a boardwalk in a former tourist cave in Western Australia from 1911 to 1992 (Treble *et al*., 2003). High-resolution analysis of trace element concentrations within the speleothem revealed that Ba in particular, but also Sr, Mg, P, Na and U, highlighted the annual banding of the speleothem. It was also noted that concentrations of P, U and Mg responded to the observed 20% decrease in local mean annual rainfall since 1965. In a subsequent study, stable isotope data for the same stalagmite were presented (Treble *et al*., 2005). Seasonal shifts in speleothem $\delta^{18}O$ mirrored the difference between the $\delta^{18}O$ of winter and summer precipitation, however the authors could not relate shifts in isotopic values to events observed in the meteorological records from the region. The second speleothem is a soda-straw stalactite from southeastern Australia that grew between 1766 and 1996 A.D. (Desmarchelier *et al*., 2006). Ratios of Ba, Sr, Mg and U to Ca revealed high-frequency (potentially annual) oscillations superimposed on longer-term trends. No inferences on climate change during the period of record were attempted from these data.

2.3.3.7 Summary

There are a significant number of Australian speleothem records in the literature. The datasets provide climate information discontinuously from the present day back several million years across a broad range of resolutions. The

poor temporal coverage of the Holocene and the last glacial period are significant for this study as few reliable trans-Tasman comparisons will be able to be made.

Of further significance to this study, it appears that $\delta^{18}O$ values in speleothems from Tasmania, and perhaps also from parts of the southern mainland of Australia, were dominated by precipitation, such that less negative values occurred during cool phases in Earth history. A similar pattern has been observed at several locations in New Zealand.

2.3.4 Southern Africa

2.3.4.1 Introduction

Tyson *et al*. (1997) established that a teleconnection between South Africa and the West Coast of New Zealand operated during at least the 20th century. It is therefore important in this study to consider speleothem and other proxy records from southern Africa. A review of research presenting data from southern African speleothems is presented in the following sections.

The potential applications of speleothems to South African research was first realized by Talma *et al*. (1974) who followed the early work on speleothems by Hendy and Wilson (1968) and several European researchers (Galimov and Grinenko, 1965; Duplessy *et al*., 1970; Fantidis and Ehhalt, 1970). However, strong interest in the topic never took hold and speleothem-related publications were few and far between until the mid-1990s. Furthermore, rather than look at isotopic variability in speleothem calcite, many early studies were focused upon dating previously active speleothem formation in dry, desert caves. Post-1995, and the input of European interest and expertise, there has been a raft of studies employing a broad range of proxies to reconstruct past environments.

The distribution of sites of speleothem-based research is largely confined to South Africa and Botswana (Figure 2.9). This is a consequence of both a lack of karst regions on the continent as a whole and limited exploration (Middleton and Waltham, 1992).

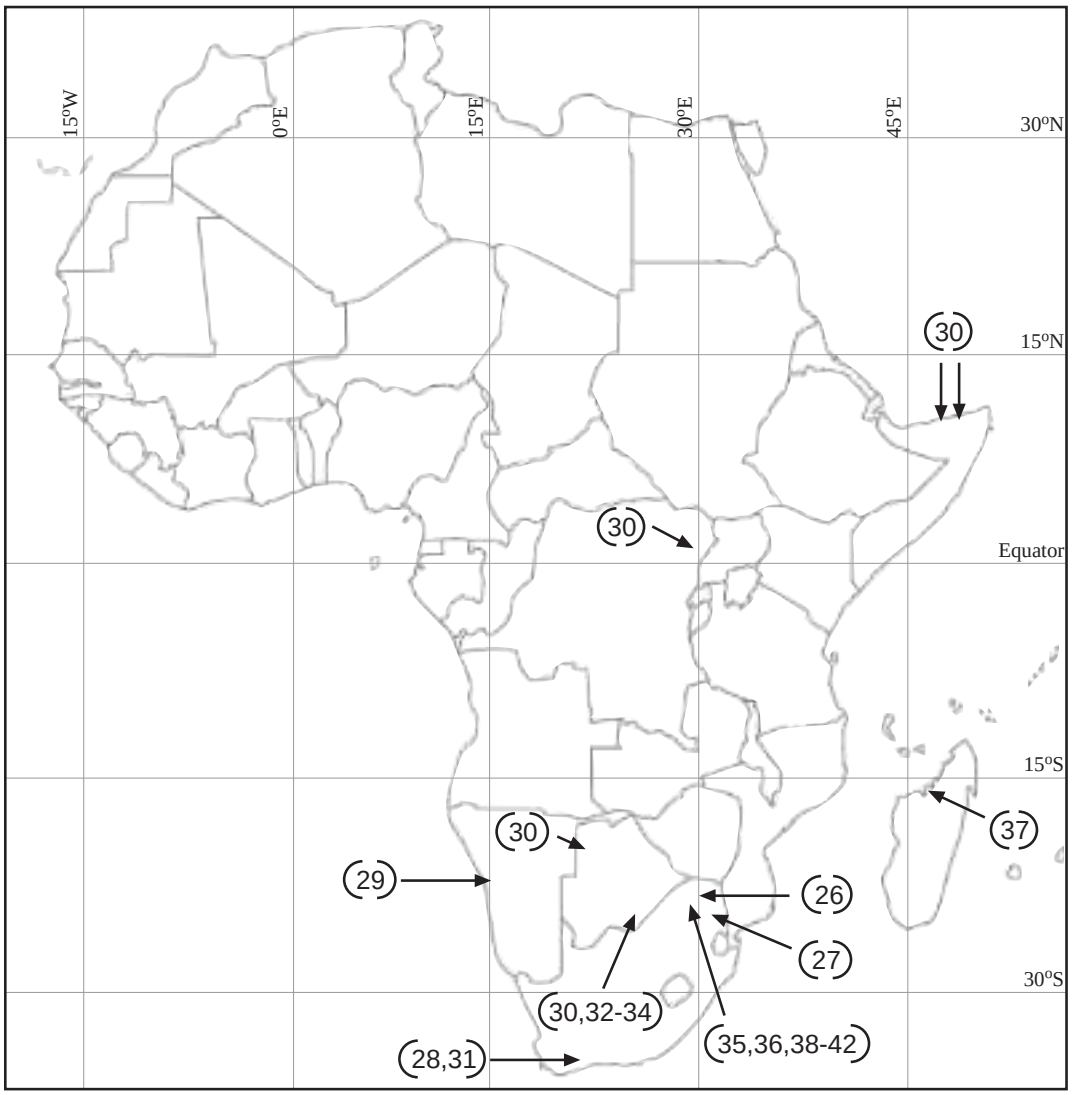

Figure 2.9: Locations of caves in southern Africa for which records of past climate change have been developed. The numbers within the figure are linked to references and supplementary information provided in Table 2.1.

2.3.4.2 Late Pleistocene

Caves of the Namib, Kalahari and Somali deserts contain speleothems of which none are presently active. Similar to arid karst regions in Australia and Brazil, most speleothems sampled for dating turn out to be greater than 100 kyr old (Heine and Geyh, 1984; Brook *et al*., 1990). These formations point to times in the past when rainfall was more plentiful. Through collection of dates on the initiation and termination of speleothem formation in many caves located across a wide area, broad-brush conclusions are drawn on wet and dry phases in the region's climate history (Brook, 1982).

2.3.4.3 Last Glacial Period

Early studies of southern African speleothems that formed during the last glacial period provided intriguing information on climate changes but were hamstrung by use of the radiocarbon dating method to gain a chronology (Talma *et al*., 1974; Brook, 1982; Talma and Vogel, 1992). Vogel (1983) attempted to determine the 'reservoir effect' inherent in all speleothem radiocarbon dates from a stalagmite from Cango Caves (#28 and 31 in Table 2.1), but later studies on the same stalagmite (Talma and Vogel, 1992; Vogel and Kronfeld, 1997) demonstrated that the magnitude of the reservoir effect could not be relied upon to remain constant. The same conclusion was reached by Holmgren *et al*. (1994) on a stalagmite from Lobatse II Cave, Botswana (#32 in Table 2.1).

Despite the uncertainty in the chronology it can still be determined that during the period 50-10 kyr B.P. there were marked climate changes across southern Africa. In general, cool and wet conditions were inferred, based on both the growth frequency of formations and stable isotope measurements (Brook *et al*., 1990; Talma and Vogel, 1992). These preliminary interpretations are supported by more recent work which benefited from uranium-thorium-based chronologies (Holmgren *et al*., 1995; Holmgren and Shaw, 1999; Holmgren *et al*., 2003). Holmgren *et al*. (1994/1995) presented stable isotope data for a speleothem from Lobatse II Cave which formed between 51 and 21 kyr B.P. with a hiatus from 43-27 kyr B.P. The periods of growth have been interpreted as periods when climate was wetter-than-present and the hiatus as a lengthy return to drier

conditions. The oxygen isotope data show some millennial-scale variability and also support the findings of Talma and Vogel (1992) that in southern Africa temperature was the dominant control on speleothem $\delta^{18}O$.

Holmgren *et al*. (2003) presented stable isotope data for two stalagmites from Cold Air Cave (#42 in Table 2.1), South Africa (Figure 2.9). One of the stalagmites (T7) was entirely Holocene in age and will be reviewed in section 2.3.4.4. A section of the second stalagmite formed between 24.4 and 12.7 kyr B.P., although the chronology suffers from several age reversals. A sampling resolution of 50 years for isotopic analysis was obtained and the resulting $\delta^{18}O$ record displays a relatively constant trend punctuated by several sub-millennial-scale fluctuations (Figure 2.10). Dry and cool conditions were inferred for the periods ~23-21, 19.5-17.5 and 15-13.5 kyr B.P. A favourable comparison has been drawn between these events and the Taylor Dome (Antarctica) oxygen isotope record where these two overlap. The authors argued that this may indicate Antarctic control of Southern Hemisphere climate to at least as far north as southern Africa during the last glacial period.

2.3.4.4 Holocene

Talma and Vogel (1992) presented an isotopic record from 5-0 kyr B.P. with an average resolution of 50 years per sample for Cango Caves, South Africa (Figure 2.9). More-or-less constant temperatures were inferred for this period from the oxygen isotopes despite some variability which appeared to represent both the Medieval Warm Period and the Little Ice Age. From the $\delta^{13}C$ record it appeared as though climate was drier between 5 and 2 kyr B.P. and remains semi-arid to the present day.

Stalagmite T7 from Cold Air Cave, which formed between 6.5 kyr B.P. and the present day, is the subject of several studies (Holmgren *et al*., 1999; Repinski *et al*., 1999; Piketh *et al*., 1999; Lee-Thorp *et al*., 2001; Finch *et al*., 2001; Holmgren *et al*., 2003). The width of annual growth bands, $\delta^{18}O$, $\delta^{13}C$, grey level and trace elements were measured and used as climate proxies. Lee-Thorp *et al*. (2001) noted that the LIA was present in the T7 record and was manifest as a long-lasting low-rainfall anomaly accompanied by cooling. The $\delta^{13}C$ record showed a steady increase from 6.5 to ~2 kyr B.P. which was completely

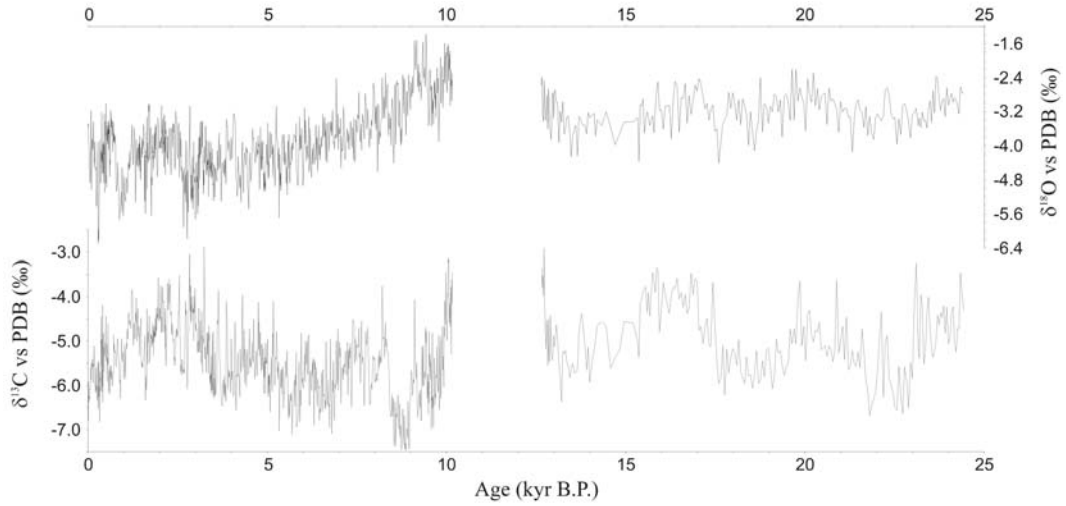

Figure 2.10: High-resolution stable isotope records from a stalagmite from Cold Air Cave, South Africa (Holmgren *et al*., 2003). No material was deposited between 12.7 and 10.4 kyr B.P.

---

independent of changes in $\delta^{18}O$, a result that closely corresponded to the findings of Talma and Vogel (1992) where the two datasets overlapped.

The only complete Holocene speleothem record for South Africa is that of stalagmite T8 from Cold Air Cave (Figure 2.10; Holmgren *et al*., 2003). The high-resolution isotopes are supported by a robust chronology, unlike the older section of this stalagmite. There was a well-defined early Holocene climate optimum in the oxygen isotope data between 10.4 and 9 kyr B.P. Furthermore, where the T8 isotope record overlaps that of T7 there is excellent agreement with only minor discrepancies. This provides greater confidence in the climate interpretations for this period made by Lee-Thorp *et al*. (2001).

Repinski *et al*. (1999) provided a short stable isotope record also from Cold Air Cave. Their stalagmite formed between 4.4-4.0 and ~0.8-0.5 kyr B.P. Despite the relatively poor dating, the authors speculated that the LIA was captured in their record as a trend toward less negative $\delta^{18}O$.

2.3.4.5 Contemporary

Brook *et al*. (1999) measured layer thickness in two stalagmites from Anjohibe Cave, Madagascar (Figure 2.9; #37 in Table 2.1). Layer counting and

several U-Th dates produced a record extending back to ~1550 A.D. which was then compared to historical indices of El Niño Southern Oscillation (ENSO). For the period 1951-1992 there appeared to be a significant correlation between layer thickness and observed ENSO variability. Furthermore, there was also reasonable correlation of the Anjohibe record with other ENSO proxy records back to ~1550 AD.

Trace element profiles of the most recently deposited calcite of Cold Air Cave stalagmites T7 and T8 were compared to observed climate records for the period 1955-1996 (Finch *et al*., 2003). General trends in strontium and barium concentrations over the recorded period were similar in both stalagmites. A comparison made with local temperature and rainfall records showed a reasonable correlation between high rainfall years and low Sr and Ba concentrations.

2.3.4.6 Concluding Remarks

Of greatest significance to this study are the findings of Holmgren *et al*. (2003) who presented results from two Botswanan speleothems covering the LGCP to the present and interpreted them within the context of global climate (a)synchrony. Following Tyson *et al*. (1997), one might expect to see similarities between the climate reconstructions of Holmgren *et al*. (2003) and any created for the same period from the West Coast of South Island, New Zealand.

2.3.5 South America

The circumpolar westerly circulation that impacts upon climate in New Zealand also has a strong influence on the climate of southern South America. The timing of maximum glacier advance at the LGCP and subsequent retreat during deglaciation in the Chilean Andes closely matches what is known of glaciers in the Southern Alps of New Zealand. This implied climate teleconnection makes it important to consider palaeoclimate records from South America as part of this research.

With the exception of several extensive karst regions in Brazil and Venezuela, South America appears to be poorly endowed in caves (Middleton and

Waltham, 1992). Within the literature there are four prominent studies on speleothems from South America (all from Brazil). These are summarised here and in Table 2.1.

Wang *et al*. (2004) visited caves within an arid region of northeastern Brazil (Figure 2.11). Although no speleothem formation is occurring at present there were many relict travertine and other speleothem deposits. These formations attest to periods in the past when climate was wetter-than-present. The authors suggested that the causes of these periods of increased precipitation were southward-shifts in the position of the Intertropical Convergence Zone (ITCZ). Furthermore, each southerly shift of the ITCZ appeared to correlate with cooling of the North Atlantic associated with Heinrich events. This relationship extended throughout the last 210 kyr.

Cruz Jr. *et al*. (2005) obtained a high-resolution (150 yr/sample) oxygen isotope record from a speleothem which formed in Caverna Botuverá (Figure 2.11; #45 in Table 2.1) from 116.2 kyr B.P. to the present day. Long-term changes are driven by insolation, highlighted by a strong influence at a precessional frequency. Superimposed on this general trend is millennial-scale variability which appeared to be influenced by D-O events. The large variability in $\delta^{18}O$ over the record (~5 ‰) indicated that insolation changes and D-O events were primarily impacting on precipitation.

A second isotope record was developed from the Caverna Botuverá by Wang *et al*. (2006) which covered the period 36-0 kyr B.P. They found that precipitation was the major driver of $\delta^{18}O$. This high-resolution (40 yr/sample) record also revealed noticeable millennial-scale variability with many events corresponding to those observed in Greenland ice cores. In addition there was close correspondence with the Asian monsoon records of Hulu and Dongge Caves (China). Interestingly, however, $\delta^{18}O$ signals in China and Brazil were of opposite polarity, indicating an anti-phasing of monsoonal climates at lower latitudes.

Bertaux *et al*. (2002) developed a 3.8 kyr palaeoclimate record from an aragonite stalagmite based on petrography of (potentially annual) layer couplets. This brief record indicated an increase in rainfall from 3.8 to 2.5 kyr B.P. which was maintained to the present day.

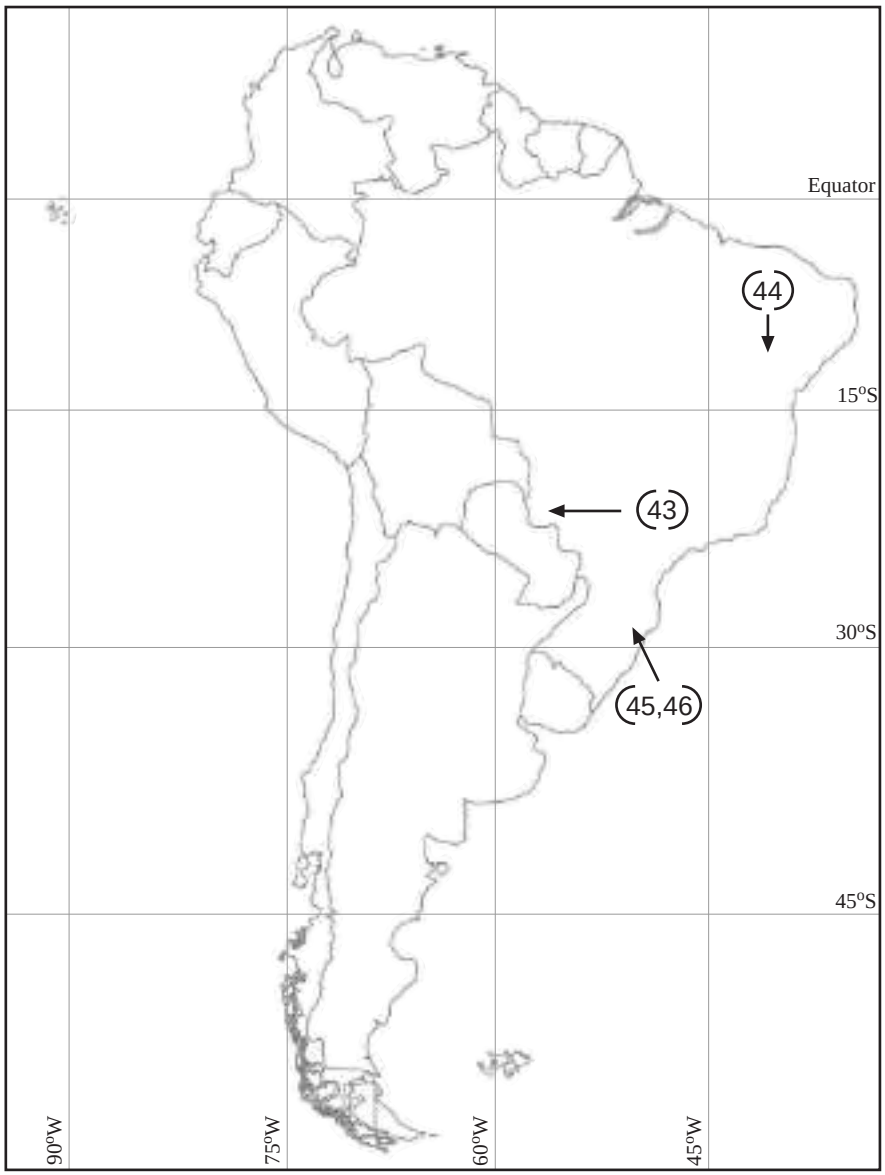

Figure 2.11: Locations of caves in South America for which records of past climate change have been developed. The numbers within the figure are linked to references and supplementary information in Table 2.1.

The potential for palaeoclimate reconstruction from speleothems has only recently been applied to South American localities. There appears to be much potential here to develop records that detail climate variability from the tropics to the sub-Antarctic. Perhaps the most interesting feature of the existing records is the impact of North Atlantic climate variability on Brazilian climate. This could suggest global synchrony of climate events. Further high-resolution studies of the last glacial period are required from the Southern Hemisphere to investigate this possibility.

2.3.6 Islands of the South Pacific

Given that many Pacific islands are composed, at least in part, of coralline limestone and receive significant ENSO-controlled rainfall there would appear to be much potential for cave development and the subsequent formation of speleothems. Furthermore, given that sea level has fluctuated by ~130 m several times over the last ~700 kyr there is also opportunity for the existence of submarine caves and speleothems which could yield information regarding the timing of relative sea level changes. However, despite this, there is only one published speleothem-based palaeoclimate record from a Pacific Island.

Rasbury and Aharon (2006) describe growth rates in four coeval, actively growing, contemporary stalagmites from Avaiki Cave on the island of Niue (19°00'S, 169°55'W) and noted a close correspondence between layer thickness and rainfall amount. Furthermore, spectral analyses of instrumental climate records and speleothem couplet thickness showed that couplet thickness was a function of ENSO variability. This record of ENSO variability covered approximately the last two centuries (Rasbury and Aharon, 2006).

Other stalagmites have been collected from Niue, specifically Matoga, Kaitanetane and Anataloa caves (C. Hendy, pers. comm. 2007). Preliminary analyses suggest that the detrital thorium in these speleothems is too great to allow meaningful U-Th dates to be obtained. Nevertheless, it may be possible to perform layer counting and use the radiocarbon spike from nuclear weapons testing to provide a tie-point for the chronology.

Caves are known on many other Pacific islands, including Fiji, Tonga and the Cook Islands (Middleton and Waltham, 1992). Furthermore the author is aware that speleothem collection has been undertaken in Papua New Guinea, Vanuatu and the Solomon Islands. The primary attraction for studying speleothems at these locations is to gain a better understanding of ENSO variability, particularly from periods prior to the instrumental era.

2.3.7 Summary

There is a long history of speleothem-based palaeoclimate research in the Southern Hemisphere, although contributions from South America have only been available for the last few years. The array of records covers periods ranging from the present day back to the limit of U-Th dating, all at a variety of resolutions from millennial to sub-annual in scale.

New Zealand has climate teleconnections between southern Australia and South Africa. Furthermore, as shown by Holmgren *et al*. (2003), there are possible climate linkages to Antarctica as well. Therefore it would be appropriate to compare records from these regions. There does not appear to be a mechanism for tying climate changes over Brazil to those of New Zealand. It is noteworthy that these speleothem records show a close correspondence to Northern Hemisphere (North Atlantic and Asia) climate variability and little influence from Antarctica.

Despite the wealth of information provided by speleothem records from the Southern Hemisphere there are still considerable temporal and spatial gaps. Furthermore, the majority of the available data are of relatively low resolution and supported by chronologies based on ^{14}C and alpha spectrometry U-Th dating. There is a clear need for new high-resolution, absolutely and precisely dated, long and continuous speleothem records from the Southern Hemisphere. For New Zealand there is sparse data covering the last glacial period, and during the LGCP and deglaciation there is disagreement at the millennial-scale between existing records.

3 Site Descriptions

3.1 West Coast, South Island

3.1.1 Introduction

The West Coast of South Island is composed of a relatively narrow strip of coastal lowland and a series of mountain ranges that make up the western side of the Southern Alps. In the south much of the lowland is covered with Late Pleistocene lateral moraines and outwash terraces. At the present day several valley glaciers descend from the mountains almost reaching the coastal lowland. During parts of the Otiran these and other glaciers expanded beyond the confines of the mountain valleys to form piedmont lobes which in many cases, all south of Hokitika, extended beyond the modern shoreline.

To the north, the main ranges of the Southern Alps are further inland and several smaller coastal ranges occur, including the Paparoa Range. It is not known if the ~1400 m high Paparoa Range supported glaciers at the LGCP although the peaks would have been close to the estimated regional snowline for this time (Shulmeister *et al*., 2005).

The climate of the West Coast of South Island is dominated by marine influences and light winds, with high rainfall and few extremes of temperature. Tasman Sea surface temperatures effectively moderate temperatures on land. As a result, mean monthly temperatures are relatively mild and vary little throughout the year. Further inland, in the Reefton and Springs Junction areas (Figure 3.1), the marine influence is diminished and a more continental climate is experienced where summers can be hot and winters cool and frosty. During the LGCP mean annual temperatures in New Zealand were estimated to be about 5 °C lower than at present (McGlone *et al*., 1993), although Drost *et al*. (2007) suggested temperatures in southern Westland could have been as much as 8-10 °C lower. This contrasts with estimated sea surface temperature decrease in the eastern Tasman Sea of 0-5 °C, relative to present day conditions, at the LGCP (Nelson *et al*., 1994; Barrows *et al*., 2007).

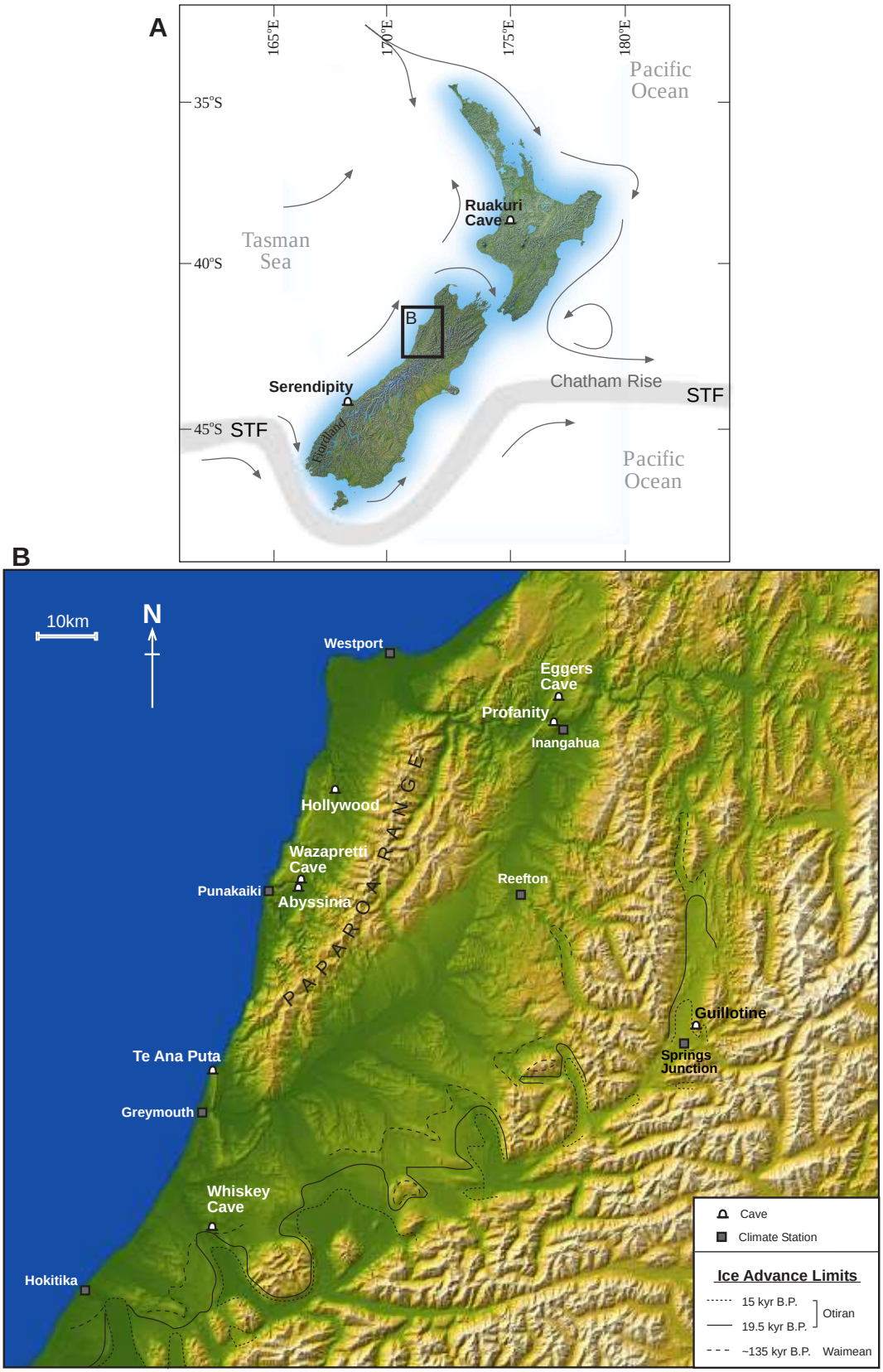

Figure 3.1: Location map of caves visited and considered for this study. In A the position of the subtropical front (grey shading) is highlighted along with a general map of local ocean currents (Nelson et al., 2000; Carter and Manighetti, 2006). In B locations where climate variables are recorded and included in this study are shown as are limits of late Quaternary ice advances [modified from Nathan et al. (2002); Suggate and Almond (2005)].

The climate of South Island is particularly sensitive to latitudinal movement of the subtropical front (STF; Figure 3.1). The STF lies immediately to the south of New Zealand and separates a strong westerly flow associated with greater rainfall and colder temperatures from temperate systems originating across the Tasman Sea. It is likely that a northward migration of the STF would lead to cooler sea surface temperatures off the West Coast, decreased temperatures on land and the potential for increased mean annual precipitation.

In the modern climate, mean annual rainfall generally increases southwards from ~2200 mm at Westport (Figure 3.1; Table 3.1) to 6500 mm in Fiordland, and considerably more at higher elevations in the Southern Alps. Most of the rainfall is precipitated from cold fronts, extending northward from storm centres to the south of the country, when they encounter the Southern Alps which rise abruptly from the coast to several peaks in excess of 3000 m. Fewer cold fronts impact the West Coast in summer than in winter due to a southerly shift in the sub-Antarctic front at this time. When conditions conspire to create southerly or easterly winds a sunny and dry climate prevails on the West Coast (NIWA, 2003). Drost *et al*. (2007) estimated that the West Coast–Fiordland region experienced a reduction in mean annual precipitation of 150 mm (~2-8 % decrease) during the LGCP. Almond *et al*. (2007) went further and suggested that annual rainfall totals on the West Coast during the period 26-33 kyr B.P. were half of present day totals, and then increased throughout the period 26-22 kyr B.P.

Today much of the West Coast is covered by temperate rainforest dominated by hardwood and broadleaf species, although some areas have been cleared during the last century to provide land for agriculture and timber plantations. In south Westland much of the forest was replaced by grassland during the LGCP (Vandergoes *et al*., 2005). Less is understood of vegetation changes in north Westland, although available evidence also suggest that forest also gave way to grassland (Moar and Suggate, 1996).

A primary aim of this study is to develop a long (> 20 kyr), continuous speleothem record of climate change for New Zealand from caves that would have been close to the maximum limits of glacier advance during the Otiran. There are few

Table 3.1: Mean annual climate data from climate stations located close to caves visited in this study (NIWA, 2006). n_t is the number of years of data used to calculate mean temperature, and n_r is the number of years of data used to calculate mean rainfall. The * indicates that the calculation is based on a mean (temperature) or sum (rainfall) of the monthly means as opposed to the average/sum of daily values.

Station	Latitude °S	Longitude °E	Elevation (m)	Period of Record	n_t	Mean Temperature (°C)	n_r	Mean Rainfall (mm)
Ruakura	37.78	175.31	40	1906-2005	82	13.4	93	1177
				1976-2005	27	13.8	30	1151
Waitomo Caves	38.26	175.10	91	1971-2005	-	-	33	1853
Te Kuiti	38.33	175.15	61	1960-2005	31	13.5	-	-
				1976-2005	17	13.6	-	-
Westport Airport	41.74	171.58	3	1938-2005	56	12.3	-	-
				1944-2005	-	-	57	2185
				1976-2005	23	12.6	26	2217
Inangahua	41.86	171.95	61	1948-1992	-	-	35	2307
Station Creek, Maruia	42.06	172.25	380	1950-2003	-	-	47	1926
				1976-2003	-	-	26	1957
Punakaiki	42.11	171.33	4	1982-2004	13	13.8	20	2584
				1982-2004*	≥ 19	13.7	≥ 20	2591
Reefton	42.12	171.86	198	1960-2005	27	11.2	43	1975
				1960-2005*	≥ 35	11.2	≥ 43	1971
				1976-2005	14	11.1	28	1967
				1976-2005*	≥ 21	11.3	≥ 28	1971
Springs Junction	42.34	172.18	421	1948-1994	-	-	33	2282
				1976-1994	3	9.3	14	2450
				1976-1994*	≥ 11	9.6	≥ 16	2401
Greymouth Airport	42.46	171.19	4	1947-2005	47	12.2	58	2446
				1976-2005	22	12.2	30	2464
Hokitika Airport	42.72	170.99	39	1963-2005	41	11.7	42	2860
				1976-2005	30	11.7	30	2883

locations in New Zealand (none on North Island) where obtaining such a continuous speleothem record from glacial margins would be possible, despite the many large areas of karst terrain (Figures 2.5a and 2.5b) and the expansion of ice across the Southern Alps during the Otiran.

Three South Island karsts (near Jacksons Bay, Springs Junction and Kumara), proximal to the limits of maximum LGCP ice extent, were selected for this study as being likely to contain caves that could yield speleothem records that would be sensitive to changes in glacier margins during the Otiran. All three of these areas are located west of the main divide. However, a potential problem when aiming to obtain records of glacial climate from speleothems in caves proximal to glacier margins is the likelihood that they will not have had continuous accumulation. Sites overridden by ice or outwash gravels, or that develop permafrost at the surface, will cease to receive seepage water. In consequence, speleothem formation will stop creating a hiatus in the record. To increase the possibility of acquiring a speleothem that had experienced continuous deposition during the Otiran, caves within three other locally occurring karsts (the Paparoa Karst, and small limestone outcrops near Inangahua and Greymouth; Figure 3.1) were also selected for this study.

The six karst areas range from Jackson's Bay in the south to Inangahua in the north, from 0-700 m elevation, and from the coast to 80 km inland (Figure 3.1). All karst areas are located at elevations below present day snow and treelines (~2000 and ~1200 m respectively) and are actively developing. Furthermore, it is likely that the same is true during the LGCP when snowlines and treelines were 600-875 m lower (Hellstrom *et al*., 1998; Denton *et al*., 1999), with the possible exception of the caves and karst at Springs Junction which could have been exposed after the descent of the treeline.

From the six karsts, nine caves were selected for consideration in this study. In the following sections I provide further details pertaining to the geology, climate, hydrology and vegetation surrounding each cave.

3.1.2 Abyssinia Cave

Abyssinia (Figure 3.1, Table 3.2) is located just south of Bullock Creek, ~6 km inland of Punakaiki. The cave is formed in Oligocene age (Duntroonian-Waitakian) Potikohua Limestone, which is a hard, white, flaggy, bryozoan biosparite with an average $CaCO_3$ content of ~90% (Anderson, 1984). The limestone extends over a wide area, including much of Paparoa National Park. Thickness varies greatly, and reaches a maximum of 130 m at Fox River (Anderson, 1984). It is locally stylobedded, most notably along the coast at the famous Punakaiki "pancake rocks" tourist attraction. The formation has extensive karst drainage and tens if not hundreds of caves, many of which are associated with the Bullock Creek polje. To date there is no published survey of Abyssinia cave. From an incomplete investigation of the cave during fieldwork it appears the cave is an extensive (>1 km) maze with passage development on multiple levels, and several large (> 20 m in both height and width) chambers. Significant speleothem development was found in only two locations despite many areas of active seepage. It is likely that the cave experiences periodic flooding associated with high-water at the polje, therefore minimizing the potential for speleothem development. Three stalagmites were cored as part of this research. Preliminary laboratory analyses on the cores revealed that the stalagmites were not suitable for testing the research aims. As a result none of the stalagmites were subsequently collected.

The vegetation above the cave is that of a tall-tree dominated temperate rainforest. There are no clear indications in the literature of what vegetation may have persisted in the area during the LGCP.

3.1.3 Eggers Cave

Six stalagmite cores were collected in Eggers Cave (Figure 3.1, Table 3.2), ~6 km north of Inangahua. The cave is formed in Oligocene-age Steel Bridge Limestone. This unit crops out on both sides of the Buller River and is known to contain several other caves, including Profanity and Damnation. Its composition varies through basal

Table 3.2: Caves for which access permits were sought for this study. Further details pertaining to each cave are provided in the text.

Cave Name	Latitude °S	Longitude °E	Elevation (masl)	Length (km)	Cave Temp. (°C)	Relative Humidity (%)	No. of cores collected	No. of stalagmites collected	Comments
Ruakuri	38° 16' 05"	175° 04' 43"	100	3.9	~12.5		0	4	
Abyssinia	42° 06'03"	171° 23'18"	~120	> 1	~9.1	~100	3	0	No survey
Eggers	41° 48'09"	171° 56'01"	~310	> 0.4	8.6-9.1	~100	6	1	No survey
Guillotine	42° 18'39"	172° 13'04"	~740	> 0.2	6.5-7.5	~100	6	1	Incomplete survey
Hollywood	41° 57'24"	171° 28'22"	~130	~4.3	10.3-10.8	~100	4	1	
Profanity	41° 50'24"	171° 55'17"	~70				0	0	Not visited
Serendipity	43° 58'20"	168° 36'15"	~60				0	0	No survey; access denied
Te Ana Puta	42° 23'01"	171° 13'09"	40	0.8	11.4-11.7	~100	6	0	
Wazapretti	42° 05'40"	171° 24'04"	~100	~0.1	9.1-9.7	~100	4	1	No survey
Whiskey	42° 35'30"	171° 11'03"	~60	~0.2			0	0	Not entered

algal grainstone to bioclastic grainstone (Nathan *et al*., 1986). This formation is a member of the Nile Group and corresponds to the Cobden and Potikohua limestones of the Greymouth and Paparoa areas of the West Coast.

There is no known published survey of Eggers Cave although our exploration showed it to be >400 m in length, composed of two main passageways (one of which contains a stream), and two entrances. Within the cave there is a slight east-to-west gradient with no significant pitches or climbs. The cave is heavily decorated at the entrance with mostly inactive stalagmites and stalactites which appear to be suffering erosion. Gypsum curls, a collection of moa bones and several metre-high hollow dirt cones, orange in colour (presumably is enriched in oxidized iron), were also observed in this area of the cave (Figure 3.2). Speleothem deposition further from the entrance is limited, potentially resulting from multiple breakdowns and periodic flooding. Six relatively short stalagmites were cored from the same dead-end chamber which was at least 10 m above the cave stream. Following laboratory analysis of the cores, one of the stalagmites, EG05-5, was subsequently collected.

Current air temperature in Eggers Cave is 8.6-9.1°C, and the humidity is 100%. The cool temperature of the cave in comparison to mean annual temperature at Westport airport (12.3°C) is likely due to the relative elevation and inland location of the cave site. However, the temperature does correspond well with other caves in the region (Abyssinia, 9.°C; Wazapretti, 9.5°C).

The cave is located on Conservation Estate, formerly forestry land. Logging and other forestry practices at the site ceased in the early 1990s. At present the vegetation above the cave is composed primarily of juvenile *Nothofagus* species.

3.1.4 Guillotine Cave

Guillotine Cave (Figure 3.1, Table 3.2), 4 km northeast of Springs Junction, is formed in a small outcrop of black marble from the Ordovician age Sluice Box Limestone (Nathan *et al*., 2002). The formation is a member of the Mount Arthur Group which is host to Nettlebed Cave and Exhaleair Cave from which speleothem-

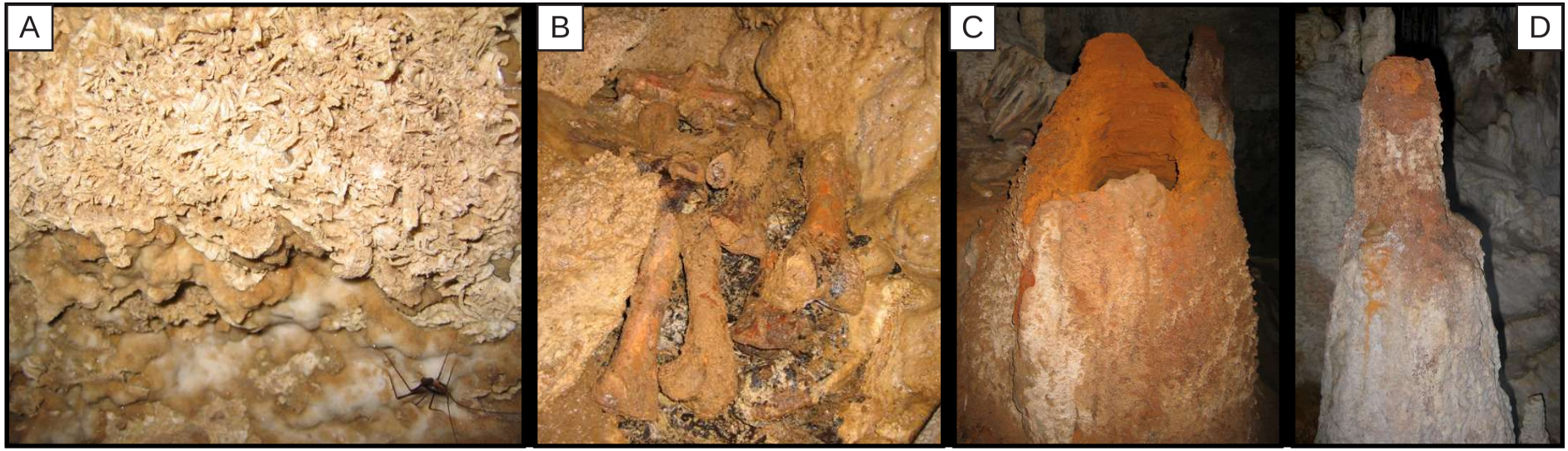

Figure 3.2: Gypsum curls (A), Moa bones (species unknown) (B), and hollow dirt cones (C and D), presumably rich in iron, found within the entrance to Eggers Cave.

based paleoclimate records extending back 31 kyr B.P. were developed by Hellstrom *et al*. (1998).

The cave is at least 200 m in length from entrance to stream sink, and over this distance a descent of ~80 m is made. The cave survey (Figure 3.3) shows the active stream passage, however there are abandoned passages above, two levels in some places, which are not shown. The cave is heavily decorated with speleothem formation, principally in the abandoned passages above stream level, with flowstones, straws, stalagmites, stalactites, shawls and cave coral. There are also banks of stratified sediments with occasional interbedded thin flowstone. The approximate locations of six stalagmites chosen for coring are shown in Figure 3.3. Several stalagmites were in upper passageways poorly depicted in the survey. On a second visit to the cave, one of these (GT05-5) was collected for further analysis.

Guillotine is located on the eastern flank of Maruia Valley. The valley is known to have hosted a glacier during the last and penultimate glacial periods (Suggate, 1965). It is not clear whether the cave would have been overridden by ice during these times. However it is likely that the area was not covered by forest, as it is today, given an estimated regional treeline lowering of 600-700 m at the LGCP (Hellstrom *et al*., 1998).

3.1.5 Hollywood Cave

Four stalagmite cores were collected in Hollywood Cave (Figure 3.1, Table 3.2), located approximately 25 km south of Westport. The cave occurs in Potikohua limestone which forms a large part of the karst in the region (Nathan *et al*., 2002) and is host to other caves visited in this study (Abyssinia and Wazapretti).

Hollywood has a surveyed length of approximately 4.3 km and is composed of a series of connected active streamways. Access to the speleothems within the cave is through a ~150 m long keyhole passage from the entrance which narrows as it approaches Streamway One (Figure 3.4). Streamway One is heavily decorated with stalagmites, stalactites and flowstones, most of which are actively accumulating. In

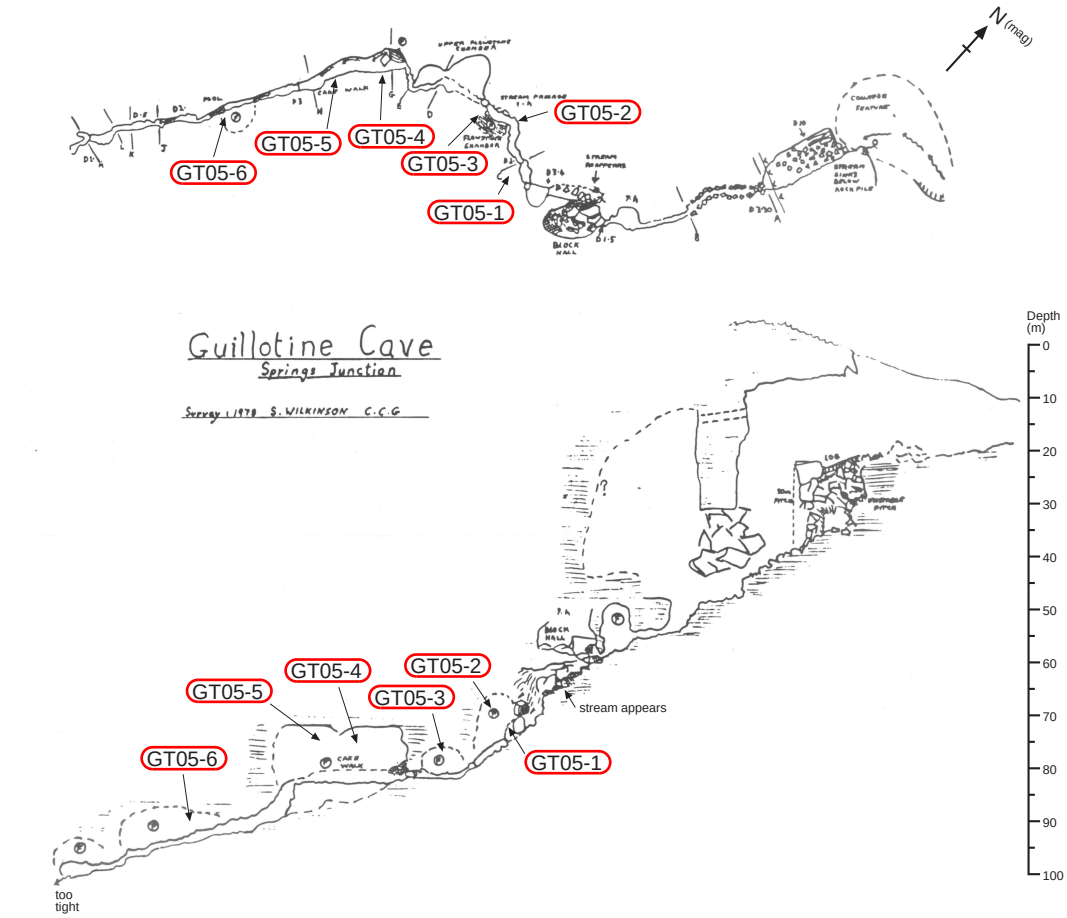

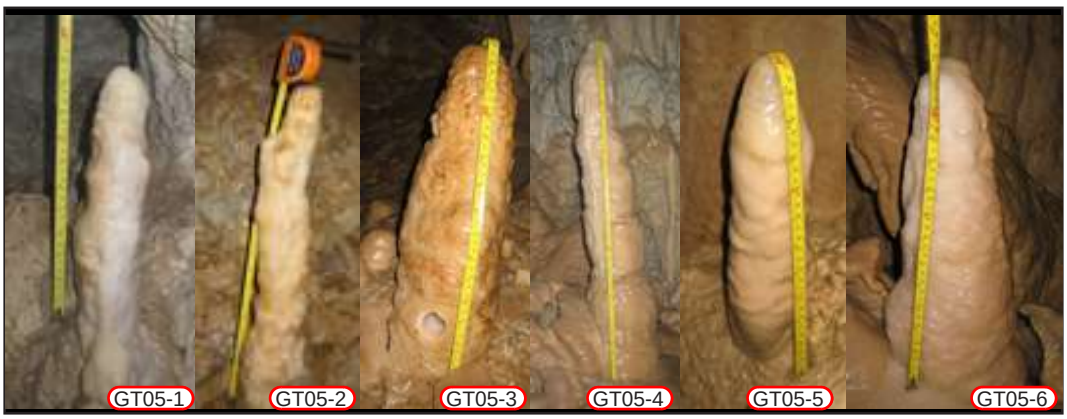

Figure 3.3: Survey of Guillotine Cave (modified from Smith, 2004). The approximate location of stalagmites cored in this study is shown on the survey. A photograph of each stalagmite is also shown.

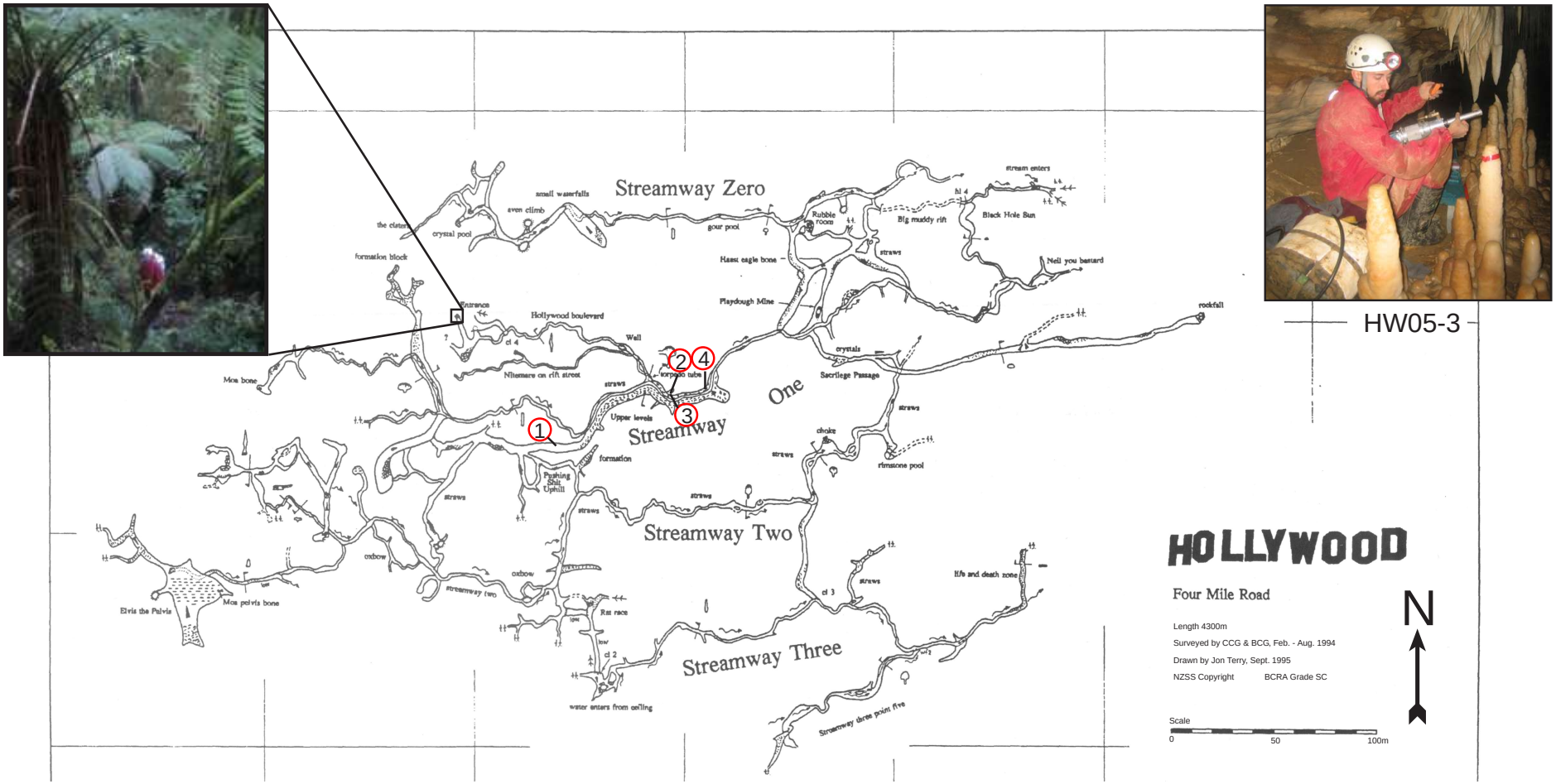

Figure 3.4: Survey of Hollywood Cave (modified from Smith, 2004). Coring sites are highlighted as numbers 1 to 4 where 1 represents HW05-1. Included are photographs of the vegetation within the entrance depression and stalagmite HW05-3 (red tape).

this part of the cave current air temperature is 10.3-10.8°C, and the humidity is 100%. No noticeable air movement was observed.

Today the vegetation above the cave entrance is primarily composed of juvenile *Nothofagus*, *Dacrydium cupressinum*, *Pinus radiata*, eucalyptus and tree ferns.

3.1.6 Te Ana Puta

Located at Point Elizabeth, ~8 km north of Greymouth (Figure 3.1, Table 3.2), is Te Ana Puta (Maori – Cave with Escape Holes). The cave is formed in the Tarapuhi Member of the Oligocene age Cobden Limestone. The limestone is a moderately cemented, fine-grained, predominantly massive, lime wackestone (Nathan, 1974). $CaCO_3$ content is generally between 70 and 75 %, the remainder being composed of mud and fine sand (Nathan, 1974; Christie *et al*., 2001). The beds dip 21° to the WSW (offshore). Solution paths within Te Ana Puta have formed along the dip and strike of the limestone creating two 'sea caves' as entrances. The cave has a total traversable length of 800 m and seven known entrances (Figure 3.5).

The vegetation directly above the cave entrance is composed of harakeke (New Zealand flax, *Phormium tenax*), ti kouka (cabbage tree, *Cordyline australis*) and gorse (*Ulex europaeus*).

Measured air temperature in the cave was 11.4-11.7°C with relative humidity ~100 %. In some chambers it was possible to feel a back-and-forth movement of air caused by waves crashing into the two sea caves. It is worth noting that during the LGCP when sea level was up to 140 m lower than today waves would not have been able to influence air movement within the cave. Furthermore, the 'sea cave' entrances may not have been formed until sea level reached its present position. It was therefore decided that there was still potential for isotope records unaffected by non-equilibrium fractionation to be obtained from Te Ana Puta. Consequently six stalagmite cores were obtained from formations in relatively sheltered locations. Preliminary laboratory analyses of the cores determined that none of the six stalagmites were appropriate for further study and as a result none were collected.

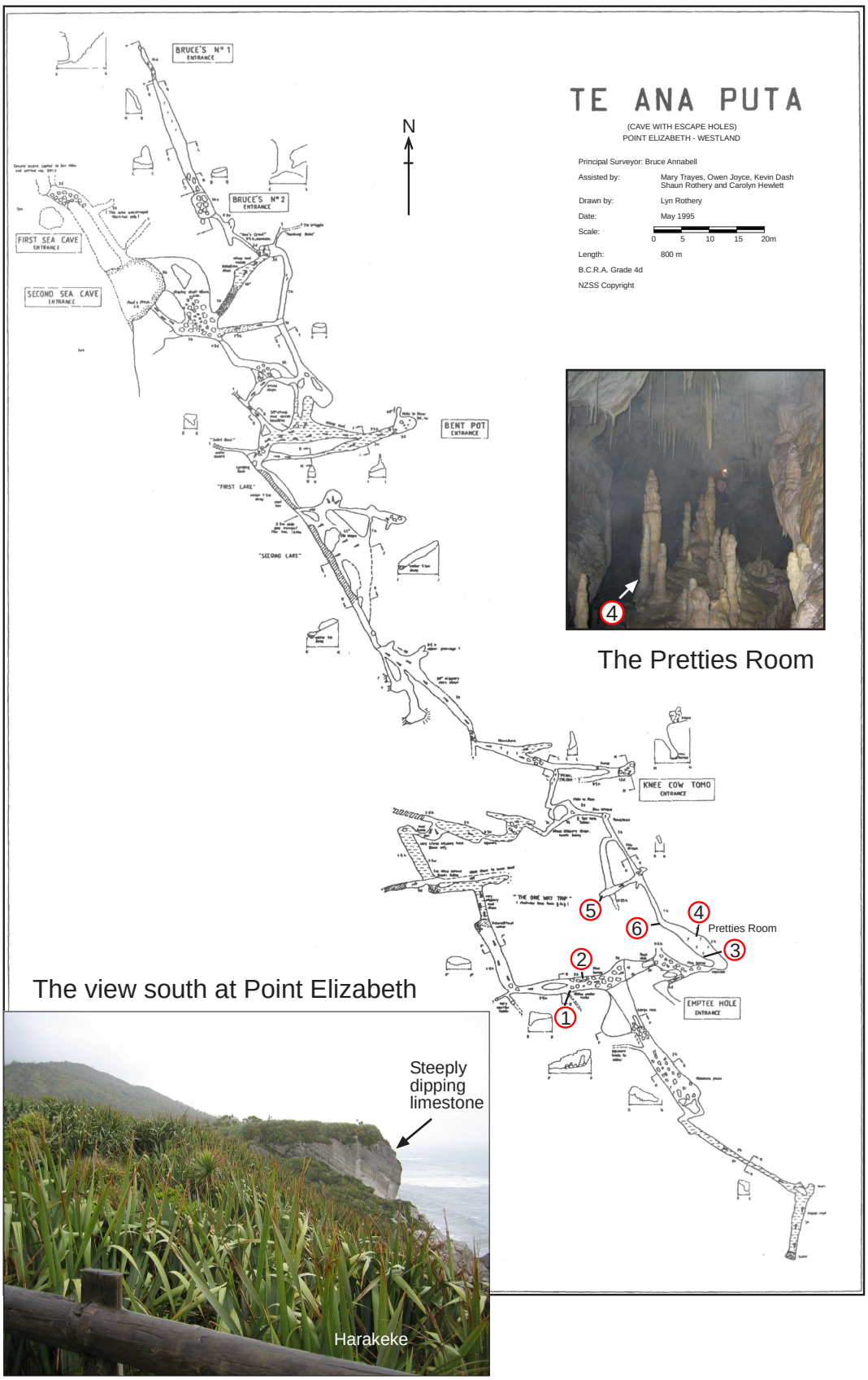

Figure 3.5: Survey of Te Ana Puta Cave (Smith, 2004) showing locations of stalagmites cored in this study. Coring sites are highlighted by numbers 1-6 where 1 represents TAP05-1. Inset photographs show speleothem development in the Pretties Room, and (looking south) the vegetation above the cave.

3.1.7 Wazapretti Cave

Four stalagmite cores were collected in Wazapretti Cave (Figure 3.1, Table 3.2). The cave is located within the Bullock Creek polje in Paparoa National Park and is hosted by the Potikohua Limestone. At the time of sampling the polje was in flood. Although no water was flowing through the cave it is clear from sediment deposits in the entrance that it does flood (or at least part of it does) on occasion. Directly above the cave entrance is a steep bank with a short limestone cliff at its summit. The vegetation on the bank is composed primarily of mixed podocarp forest and tree ferns.

There is no known published survey of Wazapretti cave. However, it is a relatively short cave (possibly ~100 m) composed of 3 large chambers behind a letter-box entrance located approximately 2-3 m above the creek bed. Each of the three chambers contain formations, but, as the cave name suggests, few are active and most are mud-coated. Cored stalagmites WZ05-1 and -2 are located in the third chamber from the entrance, and stalagmites WZ05-3 and -4 are in the middle chamber. WZ05-1 was subsequently collected as part of this study.

3.1.8 Other Caves Considered in This Study

Three other caves were also considered for sampling as part of the research, but access to each was never gained. Whiskey Cave is located in Fireball Creek, several kilometres north of Kumara on the West Coast (Figure 3.1). It lies several hundred metres outside a suite of terminal moraines dating from the LGCP (Figure 3.1). The cave is formed in a small outcrop of Cobden Limestone which at this location is thin-bedded, slightly glauconitic and crystalline (Nathan, 1974; Suggate and Waight 1999). The cave entrance, and potentially the entire cave, is liable to flooding. Several visits to the cave were thwarted by high water.

Profanity Cave, located on the southern bank of the Buller River several kilometres to the west of Inangahua (Figure 3.1), was also considered for this study. As mentioned in a previous section, Profanity is formed in Oligocene age Steel Bridge Limestone. As with Whiskey Cave, Profanity is particularly liable to flooding. Following two visits to the cave on sunny days and encountering the

cave in flood it was decided to stay safe and abandon research objectives at this site.

Serendipity Cave (Figure 3.1) is formed in a small outcrop of Oligocene age Awarua Limestone at Jackson Bay, south Westland (Mutch and McKellar, 1964; Turnbull, 2000). A previous attempt to locate the cave and collect speleothem samples was made by C. Hendy (pers. comm.) in the late 1960s without success. A second attempt was to be made as part of this study but access was denied on cultural grounds as the cave is considered a treasured site (Waahi Taonga) by local Maori.

3.2 Waitomo, North Island

3.2.1 Introduction

Arguably the most well known karst in New Zealand is that surrounding Waitomo (King Country Karst; Figure 2.5a). The region boasts hundreds of caves, many with abundant calcite and gypsum speleothem formations. For these reasons and the occurrence of glowworms (*Arachnocampa luminosa*) within the caves, tours have been operating in the region for over a century. Today more than 300,000 people visit the three main show caves (Waitomo Glowworm Cave, Aranui Cave and Ruakuri Cave) each year.

The karst has developed in limestone members of the late Eocene to early Miocene age Te Kuiti Group (Nelson, 1978). Most of the caves are formed in the Oligocene-age Orahiri Limestone and the Otorohanga Limestone of earliest Miocene age. Both formations are pure, crystalline calcarenites, generally with > 90% calcium carbonate and a few percent magnesium carbonate (Williams, 2004). The stable isotopic composition of Oligocene limestones at Waitomo varies from about -2.88‰ $\delta^{18}O$ and -1.72‰ $\delta^{13}C$ in the upper part of the sequence (Otorohanga Limestone) to -2.24‰ $\delta^{18}O$ and -0.98‰ $\delta^{13}C$ in the lower part (Orahiri Limestone) (Williams *et al*., 1999). For a thorough description of the regional karst the reader is directed to Williams (2004).

Waitomo is located about 35 km inland from the west coast of the North Island and experiences a temperate, oceanic climate. In winter, southwesterly weather dominates while in summer the region is influenced more by milder, relatively dry air of subtropical character. As a result there is a seasonal bias to the rainfall with the majority falling in the winter months. A recent model of climate conditions in western North Island during the LGCP suggests that temperatures in the region were 3°C lower than at present and that mean annual precipitation was reduced by 12.5 % (Drost *et al*., 2007).

Previous studies have used speleothems from the Waitomo area to infer past climate changes. Continuous isotopic records supported by a reliable chronology extend back to the onset of the Holocene (Williams *et al*., 2004). Two longer records based on radiocarbon dates and wiggle matching display relatively minor glacial-interglacial $\delta^{18}O$ variability (Hendy and Wilson, 1968), which could be

entirely due to changing isotopic composition of the oceans as a result of the ice volume effect.

3.2.2 Ruakuri Cave

Archaeological evidence at Ruakuri Cave (Figure 31; Table 3.2), Waitomo, suggests that it was well known to local Maori for at least the last 400 years. Translated from Maori, Ruakuri means 'den of dogs', referring to a pack of wild dogs that inhabited the cave entrance.

James Holden rediscovered the cave and opened it to tourists in 1904. The cave was the longest and most complex of the three tourist caves at Waitomo and remained a popular attraction until February 1988 when a legal and financial dispute forced its closure. In 1991 the area surrounding the cave entrance was declared Waahi Tapu (a sacred site) to protect a Maori burial site above the cave entrance.

During the closure, black-water rafting trips, following the underground Huhunui River, were still able to operate in the cave as the route taken did not include the previously used entrance. Today ~35,000 people make their way through Ruakuri on black water rafting trips.

In 2003 Tourism Holdings Ltd., operators of the Glowworm Cave and Aranui Cave tourist attractions at Waitomo, purchased a 30-year license to re-open Ruakuri Cave for guided walking tours. As part of this venture a new entrance to the cave was excavated allowing walking tours to take place without disturbing the sacred site at the former entrance. The new Ruakuri Cave experience was officially declared open in July 2005.

During excavation of the new 'drum' entrance, two stalagmites (RK05-3 and RK05-4), buried in stratified silt, were unearthed. A further two stalagmites (RK05-1 and RK05-2) were dislodged when a new tunnel was created at the back of Holden's Cavern to allow a circular walking route for the cave tours.

The 3.9 km long Ruakuri Cave (Figure 3.6) has been completely explored by the local speleological society. Members of the society found that the temperature remains fairly constant at ~11°C throughout the year (Bircham, 1975). However, Williams and Fowler (2002) report an average temperature of 12.8°C in Ruakuri

Cave from spot measurements of rock wall temperature using an infrared radiometer. Other local caves (Aranui, Gardners Gut) have air temperatures comparable to the findings of Williams and Fowler (2002). These values are comparable to the mean annual temperatures at nearby Te Kuiti and Ruakura (Table 3.1).

Above ground, a mild moist climate supports a natural vegetation of podocarp-hardwood evergreen forest. This formerly covered the entire district (Wardle, 1991), but about 80% has been cleared in the last 100 years (Williams, 2004). Local precipitation at Waitomo Caves is ~1850 mm/yr with almost 60% falling during May to October (winter). Williams and Fowler (2002) noted a distinct difference (~2.2 ‰) in the isotopic composition of winter and summer rainfall. The difference is likely the result of seasonal rainfall sources; the Southern Ocean in winter and the northern Tasman Sea and Pacific Ocean in summer. Despite this variability, cave drip waters in neighbouring Aranui Cave remained constant throughout the year at close to 5 ‰ (versus VSMOW; Williams and Fowler, 2002). One might therefore anticipate $\delta^{18}O$ (versus VPDB) of presently forming speleothem calcite from Ruakuri Cave to be close to 4-4.5 ‰.

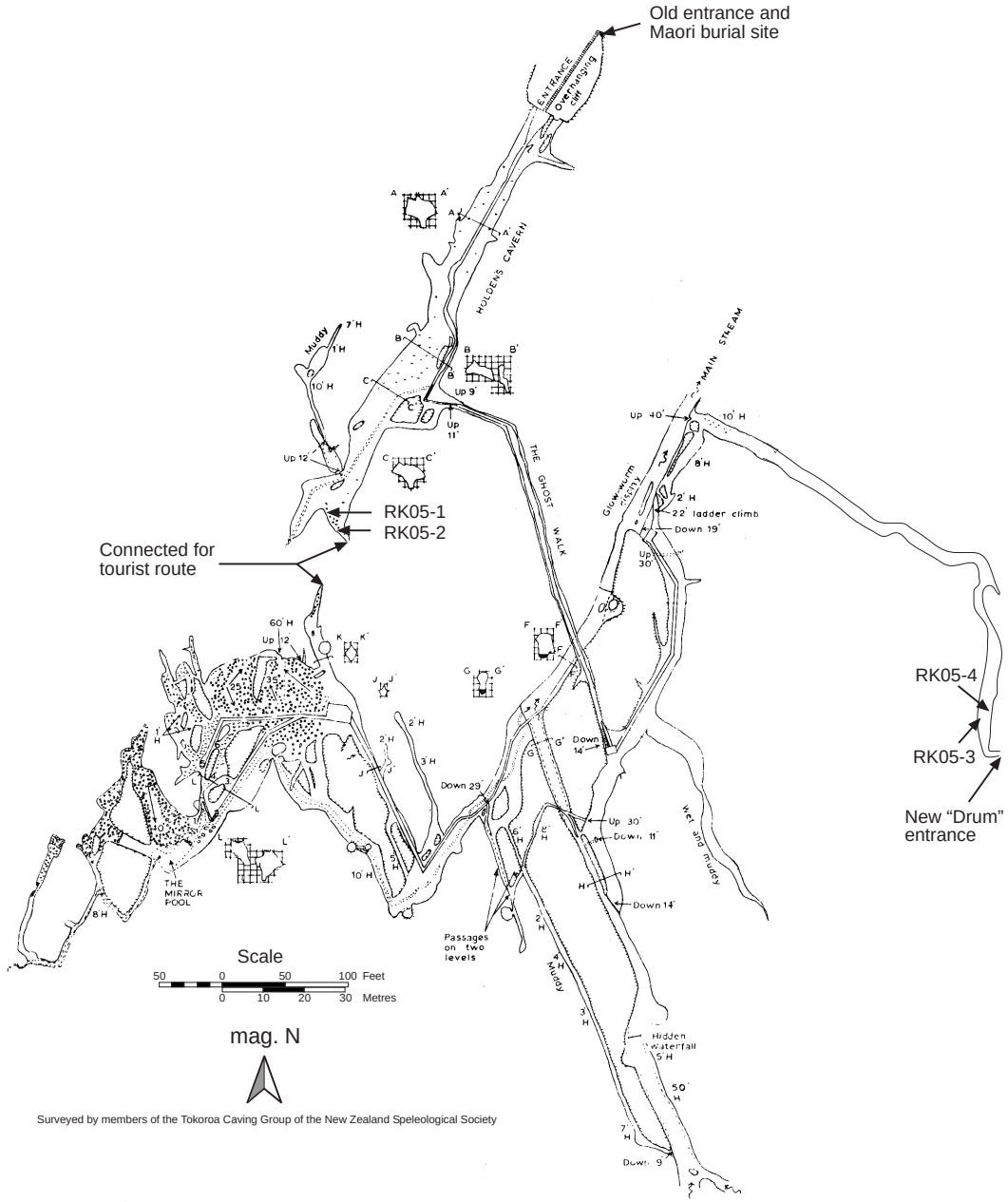

Figure 3.6: A partial map of Ruakuri Cave showing the locations of collected stalagmites [modified from Crossley (1988)].

4 Methods

4.1 Introduction

For all of the caves visited, access, particularly for research purposes, is restricted by permit. Application for permits is done through regional offices of the Department of Conservation (DoC; New Zealand Government). In turn DoC consults with cultural and recreational groups (such as local Maori (Iwi) and speleologists) that have vested interests in the caves before a decision is made. For this study the permit application process was initiated in February 2005. Permits were granted in August of the same year for seven of the eight caves applied for. Access was denied for one cave (Serendipity, near Jackson's Bay) as the cave and surrounding area are Taonga (*treasure*) of the local Iwi.

4.2 Permit Conditions

In order to conduct the research it was agreed in the permit application process with DoC and local Iwi that impact must be kept to a minimum. This necessitated developing a detailed and unambiguous research objective that could be clearly interpreted by interested parties. To minimize impact, the following measures were undertaken in the field:

1) Infrequently visited caves were selected
2) Only actively growing stalagmites were sampled
3) Only stalagmites hidden from view were sampled
4) Aesthetically pleasing stalagmites were left alone
5) Stalagmites were selected for further study based on preliminary results obtained from basal cores
6) Cores were collected using a battery-powered drill
7) Only small (<1 m tall) stalagmites were cored

Furthermore, the permit application had to demonstrate the value of the research to interested local groups, the scientific community and the general understanding of local, regional and global history.

4.3 Field Season 1 (September 2005)

4.3.1 Introduction

Sample selection and collection was carried out in two field expeditions. This was made necessary by the adoption of a coring strategy. Following preliminary laboratory analysis of the cores (see sections 4.5, 4.6 and 4.9) a second trip was required to collect the selected speleothems. In September 2005, Abyssinia, Eggers, Guillotine, Hollywood, Te Ana Puta and Wazapretti caves were visited. It was intended that Serendipity (Jacksons Bay, South Westland) also be visited, but access was not permitted. Furthermore, Profanity and Whiskey caves were also visited but on each occasion water levels at the entrances were too high to allow safe passage. Despite its promise of yielding a speleothem record from the margin of the LGCP moraines, further concerted attempts to revisit Whiskey Cave were not made as it is a relatively small cave and not renowned for its decoration.

In the six caves visited (Table 3.2) a total of 29 stalagmites were selected for coring (Abyssinia – 3; Eggers – 6; Guillotine – 6; Hollywood – 4; Te Ana Puta – 6; Wazzapretti – 4). Several criteria for their selection are outlined above and conscious efforts were also made to choose stalagmites at least 100 m from an entrance, in humid (relative humidity > 95%) passages/chambers apparently unaffected by air movement and that were thick enough to withstand the stresses of coring.

4.3.2 Temperature and Humidity

At each sampling location, prior to coring, simple measurements of temperature and humidity were made (Table 3.2). Care was taken to minimize the impact we, as thermogenic bodies, had on the cave atmosphere when readings were made. This mostly involved sending one person ahead to take a quick measurement before coring activities commenced.

4.3.3 Coring

Key amongst the measures to reduce the impact of this research on the cave environment was the novel method of extracting basal cores of active speleothems. The goal was to obtain enough material to provide for a U/Th date, conduct the Hendy Test (see section 4.6) and make preliminary judgments on the suitability of the calcite to contain a climate record based on visual observations of the structure (i.e. searching for evidence of dissolution and reprecipitation, abundant hiatuses, and degree of clay (detrital Th) contamination), while leaving the majority of the speleothem still in place. This approach allowed some information on the speleothem to be obtained prior to the irreversible process of removing it.

The coring kit consisted of a Makita (model # 6349D) battery-powered drill, fitted to a specially engineered rock coring (palaeomagnetism) set-up (Figure 4.1). The palaeomagnetism kit essentially comprises a water chamber and 200 mm long, 25 mm ID, stainless steel, diamond-tipped core barrel. Water is fed through the core barrel while drilling is underway, acting as both lubricant and coolant.

Cores were drilled horizontally through stalagmite bases and along axes that made the resulting hole observable only to those looking for it. Holes were filled with Plaster-of-Paris (90% $CaSO_4$; >5% $CaCO_3$) which at the edge of the hole was mixed with cave mud (where necessary) in an attempt to colour-match to the speleothem. In some instances fragments of previously broken speleothems were carefully used to further hide core holes. It is hoped that because only active speleothems were sampled new calcite will precipitate over the Plaster-of-Paris, hiding it permanently.

Before drilling, a prerequisite was to observe dripwater falling onto the sample to determine that is was actively growing. Also prior to drilling, absorbent towels were laid on the ground surrounding the stalagmite, particularly on any downward slopes. Excess drilling water, well mixed with calcite powder, was caught and prevented from despoiling nearby cave features. Photographs were taken of each stalagmite and its setting. The height of each sampled stalagmite was also measured.

In almost every case 20-30 minutes was required for drilling each core, which was typically achieved without exhausting a single, fully-charged 3.0 Ah battery.

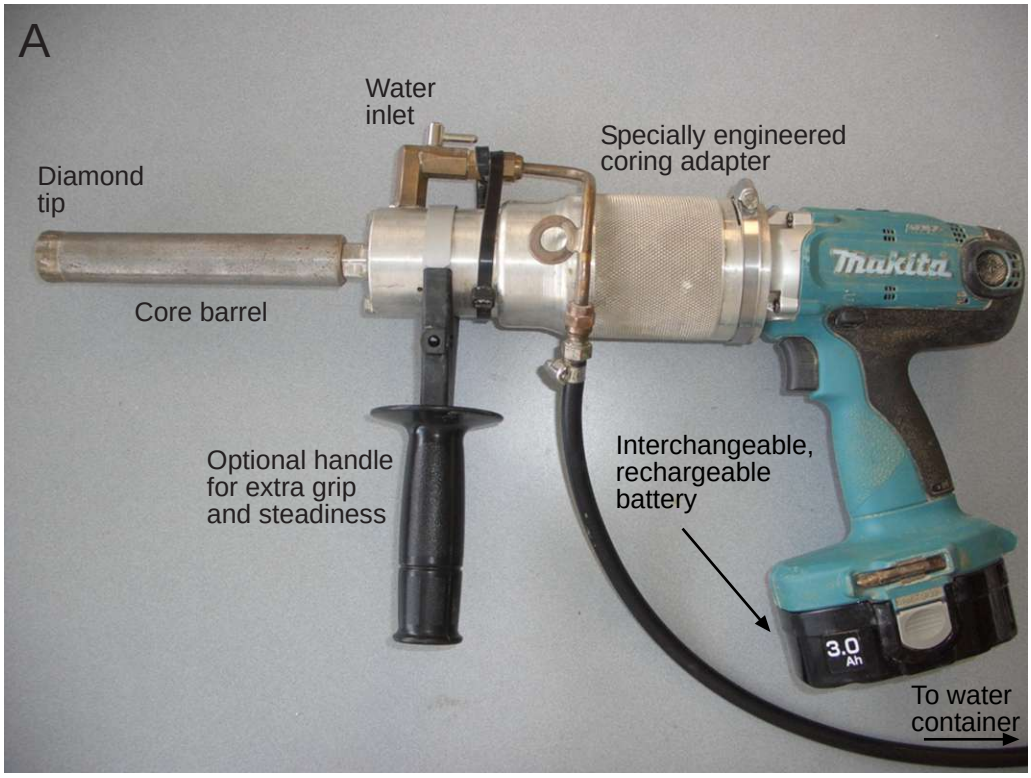

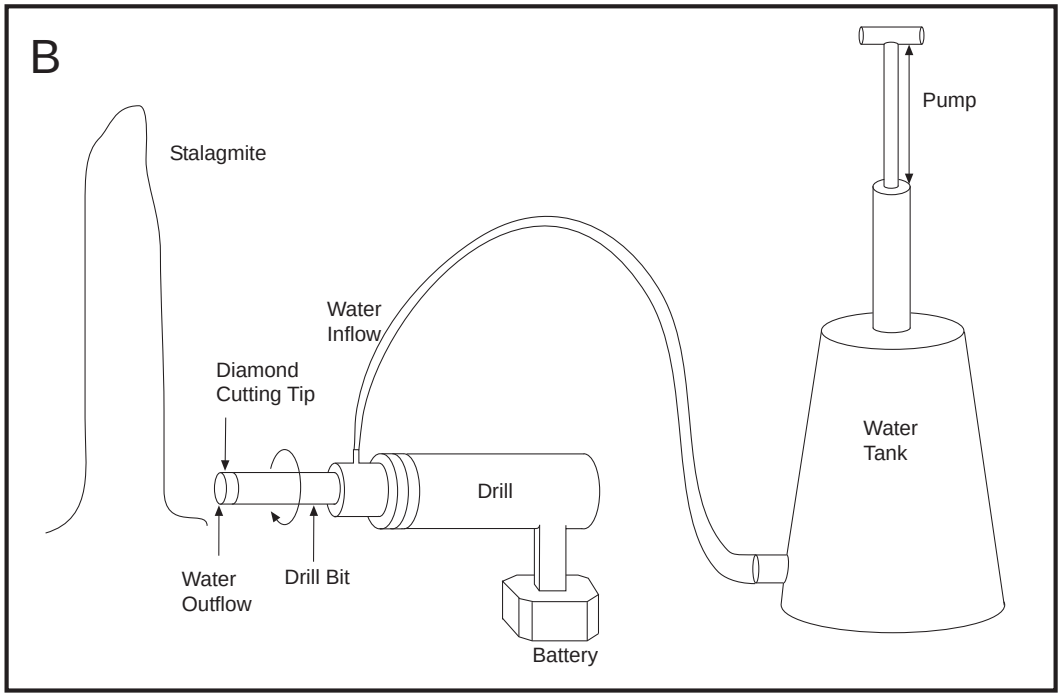

Figure 4.1: (A) Photograph of the core barrel and drill adapter and (B) sketch of speleothem coring kit and application.

4.4 Sample Sectioning

Once the cores were in the laboratory they were polished to a fine grit (to help confirm the *in situ* orientation of the sample) and photographed. Cores were sawn along the long axis as close to the growth axis as possible. It has been subsequently determined (following some coring work in Aranui Cave, Waitomo, in September 2007) that mounting the entire core sample in epoxy resin yields a cleaner cut and eliminates sample break-up during sawing (Figure 4.2).

Each core half was polished with a fine grit (1200) and photographs were taken. One half was then used for analysis and the other maintained as an archive. Analyses included visual observations of structure, stable isotope determinations (for Hendy Tests; see section 4.6) and uranium-thorium dating.

4.5 Visual Analysis

Following sectioning of the cores a visual analysis was conducted. There are several features of the calcite structure which can be observed that have implications for developing a continuous record of palaeoclimate. Chief amongst these are angular cavities, often containing small needle-like calcite crystals that grew in a direction not consistent with the growth axis (Figure 4.3), which are evidence for dissolution and reprecipitation of the calcite (J. Hellstrom, pers. comm. 2006). This process has the effect of destroying any climate signals that may have been preserved in the isotope ratios of given layers and can indicate that the sample has not remained a closed system with regards uranium-series isotopes. Discontinuous layers, particularly on the flanks of the speleothem, also indicate periods of speleothem dissolution (Figure 4.3). Although the remaining material may still yield valid climate information it is likely that there will be a hiatus in the record. Hiatuses may also be defined as clay/mud-rich horizons in the speleothem (Figure 4.3), although these breaks in calcite deposition may be short lived. As a rule, ‘dirty’ and opaque layers are more likely to contain elevated concentrations of initial (detrital) thorium. A core sample dominated by such layers will likely yield less precise uranium-thorium dates than a sample composed of clear calcite.

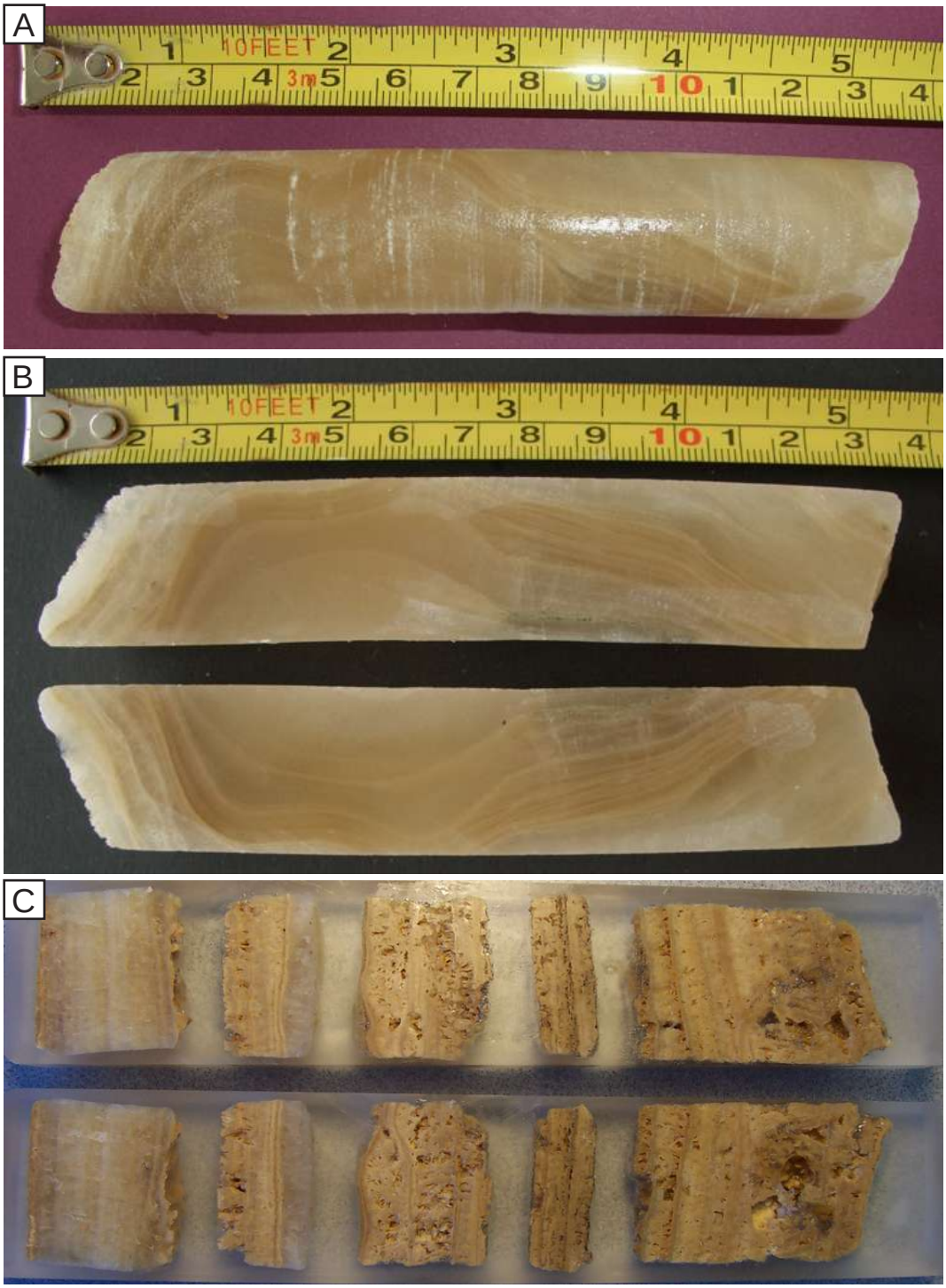

Figure 4.2: Photographs of (A) a core obtained from Hollywood Cave that was cut (B) parallel to the growth axis, as well as (C) a suite of cores of flowstone layers from Aranui Cave that was set in epoxy resin prior to being cut.

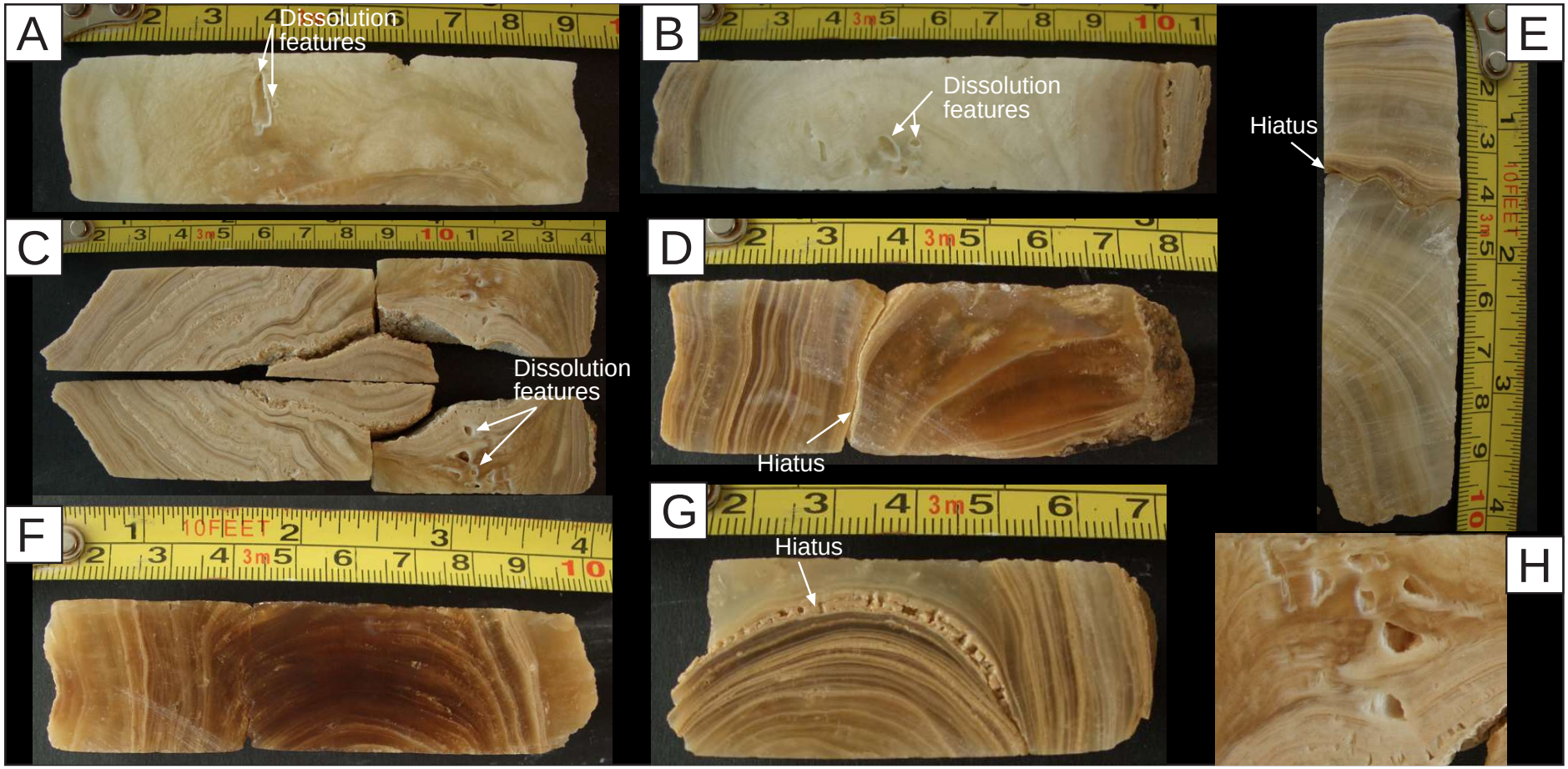

Figure 4.3: Examples of undesirable speleothem characteristics in collected speleothem cores. Dissolution features can be observed in cores A, B, C and H, where H is a close-up view of the lower right portion of C. Core C also shows evidence of abundant sediment inclusions. Cores D and E display hiatuses caused by a cessation of calcite deposition. High organic content is evident in cores D and F from the dark brown colour. Core G is an example of a hiatus caused by an interruption of calcite accumulation by a layer of sediment.

It is worth taking note of speleothem colour. Darker coloured, translucent calcite crystals contain organic compounds such as humic acids. During the course of this study it was determined that some of these compounds survived the uranium-thorium sample preparation procedures and interfered with the sample uptake capillary tube on the MC-ICP-MS. It is likely, however, that the method can be amended to mitigate or even eliminate this problem. Nevertheless, it is an observation that should be included with descriptions of samples submitted for U-Th dating.

4.6 Hendy Test

Following the methods of Hendy (1971), each core was tested to determine if non-equilibrium fractionation of stable oxygen and carbon isotopes had taken place during calcite deposition. This can occur if the precipitation rate is rapid or is driven by evaporation. The result is a distortion of the climate signal preserved within the seepage water such that confidence in interpretations of past climate from the speleothem calcite is low.

Using 400 and 600 μm tungsten carbide-tipped dental burs, driven at ~10,000 rpm by a Dremel™, 2.0-4.0 mg of calcite powder was milled from speleothem cores. Small vibrations in the bur tip position during operation resulted in a hole-width closer to 800-1000 μm. For every core at least five samples, up to a minimum distance of 25 mm from the growth axis, were milled along the same growth layer (Figure 4.4).

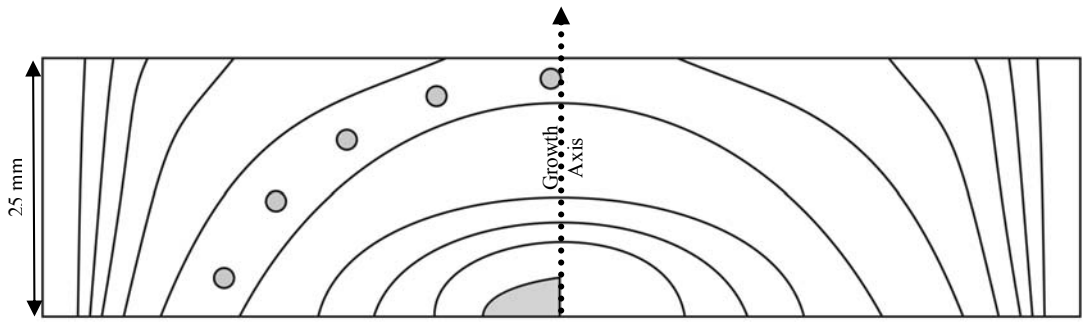

Figure 4.4: Sketch of a core half showing sampling locations for isotopic analysis (Hendy Test; filled circles) and uranium-thorium dating (shaded area at bottom).

4.7 Field Season 2 (May 2006)

Following the initial analysis of the cores (as described above) four stalagmites were deemed well suited to the research objectives. These were collected in a second field season in May 2006. The stalagmites were one each from Eggers, Guillotine, Hollywood and Wazapretti caves. Unfortunately, the foresight to take a second set of temperature and humidity measurements was not made. The removal of the stalagmites was made using hammer and chisel except in the case of the Eggers Cave stalagmite which had formed on a sediment embankment and was easily lifted off. At each site the consistency of the core filler (Plaster of Paris) was checked. In every case the exterior had hardened as a result of both drying and being covered by a very thin layer of calcite. The Plaster of Paris not exposed to the atmosphere had not hardened.

Following removal of each stalagmite a cursory tidying of the area was conducted, principally to remove loose chips of material. The surface was then left bare to allow new speleothem formation from the active seepage waters to take place over the scar. Each of the stalagmites was small enough to be able to be carried out whole, although the Wazapretti specimen weighed in excess of 30 kg.

4.8 Stable Isotopes – Continuous Sampling of the Whole Speleothem

A 10-15 mm thick slab was cut from the central growth axis of each collected speleothem. A continuous track was milled along the growth axis using a 0.6 mm diameter tungsten carbide bit effectively shaving ~3 mg at 0.22-0.25 mm increments (Figure 4.5). Track width was 2-2.5 mm and samples were milled to a depth of 2.5-3 mm. Cross sections through the track show perpendicular layers, therefore minimizing inter-layer interference at depth of 3 mm. This sampling technique homogenizes the signal for every ~0.25 mm increment, but is preferable to drilling isolated holes as it allows greater ability to identify abrupt events. Typically sample mass was ~3 mg. The small percentage (~5 %) of samples of mass > 3.5 mg were split into two with one having at least 2.1 mg.

All samples generated from the cores for Hendy Tests, and selected samples

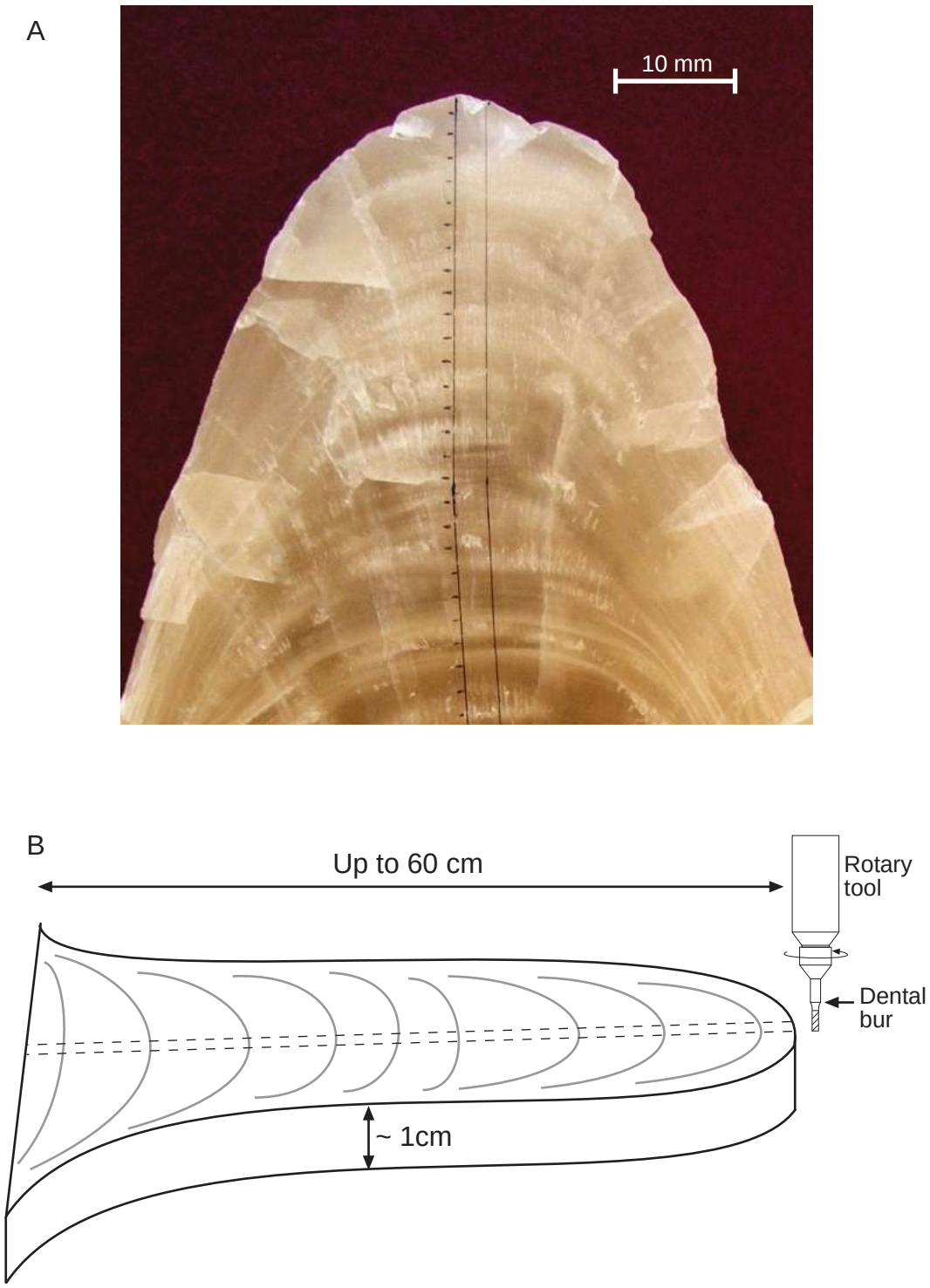

Figure 4.5: Photograph (A) and sketch (B) of continuous sampling strategy for powders obtained for stable isotope analysis. (A) A track was drawn along the length of the growth axis and divided into increments of 2 mm. (B) Powders were collected by pushing the speleothem against the cutting edge of a dental bur fitted into a vertically mounted Dremel rotary tool.

from stalagmites GT05-5, HW05-3, RK05-1 and RK05-4, were submitted for analysis at the University of Waikato. Each sample was entirely reacted with orthophosphoric acid in a Europa CAPS microcarbonate preparation device at 70°C. The evolved gas was measured for the relative abundance of ^{13}C and ^{18}O using a Europa Geo 20-20 fitted with a Europa CAPS (Carbonate Automatic Preparation System) reaction line.

Five hundred samples selected from stalagmite RK05-3 were submitted for analysis at IFM-GEOMAR (Kiel, Germany). Stable isotope ratios were determined using a Finnigan Delta-Plus Advantage mass spectrometer. Analytical precision was better than 0.051 ‰ (1σ) for $\delta^{13}C$ and better than 0.088 ‰ (1σ) for $\delta^{18}O$.

All data were normalized to Vienna Peedee Belemnite (VPDB) using National Institute of Standards reference NBS 19 ($\delta^{18}O$ = -2.20 ‰; $\delta^{13}C$ = +1.95 ‰) and in-house standard WKS for those samples run at the University of Waikato. WKS was calibrated against NBS-19, and cross-checked against NBS-20. Long term measurement of both NBS-19 and WKS at the University of Waikato yielded external precision better than ±0.06 ‰ for $\delta^{13}C$ and ± 0.12 ‰ for $\delta^{18}O$.

4.9 Uranium-Series Chronology

Samples selected for uranium-thorium dating must meet three requirements before reliable data can be obtained. First, the sample must have contained sufficient initial U to enable measurement of its accumulated daughter products. However, given modern analytical techniques this requirement is becoming less critical. Second, the sample must have contained an insignificant or known activity of ("detrital") ^{230}Th at the time of formation. The greater the unknown quantity of detrital thorium the larger the correction and errors on the sample age. Third, the sample must have remained a closed system, with respect to uranium and thorium, from the time of formation to the time of analysis. Unlike other materials such as bone and shell, speleothems do usually act as closed systems with respect to uranium-series isotopes (Hellstrom, 2006).

The ages of the oldest datable material in the collected stalagmite cores and the chronology of individual speleothems were established by uranium-series dating milled calcite samples on a Nu-instruments Nu Plasma MC-ICP-MS (Multi Collector Inductively Coupled Plasma Mass Spectrometer) at the University of Melbourne, Australia.

Samples obtained from the cores were in powder form after being ground out using an 800 μm tungsten-carbide, ball-tip dental bit. Optimal samples should contain ~10 ng of uranium. It is well documented that New Zealand speleothems typically have low (< 100 ppb) uranium concentrations (Hendy, pers. comm.; Hellstrom *et al*., 1998; Williams, 1996; Williams *et al*., 2004, 2005), so that at least 100 mg of speleothem calcite is needed to meet this target. Erring on the side of caution, sample sizes ranged between 180 and 250 mg for all core samples.

Once uranium concentrations were determined for cores of collected stalagmites and a more comprehensive understanding of the dating technique was acquired, subsequent samples submitted for dating were in solid crystal form and in the range 40-110 mg.

Sample preparation begins with dissolution in nitric acid and is then equilibrated with a $^{229}Th/^{233}U$ mixed spike solution. U and Th are then separated from the matrix by adsorption onto Eichrom TRU-Spec resin. Next the U and Th are stripped from the resin using a small quantity of hydrofluoric acid. The resulting solution is dried and a new running solution is prepared for introduction of the sample to the mass spectrometer. Further details on sample preparation and instrumental procedures are presented by Hellstrom (2003), although it should be noted that these methods have been continually refined up to the present day.

Raw (or uncorrected) ages of speleothems are calculated iteratively using the following equation, modified from Kaufman and Broecker (1965):

$$\left[\frac{^{230}Th}{^{238}U}\right] = 1 - e^{-\lambda_{230}T} + \left(\frac{\delta^{234}U_{(m)}}{1000}\right)\cdot\left(\frac{\lambda_{230}}{\lambda_{230}-\lambda_{234}}\right)\cdot\left(1 - e^{(\lambda_{234}-\lambda_{230})T}\right)$$

where $[^{230}Th/^{238}U]$ is the activity ratio between ^{230}Th and ^{238}U as measured by the mass spectrometer, λ_{230} is the ^{230}Th decay constant (9.1577 x 10^{-6} yr^{-1}; Cheng *et al*., 2000), λ_{234} is the ^{234}U decay constant (2.8263 x 10^{-6} yr^{-1}; Cheng *et al*., 2000),

$\delta^{234}U_{(m)} = ([^{234}U/^{238}U]-1)x1000$ as measured by the mass spectrometer, and T is age (in years).

The amount of initial ^{234}U must also be considered when calculating an age from uranium series isotope abundances as this has an effect on $[^{230}Th/^{238}U]$ at all ages (Edwards *et al*., 1987). Even if initial ^{234}U has been taken into account the calculated age is still based on another assumption: that initial activity of ^{230}Th was zero. This assumption is based on the extremely low solubility of thorium ions in surface waters, which ought to lead to negligible thorium in solutions from which speleothem calcite is precipitated. However, thorium strongly adsorbs onto surfaces and therefore can be incorporated in speleothem calcite with the inclusion of detrital materials, such as clays. Initial thorium concentrations can be estimated using the $^{230}Th/^{232}Th$ activity ratio as an indication.

4.10 Trace Elements

Thick sections (up to 5 mm) were cut from the growth axes of speleothems for trace element analysis by laser ablation (LA) ICP-MS. The maximum area for thick sections, as determined by the size of the laser sample chamber, is 26 x 54 mm. Therefore even relatively short speleothems demanded the cutting of many thick sections.

The sample is ablated using a New Wave UP which is equipped with a Nd:YAG laser which operates at a wavelength of 213 nm. Once ablated, the sample is carried to the ICP-MS within a mixed Argon-Helium flow. The ICP-MS used in this study is a Perkin-Elmer SCIEX ELAN DRC II.

Continuous scans and lines of spot analyses were conducted parallel to the growth axis. A typical set up for analysis was a spot size of 60 μm, power output of 0.2 W and with pulsing set at 10 Hz. For spot analyses the dwell time at each ablation site was 60 seconds.

Absolute concentrations of trace elements measured by spot analysis were calculated using the GLITTER software application and trace element measurements of the National Institute of Standards and Technology (NIST) 612 glass. One sigma (1 σ) errors better than ±5 % were consistently achieved for analyses of ^{42}Ca, ^{87}Sr, ^{138}Ba and ^{232}Th concentrations in NIST 612, and better than

±10 % for ^{23}Na, ^{24}Mg and ^{238}U. However, 1 σ errors on measurements of ^{31}P were always worse than ±50 %.

5 Results

5.1 South Island Stalagmites

5.1.1 Core Collection

During the first field-season, basal cores were extracted from 29 stalagmites located in six north Westland caves. Once sectioned and polished, one half of each core was archived and the other half subject to visual analysis, the Hendy Test and age determination by the uranium-thorium disequilibrium technique. The results of these analyses are presented in the following sections and were used to select stalagmites that would likely yield palaeoclimate records worthy of the project objectives. Supplementary to the analyses, photographs of each core were taken and are provided in Appendix B.

5.1.1.1 Visual Observations

Internal structural features of speleothems, including cavities, colour, clarity, mineralogy (e.g. calcite or aragonite), crystal size and hiatuses, can reveal useful information about the cave environment at the time of calcium carbonate deposition. Furthermore, it is also possible to recognise evidence of any post-depositional alteration of the speleothem, such as that caused by dissolution and recrystallisation. It is important to be able to identify and document these features before progressing with destructive (and expensive) analyses as they may aid subsequent interpretations of proxy data, or allow unsuitable speleothems to be avoided.

Evidence suggestive of dissolution and recrystallisation of speleothem calcite was apparent in six of the 29 cores (Table 5.1; Figures B.1, B.3 and B.4 in Appendix B). Each displayed angular cavities containing randomly-oriented calcite crystals. Three of four stalagmites cored in the relatively short Wazapretti Cave and two of six stalagmites cored in Te Ana Puta were among the six. These stalagmites were thus not considered for collection.

At least four of the cores contained hiatuses (Table 5.1). These were identified by core sections that separated easily without breaking crystals, typically leaving smooth undulating surfaces on both sides of the hiatus (e.g.

Table 5.1: Visual observations and Hendy Test results of core halves from north Westland stalagmites.

Cave	Stalagmite	Stalagmite Height (mm)	Basal Core Observations	Hendy Test	Selected for further study
Abyssinia	AB05-1	230		Pass	
	AB05-2	350	Hiatuses; high detrital content	Pass	
	AB05-3	290	Dissolution-recrystallisation?	Pass	
Eggers	EG05-1	500		Pass	
	EG05-2	300	Hiatuses	Pass	
	EG05-3	160	High organic content	Pass	
	EG05-4	200	Hiatus; high organic content	Pass	
	EG05-5	480	High organic content	Pass	Yes
	EG05-6	300	High organic content	**Fail**	
Guillotine	GT05-1	280	Opaque crystals	Pass	
	GT05-2	510		Pass	
	GT05-3	380		Pass	
	GT05-4	770		Pass	
	GT05-5	300	Hiatus	Pass	Yes
	GT05-6	370		Pass	
Hollywood	HW05-1	425		Pass	
	HW05-2	530		**Fail**	
	HW05-3	627		Pass	Yes
	HW05-4	300		Pass	
Te Ana Puta	TAP05-1	250	Opaque crystals; sandy at base	Pass	
	TAP05-2	230	Dissolution-recrystallisation	Pass	
	TAP05-3	450	Opaque crystals	Pass	
	TAP05-4	500	Very finely laminated	**Fail**	
	TAP05-5	130	Dissolution-recrystallisation?	**Fail**	
	TAP05-6	490	Opaque, detrital mineral rich	Pass	
Wazapretti	WZ05-1	610		Pass	Yes
	WZ05-2	510	Dissolution-recrystallisation	Pass	
	WZ05-3	300	Dissolution-recrystallisation?	Pass	
	WZ05-4	340	Dissolution-recrystallisation; detrital mineral rich	Pass	

EG05-4; Figure B.1). Breaks in deposition were also present in several cores as layers of detrital mineral rich calcite (e.g. EG05-2). These latter hiatuses were more robust than those mentioned above, indicating that cessation of calcite deposition was potentially relatively brief. Several stalagmite cores contained multiple detrital mineral rich layers (Table 5.1; Appendix B). This indicates a dynamic cave environment (e.g. flooding, intermittent strong air movements) in contrast to the settled conditions necessary for development of speleothems containing uninterrupted palaeoclimate records. Therefore, stalagmites whose cores contained multiple hiatuses were not considered for collection.

Colour of collected stalagmite cores ranged from almost clear (e.g. GT05-6) to dark brown (e.g. EG05-5; Figures B.1 and B.2, Appendix B). The brown colouring is most likely attributable to the inclusion of organic compounds and trace elements such as iron and manganese within the calcite structure. Darker tones indicate greater concentrations of these materials. Of all the stalagmites cored, those in Eggers Cave were the darkest brown, while several Guillotine samples were almost colourless. Although no stalagmites were discarded from the list of those to collect based on colour, it was noted that samples prepared for uranium-series analysis from darker calcite produced a viscous liquid that occasionally blocked the capillary tube used for uptake into the ICP-MS.

5.1.1.2 Hendy Tests

To discriminate samples likely affected by kinetic fractionation of oxygen and carbon stable isotopes, the Hendy Test (Hendy, 1971) was performed on a single, long (≥ 20 mm), continuous layer from each core (Figures 5.1 to 5.6). Of the 29 cores, four (EG05-6, HW05-2, TAP05-4 and TAP05-5) displayed enrichment of oxygen and carbon isotope ratios with increasing distance from the growth axis (Figures 5.2f, 5.4b and 5.5d,e; Table 5.1). Furthermore, in each case the increase in $\delta^{13}C$ was approximately three times greater than the increase in $\delta^{18}O$ as calculated by Hendy (1971) for samples affected by kinetic fractionation. Therefore these stalagmites failed the test and were removed from the list of samples worth collecting as they were unlikely to yield reliable palaeoclimate information.

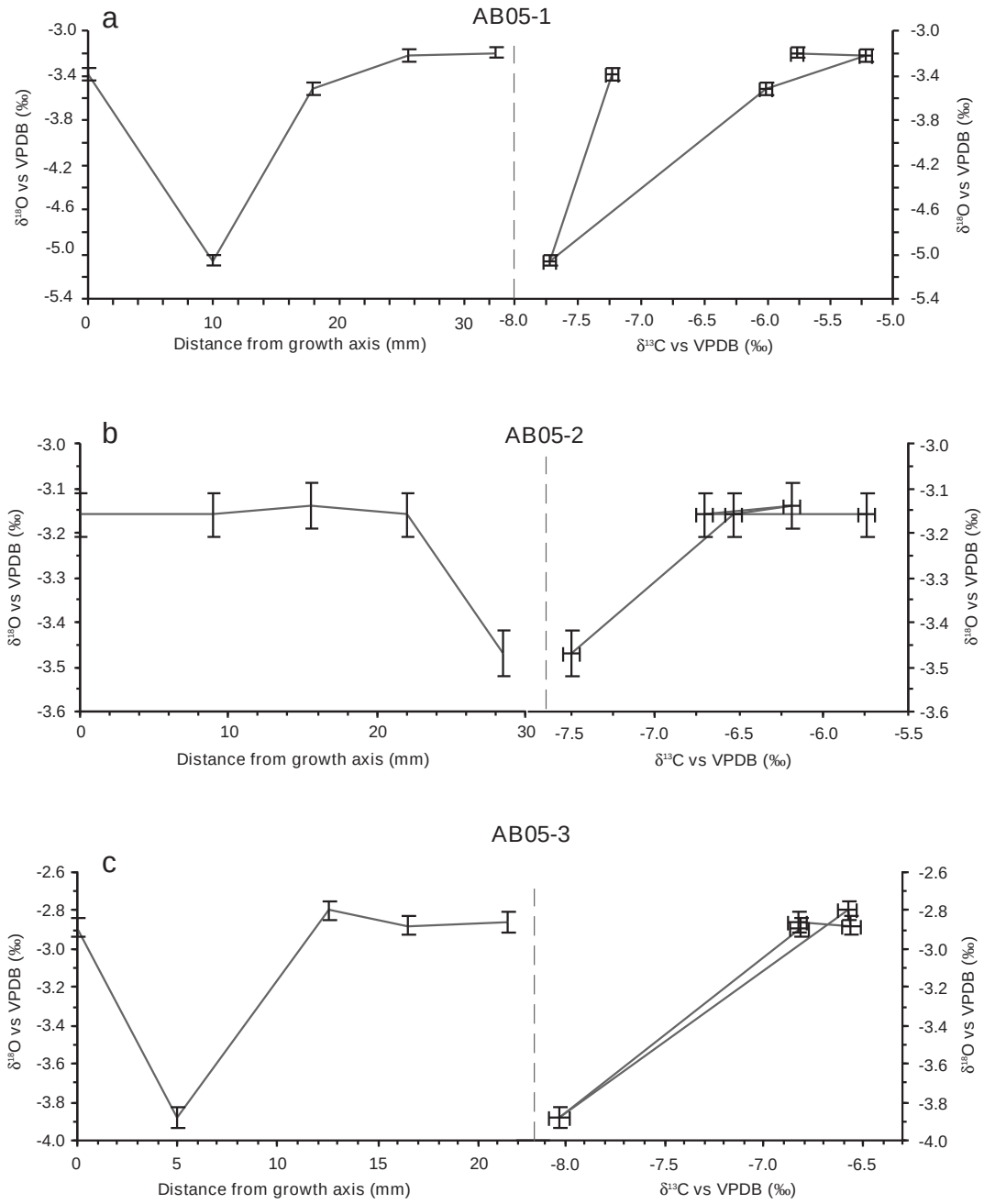

Figure 5.1: Hendy Test results for three cores obtained from stalagmites in Abyssinia Cave. The problem of sampling only one layer are highlighted in the results of (a) AB05-1 and (c) AB05-3 which show significant deviations from a general trend.

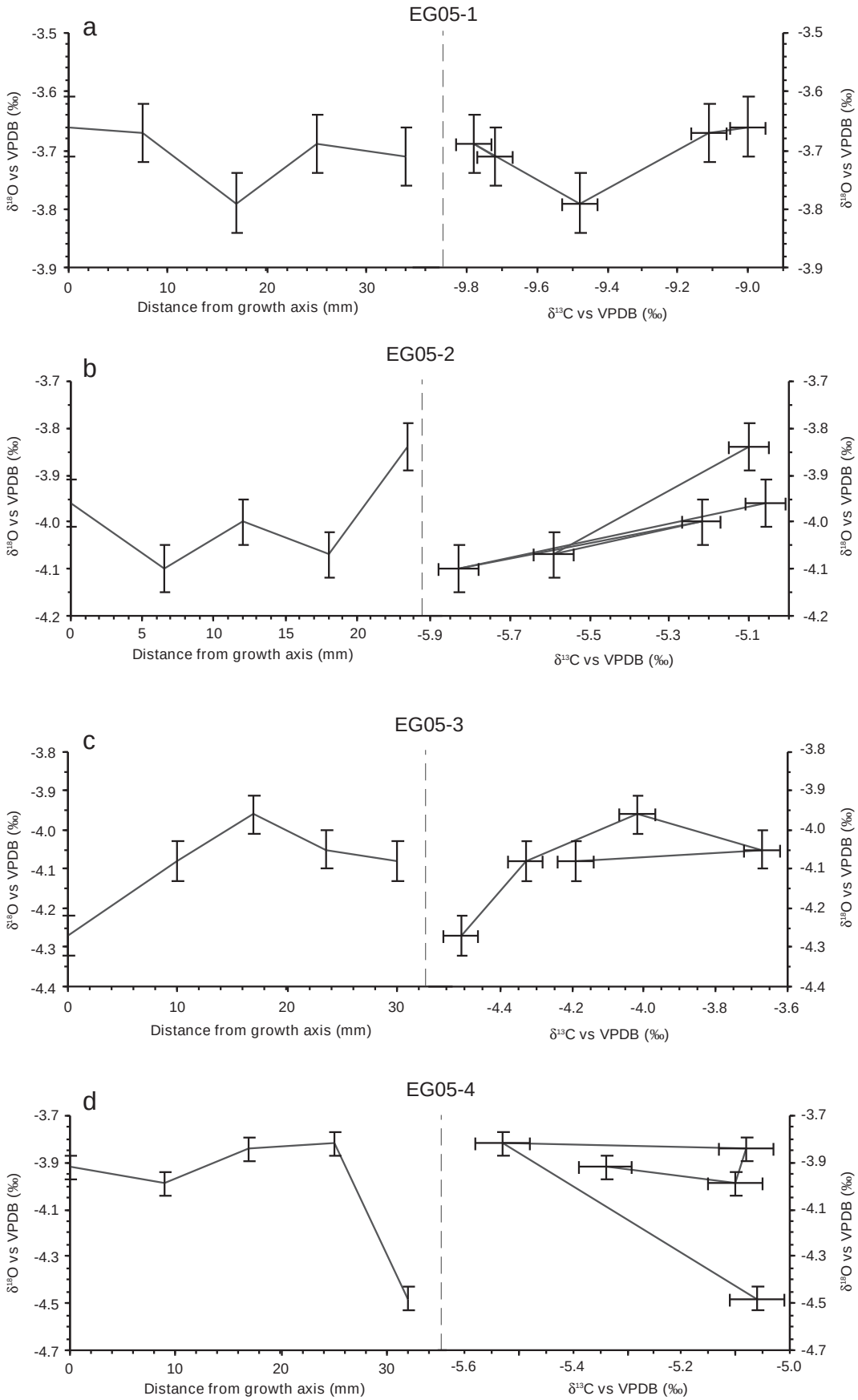

Figure 5.2: Hendy Test results for six cores obtained from stalagmites in Eggers Cave. Core EG05-6 (f) displayed increasing $\delta^{18}O$ and $\delta^{13}C$ with distance from the growth axis, and therefore 'failed' the test.

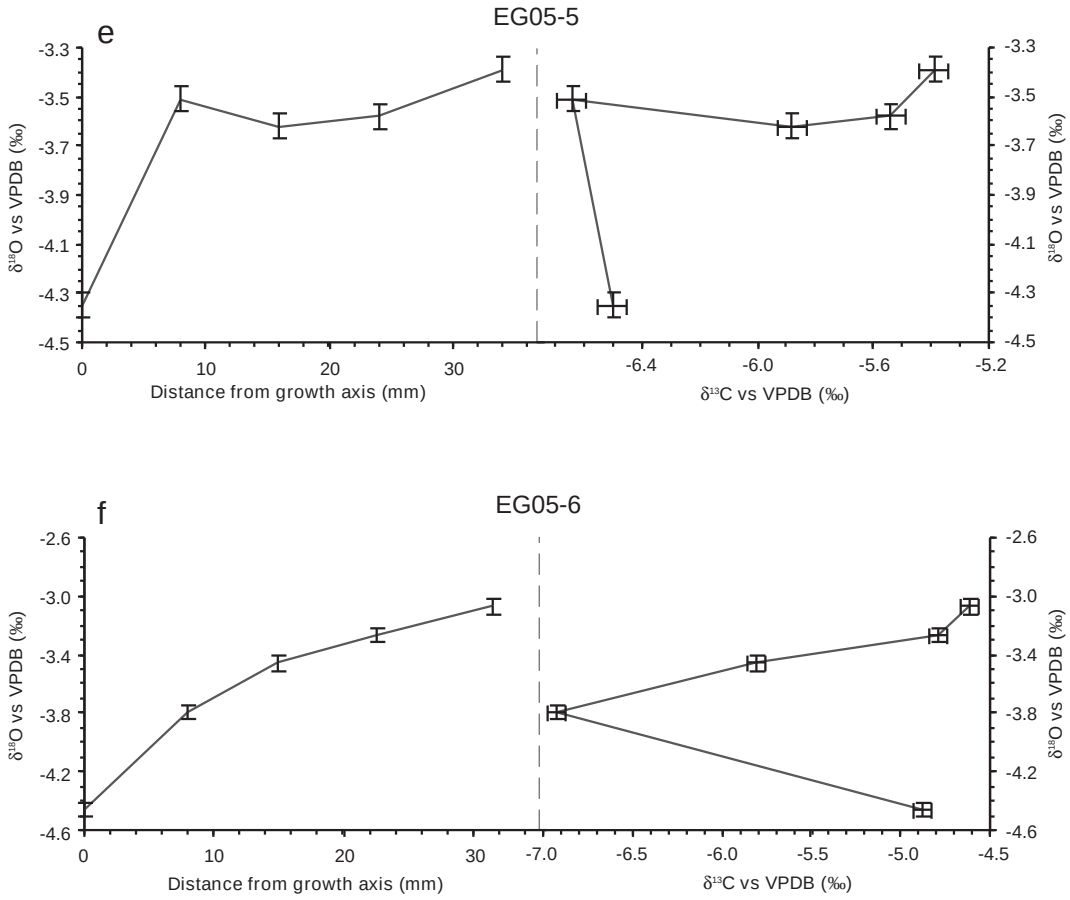

Figure 5.2 (continued)

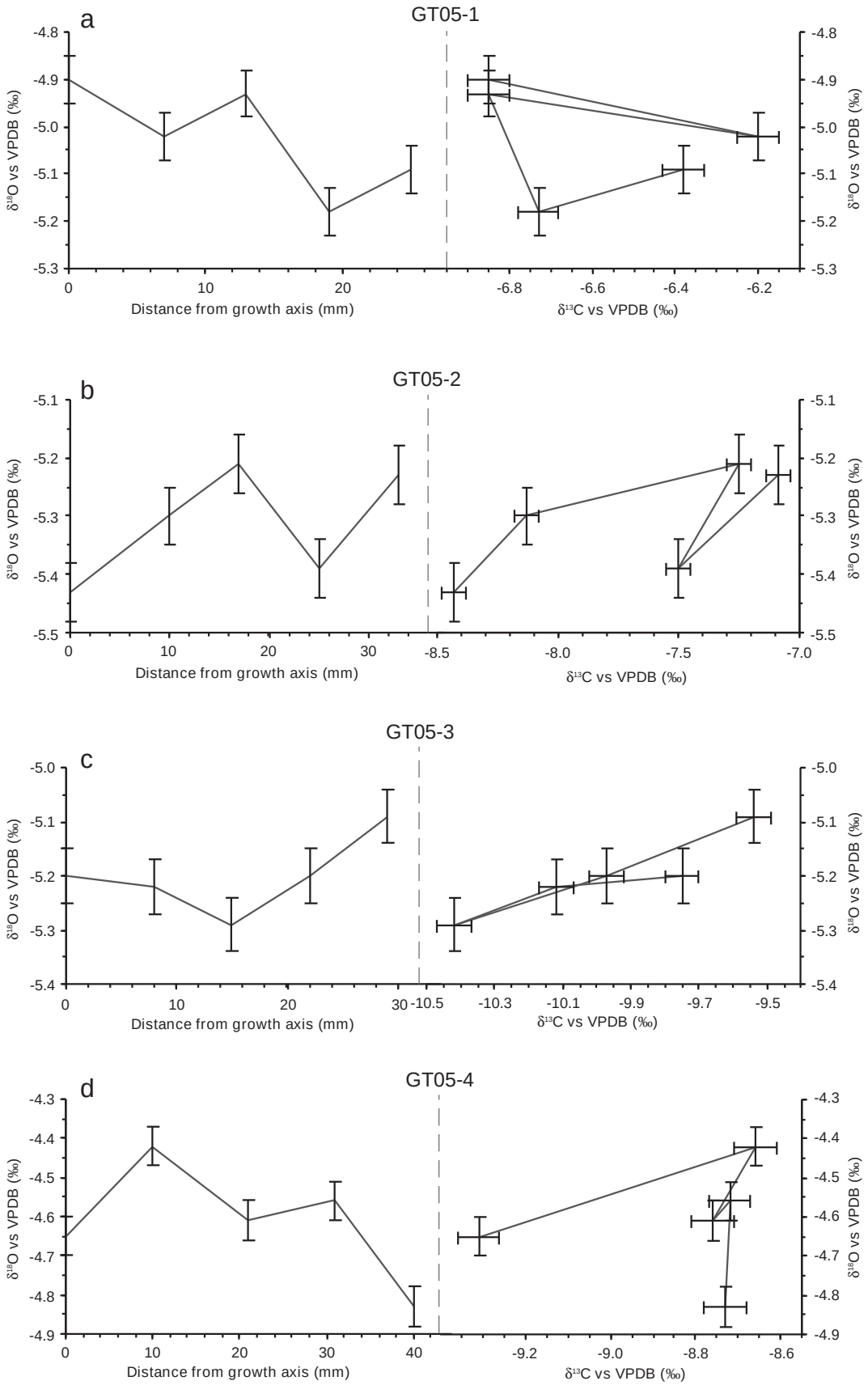

Figure 5.3: Hendy Test results for six cores obtained from stalagmites in Guillotine Cave.

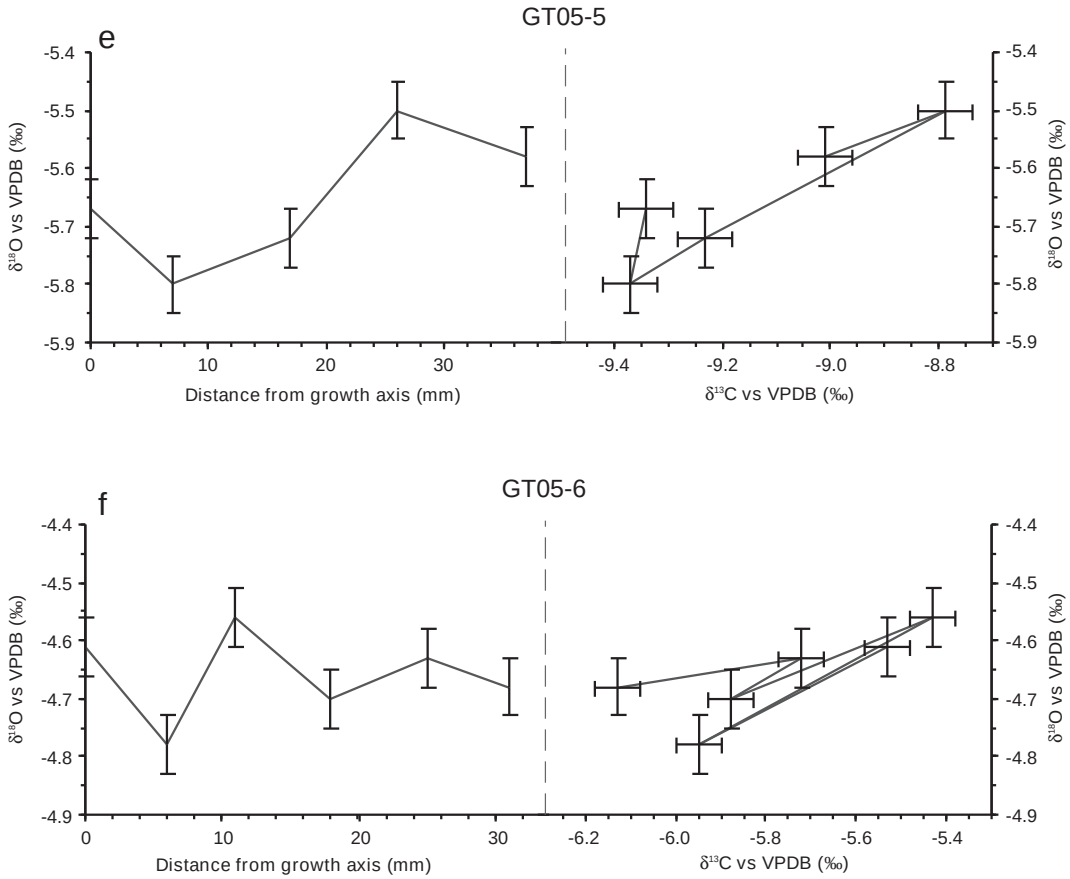

Figure 5.3 (continued)

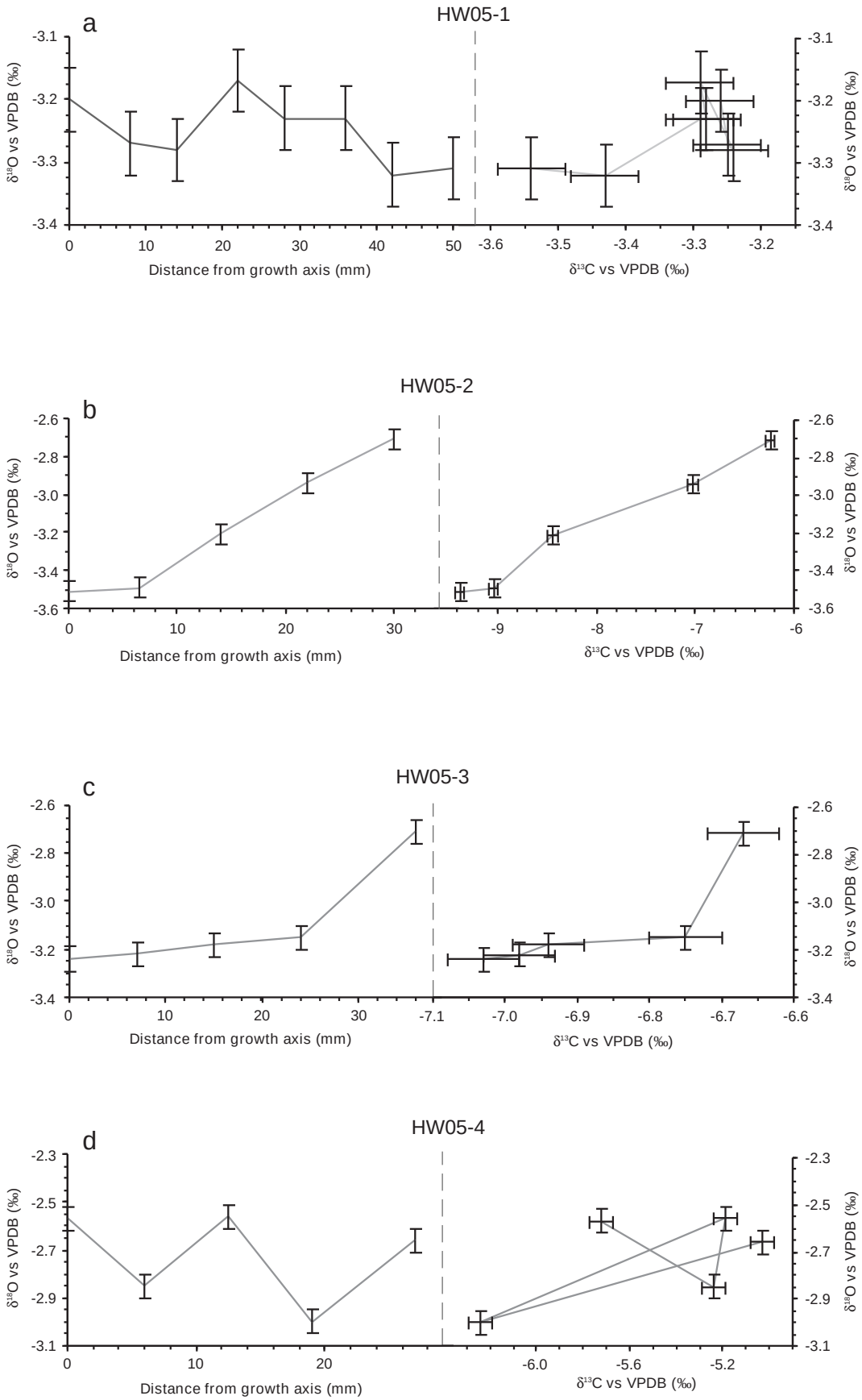

Figure 5.4: Hendy Test results for four cores obtained from stalagmites in Hollywood Cave. Core HW05-2 (b) displayed increasing $\delta^{18}O$ and $\delta^{13}C$ with distance from the growth axis, and therefore 'failed' the test.

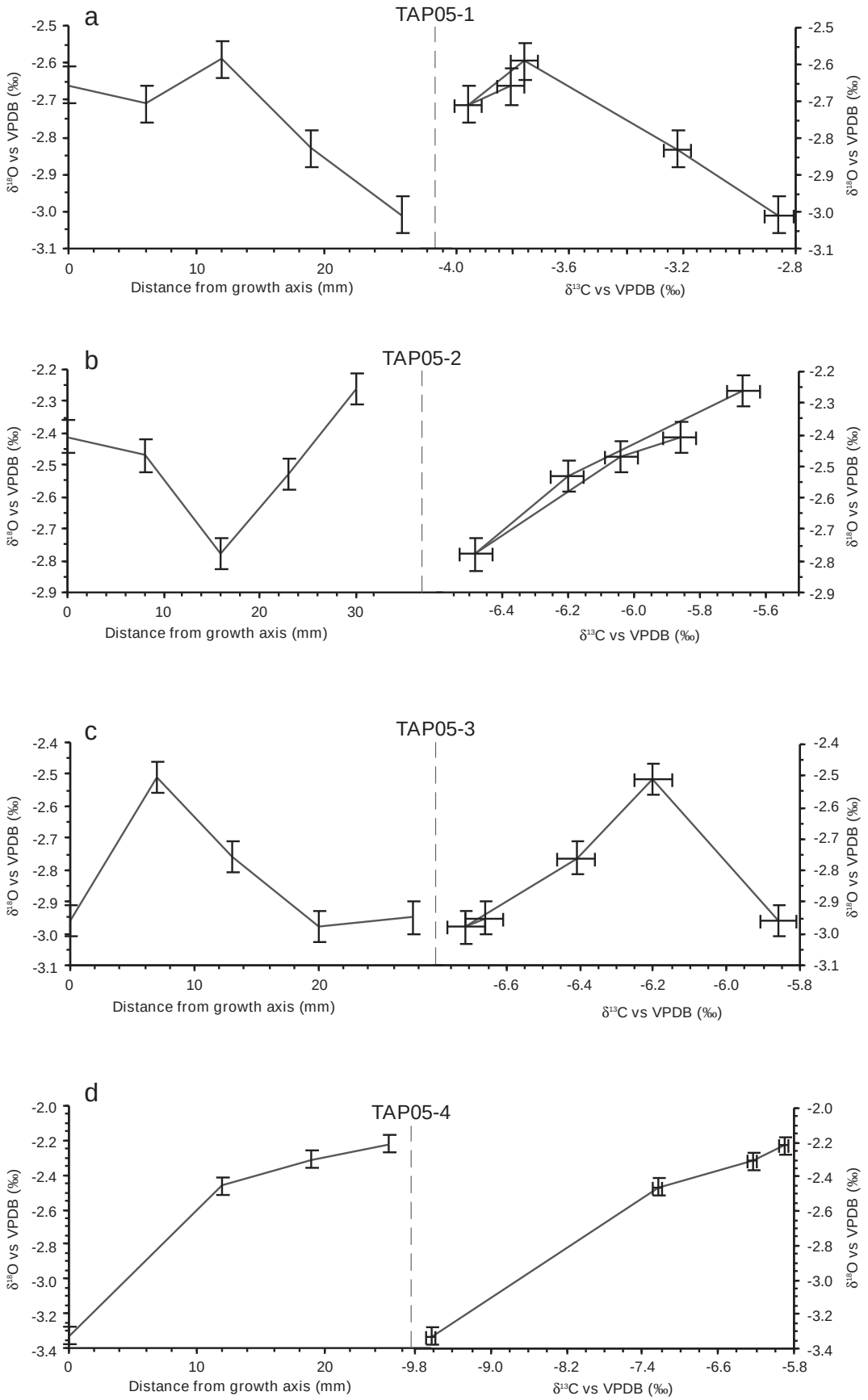

Figure 5.5: Hendy Test results for six cores collected from stalagmites in Te Ana Puta. Cores TAP05-4 (d) and TAP05-5 (e) displayed increasing $\delta^{18}O$ and $\delta^{13}C$ with distance from the growth axis, and therefore 'failed' the test.

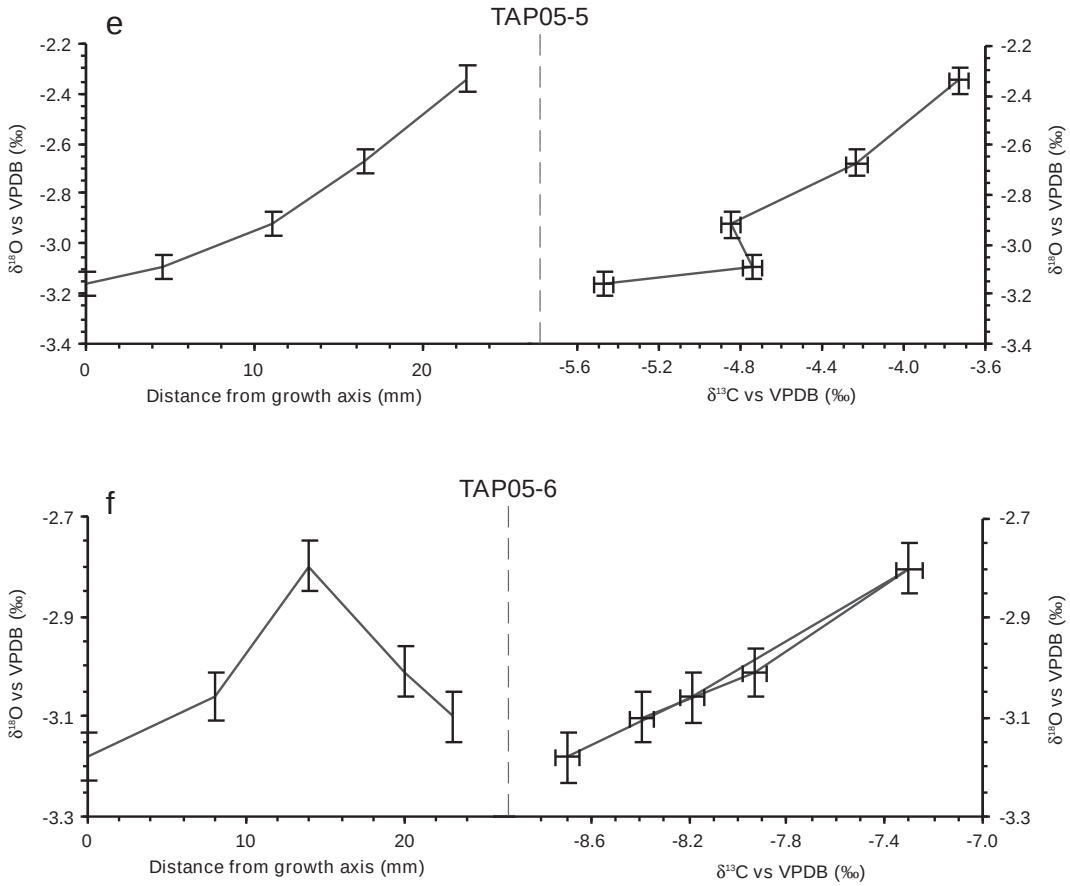

Figure 5.5 (continued)

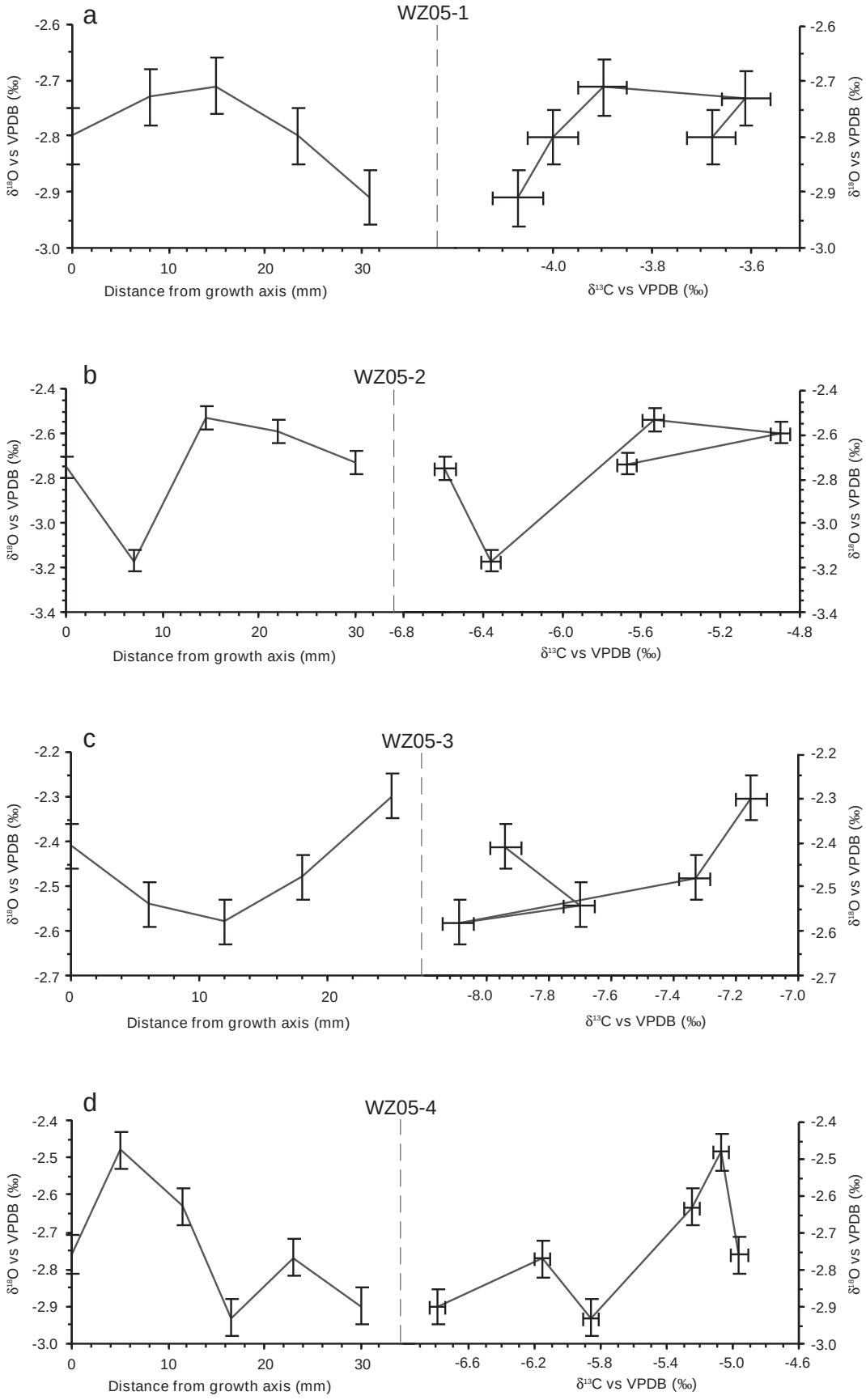

Figure 5.6: Hendy Test results for four cores obtained from stalagmites in Wazapretti Cave.

The layer chosen for analysis in core HW05-3 also displayed enrichment in $\delta^{18}O$ with distance from the growth axis (Figure 5.4). However, most of the apparent enrichment (~0.5 ‰) occurred between the two points furthest from the growth axis. This could be the result of sampling multiple layers, a problem encountered when layers are thinner than the milling tool (such as occurs at increased distance from the growth axis). It is also significant that the relationship between $\delta^{13}C$ and $\delta^{18}O$ pairs did not demonstrate a 3:1 ratio. Therefore it is likely that the isotopic composition of HW05-3 calcite was unmodified by kinetic fractionation processes.

The remaining 24 cores all passed the Hendy Test. Some appeared to be affected by sampling of more than one layer during micro-drilling which led to large (> 1 ‰) jumps in $\delta^{18}O$ between data points (Figure 5.1a,c). As mentioned above, this is a recognized limitation of the Hendy Test (Treble *et al*., 2005).

Calcite milled from Guillotine Cave (GT) core samples yielded the most negative $\delta^{18}O$ values. This cave is located at a much greater elevation (~740 masl) than the other caves from which cores were obtained. Cores from Eggers Cave, the second highest cave visited, had the next-most depleted $\delta^{18}O$ values. However, it ought to be noted that the material sampled in each core was not of the same age and therefore some or all of the difference could be accounted for by changes in the magnitude of the ice volume effect and climate.

5.1.1.3 Uranium-Thorium Dating

Uranium and thorium isotope concentrations were determined for samples milled from the oldest layers of each speleothem core. Results were obtained for 28 of 29 cores, and nine analyses were repeated (Table 5.2). Analysis of TAP05-1 was abandoned due to excessively high thorium content which prevented the calculation of accurate and precise ages.

Total uranium concentrations [U] ranged between 62 and 1377 ppb across the 29 cores. The majority of concentrations were in the range 100-300 ppb as is commonly the case for New Zealand speleothems (Hellstrom *et al*., 1998; Williams *et al*., 2004, 2005). Within each cave the uranium concentrations varied by a factor of 2.5 to 5. Uranium concentrations were significantly higher (397-1377 ppb) in Te Ana Puta than the other caves.

Table 5.2: Uranium-thorium data for 29 stalagmite cores obtained from six West Coast caves. All ages are given with 2σ errors. rpt = repeat.

Cave	Core	U (ppm)	$^{234}U/^{238}U$ activity	$^{230}Th/^{238}U$ activity	Raw Age (yr)	$^{230}Th/^{232}Th$ activity	Corrected Age (yr)
Abyssinia	AB05-1	0.140	1.090 ± 0.002	0.088 ± 0.001	9134 ± 81	7.8	7649 ± 919
	AB05-2	0.239	1.649 ± 0.003	0.133 ± 0.002	9098 ± 105	4.5	6528 ± 1595
	AB05-3	0.352	1.674 ± 0.004	0.168 ± 0.001	11,432 ± 94	128.5	11,324 ± 120
Eggers	EG05-1	0.128	1.184 ± 0.011	0.176 ± 0.005	17,374 ± 563	4.1	12,161 ± 3392
	EG05-1 rpt	0.130	1.194 ± 0.002	0.162 ± 0.001	15,846 ± 95	10.3	14,558 ± 996
	EG05-2	0.234	0.972 ± 0.002	0.104 ± 0.001	12,314 ± 148	7.4	10,265 ± 1304
	EG05-2- rpt	0.242	0.968 ± 0.002	0.098 ± 0.02	11,603 ± 240	12.9	10,843 ± 657
	EG05-3	0.318	0.919 ± 0.002	0.027 ± 0.001	3260 ± 95	5.9	2553 ± 453
	EG05-4	0.347	1.010 ± 0.003	0.036 ± 0.001	3946 ± 83	9.4	3403 ± 346
	EG05-5	0.661	0.970 ± 0.002	0.127 ± 0.001	15,304 ± 86	215.7	15,244 ± 102
	EG05-6	0.340	1.007 ± 0.002	0.130 ± 0.001	15,029 ± 117	13.2	13,630 ± 882
	EG05-6 rpt	0.315	1.006 ± 0.002	0.125 ± 0.001	14,441 ± 77	37.5	14,127 ± 260
Guillotine	GT05-1	0.148	1.187 ± 0.003	0.053 ± 0.001	4917 ± 56	41.7	4797 ± 102
	GT05-2	0.120	1.167 ± 0.002	0.030 ± 0.001	2871 ± 63	30.1	2748 ± 100
	GT05-3	0.341	1.284 ± 0.003	0.120 ± 0.001	10,585 ± 120	242.1	10,532 ± 129
	GT05-4	0.262	1.258 ± 0.003	0.147 ± 0.001	13,470 ± 76	3.6	8697 ± 2963
	GT05-4 rpt	0.179	1.257 ± 0.003	0.128 ± 0.001	11,664 ± 70	28.4	11,321 ± 274
	GT05-5	0.131	1.104 ± 0.003	0.823 ± 0.007	143,359 ± 2497	2.0	100,572 ± 41,558
	GT05-5 rpt	0.064	1.152 ± 0.003	0.575 ± 0.003	74,021 ± 543	109.8	73,620 ± 655
	GT05-6	0.062	1.162 ± 0.003	0.086 ± 0.001	8378 ± 105	17.0	7757 ± 393
Hollywood	HW05-1	0.267	1.263 ± 0.003	0.641 ± 0.003	74,773 ± 500	794.9	74,460 ± 554
	HW05-2	0.142	1.377 ± 0.003	0.741 ± 0.004	80,492 ± 654	26.3	77,978 ± 1671
	HW05-2 rpt	0.110	1.357 ± 0.005	0.695 ± 0.004	75,228 ± 607	803	75,175 ± 685

Continued on next page

Table 5.2 (continued)

Cave	Core	U (ppm)	$^{234}U/^{238}U$ activity	$^{230}Th/^{238}U$ activity	Raw Age (yr)	$^{230}Th/^{232}Th$ activity	Corrected Age (yr)
	HW05-3 rpt	0.168	1.426 ± 0.004	0.719 ± 0.004	73,080 ± 506	710.5	73,018 ± 574
Hollywood	HW05-4	0.172	1.784 ± 0.005	0.019 ± 0.001	1179 ± 42	14.0	1080 ± 71
Te Ana Puta	TAP05-1	*Abandoned due to extremely high Th concentration. Sample measurement not repeated.*					
	TAP05-2	0.488	1.625 ± 0.004	0.019 ± 0.001	1285 ± 57	6.5	1029 ± 168
	TAP05-3	0.452	1.352 ± 0.004	0.017 ± 0.001	1380 ± 81	22.7	1308 ± 97
	TAP05-4	0.397	1.238 ± 0.005	0.154 ± 0.001	14,385 ± 125	2.4	6763 ± 4912
	TAP05-5	1.377	1.625 ± 0.003	0.012 ± 0.001	821 ± 30	6.9	667 ± 99
	TAP05-6	1.286	1.599 ± 0.003	0.126 ± 0.001	8866 ± 98	3.2	5686 ± 1895
Wazapretti	WZ05-1	0.522	1.780 ± 0.003	0.436 ± 0.001	29,935 ± 107	165.5	29,789 ± 160
	WZ05-2	0.147	1.133 ± 0.002	0.101 ± 0.001	10,122 ± 80	29.0	9685 ± 281
	WZ05-3	0.163	1.434 ± 0.003	0.172 ± 0.001	13,791 ± 82	68.1	13,563 ± 160
	WZ05-4	0.137	1.309 ± 0.002	0.213 ± 0.001	19,219 101	11.9	17,447 ± 1038
	WZ05-4 rpt	0.138	1.311 ± 0.004	0.167 ± 0.002	14,719 ± 216	193	14,654 ± 232

Raw ages for the cores ranged from 821 ± 30 yr B.P. to 143,359 ± 2497 yr B.P. However, all ages were corrected for detrital thorium. An *a priori* estimate of the isotopic (^{230}Th and ^{232}Th) composition of the contaminating phase of 1.5 ± 1.5 was used following the argument presented by Hellstrom (2006). Applying this correction had a substantial impact on many results as ^{230}Th/^{232}Th activity was typically low (Table 5.2). Of 38 analyses, 28 had ^{230}Th/^{232}Th ratios of less than 100 and 12 of those had ratios < 10. The highest ^{230}Th/^{232}Th ratios (~800) were measured in Hollywood Cave cores HW05-1 and HW05-3, while thorium isotope ratios in Te Ana Puta and Eggers Cave cores (with one exception) were the lowest (Table 5.2).

The range of corrected ages of speleothem basal core samples was 667 ± 99 yr B.P. to 100,572 ± 41,558 yr B.P. (all dates are stated with a 2σ error). However, this oldest date was subsequently repeated yielding a younger age of 73,620 ± 655 yr B.P. Fourteen of the 28 basal cores yielded dates within the Holocene. Given the objective of this study to develop a record spanning at least the last glacial coldest period (LGCP) these fourteen stalagmites were not considered for collection. Four stalagmites, including three from Hollywood Cave, had ages clustered around 75,000 yr B.P. and therefore likely contain complete records of the LGCP as well as much of the Otiran. Core WZ05-1 returned an age of 29,789 ± 160 yr B.P. suggesting that this stalagmite may also have captured climate variability throughout the LGCP.

5.1.1.4 Summary

Collection and analysis of basal cores from stalagmites in six South Island caves yielded useful information leading to the selection of whole stalagmites from which to develop a record of past climate covering at least the LGCP. Of the 29 stalagmites cored, four were subsequently collected.

On the basis of Hendy Tests, visual observations and uranium-thorium ages stalagmites HW05-1, HW05-3 and WZ05-1 were deemed most suitable for this study, along with GT05-5 despite its hiatus. Of the two Hollywood Cave stalagmites, HW05-3 was chosen for collection. This decision was based on it being the taller of the two (by 200 mm; Table 5.1), thus providing a potentially higher resolution record. Furthermore, due to its position at the back of a cluster

of taller speleothems, its removal for this study would be far less obvious to regular visitors of the cave than the collection of HW05-1 which stood alone.

When the GT05-5 speleothem was collected the duration of its hiatus was not known and it was thought that a stalagmite from a high elevation cave site within the vicinity of last glacial period glacier margins would be a valuable addition to this study.

During the retrieval of WZ05-1 from Wazapretti Cave mud surrounding the base of the speleothem was excavated. This revealed an extra 200 mm of partially dissolved speleothem calcite was below where the core was drilled. As a result the length of record that could be obtained from WZ05-1 ranged from somewhere in excess of the date of the core material (29,789 ± 160 yr B.P.) to the present day. Unfortunately, due to time constraints, lack of funds and a keener interest in the records from the Hollywood and Ruakuri samples, stable isotope curves were not developed for this stalagmite.

Lastly, in an attempt to have greater geographic coverage and insurance against the others not being as useful as anticipated, a fifth stalagmite EG05-5 (15,244 ± 102 years old), was also collected. Despite not forming during the LGCP, this 480 mm tall stalagmite should allow a detailed examination of late glacial climate on South Island. Furthermore, upon collection and sectioning of the stalagmite it was discovered that there was an extra 50 mm of speleothem growth below where the core had been taken. Therefore, EG05-5 began growing prior to 15,244 ± 102 yr B.P. Visual analysis of the sectioned stalagmite revealed characteristics of rapid calcite precipitation in much of the upper half and it may therefore not be useful for further analysis. However, the lower part appears suitable for further study.

5.1.2 Stalagmite GT05-5

Stalagmite GT05-5 was retrieved from Guillotine Cave, Maruia Valley (Figures 3.1 and 3.3). Four U-Th dates, and the knowledge that the speleothem was actively forming at the time of collection in May 2006, were used to constrain growth history and provide a chronology for palaeoclimate datasets. Activity ratios and calculated ages for U-Th dates are included in Table 5.3.

Table 5.3: Uranium-thorium data for stalagmites collected in this study. All ages are given with 2σ errors. rpt = repeat.

Stalagmite	Depth Below Top (mm)	U (ppm)	$^{234}U/^{238}U$ activity	$^{230}Th/^{238}U$ activity	Raw Age (yr)	$^{230}Th/^{232}Th$ activity	Corrected Age (yr)	Comments
South Island								
EG05-5		0.661	0.970 ± 0.002	0.127 ± 0.001	15,304 ± 86	215.7	15,244 ± 102	Basal core
GT05-5	56		1.155 ± 0.003	0.009 ± 0.001	822 ± 57	7.1	654 ± 182	
	168		1.185 ± 0.003	0.064 ± 0.001	6038 ± 76	7.7	4887 ± 1167	
	197	0.221	1.195 ± 0.002	0.103 ± 0.001	9752 ± 127	17.6	9277 ± 371	
	198	0.131	1.104 ± 0.003	0.823 ± 0.007	143,359 ± 2497	2.0	100,572 ± 41,558	Basal core
	198 (rpt)	0.064	1.151 ± 0.003	0.576 ± 0.003	74,021 ± 543	109.8	73,620 ± 655	Basal core
HW05-3	9		1.752 ± 0.005	0.181 ± 0.003	11,744 ± 171	526.8	11,724 ± 181	
	71		1.744 ± 0.003	0.215 ± 0.002	14,169 ± 114	2082.6	14,162 ± 122	
	130		1.744 ± 0.004	0.239 ± 0.001	15,872 ± 99	948.8	15,857 ± 105	
	151		1.709 ± 0.004	0.315 ± 0.001	21,804 ± 104	13,928.7	21,806 ± 118	
	183		1.714 ± 0.003	0.323 ± 0.001	22,403 ± 102	3345.9	22,398 ± 109	
	219		1.656 ± 0.004	0.367 ± 0.002	26,835 ± 146	4293.1	26,830 ± 158	
	264		1.656 ± 0.004	0.384 ± 0.002	28,161 ± 137	7432.8	28,157 ± 150	
	295.5		1.643 ± 0.004	0.402 ± 0.002	29,913 ± 180	560.1	29,872 ± 199	
	319		1.637 ± 0.003	0.407 ± 0.002	30,494 ± 141	12,850.7	30,499 ± 150	
	341	0.062	1.590 ± 0.005	0.448 ± 0.003	35,236 ± 238	252.8	35,117 ± 266	
	361		1.591 ± 0.003	0.490 ± 0.003	39,033 ± 259	589.5	38,979 ± 282	
	447		1.545 ± 0.005	0.520 ± 0.003	43,435 ± 315	742.2	43,387 ± 351	
	452		1.535 ± 0.004	0.572 ± 0.004	49,163 ± 430	1807.5	49,143 ± 460	
	466		1.513 ± 0.003	0.612 ± 0.002	54,538 ± 237	277.8	54,386 ± 275	
	489		1.490 ± 0.005	0.660 ± 0.004	61,273 ± 451	295.9	61,128 ± 504	
	529		1.489 ± 0.003	0.675 ± 0.003	63,269 ± 367	505.0	63,184 ± 415	

Continued on next page

Table 5.3 (continued)

Stalagmite	Depth Below Top (mm)	U (ppm)	$^{234}U/^{238}U$ activity	$^{230}Th/^{238}U$ activity	Raw Age (yr)	$^{230}Th/^{232}Th$ activity	Corrected Age (yr)	Comments
HW05-3	595		1.465 ± 0.003	0.696 ± 0.003	67,340 ± 341	2052.2	67,317 ± 378	
	627	0.184	1.421 ± 0.003	0.727 ± 0.004	74,607 ± 609	39.6	73,360 ± 1126	Basal core
	627 (rpt)	0.168	1.426 ± 0.004	0.719 ± 0.004	73,080 ± 506	710.5	73,018 ± 574	Basal core
WZ05-1	~610	0.522	1.780 ± 0.003	0.436 ± 0.001	29,935 ± 107	165.5	29,789 ± 160	Basal core
North Island								
RK05-1	0	0.069	1.341 ± 0.002	0.528 ± 0.002	53,145 ± 280	18.3	51,140 ± 1690	
	70	0.099	1.298 ± 0.003	0.590 ± 0.003	64,164 ± 381	11.2	60,259 ± 3103	
RK05-2	0	0.065	1.381 ± 0.003	0.008 ± 0.001	623 ± 51	3.1	450 ± 143	
RK05-3	0	0.023	1.096 ± 0.006	0.305 ± 0.005	35,296 ± 713	1.1	-7.384 ± 16,428	
	29		1.095 ± 0.005	0.071 ± 0.003	7280 ± 275	193.9	7228 ± 279	
	353	0.033	1.130 ± 0.004	0.198 ± 0.002	20,894 ± 269	21.7	19,791 ± 448	
	397	0.040	1.123 ± 0.003	0.317 ± 0.003	35,812 ± 341	153.6	35,568 ± 370	
	551	0.035	1.061 ± 0.004	0.414 ± 0.003	53,479 ± 482	66.5	52,673 ± 570	
	570	0.037	1.088 ± 0.003	0.809 ± 0.004	143,650 ± 1681	3.1	106,154 ± 14,812	
RK05-4	6	0.031	1.067 ± 0.002	0.544 ± 0.003	76,787 ± 550	23.2	73,808 ± 1135	
	48		1.058 ± 0.004	0.526 ± 0.005	74,232 ± 1063	43.3	72,686 ± 1277	
	107		1.052 ± 0.005	0.540 ± 0.005	77,769 ± 1025	19.3	74,148 ± 1613	
	133	0.039	1.057 ± 0.003	0.578 ± 0.004	85,342 ± 936	8.3	76,075 ± 3212	
	146	0.057	1.076 ± 0.003	0.855 ± 0.006	166,531 ± 2864	2.2	102,325 ± 27,941	

Continued on next page

Most of the U-Th samples obtained from GT05-5 suffer from significant contributions of detrital thorium. This is demonstrated by $^{230}Th/^{232}Th$ activity ratios less than 20 for all samples except the repeat of the basal sample (198 mm; Table 5.3). As a result of the contamination the 2σ errors associated with corrected ages are large (± 4 to 28 %).

As was ultimately recognized from the core sample, stalagmite GT05-5 contains a significant hiatus (Appendix Figure B.2). Using the repeat analysis, deposition terminated 73,620 ± 655 yr B.P., and resumed approximately 64 kyr later during the early Holocene (Table 5.3). Visual analysis of the growth axis did not reveal any evidence for major breaks in deposition during the Holocene. However, this does not exclude the possibility of minor hiatuses being present. For simplicity in constructing the age model for GT05-5 it was assumed that the stalagmite grew continuously from 9277 ± 371 yr B.P. to the present day.

Age versus depth for the Holocene portion of GT05-5 is shown in Figure 5.7. Growth rate shows an accelerating trend throughout, rising from 6.6 mm/kyr in the early part of the record to an average of 86 mm/kyr over the last ~650 years. However, the paucity of dates results in this being necessarily a relatively simple age model. Further dating may yield a more complex history of growth rate changes.

Samples for stable isotope analysis were collected continuously at 0.2-0.25 mm resolution along the entire length of the growth axis. Of these a total of 187 (approximately 1 sample per millimeter) were. The differences in growth rate resulted in a temporal data resolution of ~150 yr, ~40 yr and ~11.5 yr for the periods 9.3-4.9, 4.9-0.65 and 0.65-0 kyr B.P., respectively.

Total variation of $\delta^{18}O$ in GT05-5 over the period of record is 1.81 ‰. However, this value is skewed by an outlier (Figure 5.8). The dataset is more accurately represented by a spread across the narrower range of -4.6 to -5.9 ‰.

It is necessary to consider whether the GT05-5 speleothem $\delta^{18}O$ record was affected by kinetic fractionation. During the precipitation of speleothem calcite several conditions, including rapid degassing of CO_2 from the dripwater and low relative humidity of the cave atmosphere (leading to evaporation of moisture from the dripwater), can lead to a distortion of the climate signal preserved in the $\delta^{18}O$ signature of the dripwater. Hendy (1971) observed that kinetic fractionation is apparent in affected $\delta^{18}O$ records as a close covariance of $\delta^{13}C$ and $\delta^{18}O$ along

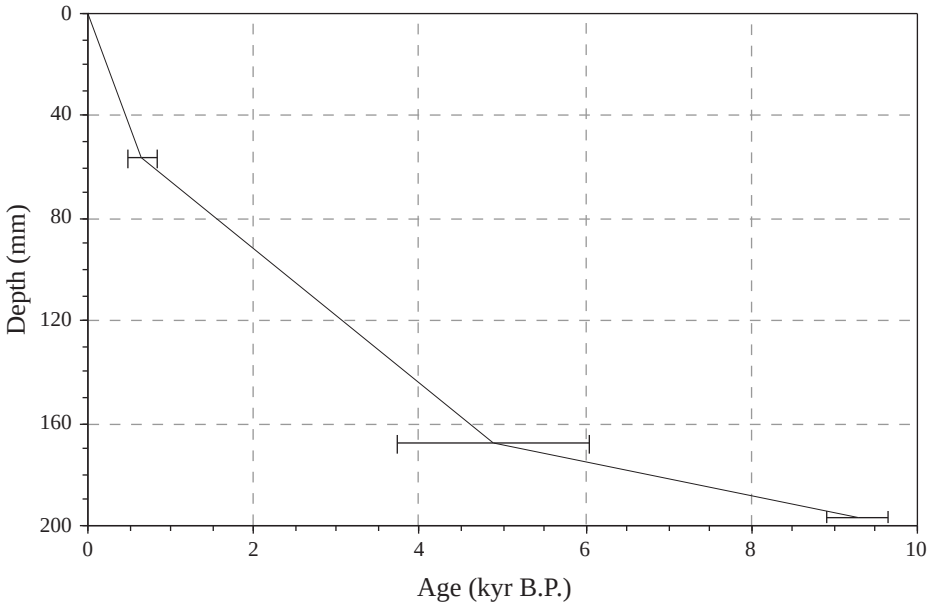

Figure 5.7: Age versus depth (below tip) for stalagmite GT05-5. Linear interpolations are applied between dates (Table 5.3) to create the age model. Dates are shown with 2σ errors.

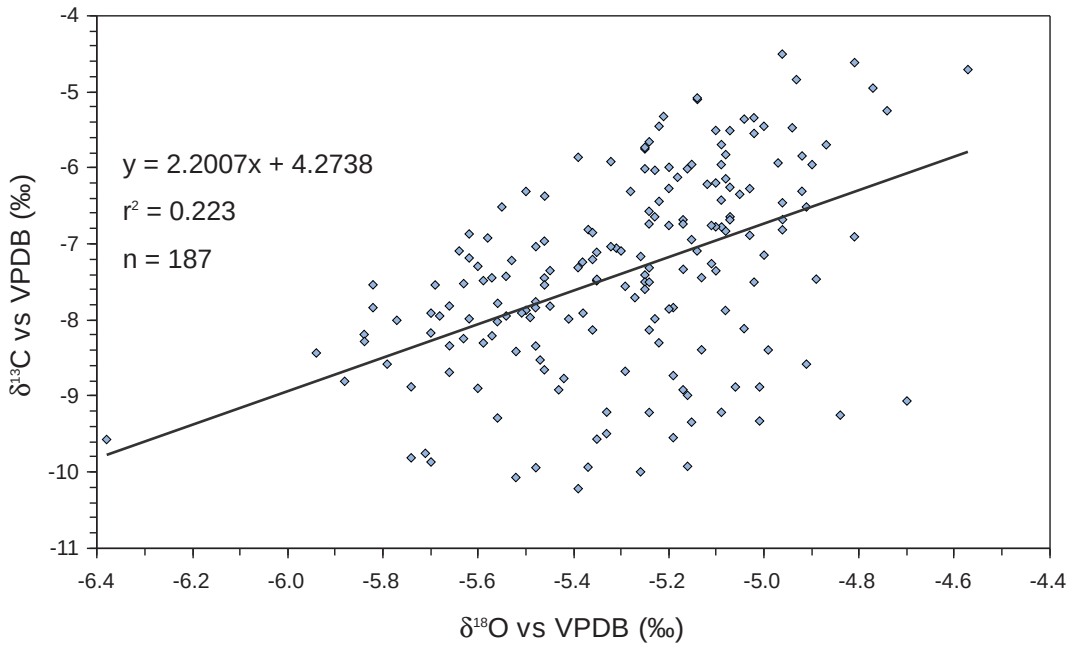

Figure 5.8: $\delta^{13}C$ versus $\delta^{18}O$ in GT05-5. The low correlation ($r^2 = 0.223$) of the data suggests that kinetic fractionation during calcite precipitation was negligible.

both individual layers and the growth axis. Although the GT05-5 core passed the Hendy Test (Figure 5.3) the material analysed was deposited prior to the hiatus. For the Holocene portion of the GT05-5 record, kinetic fractionation was tested for by observing the relationship between $\delta^{13}C$ and $\delta^{18}O$ values of samples collected along the growth axis. While there are broad correlations between GT05-5 $\delta^{13}C$ and $\delta^{18}O$ profiles, a statistical measure of the covariance within the dataset yielded an $r^2 = 0.22$ (Figure 5.8) suggesting the record is free of the effects of kinetic fractionation of stable isotopes.

In Figure 5.9a raw GT05-5 $\delta^{18}O$ data are plotted against the devised age/depth model. Data resolution for the period 9.0-4.85 kyr B.P. is relatively low, however, several broad scale events can be defined. After reinitiation of growth, ~9.3 kyr B.P., $\delta^{18}O$ was constant at -5.20 ‰ until 8.66 kyr B.P. at which time there was an abrupt 0.5 ‰ rise. Within several centuries, $\delta^{18}O$ reached a maximum for the period of record. Values then decreased, and from 7.8-4.8 kyr B.P. $\delta^{18}O$ were mostly within the range -5.0 to -5.1 ‰.

At ~4.6 kyr B.P. there was an abrupt decrease in $\delta^{18}O$ values initiating the first of four prominent, multi-centennial-scale oscillations, each with a magnitude of ~0.4 ‰. The last event terminated within the most recent 100 years of record. Troughs in each cycle occurred at 4.6-3.3, 2.7-2.4, 1.9-1.7 and 0.8-0.15 kyr B.P. and are represented by $\delta^{18}O$ values close to -5.5 ‰.

During the early part of the Holocene, sea level was as much as 40 m below the present level (Lambeck and Chappell, 2001). Therefore an adjustment has been made to the early part of the GT05-5 record to account for an ice volume effect (Figure 5.9b). Using the sea-level record of Lambeck and Chappell (2001) and a maximum sea-level lowering being equivalent to a 1.1 ‰ increase in seawater $\delta^{18}O$ (Duplessy *et al*., 2002; Schrag *et al*., 2002), a correction of ~0.25‰ has been applied to the start of the record. By 5 kyr B.P. the sea level was approximately the same as at present and any further modification of the isotopic composition of the ocean by meltwater input is considered negligible. Therefore no adjustments have been applied to the GT05-5 data that lie within the last 5 kyr of the record.

Carbon isotope ratios in GT05-5 calcite ranged between -10.2 and -4.5 ‰ (Figure 5.8). Values were least negative in the early part of the record and became more negative throughout the Holocene in a stepwise fashion (Figure 5.10).

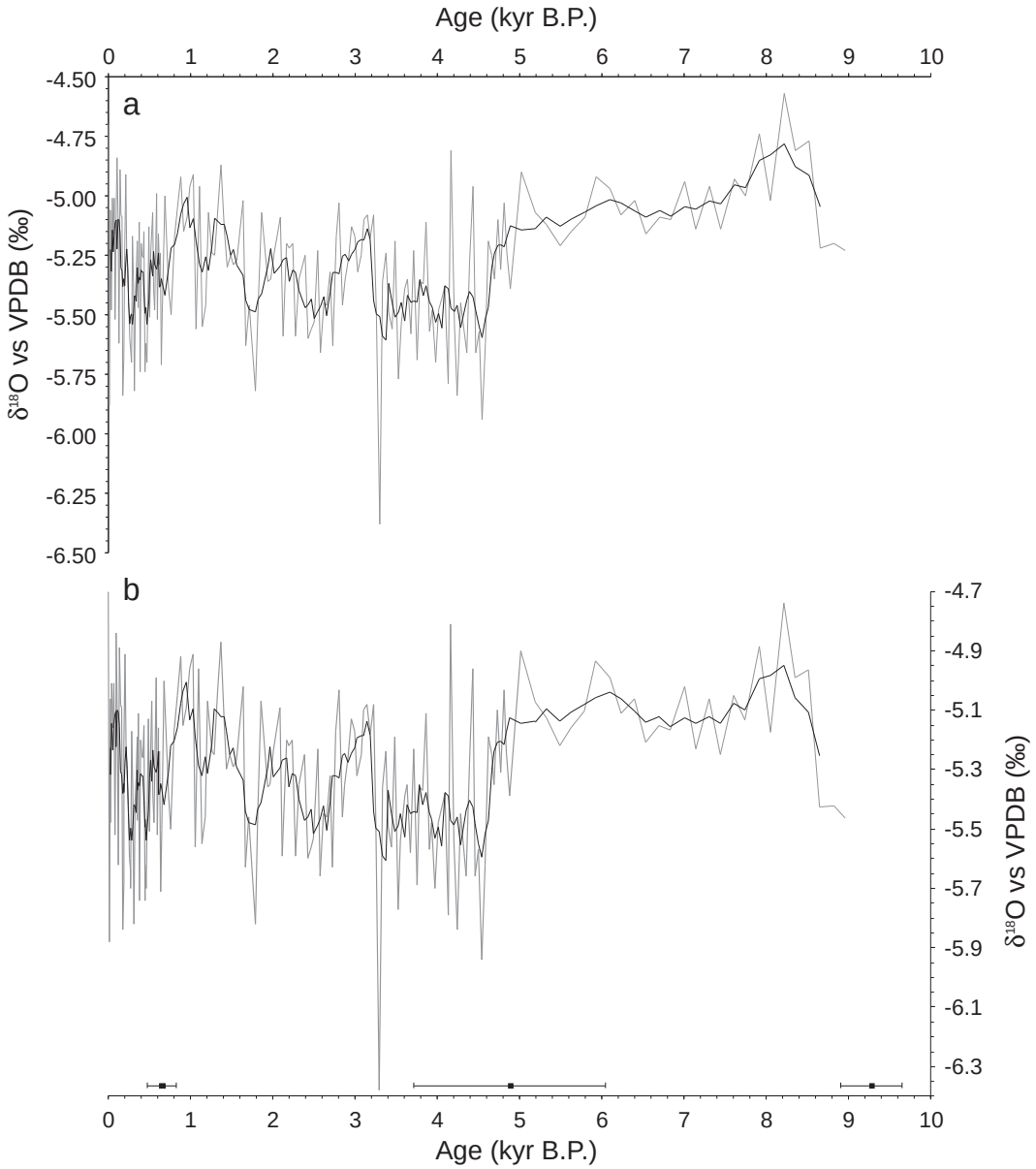

Figure 5.9: GT05-5 oxygen isotope profile. Shown are (a) raw data, and (b) ice volume adjusted data (from 5-9.3 kyr B.P.). In each, grey lines represent individual data points and black lines are 5 point running means of the data. U-Th dates are displayed as black squares with 2σ error bars.

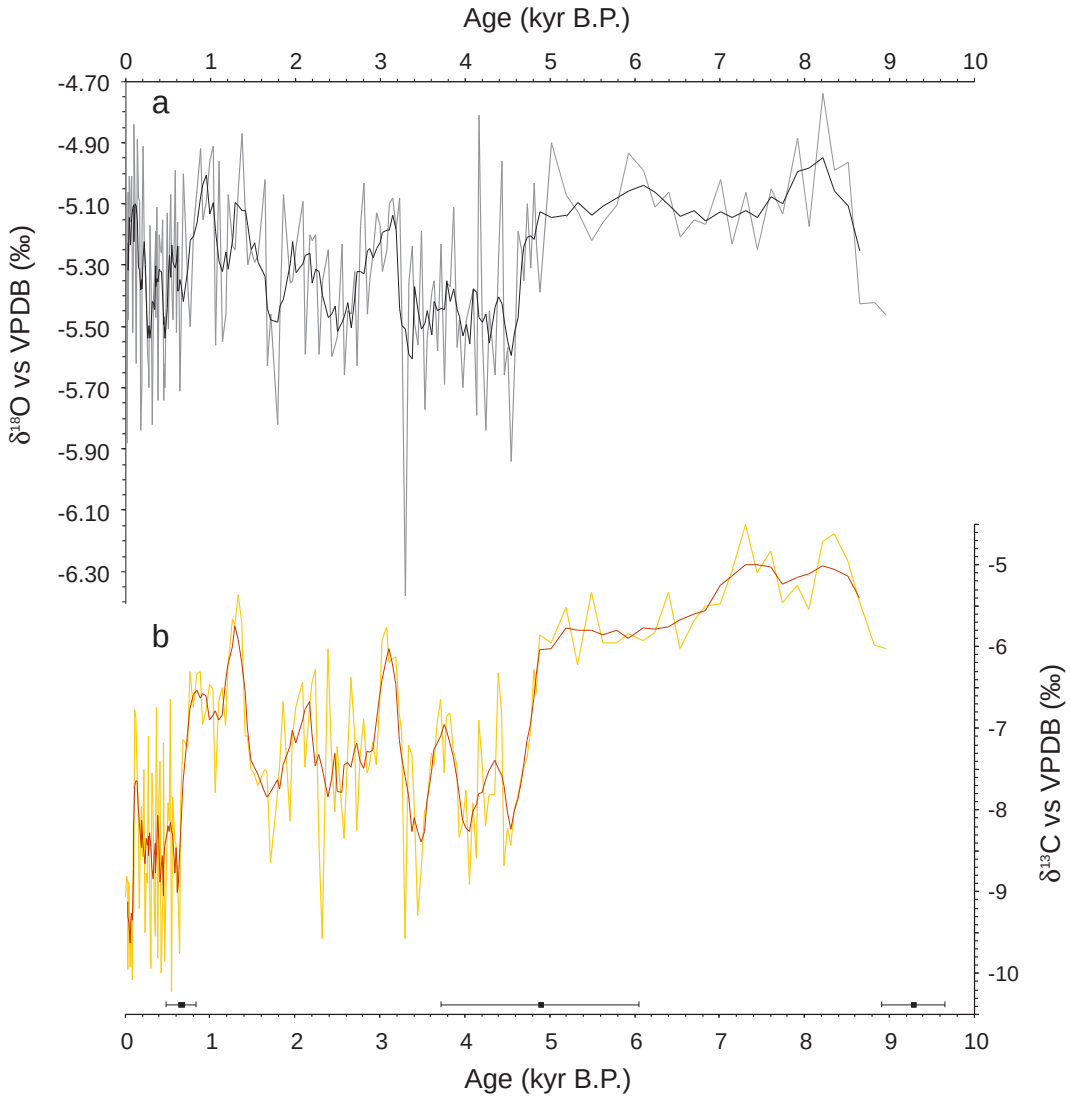

Figure 5.10: (a) $\delta^{18}O$ and (b) $\delta^{13}C$ profiles for stalagmite GT05-5. Note that the $\delta^{18}O$ profile is that adjusted for the ice volume effect (as in Figure 5.9b). U-Th dates are displayed as black squares with 2σ error bars.

Significant steps occurred at 4.8, 0.7 and 0.1 kyr B.P. The first two of these changes was synchronous with prominent decreases in the $\delta^{18}O$ record, but the most recent is associated with a rise in $\delta^{18}O$. There is further agreement between proxies at the millennial-scale, with peaks at 1.3-1.4, 1.9-2.2, 3.0-3.2, 3.6-3.9, 7.1-7.6 and 8.2-8.5 kyr B.P. common to both records (Figure 5.10).

5.1.3 HW05-3

The 627 mm tall stalagmite HW05-3 (Figure 5.11) began to form ~73 kyr B.P. (Table 5.3). Precipitation of calcite on HW05-3 continued until shortly after 11,720 ± 183 yr B.P. However, the stalagmite was obtained on the basis that it was still active. Drips were observed falling onto the stalagmite tip during coring and collection of the stalagmite. Either a significant hiatus exists at the top of HW05-3 or the dripwater pCO_2 is balanced with that of the cave atmosphere leading to no calcite precipitation (and no erosion either).

Eighteen uranium-series dates were used to create a growth history for HW05-3 (Table 5.3; Figure 5.12). All of the dates were in sequence. Age errors (2σ) are small with all but one being less than ± 1.0 % of the corrected age. Uranium concentrations within the speleothem calcite are relatively low and fall within the 50-200 ppb range. Therefore small age errors are primarily a result of the calcite being free of detrital material as shown by $^{230}Th/^{232}Th$ activity ratios between 250 to ~14,000 for all samples. The thorium activity ratios measured from HW05-3 calcite are considerably greater than any other speleothem obtained for this study (Table 5.3).

The acquired ages demonstrate that growth rate varied during the formation of HW05-3 (Figure 5.12b). Calcite accumulated at rates less than 10 mm/kyr throughout much of its formation. Minimum growth rates occurred during the period 49.1-43.4 kyr B.P. when they were as low as 0.8 mm/kyr. However, during the periods 67.3-61.1, 43.4-39.0, 30.5-26.8, 22.4-21.8 and 15.9-11.4 kyr B.P. growth rates were much greater, as much as 54 mm/kyr.

From these results it can be seen that growth rates differed between last glacial period stadials MIS4 and MIS2. During MIS4 growth rates increased (16-

Figure 5.11: Photograph of stalagmite HW05-3. The straight cut at the base was created when drilling the core.

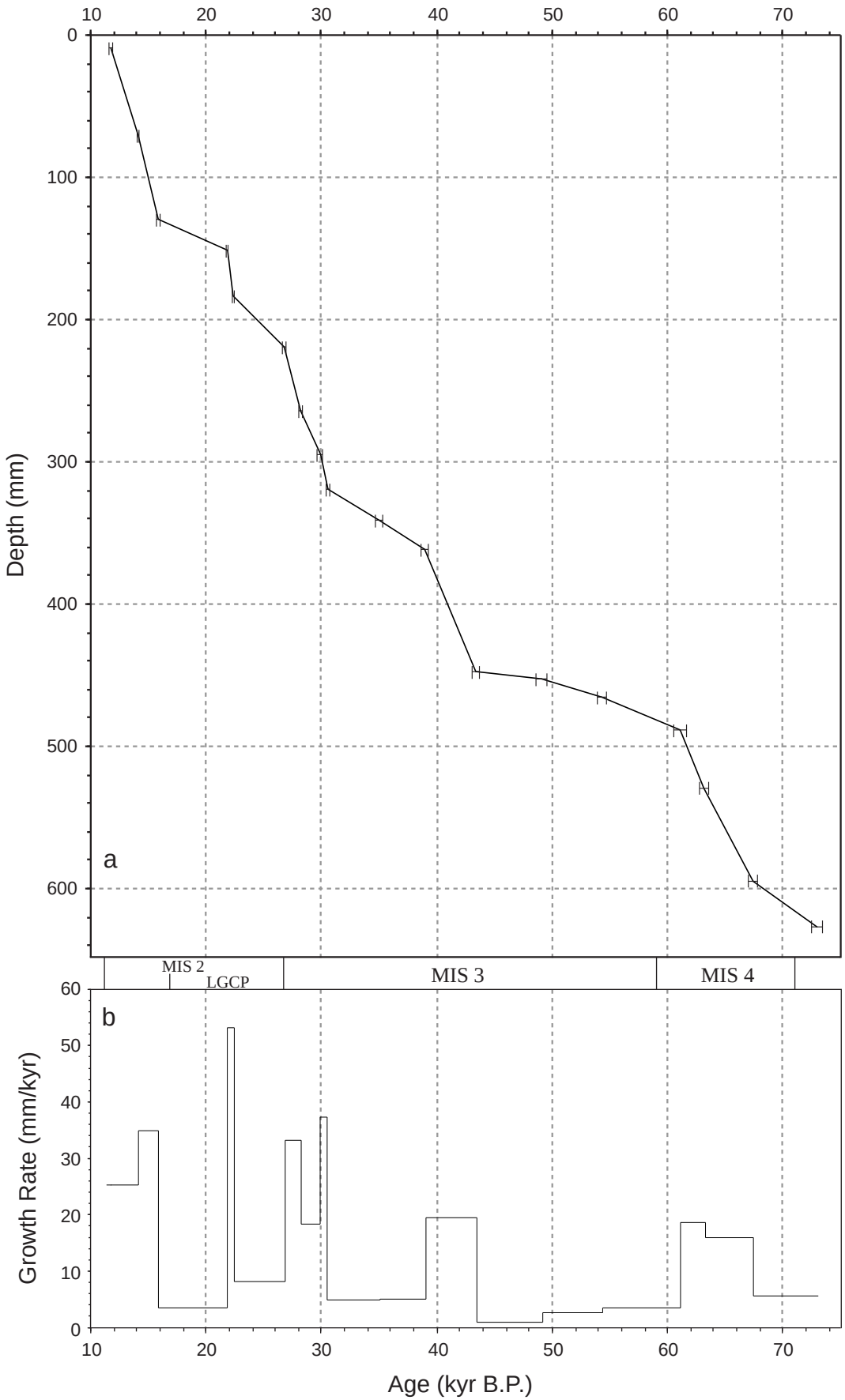

Figure 5.12: (a) Age versus depth and (b) growth rates for stalagmite HW05-3. Dates are shown with 2σ errors.

18 mm/kyr) from the background, but during much of MIS2, calcite accumulated at rates < 10 mm/kyr.

A total of 720 calcite samples from HW05-3, each representing ~0.2 mm of deposition along the growth axis, were submitted for stable isotope analysis. This yielded a resolution of 1 sample per millimeter except for depth interval 440-470 mm for which every collected sample was submitted, providing continuous results. As a result of this sampling strategy the temporal data resolution ranged between 20 and 290 years.

The paired $\delta^{18}O$ and $\delta^{13}C$ results were used to test for non-equilibrium fractionation of isotopes during the precipitation of HW05-3 calcite (Figure 5.13). A positive correlation was observed between stable isotope pairs ($r^2 = 0.427$), with the slope of the regression between the datasets being ~1.6. While a moderate correlation could be the result of kinetic fractionation it could also result from common forcing of variability of both isotope ratios (e.g. by climate; Treble *et al*., 2005). Therefore it is not possible to make a judgment based solely on the strength of the correlation. It has been calculated that under non-equilibrium conditions enrichment of $\delta^{13}C$ occurs 3 times more rapidly than the enrichment of $\delta^{18}O$ in speleothem calcite (Hendy, 1971). Such a relationship is roughly twice as large as the slope of the regression in the HW05-3 dataset. This would tend to support a shared driver of stable carbon and oxygen isotope variability rather than kinetic fractionation.

The HW05-3 $\delta^{18}O$ record extends from 73.22 to 11.37 kyr B.P. (Table 5.3). Raw $\delta^{18}O$ values ranged between about -1.2 and -4.6 ‰. The most negative values occur during the periods 67.3-61.3, 25.6-24.4, 22.5-21.5, 20.1-19.9, 15.8-15.4 and 14.1-14.0 kyr B.P. (Figure 5.14a). The earliest of these periods, which coincides with MIS4, is well defined by a sharp onset and even more abrupt termination. The periods 35.3-33.4, 32.2-31.1, 12.5-12.0 and 11.8-11.37 kyr B.P. display the least negative values (-1.9 to -3.0 ‰). While millennial-scale variability is common throughout the record it is most noticeable in the interval 35.3-26.4 kyr B.P. which is characterized by frequent, large (> 1 ‰) events.

Throughout the period of time represented by this record there were significant changes in ice volume and sea level (Lambeck and Chappell, 2001; Siddall *et al*., 2003). In Figure 5.14b the raw $\delta^{18}O$ values have been replotted following an adjustment for changes in ice volume represented by the global sea

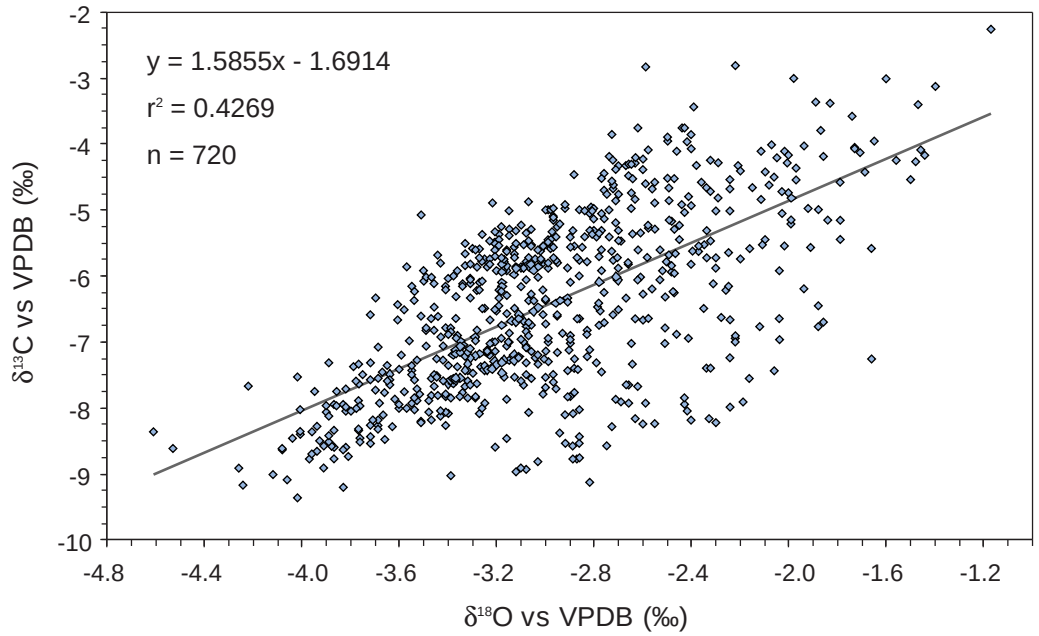

Figure 5.13: $\delta^{13}C$ versus $\delta^{18}O$ in HW05-3. The spread data yields a significant positive correlation ($r^2 = 0.427$) displaying a linear trend with a slope of ~1.6. If non-equilibrium fractionation occurred during precipitation of calcite on stalagmite HW05-3, a slope of ~3 would be anticipated.

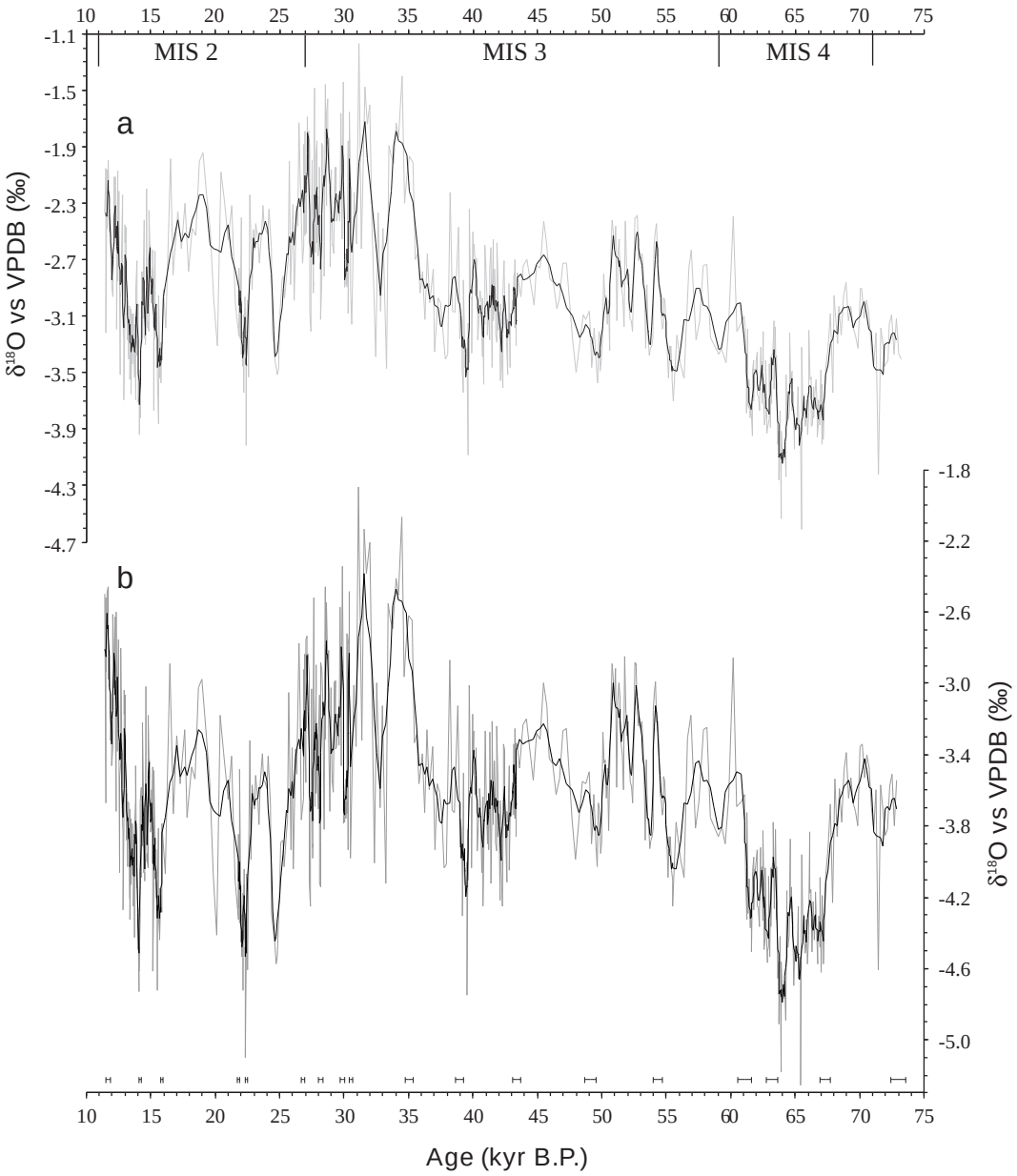

Figure 5.14: $\delta^{18}O$ profile for stalagmite HW05-3. Displayed are (a) the raw data (gray line) with 5-point running mean (black line), and (b) the ice-volume adjusted data (gray line) also with a 5-point running mean (black line). Ice volume correction is applied using sea level data presented in Lambeck and Chappell (2001) and the assumption that maximum sea level lowering was equivalent to a 1.1 ‰ change in sea water $\delta^{18}O$. U-Th dates, including 2σ errors, are represented by bars at the base of the figure.

level curve developed by Lambeck and Chappell (2001). Corrections for the ice volume effect range between -0.37 and -1.10 ‰ (Appendix E). The largest adjustments correspond with the LGCP. The changes have the effect of amplifying many of the relative changes in the HW05-3 record, although the total range of $\delta^{18}O$ values decreases slightly from 3.44 to 3.35 ‰.

Stadials MIS 2 and MIS 4 in the HW05-3 $\delta^{18}O$ profile have different isotopic signatures. The earlier MIS 4 was characterized by $\delta^{18}O$ values in the range -4.0 to -4.8 ‰, while values in MIS 2 were generally between -3.0 and -3.8 ‰, excepting several brief negative excursions noted earlier.

Measured $\delta^{13}C$ in the 720 HW05-3 samples fell in the range -9.4 to -2.3 ‰. Variability in carbon isotope profile broadly paralleled changes in $\delta^{18}O$ values, by displaying relatively negative ratios from 67.3-61.3 followed by an abrupt increase to a broad interval of enriched $\delta^{13}C$ values spanning the period 61.3-16.6 kyr B.P. (Figure 5.15). Between 16.6 and 12.8 kyr B.P. the $\delta^{13}C$ values decreased again prior to a rise at the end of the record. However, as well as the similarities to the $\delta^{18}O$ record there were also some noteable differences. Firstly, in the early part of the record (72.2-67.3 kyr B.P.) $\delta^{13}C$ values of -6.5 to -9.3 ‰ were relatively more negative than corresponding values in the $\delta^{18}O$ record. Secondly, during the period 30.9 to 30.5 kyr B.P. $\delta^{13}C$ displayed a sharp decrease from -2.83 to -8.45 ‰ succeeded by a general increasing trend to values close to -5 ‰ at 16.5 ka. Thirdly, there was a significant negative excursion in $\delta^{13}C$ from 12.2 to 11.8 kyr B.P. which did not appear in the $\delta^{18}O$ record.

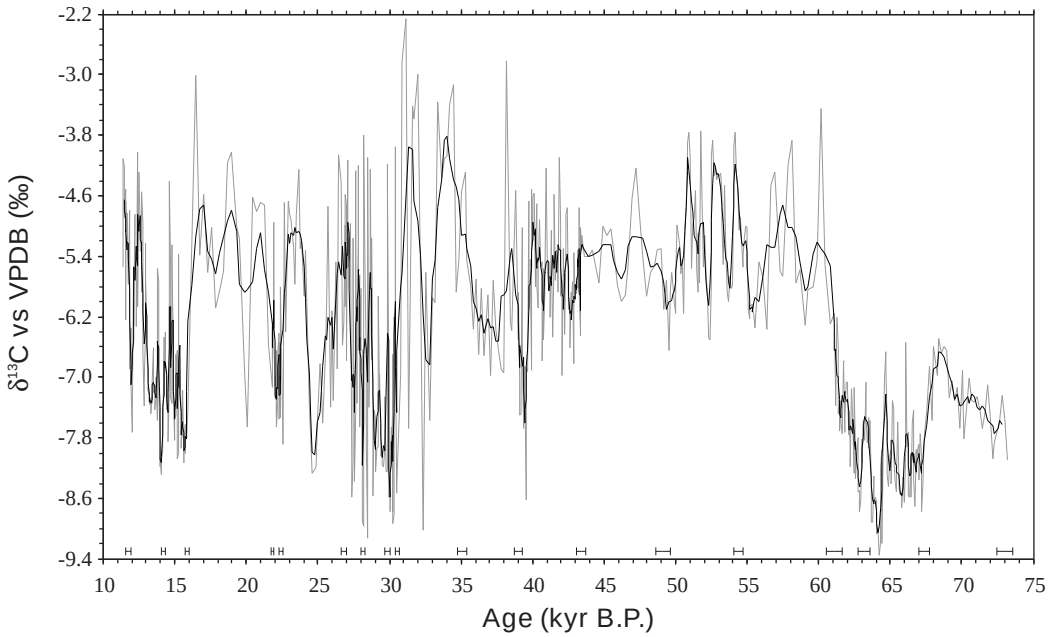

Figure 5.15: $\delta^{13}C$ profile for stalagmite HW05-3. U-Th age data are shown with 2σ error at the bottom of the figure.

5.2 Ruakuri Stalagmites

5.2.1 RK05-1

Stalagmite RK05-1 formed at the back of Holden's Cavern, Ruakuri Cave (Figures 3.1 and 3.6). The stalagmite has a rough surface and much of it is friable and porous. This indicates that the calcite from which it was formed was either precipitated rapidly (potentially as a result of drafty conditions or low humidity of the cave atmosphere) or has suffered post-depositional alteration. However, at the base of the stalagmite there is ~ 70 mm (height) of dense, finely laminated, crystalline calcite. Unfortunately, due to an error of judgment when sectioning the stalagmite this material was cut in two. This resulted in approximately 2 mm (46-48 mm depth) being lost from the RK05-1 record.

Two uranium-series ages (60,259 ± 3103 and 51,140 ± 1690 yr B.P.), one each from the topmost and bottommost layers of the stalagmite (Table 5.3), were used to create a simple chronology for the RK05-1 stable isotope and trace element records. Linear interpolation between the dates yields a growth rate of 7.8 ± 1.2 mm/kyr, and allows limited depth-to-age conversions to be made. Further dating of RK05-1 may yield a more complex growth history.

Uranium concentrations of the dated samples were less than 100 ppb. This is common for speleothems obtained from caves in the Waitomo district (Table 5.3; Williams *et* al., 2004). In addition there was significant contamination by detrital thorium. These two properties led to relatively high 2σ errors (± 3-5%) in the acquired dates.

Two separate layers of RK05-1 calcite were subject to the Hendy Test (Figure 5.16a,b). Each layer was followed for > 35 mm from the growth axis. Values for $\delta^{18}O$ remain almost unchanged, and no discernible trend was apparent when $\delta^{13}C$ is plotted against $\delta^{18}O$. These results indicate that at least these layers, if not the whole stalagmite, were deposited under isotopic equilibrium conditions.

Of the 295 samples collected along the growth axis, 68 were analyzed for stable isotope ratios. This yields a data resolution of one sample per millimeter, equivalent to ~130 years temporal resolution over the entire record.

To further investigate isotopic equilibrium conditions during the deposition of the 70 mm of crystalline calcite in RK05-1, $\delta^{13}C$ was plotted against $\delta^{18}O$ (Figure

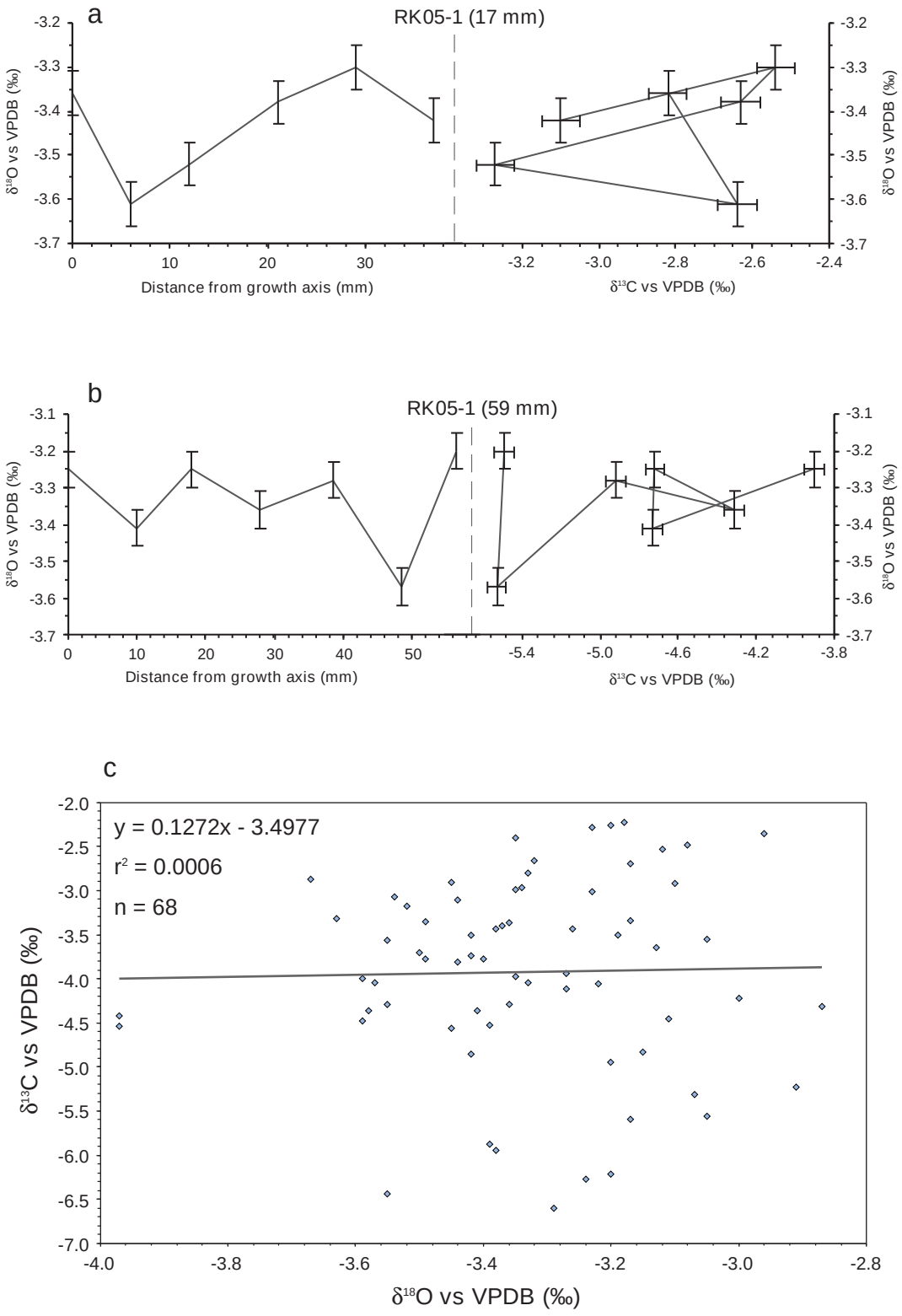

Figure 5.16: Testing for kinetic isotope fractionation in Ruakuri Cave stalagmite RK05-1. Hendy Tests along (a) a layer 17 mm below the stalagmite tip, and (b) a layer 59 mm below the tip both suggest that kinetic effects are unlikely to affect RK05-1 $\delta^{13}C$ and $\delta^{18}O$ profiles. A third test (c) displays isotope ratios of calcite obtained from a 68 mm long transect of the growth axis. No correlation between $\delta^{13}C$ and $\delta^{18}O$ supports the results of the Hendy Tests that kinetic isotope fractionation is negligible in RK05-1.

5.16c). There is almost no relationship between the two proxies ($r^2 = 0.0006$), a strong indication that isotopic equilibrium was maintained throughout the period of deposition.

Total variability in $\delta^{18}O$ is 1.10 ‰ around a mean of -3.33 ‰. The least negative values occur in the early part of the record (60-56.5 kyr B.P.). Some minor millennial-scale variability is apparent during this time. Between 56.5 and 54.5 kyr B.P. values decreased ~0.6 ‰ before beginning a steady rise of 0.5 ‰ which terminated at the end of the record (Figure 5.17a).

Oxygen isotope ratios in RK05-1 calcite were influenced by changes in ice volume. Lambeck and Chappell (2001) suggested that sea levels were 52-70 m below present during the period 50-62 ka. Assuming that maximum sea level lowering (~140 m) raised the $\delta^{18}O$ of ocean water by 1.1 ‰ parts of the RK05-1 record must be adjusted by -0.41 to -0.55 ‰ (Figure 5.17b). Other than shifting the curve toward more negative values there is little other effect of the correction on the data with relative differences not exceeding 0.14 ‰.

Carbon isotope ratios in RK05-1 calcite fall within the range -2.2 to -6.6 ‰. This is lower than the calculated values of -11 to -13 ‰ for the first calcite to be precipitated on modern speleothems (Hendy, 1971). Values were most negative (~-5.3 ‰) during the period 60-57.5 kyr B.P. (Figure 5.18a). This was followed by an increase of ~3.25 ‰ which occurred in a little under a millennium. There were further millennial-scale changes of 1-1.5 ‰ in the remainder of the record.

It is conspicuous that the large shift in $\delta^{13}C$ values occurred at the point at which the speleothem was cut in two. It is also noteworthy that the sample material obtained from the older part of RK05-1 is from the growth axis, while the angle of cut in the younger block resulted in samples being collected perhaps as much as 10 mm from the growth axis. Despite this distance from the growth axis the sample material was still on the upper surface of the speleothem and not the flank. Furthermore, as demonstrated by the Hendy Test result there is no evidence for enrichment of $\delta^{13}C$ with distance from the growth axis.

The lower section (0-22 mm) of RK05-1 was analysed for its trace element composition. A 38 mm track was drawn from the base of the speleothem (age ~60.3 kyr B.P.), where the lowermost isotope sample had been collected, diagonally up through the growth layers. The purpose of the diagonal track was to allow greater data resolution than the vertical 22 mm track sampled for isotopes.

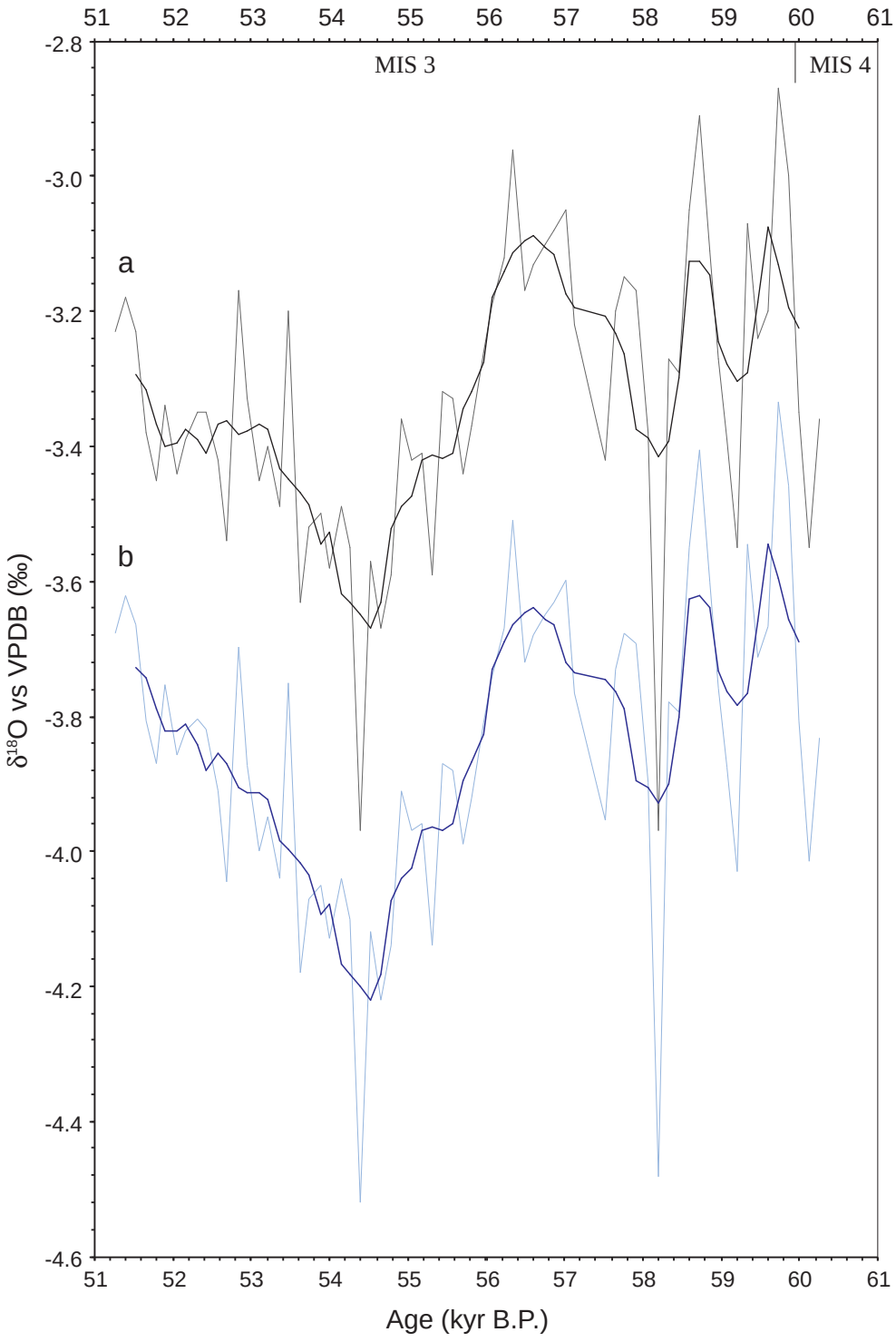

Figure 5.17: Oxygen isotope data for stalagmite RK05-1. Both the raw data (a) and the ice-volume adjusted data (b) are shown. Each profile also displays a 5-point running mean of the data (black line). Relative adjustments are based on sea level data from Lambeck and Chappell (2001) and maximum sea level lowering being equivalent to a shift of 1.1 ‰ in sea water $\delta^{18}O$.

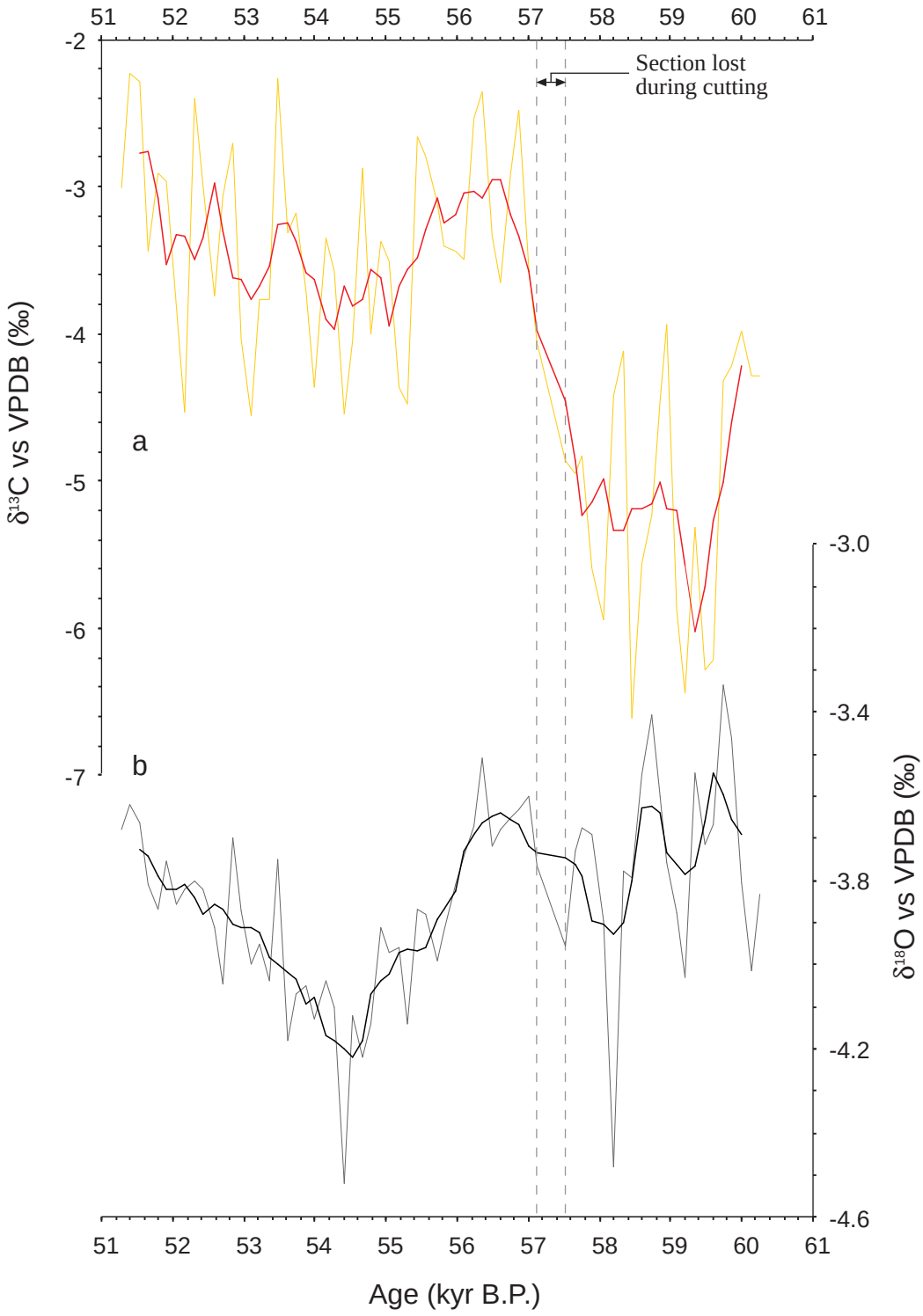

Figure 5.18: $\delta^{13}C$ and $\delta^{18}O$ profiles for stalagmite RK05-1. Note that the $\delta^{18}O$ profile is drawn using the ice-volume adjusted data.

Analysis by laser ablation was conducted twice. The first pass was a line of spots at 2 mm resolution. Having discrete sampling locations allowed the data to be imported into the GLITTER software application, and absolute concentrations to be calculated (Appendix I). Variations in the elements measured (Mg, Sr, Ba, U, Th, P and Na) are shown in Figure 5.19 with the exception of Th which was present at concentrations below detection limits at almost every sampling location. The concentration of uranium varied between 73 and 124 ppb. These values match well with those obtained from the U/Th samples (Table 5.3) and other New Zealand speleothems (Hellstrom and McCulloch, 2000; Williams *et al*., 2005). Barium, strontium, phosphorous and magnesium are present in concentrations of 10-15, 60-75, 200-450 and 500-700, ppm respectively. The range of variability in the concentration of these elements is also comparable to other New Zealand data (Hellstrom and McCulloch, 2000).

Although only a small dataset, it is possible to investigate correlation between changes in element concentrations. The strongest relationships occur between P and Sr ($r = -0.66$) and Sr and Ba ($r = 0.62$).

The second pass along the transect was a continuous line scan from 2 to 38 mm. A total of 1656 measurements were made, yielding data resolution of 22 μm (potentially a temporal resolution of ~3 years). Element concentrations could not be calculated from this dataset by the GLITTER software application. Instead raw counts were manually adjusted by first subtracting the background and then dividing by the abundance of the measured element (e.g. ^{42}Ca accounts for 0.65 % of all Ca). From these data element-to-calcium ratios have been calculated (Figure 5.20). The element-to-calcium ratios determined from the line-scan data do not agree within error with the same ratios calculated from the spot data. Furthermore, the offset between the two results is not consistent. This could be a result of the low counts (relative to background) obtained for several of the elements measured in the line scan.

High-frequency variability marks each dataset. A nine-point running mean has been used to smooth the data slightly. From these curves it can be seen that the elements split into two groups. In the first group are Na, Mg, Ba and U. They each show relatively constant base levels interspersed with peaks in intensity. Layers at 5-6, 22-24 and 29 mm show up as having increased abundances in both Mg and Ba. The strength of the relationship between the Mg and Ba nine-point

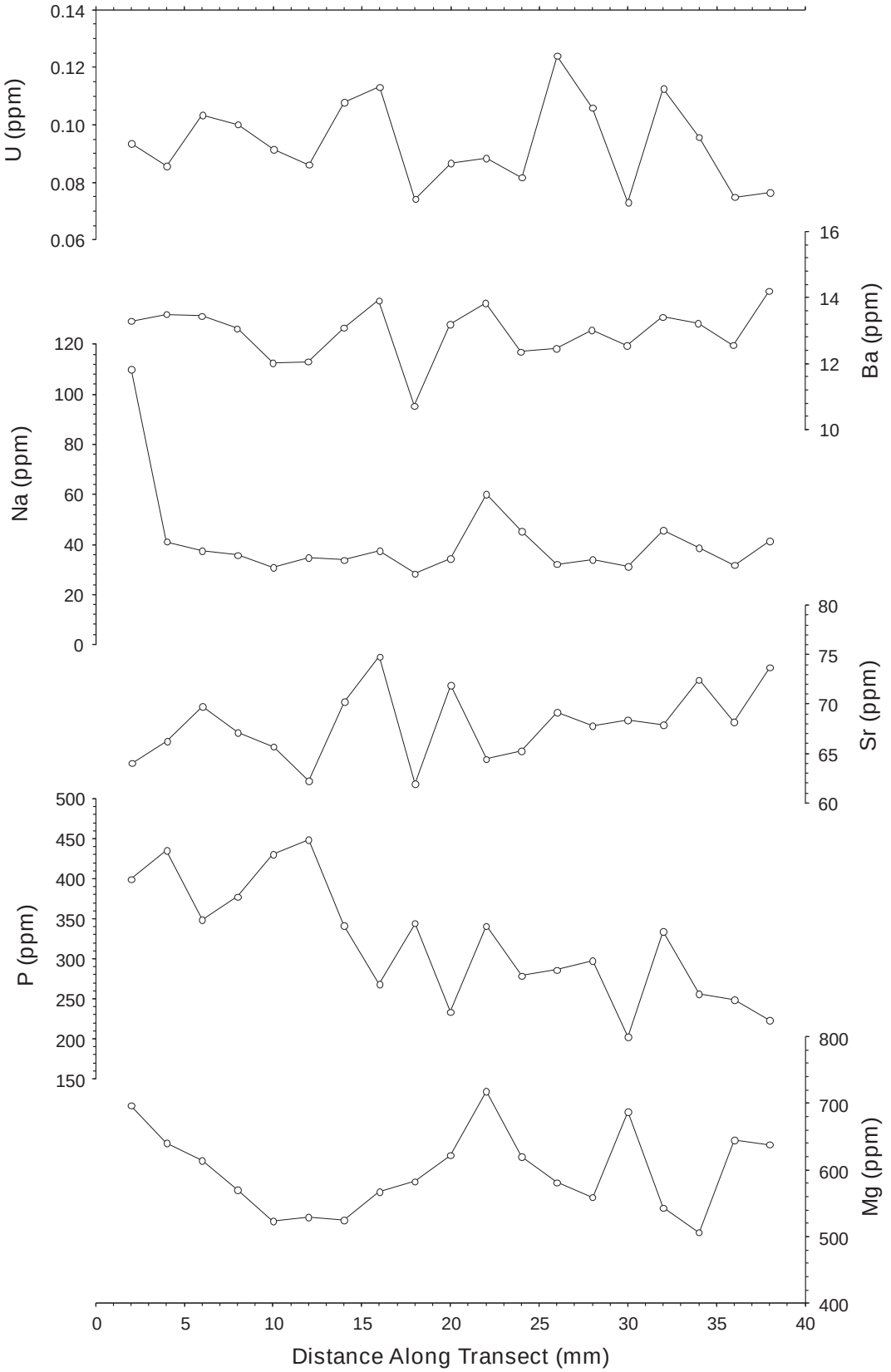

Figure 5.19: Minor and trace element concentrations in RK05-1 calcite as determined by laser ablation ICP-MS. A line of spot analyses were conducted at 2 mm intervals along a 36 mm transect on the basal portion of the stalagmite.

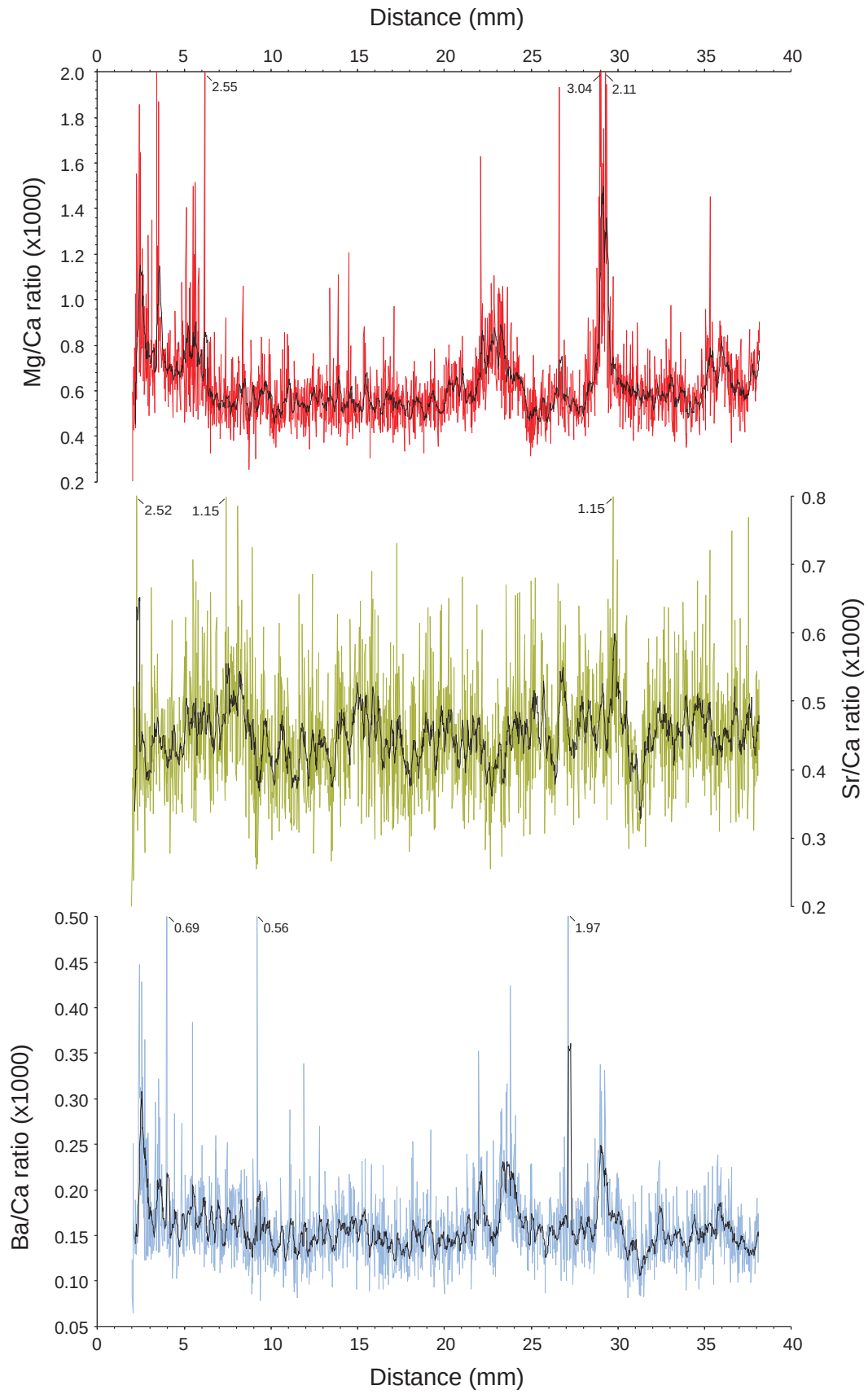

Figure 5.20: Minor and trace element-to-calcium ratios in stalagmite RK05-1. Each dataset shows the raw data and a 9-point running mean (equivalent to 0.2 mm along the transect).

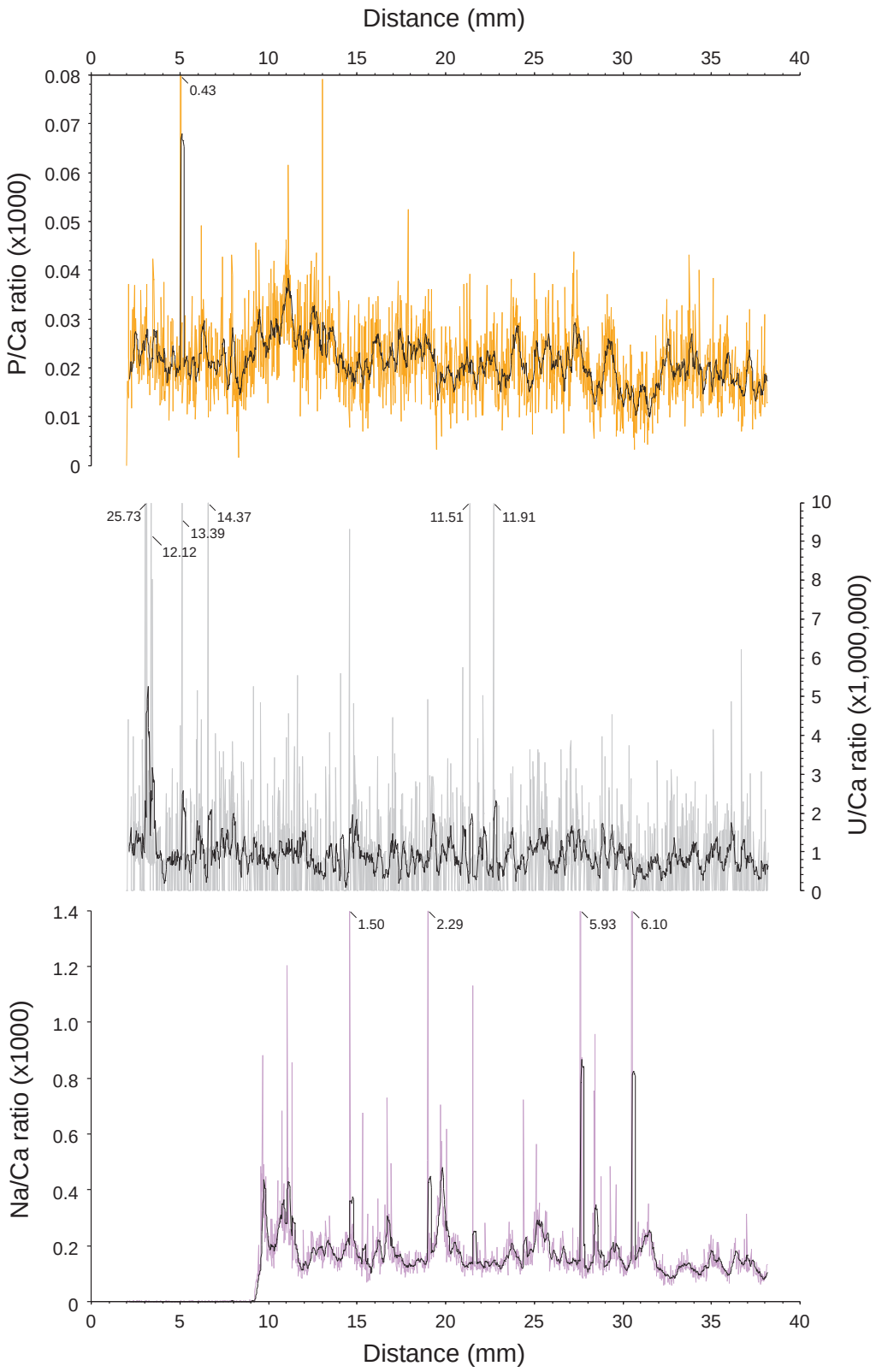

Figure 5.20 (continued)

running means is r = 0.53. The second group of elements is composed of Sr and P. This group appears to oscillate around a long-term linear trend. In the case of P the trend is toward lower values with age, while the opposite is true for Sr; this result is in broad agreement with the spot data (Figure 5.19).

5.2.2 RK05-2

Stalagmite RK05-2 was collected from approximately the same location as RK05-1 in Holden's Cavern. As with RK05-1 it was discovered that much of the structure was composed of porous and friable carbonate material (Figure 5.21). The sample was not suitable for palaeoclimate research. Nevertheless a U/Th date of 450 ± 143 yr B.P. was obtained from crystalline calcite deposited on the outer surface (Table 5.3).

5.2.3 RK05-3

The speleothem sample RK05-3 is a 570 mm tall stalagmite from the 'drum' entrance to Ruakuri Cave (Figures 3.1 and 3.6). Prior to the excavation of this entrance the passageway in which RK05-3 was deposited was a dead-end, and partially filled with sediment. RK05-3 was buried beneath laminated sediments when recovered in March of 2005. Unfortunately the depth of sediment was not recorded. Nevertheless it can be assumed that the speleothem was not recently active.

Six, in-sequence, uranium-series ages were obtained from RK05-3 calcite (Table 5.3). Samples from the tip and the base contained very low $^{230}Th/^{232}Th$ ratios (1.1 and 3.1 respectively) and as a result the calculated ages have large 2σ errors. The problem caused by the contaminant thorium was also compounded by low (< 100 ppb) uranium concentrations in each sample. However, the remaining ages have thorium isotope ratios as high as 193.9 yielding increased precision in the corrected age. Therefore only the ages of the middle four samples were used to develop a chronology for RK05-3 stable isotope profiles (Figure 5.22). It is estimated that RK05-3 started growing 54 kyr B.P. and finished ~6 kyr B.P.

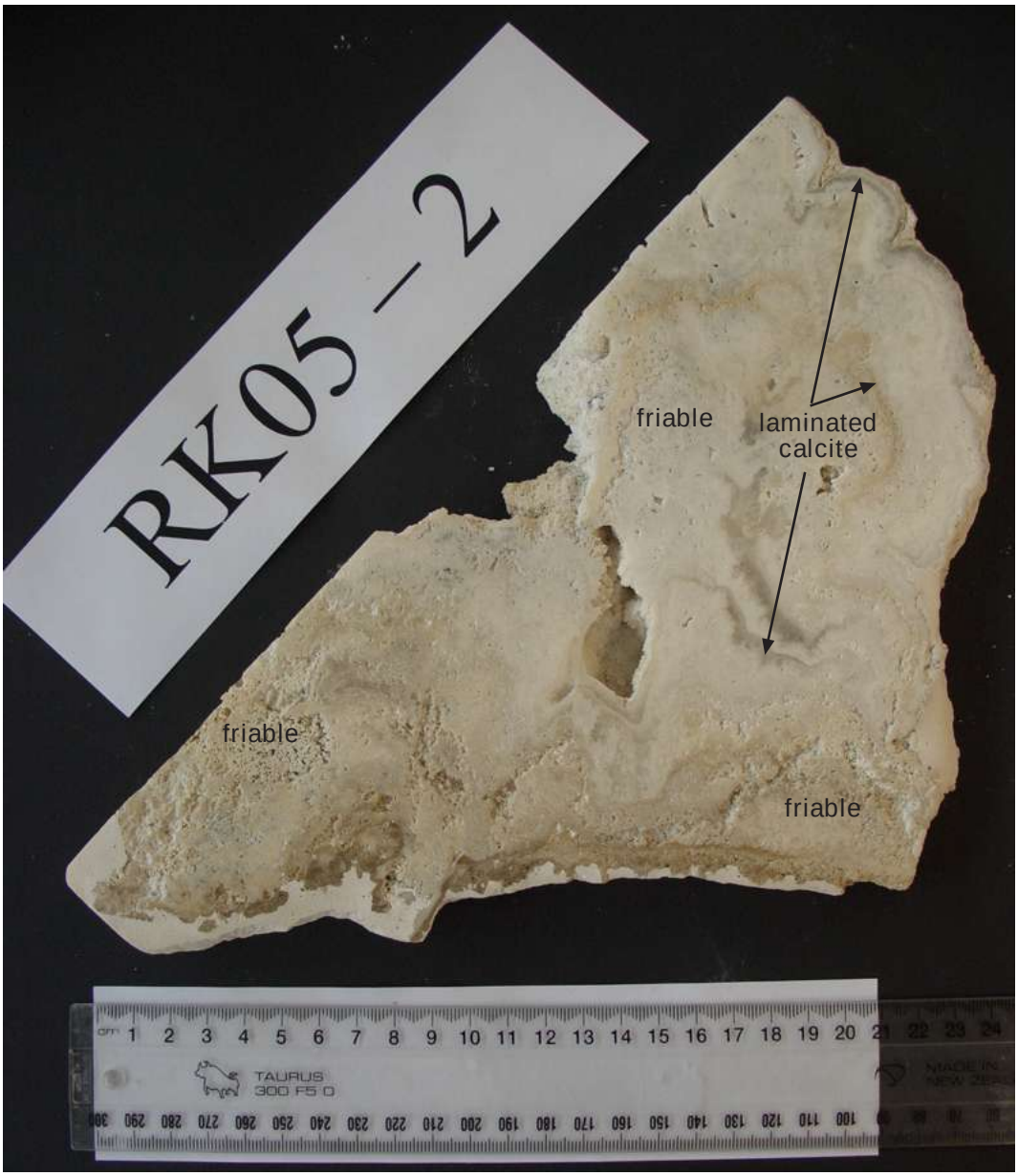

Figure 5.21: Photograph of stalagmite RK05-2 after being cut in half. It is not possible to define a clear growth axis (or axes) for this stalagmite due to the poor, or non-existent, definition of individual calcite layers. RK05-2 most likely formed under conditions that allowed evaporative water loss during calcite precipitation.

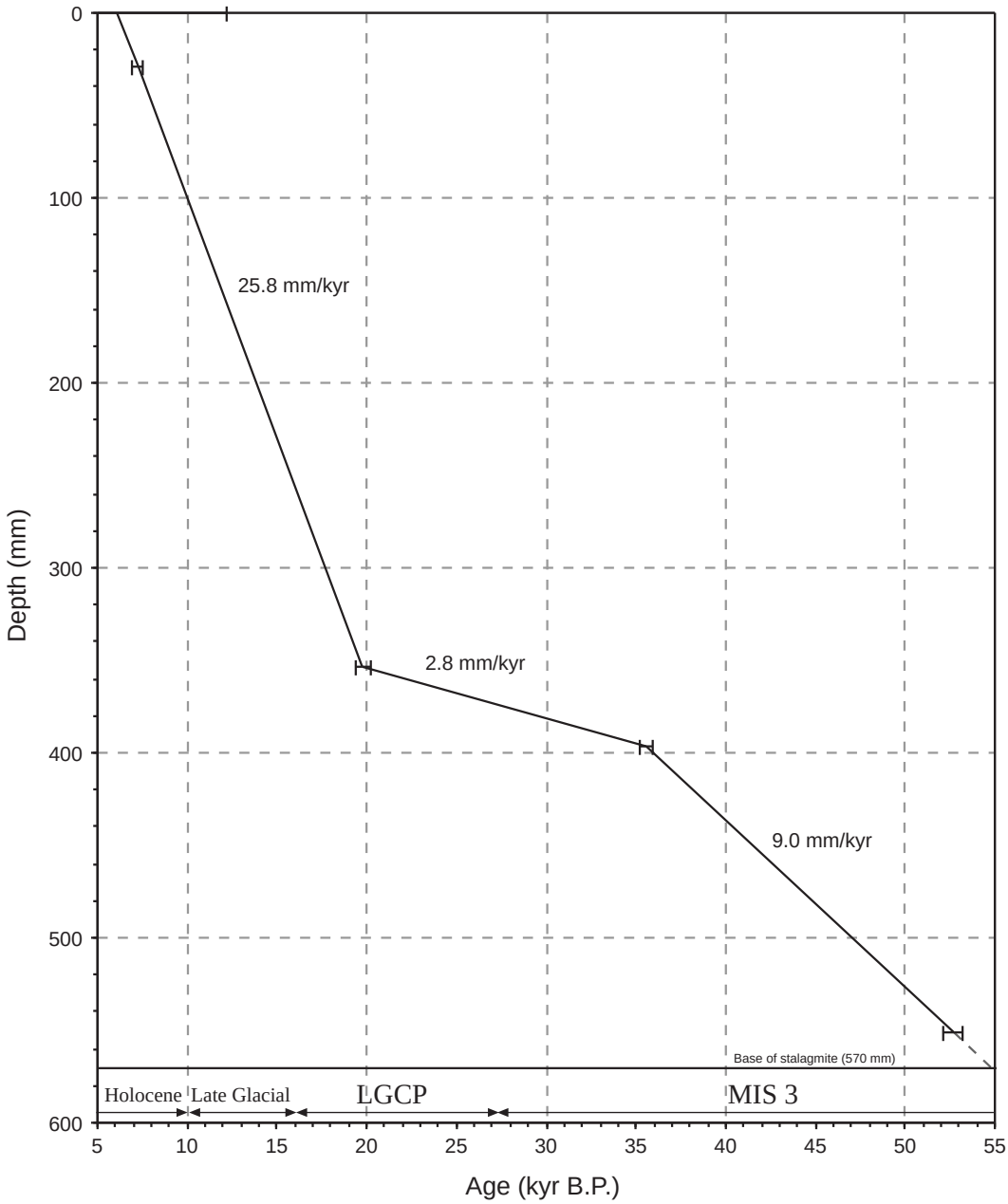

Figure 5.22: Age versus depth for Ruakuri Cave stalagmite RK05-3. Linear interpolations are applied between all dates (except the uppermost 29 mm) to create an age model. All dates are shown with 2σ errors. Average growth rates between dates are displayed on the chart.

As the dates were in sequence, a relatively straightforward accumulation rate history can be determined (Figure 5.22). Average growth rates varied from 2.8-25.8 mm/kyr with slowest growth during a period roughly equivalent to the LGCP and most rapid deposition during the late glacial and early Holocene.

Two Hendy Tests, one each from near the tip (32 mm depth) and the base (528 mm depth) of RK05-3, were conducted to determine if the calcite was deposited in isotopic equilibrium with the seepage waters (Figure 5.23). The lower layer (Figure 5.23b) was followed for 78 mm from the growth axis. For the first 62 mm $\delta^{18}O$ values are statistically identical and there was no discernible trend in the $\delta^{13}C$ data. Both results indicate that isotopic equilibrium was maintained between the dripwater and the precipitated calcite during the period of deposition. In the upper layer (Figure 5.23a) there was initially a decrease in $\delta^{18}O$ from 0-7 mm followed by a steady rise of 0.9 ‰ in the remaining 37 mm. The trend in the $\delta^{13}C$ ratios is not covariant with changes in $\delta^{18}O$. This provides further support that RK05-3 calcite was unaffected by kinetic fractionation of isotopes.

One sample every millimetre from 0-420 mm and every 2 mm from 420 to 556 mm depth was submitted for stable isotope analysis. As a result the temporal resolution of the data varies between approximately 40 and 360 years.

To further examine the assumption that stable isotope ratios in RK05-3 calcite were unaffected by kinetic fractionation processes, $\delta^{13}C$ and $\delta^{18}O$ pairs were plotted against each other (Figure 5.23c). A linear regression of the data displays a negligible ($r^2 = 0.007$) negative correlation. Both the slope and the weak relationship imply that the measured calcite was deposited in isotopic equilibrium with the dripwater from which it precipitated.

The total range of $\delta^{18}O$ in RK05-3 samples over the length of the record was -4.6 to -2.5 ‰. For much of the period of record $\delta^{18}O$ values lie within the range -3.4 ± 0.4 ‰ (Figure 5.24a). However, between 18.5 and 7.5 kyr B.P. there was a general increase in $\delta^{18}O$. The interval is composed of three main peaks separated by more negative values at 16.5-14.5 and 13-11.5 kyr B.P. Excursions toward minimum values occupied relatively brief intervals in the record and occurred ~52.5, 45.1-43.8, 38.1-37.7 and 6.5-6.1 kyr B.P.

As with other samples in this study it was important to consider the impact of changing global ice volume on speleothem $\delta^{18}O$. Despite insufficient age determinations for the RK05-3 chronology an attempt was made to adjust the

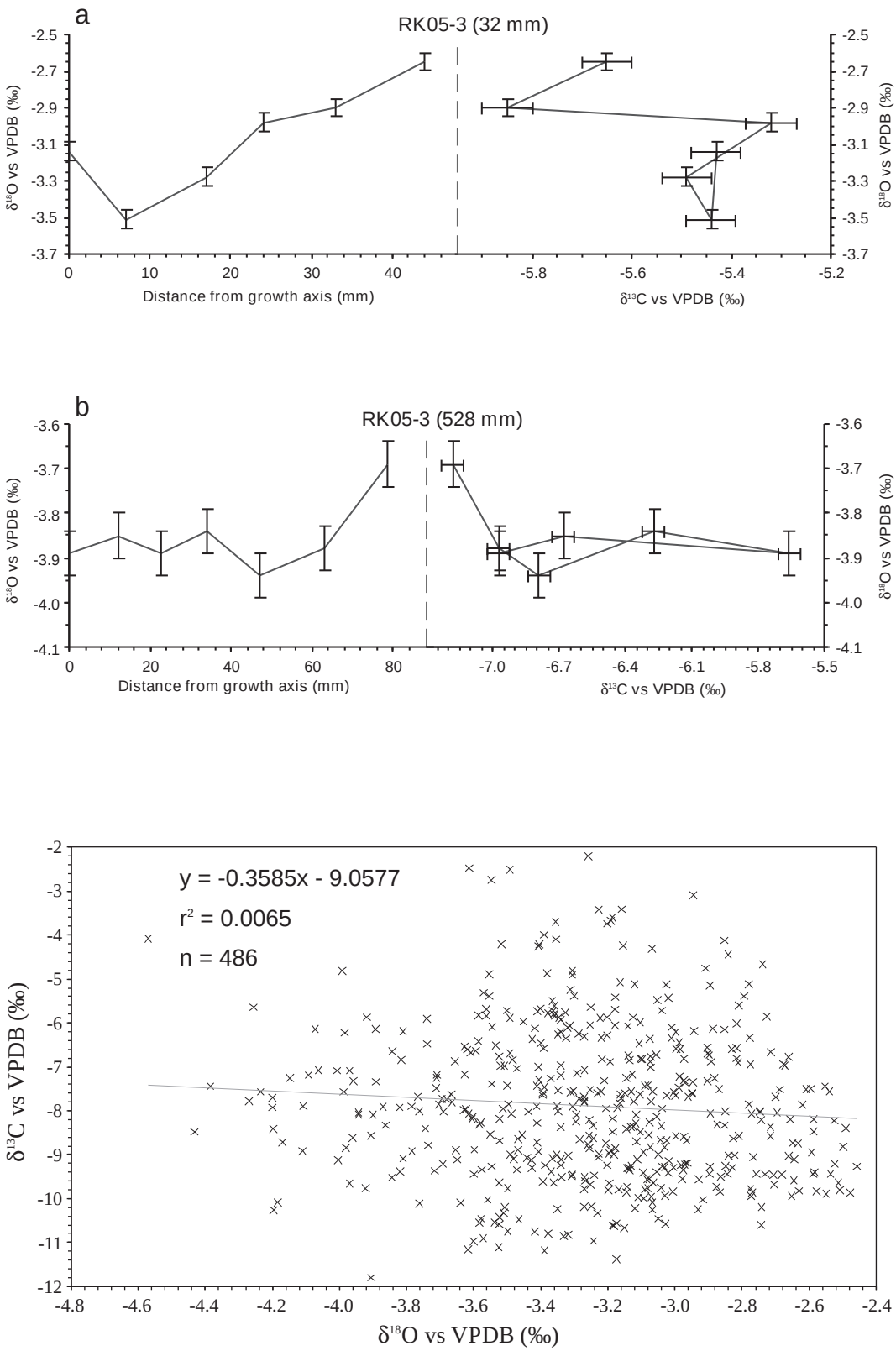

Figure 5.23: Testing for kinetic isotope fractionation in Ruakuri Cave stalagmite RK05-3. Hendy Tests along (a) a layer 32 mm below the stalagmite tip, and (b) a layer 528 mm below the tip both suggest that kinetic processes are unlikely to affect RK05-3 $\delta^{13}C$ and $\delta^{18}O$ profiles. A third test (c) displays isotope ratios of 486 calcite samples milled from the growth axis. The lack of significant correlation between $\delta^{13}C$ and $\delta^{18}O$ supports the results of the Hendy Tests.

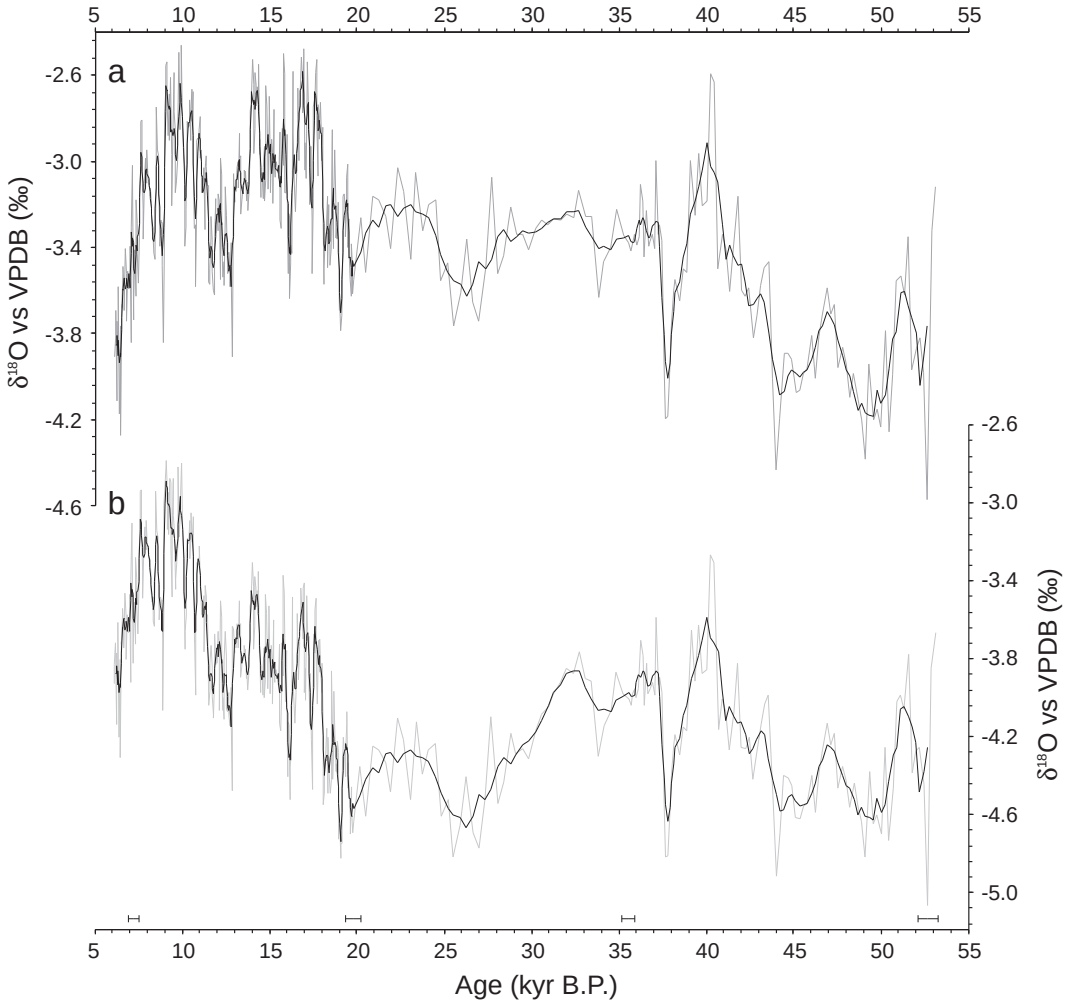

Figure 5.24: Oxygen isotope data for stalagmite RK05-3. Both the raw data (a) and the ice-volume adjusted data (b) are shown. Each profile also displays a 5-point running mean of the data (black line). Relative adjustments are based on sea level data from Lambeck and Chappell (2001) and maximum sea level lowering being equivalent to a shift of 1.1 ‰ in sea water $\delta^{18}O$. U-Th dates, including 2σ errors are shown at the base of the figure.

record for the effects of changes in global ice volume, as provided in Lambeck and Chappell (2001), for the period 54-6 kyr B.P. (Figure 5.24b). The resulting $\delta^{18}O$ curve displays a trend of increasing $\delta^{18}O$ between 44 and 40 kyr B.P. in which values become ~0.9 ‰ less negative. Following a small gap in the record and a brief minimum ~37.7 kyr B.P., $\delta^{18}O$ remained close to -4.0 ‰ until 31.6 kyr B.P. after which there was a rapid decline to -4.7 ‰ at 27 kyr B.P. Isotopic ratios remained relatively low until 18.9 kyr B.P. This event terminated abruptly as values increased 0.85 ‰ in ~1000 years to a plateau with $\delta^{18}O$ ratios close to -3.8 ‰. The increased values persisted until 11.5 kyr B.P. but were interrupted by brief negative excursions at 16.5-15.8 and 12.9-12.3 kyr B.P. A second major rise then occurred, peaking at -2.8 ‰ between 9.9 and 9.1 kyr B.P., before a general decline to ~-4.0 ‰ at 6.2 kyr B.P.

$\delta^{13}C$ in RK05-3 calcite (Figure 5.25a) fell in the range -11.8 to -2.2 ‰. This represents the greatest spread of isotopic values obtained from any speleothem in this study. In the early part of the record, between 45 and 36.6 kyr B.P., $\delta^{13}C$ varied between -7.0 and -10.3 ‰ although there were three brief positive excursions to values close to -6 ‰. Beginning at ~38 kyr B.P. there was a general increasing trend which terminated in values ~2.3 ‰ at 20 kyr B.P. This peak in $\delta^{13}C$ preceded slightly the isotopic minimum in the ice-volume adjusted $\delta^{18}O$ record (Figure 5.25b). The peak of heavy $\delta^{13}C$ ended abruptly at 19.8 kyr B.P. and was succeeded by a 900 year period where values ranged between -6.5 and -8.9 ‰. This event terminated in a sharp increase in carbon isotope ratios which then remained close to -5.0 ‰ until 17.7 kyr B.P. At this time a third, significant, rapid shift in $\delta^{13}C$ occurred as $\delta^{13}C$ decreased to -9.5 to -10.0 ‰. The remainder of the record is dominated by millennial-scale events covering the range -11.8 to -5.0 ‰. Significant events in the remainder of the record include a positive excursion from 14.4 to 12.9 kyr B.P. closely followed by a strong negative excursion lasting until 11.3 kyr B.P., and two positive excursions at 11.1 to 10.1 and 8.1 to 6.7 kyr B.P.

5.2.4 RK05-4

Stalagmite RK05-4 was recovered from the same passage (Drum Entrance) in Ruakuri Cave as stalagmite RK05-3 (Figure 3.6). It too was buried under an

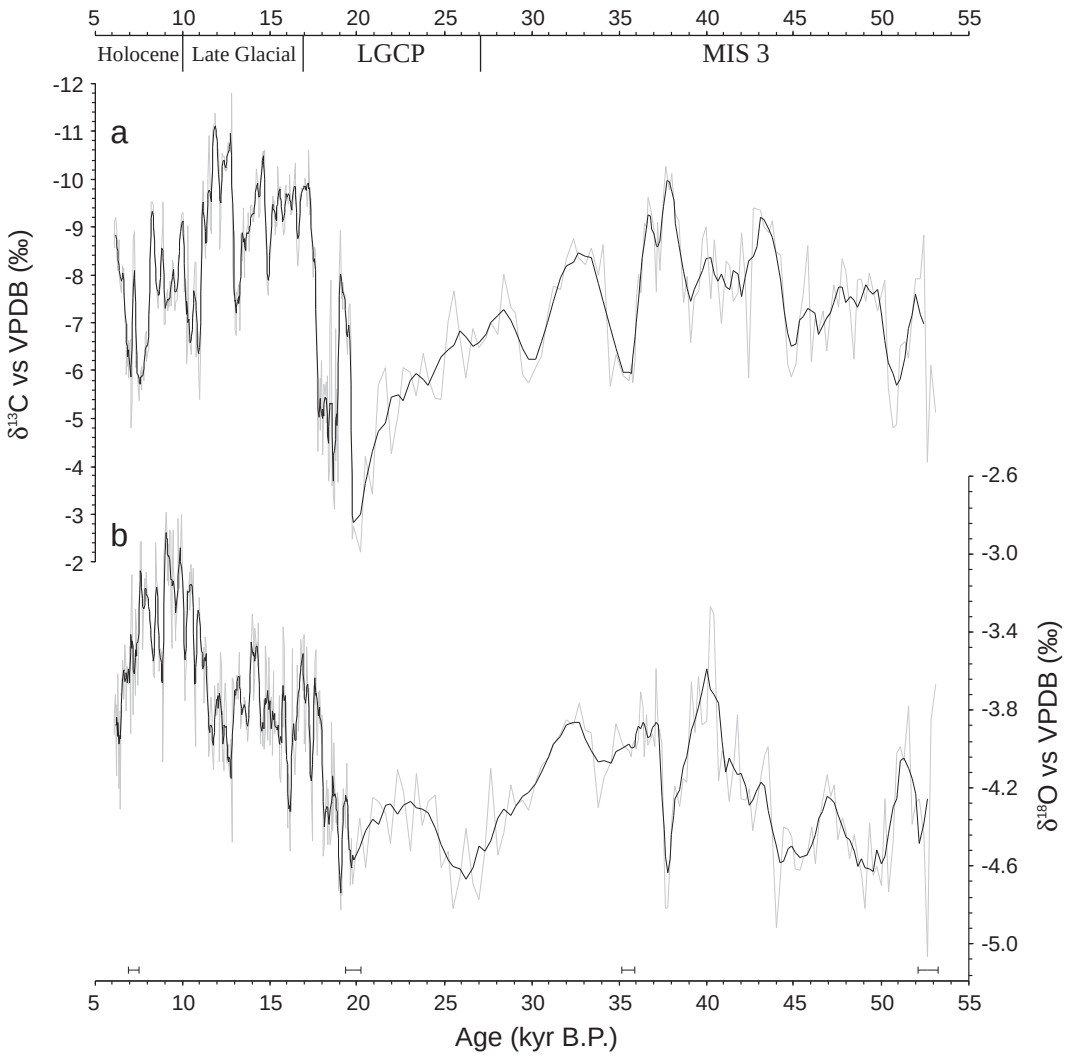

Figure 5.25: (a) RK05-3 $\delta^{13}C$ profile and (b) ice-volume adjusted $\delta^{18}O$ profile. In each record are the individual data points (gray line) and a 5-point running mean (black line). U-Th dates are displayed at the base of the figure with 2σ errors.

unknown thickness of laminated sediments, but was located deeper than RK05-3. Unlike other Ruakuri stalagmites in this study, RK05-4 has pronounced colouration (Figure 5.26). Much of the speleothem is dark brown. Also noteworthy are the abundance of 'bubbles' that characterize the upper half of the stalagmite.

Age data for five RK05-4 samples submitted for uranium-series dating are presented in Table 5.3. The dates are in sequence with the exception of the topmost sample and show that the stalagmite began growing around 100 kyr B.P. and terminated 70 kyr B.P. Given the reversal in the age-depth relationship it is not straightforward to construct a chronology for RK05-4. Furthermore, there is considerable uncertainty (± 27 %, 2σ) in the basal age of RK05-4 (Table 5.3). However, the uppermost four ages overlap within the 2σ uncertainties of the dates. This allows an age-depth curve to be constructed that still falls within the margins of error on each age (Figure 5.27). It also demonstrates that much of the calcite that composes RK05-4 was deposited within the relatively brief period from 76.1-72.6 kyr B.P.

The poor precision with which the dates on RK05-4 calcite could be determined is controlled by with the relatively low abundance of uranium and high concentrations of thorium. Uranium concentrations within the five samples fall within the range 30-60 ppb and are similar to concentrations in other Ruakuri Cave speleothems (Table 5.3). The $^{230}Th/^{232}Th$ ratios (2.2 to 43.3) are low and thus demonstrate significant contamination of dated samples by detrital thorium.

Deposition of the speleothem calcite was interrupted on several occasions by light brown, calcite-rich layers of mud. Given that the stalagmite was buried by laminated sediments it is likely that these hiatuses record flood events within the cave. Should this be the case it is unlikely that the layers represent significant temporal breaks in deposition. However, the relative frequency of mud layers may indicate that much of the speleothem is contaminated by detrital thorium so that obtaining a 'clean' sample may not be possible.

One layer of RK05-4 was subject to the Hendy Test (Figure 5.28a). There are no clear trends in either the $\delta^{13}C$ or $\delta^{18}O$ ratios with distance along the chosen layer suggesting that kinetic fractionation of isotopes has not distorted the climate record archived within the speleothem.

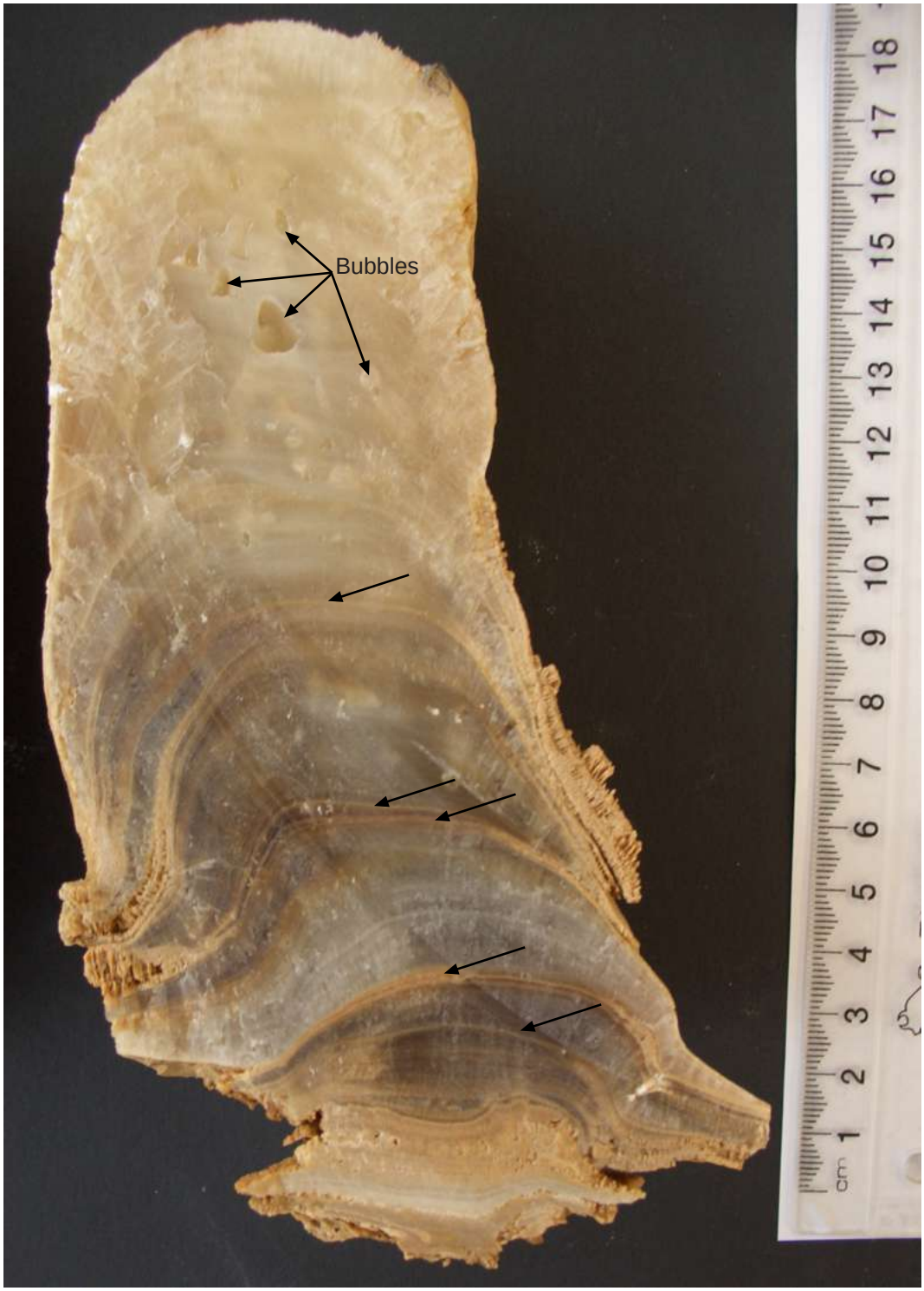

Figure 5.26: Photograph of stalagmite RK05-4. Five detrital mineral-rich laminae are indicated by arrows on the photograph. Locations of some bubbles are also shown.

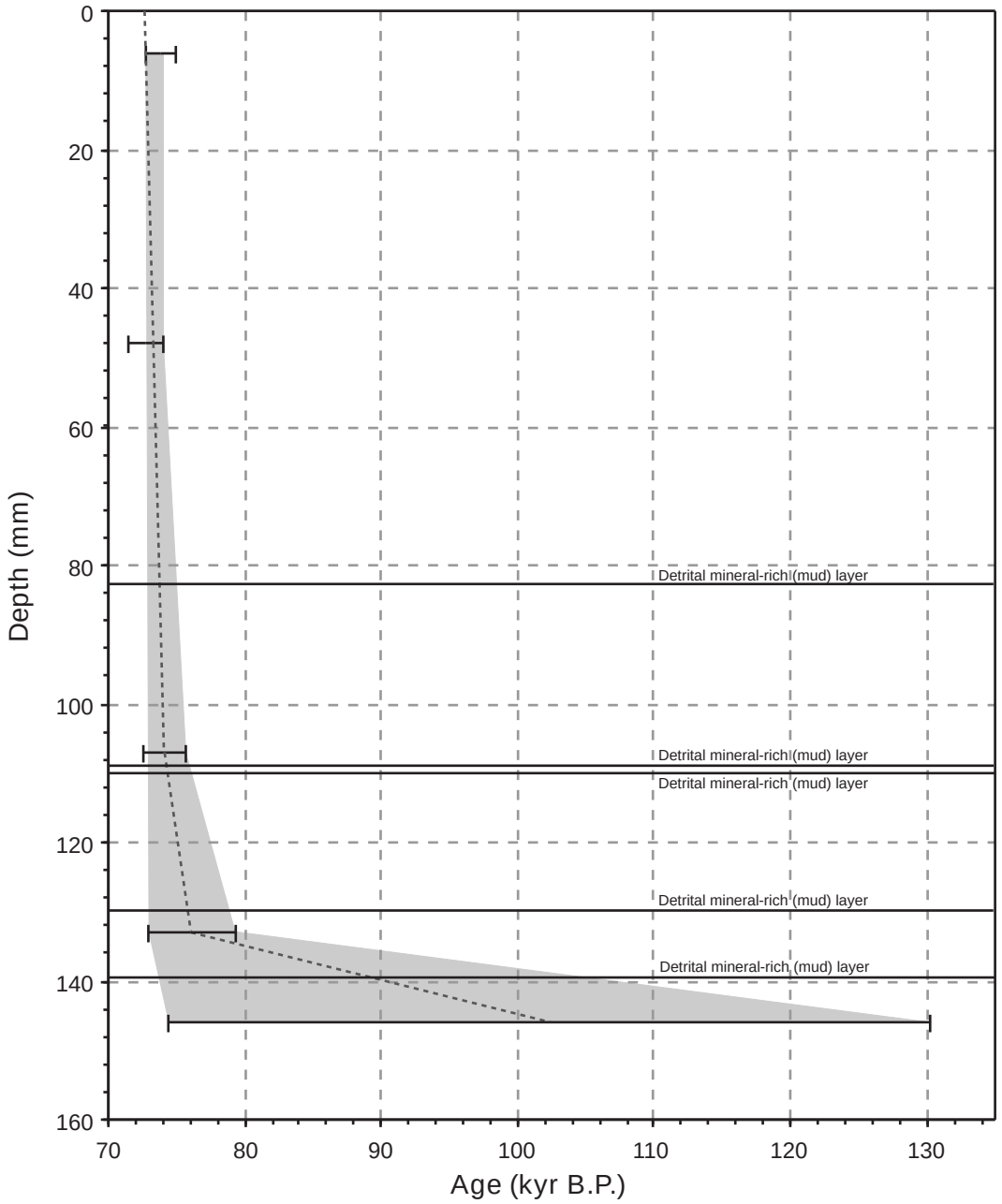

Figure 5.27: Age versus depth for Ruakuri Cave stalagmite RK05-4. All ages are given with 2σ errors. The age of the topmost date creates a minor reversal in the chronology. The grey area represents the best estimate of the possible age for any given depth. The dashed black line represents the age model used to plot measured stable isotope ratios. Also marked on the figure are the depths at which mud-rich layers occur.

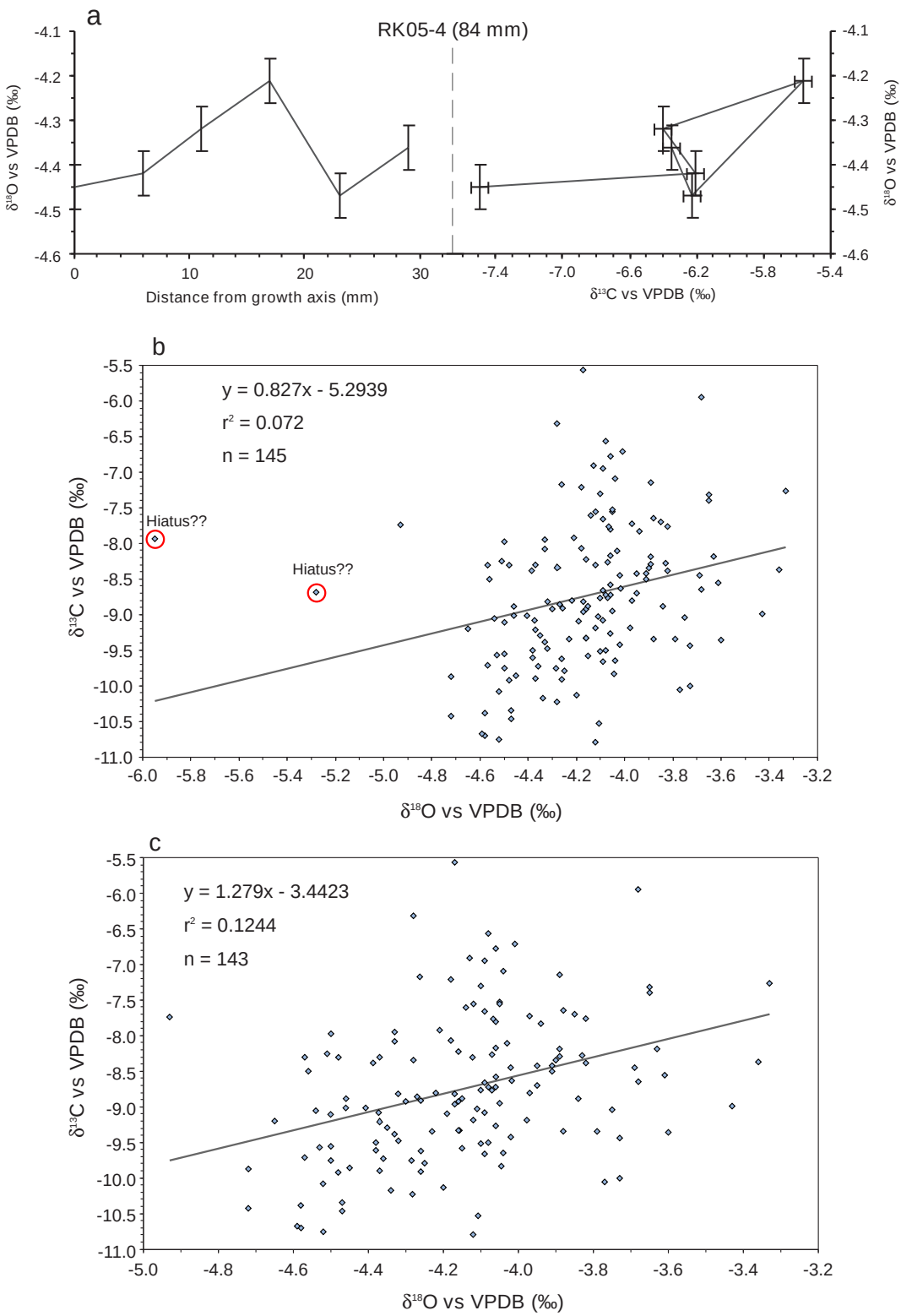

Figure 5.28: Testing for kinetic isotope fractionation in Ruakuri Cave stalagmite RK05-4. (a) Hendy Test results from a layer 84 mm below the tip of RK05-4. The lack of a trend indicates that kinetic processes have not interfered with the climate signal preserved in RK05-4 calcite. A second test (b) displays $\delta^{13}C$ versus $\delta^{18}O$ of calcite samples milled along the growth axis. However, the regression may be skewed by two outliers, both of which came from samples associated with hiatuses. These are removed in (c). The poor correlation of $\delta^{13}C$ and $\delta^{18}O$ in (c) is a further indication that the impact of kinetic fractionation effects is negligible.

Calcite was milled in ~0.25 mm increments continuously along 146 mm of the growth axis. One sample per millimeter was submitted for stable isotope analysis. These results are used to test for conditions of isotopic equilibrium at the time of calcite precipitation (Figure 5.28b,c). The strength of the relationship between $\delta^{13}C$ and $\delta^{18}O$ is low ($r^2 = 0.124$), and therefore it is likely that the isotopic composition of RK05-4 calcite has not been affected by non-equilibrium fractionation processes.

The full range of $\delta^{18}O$ is -6 to -3.3 ‰. However, two results are considerably more negative than the remainder of the dataset. These data points correspond to samples collected from hiatuses. If these two data points are rejected as outliers, the range in $\delta^{18}O$ narrows to -4.9 to -3.3 ‰ (Figure 5.28c).

For the period 102-76 kyr B.P. data resolution and age uncertainty is too great to allow interpretation of the climatic significance of the record other than to comment that the range in $\delta^{18}O$ is the same in this interval as it is in the remainder of the record (Figure 5.29). During the period 76-73.6 kyr B.P. oxygen isotope values were close to -4.2 ‰, with exceptions for the two data points corresponding to the detritus rich layers. This relatively stable period was succeeded first by a ~200 year-long minor positive excursion and second by an equally long, small negative excursion. The increasing trend following termination of this negative event continued until the end of the RK05-4 record at 72.6 kyr B.P. Over this 700 year period $\delta^{18}O$ rose 0.8 ‰, representing the largest change in the profile.

Compensation of the RK05-4 $\delta^{18}O$ record for changes in global ice volume (Lambeck and Chappell, 2001) was not attempted. This is for two reasons. First, there is considerable uncertainty in the age model. Second, during the interval 72-76 kyr B.P., the period covering almost all of the obtained data, any adjustments for ice-volume effect would create only minor differences (< 0.2 ‰) in the Figure 5.29 record.

The full range of $\delta^{13}C$ in the samples analysed was -10.8 to -5.6 ‰. This spread is unaffected by the removal of the two data points (outliers) which correspond to hiatuses. The most negative values occurred in the early part of the record following which there was a general trend toward less negative $\delta^{13}C$ (Figure 5.30). The period 75.7-74.3 kyr B.P. produced invariant $\delta^{13}C$ values of 8.5 ± 1 ‰. The youngest part of the record (74.3-72.5 kyr B.P.) was characterized by

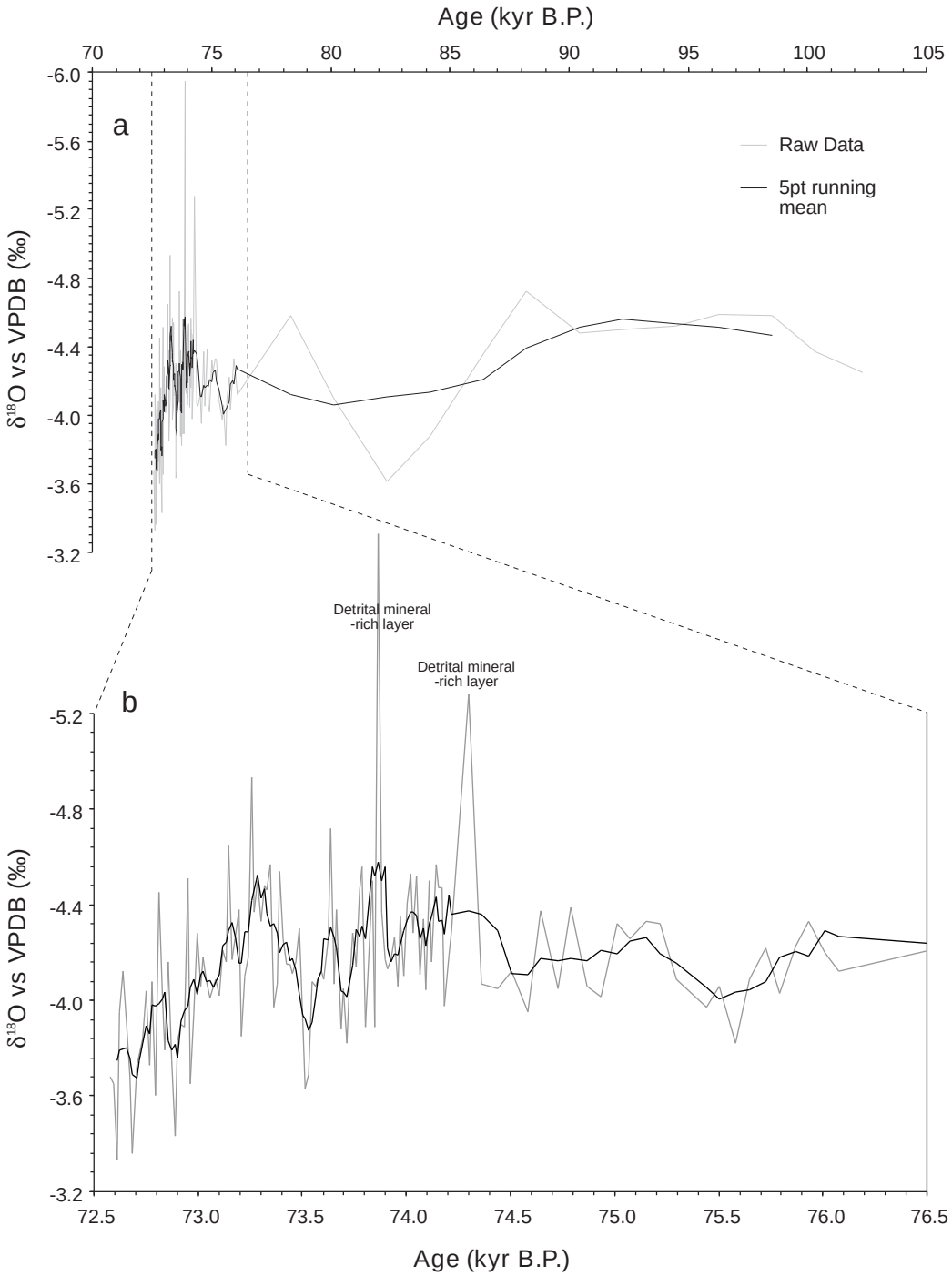

Figure 5.29: $\delta^{18}O$ values along the growth axis of stalagmite RK05-4. Two strongly negative results are associated with detritus-rich layers in the speleothem. Note that y axis values are plotted in reverse order, and that no corrections are made for changes in ice volume.

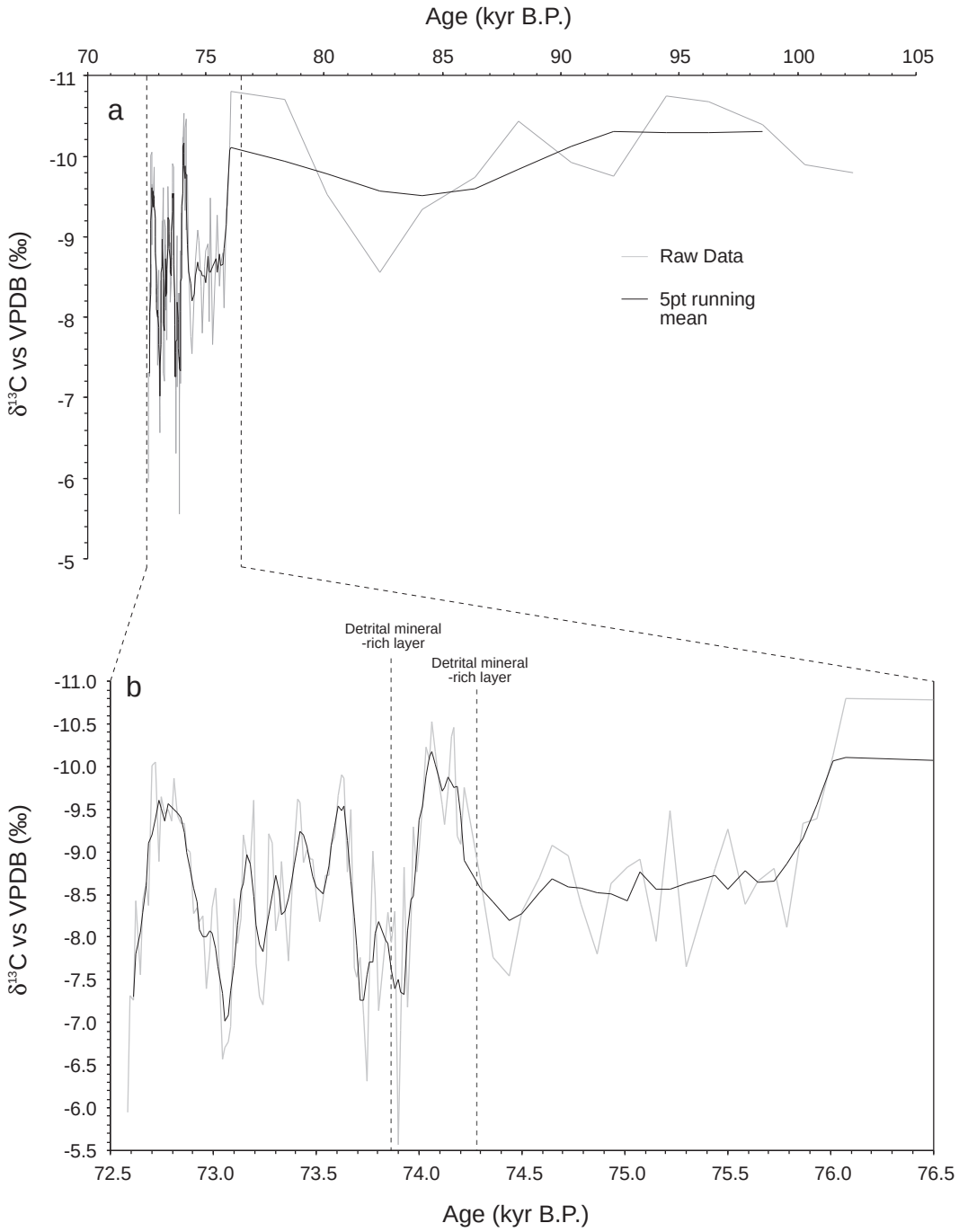

Figure 5.30: RK05-4 $\delta^{13}C$ profile. Raw data (gray line) and a 5-point running mean of the data (black line) are fit to the age model displayed in Figure 5.27.

more pronounced centennial-scale variability with values in the range -10.5 to -5.6 ‰. This period contained three intervals of more negative $\delta^{13}C$ values (74.3-74.0, 73.6-73.1 and 72.85-72.6 kyr B.P.) separated by two excursions to less negative values.

6 Discussion

Interpretations of the results obtained in this study are presented here as a series of seven sections. These begin in section 6.1 with discussions of growth rates of speleothems studied as part of this research. Next are two sections which explain how the stable isotope profiles are interpreted (section 6.2), and which investigate various methods by which the 'ice-volume' or 'source-water' effect might be removed from $\delta^{18}O$ values measured in speleothem calcite (section 6.3). With these as background, the stable isotope profiles of GT05-5 (Guillotine Cave, South Island), HW05-3 (Hollywood Cave, South Island) and Ruakuri Cave (North Island) stalagmites are discussed in sections 6.4, 6.5 and 6.6 respectively. Comparisons are made between records where they overlap and also with existing palaeoclimate records from New Zealand and elsewhere across the globe. In the last section, 6.7, opportunities for further research are explored.

6.1 Speleothem Growth Rates

Changes in growth rates of speleothems are caused by changes in climate conditions (precipitation and temperature) and soil carbon dioxide concentration, itself an indirect function of climate (Kaufmann and Dreybrodt, 2004). Therefore changes in growth rate offer the possibility of investigating past climate change. Kaufmann and Dreybrodt (2004) suggested that as speleothem stratigraphy and external morphology is controlled by growth rate variability they should therefore also preserve a record of past climate. A simpler, but lower resolution alternative is to study average growth rates between uranium-series ages (Zhao *et al*., 2001). This latter technique has been applied to the stalagmites collected for this research.

Stalagmite growth rates determined in this research, 0.4 – 85.6 mm/kyr, overlap with the lower end of the range for published speleothem records from New Zealand (~5-480 mm/kyr) and elsewhere around the world (Figure 6.1). However, growth rates of less than 1 mm/kyr are unusually slow. In this study, low rates were determined for the basal sections of RK05-3 and RK05-4, stalagmites from Ruakuri Cave. Age control at these points is particularly poor

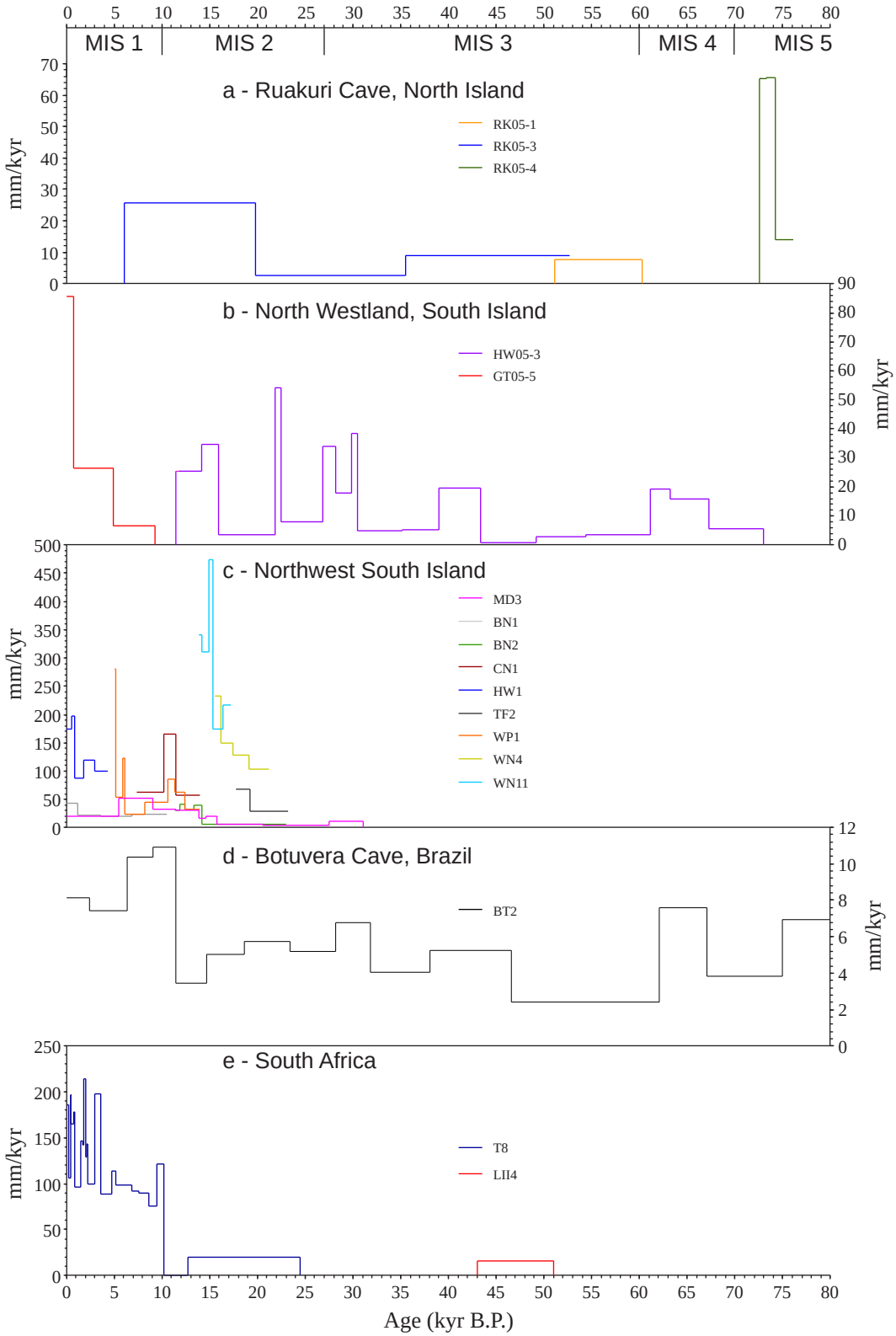

Figure 6.1: Growth rates of some Southern Hemisphere speleothems from (a) Ruakuri Cave, North Island (this study), (b) north Westland, South Island (this study), (c) northwest South Island (Hellstrom et al., 1998; Williams et al., 2005), (d) Botuvera Cave, Brazil, South America (Cruz Jr. et al., 2005), and (e) Cold Air Cave and Lobatse II Cave, South Africa (Holmgren et al., 1995; Holmgren et al., 2003). Further details pertaining to speleothem records in c, d and e are presented in Table 2.1 (pages 54-56).

due to imprecise dates (± 14-27 %) and, as a result, growth rates inherit similar uncertainties.

Low growth rates also occur in the mid-section of the relatively well-dated stalagmite HW05-3 from the West Coast region of South Island. A growth rate of 0.9 mm/kyr occurred from 49.1 to 43.4 kyr B.P. following a ~12 kyr period when growth rate was also relatively slow (<3.4 mm/kyr). Most likely this occurred in response to particularly dry, and perhaps frosty (in winter), conditions in north Westland, a hypothesis supported by weakly negative stable isotope ratios of HW05-3 calcite deposited during this interval (see section 6.6).

Low growth rates were also observed in other Southern Hemisphere speleothem records that cover the period ~60-43 kyr B.P. (Figure 6.1; Cruz *et al*., 2005; Wang *et al*., 2007). Furthermore, a South African speleothem (LII4) began growing 51 kyr B.P. suggesting that this region began to receive more rainfall while parts of New Zealand and Brazil were drying. Growth of LII4 ceased ~43 kyr B.P. suggesting that a return to dry and/or cold conditions in South Africa occurred synchronously with increasing mean annual precipitation in New Zealand (Holmgren *et al*., 1995).

In the Northern Hemisphere there is no clear consensus as to whether growth rates were reduced during the early part of MIS 3. In several Chinese speleothems, growth rates were higher in MIS 3 than MIS 4 (Wang *et al*., 2001), to the reverse of that observed in the HW05-3 Westland record. However, a French speleothem ceased growing between ~56 and 52 kyr B.P. (Genty *et al*., 2003), perhaps indicating dry climate at the onset of MIS 3. Other speleothem records from the Northern Hemisphere also capture part of this interval (Burns *et al*. 2003; Spötl *et al*., 2006), but a consistent pattern of growth periods is absent.

Slowest growth rates (~5 mm/kyr) in published New Zealand speleothem records within the interval 31-0 kyr B.P., occurred during the LGCP (Hellstrom *et al*., 1998; Williams *et al*., 2005). In this study, stalagmites HW05-3 and RK05-3, which both capture the LGCP, display comparable growth rates of 2.8-3.5 mm/kyr at this time. This phenomenon is not limited to New Zealand, with growth rates being relatively reduced in other speleothems from the Southern Hemisphere during the LGCP (Figure 6.1; Holmgren *et al*., 2003; Cruz Jr. *et al*., 2005). This is not surprising given the findings of Hennig (1983), Gascoyne (1992) and Richards and Dorale (2003) who each demonstrated that cooling of mid- to high-latitudes

during the last glacial period was sufficient to halt or severely diminish speleothem growth in many caves.

Significantly, growth rates in HW05-3 throughout the LGCP (3.5-8.1 mm/kyr) were lower than during MIS 4, the other intense and prolonged stadial of the last glacial period, which was characterized by relatively high growth rates (16.0-19.5 mm/kyr). This provides a strong indication that climate was considerably wetter in north Westland during MIS 4 than the LGCP.

The speleothems in this study each display a relationship between low growth rate and heavier stable isotope ratios. This is most clearly exhibited in the high-resolution, well-dated stalagmite HW05-3 from the West Coast (Figure 6.2). Such a relationship was also observed in an Italian speleothem that formed during part of MIS 5 (Drysdale *et al*., 2007). Unfortunately, as it is uncommon for both $\delta^{18}O$ and $\delta^{13}C$ to be published it is not possible to determine if heavy stable isotopes and low growth rate are also commonly related. In addition, the density of uranium-series dates in published speleothem records is not always sufficient to allow significant determination of growth rate variability.

Growth rates in HW05-3 during the last glacial period (73-11 kyr B.P.) were typically low although frequently interrupted by brief episodes of considerably more rapid accumulation. Each of these high growth rate events likely indicates increased mean annual rainfall above the cave, a suggestion supported by concurrent decrease of stable isotope ratios. Furthermore, the brief intervals of rapid accumulation coincide with the timing of Heinrich events (Hemming, 2004; Figure 6.2). Events H1-H4 and H6 are particularly well represented in the HW05-3 record. This suggests that Heinrich events drove the climate over the West Coast of South Island to become wetter. The lack of H5 and H5a signals in the growth rate record is most likely due to low-resolution of uranium-series ages in a part of the speleothem that accumulated extremely slowly. However, it may also be the case that these Heinrich events were associated with only minor increases in annual rainfall amount as suggested by the $\delta^{13}C$ data (Figure 6.2).

Drysdale *et al*. (2007) and Wang *et al*. (2004) also identified a link between Heinrich events and speleothem growth rate. In Italy, Heinrich events coincided with dry climate (Drysdale *et al*., 2007), while in Brazil speleothem growth occurred only during Heinrich events indicating wetter-than-normal climate (Wang *et al*., 2004).

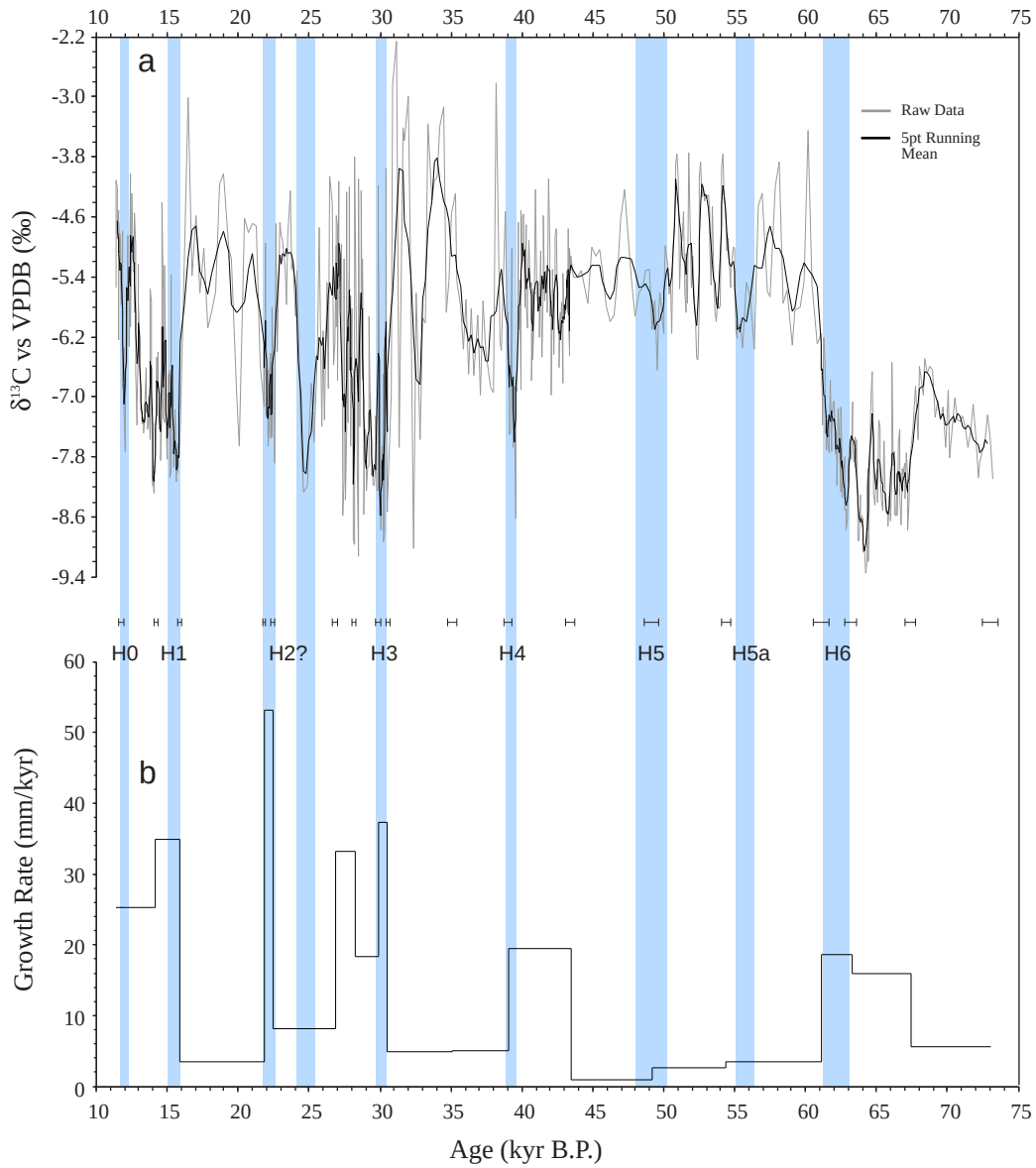

Figure 6.2: (a) Axial $\delta^{13}C$ profile and (b) growth rate of South Island stalagmite HW05-3 compared to the approximate timing of Heinrich events (blue shading) following Hemming (2004). U-Th dates, including 2σ errors (black bars), are shown.

In summary, the New Zealand stalagmite growth rate and stable isotope data appear to demonstrate a significant positive relationship. This is a strong indication that changes in growth rate are linked to variability in annual rainfall amount. As a result, high annual rainfall amounts on the West Coast, South Island, during the last glacial period are inferred from stalagmite HW05-3 for periods coinciding with MIS 4 and Heinrich events 1-4 and 6 in the North Atlantic.

6.2 Interpretation of Stable Isotope Signals

6.2.1 Temperature-$\delta^{18}O$ Relationship

There are three significant climatic influences on the $\delta^{18}O$ of speleothems precipitated under conditions of isotopic equilibrium; the so-called "cave-temperature effect", the "precipitation effect" and "ice volume effect". The second effect is in fact temperature driven but, significantly, it drives $\delta^{18}O$ in the opposite direction to the cave temperature effect. The third of these effects is discussed separately in section 6.3.

The "cave temperature effect" is set by thermodynamics and in the range of temperatures found in New Zealand caves amounts to -0.24 ‰/°C (O'Neil *et al*., 1975; Friedman and O'Neil, 1977). The magnitude of the "precipitation effect", however, is not so easily defined. In an early study, Dansgaard (1964) demonstrated that $\delta^{18}O$ of atmospheric precipitation in maritime climates decreased with increasing latitude (equivalent to decreasing mean annual temperature). This relationship could be simulated by progressively cooling and precipitating (by Rayleigh Distillation) water from a body of water vapour evaporated from seas with water temperatures of 20-25 °C (typical of the trade wind belts). The result was a linear relationship between the $\delta^{18}O$ of rain and mean annual temperature with a slope of approximately 0.69 ‰/°C.

The Dansgaard model assumes that the temperature of atmospheric precipitation is related to mean annual surface temperatures. This relationship breaks down most dramatically in regions that experience monsoonal rainfall. Here the temperature of atmospheric precipitation is controlled by the altitude to which the moisture laden air masses are uplifted.

Several local studies have determined that Dansgaard's relationship may not accurately represent oxygen isotope variability of atmospheric precipitation in New Zealand despite the maritime climate that prevails over most of the country. Instead, New Zealand specific values have been obtained based on calculations using local climate data. These include Hellstrom *et al*. (1998), who found a value of 0.19 ‰/°C at Mt. Arthur on South Island, and Williams *et al*. (2005) who determined a value of 0.35 ‰/°C also for northwest South Island. Due to the inconsistency between findings and the uncertainty of whether this effect is

greater or less than the temperature effect (0.24 ‰/°C), an additional attempt is made here to ascertain a value for the precipitation effect in New Zealand. This is achieved using the method of Williams *et al*. (2005), essentially comparing weighted $\delta^{18}O$ of precipitation and mean annual temperatures at far northern (Kaitaia) and southern (Invercargill) New Zealand locations, and an extended dataset from the Global Network of Isotopes in Precipitation (IAEA/WMO, 2004). The difference in mean annual temperatures between locations is 5.5 °C (Kaitaia = 15.32 °C; Invercargill = 9.82 °C) and between weighted $\delta^{18}O$ of precipitation is 2.3 ‰ (Kaitaia = -4.88 ‰; Invercargill = -7.18 ‰). Therefore the change in the isotopic value of precipitation with change in temperature $[d(\delta^{18}O_p)/dT]$ for New Zealand is 0.42 ‰/°C. This result is comparable to that determined by Williams *et al*. (2005), and likewise also exceeds the cave temperature effect. Therefore, provided that both the source of the water and the temperature at which it was evaporated are invariant, changes in mean annual temperature should, in general, be positively correlated with changes in speleothem $\delta^{18}O$.

While a positive relationship may be true for the present day it is necessary to determine whether this holds for the past. In this study the Waitomo, North Island, stalagmite RK05-3 provides the only record spanning the transition from the LGCP to the Holocene and therefore allows a comparison of isotopic values at times of maximum cooling and maximum warmth. Mean $\delta^{18}O$ of calcite deposited during the LGCP (18-30 kyr B.P.) was -4.39 ‰ while during that part of the Holocene captured in the record (6-10 kyr B.P.) $\delta^{18}O$ averages -3.38 ‰. The warmer Holocene has $\delta^{18}O$ values enriched by 1.0 ‰ over those of the colder LGCP indicating that a positive temperature-isotope relationship also held in the past on North Island. A similar result was achieved by Williams *et al*. (2005) for a composite South Island speleothem record also spanning the LGCP-Holocene transition. Furthermore, a positive temperature-$\delta^{18}O$ relationship is also observed in speleothems from caves in Tasmania, a region geographically and climatically similar to that of South Island (Goede *et al*., 1990b; Xia *et al*., 2001).

Another approach was taken to evaluate the relationship between air temperature and oxygen isotope ratios in New Zealand speleothems. It can be demonstrated from data presented in this and previous studies that the $\delta^{18}O$ of speleothems in South Island decreases with altitude, and therefore also mean

annual temperature, opposite to that implied by the cave temperature effect. Two high-elevation speleothems from Mt Arthur have Holocene $\delta^{18}O$ values in the range -5 to -6.7 ‰ (Hellstrom *et al*., 1998) and five stalagmites from low elevation coastal sites have Holocene $\delta^{18}O$ values between -2.6 and -4.0 ‰ (Hendy, 1969; Williams *et al*., 2005). At Guillotine Cave, ~740 m elevation, the range in $\delta^{18}O$ during the Holocene is -4.7 to -6.3 ‰, comparable to those values obtained from the Mt Arthur specimens. The same altitude-isotope relationship can be seen in the $\delta^{18}O$ values of collected cores from this study. Although only a crude test (being based on only one data point per speleothem), it nevertheless shows that Holocene-age stalagmites from coastal, low-elevation caves (e.g. Abyssinia and Te Ana Puta) have enriched $\delta^{18}O$ in comparison to stalagmites that formed in caves at higher elevation (e.g. Eggers Cave and Guillotine Cave).

While there is strong evidence for a positive relationship between temperature and speleothem $\delta^{18}O$ in this study it is unlikely that changes in temperature can account for all of the variability in the records. It may also be necessary to consider atmospheric and oceanic conditions at the moisture source and along the path taken by the evaporated moisture to the cave. In particular changes in sea surface temperature may influence $\delta^{18}O$ of evaporated water vapour. Several studies have identified that sea surface temperatures to the east and west of New Zealand were as much as 6°C below present during the LGCP (Pahnke *et al*., 2003; Pahnke and Sachs 2006; Barrows *et al*., 2007). This would result in $\delta^{18}O$ of evaporated moisture being 0.5-0.7 ‰ heavier than at present (Bottinga and Craig, 1969; Majoube, 1971; Kakiuchi and Matsuo, 1979) and assuming only locally evaporated moisture was precipitated above the cave its effect would be to reduce the difference in $\delta^{18}O$ of speleothem calcite between warm and cold intervals. Furthermore, it is likely, given the strong maritime influence on the New Zealand climate, that any sea surface temperature changes in the Tasman Sea would be matched by similar changes in air temperatures above land. Due to the cave temperature effect, lower mean annual temperatures would yield increased $\delta^{18}O$ in speleothem calcite, compounding the change caused by sea surface temperatures. However, another study found evidence for only minor (<1 °C) cooling of the Tasman Sea during the last glacial maximum (Nelson *et al*., 1994). If it is assumed that the Tasman Sea was the source for all moisture falling above the caves in this study, a realistic hypothesis given the strong westerly flow across

New Zealand and that these caves occur along the west coasts of North and South Islands, this would suggest that sea surface temperatures had a negligible impact on $\delta^{18}O$ of atmospheric precipitation. As a result, the variability would be almost solely the product of changes in air temperature and prior precipitation along the route taken by the water vapour.

At tropical and subtropical latitudes the oxygen isotopic composition of rainfall may be affected by the amount effect, which is the phenomenon whereby isotopically light precipitation is generated when an air mass is driven to higher altitudes, typically during convective thunderstorms or through orogenic uplift. In New Zealand, Williams and Fowler (2002) identified a weak influence of the amount effect in Northland, but with increasing distance south the effect was diminished such that it is thought to be of negligible significance on South Island. Therefore $\delta^{18}O$ records developed from South Island speleothems are unlikely to be affected by the amount effect (Williams *et al*., 2005).

In summary, the available evidence strongly points to the precipitation effect being the primary control of speleothem $\delta^{18}O$ in New Zealand. Therefore, shifts in $\delta^{18}O$ are positively correlated with changes in air temperature both above the cave and at the moisture source region.

6.2.2 Climatic Influence on Speleothem $\delta^{13}C$

The range in $\delta^{13}C$ values observed in this study is -2.21 to -11.80 ‰. This is similar to the range of previously obtained $\delta^{13}C$ data from New Zealand speleothems (~+1 to -12 ‰; Hellstrom *et al*., 1998; Williams *et al*., 2004; 2005). Hendy (1971) predicted that the $\delta^{13}C$ of the initial calcite precipitated on presently forming speleothems in caves of the Waitomo district (of which Ruakuri Cave is one) to be in the range -13.2 to -10.5 ‰, depending on the degree to which the seepage water was influenced by open or closed system conditions within the epikarst. Significantly, this range overlaps with less than two percent of the carbon isotope data obtained in this study. Therefore it is necessary to consider what factors could lead to heavy carbon isotope ratios in New Zealand speleothems.

In several previous studies positive carbon isotope ratio excursions were attributed to a relative increase in vegetation above the cave that utilize the C_4 photosynthetic pathway (Talma and Vogel, 1992; Dorale *et al*., 1998). However, all native New Zealand flora, with the exception of two coastal, dune-dwelling species, use the C_3 photosynthetic pathway (Troughton *et al*., 1971, 1974; Wardle, 1991). Therefore the total variation in speleothem $\delta^{13}C$ is the result of factors influencing carbon fixation during photosynthesis in the local vegetation, and inorganic processes taking place within the soil and epikarst.

Plants that fix carbon via the C_3 pathway typically have $\delta^{13}C$ values in the range -26 to -28 ‰, although the full range of variability is captured by a range extending from -22 to -38 ‰ (Tieszen, 1991; Arens *et al*., 2000). The less negative end of this range is of interest here.

Arens *et al*. (2000) note along a transect from "cool mixed hardwood and conifer" through "C_3 grassland/shrub" to "C_3 semidesert" that plant $\delta^{13}C$ becomes enriched by almost 5 ‰. In a temporal sense the transect could be used to represent a transition from moist to dry climate, such as has been proposed for parts of New Zealand (including the Waitomo region) during the last glacial period (Newnham *et al*., 1989; Drost *et al*., 2007). Therefore increasing water stress could account for a portion of observed increases in $\delta^{13}C$.

In comparing glacial and interglacial $\delta^{13}C$ values it may also be necessary to consider the influence of temperature on carbon isotope fractionation during photosynthesis. Turney *et al*. (1997) found carbon isotope ratios of plant macrofossils preserved in northern European deglacial peat sequences displayed temporal variability akin to that of $\delta^{18}O$ in the Greenland ice cores. The conclusion that cooler mean annual temperatures cause lower $\delta^{13}C$ in land plants was thus drawn. Subsequently, in a comprehensive review, Arens *et al*. (2000) also report that low air temperatures generally correlate with decreased carbon isotope ratios in plants. However the magnitude of this effect is typically small at low latitude (and altitude) locations as temperatures well below the plant's optimum growing conditions occur less frequently (Tieszen, 1991). Furthermore it was suggested that plants growing in cool climates are adapted to such conditions and are therefore less likely to display variations in $\delta^{13}C$ (Tieszen, 1991).

Of the inorganic processes able to influence speleothem $\delta^{13}C$ it is understood that lower pCO_2 of the soil atmosphere will lead to increased speleothem $\delta^{13}C$

(Dulinksi and Rozanski, 1990). Carbonate solutions formed under lower partial pressures of CO_2 precipitate $CaCO_3$ more slowly and with higher $\delta^{13}C$ than from solutions formed under higher pCO_2 values. Such conditions are likely to occur in arid soils, following a thinning of the vegetation cover and the subsequent decrease in the contribution of organic material to the soil, and as a result of enhanced soil aeration.

Hendy (1971) provided further support for heavy $\delta^{13}C$ values from dry soils. Rapid percolation and relatively low soil pCO_2 could result in dripwater solutions with carbon dioxide concentrations of ≥1000 ppm. Under this scenario the effects of isotopic exchange between carbon dioxide in solution and that of the cave atmosphere predominate over those caused by Rayleigh-type distillation. Given that the $\delta^{13}C$ of carbon dioxide in the cave atmosphere reflects that of the atmosphere above ground (~-8 ‰) a limited amount of gas loss or exchange would lead to significant decrease in the $\delta^{13}C$ of species in the dripwater solution. Furthermore, low flow conditions would yield slow drip rates and therefore an increased time interval during which isotopic exchange could take place.

Evidence to support this hypothesis is available from the data collected in this study. In South Island stalagmite HW05-3 there is a clear relationship between low growth rates and less negative $\delta^{13}C$ (Figure 6.2). The same relationship also occurs in the GT05-5 record, also from South Island, although confidence in this interpretation is lessened by the low density of age data.

In summation it can be demonstrated that increased $\delta^{13}C$ of speleothem calcite in New Zealand is strongly linked to dry climate and the associated stress on plant productivity. This observation has the potential of adding a powerful new tool to the range of palaeoclimate proxies available from speleothems.

6.3 Removing the Source Water Effect from Speleothem $\delta^{18}O$

In this study, oxygen isotope ratios of speleothem calcite deposited during the last glacial period, including deglaciation, and early Holocene have been 'corrected' for the ice-volume effect. This is done in an attempt to account for changes in sea-water $\delta^{18}O$ at moisture source regions and thus allow interpretation of changes in speleothem $\delta^{18}O$ in terms of local and regional climate variability.

Global ice volume during the Quaternary has waxed and waned to such an extent that sea levels responded by fluctuating as much as 150 m (Lambeck *et al*., 2002; Siddall *et al*., 2003). Significantly, during evaporation of ocean water and subsequent precipitation of a portion of that moisture upon an ice sheet there is fractionation of oxygen isotopes. $\delta^{18}O$ of ice from cores drilled in Greenland and Antarctic ice sheets reveal values in the range -34 to -54 ‰ relative to modern sea water (0 ‰ VSMOW) for parts of the last glacial period (NGRIP Members, 2004; EPICA Community Members, 2006).

The large volume of isotopically light water locked up in the ice sheets during periods of increased ice volume was counterbalanced by isotopically heavier sea water. A number of studies have determined that during the LGCP, when global ice volume achieved a maximum, mean ocean $\delta^{18}O$ was 1.1 ± 0.1 ‰ greater than at present (Shackleton and Opdyke, 1973; Shackleton, 1987; Fairbanks, 1989; Schrag *et al*., 1996; Shackleton, 2000; Lea *et al*., 2000; Schrag *et al*., 2002; Duplessy *et al*., 2002) although if the extreme sea-level lowering is combined with the extreme $\delta^{18}O$ observed in the Antarctic ice sheets this figure could exceed 1.7 ‰. It is likely that the bulk of the sea-level lowering resulted from ice deposited on lower latitude ice sheets, from which there is no longer ice to be measured. Oxygen isotope fractionation was likely less extreme on these ice sheets than that currently observed in Greenland and Antarctica. Provided that the same fractionation persisted between its sea water source and the meteoric precipitation over the region of interest, the rainfall would be 1.1 ± 0.1 ‰ heavier than at present. At the LGCP sea level was lower by 120-140 m compared to the present (Lambeck and Chappell, 2001). This will have resulted in adiabatic cooling of the site by about 1 °C, the net result of which is likely to decrease the $\delta^{18}O$ of the meteoric precipitation by a further 0.45 to 0.7 ‰. Therefore a detailed

history of oceanic $\delta^{18}O$ variability is required if an accurate 'correction' for ice volume is to be applied to speleothem records.

Several methods allow estimates of global ice volume fluctuations over the last glacial period to be made. Initial work used benthic foraminifera from marine sediment cores (Shackleton and Opdyke, 1973). This method provides an almost continuous record of sea level change, although the timing of changes cannot be easily determined independently but instead is tuned to variations in Earth's orbital parameters (Shackleton and Opdyke, 1973) or ice core records (Shackleton *et al*., 2000; Siddall *et al*., 2003). It also relies on the assumption that the temperature of bottom waters above the core location did not change, and that there is a linear relationship between $\delta^{18}O$ and sea level. Adkins *et al*. (2002) and Siddall *et al*. (2003) suggest that estimating sea levels by this method leads to uncertainties of up to ± 30 m (or 20-25% of the $\delta^{18}O$ correction if used in reverse).

Uranium-series dating of fossil coral terraces can also yield records of past sea-level change (Broecker *et al*., 1968; Bard *et al*., 1990, 1996; Chappell and Polach, 1991). Each terrace represents a period, when sea level rose at the same rate as the underlying coast was uplifted, long enough for a reef to form. At these locations (e.g. Barbados and Huon Peninsula, Papua New Guinea) tectonic uplift must be accounted for to obtain accurate estimates of past sea levels. Once achieved, accurate determinations of past sea level elevations can be made. However, due to the corals only recording relative stillstands, the record is fragmentary, unlike data from marine sediment cores.

Growth histories of presently submerged speleothems can also provide records of past sea level changes (Richards *et al*., 1994). Periods of growth indicate times when sea level was below that of the cave. As with the coral terraces, this method provides absolutely dated, fragmentary sea level data.

In order to maintain comparability with studies of New Zealand speleothems by Williams *et al*. (2004, 2005), this study has used the paleo-sea level curve developed from coral terraces by Lambeck and Chappell (2001). It also has the advantage of having an absolute and independent chronology. The sea level curve is particularly well constrained for the period 20-0 kyr B.P. with as many as six independent records yielding similar (± 5 m, equivalent to ± 0.04 ‰ $\delta^{18}O$ of seawater) sea level curves. Between 80 and 20 kyr B.P., approximately the remainder of the period recorded by speleothems in this study, there is less

confidence in past sea levels primarily due to coarse data resolution, but also increasing uncertainty in uplift rates and age errors.

Maximum sea level lowering in the Lambeck and Chappell (2001) dataset is -140 m. Williams *et al*. (2005) set this equal to the maximum change in mean ocean $\delta^{18}O$, namely 1.1 ‰. If it is assumed that there is a simple linear relationship between sea level and $\delta^{18}O$ of seawater, the sea-level curve of Lambeck and Chappell (2001) can be re-interpreted in terms of an isotope ratio (Figure 6.3). Using linear interpolations between data pints in the sea-level/seawater-$\delta^{18}O$ curve, the mean ocean $\delta^{18}O$ at any time in the past can be calculated. This method was used to generate values that were subtracted (because the glacial ocean was enriched in ^{18}O relative to the present) from the raw HW05-3 $\delta^{18}O$ data to adjust for the ice-volume effect (Figure 6.4).

Due to the coarse data resolution and significant uncertainty in the timing and magnitude of sea level changes in the Lambeck and Chappell (2001) curve during much of the period of interest in this research (10-75 kyr B.P.), alternative sea level proxy records were considered. Siddall *et al*. (2003) model global sea level changes for the past glacial-interglacial cycle based on the oxygen isotopic composition of planktonic foraminifera from Red Sea sediments and a model of water residence time in the Red Sea for different sea levels. The resulting curve has a data resolution of 200 years, and sea level estimates are accurate to ± 12 m, thus overcoming the limitations presented by the Lambeck and Chappell (2001) dataset. This could allow improved assessment of whether abrupt, short-term changes in the HW05-3 speleothem record might be forced by changes in ice volume.

A lack of planktonic foraminifera in sediments that accumulated between 21 and 12.3 kyr B.P. creates a hiatus in the Siddall *et al*. (2003) sea level record. A maximum lowering of global sea level at this time, and for the period of record investigated here, of 120 ± 12 m is suggested. As with the coral-terrace model, sea level was again converted to $\delta^{18}O$ values using enrichment in mean ocean $\delta^{18}O$ of 1.1 ‰ equivalent to the LGCP lowstand (here 120 m; Figure 6.3).

The application of the high-resolution record of Siddall *et al*. (2003) to the HW05-3 record produces similar results to the coral-terrace model (Figure 6.4). Two notable differences created by the Red Sea model are more negative values

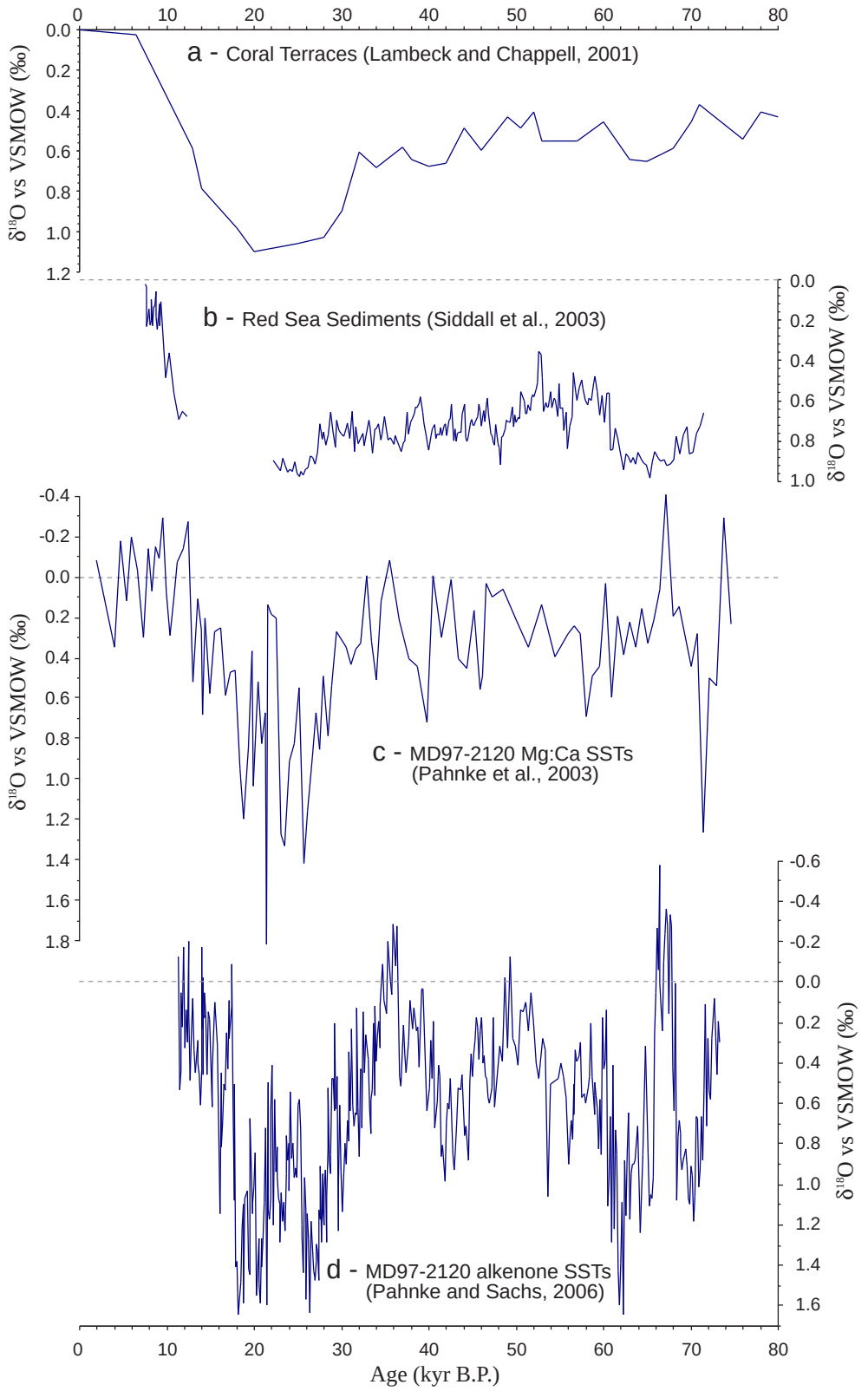

Figure 6.3: Models of seawater $\delta^{18}O$ during the last glacial period at moisture source regions affecting Hollywood Cave, South Island. Individual models are based on (a) palaeo-sea level determinations from coral terraces and (b) Red Sea sediments. In both (c) and (d), Mg:Ca and alkenone concentrations, respectively, derived sea surface temperature (SST) estimates are used with planktonic foraminifera $\delta^{18}O$ from the same site (MD97-2120; Chatham Rise) to calculate seawater $\delta^{18}O$.

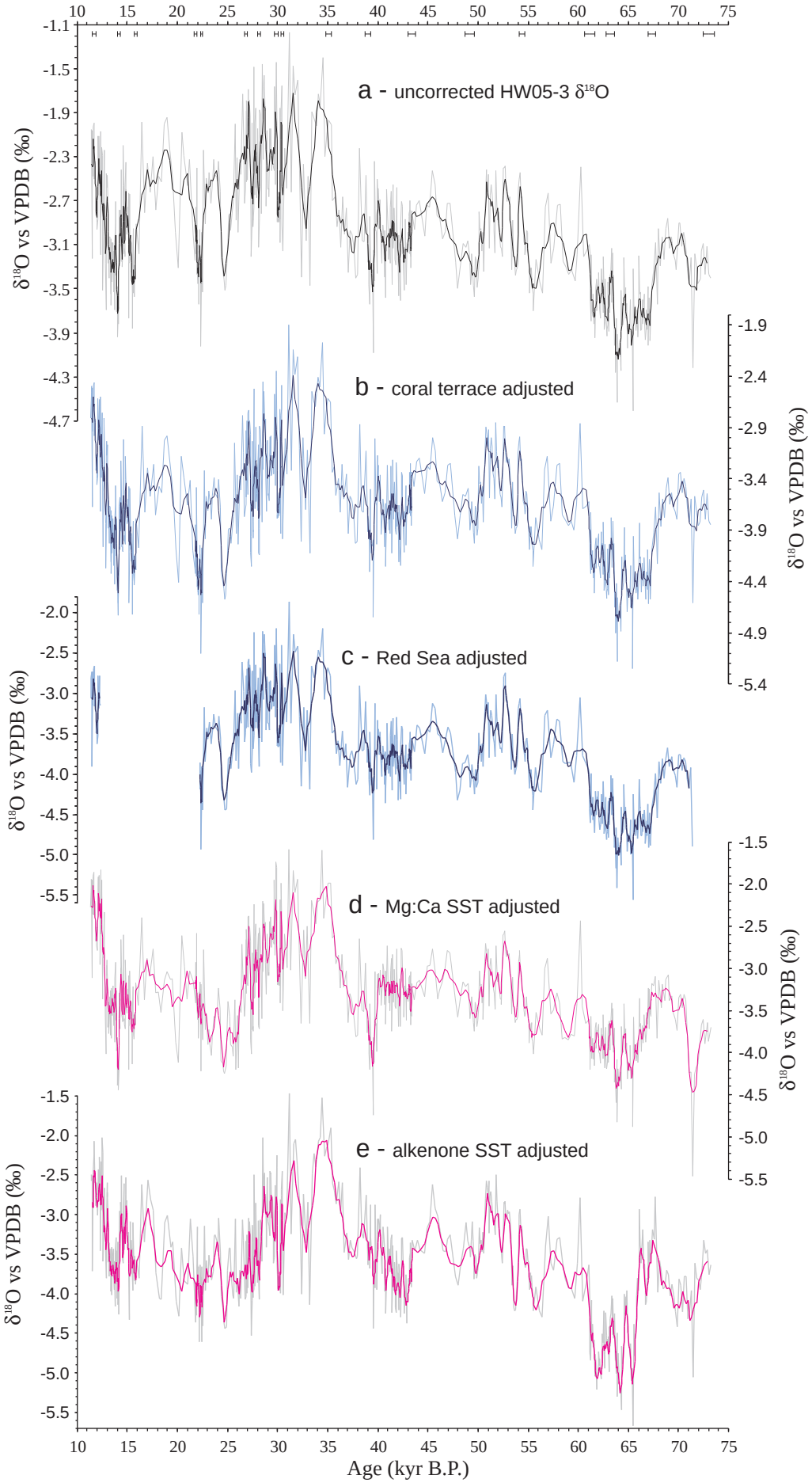
a - uncorrected HW05-3 δ18O
b - coral terrace adjusted
c - Red Sea adjusted
d - Mg:Ca SST adjusted
e - alkenone SST adjusted
δ18O vs VPDB (‰)
Age (kyr B.P.)

Figure 6.4: Comparison of (a) the raw HW05-3 $\delta^{18}O$ profile, to profiles adjusted for changes in ice-volume or local sea-surface $\delta^{18}O$. Shown in each model are all of the data (light-coloured line) as well as a 5-point running mean (heavy line). (b) The HW05-3 $\delta^{18}O$ profile adjusted for the coral terrace sea-level curve of Lambeck and Chappell (2001), converted to $\delta^{18}O$ values by assuming modern sea level is equivalent to 0.0 ‰ and tha LGM lowstand is equal to +1.1 ‰. (c) The HW05-3 $\delta^{18}O$ profile adjusted for the high-resolution sea level curve derived from Red Sea sediments (Siddall et al., 2003). Due to the lack of a sea level minimum in the Red Sea record (the aplanktonic zone covering the period 22.2-12.9 kyr B.P.) the lowstand is arbitrarily set to -120 m, which is assumed to be equivalent to +1.1 ‰ seawater $\delta^{18}O$. The other two models, d and e, utilise sea-surface temperature (SST) estimates from marine sediment core MD97-2120 to adjust planktonic foraminifer $\delta^{18}O$ (from the same core) to yield past seawater $\delta^{18}O$. (d) is calculated from SSTs derived from Mg:Ca ratios and $\delta^{18}O$ of Globigerina bulloides (Pahnke et al., 2003), while (e) is calculated using alkenone (Uk^{37})-derived SSTs (Pahnke and Sachs, 2006) and $\delta^{18}O$ of Globigerina bulloides. Of the four models, b-e, b is the preferred option and is used throghout this manuscript. Uranium-thorium age data for stalagmite HW05-3 are presented at the top of the figure with 2σ error bars.

during MIS 4, further highlighting this event, and a less gradual transition into the LGCP. All other differences fall within the margins of error in each dataset.

The Siddall *et al*. (2003) model also has its limitations. The most obvious is the lack of data during the late-glacial. This yields an incomplete modification of the HW05-3 record. Also, the chronology of the record beyond the limit of radiocarbon dating has been 'tuned' to other records. Siddall *et al*. (2003) demonstrated age offsets in excess of 1500 years between curves applied to chronologies from Northern and Southern Hemisphere profiles. However, the age uncertainty of coral terraces during this interval is of a similar magnitude. Moreover, the model relies on some of the same assumptions as the coral-terrace model regarding the relationship between sea water $\delta^{18}O$ and global ice volume.

When adjusting speleothem $\delta^{18}O$ profiles with records of global sea level change two significant assumptions are made:-

First, it is assumed that changes to the isotopic compositions of the world's oceans caused by fluctuations in global ice volume are equal and occur simultaneously regardless of where water is added or removed. Because the mixing time of the global ocean is ~ 1500 years this becomes particularly problematic when attempting to interpret millennial and sub-millennial scale events, such as those documented in this research. Due to the greater point-source nature of meltwater inputs compared to sites of ocean evaporation, inter-basin $\delta^{18}O$ differences are likely to be greatest at times of sea level rise. Ice build-up on Antarctica is suggested to have accounted for 25% of the total drop in sea level (Lambeck and Chappell, 2001), with most of the remaining 75% due to accumulation of ice in high latitudes of the Northern Hemisphere. Therefore, during melting associated with warm phases, potentially much of the ^{18}O-depleted water added to the oceans would be derived from Northern Hemisphere ice sheets (Cordilleran, Greenland, Laurentide and Fennoscandian) and thus have drained almost exclusively into the North Atlantic. If, as suggested, discharge of large volumes of glacial meltwater reduces the strength of the thermohaline circulation (Broecker, 2003) then mixing of this water across all basins could take in excess of 1500 years.

Under these conditions, rain water in New Zealand, being derived from moisture sources on the opposite side of the globe to the North Atlantic, may not

have been influenced by such significant shifts in sea water $\delta^{18}O$ as predicted by models of global sea level change.

Second, it is assumed that there is a linear relationship between changes in ice volume and sea-water $\delta^{18}O$, ignoring the fact that the isotopic composition of an ice sheet is not constant, but varies with thickness, areal extent and maturity. Because at least three large ice sheets (Cordilleran, Laurentide and Fennoscandian) which formed during the last glacial period are no longer in existence, it is not possible to directly test this assumption. Nevertheless, theoretically during the early stages of ice sheet formation the isotopic composition of atmospheric precipitation deposited on the ice surface will be relatively heavy (say -15 ‰ VSMOW) due to the low elevation of the ice sheet (Figure 6.5). Therefore the initial accumulation of ice will have a smaller impact on sea water $\delta^{18}O$ than under mature conditions. In terms of the assumed linear relationship, the estimated isotopic change in sea water $\delta^{18}O$ as determined from a sea-level record will overestimate the true change. This phenomenon can be observed (from the opposite perspective) in the offset between sea level reconstruction and benthic $\delta^{18}O$ during MIS 4 (as presented in Siddall *et al*. (2003) Figure 4) where benthic $\delta^{18}O$ underestimates sea-level lowering by as much as 20 m.

A larger, mature ice sheet has a lighter stable oxygen isotope signature (Figure 6.5). Although much of the precipitation falling on the ice sheet is relatively heavy, most falls around the margins and is rapidly returned to the oceans. Isotopically light snow that gradually accumulated in the centre of the ice sheet takes significantly longer to be recycled. Currently ice accumulates at Vostok, near the centre of the East Antarctic ice sheet, at 2.0 cm/yr and appeared to accumulate at rates of less than 1cm/yr during the LGM (Petit *et al*., 1999). Therefore changes in ice volume once large ice sheets have become established will result in greater enrichment of seawater $\delta^{18}O$ than predicted by a linear relationship between sea level and sea-water $\delta^{18}O$. Siddall *et al*. (2003, Figure 4) present evidence to suggest that during the LGCP benthic $\delta^{18}O$ indeed indicates sea levels were lower than is estimated by other proxies.

Furthermore, as an ice sheet ablates, the last ice to melt will largely be from the most isotopically depleted centre. This has implications for interpreting the change in sea-water $\delta^{18}O$ during deglaciation.

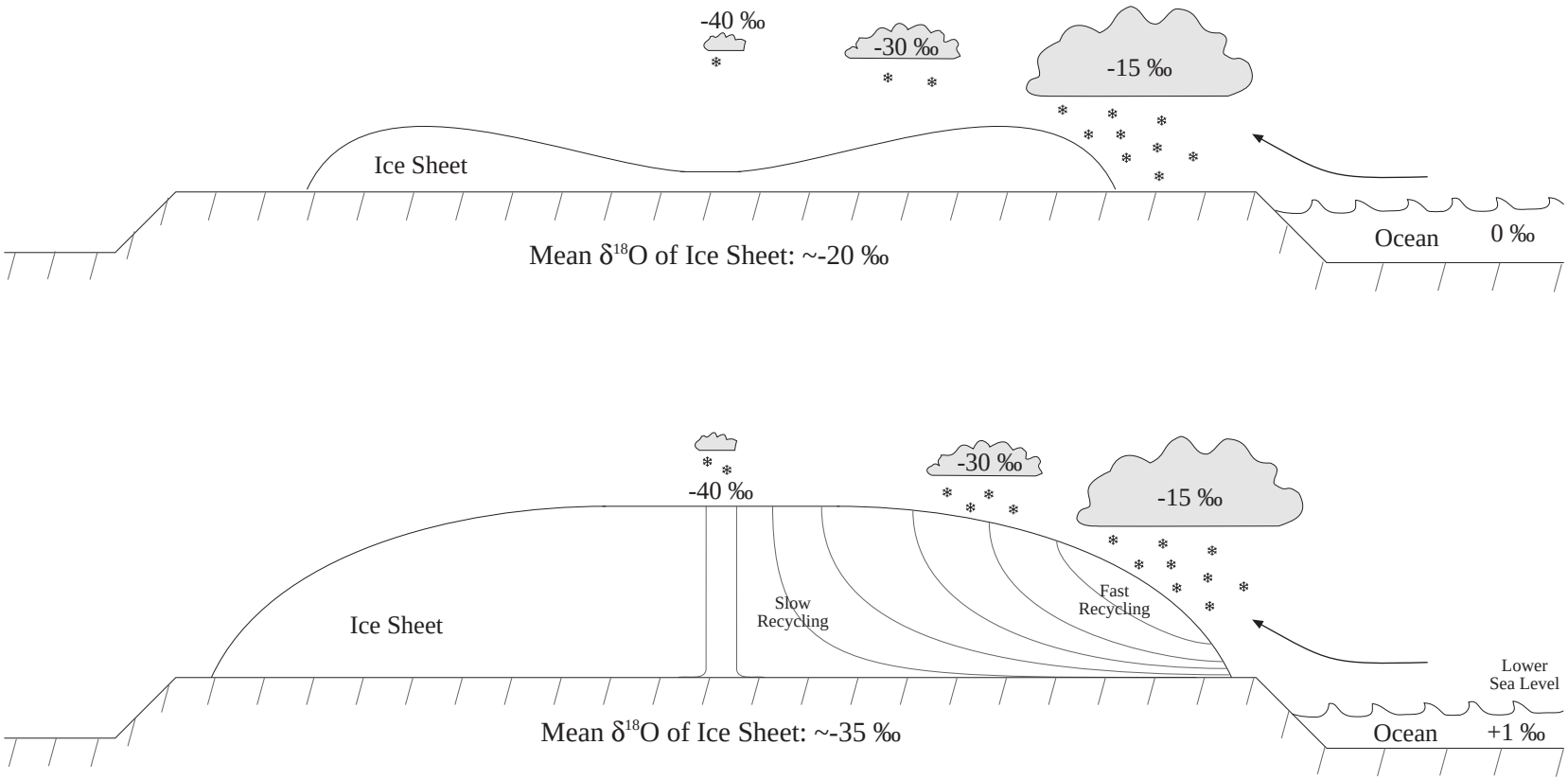

Figure 6.5: The oxygen isotopic compositions of (a) a continental ice sheet in the early phase of development, and (b) a mature ice sheet.

An additional limitation of global ice volume corrections is that they do not account for changes in sea surface temperature at the moisture source region, a variable that can have a significant impact on the $\delta^{18}O$ of meteoric precipitation. This limitation can be overcome, and the assumptions described above ignored, if records of surface ocean $\delta^{18}O$ can be found for the moisture source region of precipitation falling above the cave.

In Figure 6.3c,d two models are generated from high-resolution marine sediment data from core MD97-2120 retrieved from Chatham Rise, east of South Island (Pahnke *et al*., 2003; Pahnke and Zahn, 2005; Pahnke and Sachs, 2006). These data include $\delta^{18}O$ of planktonic foraminifer *Globigerina bulloides* (hereafter *Gg. bulloides*), and sea surface temperature (SST) estimates determined from the Mg/Ca ratio of *Gg. bulloides* tests and from alkenone paleothermometry. The $\delta^{18}O$ of a planktonic foraminifer test reflects the isotopic composition of the water in which it was formed and the temperature of that water ("vital effects" can be ignored as a single species is used to create the dataset).

The temperature effect on oxygen isotope fractionation between water and calcium carbonate is -0.24 ‰/°C. Therefore the Mg/Ca and alkenone SST estimates can be used to remove the temperature effect from foraminifer $\delta^{18}O$ leaving a value for $\delta^{18}O$ of past surface water at that site (provided that the foraminifera do not change their water mass, depth or seasonality in response to climate change (Nelson *et al*., 2000)). To simplify the relative changes in SST a mid- to late-Holocene (0-6 kyr B.P.) mean SST was calculated and all other SSTs were normalized to this value.

There are still significant assumptions built into this model. Whereas the alkenone temperatures are derived from coccoliths living at the sea surface, *Gg. bulloides* is not a surface-dwelling species but rather inhabits mid-depth waters. Furthermore, this species has been shown to exhibit changes in depth with seasons, glacial-interglacial climate shifts and the strength of upwelling of nutrient-rich bottom waters (Nelson *et al*., 2000).

The Mg/Ca SST data from core MD97-2120 has an average resolution of 670 years over the period captured in the HW05-3 isotope profile. The seawater $\delta^{18}O$ curve calculated using the above method varies across 2.2 ‰ during the period 10-75 kyr B.P. (Figure 6.3c). This is three times that determined for the change in global mean seawater $\delta^{18}O$ from fluctuations in global ice volume for the same

interval. However, for much of the period of interest, seawater $\delta^{18}O$ was less than 0.5 ‰ greater than the late-Holocene mean. Exceptions occur at 73-71.4, 28.9-23 and 21.5-17.8 kyr B.P. when sea water $\delta^{18}O$ briefly exceeded +1.1 ‰ VSMOW. The dataset is characterized by large (> 0.5 ‰) millennial-scale shifts. These are typically supported by only single data points and are largely eliminated if a 3- or 5-point running mean is applied to the data. The application of a 3-point running mean reduces the total range in calculated seawater $\delta^{18}O$ from 2.23 to 1.35 ‰. This figure is close to the estimated glacial-interglacial change in mean ocean $\delta^{18}O$ of 1.1 ± 0.1 ‰, providing confidence in applying this method to the HW05-3 $\delta^{18}O$ profile.

The Mg/Ca and planktonic $\delta^{18}O$ data yield smaller corrections during MIS 4 and MIS 3 than the sea level models, but similar corrections during the LGCP. As a result, the relatively heavy $\delta^{18}O$ during the LGCP and strongly negative values during MIS 4, prominent in the raw HW05-3 data, appear diminished (Figure 6.4d).

Surface ocean $\delta^{18}O$ at MD97-2120 was also calculated using the alkenone SST and planktonic foraminifer $\delta^{18}O$ data (Figure 6.3d). The high resolution of the resultant curve (~215 yr timesteps) is comparable to the Siddall *et al*. (2003) dataset but has the advantage of covering the entire period of interest.

Similar to the Mg/Ca model, the alkenone model of sea-water $\delta^{18}O$ was also found to vary by 2.2 ‰, with the greatest enrichment occurring during the LGCP (Figure 6.3d). However, there are few other similarities between the models. Sea water corrections were greater than 0.5 ‰ more frequently and for considerably longer intervals than in the Mg/Ca model, and corrections greater than 1.1 ‰ (the maximum assumed for the sea level models) occurred during the late stages of MIS 4, and much of the LGCP.

Another feature of the alkenone SST data are periods during MIS 4, MIS 3 and deglaciation when the surface water $\delta^{18}O$ was depleted relative to the mid-to-late Holocene mean. This result could not occur in the Lambeck and Chappell (2001) and Siddall *et al*. (2003) models, as there is presently no evidence to indicate that sea levels were higher during the last glacial period. This result therefore highlights another limitation imposed by assuming that variability in sea-water $\delta^{18}O$ is tied exclusively to ice volume.

The MD97-2120 alkenone model implies that seawater $\delta^{18}O$ underwent considerably greater variability than has been estimated for the mean global ocean from changes in ice volume (cf. Figures 6.3a and 6.3d). Part of the large variability could be the result of an underestimate of the glacial-interglacial SST change at the site. The difference between the Holocene average, to which all other data are normalized, and the LGCP is 1.5-3.5 °C. These are relatively low figures in comparison to the Mg/Ca SST data from the same core as well as other glacial-interglacial temperature change estimates for the New Zealand region (Barrows *et al*., 2007; Drost *et al*., 2007 and references therein). The MIS 5e SSTs in MD97-2120 are ~4.5 °C higher than the mid-to-late Holocene average used to normalize the data, although there are no other proxy data to support such a large difference.

Some of the seawater $\delta^{18}O$ variability could have been caused by influx of water masses with different isotopic signatures. Sea surface salinity changes at MD97-2120 provide evidence for increased incursion of Southern Ocean water over the site during cold intervals (Pahnke *et al*., 2003). The impact on seawater $\delta^{18}O$ of changing the balance of sub-tropical and polar waters is not well known, but potentially could account for up to 0.5 ‰.

As well as the uncertainty in the magnitude of the temperature changes at MD97-2120, use of the calculated seawater $\delta^{18}O$ profiles to adjust the HW05-3 stable isotope record has several other drawbacks. These include: (1) Chatham Rise is unlikely to have been a moisture source region for meteoric precipitation above Hollywood Cave (i.e. a high-resolution marine record from the north Tasman Sea would be better); (2) the chronology of the core is reasonably robust up to the limit of radiocarbon dating, but the remainder of the record was tuned to a North Atlantic marine sediment core (itself tuned to a Greenland ice core chronology) which not only introduces further age uncertainty but also provides a bias towards Northern Hemisphere timing of climate events; (3) the planktonic foraminifer *Gg. bulloides* does not dwell exclusively in the surface ocean (Nelson *et al*., 2000; Barrows *et al*., 2007) and therefore the planktonic $\delta^{18}O$ signature may not truly represent sea surface conditions; and (4) it is assumed that there was only one moisture source for precipitation above Hollywood Cave, or that all moisture sources had identical $\delta^{18}O$ at all times.

Despite the various limitations and assumptions that accompany each model, all are applied to the HW05-3 profile (Figure 6.4b-e). This allows identification of events common to each record, which would therefore likely be the result of climate changes, and events in the raw HW05-3 profile that disappear following adjustment by each model. The latter of these would indicate changes in $\delta^{18}O$ in the moisture source region as being the primary driver of $\delta^{18}O$ variability in HW05-3 calcite.

MIS 4 is consistently represented by the most negative isotopic values. However its duration in the MD97-2120 alkenone SST model is reduced. In addition, the least negative values occurred during the interval lasting from 35-27 kyr B.P. Values begin to decrease earliest in the alkenone SST model. Each model also presents evidence for an extended LGCP, which covered the period ~27 to 13 kyr B.P. Interestingly, the alkenone SST model also significantly reduced all of the enriched $\delta^{18}O$ values that occurred during the LGCP in the raw data, so creating a longer isotopic minimum than the other models.

Ultimately the models described here demonstrate that considerable care needs to be taken when (1) choosing a source water or ice volume correction to apply to speleothem $\delta^{18}O$ profiles, and (2) interpreting events, particularly those of short ($\leq$1 kyr) duration, in records where a correction has been applied.

The coral terrace derived sea-level model (Figure 6.4b) is the preferred option in this study. The main reason for this is that it allows direct comparison to previously published speleothem records from New Zealand which were also adjusted in this manner. This model was previously used here in section 5 (Results) and will be used further in the forthcoming sections.

6.4 Guillotine Cave, South Island

6.4.1 Climate reconstruction

The high elevation Guillotine Cave, from which stalagmite GT05-5 was obtained, lies within the limits of Quaternary glaciation in the Southern Alps (Suggate, 1965; Nathan *et al*., 2002). The hiatus in calcite deposition within GT05-5 from ~73-9 kyr B.P. (Table 5.3) is therefore most likely the result of glacial ice expanding over the cave and blocking the supply of seepage water. It is understood that glacial ice overrode the cave during MIS 6 and the LGCP but there is no clear indication of the position of ice margins during MISs 4 or 3. However, further south the Loopline moraine (MIS 4) clearly lies significantly beyond the Larrikins (34-28 and 24.5-21.5 kyr B.P.) and Moana (20.5-19 kyr B.P.) moraines of the LGCP (Suggate and Almond, 2005; Preusser *et al*., 2005). Furthermore, cooling of the regional climate following the penultimate interglacial (MIS 5) began as early as 81.5 kyr B.P. allowing time for extensive valley glaciers to form in the Southern Alps (Pahnke *et al*., 2003).

The interval 73 ± 2 kyr is also significant amongst speleothems collected in this and other New Zealand studies. At low-elevation, coastal Hollywood Cave uranium-series dates of basal material indicate that formation of three stalagmites (of four sampled) began at this time. Flowstone in high elevation Exhaleair Cave, Mt Arthur, contains a hiatus from 73-16 kyr B.P. (Hellstrom *et al*., 1998). On North Island, stalagmite RK05-4 (this study) also ceased forming ~72 kyr B.P., although more likely in response to dry climate than being overridden by ice.

Retreat of glacier margins from their LGCP extent began close to 17.5 kyr B.P. (Schaefer *et al*., 2006). Guillotine Cave could have been ice free as early as ~15 kyr B.P. (Figure 3.1; Nathan *et al*., 2002). Immediate reinitiation of calcite deposition in the cave is unlikely. Establishment of vegetation and the formation of a soil above the cave would be necessary to generate seepage waters with pCO_2 greater than that of the cave atmosphere. However, this process would not have taken ~6 kyr as suggested by the basal date of GT05-5. This is confirmed by basal dates from other Guillotine Cave stalagmites which demonstrate speleothem formation in the cave was underway by 11.32 kyr B.P. One possible cause for the delay in the onset of growth could be a blockage, potentially caused by glacial

debris, within the flow path preventing seepage water from reaching the stalagmite. Resumption of GT05-5 calcite deposition 9.3 kyr B.P. would therefore indicate when the blockage was breached. Alternatively, precipitation of calcite from the seepage water earlier in the flowpath may have occurred. In this scenario deposition may have begun at GT05-5 only once the concentration of carbonate in solution was sufficiently high that it could not all precipitate out in the earlier cavity. Such a mechanism would result in the calcite precipitated on GT05-5 having relatively enriched $\delta^{13}C$. While carbon isotope values are relatively heavy at the start of the GT05-5 record (Figure 6.6a) these may also be the result of dry climate or unproductive soil at this time.

Previous studies of New Zealand speleothems have indicated that a positive relationship exists between $\delta^{18}O$ and mean annual temperature (Williams *et al*., 2004, 2005). Due to noticeable covariation in the $\delta^{18}O$ and $\delta^{13}C$ of South Island speleothems collected in this study and by others (Williams *et al*., 2005), an expanded hypothesis is proposed. Decreased $\delta^{18}O$ (and $\delta^{13}C$) in speleothems from Westland likely indicates significant winter contribution to mean annual rainfall due to strong circumpolar westerly circulation. This likely would also bring cooler mean annual temperatures to the region. Under weaker westerly circulation the occurrence of southerly airflow is enhanced leading to decreased winter rainfall volumes. The drier climate would cause $\delta^{13}C$ to become enriched.

The Holocene stable isotope records from stalagmite GT05-5 (Figure 6.6a) are therefore interpreted primarily in terms of annual precipitation totals. In addition the data also allows inferences to be made regarding changes to the seasonal distribution of rainfall.

The early part of the GT05-5 record, 8.7-4.7 kyr B.P., is marked by relatively dry conditions due to decreased winter rainfall totals. This broad interval correlates with a period when almost all glaciers in the Southern Alps were at standstill or retreat (Gellatly *et al*., 1988) suggesting low rainfall totals and/or increased mean annual temperatures (Figure 6.6c). Warm conditions at this time are also indicated by increased SSTs at marine site MD97-2121 (Figure 6.6b), east of North Island (Pahnke and Sachs, 2006), as well as in air temperatures at Taylor Dome, Antarctica (Steig *et al*., 2000; Figure 6.6e). A link between events in New Zealand and Antarctica would implicate the circumpolar westerly circulation as the primary driver of climate change in the southwest Pacific.

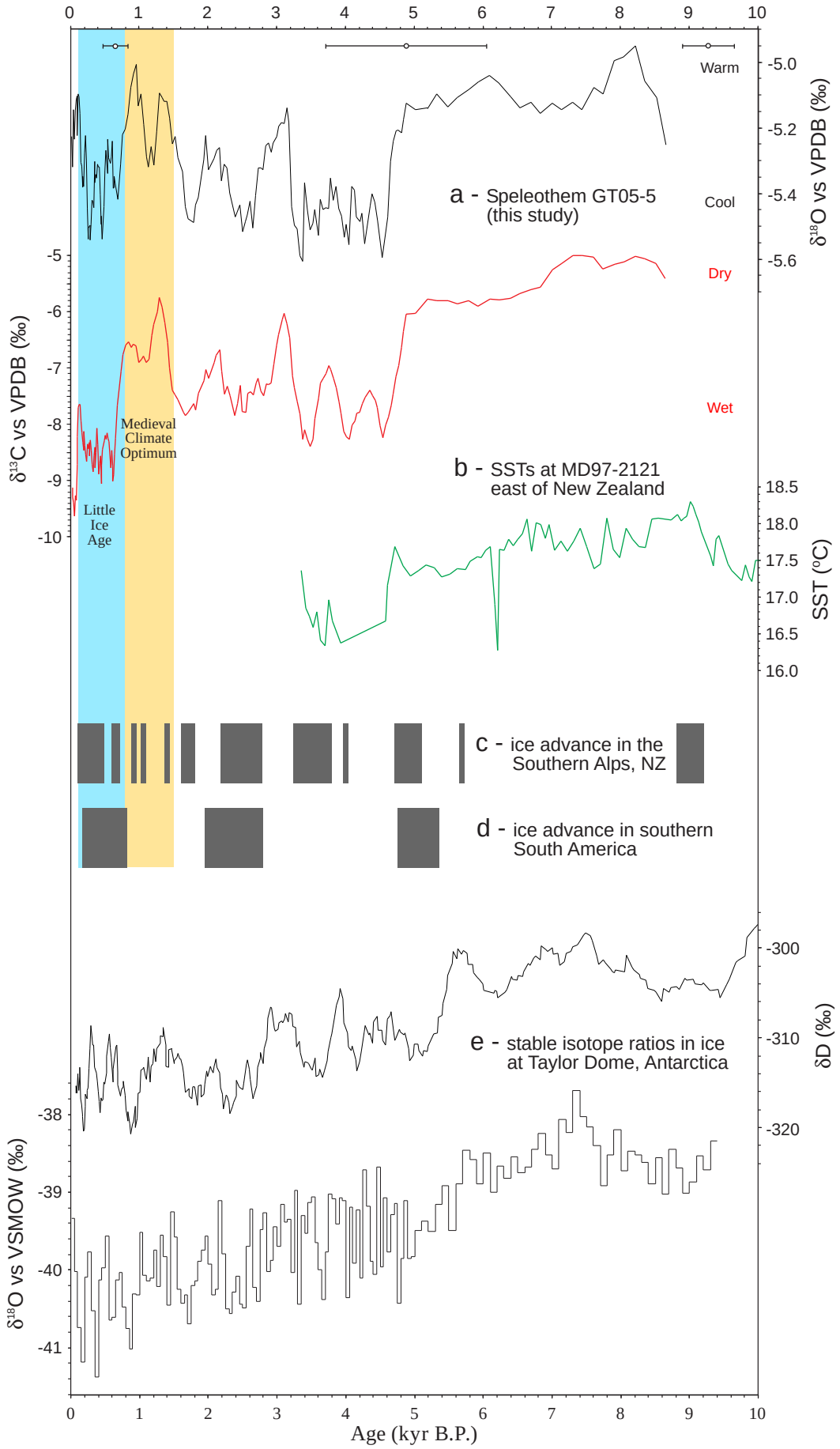
Warm
Cool
Dry
Wet
a - Speleothem GT05-5 (this study)
b - SSTs at MD97-2121 east of New Zealand
c - ice advance in the Southern Alps, NZ
d - ice advance in southern South America
e - stable isotope ratios in ice at Taylor Dome, Antarctica
Medieval Climate Optimum
Little Ice Age
δ13C vs VPDB (‰)
δ18O vs VPDB (‰)
SST (°C)
δD (‰)
δ18O vs VSMOW (‰)
Age (kyr B.P.)

Figure 6.6: Comparison of (a) GT05-5 $\delta^{13}C$ and $\delta^{18}O$ profiles (5-point running means displayed) to local, regional and hemispheric climate proxies. Uranium-series ages obtained for GT05-5 are shown at the top of the figure with 2σ error bars. Shown are (b) SSTs off the east coast of North Island (site MD97-2121; Pahnke and Sachs, 2006); (c) glacier advance in the Southern Alps (Gellatly et al., 1988); (d) glacier advance in southern South America (Mercer, 1976); and (e) δD and $\delta^{18}O$ of ice at Taylor Dome, Antarctica (Steig et al., 2000). Timing of glacier advances are converted from radiocarbon timescales using INTCAL04 (Reimer et al., 2004). Taylor Dome $\delta^{18}O$ data are presented as 50 year and 100 year means for the periods 0-5 and 5-10 kyr B.P. respectively. The δD curve is a 9-point running mean of the raw data.

The transition toward a wetter, and potentially cooler, climate following ~4.7 kyr B.P. in the GT05-5 record marks rapid onset of the Neoglacial in New Zealand. The Neoglacial is recognized as a broad period of cool climate that persisted throughout the mid-to-late Holocene (Denton and Karlén, 1973). Evidence for the cooling came largely from moraine records from North America, Europe and South America which identify the onset of the Neoglacial ~ 5 kyr B.P. as a time of advancing glaciers (Denton and Karlén, 1973; Mercer, 1976; Röthlisberger, 1986; Gellatly *et al*., 1988; Grove, 2004). The wide distribution of these records suggests that Neoglacial cooling was a global phenomenon. Decreases in GT05-5 stable isotope ratios at ~4.7 kyr B.P. add strength to these suggestions. In addition, sea surface temperatures east of New Zealand show an abrupt decrease synchronous with the decrease in isotopic values at Guillotine Cave (Figure 6.6b). Globally synchronous climate change is also supported by rapid cooling at Taylor Dome, Antarctica (Figure 6.6e). Notably this event occurs ~800 years earlier at Taylor Dome than at GT05-5 and MD97-2121, but this could be accounted for by uncertainty in the timescales used.

The Neoglacial period has continued to the present day although with three oscillations between warm and cool phases (Denton and Karlén, 1973; Grove, 2004). From 4.7 kyr B.P. to the present day the GT05-5 stable isotope profiles also contain a record of three full oscillations between isotopic maxima and minima. Minima (relatively wetter intervals) occurred at 4.7-3.2, 2.75-1.6 and 0.8-0.2 kyr B.P., each separated by well-defined maxima (relatively drier intervals). Each wet interval matches closely with known phases of glacier advance in the Southern Alps, South America (Figure 6.6c,d) and the Northern Hemisphere (Denton and Karlén, 1973; Mercer, 1976; Röthlisberger, 1986; Gellatly *et al*., 1988). The earliest oscillation was also recorded as a period of cool SSTs east of New Zealand (Pahnke and Sachs, 2006; Figure 6.6b).

A pronounced peak in $\delta^{18}O$ from 1.5-0.8 kyr B.P., followed by a trough which lasted until the early 19th century, represents the most recent, and briefest, Neoglacial oscillation in the GT05-5 record (Figure 6.6a). In addition, the significant negative excursion in stable isotope ratios indicate that the 'cool' phase was the wettest of the three that occur during the Neoglacial. Significantly, the dry and wet intervals coincide with the timing of the Medieval Climate Optimum (MCO) and Little Ice Age (LIA) respectively (Figure 6.6; Grove, 2004).

New Zealand glaciers responded to a dry MCO and wet LIA (Figure 6.7a-c). There is only sparse evidence for glacier advance during the interval 1.5-0.7 kyr B.P., but significant advances are documented after 0.7 kyr B.P. across the Southern Alps (Gellatly *et al*., 1988). LIA glaciers approached maximum extent ~1750 A.D., although they were still extensive, relative to today, in 1850 A.D. Considerable retreat has occurred in most glaciers of the Southern Alps since this time (Gellatly *et al*., 1988). Evidence for a LIA affecting the climate of South Island, New Zealand, has also been documented in previous speleothem studies (Wilson *et al*., 1979; Williams *et al*., 2005; Figure 6.7d-f). The onset of the LIA differs in each record, and is different again in the GT05-5 chronology, which shows the earliest onset (Figure 6.7a,b). However, uncertainty in the GT05-5 chronology, due to an age of 654 ± 182 yr B.P. on material which marginally post-dates the MCO/LIA transition, could account for the apparent early onset of the LIA at Guillotine Cave.

Calcite deposited on GT05-5 within the last century displays a divergence of $\delta^{13}C$ and $\delta^{18}O$ trends, a feature uncharacteristic of the entire GT05-5 record to this point. Following the termination of the LIA ~0.2 kyr B.P. $\delta^{13}C$ values increased until the onset of the 20th century at which point there is an abrupt negative shift and $\delta^{13}C$ values become 2.7 ‰ lighter (Figure 6.7b). Similarly light values are maintained until the end of the record (2006 A.D., when GT05-5 was collected), creating the longest period of such light isotopic values in the 9300 year profile. The abrupt shift to lighter $\delta^{13}C$, without a coincident change in $\delta^{18}O$, argues against a climate change and instead suggests a change in the vegetation above the cave. The abrupt vegetation change coincides with the beginning of open settlement and agricultural practices in Maruia Valley in 1907 (Tasman District Council, 2008), suggesting that the isotopic signal recorded anthropogenic influences.

6.4.2 Implications for Regional and Global Climate Change

The positive relationship between GT05-5 stable isotope profiles and changes in glacier mass balance in the Southern Alps (Figures 6.6 and 6.7) provides support for the suggestion that South Island speleothems record variability in

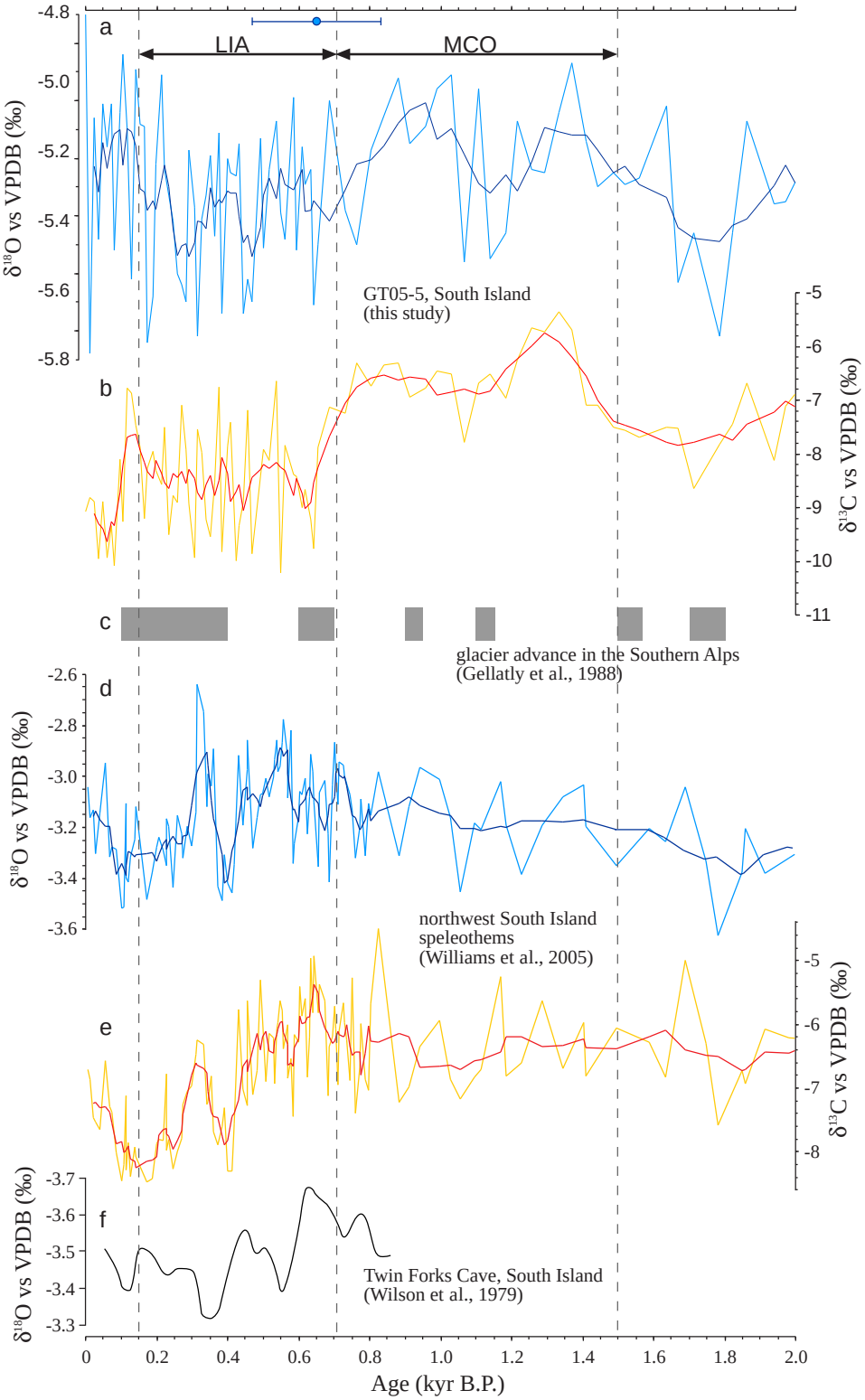

Figure 6.7: Timing of Medieval Climate Optimum (MCO) and Little Ice Age (LIA) events in GT05-5 compared to other late-Holocene palaeoclimate records from New Zealand. Shown are (a) GT05-5 $\delta^{18}O$; (b) GT05-5 $\delta^{13}C$; (c) periods of glacier advance in the Southern Alps (Gellatly et al., 1988); (d and e) northwest South Island stacked speleothem $\delta^{18}O$ and $\delta^{13}C$ records respectively (Williams et al., 2005), and (f) Twin Forks Cave, South Island, $\delta^{18}O$ (Wilson et al., 1979). Age data for the GT05-5 record is shown at the top of the figure (blue circle) with 2σ error.

precipitation volumes and rainfall seasonality. Westland climate dominated by southwesterly flow would experience wetter winters, and likely greater mean annual precipitation, than under any other predominant wind direction. This increase would promote positive mass balance in Southern Alps glaciers (Hooker and Fitzharris, 1999). In addition, if southwesterly airflow persisted during summer there would be fewer cloudless days and cooler temperatures. Such conditions would lead to reduced ablation of glaciers, raising the potential for ice advance in the Southern Alps (Anderson and Mackintosh, 2006).

Glacier advances in South America (Mercer, 1976) and cool temperatures in Antarctica (Steig *et al*., 2000; Masson-Delmotte *et al*., 2004) synchronous with wet/cool intervals in New Zealand implicate the circumpolar westerly circulation, operating in the southern mid-to-high latitudes, as the main driver of climate variability in South Island. Increased strength of the circulation leads to greater frequency of synoptic weather patterns associated with southwesterly airflow across South Island. When the circulation is operating in a weakened state, the predominant wind in South Island is a southerly (Almond *et al*., 2007). Water vapour borne by these winds would be precipitated as the air mass was forced over the Southern Alps. Once reaching the West Coast, on the other side of the ranges, potential for further rainfall would be low allowing a relatively drier climate to develop.

Many of the events in the GT05-5 stable isotope profiles (e.g. Neoglacial, MCO and LIA) were first recognized in Northern Hemisphere palaeoclimate records. The synchronous occurrence of these events, at multiple locations in both Northern and Southern Hemispheres, strongly argues for atmospheric fluctuations being rapidly transmitted across the globe. The abruptness of the onset and/or termination of some events argues further that the atmosphere, not the oceans, is the primary driver of change.

6.5 Hollywood Cave, South Island

$\delta^{13}C$ and $\delta^{18}O$ profiles developed from Hollywood Cave speleothem HW05-3 have an average temporal resolution of 86 years (Figures 5.14 and 5.15). As such they represent the best resolved terrestrial palaeoclimate records of the last glacial period from New Zealand and should therefore allow favourable comparison with other long, high-resolution records from the region and around the world. In so doing elucidation of local, hemispheric and global climate patterns should be possible. In the following sections the Hollywood Cave palaeoclimate record is discussed, beginning with the earliest part of the record and ending with the most recent.

6.5.1 MIS 4 (~70-61 kyr B.P.) Climate Reconstruction

The most prolonged period of strongly negative stable isotope ratios (both $\delta^{18}O$ and $\delta^{13}C$) in the 64 kyr HW05-3 record corresponds to marine oxygen isotope stage (MIS) 4 (Figures 5.14 and 5.15). In addition, as previously discussed (see section 6.1), this was also a period of relatively high growth rate (Figure 6.2). In combination, these proxies indicate that West Coast climate was wet (perhaps as wet as, or wetter than, at present) and cold at this time.

As demonstrated in section 6.2 there is robust evidence to suggest that cool climate intervals are represented in South Island speleothem calcite as negative $\delta^{18}O$ excursions. To confirm that this is also the case for the HW05-3 record it would be appropriate to compare ratios at known warm and cold intervals (e.g. between the Holocene and the LGCP). Unfortunately the HW05-3 record does not span a full glacial-interglacial transition. However, a late Holocene (0-4.2 kyr B.P.) specimen from Hollywood Cave has previously been analysed and the data published (Williams *et al*., 2005). During MIS 4, following the adjustment for the ice volume effect, $\delta^{18}O$ in HW05-3 is -4.3 ± 0.3 ‰. Late Holocene $\delta^{18}O$ values from the Williams *et al*. speleothem are -3.4 ± 0.4 ‰ (Williams *et al*., 2005). Making the assumption that both stalagmites would produce identical $\delta^{18}O$ under the same environmental conditions, this result indicates that MIS 4 was colder than present.

When carbon isotope ratios are compared between these Hollywood Cave speleothems for this same interval the ranges overlap [-8.0 ± 0.6 ‰ (this study) and -7 to -9 ‰ (Williams *et al*. 2005)]. This result, in conjunction with increased growth rate at this time, strongly indicates that rainfall amounts were similar to the present day during MIS 4.

A cold and wet climate in New Zealand during MIS 4 is supported by a number of previous studies. Extensive glaciation at a number of locations on both sides of the Southern Alps is inferred from the extended locations of terminal moraines (Loopline; Balmoral), extensive glacier outwash plains and loess accumulations assigned MIS 4 age from stratigraphic relationships and, more recently, exposure age dates (Suggate, 1990; Almond *et al*., 2001; Preusser *et al*., 2005).

The position of MIS 4 moraines outside those deposited during the LGCP agrees well with the isotopic values in HW05-3 calcite which indicate that MIS 4 was wetter than the LGCP, as well as being colder than at present. I also note here that the ice volume correction derived from the Lambeck and Chappell (2001) sea-level curve applied to this dataset has a conservative lowering estimate for MIS 4. If the Siddall *et al*. (2003) Red Sea data are employed to generate an ice volume correction a further decrease of MIS 4 $\delta^{18}O$ of 0.25-0.4 ‰ would occur, increasing the difference between MIS 4 and LGCP isotopic values.

Sea surface temperatures off the east and west coasts of South Island, as determined from Mg/Ca ratios of planktonic foraminifera and of di- and tri-unsaturated alkenones in marine algae, were colder-than-present, by ~3-6 °C, during MIS 4 (Pahnke *et al*., 2003; Pahnke and Sachs, 2006; Barrows *et al*., 2007). Given the strong maritime influence on New Zealand climate it is likely that mean annual temperatures on land were similarly decreased. Burge and Shulmeister (2007) inferred a 3-5°C cooling in north Westland from beetle assemblages over a period of record that potentially represents MIS 4.

The suggestion that MIS 4 was cold and wet is further supported by West Coast fossil pollen assemblages. Vandergoes *et al*. (2005) interpreted a minor shift toward increased herb pollen abundance at a coastal site during an interval approximately dated as MIS 4 in age as a cool interval, while Moar and McKellar (2001) reported pollen assemblages which indicated that the MIS 4 landscape was that of an open grassland developed on locally waterlogged soils.

At similar latitudes in Australia there is evidence for significant advance of glacier ice (Barrows *et al*., 2001; Kiernan *et al*., 2004) during MIS 4. In addition a Tasmanian speleothem record covering the period 84-56.5 kyr B.P. displays a signal for MIS 4 similar in length, magnitude and sense of change to that developed from HW05-3 (Goede *et al*., 1998).

The density of $\delta^{18}O$ analyses through the interval of HW05-3 corresponding to MIS 4 (67.7-61.3 kyr B.P.) yields a temporal data resolution of 50-65 years. This high resolution allows investigation of the structure and timing of millennial-scale events within MIS 4.

The most noticeable features of MIS 4 in the HW05-3 record are the sharp (~500 year) onset and even more abrupt termination (~150 year) (Figure 6.8e). Such rapid climate shifts are comparable to the abrupt events first observed in the Greenland ice cores, and since replicated in several other proxy records (Wang *et al*., 2001; Siddall *et al*., 2003). Furthermore, $\delta^{18}O$ of ice at Taylor Dome, Antarctica, also displays sudden climate shifts at the onset and termination of MIS 4 (Grootes *et al*., 2001), which are similar to those in the HW05-3 record (Figure 6.8g).

The duration of MIS 4 on the West Coast was shorter (~6.4 kyr) than has been suggested in other independently-dated palaeoclimate records, which typically span 8-10 kyr (Figure 6.8; Goede *et al*., 1998; Wang *et al*., 2001; Lambeck and Chappell, 2001). The onset and termination of MIS 4 are precisely dated in HW05-3 and age uncertainties are not large enough to account for the discrepancy. However, MIS 4 in HW05-3 exactly matches the length of a hiatus in a stalagmite from Villars Cave, France, referred to as the "Villars cold phase" (Figure 6.8c; Genty *et al*., 2003). The hiatus which lasted from 67.4 ± 0.9 to 61.2 ± 0.6 kyr B.P. is determined to have been caused by extremely low mean annual temperatures, associated with Heinrich event 6, which prevented continued growth of the stalagmite.

The high-resolution data reveal that West Coast climate during MIS 4 was not uniform but rather underwent millennial-scale fluctuations. The isotopic record displays five cycles of alternating cold/wet and cool/moist climatic conditions (Figure 6.8e). The first cycle began with the onset of MIS 4 cooling at 67.7 kyr B.P. and the last oscillation terminated synchronously with warming in the Northern Hemisphere associated with Greenland Interstadial (GIS) 17 (Figure

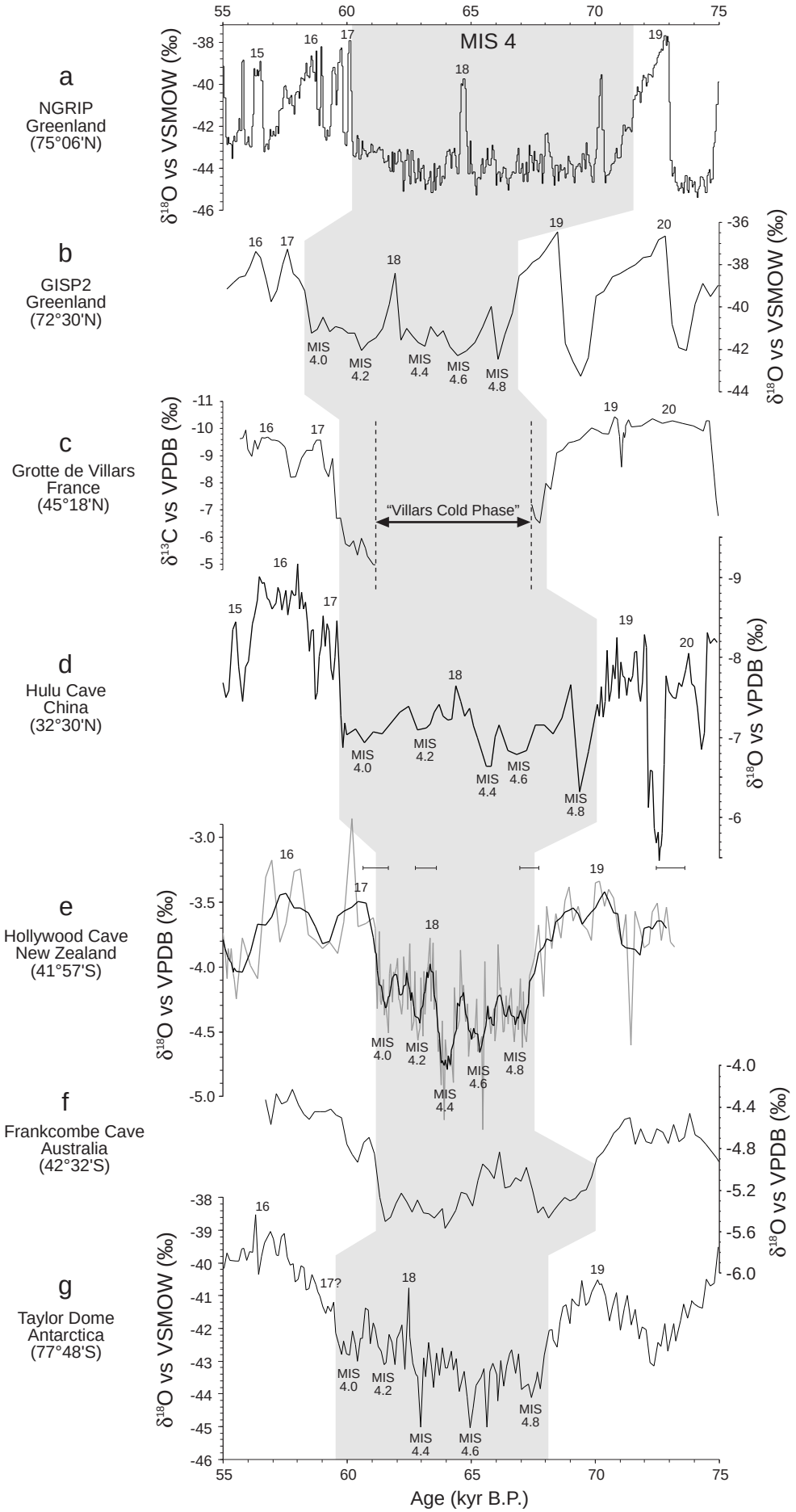
a
NGRIP
Greenland
(75°06'N)
b
GISP2
Greenland
(72°30'N)
c
Grotte de Villars
France
(45°18'N)
d
Hulu Cave
China
(32°30'N)
e
Hollywood Cave
New Zealand
(41°57'S)
f
Frankcombe Cave
Australia
(42°32'S)
g
Taylor Dome
Antarctica
(77°48'S)
MIS 4
"Villars Cold Phase"
MIS 4.0
MIS 4.2
MIS 4.4
MIS 4.6
MIS 4.8
δ18O vs VSMOW (‰)
δ13C vs VPDB (‰)
δ18O vs VPDB (‰)
Age (kyr B.P.)

Figure 6.8: Comparison of (e) the West Coast, South Island, Hollywood Cave stalagmite HW05-3 $\delta^{18}O$ profile to high-resolution speleothem and Greenland and Antarctic ice core records spanning MIS 4 (grey shading). The records are arranged in order of latitude, and include (a) NGRIP ice core $\delta^{18}O$ (on the GRIP ss09sea chronology; Johnsen et al., 2001; NGRIP Members, 2004); (b) GISP2 ice core $\delta^{18}O$ (Grootes et al., 1993); (c) Villars Cave stalagmite Vil9 $\delta^{13}C$ (Genty et al., 2003); (d) Hulu Cave stalagmite MSL $\delta^{18}O$ (Wang et al., 2001); (f) Frankcombe Cave stalagmite FT $\delta^{18}O$ (Goede et al., 1998); and (g) Taylor Dome ice core $\delta^{18}O$ (Steig et al., 2000). U-Th dates for stalagmite HW05-3 are shown with 2σ errors. Where recognised, Greenland interstadials (GIS) are numbered on each record. In accordance with MIS substage nomenclature, even numbers are used to denote the cold phases within MIS 4 that follow a ~1500 year cycle.

6.8). The length of each oscillation (peak to peak) is 1.2-1.6 kyr, with a mean duration of ~1.5 kyr.

The events are unrecognized in the existing literature. An attempt is made here to name the coolings associated with each cycle. The nomenclature suggested follows that previously used for the division of marine oxygen isotope stages into sub-stages, in that even numbers denote the relatively colder intervals. The youngest event is designated MIS 4.0 and the oldest MIS 4.8 (Figure 6.8e).

The effort has been made to name these events in light of similar cyclicity apparent in other climate records, from both Northern and Southern Hemispheres, which span MIS 4 (Figure 6.8). A particularly close match occurs between the $\delta^{18}O$ events in MIS 4 from Taylor Dome and HW05-3. The offset in age can be accounted for by the uncertainty in the Taylor Dome chronology, with estimated age errors greater than ±5 % at this time (Steig *et al*., 2000). Hulu Cave speleothem MSL also shows millennial-scale changes that broadly mirror the changes in HW05-3, although the comparison is limited by low data resolution through MIS 4.

Should the occurrence of these millennial-scale events in the Greenland ice core records be confirmed, they could be used to further develop the chronology of MIS 4 ice. There is a clear need for improvement in the chronologies given the large offsets in the timing of stadials and interstadials between the GISP2 and GRIP/NGRIP in this interval (Figure 6.8a,b).

The ~1500 year length of each cycle in the HW05-3 stable isotope records may be significant. A ~1500 year cycle has previously been identified in Holocene age North Atlantic sediments (Bond *et al*., 1997) and Greenland ice core geochemistry (O'Brien *et al*., 1995). Furthermore, the Dansgaard-Oeschger cycles in Greenland ice cores follow a 1470 year pacing that persisted throughout the glacial period. Beyond that, Bond *et al*. (2001) found evidence for a ~1500 cycle during the last interglacial. As suggested by Bond *et al*. (1997) the 1500 year cycle is likely a "pervasive component of Earth's climate system" and therefore ought to be present in palaeoclimate records from previous glacial and interglacial stages. The replication of the MIS 4 1500 year cycles in the Hollywood Cave and Taylor Dome records, along with Northern Hemisphere records, lends strong support for this hypothesis.

6.5.2 MIS 3 (~61-27 kyr B.P.) Climate Reconstruction

The MIS 4/3 transition is clearly defined in HW05-3 stable isotope profiles as an abrupt shift toward drier conditions ~61 kyr B.P. The termination of MIS 3 is less well defined, but is taken to be ~27 kyr B.P., synchronous with the conclusion of a prolonged period of enriched $\delta^{18}O$ values (Figure 6.9b,c).

In comparison to MIS 4, the climate during MIS 3 was relatively dry. In addition it is likely that annual temperatures were higher than during MIS 4, although still lower than at present (Barrows *et al*., 2007). These changes across the MIS 4/3 boundary were likely driven by a shift toward greater seasonality of climate on the South Island West Coast.

This hypothesis is based on greatly reduced growth rate and enriched isotope ratios in HW05-3 calcite deposited during MIS 3. Accumulation of calcite on HW05-3 at this time, but particularly between 61 and 43 kyr B.P., was the slowest for the entire period captured in the HW05-3 record (Figure 6.2). As discussed in section 6.1, factors leading to reduced growth rate include (1) decreased mean annual precipitation volumes, (2) a reduction of mean annual or winter temperatures leading to increased occurrence of ground frosts limiting the availability of seepage waters, and/or (3) depleted soil carbon dioxide concentration (which could occur as a result of dry soils and decreased plant productivity, again in response to low rainfall amounts and also cooler mean annual temperatures).

Low annual rainfall volumes on the West Coast could also explain the enriched $\delta^{13}C$ values in HW05-3. Drying of the soil would allow increased exchange of carbon dioxide between the soil atmosphere and the bulk atmosphere, lowering soil pCO_2. This would act to reduce the rate of calcite precipitation producing a deposit enriched in ^{13}C (Hendy, 1971; Dulinski and Rozanski, 1990). In addition, dry climates encourage plant $\delta^{13}C$ (and therefore the $\delta^{13}C$ of organic input to the soil) to rise due to water stress, compounding the inorganically driven isotopic change.

In addition to reduced growth rate and increased $\delta^{13}C$ values, the MIS 3 record in HW05-3 is also characterized by elevated $\delta^{18}O$ values (Figure 6.9b). There are three mechanisms which may have resulted in deposition of relatively enriched $\delta^{18}O$ calcite. First, warmer air temperatures above the cave. This is

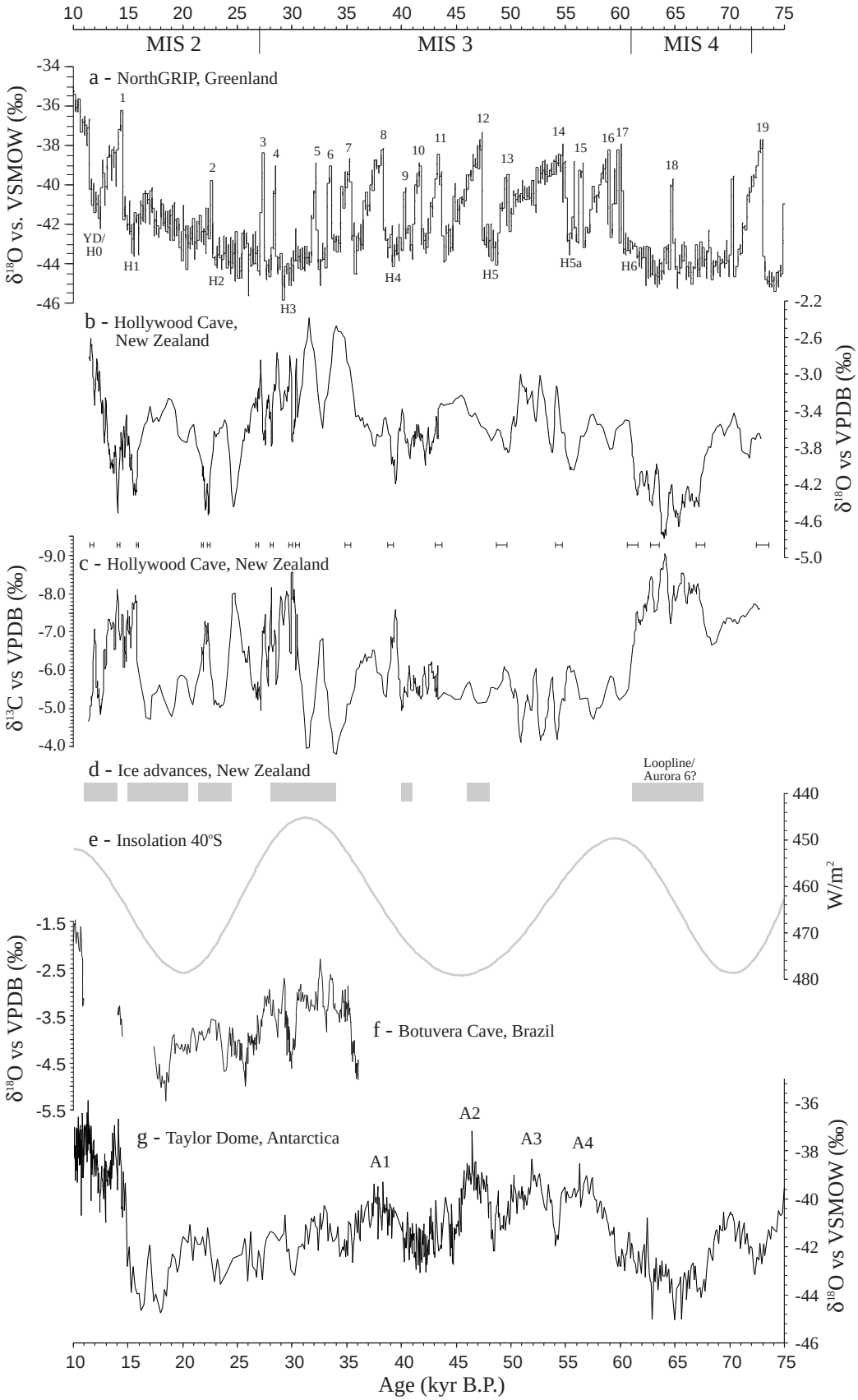
MIS 2
MIS 3
MIS 4
a - NorthGRIP, Greenland
δ18O vs. VSMOW (‰)
YD/ H0
H1
H2
H3
H4
H5
H5a
H6
b - Hollywood Cave, New Zealand
δ18O vs VPDB (‰)
c - Hollywood Cave, New Zealand
δ13C vs VPDB (‰)
d - Ice advances, New Zealand
Loopline/ Aurora 6?
e - Insolation 40°S
W/m2
f - Botuvera Cave, Brazil
δ18O vs VPDB (‰)
g - Taylor Dome, Antarctica
A1
A2
A3
A4
δ18O vs VSMOW (‰)
Age (kyr B.P.)

Figure 6.9: Comparison of HW05-3 (b) $\delta^{18}O$ and (c) $\delta^{13}C$ profiles with local, regional and global climate records. Uranium-series ages for the Hollywood Cave stalagmite HW05-3are shown, with 2s error bars, between (b) and (c). Comparisons are made with (a) $\delta^{18}O$ of ice at NorthGRIP, Greenland (NGRIP Members, 2004); (d) periods of glacier advance in New Zealand (Williams, 1996; Suggate and Almond, 2005; Schaeffer et al., 2006; Putnam et al., 2007; Kaplan et al., 2007); (e) mean summer (Dec-Jan-Feb) insolation at 40^{o}S (Berger and Loutre, 1991); (f) speleothem $\delta^{18}O$ from Botuvera Cave (Brazil; Wang et al., 2006); and (g) $\delta^{18}O$ of ice at Taylor Dome (Antarctica; Steig et al., 2000). The timing of GIS events (Greenland Interstadials) 1-19 and Heinrich events H0-6 are displayed on the NorthGRIP record, and Antarctic Interstadials A1-4 are shown on the Taylor Dome record.

explained by the positive $\delta^{18}O$-temperature relationship previously documented for Hollywood Cave (section 6.2). The difference between the precipitation effect (0.35-0.7 ‰/°C; Dansgaard, 1964; Williams *et al*., 2005; this study) and the cave temperature effect (-0.24‰/°C) is estimated to be ~0.1-0.45 ‰/°C. The total range in $\delta^{18}O$ in MIS 3 is ~2.6 ‰ which via this hypothesis would suggest mean annual temperatures varied as much as 6-26°C. Such temperature variability, even at the lower bound, exceeds current estimates of local and regional temperature changes not only during MIS 3 but also for the last glacial-interglacial cycle as a whole (Pahnke *et al*., 2003; Pahnke and Sachs, 2006; Barrows *et al*., 2007). Furthermore, this interpretation would also require that the warmest interval of the last glacial period occurred 35-31 kyr B.P., a hypothesis also unsupported by palaeotemperature reconstructions.

A second hypothesis for the relatively high $\delta^{18}O$ values is a reduction in winter rainfall amounts with the result being a shift toward summer-dominated annual precipitation. Warmer temperatures during summer, relative to winter, are accompanied by isotopically heavier precipitation. This is demonstrated for the present day using measurements of precipitation $\delta^{18}O$ at Invercargill in southern South Island. At Invercargill $\delta^{18}O$ of precipitation is heavier in summer than in winter by as much as 3 ‰ in association with mean summer temperatures 7-8 °C warmer than winter temperatures (IAEA & WMO, 2004). Therefore a shift toward annual precipitation volumes dominated by summer rainfall would lead to increased $\delta^{18}O$ of annually averaged cave seepage waters, potentially of a great enough magnitude to explain the observed changes in HW05-3.

Furthermore, under a relatively dry climate where annual precipitation is biased toward summer there is increased potential for the effect of evaporation to further reduce the volume of seepage water migrating into the cave and to raise the $\delta^{18}O$ of soil moisture via Rayleigh distillation.

A third hypothesis to explain an increase in the isotopic composition of HW05-3 calcite during MIS 3 is a change in the relative contributions of precipitation originating from isotopically different moisture sources. Two significant moisture supply regions for HW05-3 are the Southern Ocean and the Tasman Sea. The difference in the isotopic compositions of the seawater at these sites is unlikely to be great enough to explain the ~2.6 ‰ variance in the speleothem $\delta^{18}O$. However, this shortfall could be accounted for by rainout along

the moisture transport routes. Ultimately the isotopic composition of rainfall from a Southern Ocean (polar/sub-polar) source would be depleted in ^{18}O relative to rainfall from a (northern) Tasman Sea (tropical/sub-tropical) source. Therefore relatively enriched $\delta^{18}O$ in MIS 3 calcite could represent a climate shift where the bulk of precipitation subsequently came from the northern Tasman Sea.

The preferred hypothesis is that of increased seasonality of precipitation. Not only is it able to account for increased $\delta^{18}O$, it helps explain slow growth rates and elevated $\delta^{13}C$ as well. It is worth noting, however, that summer-biased precipitation could occur in harmony with a reduction in Southern Ocean sourced precipitation in the annual rainfall budget, highlighting the fact that the aforementioned three hypotheses support one another and a fourth hypothesis could be that all occur together and synchrony.

It is unclear as to what could cause the climate above Hollywood Cave to become drier. Drost *et al*. (2007) proposed that more frequent southerlies (at the expense of southwesterlies), particularly during winter, would lead to a decrease in annual precipitation volumes on the West Coast of South Island. It is anticipated that this would also amplify seasonal climate differences on the West Coast (Almond *et al*., 2007). Under an increased seasonality scenario the southerly flow dominating West Coast winters would lead to clear skies and lower temperatures. In turn, the occurrence of ground frosts would increase, preventing moisture penetration to the cave and raising the potential for reduced growth rates.

Unfortunately there is a lack of palaeoclimate data from South Island that could be used to investigate the hypothesis that West Coast climate during MIS 3 displayed greater seasonality and drier climate than at present. However, a late-MIS 3 palaeoprecipitation record from Westport (Figure 3.1), less than 25 km north of Hollywood Cave, does indicate that mean annual rainfall was reduced from present volumes by up to 50% at this time (Almond *et al*., 2007).

The suggestion that a climate pattern unique in the last glacial period to phases of MIS 3 is lent some credence from a number of Australian palaeoclimate profiles. In southern and central Australia MIS 3 was notably wetter than the preceding and subsequent stadials (MISs 2 and 4) as demonstrated by the formation and maintenance of large lakes in the central deserts (Chappell, 1991), renewed growth of speleothems (Ayliffe *et al*., 1998), and decreased dust transport to the Tasman Sea (Hesse 1994; Hesse and McTainsh, 1999). In

addition, there is a lack of speleothem records from Tasmania that capture MIS 3, suggesting that like the west coast of South Island this presently humid region was then dry. Although this evidence relies on the assumption that the lack of published MIS 3 records is due to there being no MIS 3 speleothems to collect, Goede *et al*. (1998) noted that a speleothem from Frankcombe Cave, northern Tasmania, ceased growing at the onset of MIS 3 after continuous formation through the later stages of MIS 5 and MIS 4.

Although Milankovitch cycles offer a mechanism by which seasonal climate may be modified, maxima and minima in insolation (determined for 40°S; Berger and Loutre, 1991) occur without any concurrent change in isotopic values in HW05-3 (Figure 6.9e). This is particularly clear in the interval 61-36 kyr B.P. Therefore, changes in the degree of seasonality in Westland during MIS 3 are unlikely to have been driven by orbital forcing.

Superimposed upon the broad scale changes during MIS 3 are millennial-scale fluctuations with amplitudes often reaching ~1.0 ‰ (Figure 6.9b,c). These suggest that the climate of Westland underwent frequent, abrupt, short-duration changes that bear some resemblance to the isotopic fluctuations in polar ice cores. A strong association between dry climate at Hollywood Cave and increased mean annual temperatures over both Antarctica and Greenland occurred during the period ~40-60 kyr B.P. (Figure 6.9a,g). At this time Antarctic warming events A2-A4 (equivalent to Antarctic Isotope Maxima (AIM) 12, 14 and 17) and Dansgaard-Oeschger (D-O) events 9-17 in Greenland were matched by positive isotopic excursions (dry episodes) in HW05-3 calcite. Conversely, cooler climates at the poles, indicated by decreased ice core $\delta^{18}O$, were matched by wet periods on the West Coast of South Island.

An hypothesis for a teleconnection between Antarctica and New Zealand could be that cooling of Antarctica drove northward migration of the polar front, increasing the temperature gradient across mid-southern latitudes. This in turn would strengthened the westerly circulation, increasing the frequency of southwesterly flow across South Island and therefore delivered greater precipitation to the West Coast and Hollywood Cave.

Significantly, the wettest intervals identified in the HW05-3 record occurred almost synchronously with the Heinrich events in the North Atlantic (Figure 6.2). Events H5a, H5, H4, and H3 occurred 56-55, 50.5-48, 40-39 and 29-30 kyr B.P.

in the Hollywood chronology. Further discussion of Heinrich events in the HW05-3 record is presented in section 6.5.5.

During the interval 39-27 kyr B.P. the association between climate events at the poles and those that occurred on the West Coast of South Island is less clear. Following the termination of H4, the signature of D-O/AIM 8 in HW05-3 was minor with respect to its ice core counterparts. Furthermore, two broad peaks in HW05-3 isotopic values between 35 and 31 kyr B.P., equivalent in timing to D-O/AIMs 7-5, were exaggerated relative to other D-O events. These peaks represent the driest conditions, either annually or only the winter season, at Hollywood Cave.

Almond *et al*. (2007) found that the West Coast was 50% drier than present during the interval 33-26 kyr B.P. At the same time the east coast of South Island was as wet as, and probably cooler than, present leading to extensive glaciation at southward-facing Lake Ohau on the eastern side of the Southern Alps (Putnam *et al*., 2007). The position of the ~30 kyr B.P. Lake Ohau moraines outside those deposited during the LGM supports a hypothesis that the least negative isotopic values in HW05-3 calcite at 35-30.5 kyr B.P. were driven by a prolonged period of climate dominated by cold (winter) southerlies during which time the South Island's west coast became drier and the east coast was relatively damp.

Isotope maxima were observed for this period in insolation driven $\delta^{18}O$ variability of two Brazilian speleothems (Cruz *et al*., 2005; Wang *et al*., 2006; Figure 6.9f). They also showed abrupt increases in $\delta^{18}O$ at ~35 kyr B.P. lasting until the onset of H3 at 30.5 kyr B.P. As previously argued, a link between isotopic variability in HW05-3 and insolation was not evident in the period of record discussed thus far (Figure 6.9e). Therefore the correlation of the peaks may be coincidence. It is possibile that the effect of insolation became significant during the unusually dry conditions that occurred between 35 and 30.5 kyr B.P. and acted to amplify the signal. A summer insolation minimum at 40°S occurred 32 kyr B.P. (Berger and Loutre, 1991). This could have led to a lengthened, southerly-dominated, dry winter season and reduced opportunity to receive summer precipitation.

6.5.3 Last Glacial Coldest Period (LGCP) Climate Reconstruction

The last glacial maximum (LGM) as defined by the EPILOG (Environmental Processes of the Ice Age: Land, Oceans, Glaciers) group (Mix *et al*., 2001) refers to the period 21 ± 3 kyr B.P., when global ice volume appears to have reached a maximum for the last glacial-interglacial cycle. However, recent studies have found that this interval, and therefore the term LGM, is not truly representative of the period of maximum cooling that affected New Zealand (Suggate and Almond, 2005; Vandergoes *et al*., 2005; Alloway *et al*., 2007; Newnham *et al*., 2007a). The onset of full glacial conditions is thought to have occurred as early as 29 kyr B.P. and may have lasted until 17.4 ± 1.0 kyr B.P. (Schaefer *et al*., 2006). These findings have led to the terms "extended LGM" (eLGM) and "last glacial coldest period" (LGCP) being adopted in recent studies of New Zealand palaeoclimate (Newnham *et al*., 2007a; Alloway *et al*., 2007).

It is not possible to clearly determine the timing of thermal minima at Hollywood Cave from the stable isotope data. However, a decline in $\delta^{18}O$ values at ~27 kyr initiates a period punctuated by multiple cold, wet intervals. This somewhat arbitrary definition for the onset of the LGCP is largely based on the similarity of $\delta^{13}C$ values, $\delta^{18}O$ values and accumulation rates for calcite deposited during the LGCP and much of MIS 3. The climate at these times is therefore also likely to have been similar. This provides some justification for the adoption in the previous section of LGCP climate hypotheses to interpret MIS 3 isotope variability.

A cold, dry West Coast, South Island, climate is interpreted from enriched $\delta^{13}C$ and $\delta^{18}O$ values and relatively slow growth rate. These findings are in agreement with a transition from shrubland to (sub-alpine) grassland on the coastal plain and extensive glacial advance from the Southern Alps at this time (Suggate and Almond, 2005; Vandergoes *et al*., 2005). In addition, Drost *et al*. (2007) concluded that the climate of the West Coast was likely to have been 4-5°C cooler than present and significantly drier. Dryness was likely a result of increased occurrence of southerly winds (at the expense of the presently dominant southwesterly), particularly during winter. Increased frequency of southerlies

would generate increased rainfall in the southern and eastern ranges of the Southern Alps, and create a drier, sunnier climate west of the main divide.

The climate above Hollywood Cave was not uniformly dry and cold throughout the LGCP (Figure 6.10a,b). HW05-3 $\delta^{13}C$ and $\delta^{18}O$ profiles, and growth rates (see section 6.1), were punctuated by millennial-scale changes. This too is in keeping with previous studies which have identified multiple climatic events for this period (Suggate and Almond, 2005; Vandergoes *et al*., 2005; Williams *et al*., 2005; Newnham *et al*., 2007a). The relatively dry conditions were interrupted on at least two occasions by brief (~1 kyr) wet phases likely associated with strengthening of the westerly circulation and an increased contribution to annual precipitation during winter months.

The first, and most intense of these events occurred 25.5-24.3 kyr B.P. The timing coincides with glacier advance in Westland (Figure 6.10f; Suggate and Almond, 2005), a cool interval in a South Island speleothem record (Hellstrom *et al*., 1998) and changes in the composition of trees, shrubs and grasses on the landscape surrounding Okarito, South Island (Figure 6.10g; Vandergoes *et al*., 2005). Similar vegetation changes occurred at Kohuora maar crater in Auckland, suggesting the same climate shift also affected North Island (Newnham *et al*., 2007a). In addition, glacier advance occurred in South America (Denton *et al*., 1999; McCulloch *et al*., 2005), and Heinrich 2 was discharged into the North Atlantic. This suggests that this cold and wet interval on the West Coast was part of a global climate change.

A second wet phase occurred 22.6-21.6 kyr B.P. (Figure 6.10a,b). It too was equivalent in timing to decreased(increased) herb(shrub and tree) pollen abundance at Okarito and Kohuora maar crater, as well as glacier advance in Westland and Chile. However, during this period there was no corresponding climate event in the North Atlantic. Minor cooling in Antarctica at this time (Figure 6.10i) may have allowed northward migration of the polar front. This provides an alternative mechanism by which the strength of the circumpolar westerly circulation, and the frequency of southwesterly flow over South Island, may be increased.

There is also evidence in the HW05-3 record for a third wet interval at ~20 kyr B.P. Although only defined by two data points in this low-resolution part of the record it is mentioned here due to the coincidence with the last of the

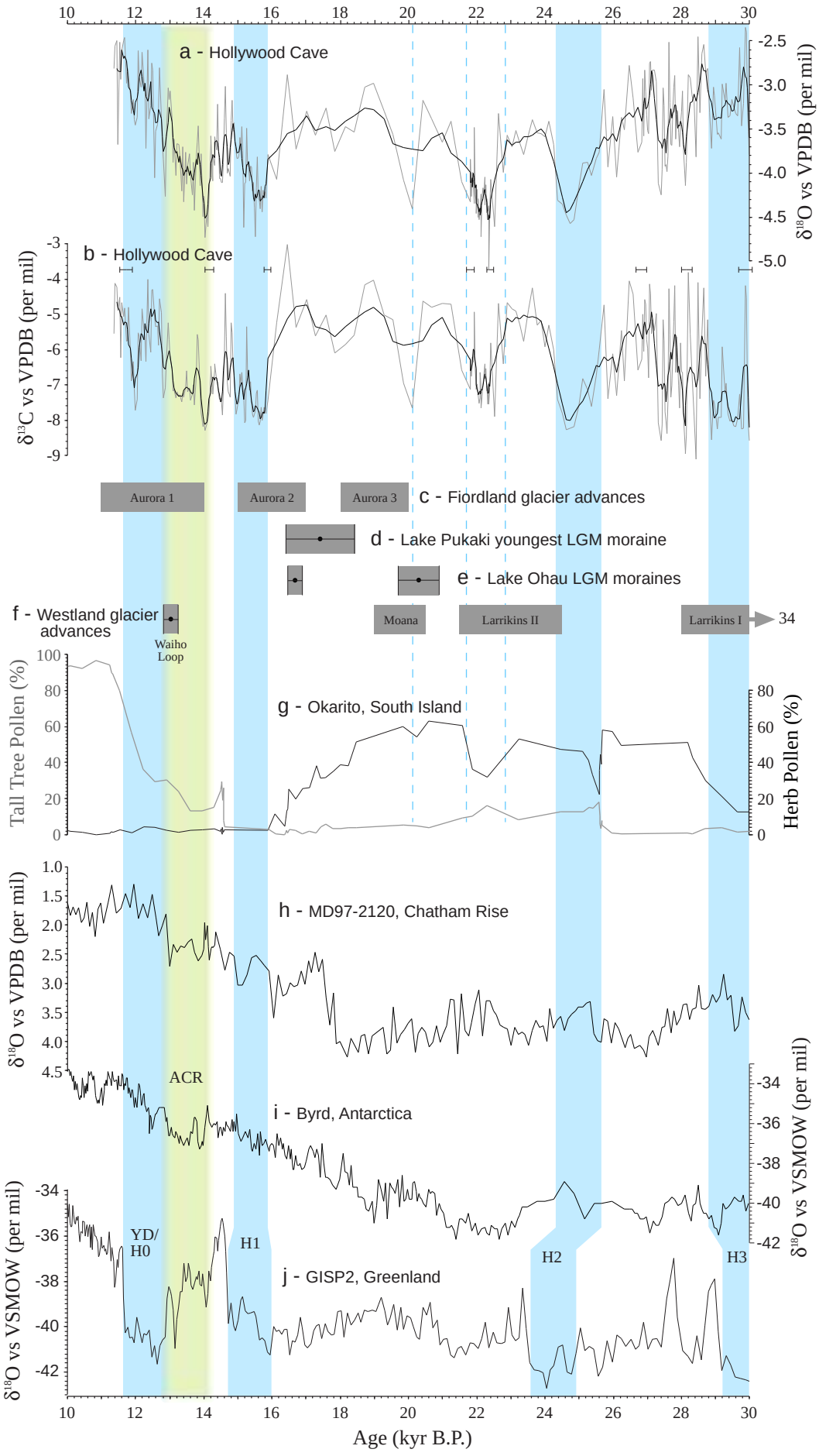
a - Hollywood Cave
b - Hollywood Cave
δ18O vs VPDB (per mil)
δ13C vs VPDB (per mil)
Aurora 1
Aurora 2
Aurora 3
c - Fiordland glacier advances
d - Lake Pukaki youngest LGM moraine
e - Lake Ohau LGM moraines
Moana
Larrikins II
Larrikins I
34
f - Westland glacier advances
Waiho Loop
Tall Tree Pollen (%)
g - Okarito, South Island
Herb Pollen (%)
h - MD97-2120, Chatham Rise
ACR
i - Byrd, Antarctica
YD/ H0
H1
H2
H3
j - GISP2, Greenland
δ18O vs VSMOW (per mil)
Age (kyr B.P.)

Figure 6.10: A composite of HW05-3 stable isotope profiles and selected palaeoclimate records covering the LGCP and deglaciation. (a) HW05-3 $\delta^{18}O$, raw data (grey line) and 5 point running mean (black line); (b) HW05-3 $\delta^{13}C$, raw data (grey line) and 5 point running mean (black line); (c) Fiordland glacier advances (Williams, 1996); (d) youngest LGCP moraines at Lake Pukaki, South Island (Schaefer et al., 2006); (e) LGCP moraines at Lake Ohau, South Island (Putnam et al., 2007); (f) LGCP moraines in Westland, South Island (Denton and Hendy, 1994; Suggate and Almond, 2005; Turney et al., 2007); (g) tall tree and herb pollen abundance in Okarito sediments, Westland (Vandergoes et al., 2005) [data on the GT timescale (Vandergoes, unpublished data)]; (h) $\delta^{18}O$ of planktonic foraminifer Globigerina bulloides at site MD97-2120, Chatham Rise (Pahnke et al., 2003); (i) $\delta^{18}O$ of ice at Byrd station, Antarctica (Blunier and Brook, 2001); and (j) $\delta^{18}O$ of ice at GISP2, Greenland (Grootes et al., 1993). Blue bars indicate the Younger Dryas Chronozone (YD) and Heinrich Events H0-H3 as they appear in the GISP2 and HW05-3 records. The green bar represents the Antarctic Cold Reversal (ACR) as defined in the Byrd record.

recognised LGCP moraines in the Westland glacial sequence (Suggate and Almond, 2005), an isotopic maximum in a northwest South Island speleothem (Hellstrom *et al*., 1998), and a minor decline in herb pollen abundance at Okarito, furthering the trend developed by the previous wet phases.

The correlation of wet phases and the timing of glacier advance on the West Coast has important implications for the understanding of the primary controlling factor of ice mass-balance in the Southern Alps. There has been some debate in the literature as to whether ice advance in the Southern Alps (particularly on the western flank) is driven primarily by increased precipitation (Hooker and Fitzharris, 1999) or decreased mean annual temperature (Anderson and Mackintosh, 2006). The results of a model of the Franz Josef Glacier, Westland, by Anderson and Mackintosh (2006) indicated that temperature had a strong effect on glacier mass balance when the volume of ice was already reduced, but its effect waned with increasing ice volume. Furthermore, to achieve a glacier long enough to have created the LGCP moraines, mean annual temperatures would have had to have been reduced by considerably more than 5°C, particularly under a drier-than-present climate as suggested by the HW05-3 stable isotope data. Such intense cooling is not supported by available palaeotemperature records for this period (Barrows *et al*., 2007). Intriguingly, however, the model presented by Anderson and Mackintosh (2006; see their Figure 3b) suggested that as mean annual temperatures decreased the length of the Franz Josef Glacier became increasingly more sensitive to changes in annual precipitation volumes. Under these conditions the longest and most intense of the wet phases (25.5-24.3 kyr B.P.) ought to have produced the most extensive glacier, and the shorter and weaker subsequent wet phases would have generated successively smaller glaciers. The moraine record at Franz Josef, and elsewhere on the West Coast, demonstrates this pattern (Suggate and Almond, 2005).

If the same model scenario is applied to the long (~6.5 kyr) and intense cool, wet phase during MIS 4 one would expect the glaciers at this time to be more extensive than during the LGCP. This is also supported in moraine records from the Southern Alps (Suggate and Almond, 2005; Preusser *et al*., 2005; Denton *et al*., unpublished data).

6.5.4 Deglaciation (~17-11 kyr B.P.)

Following the third wet phase the climate remained cold and dry at Hollywood Cave until 16.1 kyr B.P. with only minor variability apparent in the isotope proxies (Figure 6.10a,b). However, during this time deglaciation was underway. Global sea level rose (Lambeck and Chappell 2001 and references therein), Antarctica was warming (Petit *et al*., 1999; Blunier and Brook, 2001) and there was considerable retreat of glaciers from their terminal LGCP positions both on the West Coast, South Island, and elsewhere around the world (Suggate and Almond, 2005; Schaeffer *et al*., 2006; Easterbrook, 2007). In addition, Westland vegetation was changing from grassland to shrubland, further indicating amelioration of the climate (Vandergoes *et al*., 2005). The cause of the insensitivity of the HW05-3 record to regional and global warming associated with deglaciation is assumed to be a function of the proxies providing primarily a record of palaeoprecipitation rather than palaeotemperature.

Dry conditions were abruptly terminated at 16.1 kyr B.P. by a return to a wetter climate which lasted until 15.0 kyr B.P. During this period there was an increase in the abundance of tree pollen at Okarito indicating that the vegetation in the landscape was responding to further warming of the regional climate (Figure 6.10g: Vandergoes *et al*., 2005). It is not clear whether this event had an impact on glacier mass balance in the Southern Alps with only the study of Williams (1996) suggesting that glacier advance took place at this time. However, this wet phase is coeval with H1 (Figure 6.10) further demonstrating the sensitivity of West Coast climate to events in the North Atlantic.

There then occurred a brief period of slightly drier (minor increase in $\delta^{13}C$), and potentially warmer, climate which lasted until ~14.5 kyr B.P. before deglaciation was interrupted by a second wet interval lasting from 14.5-13.0 kyr B.P. This second period of increased mean annual precipitation is synchronous with expansion of glaciers in Westland (Figure 6.10; Denton and Hendy, 1994; Williams, 1996; Turney *et al*., 2007), cooling at Mt. Arthur, northwest South Island (Hellstrom *et al*., 1998) and Boundary Stream, central South Island (Vandergoes *et al*., 2008), and increases in the abundance of cold-tolerant plant species on the landscapes either side of the Southern Alps and at higher elevation sites in North Island (Newnham and Lowe, 2000; McGlone *et al*., 2004; Hajdas *et*

al., 2006; Newnham *et al*., 2007b). In addition, reconstructed marine oxygen isotope and sea surface temperatures off the east coast of South Island suggest cooling at this time (Figure 6.10h; Pahnke *et al*., 2003; Pahnke and Zahn, 2005).

Significantly, the interval of cooling and increased precipitation at Hollywood Cave and elsewhere in New Zealand is synchronous with the Antarctic Cold Reversal (ACR) (Figure 6.10; Petit *et al*., 1999; Blunier and Brook, 2001; EPICA Community Members, 2006), suggesting that the events are part of a more widespread climate change. The termination of the late-glacial reversal at 13.0 kyr B.P. in the Hollywood Cave record means that there was no overlap to the Younger Dryas chronozone such as has been observed from reversals in other New Zealand late-glacial climate records (Williams *et al*., 2005; Hajdas *et al*., 2006).

The cool and wet climate that persisted during the ACR on the West Coast was most likely generated by the same mechanisms as during previous wet phases. Earlier in this discussion it was suggested that wet intervals occurred during times of increased strength of the circumpolar westerly circulation (in this instance perhaps driven by Antarctic cooling and northward migration of the Polar Front) which delivered a greater frequency of southwesterlies, and associated heavy rainfall, to the West Coast. This would also have the effect of reducing summer temperatures, as well as seasonal climate differences. At Boundary Stream Tarn, east of the Southern Alps, a fossil chironomid study has indicated that the ACR was a period of stronger seasonality (Vandergoes *et al*., 2008). At times of southwesterly flow over South Island, Boundary Stream Tarn is located in the rain-shadow of the Southern Alps, a factor likely to have contributed to the increased seasonality that occurred during the ACR.

The drying trend that succeeded the ACR in Westland, and which continued at least until the termination of the HW05-3 record at 11.3 kyr B.P., contained a brief (300-400 year long) wet phase centred on 12 kyr B.P. This return to wetter climate may have driven late-glacial ice advance which took place 11.7 ± 0.3 kyr in the Southern Alps (Ivy-Ochs *et al*., 1999; Kaplan *et al*., 2007). However, it has been suggested that the production rate of ^{10}Be in samples selected for exposure age dating [such as those from moraines in Arthur's Pass, Irishman's Stream Valley and others from the Birch Hill moraines near Mount Cook village (11.8 ± 0.3 kyr B.P.; Denton, unpublished data)] has been overestimated by as much as

10% (G. Denton, pers. comm. 2008). If so, the true age of these moraines would lie closer to 13 kyr B.P., and thus be synchronous with the Waiho Loop advance (Figure 6.10f) on the West Coast (Denton and Hendy, 1994; Turney *et al*., 2007) and the termination of the ACR.

The timing of the wet phase places it within the YD chronozone, although its duration is considerably shorter. Given the sensitivity of the HW05-3 record to Heinrich events in the North Atlantic it would seem appropriate to anticipate wetter climate at this time. One hypothesis for the signature being diminished from that of earlier Heinrich events is that Antarctic warming, and associated southerly shift of the Polar Front, following the termination of the ACR offset southward migration of tropical and subtropical atmospheric circulation patterns caused by cooling of the Northern Hemisphere. As a result, steepening of the temperature gradient across the mid-southern latitudes and concurrent strengthening of the westerly circumpolar circulation did not occur.

6.5.5 Heinrich Events

As noted in the preceding sections there is a strong relationship between intervals of wet, cold climate on the West Coast, South Island, and massive discharges of icebergs, or Heinrich events, into the North Atlantic. This indicates that the climate of the West Coast was sensitive to global climate fluctuations.

Despite the occasionally high-amplitude (sub)millennial-scale variability displayed by HW05-3 isotope profiles, each of the eight Heinrich events (H0-H6, including H5a) that occurred during the formation of HW05-3 stand out as obvious features in the record (Figure 6.11). The timing of Heinrich events in HW05-3, as determined from growth rates and stable isotope profiles, is as follows: H6 (during MIS 4: 67.7-61.0 kyr B.P.), H5a (56-55 kyr B.P.), H5 (50.5-47.5 kyr B.P.), H4 (40-39 kyr B.P.), H3 (30.5-29 kyr B.P.), H2 (25.5-24.3 kyr B.P.), H1 (16.1-15.0 kyr B.P.) and H0 (12.2-11.8 kyr B.P.).

Increased growth rates suggest that each Heinrich event was associated with increased mean annual precipitation. The isotopic data confirm this interpretation, and further suggest that the increase in precipitation was due to higher winter rainfall amounts. In association with other proxy records the HW05-3 data may

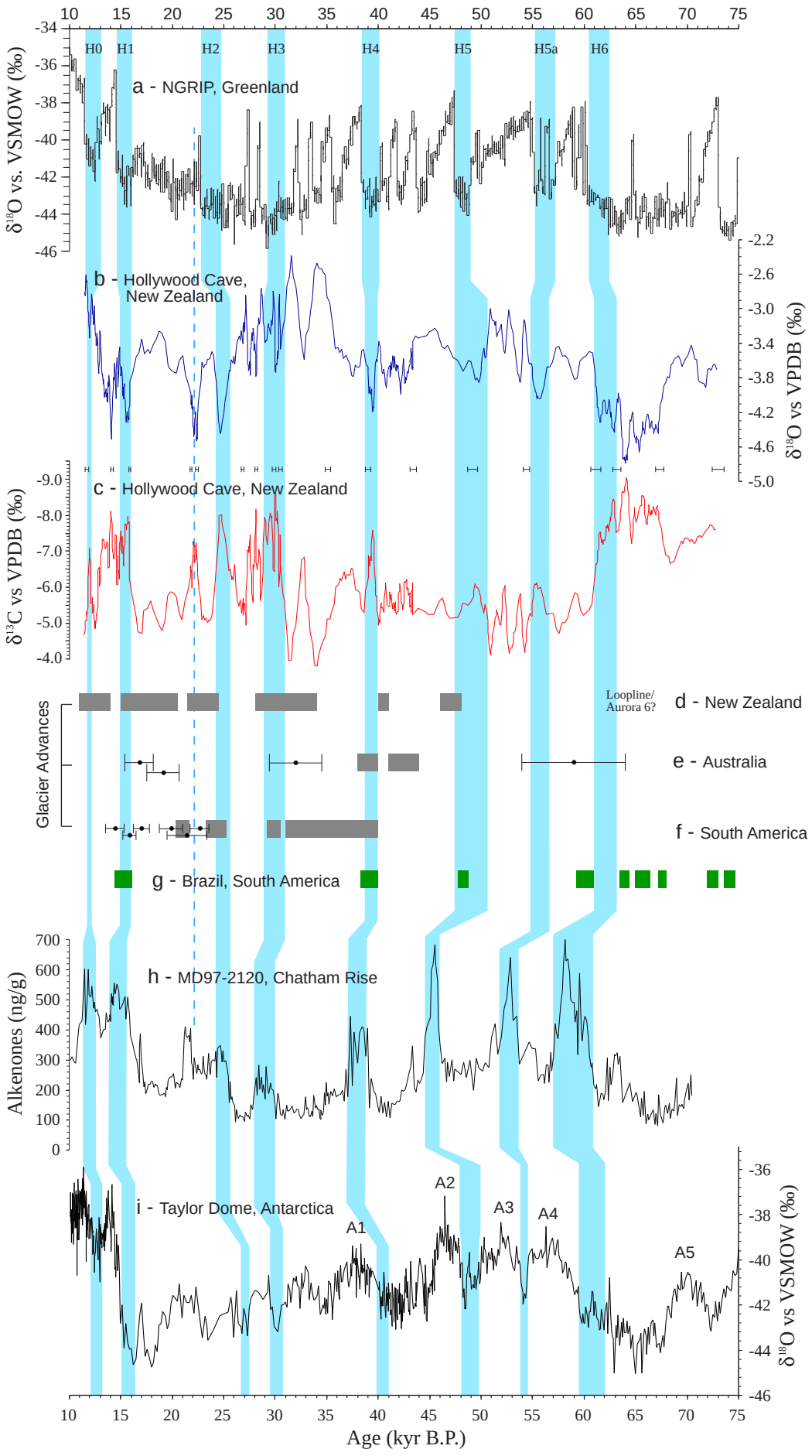
H0
H1
H2
H3
H4
H5
H5a
H6
a - NGRIP, Greenland
δ18O vs. VSMOW (‰)
b - Hollywood Cave, New Zealand
δ18O vs VPDB (‰)
c - Hollywood Cave, New Zealand
δ13C vs VPDB (‰)
Glacier Advances
Loopline/ Aurora 6?
d - New Zealand
e - Australia
f - South America
g - Brazil, South America
h - MD97-2120, Chatham Rise
Alkenones (ng/g)
i - Taylor Dome, Antarctica
A1
A2
A3
A4
A5
Age (kyr B.P.)

Figure 6.11: Occurrence and timing of Heinrich events in HW05-3 $\delta^{13}C$ and $\delta^{18}O$ profiles and comparison to other palaeoclimate records. These include (a) NGRIP ice core $\delta^{18}O$, Greenland (NGRIP Members, 2004); (b and c) HW05-3 $\delta^{18}O$ and $\delta^{13}C$ profiles respectively (black bars represent U-Th dates with 2σ error); timing of glacier advances in (d) the Southern Alps, New Zealand (Denton and Hendy, 1994; Williams, 1996; Suggate and Almond, 2005; Schaefer et al., 2006); (e) Australia (Barrows et al., 2001; Kiernan et al., 2004; Mackintosh et al., 2006); and (f) South America (Denton et al., 1999; McCulloch et al., 2005; Douglass et al., 2006); (g) timing of travertine deposition in subtropical Brazil (Wang et al., 2004); (h) alkenone concentration in sediments from core MD97-2120 (Sachs and Anderson, 2005); and (i) Talyor Dome ice core $\delta^{18}O$, Antarctica (Steig et al., 2000). Light blue bars represent the timing of Heinrich events as is suggested for (a) by NGRIP Members (2004), (b-g, i) by this study, and (h) by Sachs and Anderson (2005).

also suggest depressed mean annual temperatures, relative to today, during Heinrich events.

Between Heinrich events the climate above Hollywood Cave was drier. Almond *et al*. (2007) suggested that annual rainfall totals may have been as little as half that experienced in Westland under the current climate. They interpreted this to indicate a reduction in the strength of the band of circumpolar westerlies that affect South Island which ultimately led to increased frequency of southerlies. This shift in the prevailing wind would resulted in the West Coast falling under the rain shadow of the Southern Alps. The isotope data from HW05-3 suggest that the impact of the change to southerlies was most significant during the winter months, an hypothesis previously proposed by Drost *et al*. (2007) for climate at the LGCP. Therefore the increased rainfall events recorded in HW05-3 most likely indicate a reinvigoration of the westerly circulation.

The implication that Heinrich events effected climate change in a region antipodean to their point of origin is significant as it suggests that abrupt climate events were global in nature during the last glacial period. The global impact of Heinrich events, including the findings of this study, is presented in Figure 6.12. This is done in an to attempt better understand the mechanism(s) by which massive iceberg discharge into the North Atlantic could affect climatic change in New Zealand. However, in performing this exercise it is important to recognize the implicit assumption that Heinrich events are the trigger for change and not another symptom of change driven by an alternative forcing. Such a conundrum may only be resolved by development and comparison of further high-resolution, absolutely dated records from all regions of the globe with the aim of observing synchronous or lead-lag relationships.

The link between iceberg discharge in the North Atlantic and wet and cool conditions at Hollywood Cave more than likely involves perturbation of the Antarctic circumpolar circulation. It has previously been demonstrated in this discussion that there was a wider terrestrial response on South Island to the periods of increased mean annual precipitation captured in HW05-3 calcite. Most notably this includes the advancement of glaciers in the Southern Alps (Figure 6.11d), which are sensitive to changes in precipitation volumes. Vegetation changes also occurred and are documented at both North and South Island locations (Newnham *et al*., 2007a, 2007b). Furthermore, there is evidence for

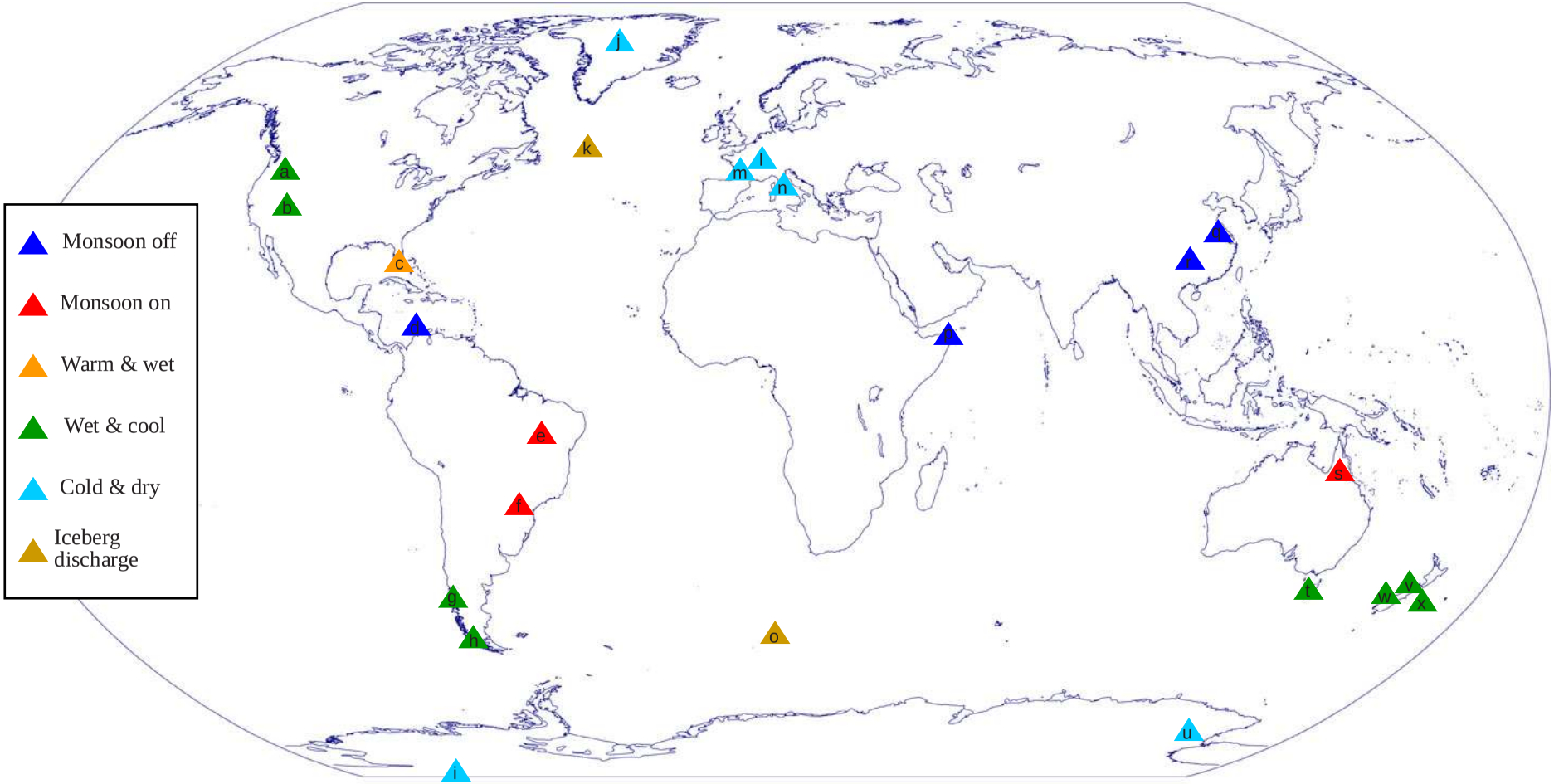
Monsoon off
Monsoon on
Warm & wet
Wet & cool
Cold & dry
Iceberg discharge
a
b
c
d
e
f
g
h
i
j
k
l
m
n
o
p
q
r
s
t
u
v
w
x

Figure 6.12: Distribution of palaeoclimate records showing changes synchronous with timing of Heinrich events. Also displayed is a key to the change observed at each locality. The cited studies are (a) Clark and Bartlein (1995), (b) Benson et al. (2003), (c) Grimm et al. (2006), (d) Peterson et al. (2000), (e) Wang et al. (2004), (f) Wang et al. (2006), (g) Lowell et al. (1995) and Denton et al. (1999), (h) McCulloch et al. (2005), (i) Blunier and Brook (2001), (j) isotope studies of ice at GRIP/GISP2/NGRIP, (k) Heinrich (1988) and others reviewed in Voelker et al. (2002) and Hemming et al. (2004), (l) Spötl et al. (2006), (m) Genty et al. (2003), (n) Drysdale et al. (2007), (o) Kanfoush et al. (2000), (p) Burns et al. (2003), (q) Wang et al. (2001), (r) Cai et al. (2006), (s) Muller et al. (2008), (t) Mackintosh et al. (2006), (u) Steig et al. (2000), (v) this study, (w) Williams (1996), and (x) Sachs and Anderson (2005).

changes in the strength of westerly circulation in association with Heinrich events leading to increased productivity of surface waters in the Pacific Ocean directly east of South Island (Figure 6.11h; Sachs and Anderson, 2005).

Palaeoclimate records from regions other than New Zealand whose climate is directly affected by the circumpolar westerly circulation also display changes toward cooler, wetter and/or windier conditions coincidental with Heinrich events in the North Atlantic. Ice cores from Antarctic sites Byrd (Blunier and Brook, 2001) and Taylor Dome (Steig *et al*., 2000) display coolings during MIS 4 and at 56-55, 50-46, ~40 and ~ 30 kyr B.P. in line with Heinrich events H6-H3 (Figure 6.11i). In addition, glacier advances in South America and southern parts of Australia also occurred at times coincident with Heinrich events (Figure 6.11e,f; Lowell *et al*., 1995; Barrows *et al*., 2001; McCulloch *et al*., 2005; Mackintosh *et al*., 2006). Kanfoush *et al*. (2000) present a record of ice rafted detritus derived from Antarctica in marine sediment cores retrieved from the South Atlantic that displays seven peaks close in timing to Heinrich events H0 and H2-H6.

Increased strength of the circumpolar westerlies would most likely occur in response to a greater latitudinal temperature gradient. Chinese, Brazilian and east African speleothems and Cariaco Basin sediment proxies document a southerly shift in the position of the intertropical convergence zone (ITCZ) during Heinrich events (Peterson *et al*., 2000; Wang *et al*., 2001; Burns *et al*., 2003; Wang *et al*., 2004; Wang *et al*., 2006; Cai *et al*., 2006). In essence this is a southerly movement of tropical air masses which, all else being equal, should steepen the temperature gradient over the southern mid-latitudes. It has been suggested this might be driven by deceased thermohaline circulation in the North Atlantic caused by the Heinrich events (Broecker, 1994). The cooling observed in Antarctic ice cores would therefore indicate increased isolation of the continent and would lead to a further increase in the latitudinal temperature gradient. The termination of the period of southwesterly dominated climate in South Island would occur as the ITCZ retreated north, potentially in response to resumption of thermohaline circulation in the North Atlantic.

6.6 Ruakuri Cave, North Island

Stable carbon and oxygen isotope profiles developed for three Ruakuri Cave, North Island, speleothems are discussed together. The combined records cover the period 102.3 to 6.1 kyr B.P. with a break from 72.6 to 60.3 kyr B.P. (Figure 6.13). RK05-4 is the only stalagmite to provide data for the early part of the record (102.3-72.6 kyr B.P.). There is significant uncertainty in the basal age of RK05-4 (102.3 ± 27.9 kyr B.P.). Because of the inadequate chronology and poor data resolution, the stable isotope ratios within the interval 102.3-76.1 kyr B.P. are not discussed further. The RK05-1 and RK05-3 datasets overlap marginally (53.1-51.3 kyr B.P.). However, there is sufficient uncertainty in the age data to allow for the possibility that the two records do not intersect. Indeed the poor correlation of $\delta^{13}C$ and $\delta^{18}O$ profiles between RK05-1 and RK05-3 where they might have overlapped would tend to support this hypothesis. Of the three speleothems, RK05-3 provides the longest record, a potentially continuous dataset spanning the period 53.1 to 6.1 kyr B.P.

The high resolution (15-70 years between datapoints) portion of RK05-4, covering the period 76.1-72.6 kyr B.P. affords the possibility of examining for sub-centennial-scale climate changes for the Waitomo region early in the last glacial period. Relatively negative $\delta^{13}C$ (mostly -7 to -10 ‰) and growth rates close to 65 mm/kyr indicate that speleothem formation was not limited by a dry and/or cold climate or lack of soil rich in organic material at the ground surface. In fact comparison of growth rates in RK05-4 to those determined for stalagmites RK05-1 and RK05-3 suggest that the period 76.1-72.6 kyr B.P. was relatively wet (Figure 6.13).

The $\delta^{18}O$ of RK05-4 calcite is isotopically light (as low as -4.9 ‰) in comparison to much of the calcite within other Ruakuri speleothems analysed in this study and also by Williams *et al*. (2004). However, it compares favourably with estimates and measurements of presently precipitating calcite in Waitomo caves (Williams *et al*., 1999; Williams and Fowler, 2002). If a correction is applied for global ice volume, which caused sea levels to be 34-71 m lower than at present during the period 72-78 kyr B.P. (Lambeck and Chappell, 2001; Siddall *et al*., 2003), $\delta^{18}O$ values have a mean of -4.6 ‰.

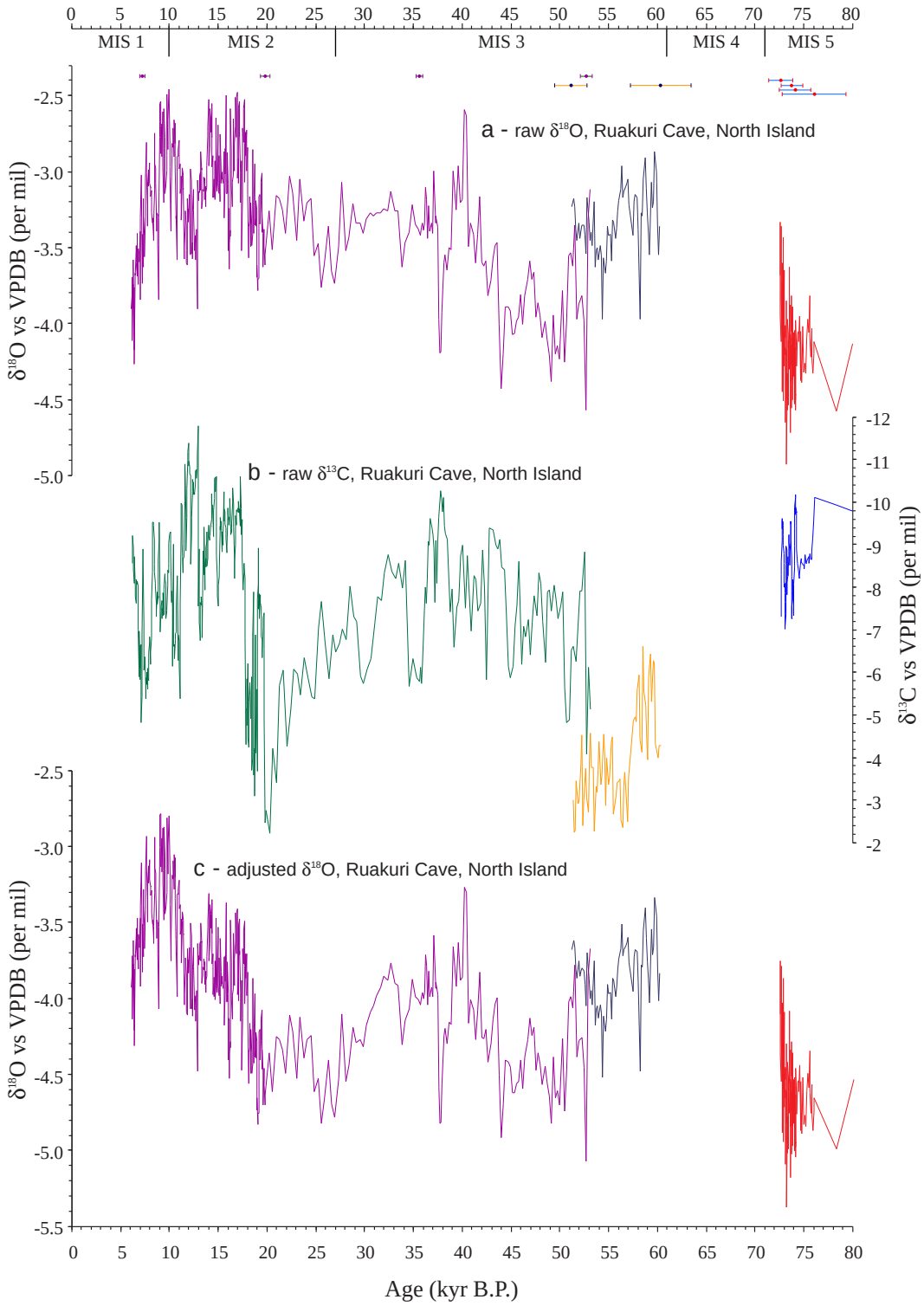

Figure 6.13: $\delta^{18}O$ and $\delta^{13}C$ of Ruakuri Cave stalagmites RK05-1, RK05-3 and RK05-4 versus age. (a) raw $\delta^{18}O$ values for RK05-1 (dark blue), RK05-3 (purple) and RK05-4 (red); (b) $\delta^{13}C$ values for RK05-1 (orange), RK05-3 (dark green) and RK05-4 (blue); and (c) ice-volume adjusted $\delta^{18}O$ values for RK05-1 (dark blue), RK05-3 (purple) and RK05-4 (red). U-Th dates are shown at the top of the figure with 2σ errors, and are colour-coded to each stalagmite.

Both $\delta^{13}C$ and $\delta^{18}O$ profiles have variability at the centennial-scale. Most noticeable are (four) abrupt shifts in $\delta^{13}C$ of greater than 2 ‰ which occurred at 74.0, 73.7, 73.1 and 72.7 kyr B.P., and a change in $\delta^{18}O$ of +0.8 ‰ over the period 73.3-72.6 kyr B.P. (Figure 5.30). What drove these changes is unclear. The present climate of western North Island is affected by El Niño-Southern Oscillation (ENSO) and the Interdecadal Pacific Oscillation (IPO), although a consistent change through multiple cycles of either index would be required to account for the observed changes in the RK05-4 record. It may also be necessary to consider the impact on $\delta^{13}C$ of disturbance of local vegetation and soils by fires and eruptions from nearby volcanic centres (e.g. Taranaki and Taupo) as well as from climate change.

Unfortunately there are no other records from New Zealand with such high data resolution to compare with the RK05-4 record. There is a small overlap (73.2-72.6 kyr B.P.) with the HW05-3 record although data resolution is 180 years between points in the South Island record at this time, preventing meaningful comparison. A general interpretation of regional climate ~75 kyr B.P. can be inferred from marine records. Sea surface temperatures at several sites to the east and west of North Island were as warm, or warmer, than present (Nelson *et al*., 1994; Pahnke and Sachs, 2006), in agreement with the interpretation of the RK05-4 stable isotope data.

The break in the Ruakuri Cave record is approximately equivalent to MIS 4. This may reflect a period of non-deposition in Ruakuri Cave, potentially caused by the cool climate of that interval, although it is equally likely to be coincidence that the termination and onset of growth of the collected specimens are close in timing to this climate event.

The RK05-1 record covers the period 60.3-51.3 kyr B.P. (Figure 6.14). Growth was initiated shortly after the onset of MIS 3, as defined in South Island speleothem HW05-3. At this time both $\delta^{18}O$ and $\delta^{13}C$ were enriched relative to the values in RK05-4. Subsequently, RK05-1 $\delta^{13}C$ values became as high as -2.2 ‰, indicating a relatively dry and cold climate or lack of soil above the cave. The growth rate of RK05-1 was also reduced relative to the earlier record of RK05-4, further suggesting that the Waitomo region was experiencing drier-than-present climate.

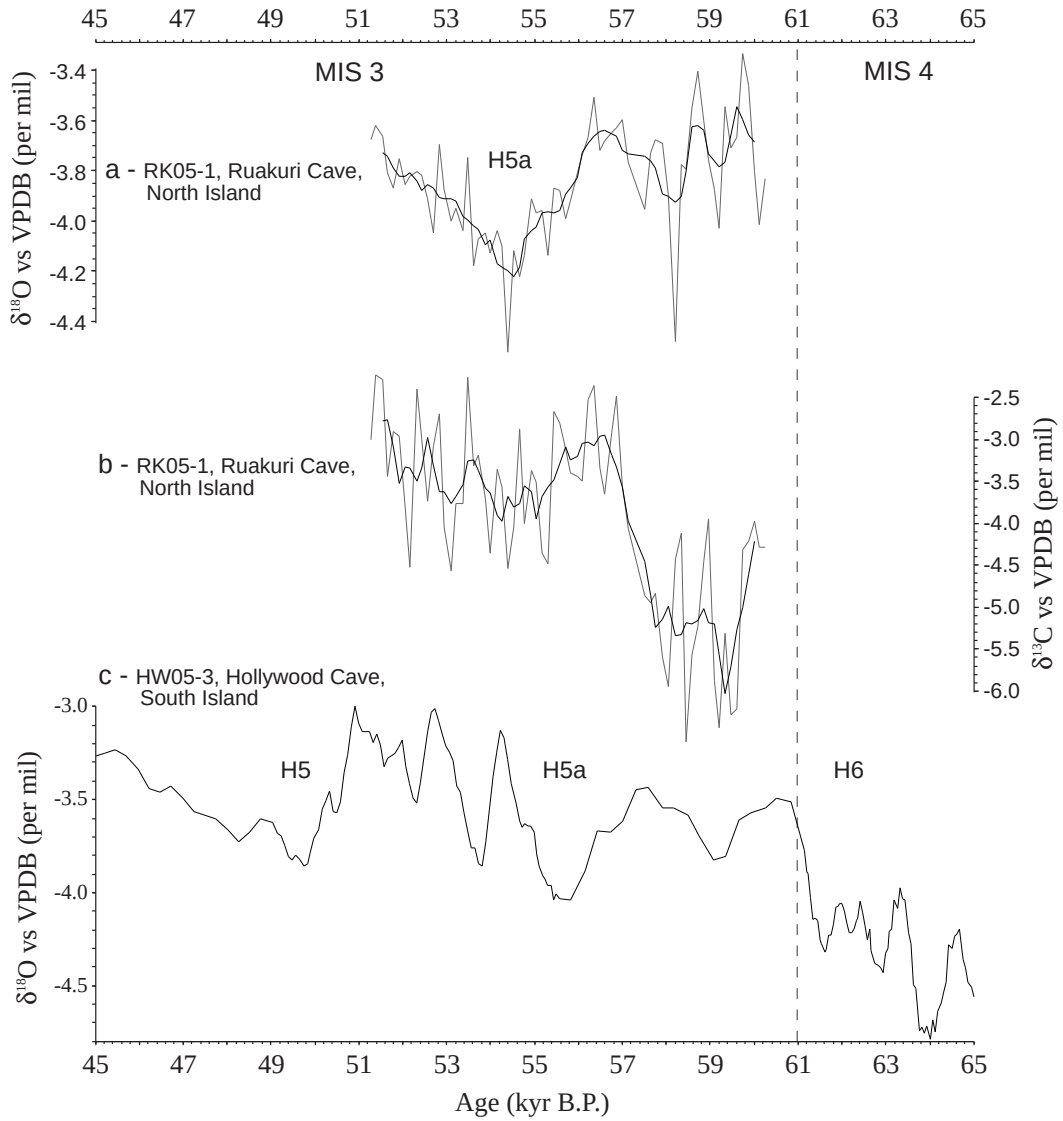

Figure 6.14: Comparison of RK05-1 and HW05-3 stable isotope profiles where the two overlap. Note that both $\delta^{18}O$ (a and c) profiles are adjusted for the ice-volume effect.

Williams *et al*. (1999, 2004) argued that the $\delta^{18}O$-temperature relationship at Waitomo is positive. Following the earlier discussion of HW05-3 isotope variability, the positive temperature relationship may be expanded to define seasonality in annual precipitation volumes on the west coasts of both islands of New Zealand. A more negative $\delta^{18}O$ will result from increased contribution to the annual rainfall budget from winter southwesterlies, while less negative $\delta^{18}O$ (particularly when in association with less negative $\delta^{13}C$) represents dry winters with increased frequency of ground frosts. In a recent study of $\delta^{18}O$ of precipitation falling above Ruakuri Cave the average 'winter' (a six month period encompassing the colder months of the year) rainfall was depleted by 2.2 ‰ relative to average 'summer' (the outstanding six months) rainfall (Williams and Fowler, 2002). This range is capable of explaining almost the entire suite of observed $\delta^{18}O$ data in the Ruakuri Cave speleothems.

During the period 60.2-51.1 kyr B.P. RK05-1 calcite was enriched in ^{18}O relative to that measured in RK05-4 and that estimated for speleothems forming in Waitomo Caves (Williams and Fowler, 2002). In combination with the relatively low growth rate and the enriched $\delta^{13}C$, the oxygen isotope data suggest that the climate at Waitomo during the period ~60-50 kyr B.P. was significantly drier than present, particularly during the winter months. This finding is consistent with the interpretation of HW05-3 stable isotope profiles, also from the west coast, which indicate a relatively dry climate prevailed at this time (Figure 6.14).

A negative excursion centred on 54.5 kyr B.P. in the RK05-1 $\delta^{18}O$ profile, taken to infer increased winter rainfall, occurred synchronously with an event displaying the same sense and similar magnitude in HW05-3, South Island (Figure 6.14). In the Hollywood Cave record the event is interpreted as being equivalent to Heinrich event H5a. The RK05-1 profile indicates that the same climate shift also affected North Island. Given the extreme distance between the locus of Heinrich events and the speleothems in this study it is anticipated that if Heinrich events affect the climate above South Island they would also affect North Island.

The remainder of the Ruakuri Cave palaeoclimate record is based on speleothem RK05-3. The raw $\delta^{18}O$ data appear to replicate the Waipuna stalactite and Gardners Gut stalagmite records of Hendy and Wilson (1968), also from the Waitomo Caves region, provided that some allowance is made for uncertainties in the respective chronologies (Figure 6.15). Should it be determined that the three

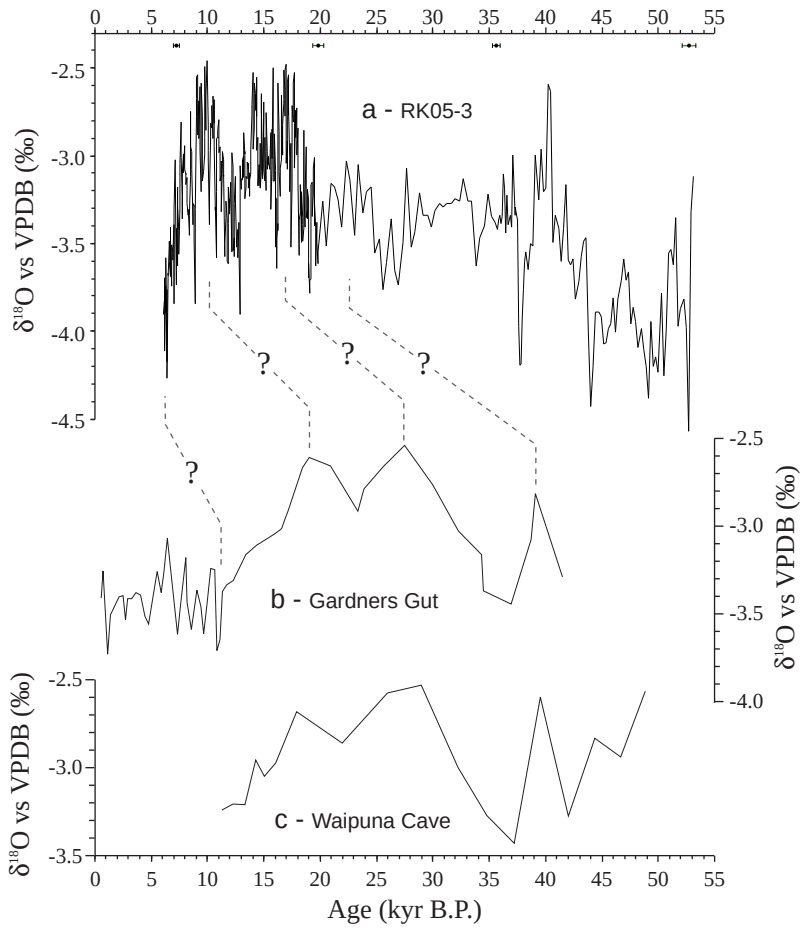

Figure 6.15: Comparison of individual speleothem $\delta^{18}O$ profiles from the Waitomo Caves area. Note that none of the profiles are adjusted for the ice volume effect. Shown are (a) stalagmite RK05-3 (this study) with uranium-series dates (black, filled circles), and (b and c) Gardners Gut stalagmite and Waipuna stalactite respectively (Hendy, 1969). The Gardners Gut and Waipuna chronologies were created using radiocarbon dates, while the 48 kyr captured in RK05-3 is only constrained by four U-Th ages. Therefore there is considerable uncertainty in the true ages of many features present in each record.

records display the same palaeoclimate signature it would suggest that idiosyncratic sensitivities to climate changes of each stalagmite are negligible, allowing greater confidence in the palaeoclimate interpretations.

The RK05-3 $\delta^{18}O$ data have also been corrected for changes in ice volume using the sea-level curve of Lambeck and Chappell (2001) and enrichment of seawater $\delta^{18}O$ of 1.1 ‰ at minimum sea level. In applying this correction the resulting curve demonstrates a close anti-correlation with mean summer insolation at 40°S (Figure 6.16). This apparent relationship is supported and extended to the present by estimates of modern $\delta^{18}O$ at Waitomo (Williams and Fowler, 2002) being equivalent to values in RK05-3 at times in the past when Ruakuri Cave experienced the same value of insolation. However, given the uncertainty of the ice volume correction (see section 6.3) and the lack of the insolation signal in the raw data, no interpretation of the correlation is attempted. The influence of insolation on Southern Hemisphere speleothem records has previously been documented from Brazil (~30°S; Cruz *et al*., 2005; Wang *et al*., 2007). In addition Vandergoes *et al*. (2005) suggested changes in insolation led to the early onset of the LGCP in New Zealand.

As with RK05-1, events in the RK05-3 $\delta^{18}O$ profile have correlatives in the HW05-3 record from South Island (Figure 6.16). Strong negative excursions in $\delta^{18}O$ in the HW05-3 record are likely correlated to Heinrich events. Therefore excursions at 50.5-47, 38-37, 27-25, 16-15 and 13-11 kyr B.P. in RK05-3 are equivalent to H5, H4, H2, H1 and H0 respectively. The lack of an event coeval with H3 may be a result of poor age control but may also be obscured by the relatively coarse data resolution in this part of the record RK05-3.

The link between Heinrich events and negative excursions in speleothem $\delta^{18}O$ is summarized here (following the full discussion in section 6.6.5). Cooling of the North Atlantic generated by the massive iceberg discharges from the Laurentide and Greenland ice sheets forced the ITCZ to migrate south. As a consequence of the shift, the temperature gradient across the mid-southern latitudes steepened, in turn causing strengthening of the circumpolar westerly circulation. This allowed a southwesterly flow across New Zealand to become more frequent, particularly in winter, leading to a bias toward winter and Southern Ocean-sources in the annual precipitation budget at Ruakuri Cave. Consequently the $\delta^{18}O$ of calcite was reduced relative to the preceding climatic interval.

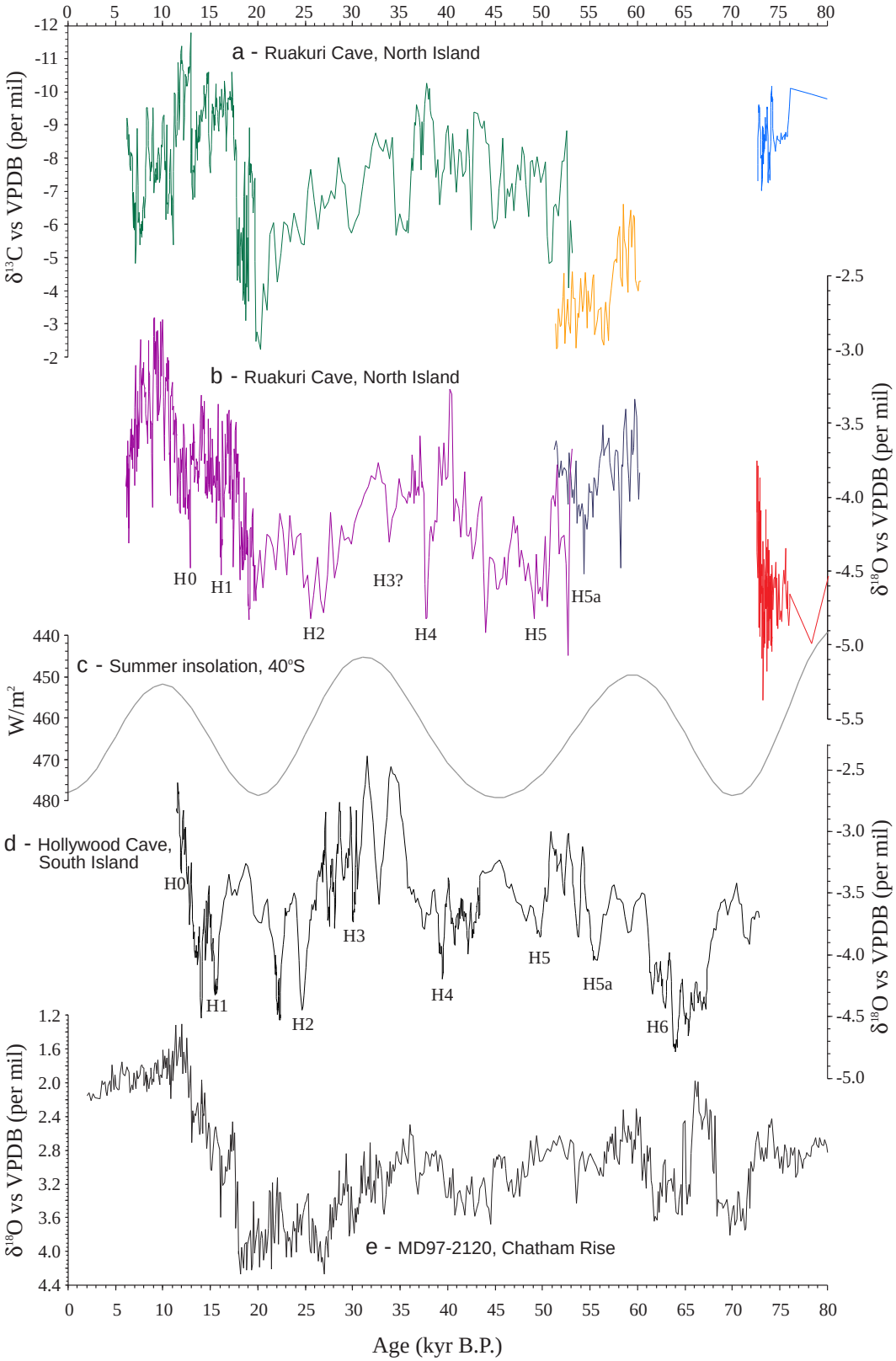

Figure 6.16: Comparison of Ruakuri Cave isotope profiles to other palaeoclimate records from the region. Show are (a and b) $\delta^{13}C$ and ice-volume adjusted $\delta^{18}O$ of Ruakuri stalagmites, respectively; (c) mean summer (Dec-Jan-Feb) insolation at 40°S (Berger and Loutre, 1991); (d) ice-volume adjusted HW05-3 $\delta^{18}O$, Hollywood Cave, South Island; and (e) planktonic $\delta^{18}O$ record from marine sediment core MD97-2120, Chatham Rise, east of South Island (Pahnke and Zahn, 2005). Heinrich events (H0-H6) are also shown.

The LGCP at Ruakuri Cave is represented by the period of relatively negative $\delta^{18}O$, enriched $\delta^{13}C$ values and low growth rates in RK05-3 extending from ~29-18 kyr B.P. This is in keeping with other interpretations of the timing of the youngest period of intense cooling (Vandergoes *et al*., 2005; Suggate and Almond, 2005; Alloway *et al*., 2007; Newnham *et al*., 2007b).

The $\delta^{18}O$ profile displays two minima during the LGCP, similar to those observed in a marine sediment proxy record from Chatham Rise (Figure 6.16d). The first occurred 27.4-24.8 kyr B.P. and is interpreted to be associated with H2. Pollen assemblages from coastal Waikato indicate that this period was one of cool and wet climate (Lees *et al*., 1998). Newnham *et al*. (2007b) interpret fluctuations in pollen assemblages in the Auckland region to indicate an amelioration of climate at this time. This could be understood to infer a brief period of increased mean annual rainfall (associated with H2) during a generally dry LGCP. The second minimum occurred between 20.9 and 18.8 kyr B.P., coincident with the maximum in the $\delta^{13}C$ profile. This event at Ruakuri Cave was driven by particularly dry and relatively cold climate. Pollen assemblages in nearby lakes and bogs also suggest dry and cold (~4°C below present) conditions at this time (Newnham *et al*., 1989; Lees *et al*., 1998). A speleothem record from Mt Arthur, South Island, also shows that climate was cold and dry at this time (Hellstrom *et al*., 1998).

In the RK05-3 $\delta^{13}C$ record, the driest conditions were succeeded by an abrupt transition to somewhat wetter conditions lasting from 19.7-18.8 kyr B.P. Similarly this event was terminated by an abrupt change to drier climate. The period of wetness affected a wide geographic area with pollen assemblages in northern Waikato also recording a wet interval extending from 17.2 to 16 ^{14}C kyr B.P. (equivalent to ~20.1 to 18.9 kyr B.P.; Lees *et al*., 1998). Dry conditions persisted briefly before a third abrupt change brought significantly wetter climate to the region at 17.6 kyr B.P. Afforestation of the region proceeded rapidly from this time, although mean annual temperatures were still cooler than present (Newnham *et al*., 1989). This most likely reflects an increase in precipitation, and potentially also an increase in mean winter temperatures (due to reduction of frostiness).

A plateau in $\delta^{18}O$ from 18.0-11.3 kyr B.P. is interrupted by brief negative excursions at 16.6-15.8 and 12.9-11.5 kyr B.P. These are correlative to Heinrich events H1 and H0 respectively, with the H0 event in the RK05-3 record closely

resembling the YD signal in the Greenland ice cores and the Hulu Cave record from China (Figure 6.17; Grootes *et al*., 1993; Wang *et al*., 2001; NGRIP Members, 2004). Correlative with both events in the $\delta^{18}O$ profile are strongly negative $\delta^{13}C$ values, the most negative for the entire record occurring in conjunction with H0, indicating wet climate. Pollen records also indicate that this period was particularly stormy, resulting in a reduction in the abundance of the dominant tall forest genus of *Dacrydium* on the Waikato landscape (Newnham *et al*., 1989). This agrees well with the cool, wet and windy conditions inferred for west coast climate during Heinrich events.

The present age control for these events is poor, being based on linear interpolation between dates at 19.8 and 7.2 kyr B.P. Order of magnitude growth rate changes have been revealed by the present suite of uranium-series ages highlighting the weakness of interpolating ages in this interval, represented by over 300 mm of deposition. Further dating is therefore recommended, particularly for the H0/YD event. Special consideration of this interval is merited due to the inconsistent evidence in previously published New Zealand palaeoclimate records for the timing and duration of cooling at this time (Denton and Hendy, 1994; Hellstrom *et al*., 1998; Singer *et al*., 1998; Ivy-Ochs *et al*., 1999; McGlone *et al*., 2004; Williams *et al*., 2005; Hajdas *et al*., 2006; Turney *et al*., 2006; Alloway *et al*., 2007; Vandergoes *et al*., 2008). The result has significant implications for the debate on past global (a)synchrony of climate change. In addition, given the clear identification of an ACR signal in South Island speleothem HW05-3, the presence of a YD in the RK05-3 record would have a profound influence on interpretations of the drivers of climate change in New Zealand.

Following the last late glacial wet interval, $\delta^{18}O$ reached an early Holocene peak. This is consistent with the findings of Newnham *et al*. (1989) of a period of maximum warmth and wetness in the Waikato region at this time. In addition a previously published Ruakuri Cave stalagmite $\delta^{18}O$ profile is very similar to the RK05-3 where the two overlap between ~11.5 and 7 kyr B.P. (Williams *et al*., 2004). An early Holocene Optimum has previously been identified in New Zealand palaeoclimate records (Alloway *et al*., 2007). The RK05-3 record suggests this period was relatively warm and dry at Waitomo.

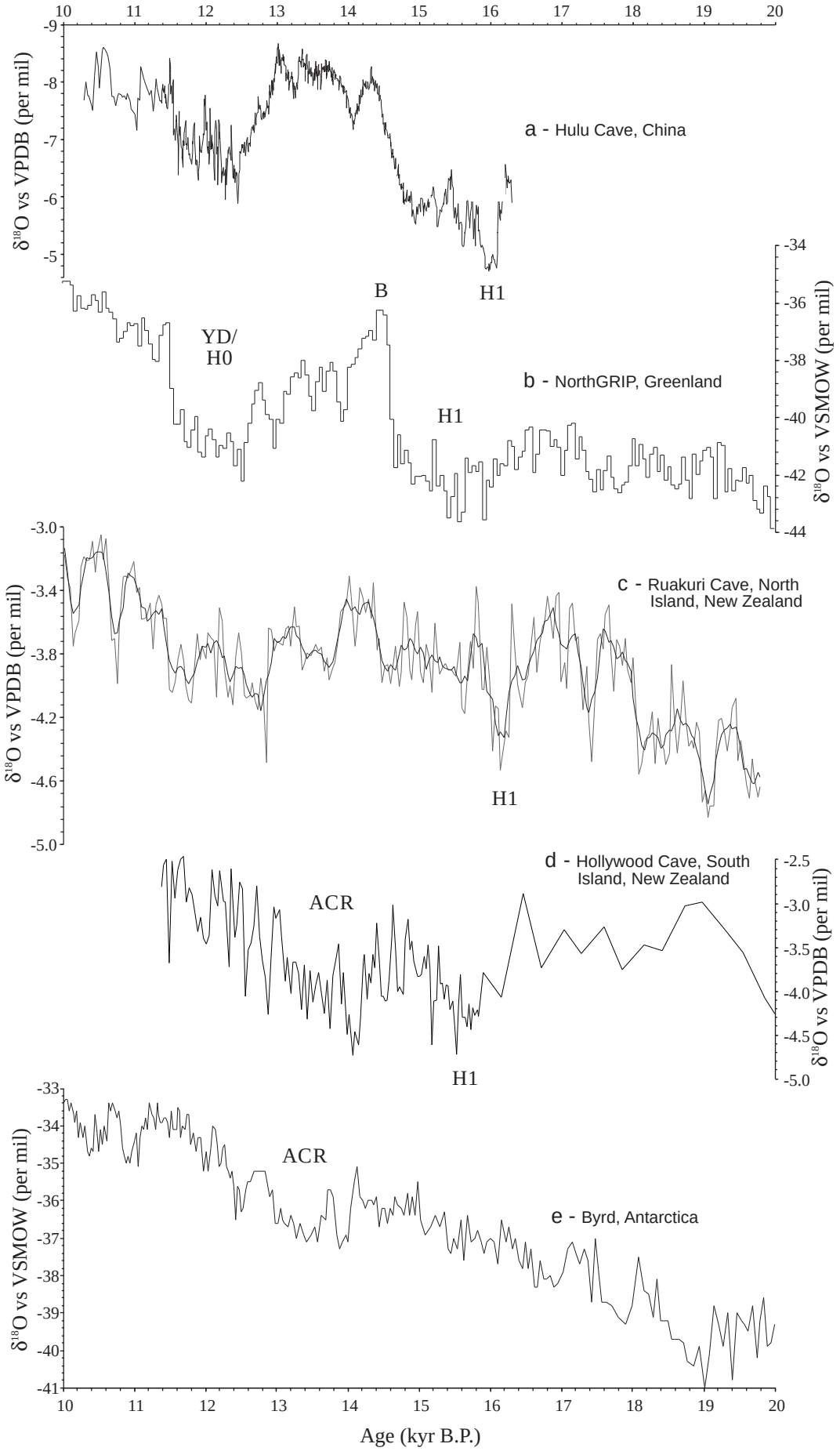
a - Hulu Cave, China
δ18O vs VPDB (per mil)
H1
B
YD/
H0
b - NorthGRIP, Greenland
H1
δ18O vs VSMOW (per mil)
c - Ruakuri Cave, North
Island, New Zealand
δ18O vs VPDB (per mil)
H1
d - Hollywood Cave, South
Island, New Zealand
ACR
H1
δ18O vs VPDB (per mil)
ACR
e - Byrd, Antarctica
δ18O vs VSMOW (per mil)
Age (kyr B.P.)

Figure 6.17: Comparison of RK05-3 late-glacial climate changes to those from other speleothem and ice core records. (a) $\delta^{18}O$ of H82, Hulu Cave, China (Wang et al., 2001); (b) $\delta^{18}O$ of ice at NorthGRIP, Greenland (NGRIP Members, 2004); (c) RK05-3 ice-volume adjusted $\delta^{18}O$, Ruakuri Cave, North Island (this study); (d) HW05-3 ice-volume adjusted $\delta^{18}O$, Hollywood Cave, South Island (this study); and (e) $\delta^{18}O$ of ice at Byrd, Antarctica (Blunier and Brook, 2001). YD = Younger Dryas Chronozone; B = Bolling; H = Heinrich event; ACR = Antarctic Cold Reversal.

6.7 Opportunities for Further Study

The data produced by this research have allowed new insights into the past climates of the west coasts of both North and South Islands, New Zealand and their significance in understanding global climate change. However, some of the conclusions drawn from the data are limited by coarse data resolution, incomplete temporal coverage of the last glacial period and Holocene, and assumptions relating to correction of the data for variability in source water $\delta^{18}O$. These limitations provide opportunities to extend and develop speleothem research in New Zealand. Some of these opportunities are identified and outlined in the following paragraphs.

Significant opportunity remains to refine the stable isotope profiles, and their respective chronologies, developed as part of this research. As an example, more than 2700 consecutive calcite samples were milled from the growth axis of HW05-3 but only 720 were used to develop the record reported here due to limitations of funding. A similar ratio of collected versus analysed samples applies to each of the other stalagmites in this study.

Given appropriate funding, the primary targets for further sample analysis would include the LGCP section of HW05-3 and the RK05-3 chronology. Current data resolution of HW05-3 during the LGCP is 283 yr/sample. Measurement of all remaining samples between 151 and 130 mm depth (a total of 70) would increase data resolution to 63 yr/sample. This would allow greater insight into the climate changes on the West Coast that led glaciers of the Southern Alps to rapidly retreat from their LGCP maximum positions.

Fast growth rates of stalagmite RK05-3 during the late glacial has allowed the development of high-resolution stable isotope profiles throughout this period. These potentially allow precise determination of the timing and structure of climate fluctuations corresponding to events recorded in polar ice cores, specifically those that occurred during the Younger Dryas chronozone and the Antarctic Cold Reversal. Such information would have significant implications for the debate surrounding the (a)synchrony of these and other late-glacial abrupt climate changes. The results might then also be compared to the timing of negative $\delta^{18}O$ excursions in the HW05-3 record from South Island, allowing any inter-island differences to be determined.

Much research is currently being invested in understanding the causes of trace element variability in speleothem calcite and the implications of these changes for interpreting past climate. Stable isotopic compositions of stalagmites GT05-5, HW05-3 and RK05-3 have been shown to provide accurate records of hemispheric and global climate changes over the past ~70 kyr B.P. These records provide platforms to investigate the response of trace elements in the soils and epikarst above the caves across glacial-interglacial boundaries and during abrupt climate shifts associated with Heinrich events. In addition, the present literature on trace element compositions of New Zealand speleothems is limited to the relatively low-resolution study by Hellstrom and McCulloch (2000). Thus there is considerable opportunity to develop this topic.

As part of this research, four stalagmites were collected from caves on the West Coast of South Island, but only two were developed into palaeoclimate records. Stalagmites EG05-5 and WZ05-1, from Eggers and Wazapretti caves respectively, were put aside while time and resources were diverted toward developing the HW05-3 and RK05-3 records. The 480 mm tall EG05-5 offers the potential to investigate late-glacial climate changes in north Westland at high-resolution. WZ05-1 began forming prior to 30 kyr B.P. and most likely contains a complete record of the LGCP. It is anticipated that stable isotope curves developed from these speleothems would replicate the changes observed in the HW05-3 and GT05-5 records. This would be particularly significant for the HW05-3 record. The correlation between $\delta^{13}C$ and $\delta^{18}O$ values in HW05-3 could be used to argue that the stable isotope profiles are affected by non-equilibrium fractionation of isotopes during calcite precipitation and therefore do not accurately represent past climate changes. Although the RK05-3 profile replicates some of the variability in the HW05-3 record, developing a second record from a north Westland cave (e.g. Wazapretti or Eggers cave) would allow an investigation into whether or not the HW05-3 isotope record accurately reflects climate changes at the surface.

Lastly, there are several opportunities for further research into the choice, application and development of *ice-volume* (or perhaps more appropriately *precipitation source water*) corrections and their application to New Zealand speleothem $\delta^{18}O$ profiles. In particular, it would be interesting to investigate, at centennial-scale resolution, sea surface $\delta^{18}O$ variability in the northern Tasman

Sea/Coral Sea, one of the major moisture source regions for meteoric precipitation on the west coasts of both North and South Islands.

Of further interest is the intriguing appearance in the long (> 40 kyr), ice-volume adjusted oxygen isotope profiles developed in this research of a signal strongly anti-correlated with insolation (at 40 °S). In addition, the lack of a pervasive insolation signal in the HW05-3 record may be significant. An hypothesis for its appearance during only the coldest part of the last glacial period is that with increased global cooling there was a gradual increase in the contribution of mean annual precipitation from moisture source regions (e.g. the subtropics) influenced by precessional forcing. Potentially the development of a long speleothem record from a cave further south than Hollywood Cave, but also on the West Coast (e.g. Serendipity Cave), would allow investigation into latitudinal influence of insolation on speleothem $\delta^{18}O$ in New Zealand.

7 Summary and Conclusions

7.1 Summary

Speleothems obtained from caves on both North and South Islands of New Zealand have been used to generate new records of past climate during the last glacial-interglacial cycle. These records allow investigation of local, regional and global patterns of climate variability. Four stalagmites were obtained from Ruakuri Cave, Waitomo, on North Island, and four stalagmites were collected (one each from four individual caves; Eggers, Guillotine, Hollywood and Wazapretti) from karsts on the West Coast of South Island (Figure 3.1).

Speleothems, from South Island caves, most likely to yield material suitable for achieving the research goals setout in chapter 1.4, were selected using a novel technique; stalagmite coring. Instead of removing entire speleothems, only cores of basal material are extracted. Each core provided sufficient material to perform isotopic equilibrium ("Hendy") tests as well as to obtain a uranium-thorium date. This technique significantly reduced the impact on the cave environment, particularly the aesthetics, caused by the traditional methods of extraction of entire speleothems without the prior knowledge of whether they covered the desired temporal range or were precipitated in isotopic equilibrium. Minimal disturbance is rapidly becoming an important consideration for researchers forced to operate within strict conservation guidelines. For further discussion on this topic the reader is directed to Appendix A.

Of the eight stalagmites obtained, the majority of this research was concentrated upon just three, one each from Guillotine (GT05-5), Hollywood (HW05-3) and Ruakuri (RK05-3) caves. These yielded continuous, high-resolution stable isotope profiles covering the periods 9-0, 73-11 and 53-6 kyr B.P. respectively. In addition, the high density of obtained ages on the Hollywood Cave stalagmite provides a detailed record of growth history.

Each of the proxies developed in this study ($\delta^{13}C$, $\delta^{18}O$ and growth rate) are interpreted primarily as indicators of palaeoprecipitation. Dry conditions are interpreted from low growth rates and less-negative isotope ratios. The

predominance of the precipitation signal above a temperature signal is highlighted by the positive relationship between isotope values and estimated palaeotemperatures, most clearly observed in the difference between glacial and interglacial age material.

In chapter 6.3 an attempt was made to remove some of the uncertainty in the palaeoclimate reconstructions developed from New Zealand speleothem $\delta^{18}O$. If the source water effect can be removed from an oxygen isotope record then the remaining variability should be dominated by the effect of changes in cave temperature. Ultimately the attempt proved unsuccessful, however each of four source water effect models used were limited either by low-resolution/discontinuous data or poor representation of moisture source regions. With the development of improved sea-level curves and/or records of Tasman Sea-surface $\delta^{18}O$ the models used in this study could be refined and potentially allow palaeotemperature curves to be developed from New Zealand speleothem $\delta^{18}O$.

Events within each of the three speleothem records developed in this study build upon and significantly improve the existing understanding of New Zealand climate history obtained from speleothems and other proxies, particularly those from the terrestrial realm.

Of the three records, that from Hollywood Cave (HW05-3; Figure 7.1) is of greatest significance to New Zealand and global palaeoclimate research. The HW05-3 record was constructed from 720 stable isotope ($\delta^{13}C$ and $\delta^{18}O$) pairs and 18 uranium-thorium dates. The data span the period ~73-11 kyr B.P., encompassing MISs 4-2, at an average temporal resolution of approximately 80-90 years (Figure 7.1). As such the HW05-3 dataset provides the highest resolution record from New Zealand for this interval, and is the only one (terrestrial or marine) covering this period that is based upon an absolute and independent chronology. The chronology also boasts high precision ($< \pm 1.0\%$ on all but one of the obtained ages), high-density of age-data and all dates being in sequence. This provides confidence in determining the timing of past events which then allows direct comparison with other similar records from around the world.

One of the primary objectives when collecting speleothems from South Island caves was to be able to observe times of glacier advance and retreat in the stable

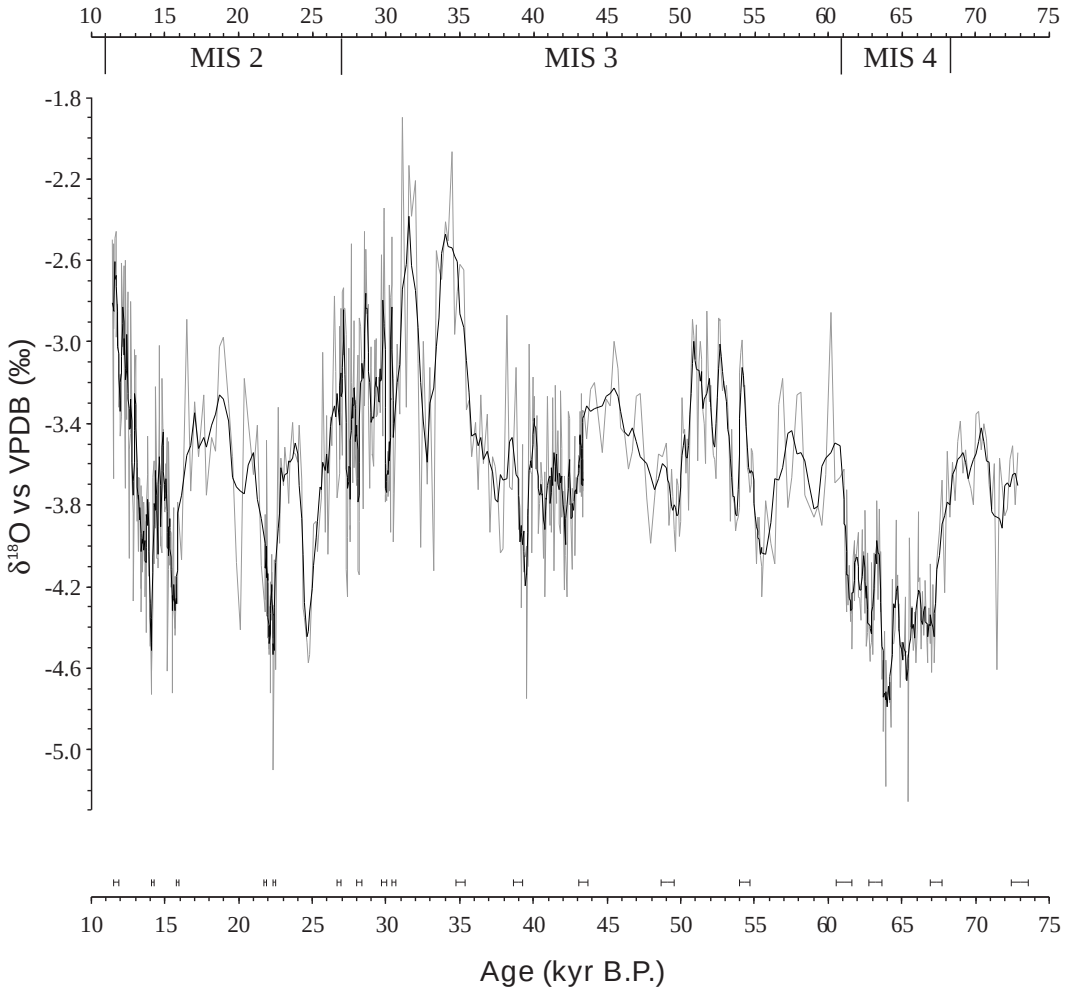

Figure 7.1: Ice-volume adjusted HW05-3 $\delta^{18}O$ profile. The raw data (gray line) is shown with a 5-point running mean (black line). Ice volume correction is applied using sea level data presented in Lambeck and Chappell (2001) and the assumption that maximum sea level lowering was equivalent to a 1.1 ‰ change in sea water $\delta^{18}O$. U-Th dates, including 2σ errors, are represented by bars at the base of the figure.

isotope records. This has been achieved successfully in both HW05-3 and GT05-5. Indeed the ability to identify periods of relatively small ice-volume changes in the Southern Alps during the Holocene GT05-5 record highlights the sensitivity of the proxy. Therefore the speleothem stable isotope records developed in this study yield significant advantages over other palaeoclimate proxies. First, the speleothem records reveal when each period of ice advance began and ended, and can therefore provide estimates of the duration of each period of ice advance or retreat. Second, ice advances older than may be dated by radiocarbon dating, and/or moraines deposited in locations unsuitable for (for example) exposure age dating can be assigned absolute and precise ages. Third, they suggest that in the past increased rainfall and cool temperatures over the Southern Alps created larger glaciers than did reduced rainfall and cold temperatures.

In this study, previously identified and dated periods of ice advance (approximately those that occurred within the last 30 kyr) are confirmed, and several older advances are assigned ages. In addition, the duration of each period of ice advance is well-constrained. Such data proved significant in demonstrating why the MIS 4 glaciers were of greater extent than those developed during the LGM. The MIS 4 climate was consistently wet and cool, whereas the LGM was mostly dry, but interspersed with millennial-scale wetter intervals.

Comparison of the Hollywood record to those developed from Ruakuri Cave, North Island, showed that long- and short-term climate changes were largely synchronous along at least the western half of New Zealand. Particularly noticeable are the simultaneous occurrence of strong negative excursions in the $\delta^{18}O$ records throughout the last glacial period.

The timing of each negative isotopic excursion is synchronous with Heinrich events in the North Atlantic. As such, the speleothem records developed in this study provide strong evidence to suggest that the climate changes experienced in New Zealand throughout the last glacial period occurred in response to shifts in the global climate system. In addition, the timing of events in the record provided by GT05-5 suggest that synchroneity of global climate change has continued into and throughout the Holocene. These findings have major implications for our understanding of global change and the mechanisms by which these changes take place. However, a simple notion of synchronous climate shifts across the Earth fails during the latter stages of the most recent deglaciation. During this time there

are two notable exceptions to the global climate change scenario. First, the Antarctic Cold Reversal (ACR) clearly present in the HW05-3 record was not global. Second is the apparent non-occurrence of a climate shift associated with Heinrich 0, also referred to as the Younger Dryas (YD), in at least the West Coast of South Island. The available evidence would suggest that neither event was global, and neither were they synchronous. The HW05-3 stable isotope record indicates that the ACR influenced at least the high and middle southern latitudes, and the RK05-3 record could indicate that the effects of YD cooling in the North Atlantic was experienced as far south as the North Island of New Zealand.

7.2 Conclusions

In this research, growth rate changes and high temporal resolution (averaging 100 years) stable carbon and oxygen isotope profiles of five speleothems from three caves located on the west coasts of South and North Islands were developed and used to reconstruct the climate for the last ~75 kyr in New Zealand. These records fill a need for long, continuous, independently dated, terrestrial palaeoclimate data from New Zealand, and the Southern Hemisphere mid-latitudes in general.

Changes in growth rate and $\delta^{13}C$ values appear to be synchronous in all stalagmites in this study where there are sufficient uranium-series dates to allow an investigation into growth rate changes. The strong relationship is interpreted to indicate that changes in $\delta^{13}C$ reflect changes in mean annual precipitation volumes. Changes in $\delta^{18}O$ are also interpreted in terms of precipitation changes, and influenced by temperature and moisture source region. The close correlation between $\delta^{18}O$ and $\delta^{13}C$ in South island stalagmites HW05-3 and GT05-5 supports regional rather than local drivers. From these results it can be inferred that there were changes in seasonality, with enriched $\delta^{18}O$ indicating drier climate and cold, frosty winters, and depleted $\delta^{18}O$ representing wet climate, and reduced precipitation and temperature differences between seasons.

The record from Hollywood Cave, South Island, spans the period ~73-11 kyr B.P. at resolutions of a few decades to three centuries (Figure 7.1). MIS 4 is prominent at the start of the record (67.7-61.3 kyr B.P.) as a prolonged period of strongly negative $\delta^{18}O$ values (wet and cool climate). MIS 3 was relatively dry, particularly during the period 61-43 kyr B.P. when growth rates were at their lowest. The last glacial coldest period (LGCP) too was dry, but likely colder than MIS 3. However, brief wet periods occur frequently throughout both of these times, indicated by significantly depleted stable isotope ratios and increased growth rate. Deglaciation was also interrupted by negative isotopic excursions.

Almost all of the wet periods identified in the Hollywood record can be correlated with times of ice advance in the Southern Alps. This indicates that the changes in the Hollywood Cave record were at least regional in scale and furthermore allows the opportunity to apply absolute ages to moraines

(particularly those on the West Coast) that are too old to be dated by the radiocarbon method. Application of this principle shows that the Loopline moraines of Westland were deposited during the period 67.7-61.3 kyr B.P. when a wet, cool climate persisted.

The HW05-3 stable isotope profiles also help explain why ice advance during MIS 4 was more extensive than during the LGCP. Wet and cool climate continued uninterrupted for ~6.5 kyr during MIS 4 allowing significant ice build-up. The climate during the LGCP, however, was mostly cold and dry, occasionally interspersed with brief (~1 kyr) wetter intervals. The moraine record indicates that glacier advances were confined to the wetter intervals, which were ultimately too brief to allow ice volumes to exceed those achieved during MIS 4.

The GT05-5 record from Guillotine Cave at high elevation in the Southern Alps demonstrates that the same relationship between wet and cool climate and glacier advance continued throughout the Holocene to the present day. A negative shift in $\delta^{18}O$ at 4.6 kyr B.P. closely matches the onset of a period of more frequent and prolonged intervals of ice advance recorded by moraines in the Mt Cook region, South Island. The $\delta^{18}O$ record displays four millennial-scale oscillations between more negative values (wet-cool) and less negative values (dry-warm climate) during the mid-to-late Holocene. The last oscillation shows a warm-dry climate persisting between 1.6 and 0.9 kyr B.P. followed by a return to wet, cool conditions from 0.8-0.15 kyr B.P. Significantly, these events are synchronous with the Medieval Climate Optimum and the Little Ice Age respectively, demonstrating an interhemispheric climate teleconnection with the North Atlantic during the late Holocene.

It is likely that the climate link between New Zealand and the Northern Hemisphere was also present throughout the last glacial period. Brief negative excursions in HW05-3 (South Island) and RK05-3 (Ruakuri Cave, North Island) $\delta^{18}O$ profiles throughout MISs 3 and 2 are synchronous with Heinrich events in the North Atlantic. The link between these antipodean locations likely operated through latitudinal displacement of wind belts (Figure 7.2). It has previously been demonstrated that cooling of the North Atlantic, associated with Heinrich events, caused the Intertropical Convergence Zone (ITCZ) to shift south (Wang *et al*., 2004, 2006). This in turn led to steepening of the temperature gradient across the mid-southern latitudes and increased intensity of the circumpolar westerly

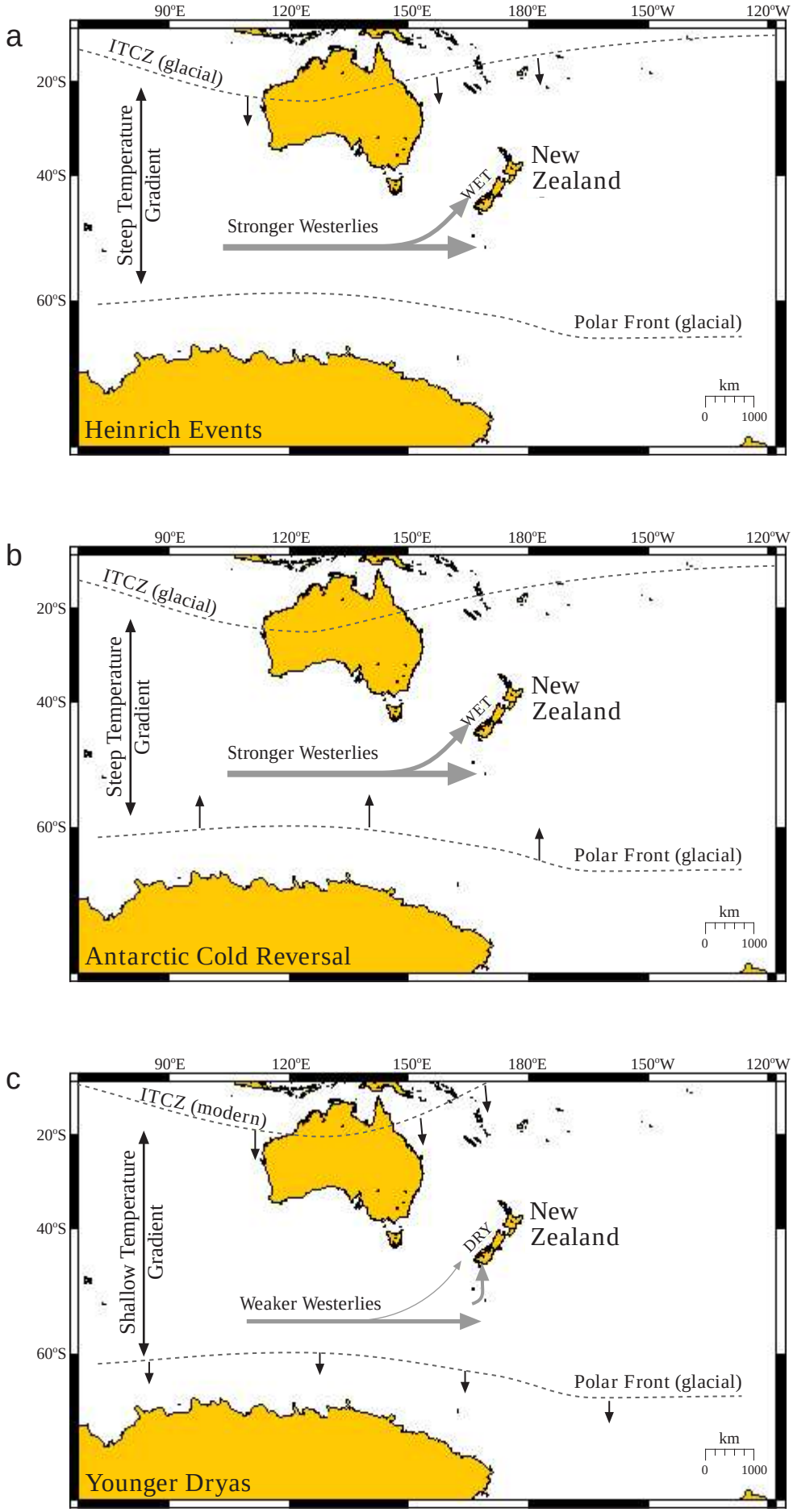
a
90°E
120°E
150°E
180°E
150°W
120°W
20°S
40°S
60°S
ITCZ (glacial)
Steep Temperature Gradient
New Zealand
WET
Stronger Westerlies
Polar Front (glacial)
km
0
1000
Heinrich Events
b
ITCZ (glacial)
Steep Temperature Gradient
New Zealand
WET
Stronger Westerlies
Polar Front (glacial)
km
0
1000
Antarctic Cold Reversal
c
ITCZ (modern)
Shallow Temperature Gradient
New Zealand
DRY
Weaker Westerlies
Polar Front (glacial)
km
0
1000
Younger Dryas

Figure 7.2: Scenarios for generating wet or dry climate on the West Coast of South Island. (a) During Heinrich events the Intertropical Convergence Zone (ITCZ) was displaced to the south, steepening the temperature gradient across the mid-southern latitudes, leading to stronger westerly circulation and a wet climate on the West Coast. (b) During the Antarctic Cold Reversal (ACR) the Polar Front was displaced to the north, steepening the temperature gradient across the mid-southern latitudes, leading to stronger westerly circulation and a wet climate on the West Coast. (c) During the Younger Dryas steepening of the temperature gradient caused by southerly displacement of the ITCZ was cancelled by poleward shift of the Polar Front in association with warming across Antarctica. As a result, westerly circulation was weak, South Island experienced a predominantly southerly flow, and the West Coast climate was relatively dry.

circulation (Figure 7.2a). Under these conditions the climate of the western side of New Zealand became dominated by rain-bearing, cold southwesterly winds. Following the termination of each Heinrich event the ITCZ retreated north and the temperature gradient across the mid-southern latitudes relaxed. Southwesterly flow was diminished and replaced by a greater frequency of southerlies. As the Southern Alps then stood between the caves and the predominant wind direction, a more continental climate was experienced on the West Coast. Mean annual rainfall totals decreased, ground-frosts became more common, and summer months were generally warm.

Late-glacial climate variability recorded in HW05-3 stable isotope ratios reveals a disconnection with the North Atlantic. Heinrich event 0, coeval with the Younger Dryas chronozone, is poorly represented, if at all, in the West Coast palaeoclimate record. However, a period of cool and wet conditions occurred immediately prior to this, between 14.5 and 13.0 kyr B.P. Significantly, this event is coincident with a return to cooler climate in Antarctic, known as the Antarctic Cold Reversal (ACR). The climate signature of the ACR on the West Coast is identical to that of Heinrich events. However, the driving force behind climate changes in New Zealand, coincident with the ACR and Heinrich events, originate from both south and north of country, respectively. This suggests that the increased strength of the circumpolar westerlies, driven by steepening of the mid-latitude temperature gradient, can also be forced by northward migration of the Polar Front during cooling in Antarctica (Figure 7.2b).

This scenario does not, however, explain why H0 (Younger Dryas) did not affect climate on the West Coast. Brazilian speleothems indicate that the ITCZ shifted to the south at this time (Wang *et al*., 2004) which should also have resulted in increased strength in the westerly circulation. An hypothesis could be that at the same time as the ITCZ shifted south, the Polar Front also shifted south as Antarctica warmed toward the early Holocene optimum following the termination of the ACR (Figure 7.2c).

A late-glacial cold reversal also affected climate above Ruakuri Cave, North Island. Unfortunately, there are insufficient dates to determine whether or not the cool and wet event was coeval with either Heinrich 0 (the Younger Dryas) or the Antarctic Cold Reversal.

In summary, the speleothem stable isotope profiles developed in this study have demonstrated sensitivity of South Island climate to events in both Antarctica and the North Atlantic. Significantly, the expression of Antarctic or Northern Hemisphere cooling in the HW05-3 isotope proxies is the same, suggesting that climate changes associated with either event are identical. These findings have significant implications for the understanding of the global climate during the last glacial period. Synchronous change at antipodean locations strongly indicates a global response to forcing of the climate system, and further that this response was transferred via the atmosphere. However, the occurrence of an Antarctic signal (the ACR) cannot be shown to have had a global impact, and may be limited to those sites in the mid-southern latitudes that are sensitive to changes in the strength of the circumpolar westerly circulation.

8 References

Abell, P. I. and Plug, I. 2000, 'The Pleistocene/Holocene transition in South Africa: evidence for the Younger Dryas event', *Global and Planetary Change*, vol. 26, pp. 173-179

Adkins, J. F., McIntyre, K. and Schrag, D. P. 2002, 'The salinity, temperature and delta O-18 of the glacial deep ocean', *Science*, vol. 298, pp. 1769-1773

Alley, R. B., Mayewski, P. A., Sowers, T., Stuiver, M., Taylor, K. C. and Clark, P. U. 1997, 'Holocene climate instability: A prominent, widespread event 8200 yr ago', *Geology*, vol. 25, pp. 483-486

Alloway, B. V., Lowe, D. J., Barrell, D. J. A., Newnham, R. M., Almond, P. C., Augustinus, P. C., Bertler, N. A. N., Carter, L., Litchfield, N. J., McGlone, M. S., Shulmeister, J., Vandergoes, M. J., Williams, P. W. and NZ-INTIMATE members 2007, 'Towards a climate event stratigraphy for new Zealand over the past 30,000 years (NZ-INTIMATE project)', *Journal of Quaternary Science*, vol. 22, pp. 9-35

Alloway, B. V., Stewart, R. B., Neall, V. E. and Vucetich, C. G. 1992, 'Climate of the last glaciation in New Zealand based on aerosolic quartz influx in an andesitic terrain', *Quaternary Research*, vol. 38, pp. 170-179

Almond, P. C., Burge, P., Shanhun, F. L., Smith, C. M. S., Shulmeister, J. and Faure, K. 2007, 'Precipitation patterns during MIS2-3 glacial advances in South Island, New Zealand', *Quaternary International*, vol. 167-168 supplement 1, p. 7

Almond, P. C., Moar, N. T. and Lian, O. B. 2001, 'Reinterpretation of the glacial chronology of South Westland, New Zealand', *New Zealand Journal of geology and Geophysics*, vol. 44, pp. 1-15

Anderson, B. and Mackintosh, A. 2006, 'Temperature change is the major driver of late-glacial and Holocene glacier fluctuations in New Zealand', *Geology*, vol. 34, pp. 121-124

Anderson, J. M. 1984, 'The sedimentology and diagenesis of an Oligocene carbonate sequence, (Nile Group), Westport to Punakaiki', *M.Sc. Thesis*, Victoria University of Wellington, New Zealand, 195 p.

Arens, N. C., Jahren, A. H. and Amundson, R. 2000, 'Can C3 plants faithfully record the carbon isotopic composition of atmospheric carbon dioxide?', *Paleobiology*, vol. 26, pp. 137-164

Ariztegui, D., Bianchi, M.M., Massaferro, J., Lafargue, E., and Niessen, F., 1997, 'Interhemispheric synchrony of Late-glacial climatic instability as recorded in proglacial Lake Mascardi, Argentina', *Journal of Quaternary Science*, vol. 12, pp. 333-338

Atkinson, T. C., Harmon, R. S., Smart, P. L. and Waltham, A. C. 1978, 'Palaeoclimatic and geomorphic implications of $^{230}Th/^{234}U$ dates on speleothems from Britain', *Nature*, vol. 272, pp. 24-28

Ayalon, A., Bar-Matthews, M. and Kaufman, A. 1999, 'Petrography, strontium, barium and uranium concentrations, and strontium and uranium isotope ratios in speleothems as palaeoclimatic proxies: Soreq Cave, Israel', *The Holocene*, vol. 9, pp. 715-722

Ayliffe, L. K., Marianelli, P. C., Moriarty, K. C., Wells, R. T., McCulloch, M. T., Mortimer, G. E. and Hellstrom, J. C. 1998, '500 ka precipitation record from southeastern Australia: Evidence for interglacial relative aridity', *Geology*, vol. 26, pp. 147-150

Baker, A., Genty, D., Dreybrodt, W., Barnes, W. L., Mockler, N. J. and Grapes, J. 1998, 'Testing theoretically predicted stalagmite growth rate with recent

annually laminated samples: implications for past stalagmite deposition', *Geochimica et Cosmochimica Acta*, vol. 62, pp. 393-404

Baker, A., Smart, P. L. and Edwards, R. L. 1995, 'Paleoclimate implications of mass spectrometric dating of a British flowstone', *Geology*, vol. 23, pp. 309-312

Baker, A., Smart, P. L., Edwards, R. L. and Richards, D. 1993, 'Annual growth banding in a cave stalagmite', *Nature*, vol. 364, pp. 518-520

Baldini, J. U. L., Baldini, L. M., McDermott, F. and Clipson, N. 2006, 'Carbon dioxide sources, sinks, and spatial variability in shallow temperate zone caves: evidence from Ballynamintra Cave, Ireland', *Journal of Cave and Karst Studies*, vol. 68, pp. 4-11

Banner, J. L., Musgrove, M. L., Asmerom, Y., Edwards, R. L. and Hoff, J. A. 1996, 'High-resolution temporal record of Holocene groundwater chemistry: tracing links between climate and hydrology', *Geology*, vol. 24, pp. 1049-1053

Bard, E., Hamelin, B., Arnold, M., Montaggioni, L., Cabioch, G., Faure, G. and Rougerie, F. 1996, 'Deglacial sea-level record from Tahiti corals and the timing of global meltwater discharge', *Nature*, vol. 382, pp. 241-244

Bard, E., Hamelin, B. and Fairbanks, R. G. 1990, 'U-Th ages obtained by mass spectrometry in corals from Barbados: Sea-level during the past 130,000 years', *Nature*, vol. 346, pp. 456-458

Bar-Matthews, M., Matthews, A. and Ayalon, A. 1991, 'Environmental controls of speleothem mineralogy in a karstic dolomitic terrain (Soreq Cave, Israel)', *Journal of Geology*, vol. 99, pp. 189-207

Barrows, T. T., Juggins, S., De Dekker, P., Calvo, E. and Pelejero, C. 2007, 'Long-term sea surface temperature and climate change in the Australian-

New Zealand region', *Paleoceanography*, vol. 22, PA2215, doi:10.1029/2006PA001328

Barrows, T. T., Stone, J. O., Fifield, L. K. and Cresswell, R. G. 2001, 'Late Pleistocene glaciation of the Kosciuszko Massif, Snowy Mountains, Australia', *Quaternary Research*, vol. 55, pp. 179-189

Bennett, K. D., Haberle, S. G., and Lumley, S. H. 2000, 'The last glacial-Holocene transition in southern Chile', *Science*, vol. 290, pp. 325-328

Benson, L., Lund, S., Negrini, R., Linsley, B. and Zic, M. 2003, 'Response of North American Great Basin Lakes to Dansgaard-Oeschger oscillations', *Quaternary Science Reviews*, vol. 22, pp. 2239-2251

Berger, A. and Loutre, M. F. 1991, 'Insolation values for the climate of the last 10 million years', *Quaternary Science Reviews*, vol. 10, pp. 297-317

Bertaux, J., Sondag, F., Santos, R., Soubiès, F., Causse, C., Plagnes, V., Le Cornec, F. and Seidel, A. 2002, 'Paleoclimatic record of speleothems in a tropical region: study of laminated sequences from a Holocene stalagmite in Central-West Brazil', *Quaternary International*, vol. 89, pp. 3-16

Bircham, D. N. 1975, *Waitomo Tourist Caves*, A. H. & A. W. Reed Ltd., Wellington, New Zealand, 30 p.

Blunier, T. and Brook, E. J. 2001, 'Timing of millennial-scale climate change in Antarctica and Greenland during the last glacial period', *Science*, vol. 291, pp. 109-112

Blunier, T., Chappellaz, J., Schwander, J., Dällenbach, A., Stauffer, B., Stocker, T. F., Raynaud, D., Jouzel, J., Clausen, H. B., Hammer, C. U. and Johnsen, S. J. 1998, 'Asynchrony of Antarctic and Greenland climate change during the last glacial period', *Nature*, vol. 394, pp. 739-743

Bond, G., Kromer, B., Beer, J., Muscheler, R., Evans, M. N., Showers, W., Hoffmann, S., Lotti-Bond, R., Hajdas, I. and Bonani, G. 2001, 'Persistent solar influence on North Atlantic climate during the Holocene', *Science*, vol. 294, pp. 2130-2136

Bond, G. C. and Lotti, R. 1995, 'Iceberg discharges into the North Atlantic on millennial time scales during the last glaciation', *Science*, vol. 267, pp. 1005-1010

Bond, G., Showers, W., Cheseby, M., Lotti, R., Almasi, P., deMenocal P., Priore, P., Cullen, H., Hajdas, I. and Bonani, G. 1997, 'A pervasive millennial-scale cycle in North Atlantic Holocene and glacial climates', *Science*, vol. 278, pp. 1257-1266

Bottinga, Y. and Craig, H., 1969, 'Oxygen isotope fractionation between CO_2 and water and the isotopic composition of marine atmospheric CO_2', *Earth and Planetary Science Letters*, vol. 5, pp. 285-295

Broecker, W. S. 1994, 'Massive iceberg discharges as triggers for global climate change', *Nature*, vol. 372, pp. 421-424

Broecker, W. 1998, 'Paleocean circulation during the last deglaciation: A bipolar seesaw?', *Paleoceanography*, vol. 13, pp. 119-121

Broecker, W. S. 2000, 'Was a change in thermohaline circulation responsible for the Little Ice Age?', *Proceedings of the National Academy of Sciences of the United States*, vol. 97, pp. 1339-1342

Broecker, W. S. 2003, 'Does the trigger for abrupt climate change reside in the ocean or in the atmosphere?', *Science*, vol. 300, pp. 1519-1522

Broecker, W. S., Thurber, D. L., Goddard, J., Ku, T., Matthews, R. K. and Mesolella, K. J. 1968, 'Milankovitch hypothesis supported by precise dating of coral reefs and deep-sea sediments', *Science*, vol. 159, pp. 1-4

Broecker, W. S. and van Donk, J. 1970, 'Insolation changes, ice volume, and the ^{18}O record in deep-sea cores', *Reviews of Geophysics and Space Physics*, vol. 8, pp. 169-198

Brook, G. A. 1982, 'Stratigraphic evidence of Quaternary climatic change at Echo Cave, Transvaal, and a paleoclimatic record for Botswana and northeastern South Africa', *Catena*, vol. 9, pp. 343-351

Brook, G. A., Burney, D. A. and Cowart, J. B. 1990, 'Desert paleoenvironmental data from cave speleothems with examples from the Chihuahuan, Somali-Chalbi, and Kalahari deserts', *Palaeogeography, Palaeoclimatology, Palaeoecology*, vol. 76, pp. 311-329

Brook, G. A., Rafter, M. A., Railsback, L. B., Sheen, S.-W. and Lundberg, J. 1999, 'A high-resolution proxy record of rainfall and ENSO since AD 1550 from layering in stalagmites from Anjohibe Cave, Madagascar', *The Holocene*, vol. 9, pp. 695-705

Burge, P. I. And Shulmeister, J. 2007, 'An MIS5a to MIS 4 (or early MIS 3) environmental and climatic reconstruction from the northwest South Island, New Zealand, using beetle fossils', *Journal of Quaternary Science*, vol. 22, pp. 501-516

Burns, S. J., Fleitmann, D., Matter, A., Kramers, J. and Al-Subbary, A. A. 2003, 'Indian Ocean climate and an absolute chronology over Dansgaard/Oeschger events 9 to 13', *Science*, vol. 301, pp. 1365-1367

Cai, Y., An, Z., Cheng, H., Edwards, R. L., Kelly, M. J., Liu, W., wang, X. and Shen C.-C. 2006, 'High-resolution absolute-dated Indian Monsoon record between 53 and 36 ka from Xiaobailong Cave, southwestern China', *Geology*, vol. 34, pp. 621-624

Carter, L. and Manighetti, B. 2006, 'Glacial/interglacial control of terrigenous and biogenic fluxes in the deep ocean off a high input, collisional margin: A 139 kyr-record from New Zealand', *Marine Geology*, vol. 226, pp. 307-322

Carter, L., Manighetti, B., Ganssen, G. and Northcote, L. 2008, 'Southwest Pacific modulation of abrupt climate change during the Antarctic Cold Reversal–Younger Dryas', *Palaeogeography, Palaeoclimatology, Palaeoecology*, vol. 260, pp. 284-298

Chappell, J. 1991, 'Late Quaternary environmental changes in eastern and central Australia, and their climatic interpretation', *Quaternary Science Reviews*, vol. 10, pp. 377-390

Chappell, J. and Polach, H. 1991, 'Post-glacial sea-level rise from a coral record at Huon Peninsula, Papua New Guinea', *Nature*, vol. 349, pp. 147-149

Charles, C. D., Lynch-Steiglitz, J., Ninnemann, U. S. and Fairbanks, R. G. 1996, 'Climate connections between the hemispheres revealed by deep sea sediment core/ice core correlations', *Earth and Planetary Science Letters*, vol. 142, pp. 19-27

Chen, J. H., Edwards, R. L. and Wasserburg, G. J. 1992, 'Mass spectrometry and application to uranium-series disequilibrium', in Uranium-Series Disequilibrium: Applications to Earth, Marine, and Environmental Sciences, 2nd Ed., Ivanovich, M. and Harmon, R. S., eds., Clarendon Press, Oxford, United Kingdom, pp. 174-206

Cheng, H., Edwards, R. L., Hoff, J., Gallup, C. D., Richards, D. A. and Asmerom, Y. 2000, 'The half-lives of uranium-234 and thorium-230', *Chemical Geology*, vol. 169, pp. 17-33

Christie, A. B., Thompson, B. N. and Brathwaite, R. L. 2001, 'Mineral Commodity Report 21: Limestone, marble and dolomite', *New Zealand Mining*, vol. 29, pp. 6-25

Clark, P. U. and Bartlein, P. J. 1995, 'Correlation of late Pleistocene glaciation in the western united States with North Atlantic Heinrich events', *Geology*, vol. 23, pp. 483-486

Crossley, P. C. 1988, *The New Zealand Cave Atlas: North Island*, New Zealand Speleological Society, Waitomo, New Zealand, 311 p.

Cruz Jr., F. W., Burns, S. J., Karmann, I., Sharp, W. D., Vuille, M., Cardoso, A. O., Ferrari, J. A., Silva Dias, P. L. and Viana Jr., O. 2005, 'Insolation-driven changes in atmospheric circulation over the past 116,000 years in subtropical Brazil', *Nature*, vol. 434, pp. 63-66

Dansgaard, W. 1964, 'Stable isotopes in precipitation', *Tellus*, vol. 16, pp. 436-468

Dansgaard, W., Clausen, H. B., Gundestrup, N., Hammer, C. U., Johnsen, S. F., Kristinsdottir, P. M. and Reeh, N. 1982, 'A new Greenland deep ice core', *Science*, vol. 218, pp. 1273-1277

Dansgaard, W., Johnsen, S. J., Clausen, H. B., Dahl-Jensen, D., Gundestrup, N. S., Hammer, C. U., Hvidberg, C. S., Steffensen, J. P., Sveinbjörnsdottir, A. E., Jouzel, J. and Bond, G. 1993, 'Evidence for general instability of past climate from a 250-kyr ice-core record', *Nature*, vol. 364, pp. 218-220

Dansgaard, W., White, J. W. C. and Johnsen, S. F. 1989, 'The abrupt termination of the Younger Dryas climate event', *Nature*, vol. 339, p. 532-534

Deines, P., Langmuir, D. and Harmon, R. S. 1974, 'Stable carbon isotope ratios and the existence of a gas phase in the evolution of carbonate ground water', *Geochimica et Cosmochimica Acta*, vol. 38, pp. 1147-1164

deMenocal, P., Ortiz, J., Guilderson, T. and Sarnthein, M. 2000, 'Coherent high- and low-latitude climate variability during the Holocene warm period', *Science*, vol. 288, pp. 2198-2202

Denton, G. H., Alley, R. B., Comer, G. C. and Broecker, W. S. 2005, 'The role of seasonality in abrupt climate change', *Quaternary Science Reviews*, vol. 24, pp. 1159-1182

Denton, G. H. and Hendy, C. H. 1994, 'Younger Dryas age advance of Franz Josef Glacier in the Southern Alps of New Zealand', *Science*, vol. 264, pp. 1434-1437

Denton, G. H., Heusser, C. J., Lowell, T. V., Moreno, P. I., Andersen, B. G., Heusser, L. E., Schlüchter, C. and Marchant, D. R. 1999a, 'Interhemispheric linkage of paleoclimate during the last glaciation', *Geografiska Annaler*, vol. 81A, pp. 107-153

Denton, G. H and Karlén, W. 1973, 'Holocene climatic variations – their pattern and possible cause', *Quaternary Research*, vol. 3, pp. 155-205

Denton, G. H., Lowell, T. V., Heusser, C. J., Schlüchter, C., Andersen, B. G., Heusser, L. E., Moreno, P. I. and Marchant, D. R. 1999b, 'Geomorphology, stratigrphy, and radiocarbon chronology of Llanquihue Drift in the area of the southern lake districtm Seno Reloncaví, and Isla Grande de Chiloé, Chile', *Geografiska Annaler*, vol. 81A, pp. 167-229

Desmarchelier, J. M., Goede, A., Ayliffe, L. K., McCulloch, M. T. and Moriarty, K. 2000, 'Stable isotope record and its palaeoenvironmental interpretation for a late Middle Pleistocene speleothem from Victoria Fossil Cave, Naracoorte, South Australia', *Quaternary Science Reviews*, vol. 19, pp. 763-774

Desmarchelier, J. M., Hellstrom, J. C. and McCulloch, M. T. 2006, 'Rapid trace element analysis of speleothems by ELA-ICP-MS', *Chemical Geology*, vol. 231, pp. 102-117

Dorale, J. A., Edwards, R. L., Alexander, E. C. Jr., Shen, C.-C., Richards, D. A. and Cheng, H. 2004, 'Uranium-series dating of speleothems: current techniques, limits, and applications', in Studies of Cave Sediments: Physical and Chemical Records of Palaeoclimate, Sasowsky, I. D. and Mylroie, J. E., eds., Kluwer Academic, New York, USA, pp. 177-197

Dorale, J. A., Edwards, R. L., Ito, E. and González, L. A. 1998, 'Climate and vegetation history of the mid-continent from 75 to 25 ka: a speleothem record from Crevice Cave, Missouri, USA', *Science*, vol. 282, pp. 1871-1874

Dorale, J. A., González, L. A., Reagan, M. K., Pickett, D. A., Murrell, M. T. and Baker, R. G. 1992, 'A high-resolution record of Holocene climate change in speleothem calcite from Cold Water Cave, northeast Iowa', *Science*, vol. 258, pp. 1626-1630

Douglass, D. C., Singer, B. S., Kaplan, M. R., Mickelson, D. M. and Caffee, M. W. 2006, 'Cosmogenic nuclide surface exposure dating of boulders on last-glacial and late-glacial moraines, Lago Buenos Aires, Argentina: Interpretive strategies and paleoclimate implications', *Quaternary Geochronology*, vol. 1, pp. 43-58

Dreybrodt, W. 1999, 'Chemical kinetics, speleothem growth and climate', *Boreas*, vol. 28, pp. 347-356

Drost, F., Renwick, J., Bhaskaran, B., Oliver, H. and McGregor, J. 2007, 'A simulation of New Zealand's climate during the Last Glacial Maximum', *Quaternary Science Reviews*, vol. 25, pp. 2505-2525

Drysdale, R. N., Zanchetta, G., Hellstrom, J. C., Fallick, A. E., McDonald, J. and Cartwright, I. 2007, 'Stalagmite evidence for the precise timing of North Atlantic cold events during the early last glacial', *Geology*, vol. 35, pp. 77-80

Dulinski, M. and Rozanski, K. 1990, 'Formation of $^{13}C/^{12}C$ isotope ratios in speleothems: a semi-dynamic model', *Radiocarbon*, vol. 32, pp. 7-16

Duplessy, J.-C., Labeyrie, J., Lalou, C., and Nguyen, H.V., 1970, 'Continental climatic variations between 130000 and 90000 years B.P.', *Nature*, vol. 226, pp. 631-633

Duplessy, J.-C., Labeyrie, J. and Waelbroeck, C. 2002, 'Constraints on the ocean oxygen isotopic enrichment between the Last Glacial Maximum and the Holocene: Paleoceanographic implications', *Quaternary Science Reviews*, vol. 21, pp. 315-330

Dykoski, C. A., Edwards, R. L., Cheng, H., Yuan, D., Cai, Y., Zhang, M., Lin, Y., Qing, J., An, Z. and Revenaugh, J. 2005, 'A high-resolution, absolute-dated Holocene and deglacial Asian monsoon record from Dongge Cave, China', *Earth and Planetary Science Letters*, vol. 233, pp. 71-86

Easterbrook, D. J. 2007, 'Late Pleistocene and Holocene glacial fluctuations: implications for the cause of abrupt global climate changes', *Geological Society of America Abstracts with Programs*, vol. 39, p. 594

Edwards, R. L., Chen, J. H. and Wasserburg, G. J. 1987, '^{238}U-^{234}U-^{230}Th-^{232}Th systematics and the precise measurement of time over the last 500,000 years', *Earth and Planetary Science Letters*, vol.81, pp. 175-192

Ek, C. and Gewelt, M. 1985, 'Carbon-dioxide in cave atmospheres – New results in Belgium and comparison with some other countries', *Earth Surface Processes and Landforms*, vol. 10, pp. 173-187

Elliot, M., Neall, V. and Wallace, C. 2005, 'A Late Quaternary pollen record from Lake Tangonge, far northern New Zealand', *Review of Palaeobotany and Palynology*, vol. 136, pp. 143-158

Emiliani, C. 1955, 'Pleistocene paleotemperatures', *Journal of Geology*, vol. 63, pp. 358-378

EPICA Community Members 2004, 'Eight glacial cycles from an Antarctic ice core', *Nature*, vol. 429, pp. 623-628

EPICA Community Members 2006, 'One-to-one coupling of glacial climate variability in Greenland and Antarctica', *Nature*, vol. 444, pp. 195-198

Fairbanks, R. G. 1989, 'A 17,000-year glacio-eustatic sea level record: influence of glacial melting rates on the Younger Dryas event and deep ocean circulation', *Nature*, vol. 342, pp. 637–642

Fairchild, I. J., Borsato, A., Tooth, A. F., Frisia, S., Hawkesworth, C. J., Huang, Y., McDermott, F. and Spiro, B. 2000, 'Contols on trace element (Sr-Mg) compositions of carbonate cave waters: implications for speleothem climate records', *Chemical Geology*, vol. 166, pp. 255-269

Fairchild, I. J., Smith, C. L., Baker, A., Fuller, L., Spötl, C., Mattey, D., McDermott, F. and E. I. M. F. 2006, 'Modification and preservation of environmental signals in speleothems', *Earth-Science Reviews*, vol. 75, pp. 105-153

Fantidis, J. and Ehhalt, D. H. 1970, 'Variations of the carbon and oxygen isotopic composition in stalagmites and stalactites: evidence of non-equilibrium isotopic fractionation', *Earth and Planetary Science Letters*, vol. 10, pp. 136-144

Faure, G. 1986, *Principles of Isotope Geology*, John Wiley and Sons, New York, U.S.A., 589 p.

Finch, A. A., Shaw, P. A., Holmgren, K. and Lee-Thorp, J. 2003, 'Corroborated rainfall records from aragonitic stalagmites', *Earth and Planetary Science Letters*, vol. 215, pp. 265-273

Finch, A. A., Shaw, P. A, Weedon, G. P. and Holmgren, K. 2001, 'Trace element variation in speleothem aragonite: potential for palaeoenvironmental reconstruction', *Earth and Planetary Science Letters*, vol. 186, pp. 255-267

Ford, D. C. and Williams, P. 1989, *Karst Hydrology and Geomorphology*, Chapman and Hall, London, United Kingdom, 601 p.

Franke, H. W. 1965, 'The theory behind stalagmite shapes', *Studies in Speleology*, vol. 1, pp. 89-95

Frappier, A. B. in press, 'A stepwise screening system to select storm-sensitive stalagmites: taking a targeted approach to speleothem sampling methodology', *Quaternary International*, available online from 4 October 2007

Frappier, A. B., Sahagian, D., Carpenter, S. J., González, L. A. and Frappier, B. R. 2007, 'Stalagmite stable isotope record of recent tropical cyclone events', *Geology*, vol. 35, pp. 111-114

Friedman, I. and O'Neil, J. R. 1977, 'Compilation of stable isotope fractionation factors of geochemical interest', *U.S. Geological Survey Professional Paper* 440-KK

Frumkin, A. and Stein, M. 2004, 'The Sahara-East Mediterranean dust and climate connection revealed by strontium and uranium isotopes in a Jerusalem speleothem', *Earth and Planetary Science Letters*, vol. 217, pp. 451-464

Galimov, E.M., and Grinenko, V.A., 1965, 'Effect of leaching under surface conditions on the isotopic composition of carbon in secondary calcite', *Geochemistry International*, vol. 1, pp. 79-82

Galy, A., Bar-Matthews, M., Halicz, L. and O'Nions, R. K. 2002, 'Mg isotopic composition of carbonate: insight from speleothem formation', *Earth and Planetary Science Letters*, vol. 201, pp. 105-115

Gascoyne, M. 1983, 'Trace element partition coefficients in the calcite-water system and their paleoclimatic significance in cave studies', *Journal of Hydrology*, vol. 61, p. 213-222

Gascoyne, M. 1992, 'Palaeoclimate determination from cave calcite deposits', *Quaternary Science Reviews*, vol. 11, pp. 609-632

Gascoyne, M., Benjamin, G. J., Schwarcz, H. P. and Ford, D. C. 1979, 'Sea-level lowering during the Illinoian glaciation: Evidence from a Bahama "Blue Hole"', *Science*, vol. 205, pp. 806-808

Gellatly, A. F., Chinn, T. J. H. and Röthlisberger, F. 1988, 'Holocene glacier variations in New Zealand: a review', *Quaternary Science Reviews*, vol. 7, pp. 227-242

Genty, D., Blamart, D., Ouahdi, R., Gilmour, M., Baker, A., Jouzel, J. and Van-Exter, S. 2003, 'Precise dating of Dansgaard-Oeschger climate oscillations in western Europe from stalagmite data', *Nature*, vol. 421, pp. 833-837

Gillieson, D. 1996, *Caves: Processes, Development, Management*, Blackwell, Oxford, United Kingdom, 324 p.

Goede, A. 1994, 'Continuous early last glacial palaeoenvironmental record from a Tasmanian speleothem based on stable isotope and minor element variations', *Quaternary Science Reviews*, vol. 13, pp. 283-291

Goede, A., Green, D. C. and Harmon, R. S. 1986, 'Late Pleistocene palaeotemperature record from a Tasmanian speleothem', *Australian Journal of Earth Sciences*, vol. 33, pp. 333-342

Goede, A., Harmon, R. S., Atkinson, T. C. and Rowe, P. J. 1990a, 'Pleistocene climatic change in Southern Australia and its effect on speleothem deposition in some Nullarbor caves', *Journal of Quaternary Science*, vol. 5, pp. 29-38

Goede, A., McCulloch, M. T., McDermott, F. and Hawkesworth, C. 1998, 'Aeolian contribution to strontium and strontium isotope variations in a Tasmanian speleothem', *Chemical Geology*, vol. 149, pp. 37-50

Goede, A., McDermott, F., Hawkesworth, C., Webb, J., and Finlayson, B., 1996, 'Evidence of Younger Dryas and Neoglacial cooling in a Late Quaternary palaeotemperature record from a speleothem in eastern Victoria, Australia', *Journal of Quaternary Science*, vol. 11, pp. 1-7

Goede, A, Veeh, H. H. and Ayliffe, L. K. 1990b, 'Late Quaternary palaeotemperature records for two Tasmanian speleothems', *Australian Journal of Earth Sciences*, vol. 37, pp. 267-278

Goede, A. and Vogel, J. C. 1991, 'Trace element variations and dating of a Late Pleistocene Tasmanian speleothem', *Palaeogeography, Palaeoclimatology, Palaeoecology*, vol. 88, pp. 121-131

Goldstein, S. J. and Stirling, C. H. 2003, 'Techniques for measuring uranium-series nuclides: 1992-2002', *Reviews in Mineralogy and Geochemistry*, vol. 52, pp. 23-57

González, L. A. and Lohmann, K. C. 1988, 'Controls on mineralogy and composition of spelean carbonates: Carlsbad Caverns, New Mexico', in James, N. P. and Choquette, P. W. (Eds.), *Paleokarst*, Springer-Verlag, New York, USA, pp. 81-101

Grimm, E. C., Watts, W. A., Jacobson Jr., G. L., Hansen, B. C. S., Almquist, H. R., Dieffenbacher-Krall, A. C. 2006, 'Evidence for warm wet Heinrich events in Florida', *Quaternary Science Reviews*, vol. 25, pp. 2197-2211

Grootes, P. M., Steig, E. J., Stuiver, M., Waddington, E. D., Morse, D. L. and Nadeau, M.-J. 2001, 'The Taylor Dome Antarctic ^{18}O record and globally synchronous changes in climate', *Quaternary Research*, vol. 56, pp. 289-298

Grootes, P. M., Stuiver, M., White, J. W. C., Johnsen, S. and Jouzel, J. 1993, 'Comparison of oxygen isotope records from the GISP2 and GRIP Greenland ice cores', *Nature*, vol. 366, pp. 552-554

Grossman, E. L. and Ku, T.-L. 1986, 'Oxygen and carbon isotope fractionation in biogenic aragonite: temperature effects', *Chemical Geology*, vol. 59, pp. 59-74

Grove, J. M. 2004, *Little ice ages: ancient and modern*, 2nd Ed., Routledge, London, U.K., 718 p.

Haeuselmann, P., Granger, D. E., Jeannin, P.-Y. and Lauritzen, S.-E. 2007, 'Abrupt glacial valley incision at 0.8 Ma dated from cave deposits in Switzerland', *Geology*, vol. 35, pp. 143-146

Hajdas, I., Lowe, D. J., Newnham, R. M. and Bonani, G. 2006, 'Timing of the late-glacial climate reversal in the Southern Hemisphere using high-resolution radiocarbon chronology for Kaipo Bog, New Zealand', *Quaternary Research*, vol. 65, pp. 340-345

Harmon, R. S., Schwarcz, H. P., Gascoyne, M., Hess, J. W. and Ford, D. C. 2004, 'Paleoclimate information from speleothems: the present as a guide to the past', *in* Sasowsky, I. D. and Mylroie, J. E. (Ed.s) *Studies of cave sediments:*

physical and chemical records of paleoclimate, Kluwer Academic Publishers, New York, U.S.A., pp. 199-226

Hays, J. D., Imbrie, J. and Shackleton, N. J. 1976, 'Variations in the Earth's orbit: Pacemaker of the ice ages', *Science*, vol. 194, pp. 1121-1132

Heine, K. and Geyh, M. A. 1984, 'Radiocarbon dating of speleothems from Rössing cave, Namib desert, and palaeoclimatic implications', in Vogel, J.C. (Ed.) *Late Cainozoic Palaeoclimates of the Southern Hemisphere*, Balkema, Rotterdam, Netherlands, 520 p.

Heinrich, H. 1988, 'Origin and consequences of cyclic ice rafting in the Northeast Atlantic Ocean during the past 130,000 years', *Quaternary Research*, vol. 29, pp. 142-152

Hellstrom, J. 2003, 'Rapid and accurate U/Th dating using parallel ion-counting multi-collector ICP-MS', *Journal of Analytical Atomic Spectrometry*, vol. 18, pp. 1346-1351

Hellstrom, J. C. and McCulloch, M. T. 2000, 'Multi-proxy constraints on the climatic significance of trace element records from a New Zealand speleothem', *Earth and Planetary Science Letters*, vol. 179, pp. 287-297

Hellstrom, J., McCulloch, M. and Stone, J. 1998, 'A detailed 31,000-year record of climate and vegetation change, from the isotope geochemistry of two New Zealand speleothems', *Quaternary Research*, vol. 50, pp. 167-178

Hemming, S. R. 2004, 'Heinrich events: massive Late Pleistocene detritus layers of the North Atlantic and their global climate imprint', *Review of Geophysics*, vol. 42, pp. 1-43 RG1005

Hendy, C. H. 1969, 'The isotopic geochemistry of speleothems and its application to the study of past climates', *Ph.D. Thesis*, Victoria University of Wellington, New Zealand, 440 p.

Hendy, C. H. 1971, 'The isotopic geochemistry of speleothems – I. The calculation of the effects of different modes of formation on the isotopic composition of speleothems and their applicability as palaeoclimatic indicators', *Geochimica et Cosmochimica Acta*, vol. 35, pp. 801-824

Hendy, C. H. and Wilson, A. T. 1968, 'Palaeoclimatic data from speleothems', *Nature*, vol. 219, pp. 48-51

Hendy, I. L. and Kennett, J. P. 2003, 'Tropical forcing of North Pacific intermediate water distribution during Late Quaternary rapid climate change?', *Quaternary Science Reviews*, vol. 22, pp. 673-689

Hennig, G. J., Grün, R. and Brunnacker, K. 1983, 'Speleothems, travertines, and paleoclimates', *Quaternary Research*, vol. 20, pp. 1-29

Hesse, P. 1994, 'The record of continental dust from Australia in Tasman Sea sediments', *Quaternary Science Reviews*, vol. 13, pp. 257-272

Hesse, P. and McTainsh, G. H. 1999, 'Last glacial maximum to early Holocene wind strength in the mid-latitudes of the southern hemisphere from aeolian dust in the Tasman Sea', *Quaternary Research*, vol. 52, pp. 343-349

Holmgren, K., Karlén, W., Lauritzen, S.-E., Lee-Thorp, J. A., Partridge, T. C., Piketh, S., Repinski, P., Stevenson, C., Svanered, O. and Tyson, P. D. 1999, 'A 3000-year high-resolution stalagmite-based record of palaeoclimate for northeastern South Africa', *The Holocene*, vol. 9, pp. 295-309

Holmgren, K., Karlén, W. and Shaw, P. A. 1995, 'Paleoclimatic significance of the stable isotopic composition and petrology of a Late Pleistocene stalagmite from Botswana', *Quaternary Research*, vol. 43, pp. 320-328

Holmgren, K., Lauritzen, S.-E. and Possnert, G. 1994, '$^{230}Th/^{234}U$ and ^{14}C dating of a Late Pleistocene stalagmite in Lobatse II Cave, Botswana', *Quaternary Geochronology* (*Quaternary Science Reviews*), vol. 13, pp. 111-119

Holmgren, K., Lee-Thorp, J. A., Cooper, G. R. J., Lundblad, K., Partridge, T.C., Scott, L., Sithaldeen, R., Talma, A. S. and Tyson, P. D. 2003, 'Persistent millennial-scale climatic variability over the past 25,000 years in Southern Africa', *Quaternary Science Reviews*, vol. 22, pp. 2311-2326

Holmgren, K. and Shaw, P. 1998-1999, 'Palaeoenvironmental interpretation of cores from large stalagmites: an example from Lobatse II cave, Botswana', *Theoretical and Applied Karstology*, vol. 11-12, pp. 23-34

Hooker, B. L. and Fitzharris, B. B. 1999, 'The correlation between climatic parameters and the retreat and advance of Franz Josef Glacier, New Zealand', *Global and Planetary Change*, vol. 22, pp. 39-48

Huang, Y. and Fairchild, I. J. 2001, 'Partitioning of Sr^{2+} and Mg^{2+} into calcite under karst-analogue experimental conditions', *Geochimica et Cosmochimica Acta*, vol. 65, pp. 47-62

Huang, Y., Fairchild, I. J., Borsato, A., Frisia, S., Cassidy, N. J., McDermott, F. and Hawkesworth, C. J. 2001, 'Seasonal variations in Sr, Mg and P in modern speleothems (Grotta di Ernesto, Italy)', *Chemical Geology*, vol. 175, pp. 429-448

Hughen, K. A., Overpeck, J. T., Peterson, L. C. and Trumbore, S. 1996, 'Rapid climate changes in the tropical Atlantic region during the last deglaciation', *Nature*, vol. 380, pp. 51-54

IAEA/WMO, 2004, Global Network of Isotopes in Precipitation. The GNIP Database. Accessible at: http://isohis.iaea.org

Imbrie, J. and Imbrie, J. P. 1979, *Ice Ages: Solving the Mystery*, Enslow Publishers, New Jersey, U. S. A., 224 p.

IPCC 2007, *Climate Change 2007: The Physical Science Basis*, Contribution of Working Group I to the Fourth Assessment Report of the Intergovernmental Panel on Climate Change; Solomon, S., Qin, D., Manning, M., Chen, Z., Marquis, M., Averyt K. B., Tignor, M. and Miller, H. L. (eds.), Cambridge University Press, Cambridge, United Kingdom, 996 p.

Iversen, J. 1954, 'The late-glacial flora of Denmark and its relationship to climate and soils', *Danmarks Geologiske Undersøgelse*, vol. 80, pp. 87–119

Ivy-Ochs, S., Schlüchter, C., Kubik, P. W. and Denton, G. H. 1999, 'Moraine exposure dates imply synchronous Younger Dryas glacier advances in the European Alps and in the Southern Alps of New Zealand', *Geografiska Annaler*, vol. 81A, pp. 313-324

Johnsen, S. J., Clausen, H. B., Dansgaard, W., Fuhrer, K., Gundestrup, N., Hammer, C. U., Iversen, P., Jouzel, J., Stauffer, B. and Steffensen, J. P. 1992, 'Irregular glacial interstadials recorded in a new Greenland ice core', *Nature*, vol. 359, pp. 311-313

Johnsen, S. J., Dahl-Jensen, D., Gundestrup, N., Steffensen, J. P., Clausen, H. B., Miller, H., Masson-Delmotte, V., Sveinbjörnsdottir, A. E. and White, J. 2001, 'Oxygen isotope and palaeotemperature records from six Greenland ice-core stations: Camp Century, Dye-3, GRIP, GISP2, Renland and NorthGRIP', *Journal of Quaternary Science*, vol. 16, pp. 299-307

Kakiuchi, M. and Matsuo, S. 1979, 'Direct measurements of D/H and $^{18}O/^{16}O$ fractionation factors between vapor and liquid water in the temperature range from 10 to 40°C', *Geochemical Journal*, vol. 13, pp. 307–311

Kanfoush, S. L., Hodell, D. A., Charles, C. D., Guilderson, T. P., Mortyn, P. G. and Ninnemann, U. S. 2000, 'Millennial-scale instability of the Antarctic ice sheet during the last glaciation', *Science*, vol. 288, pp. 1815-1818

Kaplan, M., Schaefer, J., Andersen, B., Barrell, D., Denton, G., Doughty, A., Finkel, R., Putnam, A. and Schwartz, R. 2007, '^{10}Be chronology of moraines in the Irishman's Stream Valley, Ben Ohau Range, New Zealand', Comer Fellows Meeting, New York, 2-5 May 2007

Kaufman, A. and Broecker, W. 1965, 'Comparison of ^{230}Th and ^{14}C ages for carbonate materials from Lakes Lahontan and Bonneville', *Journal of Geophysical Research*, vol. 70, pp. 4039-4054

Kaufmann, G. and Dreybrodt, W. 2004, 'Stalagmite growth and palaeo-climate: an inverse approach', *Earth and Planetary Science Letters*, vol. 224, pp. 529-545

Kiernan, K., Fifield, L. K. and Chappell, J. 2004, 'Cosmogenic nuclide ages for Last Glacial Maximum moraine at Schnells Ridge, Southwest Tasmania', *Quaternary Research*, vol. 61, pp. 335-338

Klimchouk, A. 2005, 'Gypsum caves', in *Encyclopedia of Caves*, Ed.s Culver, D. C. and White, W. B., Elsevier Academic Press, London, United Kingdom, 674 p.

Köppen, W. and Wegener, A. 1924, *Die Klimate der geologischen Vorzeit*, Berlin, Germany, 256 p.

Lamb, H. H. 1965, 'The early medieval warm epoch and its sequel', *Palaeogeography, Palaeoclimatology, Palaeoecology*, vol. 1, pp. 13-37

Lambeck, K. and Chappell, J. 2001, 'Sea level change through the last glacial cycle', *Science*, vol. 292, pp. 679-686

Lambeck, K., Yokoyama, Y. and Purcell, T. 2002, 'Into and out of the Last Glacial Maximum: sea-level change during Oxygen Isotope Stages 3 and 2', *Quaternary Science Reviews*, vol. 21, pp. 343-360

Lauriol, B., Ford, D. C., Cinq-Mars, J. and Morris, W. A. 1997, 'The chronology of speleothem deposition in northern Yukon and its relationships to permafrost', *Canadian Journal of Earth Science*, vol. 34, pp. 902-911

Lauritzen, S.-E. and Lundberg, J. 1999, 'Speleothems and climate: a special issue of The Holocene', *The Holocene*, vol. 9, pp. 643-647

Lea, D. W., Pak D. K. and Spero, H. J. 2000, 'Climate impact of late Quaternary equatorial Pacific sea surface temperature variations', *Science*, vol. 289, pp. 1719-1724

Lee-Thorp, J. A., Holmgren, K., Lauritzen, S.-E., Linge, H., Moberg, A., Partridge, T. C., Stevenson, C. and Tyson, P. D. 2001, 'Rapid climate shifts in the southern African interior throughout the mid to late Holocene', *Geophysical Research Letters*, vol. 28, pp. 4507-4510

Lees, C. M., Neall, V. E. and Palmer, A. S. 1998, 'Forest persistence at coastal Waikato, 24 000 years BP to present', *Journal of the Royal Society of New Zealand*, vol. 28, pp. 55-81

Li, W. X., Lundberg, J., Dickin, A. P., Ford, D. C., Schwarcz, H. P., McNutt, R. and Williams, D. 1989, 'High-precision mass-spectrometric uranium-series dating of calcite deposits and implications for palaeoclimate studies', *Nature*, vol. 339, pp. 534-536

Lockwood, J. G. 2001, 'Abrupt and sudden climatic transitions and fluctuations: a review', *International Journal of Climatology*, vol. 21, pp. 1153-1179

Lowell, T.V., Heusser, C.J., Andersen, B.G., Moreno, P.I., Hauser, A., Denton, G.H., Heusser, L.E., Schluchter, C., and Marchant, D., 1995,

'Interhemispheric correlation of Late Pleistocene glacial events', *Science*, vol. 269, pp. 1541-1549

Mackintosh, A. N., Barrows, T. T., Colhoun, E. A. and Fifield, L. K. 2006, 'Exposure dating and glacial reconstruction at Mt. Field, Tasmania, Australia, identifies MIS 3 and MIS 2 glacial advances and climatic variability', *Journal of Quaternary Science*, vol. 21, pp. 363-376

Majoube, M. 1971, 'Fractionnement en oxygene-18 et en deuterium entre l'eau et sa vapeur', *Journal de Chimie Physique et de Physico-Chimie Biologique*, vol. 68, pp. 1423-1436

Mangerud, J., Andersen, S. T., Berglund, B. E. and Donner, J. J. 1974, 'Quaternary stratigraphy of Norden, a proposal for terminology and classification', *Boreas*, vol. 3, pp.109-126

Marino, B. D., McElroy, M. B., Salawitch, R. J. and Spauling, W. H. 1992, 'Glacial-to-interglacial variations in the carbon isotopic composition of atmospheric CO_2', *Nature*, vol. 357, pp. 461-466

Masson-Delmotte, V., Stenni, B. and Jouzel, J. 2004, 'Common millennial-scale variability of Antarctic and Southern ocean temperatures during the past 5000 years reconstructed from the EPICA Dome C ice core', *The Holocene*, vol. 14, pp. 145-151

Mayewski, P. A., Meeker. L. D., Twickler, M. S., Whitlow, S., Ynag, Q., Lyons, W. B. and Prentice, M. 1997, 'Major features and forcing of high-latitude northern hemisphere atmospheric circulation using a 110,000-year-long glaciochemical series', *Journal of Geophysical Research*, vol. 102, pp. 26,345-26,366

McCulloch, R. D., Fogwill, C. J., Sugden, D. E., Bentley, M. J. and Kubik, P. W. 2005, 'Chronology of the last glaciation in central Strait of Magellan and

Bahía Inútil, southernmost South America', *Geografiska Annaler*, vol. 87A, pp. 289-312

McDermott, F. 2004, 'Palaeo-climate reconstruction from stable isotope variations in speleothems: a review', *Quaternary Science Reviews*, vol. 23, pp. 901-918

McGlone, M. S. 1995, 'Lateglacial landscape and vegetation change and the Younger Dryas climatic oscillation in New Zealand', *Quaternary Science Reviews*, vol. 14, pp. 867-881

McGlone, M. S., Salinger, M. J. and Moar, N. T. 1993, ' Paleovegetation studies of New Zealand's climate since the Last Glacial Maximum', in Wright, H. E., Kutzbach, J. E., Webb, T. III, Ruddiman, W. F., Street-Perrott, F. A. and Bartlein, P. J. (Eds.), *Global climates since the Last glacial Maximum*, University of Minnesota Press, Minneapolis, USA, pp. 294-317

McGlone, M. S., Turney, C. S. M. and Wilmshurst, J. M. 2004, 'Late-glacial and Holocene vegetation and climatic history of the Cass Basin, central South Island, New Zealand', *Quaternary Research*, vol. vol. 62, pp. 267-279

McManus, J. F., Bond, G. C., Broecker, W., Johnsen, S., Labeyrie, L. and Higgins, S. 1994, 'High-resolution climate records from the North Atlantic during the last interglacial', *Nature*, vol. 371, pp. 326-329

Mercer, J. H. 1976, 'Glacial history of southernmost South America', *Quaternary Research*, vol. 6, pp. 125-166

Mickler, P. J., Ketcham, R. A., Colbert, M. W. and Banner, J. L. 2004, 'Application of high-resolution X-Ray computed tomography in determining the suitability of speleothems for use in paleoclimatic, paleohydrologic reconstructions', *Journal of Cave and Karst Studies*, vol. 66, pp. 4-8

Middleton, J. and Waltham, T. 1992, *The Underground Atlas: A Gazetteer of the World's Cave Regions*, The Promotional Reprint Company, Leicester, United Kingdom, 239 p.

Mix, A. C., Bard, E. and Schneider, R. 2001, 'Environmental processes of the ice age: land, oceans, glaciers (EPILOG)', *Quaternary Science Reviews*, vol. 20, pp. 627-657

Moar, N. T. and McKellar, I. C. 2001, 'Interglacial vegetation in South Westland, South Island, New Zealand', *New Zealand Journal of Geology and Geophysics*, vol. 44, pp. 17-24

Moar, N. T. and Suggate, R. P. 1996, 'Vegetation history from the Kaihinu (last) interglacial to the present, West Coast, South Island, New Zealand', *Quaternary Science Reviews*, vol. 15, pp. 521-547

Moreno, P. I., Jacobson Jr., G. L., Lowell, T. V. and Denton, G. H. 2001, 'Interhemispheric climate links revealed by late-glacial cooling episode in southern Chile', *Nature*, vol. 409, pp. 804-808

Moreno, P.I., and León, A.L., 2003, 'Abrupt vegetation changes during the last glacial to Holocene transition in mid-latitude South America', *Journal of Quaternary Science*, vol. 18, pp. 787-800

Morgan, V., Delmotte, M., van Ommen, T., Jouzel, J., Chappellaz, J., Woon, S., Masson-Delmotte, V. and Raynaud, D. 2002, 'Relative timing of deglacial climate events in Antarctica and Greenland', *Science*, vol. 297, pp. 1862-1864

Muller, J., Kylander, M., Wüst, R. A. J., Weiss, D., Martinez-Cortizas, A., LeGrande, A. N., Jennerjahn, T., Behling, H., Anderson, W. T. and Jacobson, G. 2008, 'Possible evidence for wet Heinrich phases in tropical NE Australia: the Lynch's Crater deposit', *Quaternary Science Reviews*, vol. 27, pp. 468-475

Mutch, A. R. and McKellar, I. C. 1964, *Sheet 19 Haast*, (1st Ed.) Geological Map of New Zealand 1:250,000, Department of Scientific and Industrial research, Wellington, New Zealand

Nathan, S. 1974, 'Stratigraphic nomenclature for the Cretaceous-Lower Quaternary rocks of Buller and north Westland, West Coast, South Island, New Zealand', *New Zealand Journal of Geology and Geophysics*, vol. 17, pp. 423-445

Nathan, S., Anderson, H. J., Cook, R. A., Herzer, R. H., Hoskins, R. H., Raine, J. I. and Smale, D. 1986,*Cretaceous and Cenozoic sedimentary basins of the West Coast Region, South Island, New Zealand*, New Zealand Geological Survey Basin Studies 1, Department of Scientific and Industrial research, Wellington, New Zealand

Nathan, S., Rattenbury, M. S. and Suggate R. P. (compilers) 2002, *Geology of the Greymouth area*, Institute of Geological and Nuclear Sciences 1:250 000 geological map 12, 1 sheet and 58 p., Lower Hutt, New Zealand

Nelson, C. S. 1978, 'Stratigraphy and paleontology of the Oligocene Te Kuiti Group, Waitomo County, South Auckland, New Zealand', *New Zealand Journal of Geology and Geophysics*, vol. 21, pp. 553-594

Nelson, C. S., Cooke, P. J., Hendy, C. H. and Cuthbertson, A. M. 1993, 'Oceanographic and climatic changes over the past 160 000 years at Deep Sea Drilling Project Site 594 off southeastern New Zealand, Southwest Pacific Ocean', *Paleoceanography*, vol. 8, pp. 435-458

Nelson, C. S., Hendy, C. H. and Cuthbertson, A. M. 1994, 'Oxygen isotope evidence for climatic contrasts between Tasman Sea and Southwest Pacific Ocean during the late Quaternary', in van der Lingen, G. J., Swanson, K. M. and Muir, R. J. (Eds.), *Evolution of the Tasman Sea Basin*, A. A. Balkema, Rotterdam, The Netherlands, pp. 181-196

Nelson, C. S., Hendy, I. L., Neil, H. L., Hendy, C. H. and Weaver, P. P. E. 2000, 'Last glacial jetting of cold waters through the Subtropical Convergence zone in the Southwest Pacific off eastern New Zealand, and some geological implications', *Palaeogeography, Palaeoclimatology, Palaeoecology*, vol. 156, pp. 103-121

Newnham, R. M., Lowe, D. J. and Green, J. D. 1989, 'Palynology, vegetation and climate of the Waikato lowlands, North Island, New Zealand, since *c*. 18,000 years ago', *Journal of the Royal Society of New Zealand*, vol. 19, pp. 127-150

Newnham, R.M., and Lowe, D.J., 2000, 'Fine-resolution pollen record of late-glacial climate reversal from New Zealand', *Geology*, vol. 28, pp. 759-762

Newnham, R. M., Lowe, D. J., Giles, T. and Alloway, B. V. 2007a, 'Vegetation and climate of Auckland, since ca. 32,000 cal. yr ago: support for an extended LGM', *Journal of Quaternary Science*, vol. 22, pp. 517-534

Newnham, R. M., Vandergoes, Hendy, C. H., M. J., Lowe, D. J. and Preusser, F. 2007b, 'A terrestrial palynological record for the last two glacial cycles from southwestern New Zealand', *Quaternary Science Reviews*, vol. 26, pp. 517-535

NGRIP (North Greenland Ice Core Project) Members 2004, 'High-resolution record of Northern Hemisphere climate extending into the last interglacial period', *Nature*, vol. 431, pp. 147-151

NIWA 2003, 'West Coast climate summary: climatological statistics from 1969-1998', National Institute for Water and Atmospheric Research, Wellington, New Zealand

NIWA 2006, CliFlo: NIWA's National Climate Database on the Web (http://cliflo.niwa.co.nz/). Data retrieved 15 June 2006.

O'Brien, S. R., Mayewski, P. A., Meeker, L. D., Meese, D. A., Twickler, M. S. and Whitlow, S. I. 1995, 'Complexity of Holocene climate as reconstructed from a Greenland ice core', *Science*, vol. 270, pp. 1962-1964

O'Neil, J. R., Adami, L. H. and Epstein, S. 1975, 'Revised value for the ^{18}O fractionation factor between H_2O and CO_2 at 25°C', *Journal of Research of the United States Geological Survey*, vol. 3, pp. 633-644

O'Neil, J. R., Clayton, R. N. and Mayeda, T. K. 1969, 'Oxygen isotope fractionation in divalent metal carbonates', *Journal of Chemical Physics*, vol. 51, pp. 5547-5558

Osborn, T. J. and Briffa, K. R. 2006, 'The spatial extent of 20th-century warmth in the context of the past 1200 years', *Science*, vol. 311, pp. 841-844

Oster, J. L., Montañez, I. P., Sharp, W. D., Spero, H. J. and Fairchild, S. 2006, 'Sierra Nevada speleothems: potential as high-resolution archives of atmospheric circulation over western North America', *Geological Society of America Abstracts with Programs*, vol. 38, p. 24

Pahnke, K. and Sachs, J. P. 2006, 'Sea surface temperatures of southern midlatitudes 0-160 kyr B.P.', *Paleoceanography*, vol. 21, PA2003, doi:10.1029/2005PA001191

Pahnke, K. and Zahn, R. 2005, 'Southern Hemisphere water mass conversion linked with North Atlantic climate variability', *Science*, vol. 307, pp. 1741-1746

Pahnke, K., Zahn, R., Elderfield, H. and Schulz, M. 2003, '340,000-year centennial-scale marine record of Southern Hemisphere climatic oscillation', *Science*, vol. 301, pp. 948-952

Pelejero, C., Calvo, E., Barrows, T. T., Logan, G. A. and De Dekker, P. 2006, 'South Tasman Sea alkenone palaeothermometry over the last four glacial/interglacial cycles', *Marine Geology*, vol. 230, pp. 73-86

Peterson, L. C., Haug, G. H., Hughen, K. A. and Röhl, U. 2000, 'Rapid changes in the hydrological cycle of the tropical Atlantic during the last glacial', *Science*, vol. 290, pp. 1947-1951

Petit, J. R., Jouzel, J., Raynaud, D., Barkov, N. I., Barnola, J.-M., Basile, I., Bender, M., Chapellaz, J., Davis, M., Delaygue, G., Delmotte, M., Kotlyakov, V. M., Legrand, M., Lipenkov, V. Y., Lorius, C., Pépin, L., Ritz, C., Saltzman, E. and Stievenard, M. 1999, 'Climate and atmospheric history of the past 420,000 years from the Vostok ice core, Antarctica', *Nature*, vol. 399, pp. 429-436

Piketh, S. J., Sideras-Haddad, E., Holmgren, K. and Tyson, P. D. 1999, 'Proton micro-probe analysis of a speleothem from South Africa', *Nuclear Instruments and Methods in Physics Research B*, vol. 158, pp. 606-611

Polyak, V. J., Rasmussen, J. B. T. and Asmerom, Y. 2004, 'Prolonged wet period in the southwestern United States through the Younger Dryas', *Geology*, vol. 32, pp. 5-8

Preusser, F., Anderson, B. G., Denton, G. H. and Schluchter, C. 2005, 'Luminescence chronology of Late Pleistocene glacial deposits in north Westland, New Zealand', *Quaternary Science Reviews*, vol. 24, pp. 2207-2227

Putnam, A., Schaefer, J., Denton, G. H., Barrell, D., Andersen, B., Kaplan, M., Doughty, A., Finkel, R. And Schwartz, R. 2007, '^{10}Be chronology of moraines deposited during the Last Glacial Maximum in the Lake Ohau basin, New Zealand', Comer Fellows Meeting, New York, 2-5 May 2007

Rasbury, M. and Aharon, P. 2006, 'ENSO-controlled rainfall variability records archived in tropical stalagmites from the mid-ocean island of Niue, South Pacific', *Geochemistry, Geophysics, Geosystems*, vol. 7, Q07010, doi:10.1029/2005GC001232, 15 p.

Rashid, H., Hesse, R. and Piper, D. J. W. 2003, 'Evidence for an additional Heinrich event between H5 and H6 in the Labrador Sea', *Paleoceanography*, vol. 18, 1077, doi:10.1029/2003PA000913, 15 p.

Reimer, P. J., Baillie, M. G. L., Bard, E., Bayliss, A., Beck, J. W., Bertrand, C., Blackwell, P. G., Buck, C. E., Burr, G., Cutler, K. B., Damon, P. E., Edwards, R. L., Fairbanks, R. G., Friedrich, M., Guilderson, T. P., Hughen, K. A., Kromer, B., McCormac, F. G., Manning, S., Ramsey, C. B., Reimer, R. W., Remmele, S., Southon, J. R., Stuiver, M., Talamo, S., Taylor, F. W., van der Plicht, J. and Weyhenmeyer, C. E. 2004, 'IntCal04 terrestrial radiocarbon age calibration, 0-26 Cal Kyr BP', *Radiocarbon*, vol. 46, pp. 1029-1058

Repinski, P., Holmgren, K., Lauritzen, S.-E. and Lee-Thorp, J. A. 1999, 'A late Holocene climate record from a stalagmite, Cold Air Cave, Northern Province, South Africa', *Palaeogeography, Palaeoclimatology, Palaeoecology*, vol. 150, pp. 269-277

Richards, D. A. and Dorale, J. A. 2003, 'Uranium-series chronology and environmental applications of speleothems', *Reviews in Mineralogy and Geochemistry*, vol. 52, pp. 407-460

Richards, D. A., Smart, P. L. and Edwards, R. L. 1994, 'Maximum sea levels for the last glacial period from U-series ages of submerged speleothems', *Nature*, vol. 367, pp. 357-360

Roberts, M. S., Smart, P. and Baker, A. 1998, 'Annual trace element variations in a Holocene speleothem', *Earth and Planetary Science Letters*, vol. 154, pp. 237-246

Roberts, M. S., Smart, P. L., Hawkesworth, C. J., Perkins, W. T. and Pearce, N. J. G. 1999, 'Trace element variations in coeval Holocene speleothems from GB Cave, southwest England', *The Holocene*, vol. 9, pp. 707-713

Rohling, E. J. and Pälike, H. 2005, 'Centennial-scale climate cooling with a sudden cold event around 8,200 years ago', *Nature*, vol. 434, pp. 975-979

Röthlisberger, F. 1986, *10000 Jahre Gletschergeschichte der Erde*, Verlag Suaerländer, Frankfurt-am-Main, Germany, 416 p.

Sachs, J. P. and Anderson, R. F. 2005, 'Increased productivity in the subantarctic ocean during Heinrich events', *Nature*, vol. 434, pp. 1118-1121

Sandiford, A., Newnham, R. M., Alloway, B. V. and Ogden, J. 2003, 'A high resolution, southern hemisphere mid-latitude LGM to Holocene record of vegetation and climate change from northern New Zealand', *Palaeogeography, Palaeoclimatology, Palaeoecology*, vol. 201, pp. 235-247

Schaefer, J. M., Denton, G. H., Barrell, D. J. A., Ivy-Ochs, S., Kubic, P. W., Anderson, B. G., Phillips, F. M., Lowell, T. V. and Schluchter, C. 2006, 'Mid-latitude moraines reveal near-synchronous interhemispheric termination of the Last Glacial Maximum', *Science*, vol. 312, pp. 1510-1513

Schrag, D. P., Adkins, J. F., McIntyre, K., Alexander, J., Hodell, D. A., Charles, C. D. and McManus, J. F. 2002, 'The oxygen isotopic composition of seawater during the Last Glacial Maximum', *Quaternary Science Reviews*, vol. 21, pp. 331-342

Schrag, D. P., Hampt, G. and Murray, D. W. 1996, 'The temperature and oxygen isotopic composition of the glacial ocean', *Science*, vol. 272, pp. 1930–1932

Shackleton, N. J. 1967, 'Oxygen isotope analyses and Pleistocene temperatures re-assessed', *Nature*, vol. 215, p. 15-17

Shackleton, N. J. 1987, 'Oxygen isotopes, ice volume and sea level', *Quaternary Science Reviews*, vol. 6, pp. 183-190

Shackleton, N. J. 2000, 'The 100,000-year Ice-Age cycle identified and found to lag temperature, carbon dioxide, and orbital eccentricity', *Science*, vol. 289, pp. 1897-1902

Shackleton, N. J., Hall, M. A. and Vincent, E. 2000, 'Phase relationships between millennial-scale events 64,000-24,000 years ago', *Paleoceanography*, vol. 15, pp. 565-569

Shackleton, N. J. and Opdyke, N. D. 1973, 'Oxygen isotope and paleomagnetic stratigraphy of equatorial Pacific core V28-238: oxygen isotope temperatures and ice volumes on 10^5 and 10^6 year scale', *Quaternary Research*, vol. 3, pp. 39-55

Shopov, Y. Y., Ford, D. C. and Schwarcz, H. P. 1994, 'Luminescent microbanding in speleothems: high-resolution chronology and palaeoclimate', *Geology*, vol. 22, pp. 407-410

Shulmeister, J., Fink, D. and Augustinus, P. C. 2005, 'A cosmogenic nuclide chronology of the last glacial transition in North-West Nelson, New Zealand – new insights in Southern Hemisphere climate forcing during the last deglaciation', *Earth and Planetary Science Letters*, vol. 233, pp. 455-466

Siddall, M., Rohling, E. J., Almogi-Labin, A., Hemleben, C., Meischner, D., Schmelzer, I. and Smeed, D. A. 2003, 'Sea-level fluctuations during the last glacial cycle', *Nature*, vol. 423, pp. 853-858

Singer, C., Shulmeister, J. and McLea, W. 1998, 'Evidence against a significant Younger Dryas cooling event in New Zealand', *Science*, vol. 281, pp. 812-814

Smith, N. 2004, *The New Zealand Cave Atlas. Volume 2: South Island*, New Zealand Speleological Society, Waitomo, New Zealand

Spötl, C., Mangini, A., Frank, N., Eichstädter, R. and Burns, S. J. 2002, 'Start of the last interglacial period at 135 ka: Evidence from a high Alpine speleothem', *Geology*, vol. 30, pp. 815-818

Spötl, C., Mangini, A. and Richards, D. A. 2006, 'Chronology and paleoenvironment of Marine Isotope Stage 3 from two high-elevation speleothems, Austrian Alps', *Quaternary Science Reviews*, vol. 25, pp. 1127-1136

Steig, E. J., Brook, E. J., White, J. W. C., Sucher, C. M., Bender, M. L., Lehman, S. J., Waddington, E. D., Morse, D. L. and Clow, G. D. 1998, 'Synchronous climate changes in Antarctica and the North Atlantic', *Science*, vol. 282, pp. 92-95

Steig, E. J., Morse, D. L., Waddington, E. D., Stuiver, M., Grootes, P. M., Mayewski, P. A., Whitlow, S. L. and Twickler, M. S. 2000, 'Wisconsinan and Holocene climate history from an ice core at Taylor Dome, western Ross Embayment, Antarctica', *Geografiska Annaler*, vol. 82A, pp. 213-235

Suggate, R. P. 1965, 'Late Pleistocene geology of the northern part of the South Island, New Zealand', New Zealand Geological Survey Bulletin 77

Suggate, R. P. 1990, 'Late Pliocene and Quaternary glaciations of New Zealand', *Quaternary Science Reviews*, vol. 9, pp. 175-197

Suggate, R. P. and Almond, P. C. 2005, 'The Last Glacial Maximum (LGM) in western South Island, New Zealand: implications for the global LGM and MIS 2', *Quaternary Science Reviews*, vol. 24, pp. 1923-1940

Suggate, R. P. and Waight, T. E. 1999, *Geology of the Kumara-Moana area, scale 1:50 000*, Institute of Geological and Nuclear Sciences geological map 24, 1 sheet and 124 p., Lower Hutt, New Zealand

Talma, A. S. and Vogel, J. C. 1992, 'Late Quaternary paleotemperatures derived from a speleothem from Cango Caves, Cape province, South Africa', *Quaternary Research*, vol. 37, pp. 203-213

Talma, A. S., Vogel, J. C. and Partridge, T. C. 1974, 'Isotopic contents of some Transvaal speleothems and their palaeoclimatic significance', *South African Journal of Science*, vol. 70, pp. 135-140

Tarutani, T., Clayton, R. N. and Mayeda, T. K. 1969, 'The effect of polymorphism and magnesium substitution on oxygen isotope fractionation between calcium carbonate and water', *Geochimica et Cosmochimica Acta*, vol. 33, pp. 987-996

Tasman District Council 2008, *Celebrating a century of settlement in Maruia Valley*, viewed 29 January 2008, http://www.tdc.govt.nz/index.php?Greatnewhalldownsouth!

Tieszen, L. L. 1991, 'Natural variations in the carbon isotope values of plants: implications for archaeology, ecology, and paleoecology', *Journal of Archaeological Science*, vol. 18, pp. 227-248

Treble, P.C., Chappell, J., Gagan, M.K., McKeegan, K.D., and Harison, T.M., 2005, 'In situ measurement of seasonal $\delta^{18}O$ variations and analysis of isotopic trends in a modern speleothem from southwest Australia', *Earth and Planetary Science Letters*, vol. 233, pp. 17-32

Treble, P. C., Shelley, J. M. G., and Chappell, J. 2003, 'Comparison of high resolution sub-annual records of trace elements in a modern (1911-1992) speleothem with instrumental data from southwest Australia', *Earth and Planetary Science Letters*, vol. 216, pp. 141-153

Troughton, J. H., Hendy, C. H. and Card, K. A. 1971, 'Natural carbon isotope fractionation in some indigenous Australian, New Zealand and European *Atriplex* species', *Zeitschrift fur Pflanzenphysiologie*, vol. 65, p. 461

Troughton, J. H., Hendy, C. H. and Card, K. A. 1974, 'Photosynthetic pathways and carbon isotope discrimination by plants', *Carnegie Institute Year Book*, vol. 73, pp. 768-780

Turnbull, I. M. (compiler) 2000, *Geology of the Wakatipu area*, Institute of Geological and Nuclear Sciences 1:250 000 geological map 18, 1 sheet and 72 p., Lower Hutt, New Zealand

Turney, C. S. M., Beerling, D. J., Harkness, D. D., Lowe, J. J. and Scott, E. M. 1997, 'Stable carbon isotope variations in northwest Europe during the last glacial-interglacial transition', *Journal of Quaternary Science*, vol. 12, pp. 339-344

Turney, C. S. M., Haberle, S., Fink, D., Kershaw, A. P., Barbetti, M., Barrows, T. T., Black, M., Cohen, T. J., Corrège, T., Hesse, P. P., Hua, Q., Johnston, R., Morgan, V., Moss, P., Nanson, G., van Ommen, T., Rule, S., Williams, N. J., Zhao, J.-X., D'Costa, D., Feng, Y.-X., Gagan, M., Mooney, S. and Xia, Q. 2006, 'Integration of ice-core, marine and terrestrial records for the Australian Last Glacial Maximum and Termination: a contribution from the OZ INTIMATE group', *Journal of Quaternary Science*, vol. 21, pp. 751-761

Turney, C.S.M., McGlone, M.S., Wilmshurst, J.M., 2003, 'Asynchronous climate change between New Zealand and the North Atlantic during the last deglaciation', *Geology*, vol. 31, pp. 223-226

Turney C. S. M., Roberts, R. G., de Jonge, N., Prior, C., Wilmshurst, J. M., McGlone, M. S. and Cooper, J. 2007, 'Redating the advance of the New Zealand Franz Josef Glacier during the Last Termination: evidence for asynchronous climate change', *Quaternary Science Reviews*, vol. 26, pp. 3037-3042

Tyson, P. D., Sturman, A. P., Fitzharris, B. B., Mason, S. J. and Owens, I. F. 1997, 'Circulation changes and teleconnections between glacial advances on the West Coast of New Zealand and extended spells of drought years in South Africa', *International Journal of Climatology*, vol. 17, pp. 1499-1512

Urey, H. C. 1947, 'The thermodynamic properties of isotopic substances', *Journal of the Chemical Society*, (London), pp. 562-581

Vandergoes, M. J., Newnham, R. M., Preusser, F., Hendy, C. H., Lowell, T. V., Fitzsimons, S. J., Hogg, A. G., Kasper, H. U. and Schluchter, C. 2005, 'Regional insolation forcing of late Quaternary climate change in the Southern Hemisphere', *Nature*, vol. 436, pp. 242-244

Vandergoes M. J., Dieffenbacher-Krall, A. C., Newnham, R. M., Denton, G. H. and Blaauw, M. 2008, 'Cooling and changing seasonality in the Southern Alps, New Zeland, during the Antarctic Cold Reversal', *Quaternary Science Reviews*, vol. 27, pp. 589-601

Verheyden, S. 2004, 'Trace elements in speleothems: a short review of the state of the art', *International Journal of Speleology*, vol. 33. pp. 95-101

Voelker, A. H. L. and workshop participants 2002, 'Global distribution of centennial-scale records for Marine Isotope Stage (MIS) 3: a database', *Quaternary Science Reviews*, vol. 21, pp. 1185-1212

Vogel, J. C. 1983, '^{14}C variations during the Upper Pleistocene', *Radiocarbon*, vol. 25, pp. 213-218

Vogel, J. C. and Kronfeld, J. 1997, 'Calibration of radiocarbon dates for the Late Pleistocene using U/Th dates on stalagmites', *Radiocarbon*, vol. 39, pp. 27-32

Wang, X., Auler, A. S., Edwards, R. L., Cheng, H., Cristalli, P. S., Smart, P. L., Richards, D. A. and Shen, C.-C. 2004, 'Wet periods in northeastern Brazil over the past 210 kyr linked to distant climate anomalies', *Nature*, vol. 432, pp. 740-743

Wang, X., Auler, A. S., Edwards, R. L., Cheng, H., Ito, E. and Solheid, M. 2006, 'Interhemispheric anti-phasing of rainfall during the last glacial period', *Quaternary Science Reviews*, vol. 25, pp. 3391-3403

Wang, X., Auler, A. S., Edwards, R. L., Cheng, H., Ito, E., Wang, Y., Kong, X. and Solheid, M. 2007, 'Millennial-scale precipitation changes in southern Brazil over the past 90,000 years', *Geophysical Research Letters*, vol. 34, L23701, doi:10.1029/2007/GL031149

Wang, Y. J., Cheng, H., Edwards, R. L., An, Z. S., Wu, J. Y., Chen, C.-C. and Dorale, J. A. 2001, 'A high-resolution absolute-dated late Pleistocene monsoon record from Hulu Cave, China', *Science*, vol. 294, pp. 2345-2348

Wardle, P. 1991, *Vegetation of New Zealand*, Cambridge University Press, Cambridge, England, 672 p.

Watanabe, O., Jouzel, J., Johnsen, S., Parrenin, F., Shoji, H. and Yoshida, N. 2003, 'Homogeneous climate variability across East Antarctica over the past three glacial cycles', *Nature*, vol. 422, pp. 509-512

White, W. B. and Culver, D. C. 2005, 'Cave, Definition of', in *Encyclopedia of Caves*, Ed.s Culver, D. C. and White, W. B., Elsevier Academic Press, London, United Kingdom, 674 p.

Williams, P. W. 1982, 'Speleothem dates, Quaternary terraces and uplift rates in New Zealand', *Nature*, vol. 298, pp. 257-260

Williams, P. W. 1992, 'Karst in New Zealand', in *Landforms of New Zealand*, Soons, J. M. and Selby, M. J. (Ed.s), Longman Paul, Auckland, New Zealand. pp. 187-209

Williams, P. W. 1996, 'A 230 ka record of glacial and interglacial events from Aurora Cave, Fiordland, New Zealand', *New Zealand Journal of Geology and Geophysics*, vol. 39, pp. 225-241

Williams, P. W. 2004, 'Polygonal karst and palaeokarst of the King Country, North Island, New Zealand', *Zeitschrift für Geomorphologie*, Supplementary Vol. 136, pp. 45-67

Williams, P. W. and Fowler, A. 2002, 'Relationship between oxygen isotopes in rainfall, cave percolation waters and speleothem calcite at Waitomo, New Zealand', *Journal of Hydrology (New Zealand)*, vol. 41, pp. 53-70

Williams, P. W., King, D. N. T., Zhao, J.-X. and Collerson, K. D. 2004, 'Speleothem master chronologies: combined Holocene ^{18}O and ^{13}C records from the North Island of New Zealand and their palaeoenvironmental interpretation', *The Holocene*, vol. 14, pp. 194-208

Williams, P. W., King, D. N. T., Zhao, J.-X. and Collerson, K. D. 2005, 'Late Pleistocene to Holocene composite speleothem ^{18}O and ^{13}C chronologies from South Island, New Zealand – did a global Younger Dryas really exist?', *Earth and Planetary Science Letters*, vol. 230, pp. 301-317

Williams, P. W., Marshall, A., Ford, D. C. and Jenkinson, A. V. 1999, 'Palaeoclimatic interpretation of stable isotope data from Holocene speleothems of the Waitomo district, North Island, New Zealand', *The Holocene*, vol. 9, pp. 649-657

Wilson, A. T. and Hendy, C. H. 1971, 'Past wind strength from isotope studies', *Nature*, vol. 234, pp. 344-345

Wilson, A. T., Hendy, C. H. and Reynolds, C. P., 1979, 'Short-term climate change and New Zealand temperatures during the last millennium', *Nature*, vol. 279, pp. 315-317

Woodhead, J., Hellstrom, J., Maas, R., Drysdale, R., Zanchetta, G., Devine, P. and Taylor, E. 2006, 'U-Pb geochronology of speleothems by MC-ICPMS', *Quaternary Geochronology*, vol. 1, pp. 208-221

Woodward, C. A. and Shulmeister, J. 2007, 'Chironomid-based reconstructions of summer air temperature from lake deposits in Lyndon Stream, New Zealand spanning the MIS 3/2 transition', *Quaternary Science Reviews*, vol. 26, pp. 142-154

Wurth, G., Niggemann, S., Richter, D. K. and Mangini, A. 2004, 'The Younger Dryas and Holocene climate record of a stalagmite from Hölloch Cave (Bavarian Alps, Germany)', *Journal of Quaternary Science*, vol. 19, pp. 291-298

Xia, Q., Zhao, J.-X. and Collerson, K. D. 2001, 'Early-Mid Holocene climatic variations in Tasmania, Australia: multi-proxy records in a stalagmite from Lynds Cave', *Earth and Planetary Science Letters*, vol. 194, pp. 177-187

Yonge, C. J., Ford, D. C., Gray, J. and Schwarcz, H. P. 1985, 'Stable isotope studies of cave seepage water', *Chemical Geology*, vol. 58, pp. 97-105

Zhao, J.-X., Xia, Q. and Collerson, K. D. 2001, 'Timing and duration of the Last Interglacial inferred from high resolution U-series chronology of stalagmite growth in Southern Hemisphere', *Earth and Planetary Science Letters*, vol. 184, pp. 635-644

APPENDICES

Appendix A: Speleothem Coring

The number of studies presenting proxy records of past climate from speleothems has seen a remarkable increase in recent years (Fairchild *et al*., 2006). Although there has been significant advancement of scientific understanding of palaeoclimate, karst fluid dynamics and the transport of solutes amongst many other things as a result of this work, one must also consider whether there has been a correlative rise in the human impact of cave environments. Frappier (2007) present a screening process for speleothem selection which will hopefully reduce the impact of future palaeoenvironmental investigations.

Although sampling of speleothems by coring has been undertaken in a number of previous studies (references) we believe this is the first application of the method to the process of sample selection. Prior to undertaking fieldwork and sample selection it is common for there to be a formal project proposal and/or grant application stating the study's intended goals. In the case of New Zealand, this process is then succeeded by a cave access permit application where the project outcomes must favourably balance against the aesthetic, ecological and cultural impact (as determined by land managers and local interest groups) that may be caused by the research.

Basal coring of carefully selected stalagmites, and other speleothems, offers the possibility of determining which speleothems within a cave are best suited to the original research aims with minimal impact to the cave environment. In this study 29 stalagmites were cored. It was determined from their structure, age and stable isotopic composition that only 4 met the original research aims.

The downside to this method of sample selection is the necessity of conducting two fieldtrips. Depending on how far the cave is from the research institution where the sample will be analysed this problem could be relatively minor or quite significant. One must also consider the time between fieldtrips. Each core must halved, polished, described, subject to the Hendy Test and dated before the target speleothem(s) can be determined. If each of these methods can be carried out in-house the delay caused by the coring method will likely be minimal. If, as in the case of this study, one set of analyses must be conducted at

an alternative research institution and those samples join a backlog there may be some delay to the project. A worst case scenario might occur where speleothem collection can only take place at one time during the year due, for example, to seasonal weather variations, in which case a year might pass between coring and speleothem collection.

It may also be necessary to considering any additional costs incurred by the coring method. Clearly there is additional cost associated with making two, instead of one, field excursions. The cost of this extra trip will more than likely be proportional to the distance being travelled. However, it is common in many studies for multiple trips to be made to the cave being studied in line with making monthly (for example) measurements of dripwater isotopic and element composition. In this case collection of the target speleothem could be timed to occur at the same time as dripwater samples were collected eliminating the added cost of an extra field trip.

In terms of laboratory analyses there ought to be little difference in expenditure between wholesale speleothem collection and core analysis. Whether whole speleothems or cores have been collected it will be necessary to determine whether or not the sample was deposited in isotopic equilibrium with the dripwater and if it is the correct age to allow the project aims to be achieved.

A second advantage (behind reducing impact) to the coring method is that the reduction of material being removed from the cave is a significant reduction in the weight of sample to be moved. A 200 mm long, 25 mm diameter core of calcite (density ~2.5 g/cm^3) will have a mass of ~0.25 kg. A reasonable target stalagmite might have dimensions of 500 mm tall and 150 mm diameter and weigh close to 20 kg. Transporting smaller masses should not only afford greater ease of passage in the cave environment but also reduce shipping costs between the cave and the laboratory.

Appendix B: Stalagmite Core Photographs

Core Nomenclature: Cave – Year – Sample # (e.g. AB05-2)

Cave Abbreviations: AB – Abyssinia Cave
EG – Eggers Cave
GT – Guillotine Cave
HW – Hollywood Cave
TAP – Te Ana Puta
WZ – Wazapretti Cave

Twenty-nine stalagmite bases were cored as part of this research. Four of the stalagmites (EG05-5, GT05-5, HW05-3 and WZ05-1) were later entirely removed from the cave for this study.

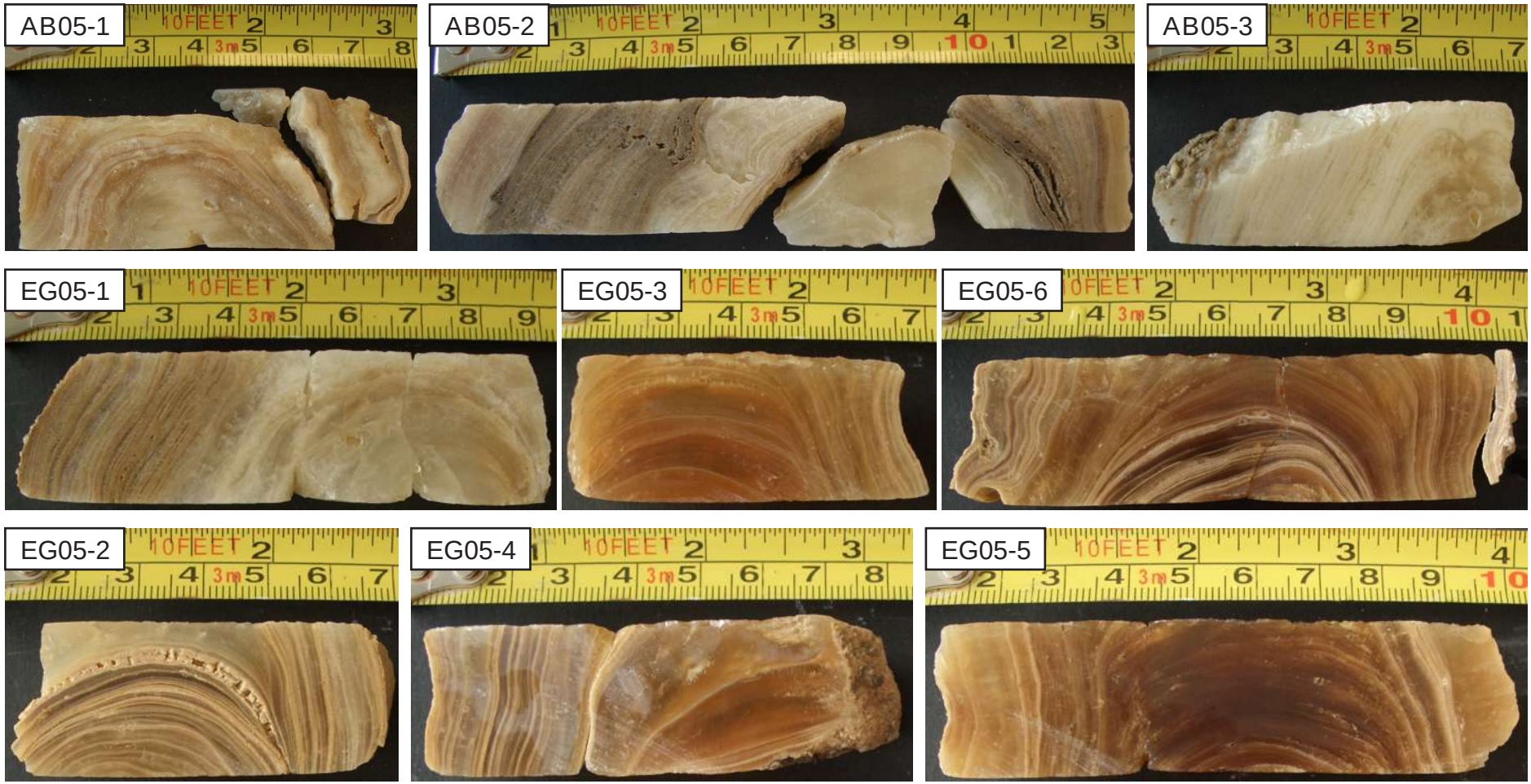

Figure B.1: Photographs of cut and polished core halves obtained from stalagmites in Abyssinia Cave and Eggers Cave.

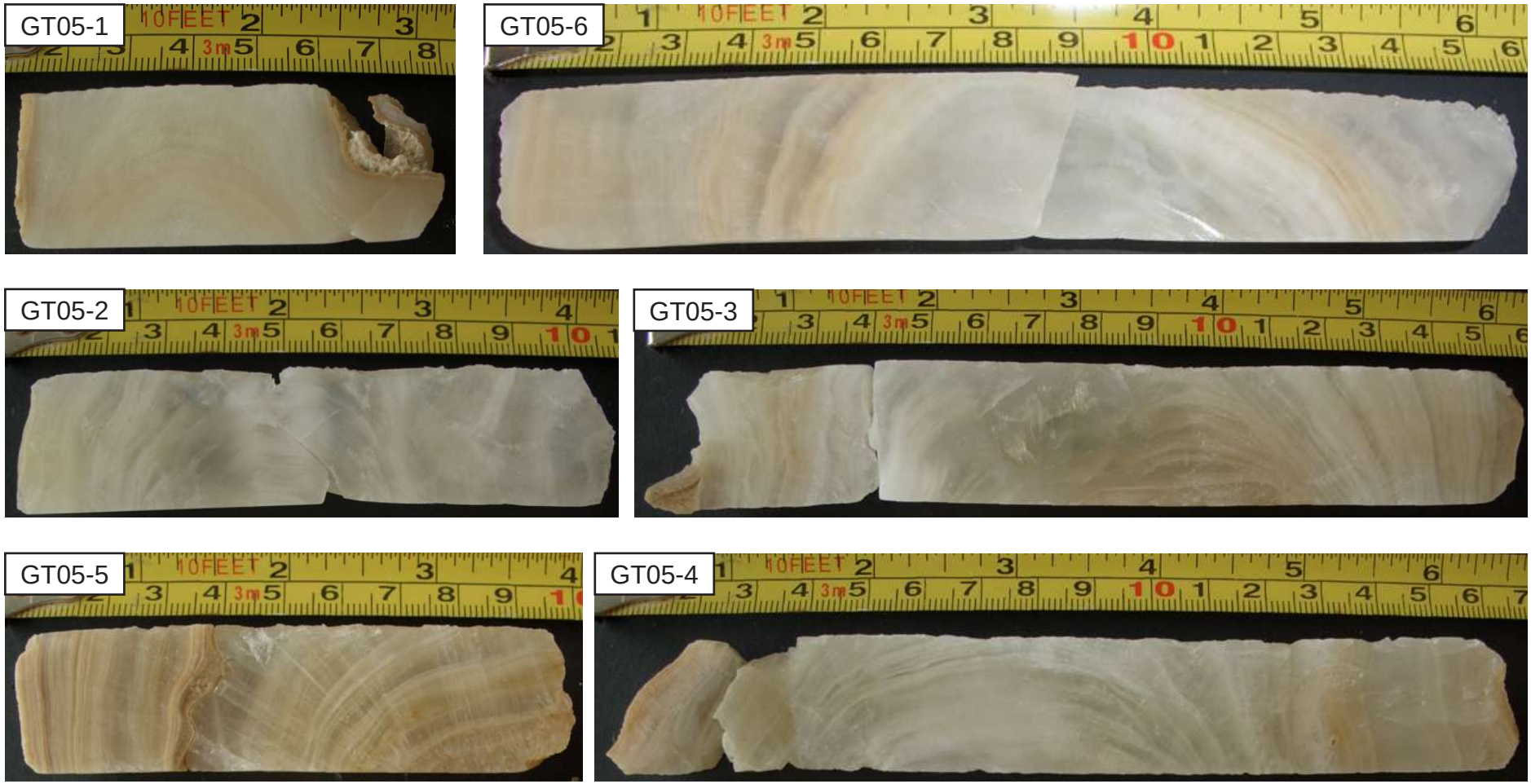

Figure B.2: Photographs of cut and polished core halves obtained from stalagmites in Guillotine Cave.

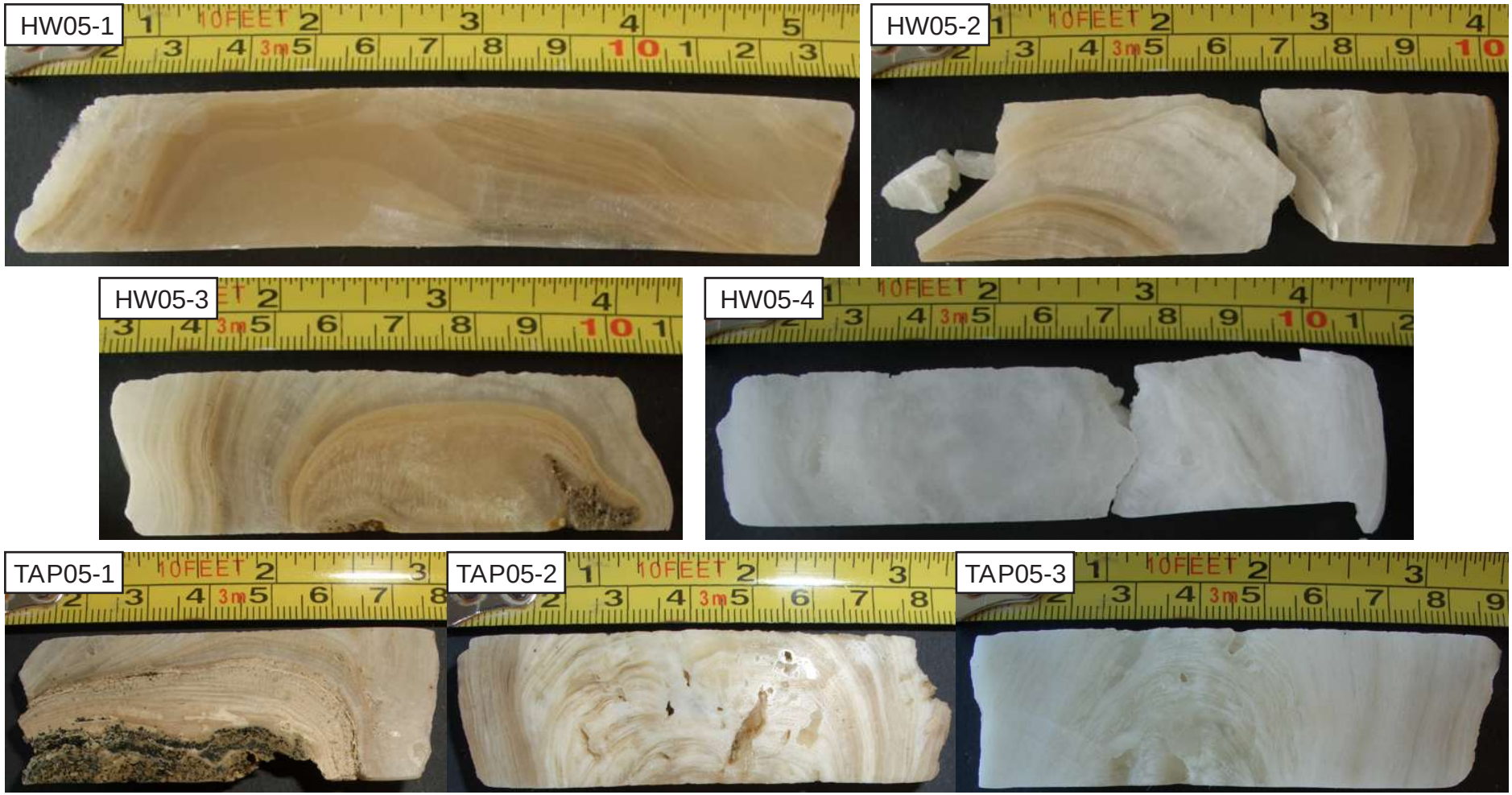

Figure B.3: Photographs of cut and polished core halves obtained from stalagmites in Hollywood Cave and Te Ana Puta.

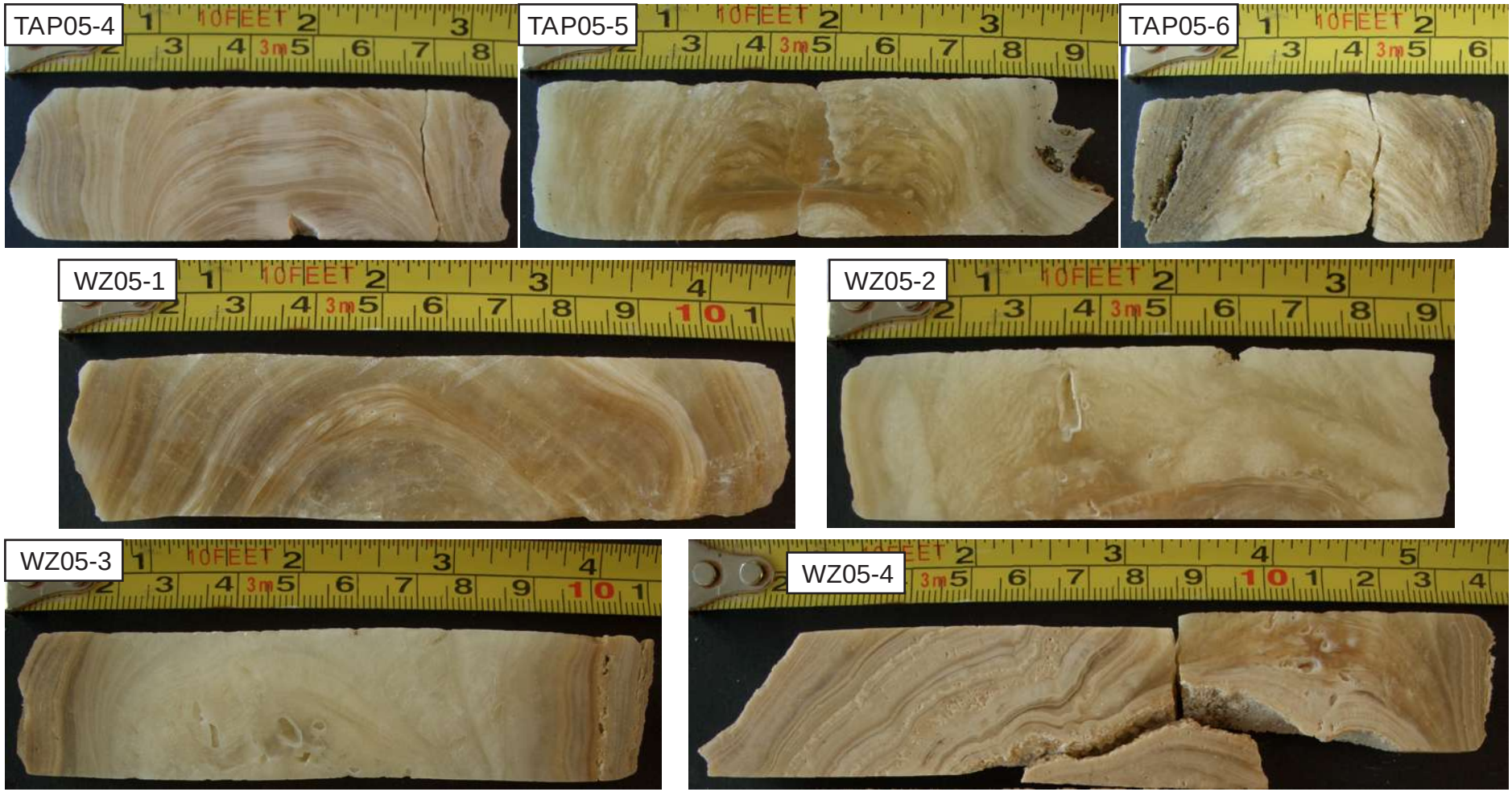

Figure B.4: Photographs of cut and polished core halves obtained from stalagmites in Te Ana Puta and Wazapretti Cave.

Appendix C: Hendy Test Stable Isotope Data

Table C.1: Stable carbon and oxygen isotope ratios from calcite milled along single growth layers in each stalagmite and stalagmite core collected in this study. Values are reported relative to Vienna Peedee Belemnite in per mil (‰) notation.

Sample		Distance from growth axis (mm)	$\delta^{13}C$ (‰)	$\delta^{13}C$ st. dev.	$\delta^{18}O$ (‰)	$\delta^{18}O$ st. dev.
AB05-1	a	0	-7.23	0.06	-3.39	0.12
AB05-1	b	10	-7.72	0.06	-5.06	0.12
AB05-1	c	18	-6.01	0.06	-3.52	0.12
AB05-1	d	25.5	-5.22	0.06	-3.22	0.12
AB05-1	e	32.5	-5.76	0.06	-3.20	0.12
AB05-2	a	0	-5.74	0.06	-3.16	0.12
AB05-2	b	9	-6.70	0.06	-3.16	0.12
AB05-2	c	15.5	-6.19	0.06	-3.14	0.12
AB05-2	d	22	-6.53	0.06	-3.16	0.12
AB05-2	e	28.5	-7.49	0.06	-3.47	0.12
AB05-3	a	0	-6.82	0.06	-2.89	0.12
AB05-3	b	5	-8.03	0.06	-3.88	0.12
AB05-3	c	12.5	-6.58	0.06	-2.80	0.12
AB05-3	d	16.5	-6.56	0.06	-2.88	0.12
AB05-3	e	21.5	-6.83	0.06	-2.86	0.12
EG05-1	a	0	-9.00	0.06	-3.66	0.12
EG05-1	b	7.5	-9.11	0.06	-3.67	0.12
EG05-1	c	17	-9.48	0.06	-3.79	0.12
EG05-1	d	25	-9.78	0.06	-3.69	0.12
EG05-1	e	34	-9.72	0.06	-3.71	0.12
EG05-2	a	0	-5.06	0.06	-3.96	0.12
EG05-2	b	6.5	-5.83	0.06	-4.10	0.12
EG05-2	c	12	-5.22	0.06	-4.00	0.12
EG05-2	d	18	-5.59	0.06	-4.07	0.12
EG05-2	e	23.5	-5.10	0.06	-3.84	0.12
EG05-3	a	0	-4.51	0.06	-4.27	0.12
EG05-3	b	10	-4.33	0.06	-4.08	0.12
EG05-3	c	17	-4.02	0.06	-3.96	0.12
EG05-3	d	23.5	-3.67	0.06	-4.05	0.12
EG05-3	e	30	-4.19	0.06	-4.08	0.12
EG05-4	a	0	-5.34	0.06	-3.92	0.12
EG05-4	b	9	-5.10	0.06	-3.99	0.12
EG05-4	c	17	-5.08	0.06	-3.84	0.12
EG05-4	d	25	-5.53	0.06	-3.82	0.12
EG05-4	e	32	-5.06	0.06	-4.48	0.12
EG05-5	a	0	-6.50	0.06	-4.35	0.12
EG05-5	b	8	-6.64	0.06	-3.51	0.12
EG05-5	c	16	-5.88	0.06	-3.62	0.12
EG05-5	d	24	-5.54	0.06	-3.58	0.12
EG05-5	e	34	-5.39	0.06	-3.39	0.12

Table C.1 (continued)

Sample		Distance from growth axis (mm)	$\delta^{13}C$ (‰)	$\delta^{13}C$ st. dev.	$\delta^{18}O$ (‰)	$\delta^{18}O$ st. dev.
EG05-6	a	0	-4.88	0.06	-4.46	0.12
EG05-6	b	8	-6.93	0.06	-3.79	0.12
EG05-6	c	15	-5.81	0.06	-3.46	0.12
EG05-6	d	22.5	-4.79	0.06	-3.27	0.12
EG05-6	e	31.5	-4.61	0.06	-3.07	0.12
GT05-1	a	0	-6.85	0.06	-4.90	0.12
GT05-1	b	7	-6.20	0.06	-5.02	0.12
GT05-1	c	13	-6.85	0.06	-4.93	0.12
GT05-1	d	19	-6.73	0.06	-5.18	0.12
GT05-1	e	25	-6.38	0.06	-5.09	0.12
GT05-2	a	0	-8.43	0.06	-5.43	0.12
GT05-2	b	10	-8.13	0.06	-5.30	0.12
GT05-2	c	17	-7.25	0.06	-5.21	0.12
GT05-2	d	25	-7.50	0.06	-5.39	0.12
GT05-2	e	33	-7.09	0.06	-5.23	0.12
GT05-3	a	0	-9.75	0.06	-5.20	0.12
GT05-3	b	8	-10.12	0.06	-5.22	0.12
GT05-3	c	15	-10.42	0.06	-5.29	0.12
GT05-3	d	22	-9.97	0.06	-5.20	0.12
GT05-3	e	29	-9.54	0.06	-5.09	0.12
GT05-4	a	0	-9.31	0.06	-4.65	0.12
GT05-4	b	10	-8.66	0.06	-4.42	0.12
GT05-4	c	21	-8.76	0.06	-4.61	0.12
GT05-4	d	31	-8.72	0.06	-4.56	0.12
GT05-4	e	40	-8.73	0.06	-4.83	0.12
GT05-5	a	0	-9.34	0.06	-5.67	0.12
GT05-5	b	7	-9.37	0.06	-5.80	0.12
GT05-5	c	17	-9.23	0.06	-5.72	0.12
GT05-5	d	26	-8.79	0.06	-5.50	0.12
GT05-5	e	37	-9.01	0.06	-5.58	0.12
GT05-6	a	0	-5.53	0.06	-4.61	0.12
GT05-6	b	6	-5.95	0.06	-4.78	0.12
GT05-6	c	11	-5.43	0.06	-4.56	0.12
GT05-6	d	18	-5.88	0.06	-4.70	0.12
GT05-6	e	25	-5.72	0.06	-4.63	0.12
GT05-6	f	31	-6.13	0.06	-4.68	0.12
HW05-1	a	0	-3.26	0.06	-3.20	0.12
HW05-1	b	8	-3.25	0.06	-3.27	0.12
HW05-1	c	14	-3.24	0.06	-3.28	0.12
HW05-1	d	22	-3.29	0.06	-3.17	0.12
HW05-1	e	28	-3.28	0.06	-3.23	0.12
HW05-1	f	36	-3.29	0.06	-3.23	0.12
HW05-1	g	42	-3.43	0.06	-3.32	0.12
HW05-1	h	50	-3.54	0.06	-3.31	0.12
HW05-2	a	0	-9.38	0.06	-3.51	0.12
HW05-2	b	6.5	-9.04	0.06	-3.49	0.12
HW05-2	c	14	-8.44	0.06	-3.21	0.12
HW05-2	d	22	-7.02	0.06	-2.94	0.12
HW05-2	e	30	-6.24	0.06	-2.71	0.12

Table C.1 (continued)

Sample		Distance from growth axis (mm)	$\delta^{13}C$ (‰)	$\delta^{13}C$ st. dev.	$\delta^{18}O$ (‰)	$\delta^{18}O$ st. dev.
HW05-3	a	0	-7.03	0.06	-3.24	0.12
HW05-3	b	7	-6.98	0.06	-3.22	0.12
HW05-3	c	15	-6.94	0.06	-3.18	0.12
HW05-3	d	24	-6.75	0.06	-3.15	0.12
HW05-3	e	36	-6.67	0.06	-2.71	0.12
HW05-4	a	0	-5.72	0.06	-2.57	0.12
HW05-4	b	6	-5.24	0.06	-2.85	0.12
HW05-4	c	12.5	-5.19	0.06	-2.56	0.12
HW05-4	d	19	-6.24	0.06	-3.00	0.12
HW05-4	e	27	-5.03	0.06	-2.66	0.12
TAP05-1	a	0	-3.81	0.06	-2.66	0.12
TAP05-1	b	6	-3.96	0.06	-2.71	0.12
TAP05-1	c	12	-3.76	0.06	-2.59	0.12
TAP05-1	d	19	-3.22	0.06	-2.83	0.12
TAP05-1	e	26	-2.86	0.06	-3.01	0.12
TAP05-2	a	0	-5.86	0.06	-2.41	0.12
TAP05-2	b	8	-6.04	0.06	-2.47	0.12
TAP05-2	c	16	-6.48	0.06	-2.78	0.12
TAP05-2	d	23	-6.20	0.06	-2.53	0.12
TAP05-2	e	30	-5.67	0.06	-2.26	0.12
TAP05-3	a	0	-5.86	0.06	-2.96	0.12
TAP05-3	b	7	-6.20	0.06	-2.51	0.12
TAP05-3	c	13	-6.41	0.06	-2.76	0.12
TAP05-3	d	20	-6.71	0.06	-2.98	0.12
TAP05-3	e	27.5	-6.66	0.06	-2.95	0.12
TAP05-4	a	0	-9.63	0.06	-3.33	0.12
TAP05-4	b	6	Sample Lost		Sample Lost	
TAP05-4	c	12	-7.24	0.06	-2.46	0.12
TAP05-4	d	19	-6.24	0.06	-2.31	0.12
TAP05-4	e	25	-5.90	0.06	-2.22	0.12
TAP05-5	a	0	-5.47	0.06	-3.16	0.12
TAP05-5	b	4.5	-4.74	0.06	-3.09	0.12
TAP05-5	c	11	-4.85	0.06	-2.92	0.12
TAP05-5	d	16.5	-4.23	0.06	-2.67	0.12
TAP05-5	e	22.5	-3.73	0.06	-2.34	0.12
TAP05-6	a	0	-8.70	0.06	-3.18	0.12
TAP05-6	b	8	-8.19	0.06	-3.06	0.12
TAP05-6	c	14	-7.30	0.06	-2.80	0.12
TAP05-6	d	20	-7.93	0.06	-3.01	0.12
TAP05-6	e	23	-8.39	0.06	-3.10	0.12
WZ05-1	a	0	-3.68	0.06	-2.80	0.12
WZ05-1	b	8	-3.61	0.06	-2.73	0.12
WZ05-1	c	15	-3.90	0.06	-2.71	0.12
WZ05-1	d	23.5	-4.00	0.06	-2.80	0.12
WZ05-1	e	31	-4.07	0.06	-2.91	0.12

Table C.1 (continued)

Sample		Distance from growth axis (mm)	$\delta^{13}C$ (‰)	$\delta^{13}C$ st. dev.	$\delta^{18}O$ (‰)	$\delta^{18}O$ st. dev.
WZ05-2	a	0	-6.59	0.06	-2.75	0.12
WZ05-2	b	7	-6.36	0.06	-3.17	0.12
WZ05-2	c	14.5	-5.54	0.06	-2.53	0.12
WZ05-2	d	22	-4.90	0.06	-2.59	0.12
WZ05-2	e	30	-5.67	0.06	-2.73	0.12
WZ05-3	a	0	-7.94	0.06	-2.41	0.12
WZ05-3	b	6	-7.70	0.06	-2.54	0.12
WZ05-3	c	12	-8.09	0.06	-2.58	0.12
WZ05-3	d	18	-7.33	0.06	-2.48	0.12
WZ05-3	e	25	-7.15	0.06	-2.30	0.12
WZ05-4	a	0	-4.96	0.06	-2.76	0.12
WZ05-4	b	5	-5.07	0.06	-2.48	0.12
WZ05-4	c	11.5	-5.25	0.06	-2.63	0.12
WZ05-4	d	16.5	-5.86	0.06	-2.93	0.12
WZ05-4	e	23	-6.15	0.06	-2.77	0.12
WZ05-4	f	30	-6.79	0.06	-2.90	0.12
RK05-1b	a	0	-3.90	0.06	-3.25	0.12
RK05-1b	b	10	-4.73	0.06	-3.41	0.12
RK05-1b	c	18	-4.72	0.06	-3.25	0.12
RK05-1b	d	28	-4.31	0.06	-3.36	0.12
RK05-1b	e	38.5	-4.92	0.06	-3.28	0.12
RK05-1b	f	48.5	-5.53	0.06	-3.57	0.12
RK05-1b	g	56.5	-5.49	0.06	-3.20	0.12
RK05-1t	a	0	-2.82	0.06	-3.36	0.12
RK05-1t	b	6	-2.64	0.06	-3.61	0.12
RK05-1t	c	12	-3.27	0.06	-3.52	0.12
RK05-1t	d	21	-2.63	0.06	-3.38	0.12
RK05-1t	e	29	-2.54	0.06	-3.30	0.12
RK05-1t	f	37	-3.10	0.06	-3.42	0.12
RK05-3	a	0	-6.97	0.06	-3.89	0.12
RK05-3	b	12	-6.68	0.06	-3.85	0.12
RK05-3	c	22.5	-5.66	0.06	-3.89	0.12
RK05-3	d	34	-6.27	0.06	-3.84	0.12
RK05-3	e	47	-6.79	0.06	-3.94	0.12
RK05-3	f	63	-6.97	0.06	-3.88	0.12
RK05-3	g	78.5	-7.18	0.06	-3.69	0.12
RK05-3	a	0	-5.43	0.06	-3.14	0.12
RK05-3	b	7	-5.44	0.06	-3.51	0.12
RK05-3	c	17	-5.49	0.06	-3.28	0.12
RK05-3	d	24	-5.32	0.06	-2.98	0.12
RK05-3	e	33	-5.85	0.06	-2.90	0.12
RK05-3	f	44	-5.65	0.06	-2.65	0.12
RK05-4	a	0	-7.49	0.06	-4.45	0.12
RK05-4	b	6	-6.21	0.06	-4.42	0.12
RK05-4	c	11	-6.40	0.06	-4.32	0.12
RK05-4	d	17	-5.56	0.06	-4.21	0.12
RK05-4	e	23	-6.23	0.06	-4.47	0.12
RK05-4	f	29	-6.35	0.06	-4.36	0.12

Appendix D: GT05-5 Stable Isotope Data

Table D.1: Stable carbon and oxygen isotope ratios from GT05-5 calcite. Values are reported relative to Vienna Peedee Belemnite in per mil (‰) notation. Ages are reported as thousands of years before present (kyr B.P.), where present is defined as 2000 AD. Ice volume adjusted $\delta^{18}O$ values (ice vol. adj.) are also given.

Sample		Depth (mm)	Age (kyr B.P.)	$\delta^{13}C$ (‰)	$\delta^{13}C$ st. dev.	$\delta^{18}O$ (‰)	$\delta^{18}O$ st. dev.	$\delta^{18}O$ ice vol. adj.
GT05-5	0-2 a	0.1	0.001	-9.07	0.06	-4.70	0.12	-4.70
GT05-5	0-2 e	1.0	0.012	-8.81	0.06	-5.88	0.12	-5.88
GT05-5	2-4 a	2.1	0.025	-8.89	0.06	-5.06	0.12	-5.06
GT05-5	2-4 e	3.0	0.035	-9.95	0.06	-5.48	0.12	-5.48
GT05-5	4-6 a	4.1	0.048	-8.88	0.06	-5.01	0.12	-5.01
GT05-5	4-6 e	5.0	0.058	-9.93	0.06	-5.16	0.12	-5.16
GT05-5	6-8 a	6.1	0.071	-9.33	0.06	-5.01	0.12	-5.01
GT05-5	6-8 e	7.0	0.082	-10.08	0.06	-5.52	0.12	-5.52
GT05-5	8-10 a	8.1	0.095	-8.11	0.06	-5.04	0.12	-5.04
GT05-5	8-10 e	9.0	0.105	-9.26	0.06	-4.84	0.12	-4.84
GT05-5	10-12 a	10.1	0.118	-6.77	0.06	-5.10	0.12	-5.10
GT05-5	10-12 e	11.0	0.128	-6.87	0.06	-5.62	0.12	-5.62
GT05-5	12-14 a	12.1	0.141	-7.47	0.06	-4.89	0.12	-4.89
GT05-5	12-14 e	13.0	0.152	-7.88	0.06	-5.08	0.12	-5.08
GT05-5	14-16 a	14.1	0.165	-9.21	0.06	-5.09	0.12	-5.09
GT05-5	14-16 e	15.0	0.175	-8.28	0.06	-5.84	0.12	-5.84
GT05-5	16-18 a	16.1	0.188	-7.95	0.06	-5.68	0.12	-5.68
GT05-5	16-18 e	17.0	0.199	-8.31	0.06	-5.22	0.12	-5.22
GT05-5	18-20 a	18.1	0.212	-8.58	0.06	-4.91	0.12	-4.91
GT05-5	18-20 e	19.0	0.222	-7.51	0.06	-5.24	0.12	-5.24
GT05-5	20-22 a	20.1	0.235	-9.50	0.06	-5.33	0.12	-5.33
GT05-5	20-22 e	21.0	0.245	-8.77	0.06	-5.42	0.12	-5.42
GT05-5	22-24 a	22.1	0.258	-8.90	0.06	-5.60	0.12	-5.60
GT05-5	22-24 e	23.0	0.269	-7.10	0.06	-5.64	0.12	-5.64
GT05-5	24-26 a	24.1	0.282	-7.91	0.06	-5.70	0.12	-5.70
GT05-5	24-26 e	25.0	0.292	-8.92	0.06	-5.17	0.12	-5.17
GT05-5	26-28 a	26.1	0.305	-9.94	0.06	-5.37	0.12	-5.37
GT05-5	26-28 e	27.0	0.315	-7.54	0.06	-5.82	0.12	-5.82
GT05-5	28-30 a	28.1	0.328	-7.98	0.06	-5.41	0.12	-5.41
GT05-5	28-30 e	29.0	0.339	-9.22	0.06	-5.33	0.12	-5.33
GT05-5	30-32 a	30.1	0.352	-9.55	0.06	-5.19	0.12	-5.19
GT05-5	30-32 e	31.0	0.362	-8.53	0.06	-5.47	0.12	-5.47
GT05-5	32-34 a	32.1	0.375	-6.75	0.06	-5.11	0.12	-5.11
GT05-5	32-34 e	33.0	0.385	-9.82	0.06	-5.74	0.12	-5.74
GT05-5	34-36 a	34.1	0.398	-7.86	0.06	-5.20	0.12	-5.20
GT05-5	34-36 e	35.0	0.409	-7.41	0.06	-5.25	0.12	-5.25
GT05-5	36-38 a	36.1	0.422	-9.99	0.06	-5.26	0.12	-5.26
GT05-5	36-38 e	37.0	0.432	-9.34	0.06	-5.15	0.12	-5.15
GT05-5	38-40 a	38.1	0.445	-8.89	0.06	-5.74	0.12	-5.74
GT05-5	38-40 e	39.0	0.455	-7.18	0.06	-5.62	0.12	-5.62
GT05-5	40-42 a	40.1	0.468	-9.86	0.06	-5.70	0.12	-5.70
GT05-5	42-44 a	42.1	0.492	-8.40	0.06	-5.13	0.12	-5.13
GT05-5	42-44 e	43.0	0.502	-7.91	0.06	-5.51	0.12	-5.51

Table D.1 (continued)

Sample		Depth (mm)	Age (kyr B.P.)	$\delta^{13}C$ (‰)	$\delta^{13}C$ st. dev.	$\delta^{18}O$ (‰)	$\delta^{18}O$ st. dev.	$\delta^{18}O$ ice vol. adj.
GT05-5	44-46 a	44.1	0.515	-8.13	0.06	-5.24	0.12	-5.24
GT05-5	46-48 a	46.1	0.539	-6.65	0.06	-5.07	0.12	-5.07
GT05-5	46-48 e	47.0	0.549	-10.22	0.06	-5.39	0.12	-5.39
GT05-5	48-50 a	48.1	0.562	-7.84	0.06	-5.48	0.12	-5.48
GT05-5	50-52 a	50.1	0.585	-8.39	0.06	-4.99	0.12	-4.99
GT05-5	50-52 e	51.0	0.596	-8.42	0.06	-5.52	0.12	-5.52
GT05-5	52-54 a	52.1	0.609	-9.00	0.06	-5.16	0.12	-5.16
GT05-5	52-54 e	53.0	0.619	-8.67	0.06	-5.29	0.12	-5.29
GT05-5	54-56 a	54.1	0.632	-9.22	0.06	-5.24	0.12	-5.24
GT05-5	54-56 e	55.0	0.642	-9.76	0.06	-5.71	0.12	-5.71
GT05-5	56-58 a	56.1	0.654	-7.87	0.06	-5.50	0.12	-5.50
GT05-5	56-58 e	57.0	0.688	-7.14	0.06	-5.00	0.12	-5.00
GT05-5	58-60 a	58.1	0.730	-7.24	0.06	-5.38	0.12	-5.38
GT05-5	58-60 e	59.0	0.763	-6.31	0.06	-5.50	0.12	-5.50
GT05-5	60-62 a	60.1	0.805	-6.74	0.06	-5.17	0.12	-5.17
GT05-5	60-62 e	61.0	0.839	-6.34	0.06	-5.05	0.12	-5.05
GT05-5	62-64 a	62.1	0.881	-6.31	0.06	-4.92	0.12	-4.92
GT05-5	62-64 e	63.0	0.914	-6.95	0.06	-5.15	0.12	-5.15
GT05-5	64-66 a	64.1	0.956	-6.78	0.06	-5.09	0.12	-5.09
GT05-5	64-66 e	65.0	0.990	-6.46	0.06	-4.96	0.12	-4.96
GT05-5	66-68 a	66.1	1.032	-6.52	0.06	-4.91	0.12	-4.91
GT05-5	66-68 e	67.0	1.066	-7.79	0.06	-5.56	0.12	-5.56
GT05-5	68-70 a	68.1	1.108	-6.68	0.06	-4.96	0.12	-4.96
GT05-5	68-70 e	69.0	1.141	-6.51	0.06	-5.55	0.12	-5.55
GT05-5	70-72 a	70.1	1.183	-6.97	0.06	-5.46	0.12	-5.46
GT05-5	70-72 e	71.0	1.217	-6.25	0.06	-5.07	0.12	-5.07
GT05-5	72-74 a	72.1	1.259	-5.66	0.06	-5.24	0.12	-5.24
GT05-5	72-74 e	73.0	1.292	-5.73	0.06	-5.25	0.12	-5.25
GT05-5	74-76 a	74.1	1.334	-5.36	0.06	-5.04	0.12	-5.04
GT05-5	74-76 e	75.0	1.368	-5.70	0.06	-4.87	0.12	-4.87
GT05-5	76-78 a	76.1	1.410	-7.10	0.06	-5.14	0.12	-5.14
GT05-5	76-78 e	77.0	1.443	-7.10	0.06	-5.30	0.12	-5.30
GT05-5	78-80 a	78.1	1.485	-7.50	0.06	-5.25	0.12	-5.25
GT05-5	78-80 e	79.0	1.519	-7.56	0.06	-5.29	0.12	-5.29
GT05-5	80-82 a	80.1	1.561	-7.70	0.06	-5.27	0.12	-5.27
GT05-5	82-84 a	82.1	1.637	-7.50	0.06	-5.02	0.12	-5.02
GT05-5	82-84 e	83.0	1.670	-7.53	0.06	-5.63	0.12	-5.63
GT05-5	84-86 a	84.1	1.712	-8.65	0.06	-5.46	0.12	-5.46
GT05-5	86-88 a	86.1	1.788	-7.83	0.06	-5.82	0.12	-5.82
GT05-5	86-88 e	87.0	1.821	-7.45	0.06	-5.46	0.12	-5.46
GT05-5	88-90 a	88.1	1.863	-6.68	0.06	-5.07	0.12	-5.07
GT05-5	90-92 a	90.1	1.939	-8.13	0.06	-5.36	0.12	-5.36
GT05-5	90-92 e	91.0	1.973	-7.11	0.06	-5.35	0.12	-5.35
GT05-5	92-94 a	92.1	2.015	-6.74	0.06	-5.24	0.12	-5.24
GT05-5	94-96 a	94.1	2.090	-6.43	0.06	-5.09	0.12	-5.09
GT05-5	94-96 e	95.0	2.124	-7.48	0.06	-5.59	0.12	-5.59
GT05-5	96-98 a	96.1	2.166	-6.75	0.06	-5.20	0.12	-5.20
GT05-5	96-98 e	97.0	2.199	-6.44	0.06	-5.22	0.12	-5.22
GT05-5	98-100 a	98.1	2.241	-6.28	0.06	-5.20	0.12	-5.20
GT05-5	98-100 e	99.0	2.275	-8.30	0.06	-5.59	0.12	-5.59
GT05-5	100-102 a	100.1	2.317	-9.57	0.06	-5.35	0.12	-5.35

Table D.1 (continued)

Sample	Depth (mm)	Age (kyr B.P.)	$\delta^{13}C$ (‰)	$\delta^{13}C$ st. dev.	$\delta^{18}O$ (‰)	$\delta^{18}O$ st. dev.	$\delta^{18}O$ ice vol. adj.
GT05-5 102-104 a	102.1	2.393	-6.02	0.06	-5.25	0.12	-5.25
GT05-5 102-104 e	103.0	2.426	-7.29	0.06	-5.60	0.12	-5.60
GT05-5 104-106 a	104.1	2.468	-8.03	0.06	-5.56	0.12	-5.56
GT05-5 104-106 e	105.0	2.502	-7.22	0.06	-5.53	0.12	-5.53
GT05-5 106-108 a	106.1	2.544	-7.98	0.06	-5.23	0.12	-5.23
GT05-5 106-108 e	107.0	2.577	-8.35	0.06	-5.66	0.12	-5.66
GT05-5 108-110 a	108.1	2.619	-7.35	0.06	-5.45	0.12	-5.45
GT05-5 108-110 e	109.0	2.653	-6.37	0.06	-5.46	0.12	-5.46
GT05-5 110-112 a	110.1	2.695	-7.04	0.06	-5.32	0.12	-5.32
GT05-5 110-112 e	111.0	2.729	-8.25	0.06	-5.63	0.12	-5.63
GT05-5 112-114 a	112.1	2.771	-7.33	0.06	-5.17	0.12	-5.17
GT05-5 112-114 e	113.0	2.804	-6.88	0.06	-5.03	0.12	-5.03
GT05-5 114-116 a	114.1	2.846	-7.55	0.06	-5.46	0.12	-5.46
GT05-5 114-116 e	115.0	2.880	-7.46	0.06	-5.35	0.12	-5.35
GT05-5 116-118 a	116.1	2.922	-7.16	0.06	-5.26	0.12	-5.26
GT05-5 116-118 e	117.0	2.955	-7.44	0.06	-5.13	0.12	-5.13
GT05-5 118-120 a	118.1	2.997	-6.68	0.06	-5.17	0.12	-5.17
GT05-5 118-120 e	119.0	3.031	-5.92	0.06	-5.32	0.12	-5.32
GT05-5 120-122 a	120.1	3.073	-5.76	0.06	-5.25	0.12	-5.25
GT05-5 120-122 e	121.0	3.106	-6.20	0.06	-5.10	0.12	-5.10
GT05-5 122-124 a	122.1	3.148	-6.15	0.06	-5.08	0.12	-5.08
GT05-5 122-124 e	123.0	3.182	-6.13	0.06	-5.18	0.12	-5.18
GT05-5 124-126 a	124.1	3.224	-6.83	0.06	-5.08	0.12	-5.08
GT05-5 124-126 e	125.0	3.258	-7.03	0.06	-5.48	0.12	-5.48
GT05-5 126-128 a	126.1	3.300	-9.58	0.06	-6.38	0.12	-6.38
GT05-5 126-128 e	127.0	3.333	-7.20	0.06	-5.36	0.12	-5.36
GT05-5 128-130 a	128.1	3.375	-7.32	0.06	-5.24	0.12	-5.24
GT05-5 128-130 e	129.0	3.409	-7.96	0.06	-5.49	0.12	-5.49
GT05-5 130-132 a	130.1	3.451	-9.29	0.06	-5.56	0.12	-5.56
GT05-5 130-132 e	131.0	3.484	-8.73	0.06	-5.19	0.12	-5.19
GT05-5 132-134 a	132.1	3.526	-8.01	0.06	-5.77	0.12	-5.77
GT05-5 132-134 e	133.0	3.560	-7.95	0.06	-5.54	0.12	-5.54
GT05-5 134-136 a	134.1	3.602	-7.31	0.06	-5.39	0.12	-5.39
GT05-5 134-136 e	135.0	3.636	-7.46	0.06	-5.35	0.12	-5.35
GT05-5 136-138 a	136.1	3.678	-6.93	0.06	-5.58	0.12	-5.58
GT05-5 136-138 e	137.0	3.711	-6.64	0.06	-5.23	0.12	-5.23
GT05-5 138-140 a	138.1	3.753	-7.55	0.06	-5.69	0.12	-5.69
GT05-5 138-140 e	139.0	3.787	-6.86	0.06	-5.36	0.12	-5.36
GT05-5 140-142 a	140.1	3.829	-6.81	0.06	-5.37	0.12	-5.37
GT05-5 140-142 e	141.0	3.862	-7.26	0.06	-5.11	0.12	-5.11
GT05-5 142-144 a	142.1	3.904	-7.44	0.06	-5.57	0.12	-5.57
GT05-5 142-144 e	143.0	3.938	-8.34	0.06	-5.48	0.12	-5.48
GT05-5 144-146 a	144.1	3.980	-8.17	0.06	-5.70	0.12	-5.70
GT05-5 144-146 e	145.0	4.014	-7.76	0.06	-5.48	0.12	-5.48
GT05-5 146-148 a	146.1	4.056	-8.91	0.06	-5.43	0.12	-5.43
GT05-5 146-148 e	147.0	4.089	-7.91	0.06	-5.38	0.12	-5.38
GT05-5 148-150 a	148.1	4.131	-8.59	0.06	-5.79	0.12	-5.79
GT05-5 148-150 e	149.0	4.165	-6.90	0.06	-4.81	0.12	-4.81
GT05-5 150-152 a	150.1	4.207	-7.42	0.06	-5.54	0.12	-5.54
GT05-5 150-152 e	151.0	4.240	-8.20	0.06	-5.84	0.12	-5.84
GT05-5 152-154 a	152.1	4.282	-7.82	0.06	-5.45	0.12	-5.45

Table D.1 (continued)

Sample	Depth (mm)	Age (kyr B.P.)	$\delta^{13}C$ (‰)	$\delta^{13}C$ st. dev.	$\delta^{18}O$ (‰)	$\delta^{18}O$ st. dev.	$\delta^{18}O$ ice vol. adj.
GT05-5 154-156 a	154.1	4.358	-7.81	0.06	-5.66	0.12	-5.66
GT05-5 154-156 e	155.0	4.391	-6.32	0.06	-5.28	0.12	-5.28
GT05-5 156-158 a	156.1	4.433	-6.82	0.06	-4.96	0.12	-4.96
GT05-5 156-158 e	157.0	4.467	-8.69	0.06	-5.66	0.12	-5.66
GT05-5 158-160 a	158.1	4.509	-8.22	0.06	-5.57	0.12	-5.57
GT05-5 158-160 e	159.0	4.543	-8.43	0.06	-5.94	0.12	-5.94
GT05-5 160-162 a	160.1	4.585	-7.99	0.06	-5.62	0.12	-5.62
GT05-5 160-162 e	161.0	4.618	-7.84	0.06	-5.19	0.12	-5.19
GT05-5 162-164 a	162.1	4.660	-7.60	0.06	-5.25	0.12	-5.25
GT05-5 162-164 e	163.0	4.694	-7.49	0.06	-5.35	0.12	-5.35
GT05-5 164-166 a	164.1	4.736	-7.36	0.06	-5.10	0.12	-5.10
GT05-5 164-166 e	165.0	4.769	-7.05	0.06	-5.31	0.12	-5.31
GT05-5 166-168 a	166.1	4.811	-6.28	0.06	-5.03	0.12	-5.03
GT05-5 166-168 e	167.0	4.845	-6.57	0.06	-5.24	0.12	-5.24
GT05-5 168-170 a	168.1	4.887	-5.86	0.06	-5.39	0.12	-5.39
GT05-5 168-170 e	169.0	5.022	-5.95	0.06	-4.90	0.12	-4.90
GT05-5 170-172 a	170.1	5.190	-5.52	0.06	-5.07	0.12	-5.07
GT05-5 170-172 e	171.0	5.324	-6.22	0.06	-5.12	0.12	-5.13
GT05-5 172-174 a	172.1	5.493	-5.33	0.06	-5.21	0.12	-5.22
GT05-5 172-174 e	173.0	5.627	-5.96	0.06	-5.15	0.12	-5.16
GT05-5 174-176 a	174.1	5.795	-5.95	0.06	-5.09	0.12	-5.10
GT05-5 174-176 e	175.0	5.930	-5.84	0.06	-4.92	0.12	-4.93
GT05-5 176-178 a	176.1	6.098	-5.93	0.06	-4.97	0.12	-4.99
GT05-5 176-178 e	177.0	6.233	-5.83	0.06	-5.08	0.12	-5.11
GT05-5 178-180 a	178.1	6.401	-5.34	0.06	-5.02	0.12	-5.06
GT05-5 178-180 e	179.0	6.535	-6.02	0.06	-5.16	0.12	-5.21
GT05-5 180-182 a	180.1	6.704	-5.69	0.06	-5.09	0.12	-5.15
GT05-5 180-182 e	181.0	6.838	-5.50	0.06	-5.10	0.12	-5.17
GT05-5 182-184 a	182.1	7.006	-5.48	0.06	-4.94	0.12	-5.02
GT05-5 182-184 e	183.0	7.141	-5.08	0.06	-5.14	0.12	-5.23
GT05-5 184-186 a	184.1	7.309	-4.51	0.06	-4.96	0.12	-5.06
GT05-5 184-186 e	185.0	7.444	-5.10	0.06	-5.14	0.12	-5.25
GT05-5 186-188 a	186.1	7.612	-4.83	0.06	-4.93	0.12	-5.05
GT05-5 186-188 e	187.0	7.746	-5.46	0.06	-5.00	0.12	-5.13
GT05-5 188-190 a	188.1	7.915	-5.25	0.06	-4.74	0.12	-4.88
GT05-5 188-190 e	189.0	8.049	-5.54	0.06	-5.02	0.12	-5.17
GT05-5 190-192 a	190.1	8.217	-4.71	0.06	-4.57	0.12	-4.74
GT05-5 190-192 e	191.0	8.352	-4.61	0.06	-4.81	0.12	-4.99
GT05-5 192-194 a	192.1	8.520	-4.95	0.06	-4.77	0.12	-4.96
GT05-5 192-194 e	193.0	8.655	-5.45	0.06	-5.22	0.12	-5.43
GT05-5 194-196 a	194.1	8.823	-5.99	0.06	-5.20	0.12	-5.42
GT05-5 194-196 e	195.0	8.957	-6.03	0.06	-5.23	0.12	-5.46

Appendix E: HW05-3 Stable Isotope Data

Table E.1: Stable carbon and oxygen isotope ratios from HW05-3 calcite. Values are reported relative to Vienna Peedee Belemnite in per mil (‰) notation. Ages are reported as thousands of years before present (kyr B.P.), where present is defined as 2000 AD. Ice volume adjusted $\delta^{18}O$ values (ice vol. adj.) are also given.

Sample		Depth (mm)	Age (kyr B.P.)	$\delta^{13}C$ (‰)	$\delta^{13}C$ st. dev.	$\delta^{18}O$ (‰)	$\delta^{18}O$ st. dev.	$\delta^{18}O$ ice vol. adj.
HW05-3	0-2 a	0.11	11.374	-5.55	0.06	-2.37	0.12	-2.81
HW05-3	0-2 e	1.00	11.409	-4.11	0.06	-2.11	0.12	-2.56
HW05-3	2-4 a	2.11	11.453	-4.22	0.06	-2.05	0.12	-2.50
HW05-3	2-4 e	3.00	11.488	-4.89	0.06	-3.22	0.12	-3.67
HW05-3	4-6 a	4.11	11.532	-4.51	0.06	-2.06	0.12	-2.52
HW05-3	4-6 e	5.00	11.567	-6.24	0.06	-2.48	0.12	-2.94
HW05-3	6-8 a	6.11	11.610	-4.66	0.06	-2.15	0.12	-2.61
HW05-3	6-8 e	7.00	11.645	-5.06	0.06	-2.03	0.12	-2.49
HW05-3	8-10 a	8.11	11.689	-4.82	0.06	-1.99	0.12	-2.46
HW05-3	8-10 e	9.00	11.724	-5.77	0.06	-2.51	0.12	-2.98
HW05-3	10-12 a	10.11	11.768	-5.72	0.06	-2.34	0.12	-2.82
HW05-3	10-12 e	11.00	11.803	-4.80	0.06	-2.41	0.12	-2.89
HW05-3	12-14 a	12.11	11.846	-6.06	0.06	-2.62	0.12	-3.10
HW05-3	12-14 e	13.00	11.881	-6.89	0.06	-2.83	0.12	-3.32
HW05-3	14-16 a	14.11	11.925	-6.34	0.06	-2.67	0.12	-3.16
HW05-3	14-16 e	15.00	11.960	-7.12	0.06	-2.90	0.12	-3.40
HW05-3	16-18 a	16.11	12.004	-7.72	0.06	-2.96	0.12	-3.46
HW05-3	16-18 e	17.00	12.039	-7.42	0.06	-2.87	0.12	-3.37
HW05-3	18-20 a	18.11	12.082	-5.53	0.06	-2.11	0.12	-2.62
HW05-3	18-20 e	19.00	12.117	-5.62	0.06	-2.40	0.12	-2.90
HW05-3	20-22 a	20.11	12.161	-6.32	0.06	-2.51	0.12	-3.02
HW05-3	20-22 e	21.00	12.196	-4.84	0.06	-2.11	0.12	-2.63
HW05-3	22-24 a	22.11	12.240	-5.45	0.06	-2.45	0.12	-2.97
HW05-3	22-24 e	23.00	12.275	-5.66	0.06	-2.47	0.12	-2.99
HW05-3	24-26 a	24.11	12.318	-6.33	0.06	-3.19	0.12	-3.72
HW05-3	24-26 e	25.00	12.353	-4.02	0.06	-2.07	0.12	-2.60
HW05-3	26-28 a	26.11	12.397	-5.56	0.06	-2.85	0.12	-3.38
HW05-3	26-28 e	27.00	12.432	-6.07	0.06	-2.70	0.12	-3.24
HW05-3	28-30 a	28.11	12.475	-4.32	0.06	-2.21	0.12	-2.75
HW05-3	28-30 e	29.00	12.510	-4.29	0.06	-2.29	0.12	-2.83
HW05-3	30-32 a	30.11	12.554	-5.08	0.06	-3.51	0.12	-4.06
HW05-3	30-32 e	31.00	12.589	-5.34	0.06	-2.98	0.12	-3.53
HW05-3	32-34 a	32.11	12.633	-5.32	0.06	-2.89	0.12	-3.45
HW05-3	32-34 e	33.00	12.668	-5.88	0.06	-2.70	0.12	-3.26
HW05-3	34-36 a	34.11	12.711	-4.55	0.06	-2.24	0.12	-2.80
HW05-3	34-36 e	35.00	12.746	-4.97	0.06	-2.81	0.12	-3.38
HW05-3	36-38 a	36.11	12.790	-6.68	0.06	-3.09	0.12	-3.66
HW05-3	36-38 e	37.00	12.825	-7.37	0.06	-3.27	0.12	-3.84
HW05-3	38-40 a	38.11	12.869	-7.08	0.06	-3.69	0.12	-4.27
HW05-3	38-40 e	39.00	12.904	-6.38	0.06	-3.05	0.12	-3.63
HW05-3	40-42 a	40.11	12.947	-5.23	0.06	-2.45	0.12	-3.03
HW05-3	40-42 e	41.00	12.982	-5.71	0.06	-2.58	0.12	-3.17

Table E.1 (continued)

Sample		Depth (mm)	Age (kyr B.P.)	$\delta^{13}C$ (‰)	$\delta^{13}C$ st. dev.	$\delta^{18}O$ (‰)	$\delta^{18}O$ st. dev.	$\delta^{18}O$ ice vol. adj.
HW05-3	42-44 a	42.11	13.026	-6.26	0.06	-2.47	0.12	-3.06
HW05-3	42-44 e	43.00	13.061	-6.53	0.06	-2.78	0.12	-3.38
HW05-3	44-46 a	44.11	13.105	-7.18	0.06	-3.27	0.12	-3.88
HW05-3	44-46 e	45.00	13.140	-7.14	0.06	-3.00	0.12	-3.61
HW05-3	46-48 a	46.11	13.183	-7.36	0.06	-3.40	0.12	-4.03
HW05-3	46-48 e	47.00	13.218	-7.19	0.06	-3.03	0.12	-3.66
HW05-3	48-50 a	48.11	13.262	-7.33	0.06	-3.03	0.12	-3.67
HW05-3	48-50 e	49.00	13.297	-7.28	0.06	-3.15	0.12	-3.80
HW05-3	50-52 a	50.11	13.341	-7.49	0.06	-3.55	0.12	-4.21
HW05-3	50-52 e	51.00	13.376	-7.23	0.06	-3.04	0.12	-3.71
HW05-3	52-54 a	52.11	13.419	-7.35	0.06	-3.65	0.12	-4.32
HW05-3	52-54 e	53.00	13.454	-7.07	0.06	-3.08	0.12	-3.76
HW05-3	54-56 a	54.11	13.498	-6.61	0.06	-3.44	0.12	-4.13
HW05-3	54-56 e	55.00	13.533	-7.20	0.06	-3.23	0.12	-3.93
HW05-3	56-58 a	56.11	13.577	-7.09	0.06	-3.08	0.12	-3.78
HW05-3	56-58 e	57.00	13.611	-7.44	0.06	-3.32	0.12	-4.03
HW05-3	58-60 a	58.11	13.655	-7.27	0.06	-3.53	0.12	-4.25
HW05-3	58-60 e	59.00	13.690	-7.00	0.06	-3.15	0.12	-3.88
HW05-3	60-62 a	60.11	13.734	-7.56	0.06	-3.69	0.12	-4.42
HW05-3	60-62 e	61.00	13.769	-6.77	0.06	-3.08	0.12	-3.82
HW05-3	62-64 a	62.11	13.812	-5.56	0.06	-2.90	0.12	-3.65
HW05-3	62-64 e	63.00	13.847	-5.73	0.06	-2.71	0.12	-3.46
HW05-3	64-66 a	64.11	13.891	-7.19	0.06	-3.38	0.12	-4.15
HW05-3	64-66 e	65.00	13.926	-7.78	0.06	-3.01	0.12	-3.78
HW05-3	66-68 a	66.11	13.970	-8.19	0.06	-3.71	0.12	-4.49
HW05-3	66-68 e	67.00	14.005	-8.06	0.06	-3.48	0.12	-4.27
HW05-3	68-70 a	68.11	14.048	-8.29	0.06	-3.94	0.12	-4.73
HW05-3	68-70 e	69.00	14.083	-8.10	0.06	-3.67	0.12	-4.46
HW05-3	70-72 a	70.11	14.127	-7.98	0.06	-3.82	0.12	-4.61
HW05-3	70-72 e	71.00	14.162	-7.80	0.06	-3.52	0.12	-4.31
HW05-3	72-74 a	72.11	14.194	-6.64	0.06	-2.87	0.12	-3.67
HW05-3	72-74 e	73.00	14.219	-6.47	0.06	-2.79	0.12	-3.58
HW05-3	74-76 a	74.11	14.251	-7.21	0.06	-3.29	0.12	-4.09
HW05-3	74-76 e	75.00	14.277	-7.26	0.06	-3.00	0.12	-3.80
HW05-3	76-78 a	76.11	14.309	-6.58	0.06	-3.11	0.12	-3.91
HW05-3	76-78 e	77.00	14.334	-6.41	0.06	-2.78	0.12	-3.58
HW05-3	78-80 a	78.11	14.366	-6.87	0.06	-2.93	0.12	-3.73
HW05-3	78-80 e	79.00	14.392	-6.94	0.06	-2.41	0.12	-3.22
HW05-3	80-82 a	80.11	14.424	-7.25	0.06	-2.88	0.12	-3.69
HW05-3	80-82 e	81.00	14.449	-7.42	0.06	-3.25	0.12	-4.06
HW05-3	82-84 a	82.11	14.481	-7.36	0.06	-3.25	0.12	-4.06
HW05-3	82-84 e	83.00	14.507	-7.47	0.06	-3.30	0.12	-4.11
HW05-3	84-86 a	84.11	14.539	-7.85	0.06	-3.29	0.12	-4.10
HW05-3	84-86 e	85.00	14.564	-7.14	0.06	-3.06	0.12	-3.87
HW05-3	86-88 a	86.11	14.596	-6.19	0.06	-2.56	0.12	-3.38
HW05-3	86-88 e	87.00	14.622	-4.41	0.06	-2.20	0.12	-3.02
HW05-3	88-90 a	88.11	14.654	-5.63	0.06	-2.73	0.12	-3.55
HW05-3	88-90 e	89.00	14.679	-6.94	0.06	-3.18	0.12	-4.00
HW05-3	90-92 a	90.11	14.711	-7.19	0.06	-3.13	0.12	-3.95
HW05-3	90-92 e	91.00	14.737	-7.27	0.06	-3.17	0.12	-3.99
HW05-3	92-94 a	92.11	14.768	-7.35	0.06	-3.21	0.12	-4.03

Table E.1 (continued)

Sample	Depth (mm)	Age (kyr B.P.)	$\delta^{13}C$ (‰)	$\delta^{13}C$ st. dev.	$\delta^{18}O$ (‰)	$\delta^{18}O$ st. dev.	$\delta^{18}O$ ice vol. adj.
HW05-3 92-94 e	93.00	14.794	-5.24	0.06	-2.58	0.12	-3.41
HW05-3 94-96 a	94.11	14.826	-5.53	0.06	-2.35	0.12	-3.18
HW05-3 94-96 e	95.00	14.851	-6.51	0.06	-2.70	0.12	-3.53
HW05-3 96-98 a	96.11	14.883	-6.67	0.06	-2.60	0.12	-3.43
HW05-3 96-98 e	97.00	14.909	-7.22	0.06	-2.83	0.12	-3.66
HW05-3 98-100 a	98.11	14.941	-7.83	0.06	-2.91	0.12	-3.74
HW05-3 98-100 e	99.00	14.966	-7.70	0.06	-3.00	0.12	-3.83
HW05-3 100-102 a	100.11	14.998	-7.53	0.06	-3.00	0.12	-3.84
HW05-3 100-102 e	101.00	15.024	-7.50	0.06	-2.97	0.12	-3.81
HW05-3 102-104 a	102.11	15.056	-6.70	0.06	-2.76	0.12	-3.60
HW05-3 102-104 e	103.00	15.081	-6.96	0.06	-2.90	0.12	-3.74
HW05-3 104-106 a	104.11	15.113	-6.65	0.06	-2.63	0.12	-3.47
HW05-3 104-106 e	105.00	15.139	-7.02	0.06	-2.90	0.12	-3.74
HW05-3 106-108 a	106.11	15.171	-7.33	0.06	-3.77	0.12	-4.61
HW05-3 106-108 e	107.00	15.196	-8.08	0.06	-3.27	0.12	-4.11
HW05-3 108-110 a	108.11	15.228	-8.01	0.06	-3.26	0.12	-4.11
HW05-3 108-110 e	109.00	15.254	-5.36	0.06	-2.64	0.12	-3.49
HW05-3 110-112 a	110.11	15.286	-6.70	0.06	-3.07	0.12	-3.92
HW05-3 110-112 e	111.00	15.311	-6.74	0.06	-3.06	0.12	-3.91
HW05-3 112-114 a	112.11	15.343	-7.15	0.06	-3.24	0.12	-4.09
HW05-3 112-114 e	113.00	15.369	-6.90	0.06	-3.07	0.12	-3.92
HW05-3 114-116 a	114.11	15.401	-7.49	0.06	-3.08	0.12	-3.93
HW05-3 114-116 e	115.00	15.426	-7.83	0.06	-3.35	0.12	-4.21
HW05-3 116-118 a	116.11	15.458	-7.93	0.06	-3.25	0.12	-4.11
HW05-3 116-118 e	117.00	15.484	-7.84	0.06	-3.54	0.12	-4.40
HW05-3 118-120 a	118.11	15.515	-7.75	0.06	-3.86	0.12	-4.72
HW05-3 118-120 e	119.00	15.541	-7.24	0.06	-3.31	0.12	-4.17
HW05-3 120-122 a	120.11	15.573	-7.16	0.06	-2.95	0.12	-3.81
HW05-3 120-122 e	121.00	15.598	-8.04	0.06	-3.43	0.12	-4.29
HW05-3 122-124 a	122.11	15.630	-8.13	0.06	-3.43	0.12	-4.30
HW05-3 122-124 e	123.00	15.656	-8.03	0.06	-3.54	0.12	-4.41
HW05-3 124-126 a	124.11	15.688	-7.63	0.06	-3.28	0.12	-4.15
HW05-3 124-126 e	125.00	15.713	-8	0.06	-3.57	0.12	-4.44
HW05-3 126-128 a	126.11	15.745	-7.85	0.06	-3.32	0.12	-4.19
HW05-3 126-128 e	127.00	15.771	-7.64	0.06	-3.40	0.12	-4.27
HW05-3 128-130 a	128.11	15.803	-7.77	0.06	-3.34	0.12	-4.21
HW05-3 128-130 e	129.00	15.828	-7.82	0.06	-3.41	0.12	-4.29
HW05-3 130-132 a	130.11	15.888	-7.44	0.06	-2.91	0.12	-3.79
HW05-3 130-132 e	131.00	16.140	-5.25	0.06	-3.18	0.12	-4.07
HW05-3 132-134 a	132.11	16.455	-3.01	0.06	-1.98	0.12	-2.89
HW05-3 132-134 e	133.00	16.707	-5.38	0.06	-2.81	0.12	-3.73
HW05-3 134-136 a	134.11	17.021	-4.59	0.06	-2.36	0.12	-3.29
HW05-3 134-136 e	135.00	17.273	-5.61	0.06	-2.62	0.12	-3.57
HW05-3 136-138 a	136.11	17.588	-5.02	0.06	-2.30	0.12	-3.26
HW05-3 136-138 e	137.00	17.840	-6.09	0.06	-2.78	0.12	-3.75
HW05-3 138-140 a	138.11	18.154	-5.85	0.06	-2.48	0.12	-3.47
HW05-3 138-140 e	139.00	18.406	-5.6	0.06	-2.53	0.12	-3.54
HW05-3 140-142 a	140.11	18.721	-4.16	0.06	-2.00	0.12	-3.02
HW05-3 140-142 e	141.00	18.973	-4.03	0.06	-1.94	0.12	-2.98
HW05-3 142-144 a	142.11	19.288	-5.02	0.06	-2.24	0.12	-3.30
HW05-3 142-144 e	143.00	19.539	-5.16	0.06	-2.49	0.12	-3.56

Table E.1 (continued)

Sample	Depth (mm)	Age (kyr B.P.)	$\delta^{13}C$ (‰)	$\delta^{13}C$ st. dev.	$\delta^{18}O$ (‰)	$\delta^{18}O$ st. dev.	$\delta^{18}O$ ice vol. adj.
HW05-3 144-146 a	144.11	19.854	-6.95	0.06	-2.99	0.12	-4.08
HW05-3 144-146 e	145.00	20.106	-7.65	0.06	-3.31	0.12	-4.41
HW05-3 146-148 a	146.11	20.421	-4.62	0.06	-2.08	0.12	-3.18
HW05-3 146-148 e	147.00	20.673	-4.81	0.06	-2.29	0.12	-3.38
HW05-3 148-150 a	148.11	20.987	-4.68	0.06	-2.56	0.12	-3.65
HW05-3 148-150 e	149.00	21.239	-4.72	0.06	-2.32	0.12	-3.41
HW05-3 150-152 a	150.11	21.554	-6.58	0.06	-3.01	0.12	-4.10
HW05-3 150-152 e	151.00	21.806	-7.13	0.06	-3.24	0.12	-4.33
HW05-3 152-154 a	152.11	21.827	-6.26	0.06	-2.76	0.12	-3.85
HW05-3 152-154 e	153.00	21.843	-6.75	0.06	-3.18	0.12	-4.27
HW05-3 154-156 a	154.11	21.864	-6.33	0.06	-2.91	0.12	-4.00
HW05-3 154-156 e	155.00	21.880	-6.21	0.06	-3.01	0.12	-4.10
HW05-3 156-158 a	156.11	21.901	-6.35	0.06	-3.00	0.12	-4.09
HW05-3 156-158 e	157.00	21.917	-6.08	0.06	-3.26	0.12	-4.34
HW05-3 158-160 a	158.11	21.938	-4.94	0.06	-2.40	0.12	-3.48
HW05-3 158-160 e	159.00	21.954	-6.56	0.06	-3.16	0.12	-4.24
HW05-3 160-162 a	160.11	21.975	-7.03	0.06	-3.23	0.12	-4.31
HW05-3 160-162 e	161.00	21.991	-7.12	0.06	-3.37	0.12	-4.45
HW05-3 162-164 a	162.11	22.012	-6.97	0.06	-3.10	0.12	-4.18
HW05-3 162-164 e	163.00	22.028	-7.27	0.06	-3.42	0.12	-4.50
HW05-3 164-166 a	164.11	22.049	-7.29	0.06	-3.21	0.12	-4.29
HW05-3 164-166 e	165.00	22.065	-7.53	0.06	-3.45	0.12	-4.53
HW05-3 166-168 a	166.11	22.086	-7.38	0.06	-3.36	0.12	-4.44
HW05-3 166-168 e	167.00	22.102	-6.64	0.06	-3.37	0.12	-4.45
HW05-3 168-170 a	168.11	22.123	-7.06	0.06	-3.16	0.12	-4.24
HW05-3 168-170 e	169.00	22.139	-7.66	0.06	-3.64	0.12	-4.72
HW05-3 170-172 a	170.11	22.160	-7.34	0.06	-3.20	0.12	-4.28
HW05-3 172-174 a	172.11	22.197	-7	0.06	-3.09	0.12	-4.17
HW05-3 172-174 e	173.00	22.213	-6.68	0.06	-3.14	0.12	-4.22
HW05-3 174-176 a	174.11	22.234	-6.41	0.06	-2.96	0.12	-4.04
HW05-3 174-176 e	175.00	22.250	-6.82	0.06	-3.28	0.12	-4.36
HW05-3 176-178 a	176.11	22.271	-6.54	0.06	-3.05	0.12	-4.13
HW05-3 176-178 e	177.00	22.287	-7.18	0.06	-3.37	0.12	-4.45
HW05-3 178-180 a	178.11	22.308	-7.01	0.06	-3.21	0.12	-4.29
HW05-3 178-180 e	179.00	22.324	-7.55	0.06	-3.35	0.12	-4.43
HW05-3 180-182 a	180.11	22.345	-6.93	0.06	-3.29	0.12	-4.37
HW05-3 180-182 e	181.00	22.361	-7.54	0.06	-4.02	0.12	-5.10
HW05-3 182-184 a	182.11	22.382	-7.05	0.06	-3.34	0.12	-4.42
HW05-3 182-184 e	183.00	22.398	-5.81	0.06	-2.99	0.12	-4.07
HW05-3 184-186 a	184.11	22.535	-7.89	0.06	-3.53	0.12	-4.61
HW05-3 184-186 e	185.00	22.644	-4.69	0.06	-2.24	0.12	-3.32
HW05-3 186-188 a	186.11	22.781	-6.4	0.06	-2.91	0.12	-3.99
HW05-3 186-188 e	187.00	22.890	-4.67	0.06	-2.49	0.12	-3.57
HW05-3 188-190 a	188.11	23.027	-4.84	0.06	-2.63	0.12	-3.71
HW05-3 188-190 e	189.00	23.137	-4.91	0.06	-2.44	0.12	-3.52
HW05-3 190-192 a	190.11	23.273	-5.28	0.06	-2.58	0.12	-3.65
HW05-3 190-192 e	191.00	23.383	-5.77	0.06	-2.72	0.12	-3.79
HW05-3 192-194 a	192.11	23.520	-4.86	0.06	-2.49	0.12	-3.56
HW05-3 192-194 e	193.00	23.629	-4.25	0.06	-2.32	0.12	-3.39
HW05-3 194-196 a	194.11	23.766	-5.3	0.06	-2.47	0.12	-3.54
HW05-3 194-196 e	195.00	23.875	-5.17	0.06	-2.48	0.12	-3.55

Table E.1 (continued)

Sample	Depth (mm)	Age (kyr B.P.)	$\delta^{13}C$ (‰)	$\delta^{13}C$ st. dev.	$\delta^{18}O$ (‰)	$\delta^{18}O$ st. dev.	$\delta^{18}O$ ice vol. adj.
HW05-3 196-198 a	196.11	24.012	-5.92	0.06	-2.52	0.12	-3.59
HW05-3 196-198 e	197.00	24.122	-5.31	0.06	-2.34	0.12	-3.41
HW05-3 198-200 a	198.11	24.258	-6.01	0.06	-2.61	0.12	-3.68
HW05-3 198-200 e	199.00	24.368	-7.42	0.06	-3.24	0.12	-4.31
HW05-3 200-202 a	200.11	24.505	-7.82	0.06	-3.29	0.12	-4.35
HW05-3 200-202 e	201.00	24.614	-8.27	0.06	-3.41	0.12	-4.47
HW05-3 202-204 a	202.11	24.751	-8.22	0.06	-3.51	0.12	-4.57
HW05-3 202-204 e	203.00	24.860	-8.19	0.06	-3.47	0.12	-4.53
HW05-3 204-206 a	204.11	24.997	-7.59	0.06	-3.10	0.12	-4.16
HW05-3 204-206 e	205.00	25.106	-6.82	0.06	-2.83	0.12	-3.89
HW05-3 206-208 a	206.11	25.243	-7.13	0.06	-2.82	0.12	-3.88
HW05-3 206-208 e	207.00	25.353	-7.61	0.06	-2.97	0.12	-4.03
HW05-3 208-210 a	208.11	25.489	-6.74	0.06	-2.78	0.12	-3.84
HW05-3 208-210 e	209.00	25.599	-6.01	0.06	-2.71	0.12	-3.77
HW05-3 210-212 a	210.11	25.736	-4.74	0.06	-2.00	0.12	-3.05
HW05-3 210-212 e	211.00	25.845	-7.4	0.06	-2.88	0.12	-3.93
HW05-3 212-214 a	212.11	25.982	-6.12	0.06	-2.31	0.12	-3.36
HW05-3 212-214 e	213.00	26.091	-7.3	0.06	-2.99	0.12	-4.04
HW05-3 214-216 a	214.11	26.228	-5.47	0.06	-2.32	0.12	-3.37
HW05-3 214-216 e	215.00	26.338	-6.88	0.06	-2.46	0.12	-3.51
HW05-3 216-218 a	216.11	26.474	-4.05	0.06	-1.73	0.12	-2.78
HW05-3 216-218 e	217.00	26.584	-4.42	0.06	-2.10	0.12	-3.15
HW05-3 218-220 a	218.11	26.721	-6.58	0.06	-2.72	0.12	-3.77
HW05-3 218-220 e	219.00	26.830	-6.28	0.06	-2.60	0.12	-3.65
HW05-3 220-222 a	220.11	26.863	-4.99	0.06	-1.88	0.12	-2.93
HW05-3 220-222 e	221.00	26.889	-6.06	0.06	-2.53	0.12	-3.58
HW05-3 222-224 a	222.11	26.922	-4.59	0.06	-1.79	0.12	-2.84
HW05-3 222-224 e	223.00	26.948	-4.72	0.06	-2.03	0.12	-3.07
HW05-3 224-226 a	224.11	26.981	-5.73	0.06	-2.30	0.12	-3.34
HW05-3 224-226 e	225.00	27.007	-5.97	0.06	-2.47	0.12	-3.51
HW05-3 226-228 a	226.11	27.040	-6.79	0.06	-2.51	0.12	-3.55
HW05-3 226-228 e	227.00	27.066	-4.13	0.06	-1.71	0.12	-2.75
HW05-3 228-230 a	228.11	27.099	-4.42	0.06	-1.69	0.12	-2.73
HW05-3 228-230 e	229.00	27.125	-5.54	0.06	-2.02	0.12	-3.06
HW05-3 230-232 a	230.11	27.158	-5.16	0.06	-1.79	0.12	-2.83
HW05-3 232-234 a	232.11	27.217	-5.45	0.06	-1.79	0.12	-2.83
HW05-3 234-236 a	234.11	27.276	-4.97	0.06	-1.92	0.12	-2.96
HW05-3 236-238 a	236.11	27.335	-8.07	0.06	-3.07	0.12	-4.11
HW05-3 238-240 a	238.11	27.394	-8.59	0.06	-3.21	0.12	-4.25
HW05-3 238-240 e	239.00	27.420	-8.11	0.06	-2.92	0.12	-3.96
HW05-3 240-242 a	240.11	27.453	-5.16	0.06	-1.99	0.12	-3.03
HW05-3 240-242 e	241.00	27.479	-5.74	0.06	-2.2	0.12	-3.24
HW05-3 242-244 a	242.11	27.512	-7.76	0.06	-2.88	0.12	-3.92
HW05-3 242-244 e	243.00	27.538	-8.02	0.06	-2.86	0.12	-3.90
HW05-3 244-246 a	244.11	27.570	-8.38	0.06	-2.94	0.12	-3.98
HW05-3 244-246 e	245.00	27.597	-7.45	0.06	-2.77	0.12	-3.81
HW05-3 246-248 a	246.11	27.629	-4.27	0.06	-1.48	0.12	-2.52
HW05-3 246-248 e	247.00	27.656	-5.59	0.06	-2.16	0.12	-3.20
HW05-3 248-250 a	248.11	27.688	-7.34	0.06	-2.64	0.12	-3.68
HW05-3 248-250 e	249.00	27.715	-7.02	0.06	-2.65	0.12	-3.69
HW05-3 250-252 a	250.11	27.747	-6.15	0.06	-2.25	0.12	-3.29

Table E.1 (continued)

Sample	Depth (mm)	Age (kyr B.P.)	$\delta^{13}C$ (‰)	$\delta^{13}C$ st. dev.	$\delta^{18}O$ (‰)	$\delta^{18}O$ st. dev.	$\delta^{18}O$ ice vol. adj.
HW05-3 250-252 e	251.00	27.774	-5.22	0.06	-1.99	0.12	-3.03
HW05-3 252-254 a	252.11	27.806	-4.19	0.06	-1.86	0.12	-2.90
HW05-3 252-254 e	253.00	27.833	-6.65	0.06	-2.58	0.12	-3.62
HW05-3 254-256 a	254.11	27.865	-5.64	0.06	-2.25	0.12	-3.29
HW05-3 254-256 e	255.00	27.892	-6.22	0.06	-2.26	0.12	-3.30
HW05-3 256-258 a	256.11	27.924	-7.02	0.06	-2.51	0.12	-3.55
HW05-3 256-258 e	257.00	27.951	-7.66	0.06	-2.67	0.12	-3.71
HW05-3 258-260 a	258.11	27.983	-5.82	0.06	-2.4	0.12	-3.43
HW05-3 258-260 e	259.00	28.010	-6.62	0.06	-2.28	0.12	-3.31
HW05-3 260-262 a	260.11	28.042	-6.64	0.06	-2.04	0.12	-3.07
HW05-3 260-262 e	261.00	28.069	-7.87	0.06	-2.71	0.12	-3.73
HW05-3 262-264 a	262.11	28.101	-8.9	0.06	-3.1	0.12	-4.12
HW05-3 262-264 e	263.00	28.128	-8.96	0.06	-3.12	0.12	-4.14
HW05-3 264-266 a	264.11	28.157	-8.43	0.06	-2.86	0.12	-3.88
HW05-3 264-266 e	265.00	28.206	-3.8	0.06	-1.87	0.12	-2.88
HW05-3 266-268 a	266.11	28.268	-5.56	0.06	-1.91	0.12	-2.92
HW05-3 266-268 e	267.00	28.317	-6.77	0.06	-2.12	0.12	-3.13
HW05-3 268-270 a	268.11	28.378	-7.9	0.06	-2.19	0.12	-3.19
HW05-3 268-270 e	269.00	28.427	-9.12	0.06	-2.82	0.12	-3.82
HW05-3 270-272 a	270.11	28.489	-4.09	0.06	-1.46	0.12	-2.46
HW05-3 270-272 e	271.00	28.538	-7.39	0.06	-2.32	0.12	-3.31
HW05-3 272-274 a	272.11	28.600	-5.58	0.06	-1.66	0.12	-2.65
HW05-3 272-274 e	273.00	28.649	-4.25	0.06	-1.56	0.12	-2.55
HW05-3 274-276 a	274.11	28.710	-6.76	0.06	-1.88	0.12	-2.86
HW05-3 274-276 e	275.00	28.759	-5.16	0.06	-1.84	0.12	-2.82
HW05-3 276-278 a	276.11	28.821	-7.39	0.06	-2.34	0.12	-3.31
HW05-3 276-278 e	277.00	28.870	-8.57	0.06	-2.75	0.12	-3.72
HW05-3 278-280 a	278.11	28.932	-7.43	0.06	-2.06	0.12	-3.03
HW05-3 278-280 e	279.00	28.981	-7.55	0.06	-2.16	0.12	-3.12
HW05-3 280-282 a	280.11	29.042	-8.25	0.06	-2.6	0.12	-3.56
HW05-3 280-282 e	281.00	29.091	-7.93	0.06	-2.59	0.12	-3.55
HW05-3 282-284 a	282.11	29.153	-7.92	0.06	-2.66	0.12	-3.61
HW05-3 282-284 e	283.00	29.202	-5.92	0.06	-2.04	0.12	-2.99
HW05-3 284-286 a	284.11	29.263	-7.24	0.06	-2.24	0.12	-3.18
HW05-3 284-286 e	285.00	29.313	-6.96	0.06	-2.04	0.12	-2.98
HW05-3 286-288 a	286.11	29.374	-7.84	0.06	-2.43	0.12	-3.37
HW05-3 286-288 e	287.00	29.423	-8.04	0.06	-2.42	0.12	-3.35
HW05-3 288-290 a	288.11	29.485	-7.98	0.06	-2.24	0.12	-3.17
HW05-3 288-290 e	289.00	29.534	-8.17	0.06	-2.33	0.12	-3.26
HW05-3 290-292 a	290.11	29.595	-8.18	0.06	-2.4	0.12	-3.32
HW05-3 290-292 e	291.00	29.645	-7.94	0.06	-2.43	0.12	-3.35
HW05-3 292-294 a	292.11	29.706	-7.26	0.06	-1.66	0.12	-2.58
HW05-3 292-294 e	293.00	29.755	-8.25	0.06	-2.55	0.12	-3.46
HW05-3 294-296 a	294.11	29.817	-8.23	0.06	-2.3	0.12	-3.21
HW05-3 294-296 e	295.00	29.872	-4.18	0.06	-1.44	0.12	-2.34
HW05-3 296-298 a	296.11	29.901	-4.54	0.06	-1.5	0.12	-2.40
HW05-3 296-298 e	297.00	29.924	-7.01	0.06	-2.22	0.12	-3.12
HW05-3 298-300 a	298.11	29.953	-8.16	0.06	-2.63	0.12	-3.53
HW05-3 298-300 e	299.00	29.977	-8.58	0.06	-2.89	0.12	-3.79
HW05-3 300-302 a	300.11	30.006	-8.53	0.06	-2.86	0.12	-3.75
HW05-3 300-302 e	301.00	30.029	-8.77	0.06	-2.89	0.12	-3.78

Table E.1 (continued)

Sample		Depth (mm)	Age (kyr B.P.)	$\delta^{13}C$ (‰)	$\delta^{13}C$ st. dev.	$\delta^{18}O$ (‰)	$\delta^{18}O$ st. dev.	$\delta^{18}O$ ice vol. adj.
HW05-3	302-304 a	302.11	30.058	-8.76	0.06	-2.86	0.12	-3.75
HW05-3	302-304 e	303.00	30.081	-8.28	0.06	-2.73	0.12	-3.61
HW05-3	304-306 a	304.11	30.110	-7.66	0.06	-2.66	0.12	-3.54
HW05-3	304-306 e	305.00	30.133	-7.91	0.06	-2.69	0.12	-3.57
HW05-3	306-308 a	306.11	30.162	-8.08	0.06	-2.89	0.12	-3.76
HW05-3	306-308 e	307.00	30.186	-7.32	0.06	-2.79	0.12	-3.66
HW05-3	308-310 a	308.11	30.215	-8.78	0.06	-2.87	0.12	-3.73
HW05-3	308-310 e	309.00	30.238	-6.7	0.06	-1.86	0.12	-2.72
HW05-3	310-312 a	310.11	30.267	-8.93	0.06	-3.08	0.12	-3.94
HW05-3	310-312 e	311.00	30.290	-8.81	0.06	-3.03	0.12	-3.88
HW05-3	312-314 a	312.11	30.319	-6.67	0.06	-2.24	0.12	-3.09
HW05-3	312-314 e	313.00	30.342	-6.2	0.06	-1.94	0.12	-2.78
HW05-3	314-316 a	314.11	30.371	-6.45	0.06	-1.88	0.12	-2.72
HW05-3	314-316 e	315.00	30.395	-3.95	0.06	-1.65	0.12	-2.49
HW05-3	316-318 a	316.11	30.424	-6.9	0.06	-2.22	0.12	-3.05
HW05-3	316-318 e	317.00	30.447	-6.5	0.06	-2.35	0.12	-3.18
HW05-3	318-320 a	318.11	30.476	-8.53	0.06	-2.92	0.12	-3.74
HW05-3	318-320 e	319.00	30.499	-8.45	0.06	-3.16	0.12	-3.98
HW05-3	320-322 a	320.11	30.732	-6.95	0.06	-2.22	0.12	-3.01
HW05-3	320-322 e	321.00	30.919	-2.83	0.06	-2.59	0.12	-3.35
HW05-3	322-324 a	322.11	31.152	-2.26	0.06	-1.17	0.12	-1.90
HW05-3	322-324 e	323.00	31.339	-7.67	0.06	-2.62	0.12	-3.32
HW05-3	324-326 a	324.11	31.572	-3.41	0.06	-1.47	0.12	-2.14
HW05-3	324-326 e	325.00	31.758	-3.58	0.06	-1.74	0.12	-2.38
HW05-3	326-328 a	326.11	31.992	-3	0.06	-1.6	0.12	-2.21
HW05-3	326-328 e	327.00	32.178	-5.68	0.06	-2.49	0.12	-3.10
HW05-3	328-330 a	328.11	32.412	-9.02	0.06	-3.39	0.12	-4.01
HW05-3	328-330 e	329.00	32.598	-5.62	0.06	-2.37	0.12	-3.00
HW05-3	330-332 a	330.11	32.831	-7.56	0.06	-3.06	0.12	-3.70
HW05-3	330-332 e	331.00	33.018	-5.94	0.06	-2.48	0.12	-3.12
HW05-3	332-334 a	332.11	33.251	-6.01	0.06	-3.47	0.12	-4.12
HW05-3	332-334 e	333.00	33.438	-3.36	0.06	-1.89	0.12	-2.55
HW05-3	334-336 a	334.11	33.671	-4.37	0.06	-1.97	0.12	-2.64
HW05-3	334-336 e	335.00	33.858	-4.11	0.06	-2.02	0.12	-2.70
HW05-3	336-338 a	336.11	34.091	-4.07	0.06	-1.73	0.12	-2.41
HW05-3	336-338 e	337.00	34.277	-3.39	0.06	-1.83	0.12	-2.51
HW05-3	338-340 a	338.11	34.511	-3.13	0.06	-1.4	0.12	-2.07
HW05-3	338-340 e	339.00	34.697	-5.88	0.06	-2.3	0.12	-2.96
HW05-3	340-342 a	340.11	34.930	-5.45	0.06	-2.1	0.12	-2.75
HW05-3	340-342 e	341.00	35.117	-4.54	0.06	-1.97	0.12	-2.62
HW05-3	342-344 a	342.11	35.332	-4.29	0.06	-2.01	0.12	-2.65
HW05-3	342-344 e	343.00	35.503	-5.46	0.06	-2.7	0.12	-3.33
HW05-3	344-346 a	344.11	35.718	-5.8	0.06	-2.66	0.12	-3.29
HW05-3	344-346 e	345.00	35.889	-6.37	0.06	-2.94	0.12	-3.56
HW05-3	346-348 a	346.11	36.104	-5.7	0.06	-2.78	0.12	-3.39
HW05-3	346-348 e	347.00	36.276	-6.69	0.06	-3.12	0.12	-3.73
HW05-3	348-350 a	348.11	36.490	-5.82	0.06	-2.66	0.12	-3.26
HW05-3	348-350 e	349.00	36.662	-6.72	0.06	-3	0.12	-3.59
HW05-3	350-352 a	350.11	36.876	-5.91	0.06	-2.77	0.12	-3.36
HW05-3	350-352 e	351.00	37.048	-6.98	0.06	-3.35	0.12	-3.93
HW05-3	352-354 a	352.11	37.263	-5.72	0.06	-2.97	0.12	-3.57

Table E.1 (continued)

Sample		Depth (mm)	Age (kyr B.P.)	$\delta^{13}C$ (‰)	$\delta^{13}C$ st. dev.	$\delta^{18}O$ (‰)	$\delta^{18}O$ st. dev.	$\delta^{18}O$ ice vol. adj.
HW05-3	352-354 e	353.00	37.434	-6.37	0.06	-3	0.12	-3.61
HW05-3	352-354 i	353.89	37.606	-6.65	0.06	-3.11	0.12	-3.73
HW05-3	354-356 e	355.00	37.820	-6.89	0.06	-3.40	0.12	-4.03
HW05-3	354-356 i	355.89	37.992	-6.94	0.06	-3.37	0.12	-4.01
HW05-3	356-358 e	357.00	38.207	-2.81	0.06	-2.22	0.12	-2.87
HW05-3	358-360 a	358.11	38.421	-6.28	0.06	-3.06	0.12	-3.71
HW05-3	358-360 e	359.00	38.593	-6.38	0.06	-3.07	0.12	-3.72
HW05-3	360-362 a	360.11	38.807	-4.53	0.06	-2.47	0.12	-3.13
HW05-3	360-362 e	361.00	38.979	-6.5	0.06	-3.26	0.12	-3.92
HW05-3	362-364 a	362.11	39.036	-5.87	0.06	-3.1	0.12	-3.76
HW05-3	362-364 e	363.00	39.082	-7.01	0.06	-3.15	0.12	-3.81
HW05-3	364-366 a	364.11	39.138	-7.5	0.06	-3.46	0.12	-4.12
HW05-3	364-366 e	365.00	39.184	-7.49	0.06	-3.64	0.12	-4.30
HW05-3	366-368 a	366.11	39.241	-5.01	0.06	-2.84	0.12	-3.50
HW05-3	366-368 e	367.00	39.287	-6.5	0.06	-3.25	0.12	-3.91
HW05-3	368-370 a	368.11	39.343	-7.68	0.06	-3.46	0.12	-4.13
HW05-3	368-370 e	369.00	39.389	-7.63	0.06	-3.38	0.12	-4.05
HW05-3	370-372 a	370.11	39.446	-6.85	0.06	-3.39	0.12	-4.06
HW05-3	370-372 e	371.00	39.492	-7.21	0.06	-3.33	0.12	-4.00
HW05-3	372-374 a	372.11	39.549	-8.61	0.06	-4.08	0.12	-4.75
HW05-3	372-374 e	373.00	39.594	-6.87	0.06	-3.15	0.12	-3.82
HW05-3	374-376 a	374.11	39.651	-6.93	0.06	-3.43	0.12	-4.10
HW05-3	374-376 e	375.00	39.697	-4.66	0.06	-2.34	0.12	-3.01
HW05-3	376-378 a	376.11	39.754	-6.1	0.06	-2.9	0.12	-3.57
HW05-3	376-378 e	377.00	39.799	-5.76	0.06	-2.96	0.12	-3.63
HW05-3	378-380 a	378.11	39.856	-5.44	0.06	-2.98	0.12	-3.65
HW05-3	378-380 e	379.00	39.902	-6.9	0.06	-3.36	0.12	-4.03
HW05-3	380-382 a	380.11	39.959	-4.52	0.06	-2.5	0.12	-3.18
HW05-3	380-382 e	381.00	40.004	-5.2	0.06	-2.71	0.12	-3.39
HW05-3	382-384 a	382.11	40.061	-4.61	0.06	-2.59	0.12	-3.27
HW05-3	382-384 e	383.00	40.107	-4.56	0.06	-2.73	0.12	-3.40
HW05-3	384-386 a	384.11	40.164	-5.81	0.06	-2.95	0.12	-3.62
HW05-3	384-386 e	385.00	40.209	-5.46	0.06	-2.69	0.12	-3.36
HW05-3	386-388 a	386.11	40.266	-4.7	0.06	-2.76	0.12	-3.43
HW05-3	386-388 e	387.00	40.312	-5.78	0.06	-3.08	0.12	-3.75
HW05-3	388-390 a	388.11	40.369	-6.09	0.06	-3.27	0.12	-3.94
HW05-3	388-390 e	389.00	40.414	-5.51	0.06	-3.12	0.12	-3.79
HW05-3	390-392 a	390.11	40.471	-4.99	0.06	-3	0.12	-3.67
HW05-3	390-392 e	391.00	40.517	-4.91	0.06	-2.92	0.12	-3.59
HW05-3	392-394 a	392.11	40.574	-5.55	0.06	-3.01	0.12	-3.68
HW05-3	392-394 e	393.00	40.619	-5.47	0.06	-3.07	0.12	-3.74
HW05-3	394-396 a	394.11	40.676	-6.79	0.06	-3.39	0.12	-4.06
HW05-3	394-396 e	395.00	40.722	-5.56	0.06	-2.97	0.12	-3.64
HW05-3	396-398 a	396.11	40.779	-6.51	0.06	-3.58	0.12	-4.25
HW05-3	396-398 e	397.00	40.824	-5.91	0.06	-3.16	0.12	-3.83
HW05-3	398-400 a	398.11	40.881	-5.85	0.06	-3.16	0.12	-3.83
HW05-3	398-400 e	399.00	40.927	-4.23	0.06	-2.6	0.12	-3.27
HW05-3	400-402 e	401.00	41.029	-5.6	0.06	-3.03	0.12	-3.70
HW05-3	402-404 a	402.11	41.086	-5.83	0.06	-3.23	0.12	-3.90
HW05-3	402-404 e	403.00	41.132	-5.8	0.06	-3.01	0.12	-3.68
HW05-3	404-406 a	404.11	41.189	-5.87	0.06	-3.09	0.12	-3.76

Table E.1 (continued)

Sample	Depth (mm)	Age (kyr B.P.)	$\delta^{13}C$ (‰)	$\delta^{13}C$ st. dev.	$\delta^{18}O$ (‰)	$\delta^{18}O$ st. dev.	$\delta^{18}O$ ice vol. adj.
HW05-3 404-406 e	405.00	41.234	-6.21	0.06	-3.27	0.12	-3.94
HW05-3 406-408 a	406.11	41.291	-5.06	0.06	-2.77	0.12	-3.44
HW05-3 406-408 e	407.00	41.337	-5.35	0.06	-2.61	0.12	-3.28
HW05-3 408-410 a	408.11	41.394	-6.47	0.06	-3.46	0.12	-4.12
HW05-3 408-410 e	409.00	41.439	-5.48	0.06	-2.99	0.12	-3.65
HW05-3 410-412 a	410.11	41.496	-4.59	0.06	-2.55	0.12	-3.21
HW05-3 410-412 e	411.00	41.542	-5.72	0.06	-3.13	0.12	-3.79
HW05-3 412-414 a	412.11	41.599	-5.58	0.06	-2.98	0.12	-3.64
HW05-3 412-414 e	413.00	41.644	-5.31	0.06	-2.77	0.12	-3.43
HW05-3 414-416 a	414.11	41.701	-5.53	0.06	-3.06	0.12	-3.72
HW05-3 414-416 e	415.00	41.747	-5.74	0.06	-3.23	0.12	-3.89
HW05-3 416-418 a	416.11	41.804	-5.87	0.06	-3.28	0.12	-3.94
HW05-3 416-418 e	417.00	41.849	-4.09	0.06	-2.58	0.12	-3.24
HW05-3 418-420 a	418.11	41.906	-4.99	0.06	-2.86	0.12	-3.52
HW05-3 418-420 e	419.00	41.952	-5.92	0.06	-3.2	0.12	-3.86
HW05-3 420-422 a	420.11	42.009	-5.72	0.06	-3.07	0.12	-3.73
HW05-3 420-422 e	421.00	42.054	-6.98	0.06	-3.56	0.12	-4.21
HW05-3 422-424 a	422.11	42.111	-5.54	0.06	-3.01	0.12	-3.66
HW05-3 422-424 e	423.00	42.157	-5.29	0.06	-3.15	0.12	-3.80
HW05-3 424-426 a	424.11	42.214	-6.22	0.06	-3.41	0.12	-4.05
HW05-3 424-426 e	425.00	42.259	-6.44	0.06	-3.61	0.12	-4.25
HW05-3 426-428 a	426.11	42.316	-5.22	0.06	-2.94	0.12	-3.57
HW05-3 426-428 e	427.00	42.362	-4.85	0.06	-2.71	0.12	-3.34
HW05-3 428-430 a	428.11	42.419	-4.75	0.06	-2.75	0.12	-3.37
HW05-3 428-430 e	429.00	42.464	-6.1	0.06	-3.18	0.12	-3.80
HW05-3 430-432 a	430.11	42.521	-5.94	0.06	-3.18	0.12	-3.79
HW05-3 430-432 e	431.00	42.567	-6.21	0.06	-3.28	0.12	-3.89
HW05-3 432-434 a	432.11	42.624	-6.61	0.06	-3.51	0.12	-4.11
HW05-3 432-434 e	433.00	42.669	-5.87	0.06	-3.12	0.12	-3.72
HW05-3 434-436 a	434.11	42.726	-6.16	0.06	-3.18	0.12	-3.78
HW05-3 434-436 e	435.00	42.772	-5.73	0.06	-2.87	0.12	-3.46
HW05-3 436-438 a	436.11	42.829	-6.82	0.06	-3.46	0.12	-4.05
HW05-3 436-438 e	437.00	42.874	-5.35	0.06	-3.08	0.12	-3.66
HW05-3 438-440 a	438.11	42.931	-5.98	0.06	-3.13	0.12	-3.71
HW05-3 438-440 e	439.00	42.977	-5.79	0.06	-3.17	0.12	-3.74
HW05-3 440-442 a	440.11	43.034	-5.89	0.06	-2.99	0.12	-3.56
HW05-3 440-442 b	440.33	43.045	-5.83	0.06	-3.07	0.12	-3.64
HW05-3 440-442 d	440.78	43.068	-5.74	0.06	-3.02	0.12	-3.59
HW05-3 440-442 e	441.00	43.079	-5.86	0.06	-3.07	0.12	-3.64
HW05-3 440-442 f	441.22	43.091	-5.86	0.06	-3.03	0.12	-3.59
HW05-3 440-442 h	441.67	43.114	-5.55	0.06	-3.06	0.12	-3.62
HW05-3 440-442 i	441.89	43.125	-5.55	0.06	-2.98	0.12	-3.54
HW05-3 442-444 a	442.11	43.136	-5.4	0.06	-2.84	0.12	-3.40
HW05-3 442-444 b	442.33	43.148	-5.32	0.06	-2.82	0.12	-3.38
HW05-3 442-444 d	442.78	43.171	-5.35	0.06	-2.78	0.12	-3.34
HW05-3 442-444 e	443.00	43.182	-5.82	0.06	-3.18	0.12	-3.74
HW05-3 442-444 f	443.22	43.193	-5.42	0.06	-2.9	0.12	-3.46
HW05-3 442-444 h	443.67	43.216	-5.83	0.06	-3.06	0.12	-3.61
HW05-3 444-446 a	444.11	43.239	-4.76	0.06	-2.7	0.12	-3.25
HW05-3 444-446 b	444.33	43.250	-4.97	0.06	-2.97	0.12	-3.52
HW05-3 444-446 c	444.56	43.262	-5.49	0.06	-3.21	0.12	-3.76

Table E.1 (continued)

Sample	Depth (mm)	Age (kyr B.P.)	$\delta^{13}C$ (‰)	$\delta^{13}C$ st. dev.	$\delta^{18}O$ (‰)	$\delta^{18}O$ st. dev.	$\delta^{18}O$ ice vol. adj.
HW05-3 444-446 d	444.78	43.273	-5.61	0.06	-3.16	0.12	-3.71
HW05-3 444-446 e	445.00	43.284	-5.88	0.06	-3.09	0.12	-3.64
HW05-3 444-446 f	445.22	43.296	-6.34	0.06	-3.31	0.12	-3.86
HW05-3 444-446 g	445.44	43.307	-6.02	0.06	-3.03	0.12	-3.58
HW05-3 444-446 h	445.67	43.319	-5.74	0.06	-3.04	0.12	-3.58
HW05-3 444-446 i	445.89	43.330	-6.45	0.06	-3.19	0.12	-3.73
HW05-3 446-448 a	446.11	43.341	-6.06	0.06	-3.08	0.12	-3.62
HW05-3 446-448 b	446.33	43.353	-5.4	0.06	-2.79	0.12	-3.33
HW05-3 446-448 c	446.56	43.364	-5.01	0.06	-2.81	0.12	-3.35
HW05-3 446-448 d	446.78	43.376	-5.31	0.06	-2.8	0.12	-3.34
HW05-3 446-448 e	447.00	43.387	-5.13	0.06	-2.8	0.12	-3.34
HW05-3 446-448 f	447.22	43.643	-5.41	0.06	-2.96	0.12	-3.48
HW05-3 446-448 g	447.44	43.899	-5.41	0.06	-2.74	0.12	-3.23
HW05-3 446-448 h	447.67	44.154	-5.32	0.06	-2.7	0.12	-3.20
HW05-3 448-450 a	448.11	44.666	-5.76	0.06	-3.02	0.12	-3.54
HW05-3 448-450 b	448.33	44.922	-5	0.06	-2.74	0.12	-3.28
HW05-3 448-450 c	448.56	45.178	-5.13	0.06	-2.76	0.12	-3.31
HW05-3 448-450 d	448.78	45.434	-5.04	0.06	-2.43	0.12	-3.00
HW05-3 448-450 e	449.00	45.689	-5.3	0.06	-2.55	0.12	-3.13
HW05-3 448-450 f	449.22	45.945	-5.79	0.06	-2.83	0.12	-3.42
HW05-3 448-450 g	449.44	46.201	-6	0.06	-2.86	0.12	-3.45
HW05-3 448-450 h	449.67	46.457	-5.91	0.06	-3.05	0.12	-3.62
HW05-3 448-450 i	449.89	46.713	-5.53	0.06	-2.98	0.12	-3.54
HW05-3 450-452 a	450.11	46.969	-4.63	0.06	-2.72	0.12	-3.26
HW05-3 450-452 b	450.33	47.224	-4.24	0.06	-2.72	0.12	-3.25
HW05-3 450-452 d	450.78	47.736	-5.38	0.06	-3.26	0.12	-3.76
HW05-3 450-452 e	451.00	47.992	-5.92	0.06	-3.5	0.12	-3.99
HW05-3 450-452 f	451.22	48.248	-5.61	0.06	-3.29	0.12	-3.76
HW05-3 450-452 g	451.44	48.503	-5.52	0.06	-3.09	0.12	-3.55
HW05-3 450-452 h	451.67	48.759	-5.32	0.06	-3.12	0.12	-3.57
HW05-3 450-452 i	451.89	49.015	-5.3	0.06	-3.06	0.12	-3.49
HW05-3 452-454 a	452.11	49.143	-5.7	0.06	-3.21	0.12	-3.65
HW05-3 452-454 b	452.33	49.226	-6.11	0.06	-3.46	0.12	-3.90
HW05-3 452-454 c	452.56	49.309	-5.92	0.06	-3.36	0.12	-3.80
HW05-3 452-454 d	452.78	49.393	-5.72	0.06	-3.18	0.12	-3.63
HW05-3 452-454 e	453.00	49.476	-6.12	0.06	-3.31	0.12	-3.76
HW05-3 452-454 f	453.22	49.559	-6.64	0.06	-3.47	0.12	-3.92
HW05-3 452-454 g	453.44	49.642	-5.86	0.06	-3.57	0.12	-4.03
HW05-3 452-454 h	453.67	49.726	-5.61	0.06	-3.21	0.12	-3.67
HW05-3 452-454 i	453.89	49.809	-5.79	0.06	-3.24	0.12	-3.70
HW05-3 454-456 a	454.11	49.892	-6.01	0.06	-3.49	0.12	-3.95
HW05-3 454-456 b	454.33	49.975	-6.15	0.06	-3.41	0.12	-3.88
HW05-3 454-456 c	454.56	50.058	-5.73	0.06	-3.27	0.12	-3.74
HW05-3 454-456 d	454.78	50.142	-4.98	0.06	-2.8	0.12	-3.27
HW05-3 454-456 e	455.00	50.225	-5.11	0.06	-2.97	0.12	-3.45
HW05-3 454-456 f	455.22	50.308	-5.25	0.06	-2.95	0.12	-3.43
HW05-3 454-456 g	455.44	50.391	-5.63	0.06	-3.16	0.12	-3.64
HW05-3 454-456 h	455.67	50.475	-5.44	0.06	-2.99	0.12	-3.48
HW05-3 454-456 i	455.89	50.558	-6.16	0.06	-3.34	0.12	-3.83
HW05-3 456-458 a	456.11	50.641	-5	0.06	-2.98	0.12	-3.46
HW05-3 456-458 b	456.33	50.724	-4.74	0.06	-2.65	0.12	-3.13

Table E.1 (continued)

Sample	Depth (mm)	Age (kyr B.P.)	$\delta^{13}C$ (‰)	$\delta^{13}C$ st. dev.	$\delta^{18}O$ (‰)	$\delta^{18}O$ st. dev.	$\delta^{18}O$ ice vol. adj.
HW05-3 456-458 c	456.56	50.807	-3.97	0.06	-2.42	0.12	-2.89
HW05-3 456-458 d	456.78	50.891	-3.9	0.06	-2.5	0.12	-2.97
HW05-3 456-458 e	457.00	50.974	-3.76	0.06	-2.62	0.12	-3.08
HW05-3 456-458 f	457.22	51.057	-4.11	0.06	-2.46	0.12	-2.92
HW05-3 456-458 g	457.44	51.140	-5.56	0.06	-3.13	0.12	-3.58
HW05-3 456-458 h	457.67	51.224	-4.97	0.06	-2.65	0.12	-3.10
HW05-3 456-458 i	457.89	51.307	-4.9	0.06	-2.55	0.12	-3.00
HW05-3 458-460 a	458.11	51.390	-4.53	0.06	-2.64	0.12	-3.08
HW05-3 458-460 b	458.33	51.473	-5.61	0.06	-2.77	0.12	-3.21
HW05-3 458-460 c	458.56	51.556	-5.88	0.06	-2.91	0.12	-3.34
HW05-3 458-460 d	458.78	51.640	-5.09	0.06	-2.97	0.12	-3.40
HW05-3 458-460 e	459.00	51.723	-5.75	0.06	-3.17	0.12	-3.59
HW05-3 458-460 f	459.22	51.806	-3.75	0.06	-2.43	0.12	-2.85
HW05-3 458-460 g	459.44	51.889	-4.68	0.06	-2.72	0.12	-3.14
HW05-3 458-460 h	459.67	51.973	-5.55	0.06	-2.88	0.12	-3.29
HW05-3 458-460 i	459.89	52.056	-5.13	0.06	-2.8	0.12	-3.21
HW05-3 460-462 a	460.11	52.139	-5.63	0.06	-3.02	0.12	-3.45
HW05-3 460-462 b	460.33	52.222	-5.89	0.06	-3.12	0.12	-3.56
HW05-3 460-462 c	460.56	52.305	-6.49	0.06	-3.13	0.12	-3.58
HW05-3 460-462 d	460.78	52.389	-6.51	0.06	-3.21	0.12	-3.67
HW05-3 460-462 e	461.00	52.472	-5.77	0.06	-2.86	0.12	-3.33
HW05-3 460-462 f	461.22	52.555	-4.07	0.06	-2.4	0.12	-2.88
HW05-3 460-462 g	461.44	52.638	-3.86	0.06	-2.4	0.12	-2.90
HW05-3 460-462 h	461.67	52.722	-4.33	0.06	-2.38	0.12	-2.89
HW05-3 460-462 i	461.89	52.805	-4.2	0.06	-2.63	0.12	-3.15
HW05-3 462-464 a	462.11	52.888	-4.39	0.06	-2.71	0.12	-3.24
HW05-3 462-464 b	462.33	52.971	-4.31	0.06	-2.65	0.12	-3.19
HW05-3 462-464 c	462.56	53.054	-4.33	0.06	-2.7	0.12	-3.25
HW05-3 462-464 d	462.78	53.138	-4.3	0.06	-2.66	0.12	-3.21
HW05-3 462-464 e	463.00	53.221	-4.53	0.06	-2.77	0.12	-3.32
HW05-3 462-464 f	463.22	53.304	-4.98	0.06	-2.92	0.12	-3.47
HW05-3 462-464 g	463.44	53.387	-5.51	0.06	-3.33	0.12	-3.88
HW05-3 462-464 h	463.67	53.471	-4.46	0.06	-2.88	0.12	-3.43
HW05-3 462-464 i	463.89	53.554	-5.33	0.06	-3.21	0.12	-3.76
HW05-3 464-466 a	464.11	53.637	-5.87	0.06	-3.24	0.12	-3.79
HW05-3 464-466 b	464.33	53.720	-5.99	0.06	-3.38	0.12	-3.93
HW05-3 464-466 c	464.56	53.803	-5.67	0.06	-3.33	0.12	-3.88
HW05-3 464-466 d	464.78	53.887	-5.82	0.06	-3.31	0.12	-3.86
HW05-3 464-466 e	465.00	53.970	-5.78	0.06	-3.26	0.12	-3.81
HW05-3 464-466 f	465.22	54.053	-4.38	0.06	-2.6	0.12	-3.15
HW05-3 464-466 g	465.44	54.136	-3.95	0.06	-2.5	0.12	-3.05
HW05-3 464-466 h	465.67	54.220	-3.76	0.06	-2.44	0.12	-2.99
HW05-3 464-466 i	465.89	54.303	-4.32	0.06	-2.67	0.12	-3.22
HW05-3 466-468 a	466.11	54.386	-4.49	0.06	-2.66	0.12	-3.21
HW05-3 466-468 b	466.33	54.451	-5.06	0.06	-2.82	0.12	-3.37
HW05-3 466-468 d	466.78	54.581	-4.88	0.06	-3.07	0.12	-3.62
HW05-3 466-468 e	467.00	54.647	-5.24	0.06	-3.1	0.12	-3.65
HW05-3 466-468 f	467.22	54.712	-5.54	0.06	-3.19	0.12	-3.74
HW05-3 466-468 g	467.44	54.777	-5.39	0.06	-3.15	0.12	-3.70
HW05-3 466-468 h	467.67	54.842	-5.16	0.06	-2.97	0.12	-3.52
HW05-3 466-468 i	467.89	54.907	-5	0.06	-2.99	0.12	-3.54

Table E.1 (continued)

Sample	Depth (mm)	Age (kyr B.P.)	$\delta^{13}C$ (‰)	$\delta^{13}C$ st. dev.	$\delta^{18}O$ (‰)	$\delta^{18}O$ st. dev.	$\delta^{18}O$ ice vol. adj.
HW05-3 468-470 a	468.11	54.972	-5.01	0.06	-3.15	0.12	-3.70
HW05-3 468-470 b	468.33	55.037	-5.37	0.06	-3.19	0.12	-3.74
HW05-3 468-470 c	468.56	55.103	-6.12	0.06	-3.34	0.12	-3.89
HW05-3 468-470 d	468.78	55.168	-6.23	0.06	-3.54	0.12	-4.09
HW05-3 468-470 e	469.00	55.233	-6.05	0.06	-3.31	0.12	-3.86
HW05-3 468-470 f	469.22	55.298	-6.04	0.06	-3.4	0.12	-3.95
HW05-3 468-470 g	469.44	55.363	-6.03	0.06	-3.31	0.12	-3.86
HW05-3 468-470 h	469.67	55.428	-6.08	0.06	-3.5	0.12	-4.05
HW05-3 468-470 i	469.89	55.493	-6.16	0.06	-3.55	0.12	-4.10
HW05-3 470-472 a	470.11	55.559	-6.34	0.06	-3.7	0.12	-4.25
HW05-3 470-472 e	471.00	55.819	-5.47	0.06	-3.23	0.12	-3.78
HW05-3 472-474 a	472.11	56.145	-5.68	0.06	-3.44	0.12	-3.99
HW05-3 472-474 e	473.00	56.405	-6.37	0.06	-3.54	0.12	-4.09
HW05-3 474-476 a	474.11	56.731	-4.45	0.06	-2.76	0.12	-3.31
HW05-3 474-476 e	475.00	56.992	-4.29	0.06	-2.63	0.12	-3.18
HW05-3 476-478 a	476.11	57.317	-5.59	0.06	-3.27	0.12	-3.81
HW05-3 476-478 e	477.00	57.578	-5.67	0.06	-3.13	0.12	-3.66
HW05-3 478-480 a	478.11	57.904	-4.19	0.06	-2.74	0.12	-3.26
HW05-3 478-480 e	479.00	58.164	-3.86	0.06	-2.73	0.12	-3.25
HW05-3 480-482 a	480.11	58.490	-5.75	0.06	-3.25	0.12	-3.75
HW05-3 480-482 e	481.00	58.750	-5.58	0.06	-3.3	0.12	-3.80
HW05-3 482-484 a	482.11	59.076	-6.31	0.06	-3.37	0.12	-3.86
HW05-3 482-484 e	483.00	59.337	-5.84	0.06	-3.33	0.12	-3.81
HW05-3 484-486 a	484.11	59.662	-5.81	0.06	-3.43	0.12	-3.90
HW05-3 484-486 e	485.00	59.923	-5.45	0.06	-3.19	0.12	-3.65
HW05-3 486-488 a	486.11	60.249	-3.45	0.06	-2.39	0.12	-2.86
HW05-3 486-488 e	487.00	60.509	-5.51	0.06	-3.21	0.12	-3.69
HW05-3 488-490 a	488.11	60.835	-6.29	0.06	-3.16	0.12	-3.66
HW05-3 488-490 e	489.00	61.128	-6.15	0.06	-3.1	0.12	-3.62
HW05-3 490-492 a	490.11	61.185	-6.23	0.06	-3.18	0.12	-3.71
HW05-3 490-492 e	491.00	61.231	-7.19	0.06	-3.59	0.12	-4.12
HW05-3 492-494 a	492.11	61.288	-7.37	0.06	-3.79	0.12	-4.32
HW05-3 492-494 e	493.00	61.334	-6.21	0.06	-3.19	0.12	-3.73
HW05-3 494-496 a	494.11	61.391	-6.58	0.06	-3.72	0.12	-4.26
HW05-3 494-496 e	495.00	61.436	-7.49	0.06	-3.75	0.12	-4.29
HW05-3 496-498 a	496.11	61.494	-7.35	0.06	-3.55	0.12	-4.10
HW05-3 496-498 e	497.00	61.539	-7.71	0.06	-3.82	0.12	-4.37
HW05-3 498-500 a	498.11	61.596	-7.31	0.06	-3.72	0.12	-4.27
HW05-3 498-500 e	499.00	61.642	-7.59	0.06	-3.78	0.12	-4.34
HW05-3 500-502 a	500.11	61.699	-7.75	0.06	-3.95	0.12	-4.51
HW05-3 500-502 e	501.00	61.745	-6.79	0.06	-3.49	0.12	-4.05
HW05-3 502-504 a	502.11	61.802	-6.78	0.06	-3.41	0.12	-3.98
HW05-3 502-504 e	503.00	61.848	-7.73	0.06	-3.7	0.12	-4.27
HW05-3 504-506 a	504.11	61.905	-7.55	0.06	-3.47	0.12	-4.04
HW05-3 504-506 e	505.00	61.950	-7.06	0.06	-3.49	0.12	-4.07
HW05-3 506-508 a	506.11	62.008	-7.06	0.06	-3.42	0.12	-4.00
HW05-3 506-508 e	507.00	62.053	-7.16	0.06	-3.35	0.12	-3.93
HW05-3 508-510 a	508.11	62.110	-7.76	0.06	-3.66	0.12	-4.25
HW05-3 508-510 e	509.00	62.156	-7.45	0.06	-3.67	0.12	-4.26
HW05-3 510-512 a	510.11	62.213	-7.88	0.06	-3.77	0.12	-4.36
HW05-3 510-512 e	511.00	62.259	-8.18	0.06	-3.69	0.12	-4.29

Table E.1 (continued)

Sample	Depth (mm)	Age (kyr B.P.)	$\delta^{13}C$ (‰)	$\delta^{13}C$ st. dev.	$\delta^{18}O$ (‰)	$\delta^{18}O$ st. dev.	$\delta^{18}O$ ice vol. adj.
HW05-3 512-514 a	512.11	62.316	-7.15	0.06	-3.32	0.12	-3.92
HW05-3 512-514 e	513.00	62.362	-7.57	0.06	-3.54	0.12	-4.14
HW05-3 514-516 a	514.11	62.419	-7.6	0.06	-3.42	0.12	-4.03
HW05-3 514-516 e	515.00	62.464	-8.26	0.06	-3.72	0.12	-4.33
HW05-3 516-518 a	516.11	62.522	-7.14	0.06	-3.21	0.12	-3.82
HW05-3 516-518 e	517.00	62.567	-7.94	0.06	-3.6	0.12	-4.22
HW05-3 518-520 a	518.11	62.624	-8.34	0.06	-3.87	0.12	-4.49
HW05-3 518-520 e	519.00	62.670	-8.05	0.06	-3.8	0.12	-4.42
HW05-3 520-522 a	520.11	62.727	-7.79	0.06	-3.41	0.12	-4.04
HW05-3 520-522 e	521.00	62.773	-8.52	0.06	-3.76	0.12	-4.39
HW05-3 522-524 a	522.11	62.830	-8.5	0.06	-3.93	0.12	-4.56
HW05-3 522-524 e	523.00	62.876	-8.78	0.06	-3.87	0.12	-4.51
HW05-3 524-526 a	524.11	62.933	-8.63	0.06	-3.83	0.12	-4.47
HW05-3 524-526 e	525.00	62.978	-7.81	0.06	-3.44	0.12	-4.08
HW05-3 526-528 a	526.11	63.036	-8.13	0.06	-3.89	0.12	-4.53
HW05-3 526-528 e	527.00	63.081	-7.58	0.06	-3.39	0.12	-4.03
HW05-3 528-530 a	528.11	63.138	-7.57	0.06	-3.72	0.12	-4.36
HW05-3 528-530 e	529.00	63.184	-7.84	0.06	-3.39	0.12	-4.04
HW05-3 530-532 a	530.11	63.254	-7.07	0.06	-3.35	0.12	-4.00
HW05-3 530-532 e	531.00	63.309	-7.53	0.06	-3.13	0.12	-3.78
HW05-3 532-534 a	532.11	63.379	-7.86	0.06	-3.62	0.12	-4.27
HW05-3 532-534 e	533.00	63.434	-7.53	0.06	-3.17	0.12	-3.82
HW05-3 534-536 a	534.11	63.504	-7.93	0.06	-3.68	0.12	-4.33
HW05-3 534-536 e	535.00	63.560	-7.56	0.06	-3.38	0.12	-4.03
HW05-3 536-538 a	536.11	63.629	-8.39	0.06	-4.01	0.12	-4.66
HW05-3 536-538 e	537.00	63.685	-8.91	0.06	-3.91	0.12	-4.56
HW05-3 538-540 a	538.11	63.755	-8.92	0.06	-4.26	0.12	-4.91
HW05-3 538-540 e	539.00	63.810	-8.31	0.06	-3.77	0.12	-4.42
HW05-3 540-542 a	540.11	63.880	-8.61	0.06	-4.53	0.12	-5.18
HW05-3 540-542 e	541.00	63.935	-8.58	0.06	-3.91	0.12	-4.56
HW05-3 542-544 a	542.11	64.005	-8.63	0.06	-4.08	0.12	-4.73
HW05-3 542-544 e	543.00	64.061	-9.08	0.06	-4.06	0.12	-4.71
HW05-3 544-546 a	544.11	64.130	-9.01	0.06	-4.12	0.12	-4.77
HW05-3 544-546 e	545.00	64.186	-9.36	0.06	-4.02	0.12	-4.67
HW05-3 546-548 a	546.11	64.256	-9.17	0.06	-4.24	0.12	-4.89
HW05-3 546-548 e	547.00	64.311	-8.2	0.06	-3.51	0.12	-4.16
HW05-3 548-550 a	548.11	64.381	-7.95	0.06	-3.83	0.12	-4.48
HW05-3 548-550 e	549.00	64.436	-9.2	0.06	-3.83	0.12	-4.48
HW05-3 550-552 a	550.11	64.506	-7.97	0.06	-3.76	0.12	-4.41
HW05-3 550-552 e	551.00	64.562	-7.01	0.06	-3.22	0.12	-3.87
HW05-3 552-554 a	552.11	64.631	-6.66	0.06	-3.61	0.12	-4.26
HW05-3 552-554 e	553.00	64.687	-6.83	0.06	-3.49	0.12	-4.14
HW05-3 554-556 a	554.11	64.756	-7.64	0.06	-3.77	0.12	-4.42
HW05-3 554-556 e	555.00	64.812	-8.29	0.06	-3.63	0.12	-4.28
HW05-3 556-558 a	556.11	64.882	-8.45	0.06	-4.04	0.12	-4.69
HW05-3 556-558 e	557.00	64.937	-8.05	0.06	-3.82	0.12	-4.47
HW05-3 558-560 a	558.11	65.007	-7.96	0.06	-3.9	0.12	-4.55
HW05-3 558-560 e	559.00	65.063	-8.41	0.06	-3.89	0.12	-4.54
HW05-3 560-562 a	560.11	65.132	-7.31	0.06	-3.89	0.12	-4.54
HW05-3 560-562 e	561.00	65.188	-7.41	0.06	-3.6	0.12	-4.25
HW05-3 562-564 a	562.11	65.257	-8.03	0.06	-4.01	0.12	-4.66

Table E.1 (continued)

Sample	Depth (mm)	Age (kyr B.P.)	$\delta^{13}C$ (‰)	$\delta^{13}C$ st. dev.	$\delta^{18}O$ (‰)	$\delta^{18}O$ st. dev.	$\delta^{18}O$ ice vol. adj.
HW05-3 562-564 e	563.00	65.313	-8.37	0.06	-3.96	0.12	-4.61
HW05-3 564-566 a	564.11	65.383	-8.51	0.06	-3.89	0.12	-4.53
HW05-3 564-566 e	565.00	65.438	-8.36	0.06	-4.61	0.12	-5.25
HW05-3 566-568 a	566.11	65.508	-7.59	0.06	-3.32	0.12	-3.96
HW05-3 566-568 e	567.00	65.564	-8.45	0.06	-3.76	0.12	-4.40
HW05-3 568-570 a	568.11	65.633	-8.47	0.06	-3.66	0.12	-4.30
HW05-3 568-570 e	569.00	65.689	-8.53	0.06	-3.72	0.12	-4.36
HW05-3 570-572 a	570.11	65.758	-8.56	0.06	-3.88	0.12	-4.52
HW05-3 570-572 e	571.00	65.814	-8.73	0.06	-3.81	0.12	-4.44
HW05-3 572-574 a	572.11	65.884	-8.32	0.06	-3.69	0.12	-4.32
HW05-3 572-574 e	573.00	65.939	-8.66	0.06	-3.94	0.12	-4.57
HW05-3 574-576 a	574.11	66.009	-8.01	0.06	-3.78	0.12	-4.41
HW05-3 574-576 e	575.00	66.065	-6.53	0.06	-3.2	0.12	-3.83
HW05-3 576-578 a	576.11	66.134	-7.92	0.06	-3.55	0.12	-4.18
HW05-3 576-578 e	577.00	66.190	-7.72	0.06	-3.53	0.12	-4.16
HW05-3 578-580 a	578.11	66.259	-8.57	0.06	-3.88	0.12	-4.51
HW05-3 578-580 e	579.00	66.315	-8.59	0.06	-3.87	0.12	-4.49
HW05-3 580-582 a	580.11	66.385	-8.01	0.06	-3.6	0.12	-4.22
HW05-3 580-582 e	581.00	66.440	-8.59	0.06	-3.82	0.12	-4.44
HW05-3 582-584 a	582.11	66.510	-7.6	0.06	-3.65	0.12	-4.27
HW05-3 582-584 e	583.00	66.566	-7.43	0.06	-3.55	0.12	-4.17
HW05-3 584-586 a	584.11	66.635	-8.34	0.06	-3.77	0.12	-4.39
HW05-3 584-586 e	585.00	66.691	-8.7	0.06	-3.96	0.12	-4.58
HW05-3 586-588 a	586.11	66.760	-7.96	0.06	-3.86	0.12	-4.47
HW05-3 586-588 e	587.00	66.816	-8.27	0.06	-3.69	0.12	-4.30
HW05-3 588-590 a	588.11	66.886	-7.95	0.06	-3.87	0.12	-4.48
HW05-3 588-590 e	589.00	66.941	-7.89	0.06	-3.48	0.12	-4.09
HW05-3 590-592 a	590.11	67.011	-8.35	0.06	-4.01	0.12	-4.62
HW05-3 590-592 e	591.00	67.067	-7.74	0.06	-3.58	0.12	-4.19
HW05-3 592-594 a	592.11	67.136	-8.06	0.06	-3.9	0.12	-4.51
HW05-3 592-594 e	593.00	67.192	-8.77	0.06	-3.97	0.12	-4.58
HW05-3 594-596 a	594.11	67.261	-8.43	0.06	-3.72	0.12	-4.32
HW05-3 594-596 e	595.00	67.317	-7.8	0.06	-3.47	0.12	-4.07
HW05-3 596-598 a	596.11	67.515	-7.43	0.06	-3.33	0.12	-3.93
HW05-3 596-598 e	597.00	67.673	-6.85	0.06	-3.08	0.12	-3.68
HW05-3 598-600 a	598.11	67.871	-7.57	0.06	-3.64	0.12	-4.23
HW05-3 598-600 e	599.00	68.030	-6.59	0.06	-2.95	0.12	-3.54
HW05-3 600-602 a	600.11	68.228	-6.98	0.06	-3.29	0.12	-3.86
HW05-3 600-602 e	601.00	68.386	-6.48	0.06	-3.03	0.12	-3.59
HW05-3 602-604 a	602.11	68.584	-6.67	0.06	-3.23	0.12	-3.78
HW05-3 602-604 e	603.00	68.742	-6.60	0.06	-2.95	0.12	-3.49
HW05-3 604-606 a	604.11	68.940	-6.64	0.06	-2.86	0.12	-3.39
HW05-3 604-606 e	605.00	69.099	-7.28	0.06	-3.13	0.12	-3.64
HW05-3 606-608 a	606.11	69.297	-7.05	0.06	-3.03	0.12	-3.53
HW05-3 606-608 e	607.00	69.455	-7.31	0.06	-3.18	0.12	-3.67
HW05-3 608-610 a	608.11	69.653	-7.14	0.06	-3.24	0.12	-3.72
HW05-3 608-610 e	609.00	69.811	-7.68	0.06	-3.33	0.12	-3.80
HW05-3 610-612 a	610.11	70.009	-6.90	0.06	-2.90	0.12	-3.35
HW05-3 610-612 e	611.00	70.168	-7.82	0.06	-2.90	0.12	-3.34
HW05-3 612-614 a	612.11	70.365	-7.22	0.06	-3.11	0.12	-3.53
HW05-3 612-614 e	613.00	70.524	-7.01	0.06	-2.99	0.12	-3.40

Table E.1 (continued)

Sample		Depth (mm)	Age (kyr B.P.)	$\delta^{13}C$ (‰)	$\delta^{13}C$ st. dev.	$\delta^{18}O$ (‰)	$\delta^{18}O$ st. dev.	$\delta^{18}O$ ice vol. adj.
HW05-3	614-616 a	614.11	70.722	-7.31	0.06	-3.08	0.12	-3.47
HW05-3	614-616 e	615.00	70.880	-7.33	0.06	-3.32	0.12	-3.70
HW05-3	616-618 a	616.11	71.078	-7.25	0.06	-3.45	0.12	-3.82
HW05-3	616-618 e	617.00	71.236	-7.41	0.06	-3.22	0.12	-3.60
HW05-3	618-620 a	618.11	71.434	-7.68	0.06	-4.22	0.12	-4.60
HW05-3	618-620 e	619.00	71.593	-7.47	0.06	-3.18	0.12	-3.57
HW05-3	620-622 a	620.11	71.791	-7.10	0.06	-3.31	0.12	-3.71
HW05-3	620-622 e	621.00	71.949	-7.51	0.06	-3.45	0.12	-3.85
HW05-3	622-624 a	622.11	72.147	-8.07	0.06	-3.41	0.12	-3.82
HW05-3	622-624 e	623.00	72.305	-7.86	0.06	-3.16	0.12	-3.57
HW05-3	624-626 a	624.11	72.503	-7.66	0.06	-3.09	0.12	-3.51
HW05-3	624-626 e	625.00	72.662	-7.58	0.06	-3.37	0.12	-3.80
HW05-3	626-628 a	626.11	72.860	-7.24	0.06	-3.11	0.12	-3.54
HW05-3	626-628 e	627.00	73.018	-7.55	0.06	-3.37	0.12	-3.81
HW05-3	628-630 a	628.11	73.216	-8.09	0.06	-3.40	0.12	-3.85

Appendix F: RK05-1 Stable Isotope Data

Table F.1: Stable carbon and oxygen isotope ratios from RK05-1 calcite. Values are reported relative to Vienna Peedee Belemnite in per mil (‰) notation. Ages are reported as thousands of years before present (kyr B.P.), where present is defined as 2000 AD. Ice volume adjusted $\delta^{18}O$ values (ice vol. adj.) are also given.

Sample	Depth (mm)	Age (kyr B.P.)	$\delta^{13}C$ (‰)	$\delta^{13}C$ st. dev.	$\delta^{18}O$ (‰)	$\delta^{18}O$ st. dev.	$\delta^{18}O$ ice vol. adj.
RK05-1t 44-46 e	1.0	51.271	-3.01	0.06	-3.23	0.12	-3.68
RK05-1t 44-46 a	1.9	51.387	-2.23	0.06	-3.18	0.12	-3.62
RK05-1t 42-44 e	3.0	51.532	-2.29	0.06	-3.23	0.12	-3.66
RK05-1t 42-44 a	3.9	51.648	-3.44	0.06	-3.38	0.12	-3.81
RK05-1t 40-42 e	5.0	51.793	-2.91	0.06	-3.45	0.12	-3.87
RK05-1t 40-42 a	5.9	51.909	-2.96	0.06	-3.34	0.12	-3.75
RK05-1t 38-40 e	7.0	52.054	-3.81	0.06	-3.44	0.12	-3.86
RK05-1t 38-40 a	7.9	52.170	-4.53	0.06	-3.39	0.12	-3.82
RK05-1t 36-38 e	9.0	52.315	-2.40	0.06	-3.35	0.12	-3.80
RK05-1t 36-38 a	9.9	52.431	-2.99	0.06	-3.35	0.12	-3.82
RK05-1t 34-36 e	11.0	52.576	-3.74	0.06	-3.42	0.12	-3.91
RK05-1t 34-36 a	11.9	52.692	-3.07	0.06	-3.54	0.12	-4.05
RK05-1t 32-34 e	13.0	52.837	-2.70	0.06	-3.17	0.12	-3.70
RK05-1t 32-34 a	13.9	52.953	-4.04	0.06	-3.33	0.12	-3.87
RK05-1t 30-32 e	15.0	53.098	-4.56	0.06	-3.45	0.12	-4.00
RK05-1t 30-32 a	15.9	53.214	-3.77	0.06	-3.40	0.12	-3.95
RK05-1t 28-30 e	17.0	53.359	-3.77	0.06	-3.49	0.12	-4.04
RK05-1t 28-30 a	17.9	53.475	-2.26	0.06	-3.20	0.12	-3.75
RK05-1t 26-28 e	19.0	53.620	-3.32	0.06	-3.63	0.12	-4.18
RK05-1t 26-28 a	19.9	53.736	-3.18	0.06	-3.52	0.12	-4.07
RK05-1t 24-26 e	21.0	53.881	-3.71	0.06	-3.50	0.12	-4.05
RK05-1t 24-26 a	21.9	53.997	-4.36	0.06	-3.58	0.12	-4.13
RK05-1t 22-24 e	23.0	54.142	-3.35	0.06	-3.49	0.12	-4.04
RK05-1t 22-24 a	23.9	54.258	-3.57	0.06	-3.55	0.12	-4.10
RK05-1t 20-22 e	25.0	54.403	-4.54	0.06	-3.97	0.12	-4.52
RK05-1t 20-22 a	25.9	54.519	-4.05	0.06	-3.57	0.12	-4.12
RK05-1t 18-20 e	27.0	54.664	-2.87	0.06	-3.67	0.12	-4.22
RK05-1t 18-20 a	27.9	54.780	-4.00	0.06	-3.59	0.12	-4.14
RK05-1t 16-18 e	29.0	54.925	-3.37	0.06	-3.36	0.12	-3.91
RK05-1t 16-18 a	29.9	55.041	-3.51	0.06	-3.42	0.12	-3.97
RK05-1t 14-16 e	31.0	55.186	-4.36	0.06	-3.41	0.12	-3.96
RK05-1t 14-16 a	31.9	55.302	-4.48	0.06	-3.59	0.12	-4.14
RK05-1t 12-14 e	33.0	55.447	-2.66	0.06	-3.32	0.12	-3.87
RK05-1t 12-14 a	33.9	55.563	-2.80	0.06	-3.33	0.12	-3.88
RK05-1t 10-12 e	35.0	55.708	-3.11	0.06	-3.44	0.12	-3.99
RK05-1t 10-12 a	35.9	55.824	-3.40	0.06	-3.37	0.12	-3.92
RK05-1t 8-10 e	37.0	55.969	-3.44	0.06	-3.26	0.12	-3.81
RK05-1t 8-10 a	37.9	56.085	-3.50	0.06	-3.19	0.12	-3.74
RK05-1t 6-8 e	39.0	56.230	-2.53	0.06	-3.12	0.12	-3.67
RK05-1t 6-8 a	39.9	56.346	-2.35	0.06	-2.96	0.12	-3.51
RK05-1t 4-6 e	41.0	56.491	-3.34	0.06	-3.17	0.12	-3.72
RK05-1t 4-6 a	41.9	56.607	-3.65	0.06	-3.13	0.12	-3.68

Table F.1 (continued)

Sample		Depth (mm)	Age (kyr B.P.)	$\delta^{13}C$ (‰)	$\delta^{13}C$ st. dev.	$\delta^{18}O$ (‰)	$\delta^{18}O$ st. dev.	$\delta^{18}O$ ice vol. adj.
RK05-1t	2-4 e	43.0	56.752	-2.92	0.06	-3.10	0.12	-3.65
RK05-1t	2-4 a	43.9	56.868	-2.48	0.06	-3.08	0.12	-3.63
RK05-1t	0-2 e	45.0	57.013	-3.55	0.06	-3.05	0.12	-3.60
RK05-1t	0-2 a	45.9	57.129	-4.06	0.06	-3.22	0.12	-3.77
RK05-1b	0-2 d	48.9	57.518	-4.86	0.06	-3.42	0.12	-3.95
RK05-1b	0-2 h	49.9	57.649	-4.95	0.06	-3.20	0.12	-3.73
RK05-1b	2-4 c	50.7	57.758	-4.83	0.06	-3.15	0.12	-3.68
RK05-1b	2-4 g	51.9	57.908	-5.59	0.06	-3.17	0.12	-3.69
RK05-1b	4-6 d	53.0	58.057	-5.95	0.06	-3.38	0.12	-3.90
RK05-1b	6-8 a	54.1	58.204	-4.42	0.06	-3.97	0.12	-4.48
RK05-1b	6-8 e	55.1	58.334	-4.12	0.06	-3.27	0.12	-3.78
RK05-1b	8-10 a	56.1	58.465	-6.61	0.06	-3.29	0.12	-3.79
RK05-1b	8-10 e	57.1	58.595	-5.56	0.06	-3.05	0.12	-3.55
RK05-1b	10-12 a	58.1	58.726	-5.23	0.06	-2.91	0.12	-3.41
RK05-1b	10-12 e	59.1	58.856	-4.45	0.06	-3.11	0.12	-3.60
RK05-1b	10-12 h	59.9	58.954	-3.94	0.06	-3.27	0.12	-3.76
RK05-1b	12-14 d	60.9	59.084	-5.88	0.06	-3.39	0.12	-3.87
RK05-1b	12-14 h	61.9	59.215	-6.44	0.06	-3.55	0.12	-4.03
RK05-1b	14-16 d	62.9	59.345	-5.31	0.06	-3.07	0.12	-3.55
RK05-1b	14-16 h	63.9	59.476	-6.28	0.06	-3.24	0.12	-3.71
RK05-1b	16-18 d	64.9	59.606	-6.22	0.06	-3.20	0.12	-3.67
RK05-1b	16-18 h	65.9	59.737	-4.32	0.06	-2.87	0.12	-3.33
RK05-1b	18-20 d	66.9	59.867	-4.22	0.06	-3.00	0.12	-3.46
RK05-1b	18-20 h	67.9	59.998	-3.98	0.06	-3.35	0.12	-3.81
RK05-1b	20-22 d	68.9	60.128	-4.29	0.06	-3.55	0.12	-4.01
RK05-1b	20-22 h	69.9	60.259	-4.29	0.06	-3.36	0.12	-3.83

Appendix G: RK05-3 Stable Isotope Data

Table G.1: Stable carbon and oxygen isotope ratios from RK05-3 calcite. Values are reported relative to Vienna Peedee Belemnite in per mil (‰) notation. Ages are reported as thousands of years before present (kyr B.P.), where present is defined as 2000 AD. Ice volume adjusted $\delta^{18}O$ values (ice vol. adj.) are also given.

Laboratory	Sample		Depth (mm)	Age (kyr B.P.)	$\delta^{13}C$ (vs. PDB)	$\delta^{13}C$ st. dev.	$\delta^{18}O$ (vs. PDB)	$\delta^{18}O$ st. dev.	$\delta^{18}O$ ice vol. adj.
GEOMAR	RK05-3	0-2 a	0.1	6.108	-8.568	0.011	-3.906	0.008	-3.928
WAIKATO	RK05-3	0-2 e	1.0	6.142	-9.09	0.06	-3.81	0.12	-3.835
GEOMAR	RK05-3	2-4 a	2.1	6.185	-9.21	0.01	-3.69	0.04	-3.719
WAIKATO	RK05-3	2-4 e	3.0	6.220	-8.92	0.06	-4.11	0.12	-4.140
GEOMAR	RK05-3	4-6 a	4.1	6.263	-8.40	0.02	-3.74	0.02	-3.776
WAIKATO	RK05-3	4-6 e	5.0	6.297	-8.09	0.06	-3.90	0.12	-3.934
GEOMAR	RK05-3	6-8 a	6.1	6.340	-8.31	0.01	-3.58	0.03	-3.619
WAIKATO	RK05-3	6-8 e	7.0	6.375	-8.72	0.06	-4.17	0.12	-4.209
GEOMAR	RK05-3	8-10 a	8.1	6.418	-8.00	0.01	-3.76	0.02	-3.804
WAIKATO	RK05-3	8-10 e	9.0	6.453	-7.78	0.06	-4.27	0.12	-4.314
GEOMAR	RK05-3	10-12 a	10.1	6.496	-7.627	0.019	-3.667	0.019	-3.714
WAIKATO	RK05-3	10-12 e	11.0	6.530	-7.74	0.06	-3.68	0.12	-3.729
GEOMAR	RK05-3	12-14 a	12.1	6.573	-8.187	0.013	-3.522	0.013	-3.574
GEOMAR	RK05-3	12-14 e	13.0	6.608	-8.073	0.013	-3.487	0.054	-3.541
GEOMAR	RK05-3	14-16 a	14.1	6.651	-8.136	0.016	-3.602	0.015	-3.659
GEOMAR	RK05-3	14-16 e	15.0	6.685	-8.017	0.011	-3.690	0.016	-3.748
GEOMAR	RK05-3	16-18 a	16.1	6.728	-7.000	0.016	-3.406	0.018	-3.468
GEOMAR	RK05-3	16-18 e	17.0	6.763	-6.973	0.012	-3.519	0.036	-3.583
GEOMAR	RK05-3	18-20 a	18.1	6.806	-5.902	0.015	-3.740	0.016	-3.806
GEOMAR	RK05-3	18-20 e	19.0	6.840	-6.973	0.012	-3.509	0.022	-3.577

Table G.1 (continued)

Laboratory	Sample		Depth (mm)	Age (kyr B.P.)	$\delta^{13}C$ (vs. PDB)	$\delta^{13}C$ st. dev.	$\delta^{18}O$ (vs. PDB)	$\delta^{18}O$ st. dev.	$\delta^{18}O$ ice vol. adj.
GEOMAR	RK05-3	20-22 a	20.1	6.883	-6.086	0.013	-3.545	0.021	-3.616
GEOMAR	RK05-3	20-22 e	21.0	6.918	-6.641	0.017	-3.593	0.017	-3.667
GEOMAR	RK05-3	22-24 a	22.1	6.961	-5.838	0.012	-3.562	0.034	-3.638
GEOMAR	RK05-3	22-24 e	23.0	6.995	-6.578	0.014	-3.391	0.031	-3.469
GEOMAR	RK05-3	24-26 a	24.1	7.038	-6.654	0.011	-3.842	0.024	-3.923
GEOMAR	RK05-3	24-26 e	25.0	7.073	-4.811	0.017	-3.306	0.031	-3.390
GEOMAR	RK05-3	26-28 a	26.1	7.116	-5.431	0.015	-3.020	0.022	-3.107
GEOMAR	RK05-3	26-28 e	27.0	7.150	-6.883	0.023	-3.073	0.035	-3.163
GEOMAR	RK05-3	28-30 a	28.1	7.193	-8.784	0.014	-3.735	0.021	-3.827
GEOMAR	RK05-3	28-30 e	29.0	7.228	-8.897	0.021	-3.653	0.031	-3.748
GEOMAR	RK05-3	30-32 a	30.1	7.271	-8.718	0.011	-3.412	0.022	-3.509
GEOMAR	RK05-3	30-32 e	31.0	7.306	-7.172	0.011	-3.627	0.020	-3.727
GEOMAR	RK05-3	32-34 a	32.1	7.349	-6.052	0.021	-3.178	0.036	-3.282
GEOMAR	RK05-3	32-34 e	33.0	7.383	-6.244	0.016	-3.287	0.028	-3.393
GEOMAR	RK05-3	34-36 a	34.1	7.426	-6.372	0.015	-3.425	0.032	-3.534
GEOMAR	RK05-3	34-36 e	35.0	7.461	-5.689	0.022	-3.563	0.041	-3.674
GEOMAR	RK05-3	36-38 a	36.1	7.504	-5.379	0.010	-3.300	0.014	-3.414
GEOMAR	RK05-3	36-38 e	37.0	7.538	-5.870	0.017	-3.124	0.023	-3.241
GEOMAR	RK05-3	38-40 a	38.1	7.581	-5.715	0.011	-3.040	0.016	-3.160
GEOMAR	RK05-3	38-40 e	39.0	7.616	-6.015	0.018	-2.816	0.026	-2.938
GEOMAR	RK05-3	40-42 a	40.1	7.659	-5.602	0.014	-2.809	0.021	-2.934
GEOMAR	RK05-3	40-42 e	41.0	7.693	-6.098	0.012	-3.010	0.013	-3.137
GEOMAR	RK05-3	42-44 a	42.1	7.736	-5.891	0.014	-3.223	0.024	-3.353
GEOMAR	RK05-3	42-44 e	43.0	7.771	-5.797	0.020	-3.361	0.042	-3.494
GEOMAR	RK05-3	44-46 a	44.1	7.814	-5.991	0.012	-3.104	0.013	-3.240
GEOMAR	RK05-3	44-46 e	45.0	7.848	-6.442	0.021	-2.987	0.048	-3.126

Table G.1 (continued)

Laboratory	Sample		Depth (mm)	Age (kyr B.P.)	$\delta^{13}C$ (vs. PDB)	$\delta^{13}C$ st. dev.	$\delta^{18}O$ (vs. PDB)	$\delta^{18}O$ st. dev.	$\delta^{18}O$ ice vol. adj.
GEOMAR	RK05-3	46-48 a	46.1	7.891	-6.721	0.016	-3.056	0.017	-3.198
GEOMAR	RK05-3	46-48 e	47.0	7.926	-6.827	0.020	-3.098	0.020	-3.242
GEOMAR	RK05-3	48-50 a	48.1	7.969	-6.180	0.018	-2.943	0.026	-3.090
GEOMAR	RK05-3	48-50 e	49.0	8.003	-6.361	0.020	-3.075	0.009	-3.225
GEOMAR	RK05-3	50-52 a	50.1	8.047	-6.468	0.010	-3.107	0.020	-3.260
GEOMAR	RK05-3	50-52 e	51.0	8.081	-6.820	0.017	-3.102	0.025	-3.259
GEOMAR	RK05-3	52-54 a	52.1	8.124	-7.718	0.011	-3.162	0.028	-3.322
GEOMAR	RK05-3	52-54 e	53.0	8.159	-8.367	0.015	-3.124	0.035	-3.287
GEOMAR	RK05-3	54-56 a	54.1	8.202	-8.972	0.012	-3.197	0.017	-3.363
GEOMAR	RK05-3	54-56 e	55.0	8.236	-9.516	0.015	-3.270	0.022	-3.439
GEOMAR	RK05-3	56-58 a	56.1	8.279	-9.516	0.017	-3.338	0.031	-3.511
GEOMAR	RK05-3	56-58 e	57.0	8.314	-9.456	0.017	-3.306	0.018	-3.482
GEOMAR	RK05-3	58-60 a	58.1	8.357	-9.124	0.012	-3.427	0.031	-3.607
GEOMAR	RK05-3	58-60 e	59.0	8.391	-8.544	0.016	-3.455	0.020	-3.639
GEOMAR	RK05-3	60-62 a	60.1	8.434	-8.369	0.009	-3.340	0.022	-3.527
GEOMAR	RK05-3	60-62 e	61.0	8.469	-8.090	0.026	-3.116	0.022	-3.305
GEOMAR	RK05-3	62-64 a	62.1	8.512	-8.014	0.016	-2.746	0.018	-2.940
GEOMAR	RK05-3	62-64 e	63.0	8.546	-7.611	0.009	-2.947	0.018	-3.144
GEOMAR	RK05-3	64-66 a	64.1	8.589	-7.302	0.013	-2.973	0.018	-3.174
GEOMAR	RK05-3	64-66 e	65.0	8.624	-7.415	0.016	-3.080	0.016	-3.284
GEOMAR	RK05-3	66-68 a	66.1	8.667	-7.890	0.014	-3.352	0.022	-3.559
GEOMAR	RK05-3	66-68 e	67.0	8.701	-7.597	0.012	-3.394	0.018	-3.604
GEOMAR	RK05-3	68-70 a	68.1	8.744	-7.801	0.009	-3.270	0.024	-3.484
GEOMAR	RK05-3	68-70 e	69.0	8.779	-7.730	0.011	-3.285	0.027	-3.502
GEOMAR	RK05-3	70-72 a	70.1	8.822	-8.648	0.007	-3.284	0.031	-3.504
GEOMAR	RK05-3	70-72 e	71.0	8.857	-9.094	0.011	-3.481	0.030	-3.704

Table G.1 (continued)

Laboratory	Sample		Depth (mm)	Age (kyr B.P.)	$\delta^{13}C$ (vs. PDB)	$\delta^{13}C$ st. dev.	$\delta^{18}O$ (vs. PDB)	$\delta^{18}O$ st. dev.	$\delta^{18}O$ ice vol. adj.
GEOMAR	RK05-3	72-74 a	72.1	8.900	-9.518	0.018	-3.844	0.029	-4.071
GEOMAR	RK05-3	72-74 e	73.0	8.934	-7.546	0.016	-3.303	0.014	-3.533
GEOMAR	RK05-3	74-76 a	74.1	8.977	-6.941	0.029	-2.775	0.041	-3.009
GEOMAR	RK05-3	74-76 e	75.0	9.012	-6.970	0.026	-2.672	0.037	-2.909
GEOMAR	RK05-3	76-78 a	76.1	9.055	-7.443	0.019	-2.553	0.022	-2.794
GEOMAR	RK05-3	76-78 e	77.0	9.089	-7.564	0.013	-2.539	0.028	-2.784
GEOMAR	RK05-3	78-80 a	78.1	9.132	-7.688	0.010	-2.700	0.054	-2.950
GEOMAR	RK05-3	78-80 e	79.0	9.167	-7.257	0.016	-2.882	0.024	-3.136
GEOMAR	RK05-3	80-82 a	80.1	9.210	-7.518	0.015	-2.687	0.031	-2.946
GEOMAR	RK05-3	80-82 e	81.0	9.244	-7.326	0.018	-2.904	0.035	-3.166
GEOMAR	RK05-3	82-84 a	82.1	9.287	-7.509	0.012	-2.609	0.038	-2.876
GEOMAR	RK05-3	82-84 e	83.0	9.322	-7.861	0.016	-2.620	0.035	-2.891
GEOMAR	RK05-3	84-86 a	84.1	9.365	-7.358	0.016	-2.969	0.029	-3.245
GEOMAR	RK05-3	84-86 e	85.0	9.399	-7.947	0.024	-3.206	0.036	-3.485
GEOMAR	RK05-3	86-88 a	86.1	9.442	-8.310	0.019	-2.875	0.020	-3.159
GEOMAR	RK05-3	86-88 e	87.0	9.477	-8.199	0.020	-2.587	0.014	-2.875
GEOMAR	RK05-3	88-90 a	88.1	9.520	-8.064	0.023	-2.772	0.023	-3.065
GEOMAR	RK05-3	88-90 e	89.0	9.554	-8.015	0.018	-2.851	0.034	-3.148
GEOMAR	RK05-3	90-92 a	90.1	9.598	-7.252	0.009	-3.144	0.031	-3.445
GEOMAR	RK05-3	90-92 e	91.0	9.632	-7.435	0.016	-3.089	0.024	-3.394
GEOMAR	RK05-3	92-94 e	93.0	9.710	-7.471	0.011	-2.989	0.015	-3.303
GEOMAR	RK05-3	94-96 a	94.1	9.753	-8.055	0.012	-2.894	0.031	-3.213
GEOMAR	RK05-3	94-96 e	95.0	9.787	-8.399	0.016	-2.491	0.028	-2.813
GEOMAR	RK05-3	96-98 a	96.1	9.830	-8.331	0.011	-2.852	0.024	-3.179
GEOMAR	RK05-3	96-98 e	97.0	9.865	-8.574	0.017	-2.716	0.028	-3.046
GEOMAR	RK05-3	98-100 a	98.1	9.908	-9.026	0.013	-2.660	0.029	-2.996

Table G.1 (continued)

Laboratory	Sample		Depth (mm)	Age (kyr B.P.)	$\delta^{13}C$ (vs. PDB)	$\delta^{13}C$ st. dev.	$\delta^{18}O$ (vs. PDB)	$\delta^{18}O$ st. dev.	$\delta^{18}O$ ice vol. adj.
GEOMAR	RK05-3	98-100 e	99.0	9.942	-9.265	0.018	-2.458	0.028	-2.797
GEOMAR	RK05-3	100-102 e	101.0	10.020	-9.293	0.022	-2.830	0.041	-3.177
GEOMAR	RK05-3	102-104 a	102.1	10.063	-9.226	0.015	-2.971	0.044	-3.321
GEOMAR	RK05-3	102-104 e	103.0	10.097	-8.828	0.014	-3.030	0.051	-3.384
GEOMAR	RK05-3	104-106 a	104.1	10.140	-7.641	0.022	-3.395	0.031	-3.752
GEOMAR	RK05-3	104-106 e	105.0	10.175	-7.911	0.011	-3.304	0.015	-3.664
GEOMAR	RK05-3	106-108 a	106.1	10.218	-7.560	0.013	-3.221	0.030	-3.585
GEOMAR	RK05-3	106-108 e	107.0	10.252	-6.135	0.013	-2.887	0.037	-3.254
GEOMAR	RK05-3	108-110 a	108.1	10.295	-6.578	0.013	-2.815	0.020	-3.185
GEOMAR	RK05-3	108-110 e	109.0	10.330	-9.022	0.021	-2.840	0.032	-3.212
GEOMAR	RK05-3	110-112 a	110.1	10.373	-6.601	0.015	-2.830	0.020	-3.206
GEOMAR	RK05-3	110-112 e	111.0	10.408	-6.664	0.020	-2.714	0.037	-3.093
GEOMAR	RK05-3	112-114 a	112.1	10.451	-6.566	0.010	-2.903	0.015	-3.285
GEOMAR	RK05-3	112-114 e	113.0	10.485	-6.328	0.019	-2.777	0.029	-3.162
GEOMAR	RK05-3	114-116 a	114.1	10.528	-6.771	0.016	-2.661	0.013	-3.050
GEOMAR	RK05-3	114-116 e	115.0	10.563	-6.901	0.015	-2.811	0.023	-3.203
GEOMAR	RK05-3	116-118 a	116.1	10.606	-6.944	0.017	-2.677	0.015	-3.072
GEOMAR	RK05-3	116-118 e	117.0	10.640	-7.343	0.019	-2.947	0.042	-3.344
GEOMAR	RK05-3	118-120 a	118.1	10.683	-7.577	0.023	-3.311	0.035	-3.712
GEOMAR	RK05-3	118-120 e	119.0	10.718	-8.248	0.008	-3.295	0.028	-3.699
GEOMAR	RK05-3	120-122 a	120.1	10.761	-8.269	0.011	-3.580	0.025	-3.987
GEOMAR	RK05-3	120-122 e	121.0	10.795	-6.280	0.016	-3.202	0.027	-3.612
GEOMAR	RK05-3	122-124 a	122.1	10.838	-6.687	0.020	-2.903	0.049	-3.316
GEOMAR	RK05-3	122-124 e	123.0	10.873	-6.880	0.018	-2.892	0.024	-3.309
GEOMAR	RK05-3	124-126 a	124.1	10.916	-6.736	0.012	-2.898	0.015	-3.318
GEOMAR	RK05-3	124-126 e	125.0	10.950	-6.147	0.019	-2.852	0.022	-3.275

Table G.1 (continued)

Laboratory	Sample		Depth (mm)	Age (kyr B.P.)	$\delta^{13}C$ (vs. PDB)	$\delta^{13}C$ st. dev.	$\delta^{18}O$ (vs. PDB)	$\delta^{18}O$ st. dev.	$\delta^{18}O$ ice vol. adj.
GEOMAR	RK05-3	126-128 a	126.1	10.993	-5.386	0.017	-2.793	0.033	-3.220
GEOMAR	RK05-3	126-128 e	127.0	11.028	-6.600	0.018	-2.984	0.044	-3.413
GEOMAR	RK05-3	128-130 a	128.1	11.071	-7.594	0.017	-2.948	0.023	-3.381
GEOMAR	RK05-3	128-130 e	129.0	11.105	-9.310	0.016	-3.143	0.021	-3.578
GEOMAR	RK05-3	130-132 a	130.1	11.149	-9.349	0.009	-3.136	0.037	-3.575
GEOMAR	RK05-3	130-132 e	131.0	11.183	-9.979	0.016	-3.111	0.030	-3.552
GEOMAR	RK05-3	132-134 a	132.1	11.226	-9.930	0.014	-3.030	0.018	-3.475
GEOMAR	RK05-3	132-134 e	133.0	11.261	-9.023	0.019	-3.319	0.028	-3.767
GEOMAR	RK05-3	134-136 a	134.1	11.304	-8.344	0.014	-3.041	0.034	-3.492
GEOMAR	RK05-3	134-136 e	135.0	11.338	-8.589	0.013	-2.973	0.026	-3.427
GEOMAR	RK05-3	136-138 a	136.1	11.381	-8.680	0.006	-3.025	0.016	-3.483
GEOMAR	RK05-3	136-138 e	137.0	11.416	-8.701	0.027	-3.115	0.029	-3.575
GEOMAR	RK05-3	138-140 a	138.1	11.459	-9.105	0.015	-3.113	0.035	-3.577
GEOMAR	RK05-3	138-140 e	139.0	11.493	-10.025	0.015	-3.558	0.054	-4.025
GEOMAR	RK05-3	140-142 a	140.1	11.536	-10.906	0.013	-3.572	0.021	-4.042
GEOMAR	RK05-3	140-142 e	141.0	11.571	-9.770	0.022	-3.499	0.034	-3.972
GEOMAR	RK05-3	142-144 a	142.1	11.614	-9.004	0.016	-3.353	0.019	-3.829
GEOMAR	RK05-3	142-144 e	143.0	11.648	-8.857	0.013	-3.256	0.042	-3.736
GEOMAR	RK05-3	144-146 a	144.1	11.691	-9.634	0.026	-3.361	0.025	-3.844
GEOMAR	RK05-3	144-146 e	145.0	11.726	-10.320	0.025	-3.511	0.030	-3.997
GEOMAR	RK05-3	146-148 a	146.1	11.769	-10.976	0.018	-3.600	0.035	-4.089
GEOMAR	RK05-3	146-148 e	147.0	11.803	-11.161	0.024	-3.618	0.052	-4.110
GEOMAR	RK05-3	148-150 a	148.1	11.846	-11.188	0.030	-3.389	0.032	-3.885
GEOMAR	RK05-3	148-150 e	149.0	11.881	-11.384	0.029	-3.175	0.041	-3.673
GEOMAR	RK05-3	150-152 a	150.1	11.924	-10.854	0.019	-3.331	0.029	-3.833
GEOMAR	RK05-3	150-152 e	151.0	11.959	-10.965	0.016	-3.243	0.041	-3.747

Table G.1 (continued)

Laboratory	Sample		Depth (mm)	Age (kyr B.P.)	$\delta^{13}C$ (vs. PDB)	$\delta^{13}C$ st. dev.	$\delta^{18}O$ (vs. PDB)	$\delta^{18}O$ st. dev.	$\delta^{18}O$ ice vol. adj.
GEOMAR	RK05-3	152-154 a	152.1	12.002	-10.821	0.018	-3.319	0.049	-3.827
GEOMAR	RK05-3	152-154 e	153.0	12.036	-10.665	0.016	-3.151	0.027	-3.662
GEOMAR	RK05-3	154-156 a	154.1	12.079	-10.616	0.025	-3.182	0.046	-3.697
GEOMAR	RK05-3	154-156 e	155.0	12.114	-9.809	0.022	-3.199	0.054	-3.717
GEOMAR	RK05-3	156-158 a	156.1	12.157	-8.536	0.027	-3.550	0.042	-4.071
GEOMAR	RK05-3	156-158 e	157.0	12.191	-9.232	0.016	-2.982	0.038	-3.506
GEOMAR	RK05-3	158-160 a	158.1	12.234	-9.636	0.015	-3.064	0.034	-3.591
GEOMAR	RK05-3	158-160 e	159.0	12.269	-10.237	0.013	-3.351	0.026	-3.881
GEOMAR	RK05-3	160-162 a	160.1	12.312	-10.540	0.019	-3.538	0.018	-4.071
GEOMAR	RK05-3	160-162 e	161.0	12.346	-10.469	0.012	-3.465	0.029	-4.002
GEOMAR	RK05-3	162-164 a	162.1	12.389	-10.460	0.010	-3.578	0.027	-4.118
GEOMAR	RK05-3	162-164 e	163.0	12.424	-10.184	0.024	-3.270	0.023	-3.813
GEOMAR	RK05-3	164-166 a	164.1	12.467	-10.219	0.014	-3.118	0.021	-3.664
GEOMAR	RK05-3	164-166 e	165.0	12.501	-10.172	0.019	-3.248	0.046	-3.797
GEOMAR	RK05-3	166-168 a	166.1	12.544	-10.200	0.018	-3.507	0.025	-4.059
GEOMAR	RK05-3	166-168 e	167.0	12.579	-10.425	0.013	-3.523	0.050	-4.078
GEOMAR	RK05-3	168-170 a	168.1	12.622	-10.748	0.019	-3.498	0.023	-4.057
GEOMAR	RK05-3	168-170 e	169.0	12.656	-10.759	0.013	-3.418	0.031	-3.980
GEOMAR	RK05-3	170-172 a	170.1	12.699	-10.584	0.031	-3.523	0.019	-4.088
GEOMAR	RK05-3	170-172 e	171.0	12.734	-10.553	0.035	-3.582	0.068	-4.150
GEOMAR	RK05-3	172-174 a	172.1	12.777	-10.794	0.009	-3.378	0.049	-3.949
GEOMAR	RK05-3	172-174 e	173.0	12.812	-11.107	0.016	-3.525	0.030	-4.099
GEOMAR	RK05-3	174-176 a	174.1	12.855	-11.800	0.021	-3.905	0.051	-4.483
GEOMAR	RK05-3	174-176 e	175.0	12.889	-8.134	0.020	-3.055	0.050	-3.636
GEOMAR	RK05-3	176-178 a	176.1	12.932	-7.561	0.043	-3.066	0.037	-3.650
GEOMAR	RK05-3	176-178 e	177.0	12.967	-8.903	0.011	-3.191	0.030	-3.777

Table G.1 (continued)

Laboratory	Sample		Depth (mm)	Age (kyr B.P.)	$\delta^{13}C$ (vs. PDB)	$\delta^{13}C$ st. dev.	$\delta^{18}O$ (vs. PDB)	$\delta^{18}O$ st. dev.	$\delta^{18}O$ ice vol. adj.
GEOMAR	RK05-3	178-180 a	178.1	13.010	-7.167	0.024	-3.127	0.070	-3.718
GEOMAR	RK05-3	178-180 e	179.0	13.044	-6.852	0.017	-3.136	0.020	-3.734
GEOMAR	RK05-3	180-182 a	180.1	13.087	-6.740	0.027	-3.139	0.033	-3.745
GEOMAR	RK05-3	180-182 e	181.0	13.122	-7.653	0.023	-3.025	0.050	-3.638
GEOMAR	RK05-3	182-184 a	182.1	13.165	-7.578	0.020	-3.004	0.027	-3.626
GEOMAR	RK05-3	182-184 e	183.0	13.199	-7.788	0.026	-3.122	0.047	-3.751
GEOMAR	RK05-3	184-186 a	184.1	13.242	-7.511	0.011	-2.868	0.015	-3.505
GEOMAR	RK05-3	184-186 e	185.0	13.277	-7.221	0.015	-2.987	0.044	-3.630
GEOMAR	RK05-3	186-188 a	186.1	13.320	-6.819	0.024	-2.973	0.027	-3.625
GEOMAR	RK05-3	186-188 e	187.0	13.354	-8.623	0.017	-3.243	0.031	-3.902
GEOMAR	RK05-3	188-190 a	188.1	13.397	-8.856	0.019	-3.178	0.032	-3.845
GEOMAR	RK05-3	188-190 e	189.0	13.432	-8.291	0.018	-3.117	0.063	-3.791
GEOMAR	RK05-3	190-192 a	190.1	13.475	-9.260	0.007	-3.130	0.026	-3.812
GEOMAR	RK05-3	190-192 e	191.0	13.510	-9.407	0.013	-3.094	0.018	-3.784
GEOMAR	RK05-3	192-194 a	192.1	13.553	-7.946	0.013	-3.038	0.027	-3.736
GEOMAR	RK05-3	192-194 e	193.0	13.587	-8.549	0.013	-3.078	0.030	-3.782
GEOMAR	RK05-3	194-196 a	194.1	13.630	-8.666	0.010	-3.043	0.014	-3.756
GEOMAR	RK05-3	194-196 e	195.0	13.665	-8.483	0.019	-3.186	0.023	-3.906
GEOMAR	RK05-3	196-198 a	196.1	13.708	-8.946	0.011	-3.094	0.028	-3.822
GEOMAR	RK05-3	196-198 e	197.0	13.742	-9.062	0.014	-3.229	0.029	-3.964
GEOMAR	RK05-3	198-200 a	198.1	13.785	-9.297	0.014	-3.138	0.026	-3.881
GEOMAR	RK05-3	198-200 e	199.0	13.820	-8.484	0.016	-3.103	0.024	-3.854
GEOMAR	RK05-3	200-202 a	200.1	13.863	-8.673	0.016	-2.965	0.037	-3.724
GEOMAR	RK05-3	200-202 e	201.0	13.897	-9.060	0.017	-2.766	0.020	-3.532
GEOMAR	RK05-3	202-204 a	202.1	13.940	-9.441	0.021	-2.731	0.024	-3.505
GEOMAR	RK05-3	202-204 e	203.0	13.975	-9.458	0.015	-2.706	0.019	-3.487

Table G.1 (continued)

Laboratory	Sample		Depth (mm)	Age (kyr B.P.)	$\delta^{13}C$ (vs. PDB)	$\delta^{13}C$ st. dev.	$\delta^{18}O$ (vs. PDB)	$\delta^{18}O$ st. dev.	$\delta^{18}O$ ice vol. adj.
GEOMAR	RK05-3	204-206 a	204.1	14.018	-9.209	0.012	-2.524	0.015	-3.310
GEOMAR	RK05-3	204-206 e	205.0	14.052	-9.102	0.019	-2.644	0.046	-3.433
GEOMAR	RK05-3	206-208 a	206.1	14.095	-9.194	0.019	-2.963	0.017	-3.753
GEOMAR	RK05-3	206-208 e	207.0	14.130	-9.433	0.016	-2.844	0.043	-3.636
GEOMAR	RK05-3	208-210 a	208.1	14.173	-9.440	0.004	-2.588	0.021	-3.382
GEOMAR	RK05-3	208-210 e	209.0	14.207	-9.589	0.017	-2.645	0.026	-3.441
GEOMAR	RK05-3	210-212 a	210.1	14.250	-10.202	0.010	-2.742	0.031	-3.540
GEOMAR	RK05-3	210-212 e	211.0	14.285	-9.941	0.017	-2.652	0.020	-3.452
GEOMAR	RK05-3	212-214 a	212.1	14.328	-9.939	0.016	-2.773	0.014	-3.574
GEOMAR	RK05-3	212-214 e	213.0	14.363	-9.895	0.014	-2.549	0.031	-3.353
GEOMAR	RK05-3	214-216 a	214.1	14.406	-9.192	0.029	-2.968	0.034	-3.774
GEOMAR	RK05-3	214-216 e	215.0	14.440	-9.277	0.018	-2.895	0.031	-3.703
GEOMAR	RK05-3	216-218 a	216.1	14.483	-9.790	0.013	-3.168	0.043	-3.977
GEOMAR	RK05-3	216-218 e	217.0	14.518	-10.085	0.016	-3.067	0.042	-3.878
GEOMAR	RK05-3	218-220 a	218.1	14.561	-10.457	0.008	-3.050	0.031	-3.863
GEOMAR	RK05-3	218-220 e	219.0	14.595	-10.558	0.018	-3.174	0.021	-3.989
GEOMAR	RK05-3	220-222 a	220.1	14.638	-10.580	0.017	-3.028	0.033	-3.845
GEOMAR	RK05-3	220-222 e	221.0	14.673	-10.243	0.019	-2.931	0.017	-3.750
GEOMAR	RK05-3	222-224 a	222.1	14.716	-10.610	0.022	-3.185	0.038	-4.006
GEOMAR	RK05-3	222-224 e	223.0	14.750	-9.792	0.020	-3.089	0.024	-3.912
GEOMAR	RK05-3	224-226 a	224.1	14.793	-8.735	0.009	-2.649	0.018	-3.474
GEOMAR	RK05-3	224-226 e	225.0	14.828	-8.213	0.014	-2.743	0.018	-3.569
GEOMAR	RK05-3	226-228 a	226.1	14.871	-7.791	0.013	-3.072	0.025	-3.900
GEOMAR	RK05-3	226-228 e	227.0	14.905	-7.561	0.020	-3.130	0.023	-3.960
GEOMAR	RK05-3	228-230 a	228.1	14.948	-7.855	0.013	-2.779	0.027	-3.611
GEOMAR	RK05-3	228-230 e	229.0	14.983	-8.040	0.016	-2.695	0.049	-3.529

Table G.1 (continued)

Laboratory	Sample		Depth (mm)	Age (kyr B.P.)	$\delta^{13}C$ (vs. PDB)	$\delta^{13}C$ st. dev.	$\delta^{18}O$ (vs. PDB)	$\delta^{18}O$ st. dev.	$\delta^{18}O$ ice vol. adj.
GEOMAR	RK05-3	230-232 a	230.1	15.026	-8.257	0.023	-3.076	0.049	-3.912
GEOMAR	RK05-3	230-232 e	231.0	15.060	-8.415	0.007	-3.145	0.026	-3.982
GEOMAR	RK05-3	232-234 a	232.1	15.104	-9.432	0.015	-2.896	0.030	-3.736
GEOMAR	RK05-3	232-234 e	233.0	15.138	-9.348	0.016	-2.975	0.013	-3.816
GEOMAR	RK05-3	234-236 a	234.1	15.181	-9.649	0.016	-3.195	0.014	-4.039
GEOMAR	RK05-3	234-236 e	235.0	15.216	-9.436	0.015	-2.757	0.012	-3.602
GEOMAR	RK05-3	236-238 a	236.1	15.259	-9.553	0.013	-2.979	0.023	-3.826
GEOMAR	RK05-3	236-238 e	237.0	15.293	-8.824	0.015	-3.074	0.020	-3.923
GEOMAR	RK05-3	238-240 a	238.1	15.336	-9.284	0.017	-3.031	0.013	-3.882
GEOMAR	RK05-3	238-240 e	239.0	15.371	-9.291	0.013	-3.004	0.029	-3.857
GEOMAR	RK05-3	240-242 a	240.1	15.414	-8.996	0.012	-3.049	0.033	-3.904
GEOMAR	RK05-3	240-242 e	241.0	15.448	-9.267	0.014	-3.038	0.029	-3.894
GEOMAR	RK05-3	242-244 a	242.1	15.491	-10.254	0.011	-3.067	0.020	-3.926
GEOMAR	RK05-3	242-244 e	243.0	15.526	-9.550	0.020	-3.076	0.027	-3.937
GEOMAR	RK05-3	244-246 a	244.1	15.569	-9.850	0.024	-2.866	0.022	-3.728
GEOMAR	RK05-3	244-246 e	245.0	15.603	-9.784	0.020	-3.271	0.029	-4.135
GEOMAR	RK05-3	246-248 a	246.1	15.646	-9.485	0.028	-3.308	0.042	-4.175
GEOMAR	RK05-3	246-248 e	247.0	15.681	-9.395	0.011	-3.054	0.032	-3.922
GEOMAR	RK05-3	248-250 a	248.1	15.724	-9.261	0.015	-2.849	0.045	-3.719
GEOMAR	RK05-3	248-250 e	249.0	15.758	-9.140	0.010	-3.018	0.022	-3.890
GEOMAR	RK05-3	250-252 a	250.1	15.801	-8.817	0.019	-2.498	0.036	-3.373
GEOMAR	RK05-3	250-252 e	251.0	15.836	-8.946	0.014	-2.592	0.040	-3.468
GEOMAR	RK05-3	252-254 a	252.1	15.879	-9.726	0.013	-3.143	0.049	-4.021
GEOMAR	RK05-3	252-254 e	253.0	15.914	-9.858	0.024	-3.145	0.047	-4.024
GEOMAR	RK05-3	254-256 a	254.1	15.957	-9.735	0.014	-2.876	0.046	-3.758
GEOMAR	RK05-3	254-256 e	255.0	15.991	-9.561	0.027	-3.084	0.018	-3.967

Table G.1 (continued)

Laboratory	Sample		Depth (mm)	Age (kyr B.P.)	$\delta^{13}C$ (vs. PDB)	$\delta^{13}C$ st. dev.	$\delta^{18}O$ (vs. PDB)	$\delta^{18}O$ st. dev.	$\delta^{18}O$ ice vol. adj.
GEOMAR	RK05-3	256-258 a	256.1	16.034	-9.637	0.011	-3.524	0.043	-4.409
GEOMAR	RK05-3	256-258 e	257.0	16.069	-9.471	0.007	-3.241	0.055	-4.128
GEOMAR	RK05-3	258-260 a	258.1	16.112	-9.678	0.010	-3.252	0.019	-4.141
GEOMAR	RK05-3	258-260 e	259.0	16.146	-10.093	0.023	-3.639	0.051	-4.530
GEOMAR	RK05-3	260-262 a	260.1	16.189	-9.344	0.027	-3.471	0.020	-4.364
GEOMAR	RK05-3	260-262 e	261.0	16.224	-9.240	0.014	-3.387	0.039	-4.282
GEOMAR	RK05-3	262-264 a	262.1	16.267	-9.296	0.034	-3.427	0.043	-4.324
GEOMAR	RK05-3	262-264 e	263.0	16.301	-9.398	0.012	-2.584	0.027	-3.482
GEOMAR	RK05-3	264-266 a	264.1	16.344	-9.506	0.008	-2.864	0.060	-3.765
GEOMAR	RK05-3	264-266 e	265.0	16.379	-9.996	0.021	-3.092	0.026	-3.995
GEOMAR	RK05-3	266-268 e	267.0	16.456	-10.334	0.025	-3.231	0.034	-4.137
GEOMAR	RK05-3	268-270 a	268.1	16.499	-9.956	0.020	-3.070	0.023	-3.979
GEOMAR	RK05-3	268-270 e	269.0	16.534	-9.417	0.013	-3.020	0.011	-3.930
GEOMAR	RK05-3	270-272 a	270.1	16.577	-8.631	0.008	-2.826	0.018	-3.738
GEOMAR	RK05-3	270-272 e	271.0	16.611	-8.196	0.018	-2.656	0.024	-3.570
GEOMAR	RK05-3	272-274 a	272.1	16.655	-8.576	0.019	-2.997	0.032	-3.913
GEOMAR	RK05-3	272-274 e	273.0	16.689	-9.011	0.014	-2.822	0.017	-3.740
GEOMAR	RK05-3	274-276 a	274.1	16.732	-9.683	0.013	-2.704	0.018	-3.624
GEOMAR	RK05-3	274-276 e	275.0	16.767	-9.449	0.020	-2.681	0.040	-3.602
GEOMAR	RK05-3	276-278 a	276.1	16.810	-9.637	0.010	-2.513	0.021	-3.436
GEOMAR	RK05-3	276-278 e	277.0	16.844	-9.822	0.019	-2.630	0.019	-3.556
GEOMAR	RK05-3	278-280 a	278.1	16.887	-9.773	0.018	-2.775	0.018	-3.702
GEOMAR	RK05-3	278-280 e	279.0	16.922	-9.810	0.018	-2.508	0.037	-3.438
GEOMAR	RK05-3	280-282 a	280.1	16.965	-9.869	0.013	-2.478	0.031	-3.409
GEOMAR	RK05-3	280-282 e	281.0	16.999	-9.759	0.024	-3.041	0.035	-3.974
GEOMAR	RK05-3	282-284 a	282.1	17.042	-10.028	0.014	-2.916	0.022	-3.851

Table G.1 (continued)

Laboratory	Sample		Depth (mm)	Age (kyr B.P.)	$\delta^{13}C$ (vs. PDB)	$\delta^{13}C$ st. dev.	$\delta^{18}O$ (vs. PDB)	$\delta^{18}O$ st. dev.	$\delta^{18}O$ ice vol. adj.
GEOMAR	RK05-3	282-284 e	283.0	17.077	-9.761	0.012	-3.080	0.037	-4.017
GEOMAR	RK05-3	284-286 a	284.1	17.120	-9.832	0.013	-2.578	0.024	-3.517
GEOMAR	RK05-3	284-286 e	285.0	17.154	-9.434	0.013	-2.536	0.034	-3.477
GEOMAR	RK05-3	286-288 a	286.1	17.197	-9.857	0.008	-2.769	0.031	-3.712
GEOMAR	RK05-3	286-288 e	287.0	17.232	-10.600	0.015	-2.743	0.022	-3.687
GEOMAR	RK05-3	288-290 a	288.1	17.275	-9.842	0.021	-3.007	0.056	-3.953
GEOMAR	RK05-3	288-290 e	289.0	17.309	-9.239	0.010	-3.202	0.015	-4.151
GEOMAR	RK05-3	290-292 a	290.1	17.352	-9.561	0.014	-2.928	0.025	-3.879
GEOMAR	RK05-3	290-292 e	291.0	17.387	-9.594	0.022	-3.267	0.028	-4.219
GEOMAR	RK05-3	292-294 a	292.1	17.430	-8.686	0.018	-3.522	0.015	-4.476
GEOMAR	RK05-3	292-294 e	293.0	17.465	-7.933	0.011	-3.171	0.024	-4.127
GEOMAR	RK05-3	294-296 a	294.1	17.508	-8.023	0.014	-2.748	0.017	-3.706
GEOMAR	RK05-3	294-296 e	295.0	17.542	-8.365	0.012	-2.715	0.026	-3.675
GEOMAR	RK05-3	296-298 a	296.1	17.585	-8.571	0.014	-2.809	0.027	-3.771
GEOMAR	RK05-3	296-298 e	297.0	17.620	-8.476	0.016	-2.587	0.021	-3.551
GEOMAR	RK05-3	298-300 a	298.1	17.663	-8.230	0.008	-2.525	0.011	-3.490
GEOMAR	RK05-3	298-300 e	299.0	17.697	-6.807	0.013	-2.816	0.044	-3.784
GEOMAR	RK05-3	300-302 a	300.1	17.740	-4.303	0.017	-3.068	0.038	-4.038
GEOMAR	RK05-3	300-302 e	301.0	17.775	-4.662	0.011	-2.738	0.024	-3.710
GEOMAR	RK05-3	302-304 a	302.1	17.818	-5.114	0.007	-2.779	0.027	-3.752
GEOMAR	RK05-3	302-304 e	303.0	17.852	-5.146	0.008	-2.896	0.021	-3.870
GEOMAR	RK05-3	304-306 a	304.1	17.895	-5.850	0.016	-2.726	0.019	-3.703
GEOMAR	RK05-3	304-306 e	305.0	17.930	-4.757	0.014	-2.909	0.034	-3.888
GEOMAR	RK05-3	306-308 a	306.1	17.973	-6.203	0.014	-2.998	0.018	-3.978
GEOMAR	RK05-3	306-308 e	307.0	18.007	-4.447	0.013	-2.841	0.013	-3.824
GEOMAR	RK05-3	308-310 a	308.1	18.050	-4.239	0.017	-3.154	0.026	-4.139

Table G.1 (continued)

Laboratory	Sample		Depth (mm)	Age (kyr B.P.)	$\delta^{13}C$ (vs. PDB)	$\delta^{13}C$ st. dev.	$\delta^{18}O$ (vs. PDB)	$\delta^{18}O$ st. dev.	$\delta^{18}O$ ice vol. adj.
GEOMAR	RK05-3	308-310 e	309.0	18.085	-5.314	0.017	-3.570	0.036	-4.557
GEOMAR	RK05-3	310-312 a	310.1	18.128	-5.717	0.021	-3.500	0.030	-4.490
GEOMAR	RK05-3	310-312 e	311.0	18.162	-5.498	0.019	-3.366	0.038	-4.357
GEOMAR	RK05-3	312-314 a	312.1	18.206	-5.760	0.013	-3.327	0.027	-4.321
GEOMAR	RK05-3	312-314 e	313.0	18.240	-4.907	0.018	-3.306	0.036	-4.303
GEOMAR	RK05-3	314-316 a	314.1	18.283	-5.079	0.021	-3.164	0.027	-4.162
GEOMAR	RK05-3	314-316 e	315.0	18.318	-5.884	0.011	-3.491	0.026	-4.492
GEOMAR	RK05-3	316-318 a	316.1	18.361	-3.736	0.014	-3.202	0.021	-4.206
GEOMAR	RK05-3	316-318 e	317.0	18.395	-3.693	0.014	-3.356	0.028	-4.361
GEOMAR	RK05-3	318-320 a	318.1	18.438	-3.993	0.014	-3.390	0.015	-4.398
GEOMAR	RK05-3	318-320 e	319.0	18.473	-6.837	0.021	-3.484	0.032	-4.494
GEOMAR	RK05-3	320-322 a	320.1	18.516	-7.896	0.014	-3.412	0.014	-4.425
GEOMAR	RK05-3	320-322 e	321.0	18.550	-4.120	0.009	-2.852	0.043	-3.866
GEOMAR	RK05-3	322-324 a	322.1	18.593	-3.593	0.011	-3.187	0.030	-4.204
GEOMAR	RK05-3	322-324 e	323.0	18.628	-4.214	0.011	-3.404	0.015	-4.423
GEOMAR	RK05-3	324-326 a	324.1	18.671	-3.420	0.012	-3.227	0.019	-4.249
GEOMAR	RK05-3	324-326 e	325.0	18.705	-3.089	0.022	-2.946	0.039	-3.970
GEOMAR	RK05-3	326-328 a	326.1	18.748	-6.886	0.018	-3.193	0.033	-4.219
GEOMAR	RK05-3	326-328 e	327.0	18.783	-4.099	0.029	-3.354	0.027	-4.382
GEOMAR	RK05-3	328-330 a	328.1	18.826	-5.241	0.015	-3.311	0.009	-4.342
GEOMAR	RK05-3	328-330 e	329.0	18.860	-5.613	0.017	-3.359	0.029	-4.392
GEOMAR	RK05-3	330-332 a	330.1	18.903	-3.670	0.016	-3.191	0.041	-4.226
GEOMAR	RK05-3	330-332 e	331.0	18.938	-5.642	0.023	-3.250	0.017	-4.288
GEOMAR	RK05-3	332-334 a	332.1	18.981	-7.733	0.011	-3.695	0.016	-4.735
GEOMAR	RK05-3	332-334 e	333.0	19.016	-8.068	0.016	-3.615	0.019	-4.657
GEOMAR	RK05-3	334-336 a	334.1	19.059	-8.922	0.015	-3.784	0.022	-4.829

Table G.1 (continued)

Laboratory	Sample		Depth (mm)	Age (kyr B.P.)	$\delta^{13}C$ (vs. PDB)	$\delta^{13}C$ st. dev.	$\delta^{18}O$ (vs. PDB)	$\delta^{18}O$ st. dev.	$\delta^{18}O$ ice vol. adj.
GEOMAR	RK05-3	334-336 e	335.0	19.093	-7.485	0.022	-3.712	0.054	-4.758
GEOMAR	RK05-3	336-338 a	336.1	19.136	-7.850	0.016	-3.705	0.039	-4.754
GEOMAR	RK05-3	336-338 e	337.0	19.171	-7.266	0.015	-3.370	0.025	-4.421
GEOMAR	RK05-3	338-340 a	338.1	19.214	-7.831	0.017	-3.164	0.017	-4.218
GEOMAR	RK05-3	338-340 e	339.0	19.248	-7.603	0.014	-3.149	0.026	-4.205
GEOMAR	RK05-3	340-342 a	340.1	19.291	-7.602	0.014	-3.230	0.034	-4.289
GEOMAR	RK05-3	340-342 e	341.0	19.326	-7.536	0.011	-3.348	0.025	-4.408
GEOMAR	RK05-3	342-344 a	342.1	19.369	-6.826	0.012	-3.217	0.014	-4.280
GEOMAR	RK05-3	342-344 e	343.0	19.403	-6.764	0.010	-3.072	0.018	-4.137
GEOMAR	RK05-3	344-346 a	344.1	19.446	-6.344	0.018	-3.011	0.026	-4.078
GEOMAR	RK05-3	344-346 e	345.0	19.481	-6.457	0.022	-3.400	0.036	-4.469
GEOMAR	RK05-3	346-348 a	346.1	19.524	-7.074	0.017	-3.269	0.028	-4.341
GEOMAR	RK05-3	346-348 e	347.0	19.558	-7.294	0.024	-3.406	0.033	-4.480
GEOMAR	RK05-3	348-350 a	348.1	19.601	-7.393	0.011	-3.545	0.033	-4.622
GEOMAR	RK05-3	348-350 e	349.0	19.636	-6.534	0.024	-3.626	0.035	-4.705
GEOMAR	RK05-3	350-352 a	350.1	19.679	-4.877	0.021	-3.381	0.019	-4.462
GEOMAR	RK05-3	350-352 e	351.0	19.713	-2.505	0.022	-3.492	0.035	-4.575
GEOMAR	RK05-3	352-354 a	352.1	19.756	-2.474	0.020	-3.614	0.027	-4.700
GEOMAR	RK05-3	352-354 e	353.0	19.791	-2.746	0.021	-3.547	0.010	-4.635
GEOMAR	RK05-3	354-356 a	354.1	20.189	-2.206	0.019	-3.258	0.036	-4.357
GEOMAR	RK05-3	354-356 e	355.0	20.508	-4.201	0.024	-3.517	0.031	-4.613
GEOMAR	RK05-3	356-358 a	356.1	20.906	-3.414	0.021	-3.159	0.030	-4.252
GEOMAR	RK05-3	356-358 e	357.0	21.225	-5.695	0.018	-3.179	0.036	-4.270
GEOMAR	RK05-3	358-360 a	358.1	21.623	-6.050	0.012	-3.253	0.043	-4.340
GEOMAR	RK05-3	358-360 e	359.0	21.942	-4.256	0.020	-3.406	0.046	-4.491
GEOMAR	RK05-3	360-362 a	360.1	22.340	-5.122	0.037	-3.026	0.045	-4.108

Table G.1 (continued)

Laboratory	Sample		Depth (mm)	Age (kyr B.P.)	$\delta^{13}C$ (vs. PDB)	$\delta^{13}C$ st. dev.	$\delta^{18}O$ (vs. PDB)	$\delta^{18}O$ st. dev.	$\delta^{18}O$ ice vol. adj.
GEOMAR	RK05-3	360-362 e	361.0	22.660	-6.072	0.031	-3.140	0.054	-4.219
GEOMAR	RK05-3	362-364 a	362.1	23.058	-5.970	0.019	-3.452	0.023	-4.528
GEOMAR	RK05-3	362-364 e	363.0	23.377	-5.479	0.020	-3.052	0.024	-4.126
GEOMAR	RK05-3	364-366 a	364.1	23.775	-6.349	0.009	-3.324	0.029	-4.395
GEOMAR	RK05-3	364-366 e	365.0	24.094	-5.871	0.021	-3.203	0.052	-4.271
GEOMAR	RK05-3	366-368 a	366.1	24.492	-5.412	0.025	-3.178	0.036	-4.243
GEOMAR	RK05-3	366-368 e	367.0	24.811	-5.387	0.029	-3.554	0.068	-4.616
GEOMAR	RK05-3	368-370 a	368.1	25.209	-7.037	0.037	-3.471	0.044	-4.530
GEOMAR	RK05-3	368-370 e	369.0	25.528	-7.676	0.045	-3.766	0.067	-4.821
GEOMAR	RK05-3	370-372 a	370.1	25.926	-6.668	0.026	-3.609	0.024	-4.660
GEOMAR	RK05-3	370-372 e	371.0	26.245	-5.838	0.034	-3.359	0.064	-4.407
GEOMAR	RK05-3	372-374 a	372.1	26.643	-6.878	0.020	-3.655	0.062	-4.699
GEOMAR	RK05-3	372-374 e	373.0	26.962	-6.477	0.014	-3.739	0.040	-4.779
GEOMAR	RK05-3	374-376 a	374.1	27.360	-6.685	0.021	-3.491	0.047	-4.527
GEOMAR	RK05-3	374-376 e	375.0	27.680	-7.007	0.028	-3.072	0.032	-4.105
GEOMAR	RK05-3	376-378 a	376.1	28.078	-6.767	0.034	-3.523	0.034	-4.548
GEOMAR	RK05-3	376-378 e	377.0	28.397	-8.027	0.014	-3.436	0.033	-4.439
GEOMAR	RK05-3	378-380 a	378.1	28.795	-7.317	0.021	-3.211	0.049	-4.187
GEOMAR	RK05-3	378-380 e	379.0	29.114	-7.193	0.025	-3.340	0.025	-4.295
GEOMAR	RK05-3	380-382 a	380.1	29.512	-5.925	0.019	-3.340	0.024	-4.269
GEOMAR	RK05-3	380-382 e	381.0	29.831	-5.734	0.039	-3.410	0.046	-4.317
GEOMAR	RK05-3	382-384 a	382.1	30.229	-6.066	0.046	-3.313	0.034	-4.176
GEOMAR	RK05-3	382-384 e	383.0	30.548	-6.311	0.017	-3.271	0.024	-4.087
GEOMAR	RK05-3	384-386 a	384.1	30.946	-7.143	0.036	-3.292	0.058	-4.050
GEOMAR	RK05-3	384-386 e	385.0	31.265	-7.778	0.010	-3.269	0.036	-3.981
GEOMAR	RK05-3	386-388 a	386.1	31.663	-7.684	0.028	-3.271	0.059	-3.925

Table G.1 (continued)

Laboratory	Sample		Depth (mm)	Age (kyr B.P.)	$\delta^{13}C$ (vs. PDB)	$\delta^{13}C$ st. dev.	$\delta^{18}O$ (vs. PDB)	$\delta^{18}O$ st. dev.	$\delta^{18}O$ ice vol. adj.
GEOMAR	RK05-3	386-388 e	387.0	31.982	-8.334	0.034	-3.244	0.036	-3.851
GEOMAR	RK05-3	388-390 a	388.1	32.380	-8.768	0.025	-3.259	0.046	-3.879
GEOMAR	RK05-3	388-390 e	389.0	32.699	-8.362	0.020	-3.133	0.037	-3.765
GEOMAR	RK05-3	390-392 a	390.1	33.097	-8.213	0.017	-3.256	0.027	-3.904
GEOMAR	RK05-3	390-392 e	391.0	33.417	-8.568	0.022	-3.256	0.040	-3.917
GEOMAR	RK05-3	392-394 a	392.1	33.815	-7.981	0.048	-3.628	0.074	-4.305
GEOMAR	RK05-3	392-394 e	393.0	34.134	-8.636	0.018	-3.467	0.022	-4.146
GEOMAR	RK05-3	394-396 a	394.1	34.532	-5.671	0.029	-3.402	0.047	-4.067
GEOMAR	RK05-3	394-396 e	395.0	34.851	-6.331	0.017	-3.220	0.030	-3.875
GEOMAR	RK05-3	396-398 a	396.1	35.249	-5.876	0.051	-3.346	0.076	-3.987
GEOMAR	RK05-3	396-398 e	397.0	35.568	-5.780	0.020	-3.379	0.026	-4.009
GEOMAR	RK05-3	398-400 a	398.1	35.691	-6.126	0.038	-3.418	0.088	-4.044
GEOMAR	RK05-3	398-400 e	399.0	35.790	-5.729	0.016	-3.363	0.033	-3.986
GEOMAR	RK05-3	400-402 a	400.1	35.913	-6.203	0.028	-3.340	0.038	-3.958
GEOMAR	RK05-3	400-402 e	401.0	36.012	-7.462	0.014	-3.389	0.026	-4.004
GEOMAR	RK05-3	402-404 a	402.1	36.136	-8.003	0.030	-3.348	0.052	-3.959
GEOMAR	RK05-3	402-404 e	403.0	36.234	-7.622	0.019	-3.104	0.028	-3.711
GEOMAR	RK05-3	404-406 a	404.1	36.358	-8.174	0.021	-3.185	0.047	-3.788
GEOMAR	RK05-3	404-406 e	405.0	36.457	-9.071	0.017	-3.441	0.037	-4.041
GEOMAR	RK05-3	406-408 a	406.1	36.580	-8.983	0.020	-3.227	0.060	-3.823
GEOMAR	RK05-3	406-408 e	407.0	36.679	-9.612	0.012	-3.394	0.018	-3.986
GEOMAR	RK05-3	408-410 a	408.1	36.802	-9.385	0.015	-3.369	0.032	-3.957
GEOMAR	RK05-3	408-410 e	409.0	36.901	-9.241	0.028	-3.340	0.032	-3.925
GEOMAR	RK05-3	410-412 a	410.1	37.024	-8.932	0.024	-3.407	0.038	-3.990
GEOMAR	RK05-3	410-412 e	411.0	37.123	-7.655	0.028	-2.998	0.050	-3.587
GEOMAR	RK05-3	412-414 a	412.1	37.246	-9.102	0.021	-3.339	0.032	-3.936

Table G.1 (continued)

Laboratory	Sample		Depth (mm)	Age (kyr B.P.)	$\delta^{13}C$ (vs. PDB)	$\delta^{13}C$ st. dev.	$\delta^{18}O$ (vs. PDB)	$\delta^{18}O$ st. dev.	$\delta^{18}O$ ice vol. adj.
GEOMAR	RK05-3	412-414 e	413.0	37.345	-8.089	0.024	-3.294	0.031	-3.897
GEOMAR	RK05-3	414-416 a	414.1	37.468	-9.084	0.017	-3.365	0.028	-3.976
GEOMAR	RK05-3	414-416 e	415.0	37.567	-9.650	0.030	-3.970	0.056	-4.587
GEOMAR	RK05-3	416-418 a	416.1	37.691	-10.260	0.028	-4.196	0.047	-4.821
GEOMAR	RK05-3	416-418 e	417.0	37.789	-10.082	0.022	-4.185	0.054	-4.816
GEOMAR	RK05-3	418-420 a	418.1	37.913	-9.770	0.019	-3.922	0.034	-4.561
GEOMAR	RK05-3	418-420 e	419.0	38.012	-10.107	0.026	-3.762	0.058	-4.406
GEOMAR	RK05-3	420-422 a	420.1	38.135	-9.444	0.022	-3.599	0.031	-4.245
GEOMAR	RK05-3	420-422 e	421.0	38.234	-9.263	0.029	-3.546	0.031	-4.194
GEOMAR	RK05-3	422-424 e	423.0	38.456	-9.118	0.026	-3.649	0.036	-4.300
GEOMAR	RK05-3	424-426 e	425.0	38.678	-7.425	0.014	-3.500	0.026	-4.155
GEOMAR	RK05-3	426-428 e	427.0	38.900	-7.956	0.022	-3.513	0.024	-4.171
GEOMAR	RK05-3	428-430 e	429.0	39.122	-6.590	0.016	-2.996	0.027	-3.658
GEOMAR	RK05-3	430-432 e	431.0	39.344	-7.520	0.022	-3.253	0.026	-3.918
GEOMAR	RK05-3	432-434 e	433.0	39.567	-7.679	0.016	-2.961	0.028	-3.630
GEOMAR	RK05-3	434-436 e	435.0	39.789	-8.748	0.020	-3.206	0.029	-3.878
GEOMAR	RK05-3	346-438 e	437.0	40.011	-8.997	0.031	-3.182	0.052	-3.857
GEOMAR	RK05-3	438-440 e	439.0	40.233	-7.501	0.009	-2.595	0.027	-3.269
GEOMAR	RK05-3	440-442 e	441.0	40.455	-8.739	0.010	-2.633	0.028	-3.305
GEOMAR	RK05-3	442-444 e	443.0	40.677	-7.853	0.023	-3.497	0.018	-4.167
GEOMAR	RK05-3	444-446 e	445.0	40.899	-6.972	0.017	-3.340	0.046	-4.008
GEOMAR	RK05-3	446-448 e	447.0	41.122	-8.275	0.024	-3.411	0.046	-4.077
GEOMAR	RK05-3	448-450 e	449.0	41.344	-8.187	0.030	-3.604	0.038	-4.269
GEOMAR	RK05-3	450-452 e	451.0	41.566	-7.438	0.022	-3.410	0.041	-4.074
GEOMAR	RK05-3	452-454 e	453.0	41.788	-7.622	0.022	-3.163	0.028	-3.825
GEOMAR	RK05-3	454-456 e	455.0	42.010	-8.886	0.027	-3.598	0.053	-4.257

Table G.1 (continued)

Laboratory	Sample		Depth (mm)	Age (kyr B.P.)	$\delta^{13}C$ (vs. PDB)	$\delta^{13}C$ st. dev.	$\delta^{18}O$ (vs. PDB)	$\delta^{18}O$ st. dev.	$\delta^{18}O$ ice vol. adj.
GEOMAR	RK05-3	456-458 e	457.0	42.232	-7.970	0.037	-3.624	0.049	-4.264
GEOMAR	RK05-3	458-460 e	459.0	42.454	-5.829	0.024	-3.586	0.032	-4.207
GEOMAR	RK05-3	460-462 e	461.0	42.677	-9.389	0.013	-3.819	0.054	-4.421
GEOMAR	RK05-3	462-464 e	463.0	42.899	-9.366	0.019	-3.717	0.028	-4.299
GEOMAR	RK05-3	464-466 e	465.0	43.121	-9.338	0.009	-3.576	0.024	-4.139
GEOMAR	RK05-3	466-468 e	467.0	43.343	-8.994	0.020	-3.491	0.026	-4.035
GEOMAR	RK05-3	468-470 e	469.0	43.565	-8.892	0.014	-3.467	0.036	-3.992
GEOMAR	RK05-3	470-472 e	471.0	43.787	-9.125	0.016	-4.004	0.030	-4.510
GEOMAR	RK05-3	472-474 e	473.0	44.009	-8.481	0.016	-4.432	0.036	-4.920
GEOMAR	RK05-3	474-476 e	475.0	44.232	-8.416	0.020	-4.197	0.021	-4.697
GEOMAR	RK05-3	476-478 e	477.0	44.454	-7.336	0.029	-3.891	0.028	-4.403
GEOMAR	RK05-3	478-480 e	479.0	44.676	-6.137	0.031	-3.893	0.035	-4.417
GEOMAR	RK05-3	480-482 e	481.0	44.898	-5.870	0.026	-3.918	0.045	-4.455
GEOMAR	RK05-3	482-484 e	483.0	45.120	-6.144	0.025	-4.072	0.049	-4.621
GEOMAR	RK05-3	484-486 e	485.0	45.342	-7.076	0.040	-4.063	0.034	-4.624
GEOMAR	RK05-3	486-488 e	487.0	45.564	-7.566	0.014	-3.987	0.043	-4.560
GEOMAR	RK05-3	488-490 e	489.0	45.787	-8.613	0.015	-3.961	0.021	-4.546
GEOMAR	RK05-3	490-492 e	491.0	46.009	-6.195	0.013	-3.810	0.023	-4.407
GEOMAR	RK05-3	492-494 e	493.0	46.231	-7.083	0.019	-4.008	0.022	-4.592
GEOMAR	RK05-3	494-496 e	495.0	46.453	-6.838	0.032	-3.816	0.029	-4.389
GEOMAR	RK05-3	496-498 e	497.0	46.675	-7.250	0.019	-3.711	0.026	-4.271
GEOMAR	RK05-3	498-500 e	499.0	46.897	-6.417	0.009	-3.585	0.034	-4.133
GEOMAR	RK05-3	500-502 e	501.0	47.119	-7.182	0.013	-3.709	0.020	-4.245
GEOMAR	RK05-3	502-504 e	503.0	47.342	-7.801	0.023	-3.664	0.030	-4.188
GEOMAR	RK05-3	504-506 e	505.0	47.564	-7.319	0.024	-3.959	0.030	-4.470
GEOMAR	RK05-3	506-508 e	507.0	47.786	-8.331	0.016	-3.863	0.016	-4.362

Table G.1 (continued)

Laboratory	Sample		Depth (mm)	Age (kyr B.P.)	$\delta^{13}C$ (vs. PDB)	$\delta^{13}C$ st. dev.	$\delta^{18}O$ (vs. PDB)	$\delta^{18}O$ st. dev.	$\delta^{18}O$ ice vol. adj.
GEOMAR	RK05-3	508-510 e	509.0	48.008	-8.085	0.017	-3.943	0.031	-4.430
GEOMAR	RK05-3	510-512 e	511.0	48.230	-7.190	0.026	-4.093	0.033	-4.567
GEOMAR	RK05-3	512-514 e	513.0	48.452	-6.227	0.012	-3.984	0.061	-4.446
GEOMAR	RK05-3	514-516 e	515.0	48.674	-7.886	0.033	-4.108	0.076	-4.558
GEOMAR	RK05-3	516-518 e	517.0	48.897	-7.923	0.016	-4.200	0.032	-4.638
GEOMAR	RK05-3	518-520 e	519.0	49.119	-7.441	0.025	-4.384	0.038	-4.821
GEOMAR	RK05-3	520-522 e	521.0	49.341	-8.045	0.023	-3.943	0.020	-4.387
GEOMAR	RK05-3	522-524 e	523.0	49.563	-7.706	0.027	-4.200	0.035	-4.653
GEOMAR	RK05-3	524-526 e	525.0	49.785	-7.253	0.024	-4.148	0.048	-4.609
GEOMAR	RK05-3	526-528 e	527.0	50.007	-7.566	0.028	-4.235	0.029	-4.704
GEOMAR	RK05-3	528-530 e	529.0	50.229	-7.897	0.013	-3.785	0.021	-4.262
GEOMAR	RK05-3	530-532 e	531.0	50.452	-5.646	0.023	-4.256	0.037	-4.741
GEOMAR	RK05-3	532-534 e	533.0	50.674	-4.812	0.013	-3.992	0.023	-4.470
GEOMAR	RK05-3	534-536 e	535.0	50.896	-4.888	0.018	-3.554	0.029	-4.021
GEOMAR	RK05-3	536-538 e	537.0	51.118	-6.512	0.020	-3.533	0.032	-3.988
GEOMAR	RK05-3	538-540 e	539.0	51.340	-6.603	0.014	-3.619	0.025	-4.062
GEOMAR	RK05-3	540-542 e	541.0	51.562	-6.259	0.015	-3.350	0.028	-3.781
GEOMAR	RK05-3	542-544 e	543.0	51.784	-7.083	0.018	-3.970	0.034	-4.389
WAIKATO	RK05-3	544-546 e	545.0	52.007	-7.91	0.06	-3.87	0.12	-4.280
WAIKATO	RK05-3	546-548 e	547.0	52.229	-7.92	0.06	-3.82	0.12	-4.261
WAIKATO	RK05-3	548-550 e	549.0	52.451	-8.84	0.06	-3.98	0.12	-4.452
WAIKATO	RK05-3	550-552 e	551.0	52.673	-4.08	0.06	-4.57	0.12	-5.074
WAIKATO	RK05-3	552-554 e	553.0	52.895	-6.11	0.06	-3.32	0.12	-3.855
WAIKATO	RK05-3	554-556 e	555.0	53.117	-5.12	0.06	-3.12	0.12	-3.670

Appendix H: RK05-4 Stable Isotope Data

Table H.1: Stable carbon and oxygen isotope ratios from RK05-4 calcite. Values are reported relative to Vienna Peedee Belemnite in per mil (‰) notation. Ages are reported as thousands of years before present (kyr B.P.), where present is defined as 2000 AD. Ice volume adjusted $\delta^{18}O$ values (ice vol. adj.) are also given.

Sample		Depth (mm)	Age (kyr B.P.)	$\delta^{13}C$ (‰)	$\delta^{13}C$ st. dev.	$\delta^{18}O$ (‰)	$\delta^{18}O$ st. dev.	$\delta^{18}O$ ice vol. adj.
RK05-4	0-2 a	0.11	72.581	-5.95	0.06	-3.68	0.12	-4.10
RK05-4	0-2 e	1.00	72.595	-7.32	0.06	-3.65	0.12	-4.07
RK05-4	2-4 a	2.11	72.612	-7.26	0.06	-3.33	0.12	-3.76
RK05-4	2-4 e	3.00	72.625	-8.43	0.06	-3.95	0.12	-4.38
RK05-4	4-6 a	4.11	72.642	-7.56	0.06	-4.12	0.12	-4.55
RK05-4	4-6 e	5.00	72.656	-8.42	0.06	-3.91	0.12	-4.34
RK05-4	6-8 a	6.11	72.673	-8.65	0.06	-3.68	0.12	-4.11
RK05-4	6-8 e	7.00	72.687	-8.37	0.06	-3.36	0.12	-3.79
RK05-4	8-10 a	8.11	72.704	-10.01	0.06	-3.73	0.12	-4.16
RK05-4	8-10 e	9.00	72.717	-10.05	0.06	-3.77	0.12	-4.20
RK05-4	10-12 a	10.11	72.734	-8.89	0.06	-3.84	0.12	-4.27
RK05-4	10-12 e	11.00	72.748	-9.65	0.06	-4.04	0.12	-4.47
RK05-4	12-14 a	12.11	72.765	-9.44	0.06	-3.73	0.12	-4.16
RK05-4	12-14 e	13.00	72.779	-9.50	0.06	-4.08	0.12	-4.51
RK05-4	14-16 a	14.11	72.796	-9.36	0.06	-3.60	0.12	-4.03
RK05-4	14-16 e	15.00	72.810	-9.86	0.06	-4.45	0.12	-4.88
RK05-4	16-18 a	16.11	72.827	-9.43	0.06	-4.02	0.12	-4.45
RK05-4	16-18 e	17.00	72.840	-9.34	0.06	-3.79	0.12	-4.22
RK05-4	18-20 a	18.11	72.857	-9.33	0.06	-4.16	0.12	-4.59
RK05-4	18-20 e	19.00	72.871	-9.04	0.06	-3.75	0.12	-4.18
RK05-4	20-22 a	20.11	72.888	-8.99	0.06	-3.43	0.12	-3.86
RK05-4	20-22 e	21.00	72.902	-8.28	0.06	-3.83	0.12	-4.27
RK05-4	22-24 a	22.11	72.919	-8.35	0.06	-3.90	0.12	-4.34
RK05-4	22-24 e	23.00	72.932	-8.19	0.06	-3.89	0.12	-4.33
RK05-4	24-26 a	24.11	72.949	-8.25	0.06	-4.51	0.12	-4.95
RK05-4	24-26 e	25.00	72.963	-7.40	0.06	-3.65	0.12	-4.09
RK05-4	26-28 a	26.11	72.980	-7.83	0.06	-3.94	0.12	-4.38
RK05-4	26-28 e	27.00	72.994	-8.34	0.06	-4.28	0.12	-4.72
RK05-4	28-30 a	28.11	73.011	-8.58	0.06	-4.06	0.12	-4.50
RK05-4	28-30 e	29.00	73.025	-8.07	0.06	-4.18	0.12	-4.62
RK05-4	30-32 a	30.11	73.042	-6.57	0.06	-4.08	0.12	-4.52
RK05-4	30-32 e	31.00	73.055	-6.71	0.06	-4.01	0.12	-4.45
RK05-4	32-34 a	32.11	73.072	-6.78	0.06	-4.06	0.12	-4.50
RK05-4	32-34 e	33.00	73.086	-6.95	0.06	-4.09	0.12	-4.53
RK05-4	34-36 a	34.11	73.103	-8.45	0.06	-4.02	0.12	-4.46
RK05-4	34-36 e	35.00	73.117	-7.93	0.06	-4.21	0.12	-4.65
RK05-4	36-38 a	36.11	73.134	-8.22	0.06	-4.16	0.12	-4.60
RK05-4	36-38 e	37.00	73.147	-9.20	0.06	-4.65	0.12	-5.09
RK05-4	38-40 a	38.11	73.164	-8.96	0.06	-4.17	0.12	-4.61
RK05-4	38-40 e	39.00	73.178	-8.86	0.06	-4.27	0.12	-4.71
RK05-4	40-42 a	40.11	73.195	-9.61	0.06	-4.38	0.12	-4.83
RK05-4	40-42 e	41.00	73.209	-7.70	0.06	-3.85	0.12	-4.30

Table H.1 (continued)

Sample		Depth (mm)	Age (kyr B.P.)	$\delta^{13}C$ (‰)	$\delta^{13}C$ st. dev.	$\delta^{18}O$ (‰)	$\delta^{18}O$ st. dev.	$\delta^{18}O$ ice vol. adj.
RK05-4	42-44 a	42.11	73.226	-7.30	0.06	-4.10	0.12	-4.55
RK05-4	42-44 e	43.00	73.240	-7.21	0.06	-4.18	0.12	-4.63
RK05-4	44-46 a	44.11	73.257	-7.74	0.06	-4.93	0.12	-5.38
RK05-4	44-46 e	45.00	73.270	-9.21	0.06	-4.37	0.12	-4.82
RK05-4	46-48 a	46.11	73.287	-9.11	0.06	-4.50	0.12	-4.95
RK05-4	46-48 e	47.00	73.301	-8.08	0.06	-4.33	0.12	-4.78
RK05-4	48-50 a	48.11	73.318	-8.31	0.06	-4.48	0.12	-4.93
RK05-4	48-50 e	49.00	73.332	-8.89	0.06	-4.46	0.12	-4.91
RK05-4	50-52 a	50.11	73.348	-8.31	0.06	-4.57	0.12	-5.02
RK05-4	50-52 e	51.00	73.362	-7.72	0.06	-3.97	0.12	-4.42
RK05-4	52-54 a	52.11	73.379	-8.27	0.06	-4.07	0.12	-4.52
RK05-4	52-54 e	53.00	73.392	-9.06	0.06	-4.54	0.12	-4.99
RK05-4	54-56 a	54.11	73.409	-9.62	0.06	-4.26	0.12	-4.71
RK05-4	54-56 e	55.00	73.423	-9.58	0.06	-4.15	0.12	-4.60
RK05-4	56-58 a	56.11	73.440	-8.88	0.06	-4.15	0.12	-4.60
RK05-4	56-58 e	57.00	73.453	-9.03	0.06	-4.11	0.12	-4.56
RK05-4	58-60 a	58.11	73.470	-8.92	0.06	-4.16	0.12	-4.61
RK05-4	58-60 e	59.00	73.484	-8.92	0.06	-4.30	0.12	-4.76
RK05-4	60-62 a	60.11	73.501	-8.50	0.06	-3.91	0.12	-4.37
RK05-4	60-62 e	61.00	73.514	-8.18	0.06	-3.63	0.12	-4.09
RK05-4	62-64 a	62.11	73.531	-8.45	0.06	-3.69	0.12	-4.15
RK05-4	62-64 e	63.00	73.545	-8.72	0.06	-4.08	0.12	-4.54
RK05-4	64-66 a	64.11	73.562	-8.72	0.06	-4.06	0.12	-4.52
RK05-4	64-66 e	65.00	73.575	-9.08	0.06	-4.09	0.12	-4.55
RK05-4	66-68 a	66.11	73.592	-9.19	0.06	-4.12	0.12	-4.58
RK05-4	66-68 e	67.00	73.606	-9.66	0.06	-4.09	0.12	-4.55
RK05-4	68-70 a	68.11	73.623	-9.91	0.06	-4.26	0.12	-4.72
RK05-4	68-70 e	69.00	73.636	-9.87	0.06	-4.72	0.12	-5.18
RK05-4	70-72 a	70.11	73.653	-8.77	0.06	-4.07	0.12	-4.53
RK05-4	70-72 e	71.00	73.667	-9.50	0.06	-4.38	0.12	-4.84
RK05-4	72-74 a	72.11	73.684	-7.64	0.06	-3.88	0.12	-4.34
RK05-4	72-74 e	73.00	73.697	-7.53	0.06	-4.05	0.12	-4.51
RK05-4	74-76 a	74.11	73.714	-7.76	0.06	-3.82	0.12	-4.28
RK05-4	74-76 e	75.00	73.728	-7.09	0.06	-4.04	0.12	-4.50
RK05-4	76-78 a	76.11	73.745	-6.31	0.06	-4.28	0.12	-4.74
RK05-4	76-78 e	77.00	73.758	-7.61	0.06	-4.14	0.12	-4.60
RK05-4	78-80 a	78.11	73.775	-9.01	0.06	-4.46	0.12	-4.93
RK05-4	78-80 e	79.00	73.789	-8.50	0.06	-4.56	0.12	-5.03
RK05-4	80-82 a	80.11	73.806	-7.14	0.06	-3.89	0.12	-4.36
RK05-4	82-84 a	82.11	73.836	-7.98	0.06	-4.50	0.12	-4.97
RK05-4	82-84 e	83.00	73.850	-8.29	0.06	-3.89	0.12	-4.36
RK05-4	84-86 a	84.11	73.867	-7.94	0.06	-5.95	0.12	-6.42
RK05-4	84-86 e	85.00	73.880	-8.31	0.06	-4.37	0.12	-4.84
RK05-4	86-88 a	86.11	73.897	-5.56	0.06	-4.17	0.12	-4.64
RK05-4	86-88 e	87.00	73.911	-6.91	0.06	-4.13	0.12	-4.60
RK05-4	88-90 a	88.11	73.927	-8.82	0.06	-4.17	0.12	-4.64
RK05-4	88-90 e	89.00	73.941	-7.18	0.06	-4.26	0.12	-4.73
RK05-4	90-92 a	90.11	73.958	-8.17	0.06	-4.06	0.12	-4.53
RK05-4	90-92 e	91.00	73.972	-9.30	0.06	-4.35	0.12	-4.82
RK05-4	92-94 a	92.11	73.988	-8.77	0.06	-4.10	0.12	-4.57
RK05-4	92-94 e	93.00	74.002	-9.02	0.06	-4.41	0.12	-4.88

Table H.1 (continued)

Sample	Depth (mm)	Age (kyr B.P.)	$\delta^{13}C$ (‰)	$\delta^{13}C$ st. dev.	$\delta^{18}O$ (‰)	$\delta^{18}O$ st. dev.	$\delta^{18}O$ ice vol. adj.
RK05-4 94-96 a	94.11	74.019	-9.57	0.06	-4.53	0.12	-5.00
RK05-4 94-96 e	95.00	74.032	-10.24	0.06	-4.28	0.12	-4.76
RK05-4 96-98 a	96.11	74.049	-10.08	0.06	-4.52	0.12	-4.99
RK05-4 96-98 e	97.00	74.063	-10.53	0.06	-4.11	0.12	-4.58
RK05-4 98-100 a	98.11	74.080	-10.17	0.06	-4.34	0.12	-4.82
RK05-4 98-100 e	99.00	74.093	-9.83	0.06	-4.05	0.12	-4.52
RK05-4 100-102 a	100.11	74.110	-9.55	0.06	-4.50	0.12	-4.98
RK05-4 100-102 e	101.00	74.124	-9.33	0.06	-4.16	0.12	-4.64
RK05-4 102-104 a	102.11	74.141	-9.71	0.06	-4.57	0.12	-5.05
RK05-4 102-104 e	103.00	74.154	-10.35	0.06	-4.47	0.12	-4.95
RK05-4 104-106 a	104.11	74.171	-10.46	0.06	-4.47	0.12	-4.95
RK05-4 104-106 e	105.00	74.185	-9.19	0.06	-3.98	0.12	-4.46
RK05-4 106-108 a	106.11	74.202	-9.09	0.06	-4.19	0.12	-4.67
RK05-4 106-108 e	107.00	74.217	-9.76	0.06	-4.28	0.12	-4.76
RK05-4 108-110 a	108.11	74.296	-8.69	0.06	-5.28	0.12	-5.76
RK05-4 108-110 e	109.00	74.360	-7.76	0.06	-4.07	0.12	-4.55
RK05-4 110-112 a	110.11	74.439	-7.55	0.06	-4.05	0.12	-4.54
RK05-4 110-112 e	111.00	74.503	-8.30	0.06	-4.12	0.12	-4.61
RK05-4 112-114 a	112.11	74.582	-8.70	0.06	-3.95	0.12	-4.44
RK05-4 112-114 e	113.00	74.646	-9.08	0.06	-4.37	0.12	-4.87
RK05-4 114-116 a	114.11	74.725	-8.95	0.06	-4.05	0.12	-4.55
RK05-4 114-116 e	115.00	74.789	-8.39	0.06	-4.39	0.12	-4.89
RK05-4 116-118 a	116.11	74.868	-7.80	0.06	-4.06	0.12	-4.56
RK05-4 116-118 e	117.00	74.932	-8.63	0.06	-4.02	0.12	-4.52
RK05-4 118-120 a	118.11	75.011	-8.82	0.06	-4.32	0.12	-4.83
RK05-4 118-120 e	119.00	75.075	-8.91	0.06	-4.26	0.12	-4.77
RK05-4 120-122 a	120.11	75.154	-7.95	0.06	-4.33	0.12	-4.84
RK05-4 120-122 e	121.00	75.217	-9.48	0.06	-4.32	0.12	-4.84
RK05-4 122-124 a	122.11	75.297	-7.66	0.06	-4.09	0.12	-4.61
RK05-4 124-126 a	124.11	75.440	-8.81	0.06	-3.97	0.12	-4.49
RK05-4 124-126 e	125.00	75.503	-9.27	0.06	-4.06	0.12	-4.58
RK05-4 126-128 a	126.11	75.583	-8.39	0.06	-3.82	0.12	-4.35
RK05-4 126-128 e	127.00	75.646	-8.66	0.06	-4.09	0.12	-4.62
RK05-4 128-130 a	128.11	75.726	-8.80	0.06	-4.22	0.12	-4.75
RK05-4 128-130 e	129.00	75.789	-8.11	0.06	-4.03	0.12	-4.56
RK05-4 130-132 a	130.11	75.869	-9.34	0.06	-4.23	0.12	-4.77
RK05-4 130-132 e	131.00	75.932	-9.39	0.06	-4.33	0.12	-4.87
RK05-4 132-134 a	132.11	76.011	-10.13	0.06	-4.20	0.12	-4.74
RK05-4 132-134 e	133.00	76.075	-10.80	0.06	-4.12	0.12	-4.66
RK05-4 134-136 a	134.11	78.319	-10.70	0.06	-4.58	0.12	-4.99
RK05-4 134-136 e	135.00	80.113	-9.52	0.06	-4.10	0.12	-4.53
RK05-4 136-138 a	136.11	82.357	-8.55	0.06	-3.61	0.12	
RK05-4 136-138 e	137.00	84.152	-9.34	0.06	-3.88	0.12	
RK05-4 138-140 a	138.11	86.396	-9.73	0.06	-4.36	0.12	
RK05-4 138-140 e	139.00	88.190	-10.43	0.06	-4.72	0.12	
RK05-4 140-142 a	140.11	90.434	-9.92	0.06	-4.48	0.12	
RK05-4 140-142 e	141.00	92.229	-9.75	0.06	-4.50	0.12	
RK05-4 142-144 a	142.11	94.472	-10.75	0.06	-4.52	0.12	
RK05-4 142-144 e	143.00	96.267	-10.67	0.06	-4.59	0.12	
RK05-4 144-146 a	144.11	98.511	-10.39	0.06	-4.58	0.12	
RK05-4 144-146 e	145.00	100.306	-9.90	0.06	-4.37	0.12	
RK05-4 146-148 a	146.11	102.325	-9.79	0.06	-4.25	0.12	

Appendix I: RK05-1 Trace Element Data

Table I.1: Trace element concentrations (in ppm) in RK05-1b calcite as determined from laser ablation 'spot' analyses.

Sample	^{23}Na	^{24}Mg	^{31}P	^{42}Ca	^{86}Sr	^{87}Sr	^{88}Sr	^{138}Ba	^{232}Th	^{238}U
NIST 612	103864.1	78.4	41.7	85263	75.1	76.4	76.4	37.7	37.3	37.5
NIST 612	103803.9	76.9	71.9	85263	77.3	76.1	76.0	37.9	37.3	37.1
RK05-1b 2mm	110.1	696.5	399.5	400233	64.8	25.3	64.0	13.3	0.0649	0.0935
RK05-1b 4mm	41.1	640.2	435.2	400233	68.4	25.5	66.2	13.5	<0.0060	0.0857
RK05-1b 6mm	37.4	614.1	348.5	400233	70.2	26.0	69.7	13.4	0.005	0.1035
RK05-1b 8mm	35.7	570.4	377.4	400233	67.4	25.3	67.1	13.1	<0.0055	0.1001
RK05-1b 10mm	30.8	523.3	430.3	400233	65.4	25.1	65.7	12.0	<0.0043	0.0914
RK05-1b 12mm	34.6	529.2	448.9	400233	62.1	23.4	62.3	12.1	<0.0054	0.0862
RK05-1b 14mm	33.8	525.2	341.4	400233	70.0	26.3	70.2	13.1	<0.0051	0.1079
RK05-1b 16mm	37.5	567.4	268.3	400233	74.2	28.0	74.8	13.9	<0.0054	0.1132
RK05-1b 18mm	28.3	583.0	344.6	400233	62.1	23.4	62.0	10.7	<0.0053	0.0742
RK05-1b 20mm	34.3	621.9	233.6	400233	73.4	27.0	71.9	13.2	<0.0056	0.0866
RK05-1b 22mm	60.1	717.8	341.0	400233	65.0	25.0	64.5	13.8	0.0235	0.0884
RK05-1b 24mm	45.3	619.7	278.9	400233	65.7	24.5	65.3	12.4	<0.0067	0.0817
RK05-1b 26mm	32.1	581.4	286.2	400233	69.1	25.8	69.1	12.5	<0.0044	0.1240
RK05-1b 28mm	34.0	559.1	297.2	400233	67.4	25.6	67.8	13.0	0.0066	0.1059
RK05-1b 30mm	31.2	687.0	202.7	400233	68.7	26.5	68.4	12.6	<0.0050	0.0730
RK05-1b 32mm	45.6	543.4	334.1	400233	67.6	25.3	67.9	13.4	<0.0060	0.1126
RK05-1b 34mm	38.6	506.6	256.2	400233	73.8	27.1	72.4	13.2	<0.0052	0.0957
RK05-1b 36mm	31.7	645.1	248.8	400233	69.2	26.2	68.2	12.6	<0.0055	0.0749
RK05-1b 38mm	41.3	638.1	222.7	400233	74.7	29.0	73.7	14.2	0.0639	0.0764
NIST 612	102242.6	76.7	48.5	85263	76.0	76.0	76.3	37.4	36.3	36.1
NIST 612	103642.5	74.7	52.0	85263	75.5	74.8	75.4	37.2	37.2	36.7

Table I.2: One standard deviation errors (in ppm) of measured trace element concentrations in RK05-1b calcite.

Sample	^{23}Na	^{24}Mg	^{31}P	^{42}Ca	^{86}Sr	^{87}Sr	^{88}Sr	^{138}Ba	^{232}Th	^{238}U
NIST 612	5808.9	5.26	30.19	2715.37	3.11	2.84	2.5	1.34	1.45	1.71
NIST 612	5799.32	5.16	48.72	2714.7	3.19	2.83	2.48	1.34	1.45	1.69
RK05-1b 2mm	6.2	45.9	259.94	12664.28	2.59	0.95	2.08	0.47	0.0072	0.0087
RK05-1b 4mm	2.35	42.32	277.43	12662.92	2.72	0.95	2.15	0.48	0.0027	0.0078
RK05-1b 6mm	2.14	40.79	217.97	12662.56	2.8	0.97	2.26	0.48	0.0026	0.0083
RK05-1b 8mm	2.05	38.14	231.91	12663.19	2.7	0.95	2.18	0.47	0.0021	0.0086
RK05-1b 10mm	1.78	35.26	260.03	12663.47	2.64	0.95	2.14	0.43	0.0023	0.0083
RK05-1b 12mm	1.99	35.99	267.08	12664.07	2.53	0.9	2.03	0.44	0.0024	0.0082
RK05-1b 14mm	1.95	36.09	200.18	12663.83	2.86	1	2.3	0.47	0.0026	0.0094
RK05-1b 16mm	2.15	39.43	155.21	12662.9	3.04	1.06	2.45	0.5	0.0024	0.0091
RK05-1b 18mm	1.64	41.02	196.88	12663	2.58	0.9	2.04	0.39	0.0025	0.0071
RK05-1b 20mm	1.97	44.35	132	12662.91	3.07	1.04	2.37	0.48	0.0027	0.0077
RK05-1b 22mm	3.41	51.94	190.59	12663.07	2.75	0.97	2.13	0.51	0.0043	0.008
RK05-1b 24mm	2.59	45.54	154.42	12663.46	2.81	0.96	2.17	0.46	0.0035	0.008
RK05-1b 26mm	1.86	43.41	157.04	12663.29	2.99	1.02	2.3	0.47	0.002	0.01
RK05-1b 28mm	1.96	42.44	161.77	12662.92	2.95	1.02	2.27	0.49	0.0027	0.0091
RK05-1b 30mm	1.81	53.05	109.55	12663.09	3.04	1.06	2.3	0.48	0.0023	0.0072
RK05-1b 32mm	2.62	42.71	179.31	12663.19	3.03	1.03	2.29	0.52	0.0025	0.0096
RK05-1b 34mm	2.23	40.54	136.75	12663.18	3.34	1.11	2.46	0.51	0.0028	0.0087
RK05-1b 36mm	1.84	52.57	132.09	12662.43	3.18	1.08	2.32	0.49	0.0027	0.0072
RK05-1b 38mm	2.39	52.98	117.69	12662.5	3.47	1.2	2.52	0.56	0.0062	0.0072
NIST 612	5814.11	6.56	25.94	2712.37	3.68	3.19	2.65	1.5	1.69	2.06
NIST 612	5908.88	6.51	27.55	2711.56	3.7	3.17	2.63	1.51	1.75	2.12

Table I.3: Minimum detection limits (in ppm; 99 % confidence) of trace elements analyzed for in RK05-1b calcite.

Sample	^{23}Na	^{24}Mg	^{31}P	^{42}Ca	^{86}Sr	^{87}Sr	^{88}Sr	^{138}Ba	^{232}Th	^{238}U
NIST 612	0.939	0.124	21.41	109.12	0.739	0.21	0.0326	0.0139	0.0147	0.0127
NIST 612	4.420	0.180	19.28	109.94	0.713	0.225	0.0496	0.0284	0.0259	0.0275
RK05-1b 2mm	0.444	0.060	9.30	50.97	0.33	0.12	0.0165	0.00734	0.00701	0.00648
RK05-1b 4mm	0.313	0.051	6.56	38.37	0.264	0.0783	0.0131	0.00553	0.00601	0.00591
RK05-1b 6mm	0.313	0.044	5.49	32.39	0.243	0.0776	0.0113	0.00573	0.00478	0.00453
RK05-1b 8mm	0.289	0.080	6.00	35.2	0.259	0.0827	0.0159	0.00593	0.00555	0.00544
RK05-1b 10mm	0.296	0.083	5.45	31.76	0.249	0.0772	0.0117	0.00659	0.00425	0.00575
RK05-1b 12mm	0.317	0.056	5.22	31.94	0.232	0.081	0.0125	0.00671	0.00538	0.00541
RK05-1b 14mm	0.309	0.060	5.35	32.58	0.272	0.0913	0.0139	0.00586	0.00509	0.00622
RK05-1b 16mm	0.278	0.060	4.80	29.71	0.25	0.0722	0.0121	0.00544	0.00537	0.00464
RK05-1b 18mm	0.269	0.084	4.80	31.26	0.255	0.0727	0.0164	0.00565	0.0053	0.00485
RK05-1b 20mm	0.294	0.103	4.80	34.14	0.246	0.0828	0.0169	0.00688	0.00564	0.00434
RK05-1b 22mm	0.294	0.065	4.73	30.15	0.241	0.0801	0.0129	0.00656	0.00568	0.00488
RK05-1b 24mm	0.301	0.087	4.75	31.19	0.257	0.0793	0.0139	0.0063	0.00666	0.0063
RK05-1b 26mm	0.314	0.085	4.67	30.56	0.253	0.0797	0.0117	0.00723	0.00444	0.00532
RK05-1b 28mm	0.306	0.085	4.31	29.59	0.249	0.0745	0.0144	0.00625	0.00449	0.00557
RK05-1b 30mm	0.305	0.092	4.50	31.02	0.254	0.086	0.0157	0.00523	0.00497	0.0051
RK05-1b 32mm	0.303	0.102	4.37	30.43	0.259	0.083	0.0143	0.0065	0.00603	0.00548
RK05-1b 34mm	0.289	0.076	3.95	27.69	0.223	0.0773	0.012	0.00615	0.00515	0.00522
RK05-1b 36mm	0.282	0.078	3.86	27.5	0.222	0.0821	0.0162	0.00597	0.00554	0.00473
RK05-1b 38mm	0.283	0.079	3.69	27.24	0.225	0.071	0.0151	0.00593	0.004	0.00382
NIST 612	0.657	0.213	8.43	63.88	0.538	0.196	0.0346	0.0147	0.0104	0.00987
NIST 612	1.840	0.112	7.44	55.72	0.517	0.151	0.0291	0.0155	0.0131	0.0116